Norwegian University of Life Sciences
Faculty of Science and Technology

Philosophiae Doctor (PhD)
Thesis 2021:25

Sustainable Fungal Biorefineries: Optimizing production of valuable metabolites in oleaginous Mucoromycota

Bærekraftige soppbioraffinerier: Optimalisering av produksjon av verdifulle metabolitter i oljeaktig Mucoromycota

Simona Dzurendova

Sustainable Fungal Biorefineries: Optimizing production of valuable metabolites in oleaginous Mucoromycota

Bærekraftige soppbioraffinerier: Optimalisering av produksjon av verdifulle metabolitter i oljeaktig Mucoromycota

Philosophiae Doctor (PhD) Thesis

Simona Dzurendova

Norwegian University of Life Sciences

Faculty of Science and Technology

Ås 2021

Thesis number 2021:25

ISSN 1894-6402

ISBN 978-82-575-1797-7

simona.dzurendova@gmail.com
Doctoral thesis

Main supervisor: Assoc. Prof. Dr. Volha Shapaval
Norwegian University of Life Sciences
Faculty of Science and Technology
volha.shapaval@nmbu.no

Co-supervisors: Dr. Boris Zimmermann
Norwegian University of Life Sciences
Faculty of Science and Technology
boris.zimmermann@nmbu.no

Prof. Dr. Achim Kohler
Norwegian University of Life Sciences
Faculty of Science and Technology
achim.kohler@nmbu.no

Prof. Dr. Svein Jarle Horn
Norwegian University of Life Sciences
Faculty of Chemistry, Biotechnology and Food Science
svein.horn@nmbu.no

Evaluation committee: Prof. Dr. Volkmar Passoth
Swedish University of Agricultural Sciences
volkmar.passoth@slu.se

Prof. Dr. Ganesh Sockalingum
University of Reims Champagne-Ardenne
ganesh.sockalingum@univ-reims.fr

Coordinator: Assoc. Prof. Dr. Kristian Berland
Norwegian University of Life Sciences
Faculty of Science and Technology
kristian.berland@nmbu.no

Table of contents

Acknowledgements

The research in the presented doctoral thesis was conducted from September 2017 to January 2021 at the Norwegian University of Life Sciences (NMBU), Faculty of Science and Technology, in the Biospectroscopy and Data Modelling group (BioSpec, Norway), in a collaboration with the Faculty of Chemistry, Biotechnology and Food Science, NMBU. The PhD work was funded by the Norwegian University of Life Sciences (NMBU) and the Norwegian Research Council (Bio4Fuels project, reference number 257622).

I would like to show my gratitude to my main supervisor Volha Shapaval and co-supervisors Boris Zimmermann and Achim Kohler for all the guidance throughout the PhD study and sharing their expertise. Thank you for always being helpful and available despite the busy schedule, for the discussions, contributions, respectful and empathetic approach, and for giving me the opportunity to be part of the BioSpec group. Many thanks to Valeria Tafintseva, not only for the contributions concerning data analysis, but also for care and helping with personal matters. I'm thankful to my co-supervisor Svein Jarle Horn for his contributions and welcoming offer to use the infrastructure of the Bioprocess technology and Biorefining group. Dag Ekeberg, Kasper Reitzel, Ulla Gro Nielsen, Dana Byrtusova, Martin Szotkowski, Ivana Marova, Milan Certik, Ondrej Slany, Benjamin Xavier Dupuy—Galet and Shaun Allan Leivers, your time and expertise which contributed to the publications presented in this thesis are highly appreciated. Johanne Solheim, thank you for being a good friend in happy and challenging times. Maren Anna Brandsrud and Eivind Seim, I appreciate the time spent with you either at work or in your welcoming home/cabin. Further, I would like to thank Vlad Blazhko for his technical time-saving solutions and interesting discussions. Volha Akulova, Margarita Smirnova, Dana Byrtusova, Johanna Blomqvist, Kai Fjær, Pernille Olsen and Anne Marie Langseter, it was pleasure to share the lab with you and spending either work- or free time together has brought a lot of great memories. I would like to acknowledge all members of Biospec group for creating a friendly working environment, Kristin Forfang and Gergely Kosa for performing groundwork for the methodology I used and Berit Hauger Lindstad for all help with PhD coordination.

Finally, I would like to thank my family for their support. Jozef, I'm grateful for all your care and companionship throughout this adventure.

Abstract

Fungal biorefineries are important players in the emerging global bioeconomy and contribute to the transition from the traditional fossil-based production to a renewable, sustainable and environment-friendly bio-production. In such biorefineries, fermentation utilizing fungi as cell factories is a central process. Development of sustainable fungal biorefineries involves optimization of fungal fermentation for efficient feedstock utilization and high product yields. Since lignocellulosic biomass is sustainable and of high abundance, lignocellulose hydrolysates are considered as key carbon sources for large scale fungal fermentation. Mucoromycota filamentous fungi are powerful cell factories able to valorize hydrolyzed lignocellulose materials into a range of marketable products, such as lipids, biopolymers, pigments, proteins, enzymes and organic acids. Currently, the use of Mucoromycota for industrial production of fungal lipids for food, feed and biofuels applications is not economically viable. Therefore, a co-production concept has been proposed where several valuable bio-products can be produced in a single fungal fermentation process.

This PhD work has focused on optimizing co-production of several metabolites in oleaginous Mucoromycota fungi by manipulation of growth media composition, with the ultimate goal of improving the economic sustainability of fungal biorefineries. The following media parameters were manipulated-type of nitrogen source, concentration of phosphorus substrate, and concentration of different metal ions. The optimization was performed using a high-throughput micro-cultivation system (Duetz- microtiter plate system) combined with different analytical techniques including vibrational spectroscopy. Total fungal lipid content was estimated either by gravimetry or gas chromatography (GC), while lipid profile was characterized by GC and nuclear magnetic resonance spectroscopy (NMR). NMR was also used for the characterization of phosphates in Mucoromycota biomass, in addition to estimation of total phosphorus by assay-based UV-visible (UV-VIS) spectroscopy. Fourier transform infrared spectroscopy (FTIR) and Fourier transform Raman spectroscopy (FT-Raman) were utilized for monitoring fungal fermentation in Duetz-MTPS and for biochemical fingerprinting of fungal biomass in order to measure the co-production of intracellular metabolites.

The influence of two nitrogen sources (yeast extract and ammonium sulphate) and different amounts of phosphate substrate on the co-production of lipids, chitin/chitosan and polyphosphate, and on the lipid accumulation, in nine oleaginous Mucoromycota fungi was studied in **Paper I** and **Paper II**,

respectively. To verify co-production, high-throughput FTIR spectroscopy was used as a main analytical method in **Paper I.** In **Paper II,** gas chromatography was used for analyzing the fatty acid profile and total lipid content was estimated gravimetrically. Strains with co-production potential and media components affecting the co-production and lipid accumulation were identified. In **Paper III,** the role of the metal ions calcium, copper, cobalt, iron, magnesium, manganese and zinc for growth of *Mucor circinelloides* was assessed. This strain was used since it is one of the most promising strains for the co-production of lipids, chitin/chitosan and polyphosphate. It was observed that calcium ions have a significant effect on the lipid accumulation in *Mucor circinelloides*. In order to investigate whether the effect of calcium ions is generally valid for other oleaginous Mucoromycota fungi, a study where six Mucoromycota fungi were grown in the presence and absence of calcium ions was performed in **Paper V**. Calcium availability was shown to affect lipid and polyphosphate accumulation under nonacidic conditions, while increased lipid accumulation was recorded mainly in acidic conditions lacking calcium ions. Analysis of fungal lipids was based on the Lewis method that utilizes simultaneous extraction and transesterification of lipids from the fungal biomass. However, since some Mucoromycota strains showed extraordinarily high lipid content while having strong cell wall structures hindering effective extraction, a modification of the Lewis method was developed in **Paper IV.** FTIR and FT-Raman spectroscopy were utilized for biochemical profiling of Mucoromycota biomass for revealing co-production of the targeted valuable metabolites, for monitoring fungal fermentation in Duetz-MTPS, and understanding the effect of the selected media components on Mucoromycota metabolism. In **Paper VI,** a comparison of the monitoring and biochemical profiling capacity of these two spectroscopies was investigated.

Overall, this PhD work has provided knowledge on how manipulation of nitrogen source, phosphorus concentration and metal ions availability allow optimizing co-production in oleaginous Mucoromycota fungi. It was shown that several oleaginous Mucoromycota fungi have a great ability to perform co-production of triglyceride lipids, chitin/chitosan and polyphosphate biopolymers, and carotenoid pigments, and therefore have the potential to be powerful microbial cell factories in sustainable fungal biorefineries. The PhD work has contributed to the development of a more efficient and reliable lipid extraction method. Moreover, it has demonstrated how utilizing of modern vibrational spectroscopy techniques allows rapid and reliable optimization of media components for production of different metabolites and monitoring of fungal fermentations.

Norsk sammendrag

Bioraffinerier er viktige aktører i den kommende globale bioøkonomien og bidrar til overgangen fra tradisjonell fossilbasert produksjon til fornybar, bærekraftig og miljøvennlig bioproduksjon. I slike bioraffinerier er gjæring ved bruk av sopp som cellefabrikker en viktig prosess. Utvikling av bærekraftige soppbioraffinerier innebærer optimalisering av soppgjæring for effektiv råstoffutnyttelse og høye produktutbytter. Siden lignocellulose er et bærekraftig råstoff det finnes mye av, er lignocellulosehydrolysater en viktig potensiell karbonkilde for soppfermentering i storskala. Mucoromycota filamentøse sopp er effektive cellefabrikker som kan foredle hydrolyserte lignocellulosematerialer til en rekke salgbare produkter, som lipider, biopolymerer, pigmenter, proteiner, enzymer og organiske syrer. I dag er ikke bruken av Mucoromycota for industriell produksjon av sopplipider for mat-, fôr- og biodrivstoffanvendelser økonomisk. Derfor er det foreslått et samproduksjonskonsept hvor flere verdifulle bioprodukter kan produseres i en enkelt soppgjæringsprosess.

Dette Doktorgradsarbeidet har fokuset ligget på å optimalisere produksjonen av flere metabolitter i oljerike Mucoromycota-sopp ved å manipulere sammensetningen av vekstmediene, med målet om å forbedre økonomien i soppbioraffinerier. Følgende parametere ble manipulert for å optimalisere vekstmediene: type nitrogenkilde, konsentrasjon av fosforsubstrat og konsentrasjon av forskjellige metallioner. Optimaliseringen ble utført ved hjelp av et mikrodyrkningssystem med stor kapasitet (Duetz-mikrotiterplatesystem) kombinert med forskjellige analytiske teknikker, inkludert vibrasjonsspektroskopi. Det totale innholdet av lipider i soppen ble estimert enten ved bruk av gravimetri eller gasskromatografi (GC), mens lipidprofilen ble bestemt ved bruk av GC og kjernemagnetisk resonansspektroskopi (NMR). NMR ble også brukt til analyse av polyfosfatinnhold i Mucoromycota-biomassen. Fourier transform infrarød spektroskopi (FTIR) og Fourier transform Raman spektroskopi (FT-Raman) ble brukt til å overvåke soppfermentering i Duetz-MTPS og for å få et biokjemisk fingeravtrykk av soppbiomasse for å måle samproduksjon av intracellulære metabolitter.

Effekten av to nitrogenkilder (gjærekstrakt og ammoniumsulfat) og forskjellige mengder fosfatsubstrat på samproduksjon av lipider, kitin/kitosan og polyfosfat, eller på lipidakkumuleringen, i ni oljeaktige Mucoromycota-sopp, ble studert i henholdsvis **Artikkel I** og **Artikkel II**. For å få bekreftet samproduksjon ble høykapasitets FTIR spektroskopi brukt som den viktigste analysemetoden i **Artikkel I**. I **Artikkel II** ble gasskromatografi brukt for å

analysere fettsyreprofilen mens det totale lipidinnholdet ble estimert gravimetrisk. Stammer med samproduksjonspotensial og mediekomponenter som påvirket samproduksjonen og lipidakkumuleringen ble identifisert. I **Artikkel III** ble rollen til metallionene kalsium, kobber, kobolt, jern, magnesium, mangan og sink i forskjellige konsentrasjoner undersøkt for *Mucor circinelloides*. Denne stammen ble brukt siden den er en av de mest lovende stammene for samproduksjon av lipider, kitin/kitosan og polyfosfat. I denne studien ble det observert at kalsiumioner har en signifikant effekt på lipidakkumuleringen i *Mucor circinelloides*. For å undersøke om effekten av kalsiumioner generelt er gyldig for andre oljeaktige Mucoromycota-sopp, ble det i **Artikkel V** dyrket et sett med seks Mucoromycota-sopp i nærvær og fravær av kalsiumioner. Kalsiumtilgjengelighet viste seg å påvirke lipid- og polyfosfatakkumulering under ikke-sure forhold, mens økt lipidakkumulering ble registrert hovedsakelig under sure forhold hvor kalsiumioner manglet. Analysen av sopplipider var basert på Lewis-metoden som benytter samtidig ekstraksjon og transesterifisering av lipider fra soppbiomassen. Siden noen Mucoromycota-stammer har et veldig høyt lipidinnhold, og noen har celleveggstrukturer som hindrer effektiv ekstraksjon, ble en modifisert Lewis-metode utviklet i **Artikkel IV**. FTIR- og FT-Raman-spektroskopi ble brukt til biokjemisk profilering av Mucoromycota-biomasse for å avdekke samproduksjon av de ønskede verdifulle metabolittene, for å overvåke soppgjæring i Duetz-MTPS, og for å forstå effekten av de utvalgte mediekomponentene på Mucoromycota-metabolismen. I **Artikkel VI** ble overvåkingskapasiteten og profileringskapasiteten til disse to spektroskopimetodene sammenlignet

Samlet sett har dette Doktorgradsarbeidet gitt kunnskap om hvordan manipulering av nitrogenkilde, fosforsubstrat og metalliontilgjengelighet muliggjør optimaliseringen av samproduksjon i oljerike Mucoromycota-sopp. Det ble vist at flere oljeaktige Mucoromycota-sopp har et stort potensial til å utføre samproduksjon av triglyseridlipider, kitin/kitosan- og polyfosfatbiopolymerer, samt karotenoidpigmenter, og kan derfor brukes som en effektiv mikrobiell cellefabrikk i bærekraftige soppbioraffinerier. Doktorgradsarbeidet har bidratt til utviklingen av en mer effektiv og pålitelig metode for utvinning av lipider. Videre har det vist hvordan bruk av moderne vibrasjonsspektroskopiteknikker muliggjør rask og pålitelig optimalisering av mediekomponenter for produksjon av forskjellige metabolitter og overvåking av soppgjæring.

List of papers

Paper I

Dzurendova, Simona; Zimmermann, Boris; Kohler, Achim; Tafintseva, Valeria; Slany, Ondrej; Certik, Milan; Shapaval, Volha**. Microcultivation and FTIR spectroscopy-based screening revealed a nutrient-induced co-production of high-value metabolites in oleaginous Mucoromycota fungi.** *PLoS ONE* 2020; 15(6): e0234870. DOI: 10.1371/journal.pone.0234870

Paper II

Dzurendova, Simona; Zimmermann, Boris; Tafintseva, Valeria; Kohler, Achim; Ekeberg, Dag; Shapaval, Volha. **The influence of phosphorus source and the nature of nitrogen substrate on the biomass production and lipid accumulation in oleaginous Mucoromycota fungi.** *Applied Microbiology and Biotechnology* 2020**;** 104, 8065–8076. DOI: 10.1007/s00253-020-10821-7

Paper III

Dzurendova, Simona; Zimmermann, Boris; Tafintseva, Valeria; Kohler, Achim; Horn, Svein Jarle; Shapaval, Volha. **Metal and phosphate ions show remarkable influence on the biomass production and lipid accumulation in oleaginous *Mucor circinelloides.*** *Journal of Fungi* 2020; 6(4), 260. DOI: 10.3390/jof6040260

Paper IV

Langseter, Anne Marie; Dzurendova, Simona; Shapaval, Volha; Kohler, Achim; Ekeberg, Dag; Zimmermann, Boris. **Evaluation and optimization of direct transesterification methods for the assessment of lipid accumulation in oleaginous filamentous fungi.** *Microbial cell factories, resubmitted after first revision.*

Paper V

Dzurendova, Simona; Zimmermann, Boris; Kohler, Achim; Reitzel, Kasper; Nielsen, Ulla Gro; Dupuy—Galet, Benjamin Xavier; Leivers, Shaun Allan; Horn, Svein Jarle; Shapaval, Volha. **Calcium affects polyphosphate and lipid accumulation in Mucoromycota fungi.** *Manuscript.*

Paper VI

Dzurendova, Simona; Shapaval, Volha; Tafintseva, Valeria; Kohler, Achim; Szotkowski, Martin; Byrtusova, Dana; Marova, Ivana; Zimmermann, Boris. **Assessment of fungal biomass by Fourier transform Raman spectroscopy for application in biotechnology and bioprocessing.** *Manuscript.*

Additional scientific contributions

Peer-reviewed research publications

Magnussen, Eirik Almklov; Solheim, Johanne Heitmann; Blazhko, Uladzislau; Tafintseva, Valeria; Tøndel, Kristin; Liland, Kristian Hovde; Dzurendova, Simona; Shapaval, Volha; Kohler, Achim. **Deep convolutional neural network recovers pure absorbance spectra from highly scatter-distorted spectra of cells.** *Journal of Biophotonics* 2020; e202000204. DOI: 10.1002/jbio.202000204

Dubava, Darya; Kohler, Achim; Deniset-Besseau, Ariane; Solheim, Johanne Heitmann; Dzurendova, Simona; Shapaval, Volha. **Multiscale analysis of lipids in dimorphic oleaginous fungi by modern vibrational spectroscopy techniques**. *Manuscript.*

Oral presentations as a main presenting author

Dzurendova, Simona; Zimmermann, Boris; Kohler, Achim; Tafintseva, Valeria; Kòsa, Gergely; Forfang, Kristin; Blomqvist, Johanna Karin Hillevi; Langseter, Anne Marie; Shapaval, Volha. **Application of Fourier transform infrared spectroscopy for developing, monitoring and control of microbial bioprocesses.** European Biotechnology Congress, 24th -26th September 2020. Prague, Czech Republic/ online.

Dzurendova, Simona; Zimmermann, Boris; Kohler, Achim; Shapaval, Volha. **The effect of phosphorus source on the lipid accumulation in oleaginous fungi grown under nitrogen limitation.** European Biotechnology Congress; 11th -13th April 2019. Valencia, Spain.

Posters as a main presenting author

Dzurendova, Simona; Zimmermann, Boris; Kohler, Achim; Hansen, Line Degn; Varnai, Aniko; Horn, Svein Jarle; Eijsink, Vincent; Shapaval, Volha. **Optimization of lignocellulose-based substrates for sustainable production of lipids by oleaginous filamentous fungi.** Bio4Fuels Days 2019: Building a Sustainable European Biofuel Industry; 4th -6th November 2019. Gothenburg, Sweden.

Dzurendova, Simona; Zimmermann, Boris; Tafintseva, Valeria; Kohler, Achim; Shapaval, Volha. **Monitoring the lipid accumulation in oleaginous fungi grown under nitrogen limitation and different phosphorus levels by FTIR spectroscopy combined with multivariate calibration**. BioSpecMLC2019 Workshop on Machine Learning and Chemometrics in Biospectroscopy. 18th-21st August 2019. Minsk, Belarus.

Dzurendova, Simona; Zimmermann, Boris; Kohler, Achim; Shapaval, Volha. **The role of phosphorus in the lipid accumulation of oleaginous fungi.** Copenhagen School of Chemometrics; 6th Mai- 7th June 2020. Copenhagen, Denmark.

Dzurendova, Simona; Zimmermann, Boris; Kohler, Achim; Shapaval, Volha. **The role of phosphorus in the lipid accumulation of oleaginous fungi.** Euro Fed Lipid; 16th – 19th September 2018. Belfast, UK.

Dzurendova, Simona; Zimmermann, Boris; Kohler, Achim; Hansen, Line Degn; Varnai, Aniko; Horn, Svein Jarle; Eijsink, Vincent; Marova, Ivana; Shapaval, Volha. **Evaluation of the lignocellulose hydrolysate materials as a substrate for the sustainable production of high-value single cell oils.** Exploring lignocellulosic biomass: challenges and opportunity for bioeconomy. 26th- 29th June 2018. Reims, France.

Other oral presentations

Magnussen, Eirik; Solheim, Johanne Heitmann; Blazhko, Uladislau; Tafintseva, Valeria; Tøndel, Kristin; Hovde Liland, Kristian; Dzurendova, Simona; Shapaval, Volha; Sandt, Christophe; Borondics, Ferenc; Kohler, Achim. **Descattering Autoencoder for Mie Scatter Correction of Infrared Microscopy Images**. SciX 2020, 11th –16th October 2020. Nugget Casino Resort, Sparks, NV, USA.

Shapaval, Volha; Kosa, Gergely; Zimmermann, Boris; Dzurendova, Simona; Kohler, Achim. **Production of low- and high-value lipids by oleaginous filamentous fungi: High-throughput screening and process development**. Invited lecture. EUROFUNG 2019, 10th – 11th October. Berlin, Germany.

Dzurendova, Simona; Zimmermann, Boris; Kohler, Achim; Kosa, Gergely; Langseter, Anne Marie; Blomqvist, Johanna; Tafintseva, Valeria; Shapaval, Volha**. Co-production of Lipids and Biopolymers in a single fermentation process – a way to improve sustainability of Microbial Lipid-based Biofuels.** Bio4Fuels Days 2019: Building a Sustainable European Biofuel Industry, 4th – 6th November 2019. Gothenburg, Sweden.

Dubava, Darya; Kohler, Achim; Deniset-Besseau, Ariane; Dzurendova, Simona; Shapaval, Volha. **Strategies for preprocessing nanospectroscopic infrared data for visualizing chemistry of lipid bodies in oleaginous filamentous fungi.** BioSpecMLC2019 Workshop on Machine Learning and Chemometrics in Biospectroscopy, 18th-21st August 2019. Minsk, Belarus.

List of abbreviations

ADP adenosine diphosphate
AMP adenosine monophosphate
ARA arachidonic acid
AS ammonium sulphate
ATP adenosine triphosphate
ATR attenuated total reflection
CPCA consensus principal component analysis
EMSC extended multiplicative signal correction
FA fatty acid
FAME fatty acid methyl ester
FTIR Fourier-transform infrared spectroscopy
GLA γ-linolenic acid
HPLC high performance liquid chromatography
HTS high-throughput screening
IR infrared
MTPS microtiter plate system
MUFA monounsaturated fatty acid
PCA principal component analysis
Pi inorganic phosphates
PLSR partial least square regression
PUFA polyunsaturated fatty acid
SAT saturated fatty acid
SCO single cell oil
TAG triacylglycerol
YE yeast extract

Aims of the thesis

The main aim of the thesis was to optimize the production of valuable metabolites in oleaginous Mucoromycota fungi by the manipulation of growth media components, for increasing sustainability of fungal biorefineries. The optimization was performed by using a high-throughput micro-cultivation system (Duetz-MTPS) combined with different analytical techniques including vibrational spectroscopy.

The sub-goals were the following:

1. To investigate the effect of nitrogen source and level of phosphorus substrate on the co-production of valuable Mucoromycota metabolites (**Paper I**).

2. To investigate the effect of nitrogen source and level of phosphorus substrate on the lipid accumulation in Mucoromycota fungi (**Paper II**).

3. To understand the role of metal ions on the growth and lipid production in Mucoromycota (**Paper III and Paper V**).

4. To optimize extraction and analysis of lipids from the oleaginous fungal biomass (**Paper IV**).

5. To utilize vibrational spectroscopy for optimizing co-production of valuable metabolites in Mucoromycota fungi (**Paper I, III, V and VI**).

1. Introduction

Our society has driven the industrial development by utilizing fossil fuels resources since around 1880, starting by the use of coal for production of electricity. Due to the environmental, economic and societal issues related to the climate change, sea and soil pollution, decline in fossil resources, growing population and decreased economical sustainability, there is an increasing need in the transition from fossil to renewable resources [1].

Biotechnological processes, utilizing microorganisms as production cell factories, are important tools in the replacement of the non-renewable feedstock and traditional fossil refineries. Microbial biorefinery is based on biotechnological processes transforming various types of biomass into a spectrum of high- and low-value marketable bioproducts by utilizing microbial fermentation [2]. Selection of the most suitable microbial cell factories, the choice of feedstock and process parameters are important steps in establishing sustainable biorefineries.

1.1 Fungal biorefinery and co-production concept

Filamentous fungi are one of the key cell factories in white and red biotechnology and are currently used in industrial bioprocesses to produce various products, such as biopolymers, pigments, lipids, polysaccharides, antibiotics, statins, steroids, ethanol, organic acids and enzymes [3,4]. Due to their versatile metabolism, filamentous fungi can utilize a broad range of renewable feedstocks such as lignocellulosic biomass, food by-products, agricultural residues, industrial waste and sludge. Therefore, filamentous fungi are versatile processing tools in biorefining and play one of the central roles in establishing sustainable biorefinery.

Lignocellulosic biomass is a renewable organic material and due to its high abundance and, currently, low price, it represents an ideal feedstock for large scale industrial biorefineries. In nature, filamentous fungi contribute significantly to decomposing lignocellulosic materials by producing lignocellulolytic enzymes. These enzymes are degrading the cellulose and hemicellulose fractions of the biomass into 5- and 6-carbon fermentable sugars. In nature, fungi are utilizing such sugars for building metabolically active fungal mycelium which is important for soil and plant health. During the last decade, the unique metabolic activity of filamentous fungi has been extensively utilized in the development of lignocellulose-based fungal

biorefineries [5]. Such biorefineries produce a range of valuable products, including biofuels, chemicals, feed and food ingredients by employing fungi [6-8]. Currently it is challenging for biorefineries to economically compete with processes based on fossil resources. In order to increase economic viability of biorefineries, a co-production approach, in which fungal fermentation results in more than one product, has recently been proposed for fungal lignocellulose-based biorefineries [2,9]. The co-produced fungal metabolites should ideally not compete for the same substrate components. Moreover, they should be easy to separate in the downstream processes and the co-production of several intra- and extracellular metabolites need to be evaluated [5,8].

Employing oleaginous Mucoromycota fungi as cell factories in lignocellulose-based biorefineries is very promising, due to the fact that these organisms are able to utilize lignocellulose sugars and co-produce several valuable metabolites [7,10-12]. For example, the following co-production concepts were reported in the literature: (i) co-production of lactic and fumaric acids along with the fungal biomass by *Rhizopus* [13], (ii) co-production of ethanol along with the fungal biomass by *Mucor* [14], and (iii) co-production of lipids and chitosan by *Mucor circinelloides* [15].

1.2 Mucoromycota fungi – powerful cell factories for fungal biorefinery

1.2.1 General characteristics of Mucoromycota fungi

Mucoromycota are common soil fungi and were historically probably among the first land colonizers. There are three subphyla in the phylum Mucoromycota: Glomeromycotina, Mucoromycotina and Mortierellomycotina. Glomeromycotina are mycorrhizal fungi that interact with plant roots, while Mucoromycotina and Mortierellomycotina fungi are either soil saprotrophic decomposers of plant materials or can live as endophytes [16]. Several Mucoromycota genera, such as *Rhizopus* [8,13,17], *Mucor* [7,18-21], *Mortierella* [22-24], *Cunninghamella* [25,26] and *Umbelopsis* [27,28] have been identified as industrially important [14,29]. Mucoromycota representatives grow well on simple sugar substrates and are able to assimilate more complex organic compounds [30]. Therefore, they are considered as powerful cell factories for lignocellulose biorefinery applications [16,31].

1.2.2 Mucoromycota intracellular metabolites of main interest

The biomass of Mucoromycota fungi has a high nutritional value because it contains several valuable components such as lipids, polysaccharides, polyphosphate, pigments and proteins. It can be utilized in its intact form, as a bio-product for fish and animal feed [32] or as bio-absorbent. Alternatively, it can be fractionated into pure single components for different applications.

Below, we provide a brief overview over the main Mucoromycota intracellular metabolites of interest, and thus the **potential metabolites for fermentation process optimization**.

Lipids. Oleaginous Mucoromycota fungi are able to accumulate lipids, or single cell oils (SCOs) with the yield up to 80% (w/w) [33]. Accumulated SCOs are stored in the globular intracellular organelles - lipid bodies (Figure 1.1 and 1.2), predominantly in the form of triacylglycerides (TAGs) [34]. Lipid accumulation (lipogenesis) in Mucoromycota occurs under the condition of high carbon-to-nitrogen ratio (C/N), when nitrogen is limited, and carbon is in high access. Depending on the nature of carbon source, two metabolically different lipogenesis processes can occur in Mucoromycota cells:

- *de novo* lipogenesis occurs when the carbon source is based on sugar. The limitation of nitrogen combined with the high access of carbon is a strict requirement for triggering lipogenesis;
- *ex novo* lipogenesis, when carbon source is lipophilic. Lipogenesis occurs along with the active cell growth, while nitrogen limitation is not a strict requirement, as for *de novo* lipogenesis.

In the case of *de novo* lipogenesis, nitrogen limitation leads to the stagnation of cell growth. Cell proliferation is terminated, the stationary growth phase is reached early and transformation of highly accessible carbon into lipids is triggered [33]. Further, inhibition of isocitrate dehydrogenase is observed leading to the overproduction of citrate which is transported from mitochondria into cytosol. In cytosol, ATP citrate lyase cleaves citrate into acetyl-CoA, which is subsequently reduced by the malic enzyme. This provides NADPH needed for the activity of fatty acid synthase [35] involved in the synthesis of fatty acids which are further built into triacylglycerides (TAGs). In *ex novo* lipogenesis, fungal cells secrete extracellular lipases breaking TAGs into FA and glycerol, which are subsequently utilized by cells for building TAGs [33].

Depending on culture conditions different Mucoromycota fungi can accumulate low and high-value SCOs. Low-value fungal SCOs have fatty acid (FA) profile similar to vegetable oils and are rich in monounsaturated (MUFA) and saturated (SAT) fatty acids such as palmitic (C16:0), stearic (C18:0) or oleic (C18:1n9) acids. They can be used to produce biodiesel, bio-coatings, cosmetics and animal feed ingredients. It has been emphasized that SCO-based biofuels provide several advantages compared to plant oil biofuels. SCOs production is faster, it is not season/geographically dependent. The controlled environment of the fermentation process provides higher and reliable yields. Moreover, since biofuel production on agricultural areas competes with food production, SCOs biofuels represent a sustainable alternative.

High-value fungal SCOs can be similar to highly nutritious and valuable fish oils with a high content of polyunsaturated fatty acids (PUFAs) [35], such as linoleic (LA; C18:2), alpha linolenic (ALA, C18:3n3) or eicosatetraenoic (arachidonic-ARA, C20:4n6) acids. PUFAs are essential for mammals for proper function of brain, heart or cellular growth [36]. An example of industrial production of nutritious PUFAs by Mucoromycota fungi is the production of ARASCO™ oil by using *Mortierella alpina* (DSM Nutritional Products, Inc., Netherlands) which can accumulate up to 9.1 g/L of ARA [22].

Figure 1.1: Hyphae of Mucor circinelloides grown under the lipid accumulation triggering conditions. The hyphae contain numerous lipid bodies. Author: Simona Dzurendova

Polysaccharides. Typical fungal cell walls are composed of 80-90% of polysaccharides, while the rest is made of proteins, lipids and polyphosphates [37] (Figure 1.2). The cell wall provides cell integrity and protects fungal cells from the environmental and chemical stress, such as osmotic pressure and pH [37,38].

The main polysaccharides of Mucoromycota cell wall are chitin, chitosan, glucans and mannans. Chitin and chitosan are unique high-value biopolymers with diverse functionalities that allow a wide range of applications in medicine, cosmetics, food industries or wastewater treatment [39,40]. Chitosan (ß-1,4-D-glucosamine) is a deacetylated form of chitin (ß-1,4-N-acetyl-D-glucosamine) [41] and both of biopolymers are typically accounting for about 0.5 g/g of the Mucoromycota cell wall [42]. Several Mucoromycota fungi showed an ability to produce a significant amount of these cell wall polysaccharides. For example, *Mucor, Absidia* and *Rhizopus* have been identified as one of the most promising chitin and chitosan producers [43,44] with a maximum reported yield of about 35% (w/w) [45]. The most common way for triggering chitin and chitosan overproduction is manipulation of the pH of the growth media [44], while some effects of different macro-nutrients, such as phosphates have been

reported as well [44,46,47]. Since the cell wall is a rest material after lipid extraction from oleaginous Mucoromycota biomass, chitin and chitosan can be considered as potential valuable co-products in fungal lipid biorefineries.

Currently, the main industrial source of chitin and chitosan are crab and shrimp shell wastes, with annual worldwide production of 1.2 million tons [48]. Mucoromycota chitin and chitosan show several advantages over their crustacean counterparts, such as higher purity, more stable physical and chemical properties. Microbial chitin and chitosan production is independent of season and climate and doesn't cause overfishing of the sea. Moreover, demineralization treatment is not required when extracting Mucoromycota chitin and chitosan, therefore, waste management in this case is cheaper and more environmentally friendly [49].

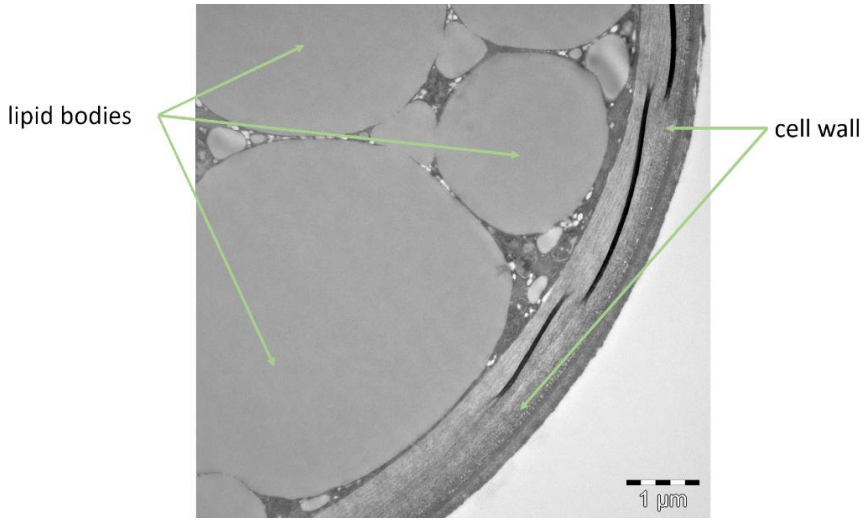

Figure 1.2: Cross section of Mucor circinelloides hyphae, TEM. Author: Lene Cecilie Hermansen, Imaging Center NMBU.

Polyphosphate. Polyphosphate is another biopolymer which can be produced and accumulated in Mucoromycota fungi. Polyphosphate is a polymer containing phosphate units connected by high-energy phospho-anhydride bonds. Polyphosphates of various length ranging from 3 to more than 1000 orthophosphate residues can be present in fungal cells. In Mucoromycota, polyphosphate can be found in the cell wall where it functions as an anion counter-ion for chitin and chitosan [50,51] and it can be stored intracellularly in

the form of granules in the connection with endoplasmic reticulum (ER) [52]. The ability of some Mucoromycota fungi to accumulate high amounts of polyphosphate is of great importance for developing phosphorus bio-recovery and recycling. It is therefore considered another potential co-product in fungal biorefinery. The emerging global shortage of phosphorus motivates developing new biotechnological processes for phosphorus recovery, where Mucoromycota fungi could play an important role [53,54].

Pigments. Some Mucoromycota fungi can synthetize and accumulate pigments represented mainly by carotenoids with β-carotene as the major carotenoid pigment produced by these fungi [55] (Figure 1.3). The main biological role of pigments in Mucoromycota cells is to protect the cells against free radicals and reactive oxygen species [56]. Synthesized pigments can be stored in the cell wall or in lipid droplets together with SCOs. Among different Mucoromycota fungi, *Mucor circinelloides* has been reported as the most promising industrial producer of β-carotene [55-57], while carotenoid production was also registered in *Mucor rouxii*, *Mucor hiemalis* and *Mucor mucedo* [58-60]. Pigment production in Mucoromycota fungi is performed through the general isoprenoid pathway and can be triggered by culture conditions, where light exposure is the most significant factor [58,61]. In addition, oxygen and temperature have been reported as factors influencing carotenogenesis [59,62]. Glucose concentration does not play any significant role in the carotenogenesis in wild-type strains, while in the *Mucor circinelloides* transformants, 2.5% glucose concentration leads to the highest carotenoid production [63]. Genetically modified *Mucor circinelloides* can produce up to 4 mg/g of β-carotene [64].

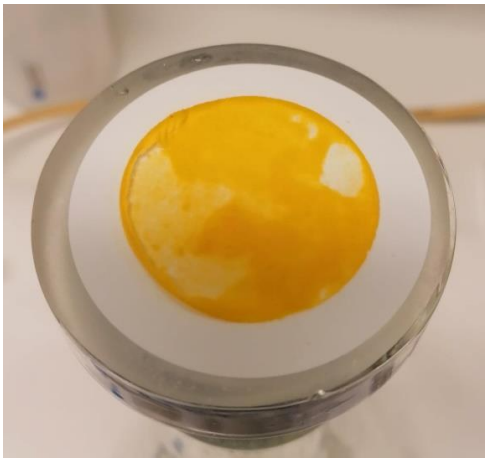

Figure 1.3: Carotenoid rich biomass of Mucor circinelloides. Author: Simona Dzurendova

Since all of the above-mentioned metabolites represent potential value-added products of fungal fermentation, their co-production was assessed in this PhD work.

1.2.3 Mucoromycota fungi selected for the PhD study

The detailed list of Mucoromycota fungi selected for the PhD study is provided in Table 1.1. The selection of fungal strains was based on the previous high-throughput screening study of hundred oleaginous Mucoromycota strains for high- and low-value lipid production [65].

All selected strains of each genus showed great oleaginous properties and were therefore used for optimizing lipid accumulation and for evaluating co-production of several intracellular metabolites such as lipids, polysaccharides and polyphosphate (**Paper I, II** and **IV**). Further, *Mucor circinelloides* was selected as a model oleaginous Mucoromycota fungus for studying the influence of different metal ions and for establishing spectroscopy-based monitoring of fungal biomass production by Fourier Transform Infrared (FTIR) and FT-Raman spectroscopies (**Paper III** and **VI**). *Mucor circinelloides* is a dimorphic fungus, has fully sequenced genome and is one of the most studied among Mucoromycota fungi. Therefore, it is generally considered as a model organism to study fungal physiology and dimorphism [66]. In addition, this fungus is known for being a good cell factory for valorizing different agricultural and lignocellulose materials and is able to produce biodiesel-grade lipids, enzymes, pigments, chitin and chitosan [21]. The physiological response of this

fungus towards different metal and phosphorus ions conditions has been studied to a higher extend in **Paper III**.

Table 1.1: List of Mucoromycota fungi selected for the PhD study

Mucoromycota fungi	Collection №	Paper
Absidia glauca	CCM[1] 451	I, II, IV
Amylomyces rouxii	CCM F220	I, II, IV, V, VI
Cunninghamella blakesleeana	CCM F705	I, II, IV
Lichtheimia corymbifera	CCM 8077	I, II, IV
Mortierella alpina	ATCC[2] 32222	I, II
Mortierella hyalina	VKM[3] F1629	I, II
Mucor circinelloides	VI[4] 04473	I, II, III, IV, V, VI
Mucor circinelloides	FRR[5] 5020	V, VI
Mucor racemosus	UBOCC[6] A 102007	V, VI
Rhizopus stolonifer	VKM F-400	I, II
Rhizopus stolonifer	CCM F445	V, VI
Umbelopsis vinacea	CCM F539	I, II, IV, V, VI

[1]Czech collection of Microorganisms (Brno, Czech Republic), [2]American Type Culture Collection (Virginia, USA), [3]All-Russian Collection of Microorganisms (Moscow, Russia), [4]Norwegian school of Veterinary Science (Oslo, Norway), [5]Food Fungal Culture Collection (FRR; North Ryde, Australia), [6]Universitè de Bretagne Occidentale Culture Collection (UBOCC; Brest, France).

1.3 Optimizing production of target metabolites in Mucoromycota fungi

1.3.1 Role of macro- and micronutrients

In order to develop a profitable fungal biorefinery for various renewable feedstocks, there is a need to optimize the chemical composition of the feedstock [67]. When optimizing chemical composition of the feedstock, understanding the influence of its main chemical components on fungal physiology and metabolism is crucial. Renewable feedstocks used in biorefinery contain the following main components: carbon (C), nitrogen (N), phosphorus (P) and sulphur (S), which are considered as the main biogenic macro-nutrients required for the fungal growth. Further, micro-nutrients and trace elements, such as metal ions magnesium (Mg), zinc (Zn), calcium (Ca), iron (Fe) are also required for supporting metabolic activity of fungi, and should be present in the biorefinery feedstocks.

Carbon and nitrogen. Usually, carbon and nitrogen are actively utilized during the logarithmic and exponential growth phases when fungal cells are proliferating. In some cases, when nitrogen is depleted, carbon can be assimilated during stationary growth phase [28]. Mucoromycota fungi can assimilate different carbon and nitrogen sources: (i) saccharides (glucose, xylose, fructose, mannose), (ii) carboxylic acids (acetic, fumaric, lactic), (iii) other C-substrates (glycerol, glycogen, dextrin) [30], (iv) inorganic N-sources (ammonium sulphate, ammonium nitrate) and (v) organic N-sources (peptone, yeast extract, urea, protein lysate) [14,17]. Carbon-to-nitrogen ratio (C/N) can considerably influence the production of metabolites in Mucoromycota fungi [68]. For example, it is well known that high C/N triggers accumulation of intracellular carbon-rich metabolites, such as lipids, polysaccharides chitin/chitosan [33] and pigments [69,70], while low C/N may lead to the high protein production [68]. While there are several studies reporting the effect of different carbon [71-74] and nitrogen sources [71,73,75,76] on the lipid accumulation in oleaginous fungi, studies reporting the influence of these two factors on the co-production of valuable metabolites in Mucoromycota fungi is limited. Glucose was assigned as the most suitable commercial C-source for lipid, carotenoid and chitin/chitosan production of Mucoromycota fungi [15,46,77-79]. Utilization of complex organic nutrient rich N-sources, such as yeast extract and peptone has shown to be beneficial for lipid and carotenoid production [15,23,24,33]. Therefore, we decided to investigate the effect of

different nitrogen sources in high access of carbon on the co-production of lipids and other valuable metabolites in Mucoromycota fungi.

Phosphorus. Phosphorus is an essential macronutrient for microorganisms. Phosphorus is a part of several key phosphorylated molecules in cells, such as energy transfer molecules adenosine mono-, di- and triphosphate (AMP, ADP and ATP), key lipogenesis enzyme ATP-citrate lyase, and reduced nicotinamide adenine dinucleotide phosphate (NADPH). Moreover, phosphorus is involved in a cell and organelles integrity, being a part of phospholipid membrane. Mucoromycota fungi are able to accumulate phosphorus in the form of polyphosphate which is localized in the cell wall, in the form of intracellular polyphosphate granules or in calciosomes [50,80]. The main function of polyphosphate in fungal cells is to control cellular homeostasis, to trap cations and amino acids and to serve as an energy source. When excess of phosphorus is present in the culture medium, some Mucoromycota fungi, as for example, *Mucor circinelloides* and *Rhizopus stolonifer*, are able to perform so called luxury phosphorus uptake in the exponential growth and accumulate extraordinary high amounts of intracellular polyphosphate [52]. Low phosphorus source concentration or phosphate-free media can benefit the chitin/chitosan production in Mucoromycota fungi [42,81], while the presence of a phosphorus source is required for carotenogenesis [79]. Studies reporting the effects of phosphorus sources on the lipogenesis are very limited. Therefore, one of the subgoals of the thesis was to assess the influence of different phosphorus source availability on the co-production of valuable metabolites in Mucoromycota fungi.

Metal ions. Metal ions are trace elements and/or micro-nutrients that are necessary for optimal fungal growth. Metal ions provide necessary redox and catalytic activities to the cellular processes and bivalent metal ions are often reported as co-factors for different cellular enzymes [82]. The following metal ions have been reported as important for supporting growth of fungi:

(i) Magnesium and zinc are involved in cell homeostasis, proper function of endoplasmic reticulum and protein folding [83];
(ii) Magnesium is controlling the level of glucose-6-phosphate, phospholipid content, carotenogenesis and oxygen delivery [79,84,85]. In addition, it has been reported that magnesium limitation promotes lipogenesis in oleaginous filamentous fungi [86,87];
(iii) Copper is a co-factor of oxygen-related enzymes [88], and together with iron, manganese and zinc its involved in lipogenesis [89-91];

(iv) Iron is involved in the central metabolic pathways [92];
(v) Manganese is involved in functioning of several cellular enzymes [93];
(vi) Calcium plays important role in fungal growth and branching of hyphal tip [94,95] and it is a signaling element in fungal cells involved in chitin synthesis, sporulation and intracellular pH signaling [96]. Furthermore, Ca is associated with endoplasmic reticulum, of which the smooth domain is responsible for cell lipogenesis. Ca-rich vacuoles adhered with phosphates could be located on ER [97-99];
(vii) Cobalt and other bivalent metal ions are involved in the synthesis of cell wall components [100-102].

The role of metal ions in Mucoromycota physiology and metabolism was studied to a limited extent. Most of the studies examined the ability of Mucoromycota fungi to absorb different metal ions and their potential application as bioremediation agents for wastewater treatment. Thus, above mentioned metal ions were selected as the optimization components in the experiments of the PhD work.

1.3.2 Detailed overview of optimization parameters used in the PhD study

In this PhD work, the main optimization parameters were nitrogen, phosphorus and metal ions. Glucose was used as C-source and C/N 100 was applied in order to trigger lipogenesis and accumulation of lipids in the studied Mucoromycota fungi. Two types of N-source, yeast extract and ammonium sulphate were evaluated. Phosphorus source was in the form of phosphate salts KH_2PO_4 and Na_2HPO_4 and six concentrations of phosphorus source were applied (Table 1.2). Seven metal ions (Ca, Co, Cu, Fe, Mg, Mn, Zn) at different concentrations were chosen for studying their effect on the metabolite production in Mucoromycota fungi (Table 1.2).

The composition of the reference medium was the following (g/L): glucose 80, yeast extract 3 or $(NH_4)_2SO_4$ 1.5, KH_2PO_4 7, Na_2HPO_4 2, $MgSO_4{\cdot}7H_2O$ 1.5, $CaCl_2{\cdot}2H_2O$ 0.1, $FeCl_3{\cdot}6H_2O$ 0.008, $ZnSO_4{\cdot}7H_2O$ 0.001, $CoSO_4{\cdot}7H_2O$ 0.0001, $CuSO_4{\cdot}5H_2O$ 0.0001, $MnSO_4{\cdot}5H_2O$ 0.0001, where the listed concentrations of the metal ions Ca, Cu, Co, Fe, Mg, Mn and Zn were assigned as reference concentrations and marked as "R" (Table 1.2). Reference medium was modified by using five relative levels of metal and phosphate ions (Table 1.2). The total concentration of KH_2PO_4 and Na_2HPO_4 is referred as “phosphates concentration” (Pi). Phosphate concentrations KH_2PO_4 7 g/L, Na_2HPO_4 2 g/L have been assigned as Pi1. In addition to Pi1 concentration, the higher –

8, 4 and 2 × Pi1 and lower – 0.5 and 0.25 × Pi1 concentrations of phosphates were assessed in the thesis as described in Table 1.2. The reference medium was based on commonly used medium for Mucoromycota fungi used in previous studies [103,104].

Table 1.2: Overview over concentrations of phosphorus and metal ions substrates

Pi	Ca	Mg	Cu	Co	Fe	Mn	Zn
0.25 0.5 Pi1 2 4 8	0 0.01 0.1 R 10	0Mg 10Ca 0.01 0.1 R	0 R 10 100 1000	0 R 10 100 1000	0 R 10 100 1000	0 R 10 100 1000	0 R 10 100 1000

The media components present in higher amounts in the reference medium, such as phosphates, Ca and Mg source, were tested in levels from 0 up to 10 times the reference concentration. In addition to above-mentioned phosphorus source biological functions, phosphates play a buffering role in the growth media. Thus, different levels of phosphates contribute to different media properties in regard to acidity. The micro-nutrients and trace elements, such as Cu, Co, Fe, Mn and Zn sources, originally present in low amounts in the reference medium, were tested in the levels from 0 up to 1000 times the reference concentration. Such high range of concentrations was chosen to make the changes related to effects of these components more prominent.

In the **Paper I and II**, the role of nitrogen sources and levels of phosphorus source on the co-production of metabolites and lipid accumulation in nine Mucoromycota fungi was evaluated. The following Pi levels have been assessed for each N- source: Pi0.25, Pi0.5, Pi1, Pi2, Pi4 and Pi8.

In the **Paper III** the influence of the selected metal ions at different concentrations (Table 1.2) on the biomass and lipid accumulation in *M. circinelloides* was assessed. Ammonium sulphate was used as N-source. Each metal condition was tested for the following Pi levels: Pi0.25, Pi0.5, Pi1, Pi2 and Pi4. In total 140 different conditions were evaluated.

In the **Paper IV** reference medium was used to culture six Mucoromycota strains (Table 1.2) for optimizing lipid extraction and transesterification.

In the **Paper V and VI**, the influence of calcium on the biomass production and lipid accumulation for a sub-set of six Mucoromycota fungi have been assessed in the media with ammonium sulphate and reference concentrations of all other metal ions. For each Ca condition three Pi levels have been applied: Pi0.5, Pi1 and Pi4.

1.4 Cultivation systems for optimizing metabolite production in fungi

Different cultivation systems may be used for optimizing metabolite production in filamentous fungi. At the beginning of the optimization process, when the role of various media components and most suitable production strains needs to be identified, a high-throughput screening approach allowing to test hundreds of conditions and strains is desirable.

High-throughput micro-cultivation systems. Miniaturization of cultivation allows rapid, reproducible, high-throughput and cost-saving screening optimization studies. There are several micro-cultivation systems available on the market with the culture volume ranging from several microliters to several milliliters. One of the most miniaturized micro-cultivation systems that is suitable for fungal cultivations is the BioLector system (m2p labs, Germany). BioLector is a high-throughput microbioreactor system with an integrated continuous monitoring of biomass growth, pH, dissolved oxygen (DO) and fluorescence. This system allows to perform up to 48 parallel cultivations with a volume 800-2400 µL in each microbioreactor [105].

An alternative is the Duetz microtiter plate system (Duetz-MTPS) (Enzyscreen, Netherlands) [104,106,107], a micro-cultivation system that was recently adapted for the screening of filamentous fungi. The Duetz-MTPS comprises of various types of deep and shallow-well microtiter plates (MTPs) with well numbers per plate ranging from 6 to 96 and sandwich covers consisting of a soft silicone layer on the bottom, 0.3 micron expanded polytetrafluoroethylene (ePTFE) and microfiber filters in the middle securing the gas transfer and stainless steel lid with pinholes on the top (Figure 1.4). The sandwich cover limits evaporation and prevents well-to-well cross-contaminations during cultivation as it is tightly attached to the microtiter plate via a clamp system. Cultivation in Duetz-MTPS is performed by mounting MTPs in the special clamp system (Figure 1.4). The culture volume of the Duetz-MTPS ranges from 0.1 ml (96-low well MTPs) to 35 ml (6 well MTPs). Recently, it has been shown that cultivations in the Duetz-MTPS are scalable up to Erlenmeyer shake flasks, 1,5L and 25L bioreactors [107].

The only disadvantage of the Duetz-MTPS is a lack of integrated monitoring of pH, dissolved oxygen and optical density.

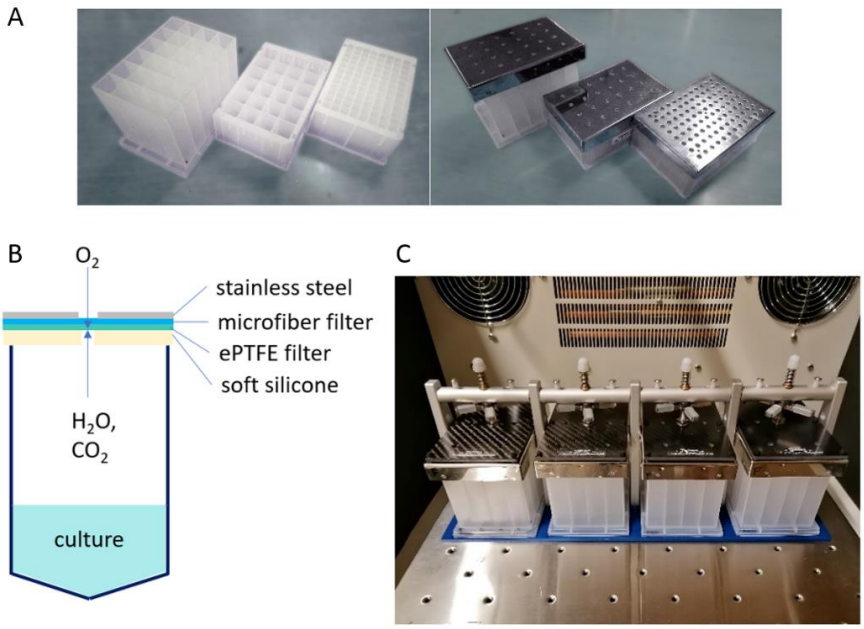

Figure 1.4: Duetz MTPs system; A- microplates with sandwich covers; B- sandwich cover layers. Adapted from Enzyscreen webpage[1]; C- clamp system for MTPs utilized in this thesis.

Recently, more advanced high-throughput micro-cultivation systems based on 'Lab-on-a-chip' technology utilizing microfluidics with real-time monitoring on a single cell level have been reported [108]. One example of such a system is the microbial microdroplet culture system (MMC) reported by Jian et al. [109]. MMC operates with a culture volume of 2 µL and is based on microfluidics with the integrated sensors allowing to monitor pH, pO_2 and optical density.

Flask system. The results from the high-throughput screening studies need to be further scaled-up for the verification. Erlenmeyer flasks are commonly employed cultivation system for a laboratory scale-up. The typical Erlenmeyer flask can be baffled or non-baffled and it has a conical body with a wider base and a cylindrical neck. Baffled Erlenmeyer flasks provide improved aeration, which is particularly useful when handling viscous cultures, e.g. filamentous fungi to prevent spore aggregation or culture pelleting [110].

[1] https://www.enzyscreen.com/sandwich_covers.htm

Normally, Erlenmeyer flasks are agitated at a certain agitation speed, thus oxygen and carbon dioxide transfer rate could be limited. The recently developed online monitoring system called Respiration Activity Monitoring System (RAMOS) enables online monitoring of oxygen and carbon dioxide transfer rate in Erlenmeyer flasks [2].

Bioreactor systems. Bioreactors are systems used for lab and industrial scale-up of fungal fermentation. There are various types of bioreactors available for fungal fermentations and the most conventional bioreactors are stirred tank bioreactors. The core component of the stirred tank bioreactor is the agitator or impeller performing heat and mass transfer, aeration, and mixing for homogenization. Stirred tank bioreactors have integrated monitoring of several process parameters such as aeration and pH control of the process. The culture volume in bioreactors varies from 250 ml (MiniBio reactors) up to 20 L. The volume of semi-industrial and industrial scale bioreactors ranges from 10 – 30 and 30 – 15000 L, respectively.

1.4.1 Cultivation systems and conditions used in the PhD work

In this PhD work, optimization of the selected media components was done in the Duetz-MTPS using 24 deep-square well polypropylene microtiter plates with a culture volume of 7 ml (**Paper I - VI**). The MTPs were mounted onto the shaking platform of MAXQ 4000 incubator (1.9 cm circular orbit, 400 rpm) using the clamp system. In addition, Erlenmeyer flask cultivation was used for **Paper IV** to produce enough biomass for optimizing lipid extraction and transesterification procedures (130 rpm). All cultivations were done at 25 °C for 7 – 14 days. Each Mucoromycota fungi on each condition were grown in 3 or 4 independent biological replicates, except for **Paper III**, where 11, 4 or 2 bioreplicates were produced for control samples, while 1 bioreplicate was used for other conditions. The pH of media before cultivation and the culture supernatants was measured.

1.5 Analytical methods for characterizing fungal metabolites

When cultivation was completed, fungal biomass was separated from the growth media by filtration or centrifugation, washed and freeze dried for cell dry weight estimation. Freeze dried biomass was further subjected to the

[2] https://www.hitec-zang.de/en/products-solutions/fermentationstechnique/bioreactor-systems/shaked-bioreactors/

metabolite analysis. In this PhD work, both traditional single-analyte reference and vibrational analytical techniques were applied for the analysis of intracellular fungal metabolites. Thus, (i) lipids were extracted by the modified Lewis methods (**Paper II, III, IV, V**) and total lipid content was estimated either gravimetrically (**Paper II**) or by gas chromatography (GC) (**Paper III, IV, V**); fatty acid profile of fungal lipids was estimated by GC (**Paper II, III, IV, V**) and the lipid composition was analyzed by nuclear magnetic resonance spectroscopy (NMR) (**Paper IV**); (ii) polyphosphates were analyzed by solid state nuclear magnetic resonance spectroscopy (**Paper V**) and total biomass phosphorus was estimated by spectrophotometric analysis (**Paper V**); (iii) biochemical profiling of fungal biomass was done by the high-throughput Fourier transform infrared (FTIR-HTS) spectroscopy and FT-Raman spectroscopy (**Paper I, III, V and VI**); (iv) cell wall was visualized by TEM microscopy of the cross-sectioned fungal hyphae (**Paper I**). In addition, the culture supernatants were monitored by FTIR Attenuated total reflection (FTIR-ATR) spectroscopy (**Paper I, V**).

1.5.1 Vibrational spectroscopy for profiling of fungal biomass and monitoring of fungal fermentation

Traditional analytical approaches for chemical analysis of fungal metabolites such as liquid or gas chromatographies, or colorimetric assays, provide detailed information on single analytes, while they are time consuming and often require tedious extraction protocols that are not compatible with the high-throughput optimization screenings. In this PhD work, optimizing of high-value metabolite production and evaluation of the co-production in Mucoromycota fungi was performed by the traditional analytical methods and by vibrational spectroscopy techniques.

Vibrational spectroscopy is an analytical technology allowing high-throughput biochemical fingerprinting and quantitative or semi-quantitative analysis of all main intracellular and extracellular fungal metabolites in a single measurement run. Quantitative analysis is obtainable via regression models. Vibrational spectroscopy analysis requires no or minimal sample preparation and can be performed in a high-throughput set-up. Therefore, it is well-suited for biotechnology screening studies. Vibrational spectroscopy techniques allow at-line and on-line measurements and can be utilized for monitoring and control of the product formation and substrate consumption during fungal fermentations [111]. The main principle of vibrational spectroscopies is the interaction of light with the chemical bonds of molecules that causes change

in their vibrational energy states and subsequent stretching or bending of the chemical bonds [112].

In the PhD work, high-throughput Fourier transform infrared (FTIR) and FT-Raman spectroscopy were applied to reveal the influence of the selected media components on the production of valuable metabolites and co-production in Mucoromycota fungi (**Paper I, III, V** and **VI**). FTIR spectroscopy was used for monitoring efficiency of lipid extraction (**Paper IV**).

Fourier transform infrared spectroscopy (FTIR)

FTIR spectroscopy is a biophysical analytical method based on the absorption of infrared (IR) radiation by chemical bonds of molecules in a sample. When polychromatic IR radiation interacts with the sample and its chemical components, chemical bonds absorb IR radiation at characteristic frequencies. In the mid-infrared region (4000-400 cm^{-1}/2.5-25 μm), we observe mainly absorption of infrared radiation by fundamental vibrations. In infrared spectroscopy, infrared radiation is strongly absorbed by polar bonds, such as C=O, N-H or O-H [113]. The resulting measured spectrum is usually presented in the unit-free quantity absorbance as a function of wavenumbers (cm^{-1}). Different absorbance bands are characteristic for different chemical components of the sample. The position of bands and probability of absorption are dependent on the polarity and strength of chemical bonds and is influenced by surroundings of the bonds. Thus, the inter and intra-molecular effects are projected in the FTIR spectrum [114]. The term 'Fourier Transform' relates to a specifically successful spectrometric principle based on a Michelson interferometer. FTIR spectroscopy has been utilized for the characterization of chemical structures since decades, and it has become popular for analysis of biological samples from the 90ties. Since then FTIR spectroscopy has been widely applied for the identification of microorganisms, as different microorganisms have specific fingerprint in the FTIR spectra [115], or in the monitoring of microbial metabolites formation [116,117].

FTIR analysis provides qualitative and semi-quantitative information about all main cellular chemical components, such as lipids, proteins, carbohydrates, polyphosphates or chitin/chitosan. In the case of lipids, the FTIR spectrum provides information about the main lipid class, the length of the fatty acid chains and unsaturation [118,119]. In the case of chitin/chitosan, FTIR spectroscopy can detect the degree of acetylation [120]. Concerning polyphosphates, their presence and to some extend the structure (i.e. chain length- polyphosphate/orthophosphate) can be estimated by FTIR [121,122].

Proteins can be analyzed with regard to their structure, folding, unfolding or reactions [114]. A summary of the main characteristic spectral regions and bands that are relevant for this PhD work can be found in Table 1.3.

In this thesis, two measurements modes of FTIR were used: (A) attenuated total reflection (ATR) measurements or (B) transmission measurements in a high throughput setup (HTS) (Figure 1.5). Both measurement modes can be utilized for the analysis of bulk samples, biomass and growth media (Figure 1.5).

Figure 1.5: Schematics of FTIR measurement modes that were utilized in this thesis; A- Attenuated total reflection, B- transmission mode employing a high throughput system.

In the PhD work, FTIR measurements were performed using a Vertex 70 FTIR spectrometer (Bruker Optik GmbH, Germany) equipped with a globar mid-IR source and a DTGS detector. For the FTIR-ATR measurements, a single reflectance-attenuated total-reflectance (SR-ATR) High Temperature Golden gate ATR Mk II (Specac, UK) accessory was used. In ATR measurements, an infrared beam is guided through a crystal and the beam is totally reflected at the surface of the crystal where the sample is located. Depending on the setup, the beam is reflected once or multiple times. At the surface, where the sample is located, the totally reflected radiation is creating and evanescing field into the sample which leads to an attenuation of the infrared beam due to absorption by the sample [123]. The main advantage of the ATR mode is the possibility to measure thicker samples as the measurement is done only at the surface of the sample with a certain penetration depth into the sample. This allows to probe liquid and solid samples. The measurements are reproducible due to the stable penetration depth of the IR beam in the ATR mode. The analysis of fungal biomass and culture supernatant by FTIR-ATR spectroscopy was performed in the following way: 10 µl of culture supernatant or approximately 1 mg of fungal biomass, was deposited on the ATR-crystal. In case of the biomass samples, a sample was pressed on the ATR crystal by using a sapphire anvil. The FTIR-ATR spectra were recorded with a total of 32 scans, spectral resolution of 4 cm^{-1}, and digital spacing of 1.928 cm^{-1}, over the range

of 4000–600 cm^{-1}, using the horizontal SR-ATR diamond prism with 45° angle of incidence. All samples were analyzed in three technical replicates. Background measurements of empty crystal were conducted between every sample measurement. FTIR-ATR spectroscopy with single reflection was utilized for the analysis of culture supernatants and estimation of residual glucose in **Paper I** and **V** and phosphate salts in **Paper I**. In addition, FTIR-ATR spectroscopy was utilized to estimate lipid extraction efficiency in **Paper IV**. Since FTIR-ATR was in this thesis mainly utilized for the monitoring of growth media, below (Figure 1.6) we show the spectra of media before and after cultivation with assigned characteristic peaks for glucose (1151, 1103, 1080, 1034, and 990 cm^{-1}) and phosphates (1157, 1076, and 937 cm^{-1}).

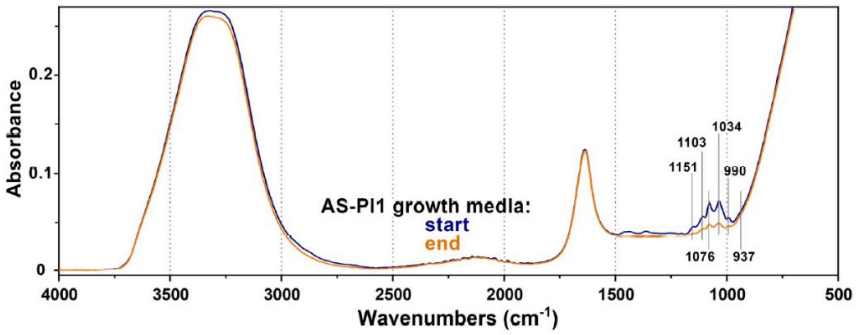

Figure 1.6: FTIR-ATR spectra of growth media containing ammonium sulphate and reference Pi concentration. Spectra of media before (blue) and after (orange) the cultivation of Mucor circinelloides are shown.

In transmission measurements an infrared beam is transmitted through a sample that is placed on a transparent sample holder. For transmission measurements, samples need to be carefully prepared as thick samples would absorb all infrared radiation. FTIR-HTS measurements in the transmission mode require dry samples and provide spectra with high signal-to-noise ratios [124]. Differences in optical pathlength caused by differently thick biofilms result in variability of IR absorption and low reproducibility, although this disadvantage could be eliminated by applying different spectra-preprocessing methods. FTIR-HTS was applied for profiling of intracellular metabolites in fungal biomass (**Papers I, III, IV** and **V**) and for monitoring of culture supernatants (**Paper I**). For FTIR-HTS analysis, fungal biomass was homogenized by beads beating. Approximately 5 mg of biomass was transferred into 2 ml polypropylene tube containing 250 ± 30 mg of acid washed glass beads and 0.5 ml of distilled water, and homogenized by Percellys

Evolution tissue homogenizer (Bertin Technologies, France) with the following set-up: 5500 rpm, 6 × 20 s cycle. 10 µl of homogenized fungal biomass of each sample was pipetted onto an IR transparent 384-well silica microplate and dried at room temperature for two hours. The HTS-FTIR spectra were recorded with a total of 64 scans, spectral resolution of 6 cm^{-1}, and digital spacing of 1.928 cm^{-1}, over the range of 4000–500 cm^{-1}, and an aperture of 5 mm. Spectra were recorded as the ratio of the sample spectrum to the spectrum of the empty IR transparent microplate.

Fourier transform Raman spectroscopy (FT-Raman)

When electromagnetic radiation impinges on the sample, it can be reflected, absorbed or scattered. While the lion's share of the radiation is scattered elastically, i.e. scattered without loss of energy or shift of frequency, or absorbed, a tiny part of the scattered radiation differs in frequency from the incident radiation and this phenomenon is called inelastic scattering. FT-Raman spectroscopy is analytical technique based on inelastic scattering of monochromatic light by chemical bonds of the sample. In Raman spectroscopy, a laser is used as an excitation source. If the scattered radiation has lower energy than incident radiation, Stokes scattering occurs, while the scattered radiation has higher frequency than the laser radiation, it is called anti-Stokes scattering [125]. Most Raman instruments are based on a grating, the Raman instrument that was available for this thesis, is based on a Michelson spectrometer, i.e. a Fourier Transform (FT) Raman instrument. An FT-Raman spectrum displays the Raman intensity of inelastic light scattered by characteristic frequencies [126] and traditionally, anti-Stokes lines are shown. FT-Raman spectroscopy characterizes mainly molecules containing non-polar chemical bonds, such as C-C, C=C or S-S etc. Thus, this method is complementary to FTIR. Resonance Raman Spectroscopy is an advanced method which utilizes lasers with frequencies close to the energy which is required for molecular transitions of the analyte and enhances the Raman intensities approximately 10^6 – fold. Thus, the sensitivity can be significantly increased, while there is a risk of damaging the sample [127].

In general, Raman scattering intensities are weak. It is difficult to detect molecules that are present in low concentration in the sample. However, if the excitation radiation is in resonance with the electronic transitions, so called resonance Raman effect will occur. In that case, the Raman scattering will be significantly enhanced, approx. 10^4-10^6 – fold, enabling detection of molecules

present in relatively low concentrations [127]. This is also the case of carotenoids, that are undetectable by FTIR [128].

Unfortunately, in addition to Raman and resonant Raman effect, excitation laser can often create resonance fluorescence effect. The fluorescence effect occurs when the energy of the excitation photon is close to the transition energy between two electronic states, resulting in intensive fluorescence. Fluorescence can significantly obstruct the detection of the Raman effect. Another problematic aspect in Raman spectroscopy is sample heating that leads to emission of longer-wavelength radiation and thermal interference to the Raman spectrum, and can even result in thermal degradation of the sample. Both fluorescence and thermal interferences can be minimised by using different excitation lasers, with simultaneous optimization of Raman effect [129,130]. In general, electronic transitions are weaker at longer wavelengths, and thus detrimental effects can be avoided by use of near-infrared (NIR) lasers, such as neodymium doped yttrium aluminium garnet (Nd:YAG) laser with excitation at 1064 nm. However, NIR excitation lasers offer significantly lower Raman sensitivity compared to ultraviolet and visible lasers, and thus they often require Fourier transform (FT) Raman spectrometers with a Michelson interferometer and a FT processor for signal enhancement. In the last decade, increased interest in utilizing FT-Raman spectroscopy in analyses of biological samples occurred [131-134]. The main advantage of FT-Raman spectroscopy is the invisibility of water and glass in the spectra [128]. This represents a great potential for screening experiments and online/inline process monitoring, where samples can be analyzed through glass walls of bioreactors/flasks in submerged cultivations. Similarly as in FTIR, main cellular components such as lipids, proteins, carbohydrates or nucleic acids can be detected. Characteristic Raman bands of filamentous fungi spectra are summarized in Table 1.3.

In this thesis, Raman spectra were recorded in backscattering geometry using MultiRAM FT-Raman spectrometer (Bruker Optik GmbH, Germany) equipped with a neodymium-doped yttrium aluminum garnet (Nd:YAG) laser (1064 nm, 9394 cm^{-1}), and germanium detector cooled with liquid nitrogen. For each measurement, 0.5 – 1 mg of freeze-dried sample was deposited in aluminium sample container and pressed with pestle. The spectra were recorded with a total of 128 scans, using Blackman–Harris 4-term apodization, spectral resolution of 4 cm^{-1}, with a digital resolution of 1.928 cm^{-1}, over the range of 3785-50 cm^{-1}, at 200 or 500 mW laser power.

The comparison of FTIR and FT Raman spectroscopies

In order to demonstrate the information contained in FTIR and FT-Raman spectra, the spectra of *Mucor circinelloides* biomass grown in 2 different substrates are plotted in Figure 1.7. The biomass chemistry is displayed in the spectra and the complementary information is presented between FTIR and FT Raman spectra. The description of characteristic peaks is summarized in Table 1.3 and peaks are assigned in Figure 1.7.

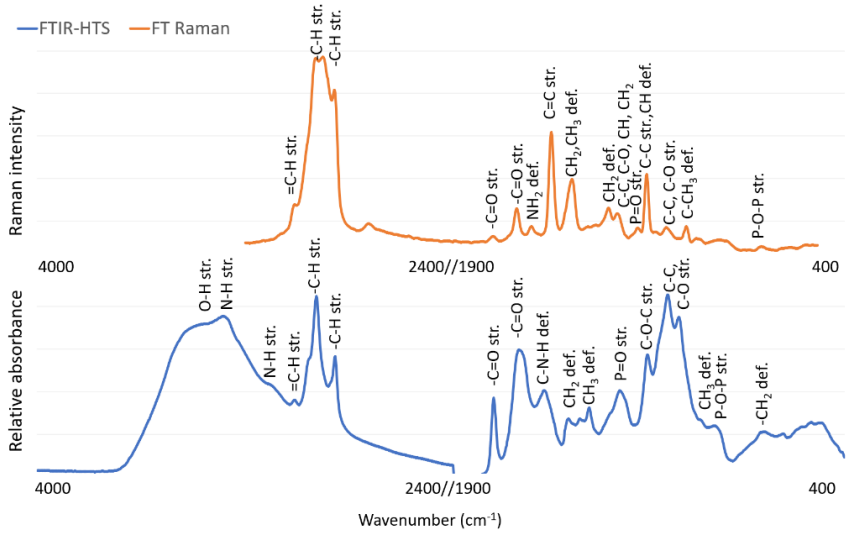

Figure 1.7: The comparison of FT Raman and FTIR-HTS spectrum of the same Mucor circinelloides biomass sample.

Table 1.3: Peak assignments of the FTIR and FT Raman spectra (str.-stretching, def.-deformation) [65,135-141]

Cell component	Infrared		Raman	
	Wavenumbers (cm^{-1})	Molecular vibration	Wavenumbers (cm^{-1})	Molecular vibration
Carbohydrates (glucosamines, glucans, glucuronans)	3300	O-H str.	2933 and 2895	-C-H str. (CH_3)
	3400-3100	N-H str., N-H_2 str.	2855	-C-H str. (CH_2, glucan)
	2879	-C-H str. (CH_3)	1680-1620	-C=O str. (Amide I, chitin)
	1730	-C=O str. (glucuronans)	1755	-C=O str. (glucuronan)
	1680-1620	-C=O str. (Amide I, chitin)	1620-1570	NH_2 def. (chitosan)
	1600-1550	NH_2 def. (chitosan)	1460-1440	CH_2 and CH_3 def.
	1554	C-N str. & NH def. (Amide II, chitin)	1377	CH_2, CH, COH def.
	1375	-CH_3 def.	1327	CH_2, CH, COH def.
	1305	C-N-H def. (Amide III, chitin)	1256	C-C, C-O, CH, CH_2
	1200-1000	C-O-C str., COH def. COC def.	1200-1150	C-O-C str.
	950	-CH_3 def.	1050-1150	C-N str. & C-C str.
			950-850	C-C str, C-O-C str. & def., COH def.
			715	O-C-O str. & CH def.
Acylglycerol lipids (triglycerides)	3010	=C-H str.	3008	=C-H str.
	2921	-C-H str. (CH_3)	2933 and 2895	-C-H str. (CH_3)
	2852	-C-H str. (CH_2)	2855	-C-H str. (CH_2)
	1743	-C=O str.	1750	C=O str.
	1463	-CH_2 def.	1660	C=C str.
	1160	C-O-C str.	1460-1440	CH_2 and CH_3 def.
	723	-CH_2 def.	1305	CH_2 def.
			1080-1060	C-C str. C-O str.
Polyphosphates	1263	P=O str (PO_2^-)	1165	P=O str. (PO_2^-)
	885	P-O-P str.	685	P-O-P str.
Proteins	1680-1630	-C=O str. (Amide I)	1660	-C=O str. (Amide I)
	1560-1530	C-N-H def. (Amide II)	1620-1580	NH_2 def.
	1310-1250	C-N-H def. (Amide III)	1605	C=C str. (phenyl ring)
			1460-1440	CH_2 and CH_3 def.
			1310-1250	C-N-H def. (Amide III)
			1005	phenyl ring def.
Carotenoids	*Not detectable at concentrations present in fungal biomass*		1525	C=C str. (polyene chain)
			1155	C-C str. & CH def.
			1005	C-CH_3 def.

1.5.2 Analysis of lipids by gas chromatography

Analysis of lipids by gas chromatography (GC) requires extraction of fungal lipids and their transesterification to fatty acid methyl esters.

Lipid extraction. Lipid extraction involves cell disintegration and solvent-based extraction. Since fungal biomass has resilient cell wall and extraction-challenging lipids, there is a need to disintegrate cells. Cell wall disintegration can be achieved by different techniques, such as ultrasonication, bead beating, grinding, agitation with abrasive, chemicals or enzymatic digestion [142]. In this PhD study bead beating in the tissue homogenizer (Percellys Evolution) was used, followed by acid treatment during transesterification. The bead beating of oleaginous fungal biomass has been optimized in the previous studies, where sonication, bead beating and acid treatment were compared for their efficiency to disrupt fungal cells for the lipid extraction [141]. The extraction of lipids is performed by applying different solvents and/or solvent mixtures. Lipid content in oleaginous Mucoromycota fungi can reach up to 80% of the cell dry weight, which is higher than in oleaginous plants. Therefore, efficient extraction of lipids is challenging, and extraction methods commonly applied to non-oleaginous fungal biomass could lead to the underestimation errors [143]. In this PhD work, hexane, methanol, chloroform and water were used as solvents d the lipid extraction.

Transesterification. The majority of fungal lipids are stored mainly in the form of acylglycerols (MAG, DAG and TAG), with smaller amount of glycerophospholipids and fatty acids [141]. The total lipid content, as well as fatty acid composition, of such lipids can be determined by GC, by converting them into fatty acid methyl esters (FAMEs) which are volatile and detectable by flame ionization detector (FID) in GC (Figure 1.8).

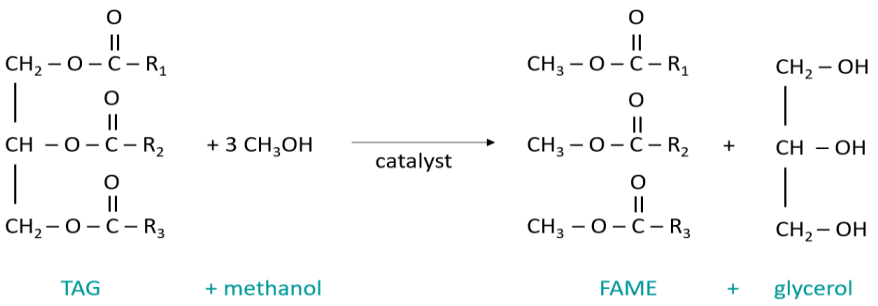

Figure 1.8: Transesterification reaction of TAG into FAME

Direct transesterification involving cell disintegration, lipid extraction and transesterification in a single operation is preferable for reducing operational errors, increasing throughput and decreasing cost. For estimating total lipid content and fatty acid profile by GC-FID, internal standards representing the main class of lipids present in the biomass and mimicking FAMEs conversion need to be added during direct transesterification. In the PhD study, the glyceryl tritridecanoate (C13:0 TAG) was used as the main internal standard and hydrochloric acid (HCl) was used as the main catalyst (Paper II, III, IV, V).

In **Paper II** and **Paper III**, direct transesterification based on the modified Lewis method [104,144] was used: 2 mL screw-cap polypropylene (PP) tube was filled with 30 ± 5 mg freeze dried biomass or vegetable oil, approx. 250 ± 30 mg (710–1180 µm diameter) acid-washed glass beads and 600 µL of methanol. The fungal biomass was homogenized in a Percellys Evolution tissue homogenizer (Bertin Technologies, France) at 5500 rpm, 6×20 s cycles. The processed biomass was transferred into a glass reaction tube by washing the PP tube with 2400 µL of methanol–chloroform–hydrochloric acid solvent mixture (7.6:1:1v/v) (3×800 µL). 1.02 mg of C13:0 TAG internal standard in 100 µL of hexane was added to the glass reaction tube (100 µL from a 10.2 mg/mL−1 glyceryl tritridecanoate ($C_{42}H_{80}O_6$, C13:0 TAG (13:0/13:0/13:0), Sigma-Aldrich, USA)). The reaction mixture was incubated at 90 °C for 1 h in a heating block, followed by cooling to room temperature and addition of 1 mL of distilled water. FAMEs were extracted by the addition of 2 mL hexane–chloroform (4:1 v/v) followed by 10 s vortex mixing. The reaction tube was centrifuged at 3000 rpm for 5 min at 4 °C, and the upper (organic) phase was collected in glass tube. The hexane–chloroform extraction (extractive workup) was performed thrice. The solvent in glass tube was evaporated under nitrogen at 30 °C, and small amount of anhydrous sodium sulphate (approx. 5 mg) was added in glass tube. FAMEs were transferred into GC vials by washing the glass tube with 1500 µL hexane (2×750 µL) containing 0.01% butylated hydroxytoluene (BHT, Sigma-Aldrich, USA) followed by 5 s vortex mixing.

After observing incompatibility between the FTIR spectra (**Paper I**) and total lipid content estimated by GC-FID according to the aforementioned Lewis 1 method [104], particularly in the cases of biomass containing extraordinary high lipid content as for *Umbelopsis vinacea*, gravimetrical determination of total lipid content was utilized (**Paper II**). According to the FTIR spectra, higher lipid content could be expected for *Umbelopsis vinacea* biomass.

To understand the reason of incompatibility between FTIR and GC-FID data, a set of direct transesterification experiments was conducted (Paper IV), involving olive oil, *Umbelopsis vinacea* and *Mucor circinelloides* biomass (grown in Erlenmeyer flasks), as control samples to optimize the method. *Mucor circinelloides* was selected due to the thick and resilient cell wall, while *Umbelopsis vinacea* was selected due to the extraordinary high lipid content. Three standard direct transesterification methods and their modifications were assessed in **Paper IV**: Lewis [144], Wahlen [145] and Lepage [146]. The main difference between the methods was the type of the acid catalyst used: hydrochloric acid in Lewis method, sulphuric acid in Wahlen method, and acetyl chloride in Lepage method. Further, transesterification according to Wahlen 1 was performed using microwave oven, while for all other methods (including Wahlen 2 method) it was performed using heating block. The methods were modified regarding the reaction times and co-solvents. The exact descriptions of methods and their modifications can be found in Paper IV. Residual lipids in the fungal biomass after extraction were assessed by FTIR spectroscopy and lipid classes were characterized by NMR spectroscopy. Further, biomass of *Mucor circinelloides, Umbelopsis vinacea, Absidia glauca, Lichtheimia corymbifera, Cunninghamella blakesleeana*, and *Amylomyces rouxii* grown in reference medium in Duetz-MTPS was used to assess the optimized method.

The optimized direct transesterification method, based on Lewis method, provided reliable estimation of total lipid content in fungal biomass; therefore, it was further applied for lipid analysis in studies presented in Paper V and VI. The extraction of lipids according to the optimized Lewis method was done in the following way: 2 mL screw-cap PP tube was filled with 30 ± 5 mg freeze dried biomass or vegetable oil, approx. 250 ± 30 mg (710–1180 µm diameter) acid-washed glass beads, and 500 µL of chloroform. 1.02 mg of C13:0 TAG internal standard in 100 µL of hexane was added to the PP tube. The fungal biomass was homogenized in a Percellys Evolution tissue homogenizer at 5500 rpm, 6×20 s cycles. The processed biomass was transferred into glass reaction tube by washing the PP tube with 2400 µL of methanol–chloroform–hydrochloric acid solvent mixture (7.6:1:1v/v) (3×800 µL). Finally, 500 µL of methanol was added into glass reaction tube. The reaction mixture was incubated at 90 °C for 90 min in a heating block, followed by cooling to room temperature and addition of 1 mL of distilled water. The fatty acid methyl esters (FAMEs) were extracted by the addition of 2 mL hexane followed by 10 s vortex mixing. The reaction tube was centrifuged at 3000 rpm for 5 min at

4 °C, and the upper (organic) phase was collected in a glass tube. The lower (water phase) was extracted two more times, but now by the addition of 2 mL hexane–chloroform mixture (4:1 v/v). The organic phase in the glass tube was dried and prepared for the GC measurement according to the Lewis 1 method.

In addition to GC-FID, vibrational spectroscopy was applied for analyzing lipid content and profile in the intact fungal biomass and lipid droplets were visualized by TEM microscopy of the cross-sectioned hyphae.

1.5.3 Analysis of fungal chitin and chitosan

Conventional analysis of fungal chitin and chitosan content requires extraction of these components that involves biomass homogenization, alkaline treatment for removing proteins and other polysaccharides, and acid reflux for separation and precipitation under alkaline conditions [147]. Instead of alkaline-acid extraction, enzymatic hydrolysis can be applied. The extracted chitin and chitosan is estimated by colorimetry N-acetyl glucosamine is measured as an indicator of the total chitin content, while free glucosamine represents total chitosan content [148]. Further, the acetylation patterns of chitosan polymers can be estimated by enzymatic- mass spectrometric fingerprinting analysis [149,150].

Conventional methods of chitin and chitosan analysis are time-consuming and require large amount of sample, and so they do not fit to the high-throughput set-up of the PhD study. Therefore, vibrational spectroscopy techniques were utilized for estimating chitin and chitosan in the studied Mucoromycota fungi (**Paper I, III, V, VI**). In addition, TEM microscopy was used for visualizing cell wall of the cross sectioned *Mucor circinelloides* hyphae (Figure 1.2) (**Paper I**).

1.5.4 Analysis of fungal polyphosphate and total phosphorus content

Estimating polyphosphate content in fungal biomass can be done by applying acid extraction at high temperature [151] or alkaline with combined EDTA and NaOH extraction [152] and the subsequent colorimetric determination [153]. Extraction based approach suffers from the low reproducibility, low efficiency and errors due to the chemical modifications and polyphosphate degradation during the extraction procedure. Solid state NMR spectroscopy is a non-destructive method that enables rapid and highly precise estimation of polyphosphate content in fungal biomass [154]. In **Paper V** solid state NMR spectroscopy method was used according to Staal et al [154]: Quantitative 31P SSNMR spectra were recorded on a 500 MHz JEOL ECZ 500R spectrometer using a 3.2 mm triple resonance magic angle spinning (MAS) NMR probe, 15

kHz spinning speed, a 45° pulse, and proton decoupling. Relaxation delays were optimized on each sample, typically 200–300 s / 410 s for a synthetic struvite, which served as an external intensity reference for spin counting experiments. The 31P SSNMR spectra were referenced relative to H3PO4 (δ(31P) = 0 ppm) and analyzed with 100 Hz line broadening using MestReNova (Mestrelab Research) by absolute integration of the spinning side band manifold. The 31P SSNMR spectra of samples extracted by water/hexanol or water were recorded on a 600 MHz Agilent spectrometer using a 3.2 mm triple resonance MAS NMR probe, 15 kHz spinning speed, 22.5° pulse and proton decoupling. NMR measurements were performed for *Mucor circinelloides* biomass only, due to the cost of the analysis.

In order to estimate the relation between Ca and polyphosphates, and the correlation between the FTIR spectra and polyphosphate content in the fungal biomass, total phosphorus was determined by assay-based UV/VIS spectroscopy. The samples were freezedried and decomposed in the muffle oven at 550° C for 16 hours. 5 mL of 6M HCl was added to each sample. Samples were boiled on a heating-plate for 20 minutes, 7.5 mL MilliQ water were added, and samples were left overnight in the acid/water mixture. Next day, samples were diluted up to 100 mL with MilliQ water, centrifuged and analyzed using RX Daytona+ with kit PH8328 (Randox) [155].

1.6 Data analysis

In this PhD work, different types of data were generated: (i) cell dry weight (CDW) in g/L; (ii) pH of growth media; (iii) gravimetrical total lipid content in % and g/L; (iv) GC-FID data of fatty acid profile and total lipid content in %; (v) FTIR-HTS and FTIR-ATR spectra of fungal biomass and growth media, respectively; (vi) FT- Raman spectra of fungal biomass; (vii) content of lipid classes in fungal lipids and olive oil and polyphosphate in *Mucor circinelloides* biomass estimated from NMR spectra; (viii) total phosphorus content in %; (ix) total content of carotenoids in µg/g estimated from HPLC data. Univariate data such as CDW, pH and total content were assessed by taking average of biological replicates and estimating standard deviation. Multivariate data, such as FA profiles and spectral data were analyzed by different multivariate data approaches, such as principal component analysis (PCA) and ANOVA PCA. Multiblock approach was used for FTIR and FT-Raman spectra, namely consensus PCA. Partial least square regression (PLSR) models were built to predict the carotenoids, lipids, polyphosphates and residual glucose. The graphical overview over the generation of data is shown in Figure 1.9.

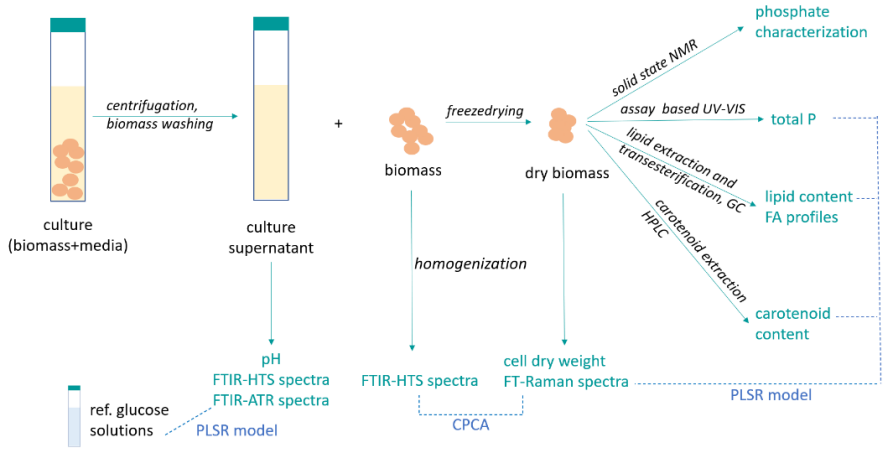

Figure 1.9: Schematics of the data acquisition. Green color indicates generated data, blue color indicates links between datasets.

For the data analysis, the following software were used:
- Unscrambler X version 10.5.1 (CAMO Analytics, Norway);
- Orange data mining toolbox version 3.16 (University of Ljubljana, Slovenia) [156];
- Matlab R2018a/R2019a (The Mathworks Inc., Natick, Ma, USA).

1.6.1 Multivariate data analysis of spectra

Vibrational spectroscopy data are multivariate data composed of a high number of collinear variables – for example infrared absorbance and Raman intensity values corresponding to the different wavelengths. Two main approaches are applied in the multivariate data analysis: data exploration and multivariate calibration. In this PhD work, the data exploration approach was utilized to explore the underlying correlations and co-variation patterns in the datasets, while multivariate calibration model was utilized for determination of residual glucose. However, spectral data can suffer from the unwanted physical effects caused by technical variations. To remove unwanted variations from the spectra, spectral preprocessing was applied. Multivariate data analysis approaches such as factor, cluster, correspondence, correlation, discriminant or regression analysis [157] are applied for exploring spectral data and finding patterns and relationships in examined samples [158].

Preprocessing of spectra. Different preprocessing methods were used for removing non-desirable distortions from the spectra, as for example, scattering, water vapor, noise, baseline shifts etc. [159]. The spectral

preprocessing procedure involves derivation of spectra by taking second derivatives using the Savitzky-Golay (SG) algorithm. Spectral derivatives allow removing baselines and noise variations. In addition, SG may enhance spectral information [160]. It must be noted that when applying SG algorithm, the window size needs to be adjusted according to the spectral features of the selected analytes and the noise level in the data. In this PhD work, when applying the SG algorithm to the spectral regions of interest, a window size of 11 points was used for lipids and chitin/chitosan spectral regions, while 61 points was used for the polyphosphate region (**Paper I, III, IV and V**).

Derivates of spectra were subjected to extended multiplicative signal correction (EMSC), a model based preprocessing method, removing multiplicative effects from spectra caused by for example optical path length variations or scattering [159]. In addition, EMSC allows to further suppress baseline variation. EMSC-preprocessed spectra were further analyzed by multivariate data analysis approaches.

In the PhD study, EMSC was applied to preprocess FTIR-HTS and FT-Raman spectra as a sole pre-processing method (**Paper I, III, IV, V, VI**) or after applying the SG algorithm (**Paper I, III, VI**). The baseline of FTIR-ATR spectra of growth media in **Paper V** was corrected by vertical offset and a water related peak at 1637 cm^{-1} was used for normalization. Detailed description of spectral preprocessing can be found in the materials and methods of the respective papers.

Principal component analysis (PCA) and Analysis of variance (ANOVA) PCA. Principal component analysis (PCA) is widely applied in the exploration of multivariate data. PCA is used for data with strong co-variation patterns and allows to detect the main covariation patterns in the data. The main co-variation patterns can then be investigated in the sample and variable space by the new latent variables, the so-called scores and loadings [161]. The main co-variation patterns are found by maximizing the co-variance of the data matrix. The first principal component (PC) represents the direction of the maximal co-variance in the data set. The second PC is found by removing the first PC from the data and then maximizing the covariance of the residual data matrix and so on. This ensures that all principal components are orthogonal to each other (Figure 1.10). Due to high covariance in infrared data, typically few PCs cover the most interesting information of an infrared dataset, while the number of significant components can be determined by, for example, cross-validation [161].

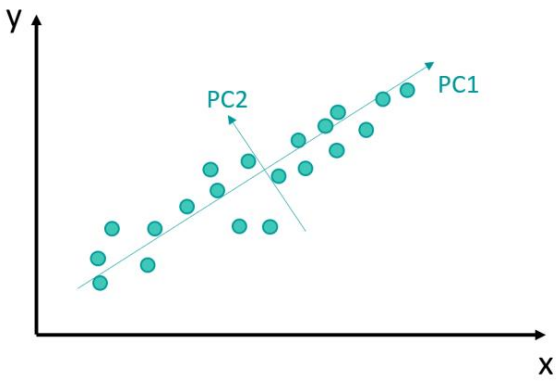

Figure 1.10: Principal component analysis

ANOVA PCA is a multivariate data analysis method applied in designed experiments to evaluate the influence of design factors. Firstly, the data is split in matrices according to the design factors and further the matrices are analyzed by component analysis [162].

Two PCA approaches have been utilized in the PhD study (i) PCA analysis of the whole spectral region (**Paper I and III**); (ii) PCA analysis of selected spectral regions corresponding to classes of target metabolites (**Paper I**).

Peak ratios. The univariate analysis based on ratios of peak heights/areas of certain bands is considered as a simplified approach to the multivariate data analysis. Before calculating band ratios, spectra need to be preprocessed to remove baseline variations [163,164]. In **Paper V and VI**, we have utilized the calculation of peak ratios for estimation of relative content of polyphosphates and lipids in Mucoromycota biomass. In **Paper V**, the amide I peak in the FTIR spectra, mainly related to proteins, was selected as a relatively stable band for estimation of relative content of cellular lipids and phosphates. The ester bond (C=O stretching at 1745 cm^{-1}) in the FTIR spectra was selected for lipids, and the phosphate functional group (P=O stretching at 1251 cm^{-1}) was used for estimating amounts of polyphosphate. In **Paper VI,** ratios of Raman intensities at different wavenumbers related to chemical constituents of fungal biomass (1747 cm^{-1} -lipids; 1163 cm^{-1}- phosphates**,** 1523 cm^{-1}-carotenoids) were used for the initial estimation of their content.

Partial Least Square Regression (PLSR). Partial least square regression (PLSR) is a commonly used technique for establishing regression models of spectroscopic data on reference data [165]. PLSR can be used for regression of

spectroscopic data (called the predictor matrix **X**) onto one reference variable (the so-called response variable). PLSR is able to handle the high collinearity as it is inherent in for example spectroscopic data. As in principle component analysis, the PLSR model is based on latent variables. The latent variables in PLSR do not only take into account the main variation pattern in the **X** data matrix as in PCA, but also the main variation patterns inherent in the reference data. PLSR was used in **Paper V** to predict the residual glucose concentration in the culture supernatants. In this case, a PLSR model was established using FTIR-ATR spectra obtained from a set of glucose solutions of known concentrations. The model was externally validated using a smaller set of standard solutions and culture supernatants from our earlier study [117], where glucose values were determined by reference analytical method (UHPLC). In **Paper VI**, PLSR was used to establish calibration models for lipids, phosphorus and carotenoids. A data set of either GC (lipids), UV/Vis (phosphorus) or HPLC (carotenoids) reference measurements (responses) were used as reference variables, which was regressed onto an **X** matrix containing FT-Raman or FTIR measurements (predictors).

Consensus Principal Component Analysis (CPCA). Consensus principal component analysis (CPCA) is a multiblock method that allows to correlate multivariate data obtained for the same set of samples, i.e. where a sample to sample correspondence can be established between the different multivariate data sets (blocks). When e.g. Raman, FTIR data and a set of reference data are obtained from the same data, CPCA can be applied. The consensus of all data blocks involved in CPCA is described by global scores. Further, block scores and block loadings which show the variations of individual samples and variables, are calculated [166]. In **Paper VI**, CPCA was used on multiblock spectral data, consisting of preprocessed derivative FTIR and FT-Raman data blocks.

2 Main results and discussions

2.1 Paper I: Microcultivation and FTIR spectroscopy-based screening revealed a nutrient-induced co-production of high-value metabolites in oleaginous Mucoromycota fungi

In **Paper I**, the micro-cultivation system Duetz-MTPS combined with FTIR spectroscopy and PCA analysis was applied to assess the influence of two types of nitrogen sources (yeast extract and ammonium sulphate) and phosphorus substrate availability (6 different concentrations) on the growth and co-production potential of nine oleaginous Mucoromycota fungi. FTIR-HTS provided a full biochemical profile of fungal biomass constituents identifying the co-production of lipids, chitin/chitosan and polyphosphate. FTIR-ATR spectroscopy was used to estimate consumption of glucose and phosphates.

Biomass production was quite uniform in the media with yeast extract (Figure 2.1). Relative lipid content in *Mortierella alpina* increased with higher phosphorus (Pi) substrate availability indicating high P requirements for this fungus, while the opposite effect was observed for *Absidia glauca*. Relative polyphosphate content increased in *Mucor circinelloides* and *Amylomyces rouxii* with higher amount of Pi substrate in the media, while in *Rhizopus stolonifer* polyphosphate accumulation was not affected by the Pi availability (Figure 2.1). The role of phosphate salts as buffering agents was highlighted when ammonium sulphate was used as a nitrogen source, due to its low buffering capacity and release of H^+ connected to its assimilation by fungi. Low P substrate availability caused acidic pH that influenced biomass production and co-production in all tested Mucoromycota strains except for *Rhizopus stolonifer*. The biomass and lipid production in PUFA producers *Mortierella alpina* and *Mortierella hyalina* were significantly increased when high concentrations of inorganic phosphorus were combined with ammonium sulphate. The fungi *Mucor circinelloides, Rhizopus stolonifer, Amylomyces rouxii, Absidia glauca* and *Lichtheimia corymbifera* showed overproduction of chitin/chitosan under the low pH conditions caused by the limitation of P substrate. The fungi *Mucor circinelloides, Amylomyces rouxii, Rhizopus stolonifer* and *Absidia glauca* were able to co-produce polyphosphate and lipids when high concentration of inorganic phosphorus was used (Figure 2.1). *Umbelopsis vinacea* reached almost double biomass concentration (22g/L) compared to other strains when yeast extract was used as nitrogen source while Pi limitation had little effect on the biomass production. Thus, the co-production inducing media compositions and fungal strains co-producing more valuable metabolites, were identified.

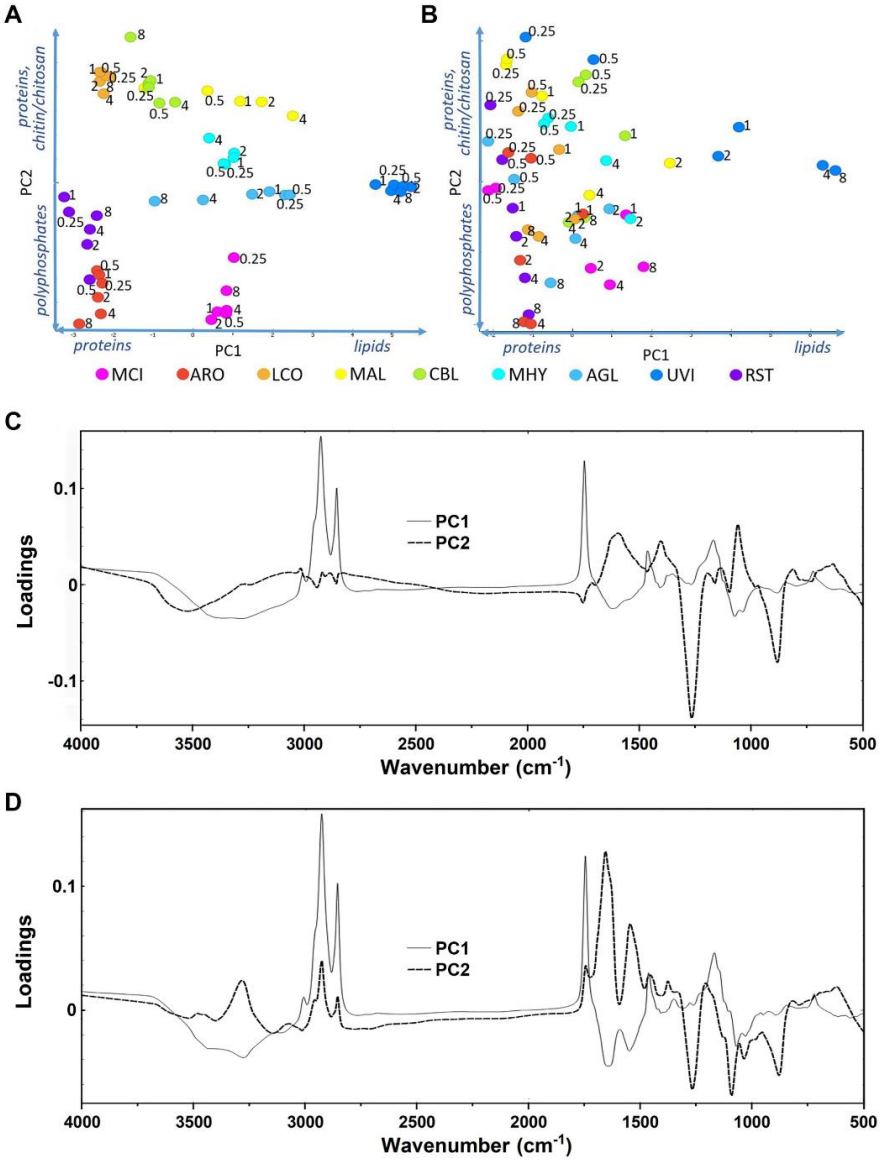

Figure 2.1: PCA score plots of FTIR-HTS spectra of fungi grown at different phosphorus concentrations on yeast extract (A) and ammonium sulphate (B). Numbers in PCA score plots indicate the Pi amounts. Vectors on axis describe an observed increase of the metabolites chitin/chitosan, polyphosphates and lipids. Below the scatter plots, loading vectors for PC1 (full line) and PC2 (dashed line) are plotted in C and D, respectively. The explained variance for the first and second principal components are 87% and 7%, respectively, for YE and 69% and 20% for AS.

2.2 Paper II: The influence of phosphorus source and the nature of nitrogen substrate on the biomass production and lipid accumulation in oleaginous Mucoromycota fungi.

In **Paper II**, the influence of phosphorus availability and type of nitrogen substrate (yeast extract or ammonium sulphate), on the biomass formation, lipid production and fatty acid profile of nine oleaginous *Mucoromycota* fungi was investigated. **Paper I** and **Paper II** share experimental design for the cultivation. GC-FID was utilized to analyse the fatty acid profiles of extracted fungal lipids. The total lipid content was estimated gravimetrically.

The influence of phosphorus source on the biomass production, lipid accumulation and fatty acid profile is strain-specific and both low and/or high phosphorus source availability can have beneficial effects (Figure 2.2). The fatty acid profile of fungal lipids produced in yeast extract media with different amounts of phosphorus substrate was quite consistent irrespective of phosphorus availability. While for biomass grown in ammonium sulphate media FA profiles varied depending on the growth phase of the fungi. Based on the biomass concentration results, it can be suggested that low pH caused by low phosphorus source availability in the ammonium sulphate media led to a delayed stationary (lipogenesis) phase of Mucoromycota fungi. Among the tested Mucoromycota fungi, the highest biomass and lipid yield (22 g/L and 63.55 %) was recorded for *Umbelopsis vinacea* grown at relatively high phosphorus source amount (Figure 2.2). High sensitivity towards high levels of phosphorus substrate was observed for *Mortierella* fungi, while at moderate amounts an increase in lipid accumulation and unsaturation was observed. Further, *Rhizopus stolonifer* showed an obvious advantage in managing the acidic pH caused by phosphorus source deficiency, since its growth, lipid accumulation and fatty acid profile was consistent under different phosphorus source amounts. Using *Umbelopsis vinacea*, *Lichtheimia corymbifera* and *Cunninghamella blakesleeana* resulted in the most suitable FA composition for biofuel applications concerning the unsaturation.

Results of **Paper II** allow to conclude that yeast extract could be used as both nitrogen and phosphorus source, possibly without additional inorganic phosphorus supplementation. The inorganic nitrogen source ammonium sulphate is cheap, while strain-specific optimization of phosphorus source amount and pH is necessary to obtain optimal lipid production and fatty acid profiles.

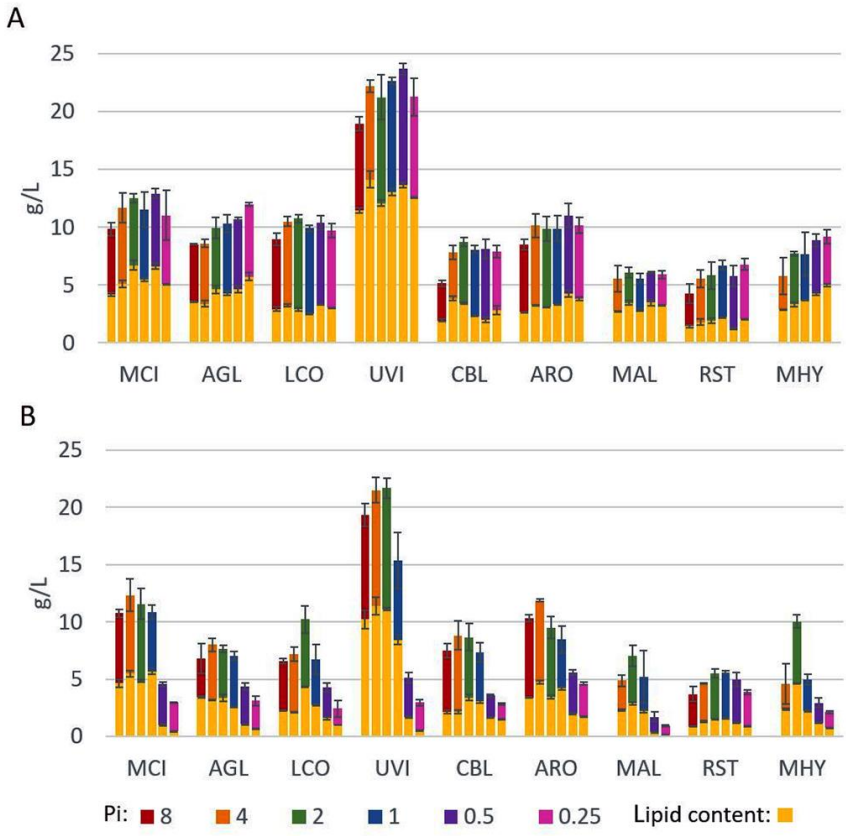

Figure 2.2: Biomass and lipid production of oleaginous Mucoromycota fungi grown in nitrogen-limited broth media based on yeast extract -YE-Pi (A) and ammonium sulphate- AS-Pi (B).

2.3 Paper III: Metal and phosphate ions show remarkable influence on the biomass production and lipid accumulation in oleaginous *Mucor circinelloides.*

In **Paper III**, the role of metal ions on the growth, lipid accumulation and co-production in *Mucor circinelloides* was investigated. In the study seven metal ions (Ca, Co, Cu, Fe, Mg, Mn, Zn) were combined in different concentrations with five levels of phosphorus substrate and with ammonium sulphate as nitrogen source resulting in 140 different media. *M. circinelloides* was selected due to its extraordinary ability to co-produce lipids, chitin/chitosan and polyphosphates. All cultivations were performed in Duetz-MTPS and the produced fungal biomass was analyzed by FTIR spectroscopy. In addition, lipids were extracted by the Lewis method and analyzed using GC-FID.

Growth of *M. circinelloides* was affected mainly by phosphorus substrate availability. A decreased growth under low phosphorus levels due to the acidic pH (Figure 2.3) was observed. Among all tested metal ions, Mg and Zn ions showed to be essential for the growth and metabolic activity of *M. circinelloides.* When these metals were lacking, no growth could be observed. In addition, FA profiles of lipids accumulated by *M. circinelloides* that were grown in media that had low amounts of Mg and Zn ions, differed from FA profiles observed for media with higher amounts of Mg and Zn ions. This may indicate that Mg availability could lead to a delay in lipogenesis. Higher concentrations of Cu, Co and Zn ions enhanced the growth of lipids and lipid accumulation, while high amount of Fe ions was toxic for *M. circinelloides* growth. Lack of Ca and Cu ions, as well as higher amounts of Zn and Mn ions, enhanced lipid accumulation in *M. circinelloides* (Figures 2.3, 2.4).

Correlation PCA loading plots of FTIR data (Figure 2.4) show, that a lack of Ca ions resulted in an increased lipid content and a decrease in polyphosphate content. Higher concentration of Ca ions in the media enhanced polyphosphate accumulation. This can be explained by the several hypotheses, where one of them is that Ca deficiency affects antilipolytic pathways resulting in increased lipid content. Another hypothesis is related to the fact that endoplasmic reticulum can be affected by lack of Ca via sterol response element binding proteins that are triggering lipid accumulation. More detailed studies are required to confirm these events in oleaginous fungi.

This study suggests that Ca ions can be considered as a key optimization parameter for improving lipid accumulation and achieving co-production of lipids and polyphosphate in *M. circinelloides*, we expect that our findings may contribute to increasing sustainability of fungal biorefineries.

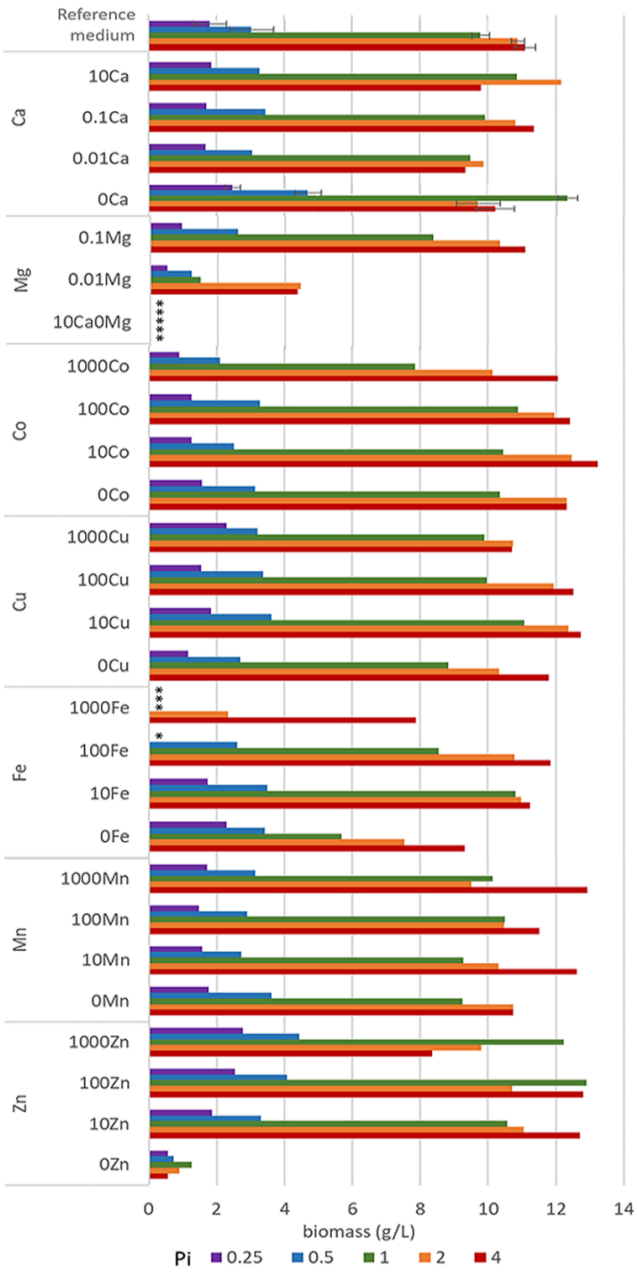

*Figure 2.3: Final biomass concentrations after 7 days of incubation of Mucor circinelloides in the media with different concentrations of metal and phosphorus ions. *Empty slots indicate no growth.*

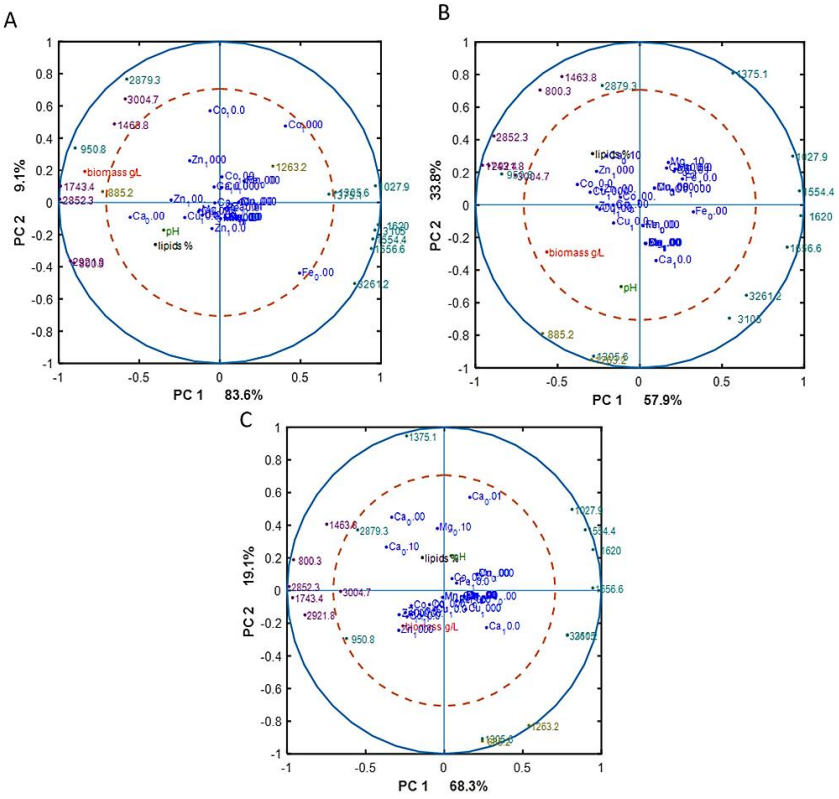

Figure 2.4: Correlation loading plots based on the PCA analysis of FTIR-HTS spectra of M. circinelloides biomass grown in metal-ions regulated media with Pi1 (A), Pi2 (B) and Pi4 (C) levels. Main peaks corresponding to the lipids (purple), chitin/chitosan (green) and polyphosphates (yellow) are presented.

2.4 Paper IV: Evaluation and optimization of direct transesterification methods for the assessment of lipid accumulation in oleaginous filamentous fungi.

Oleaginous filamentous fungi can accumulate lipids with the relatively wide yield range from 20% to 80% and many of them have thick resilient cell wall that is affecting extraction and estimation of lipids. In **Paper II** and **Paper III**, analysis of the total lipid content in fungal biomass was done by a direct transesterification according to the modified Lewis method (Lewis method 1) and the subsequent GC-FID analysis. It was observed that the employed Lewis method underestimates total lipid content especially for fungi with the high lipid content. Therefore, further optimization of the extraction and direct transesterification protocol was done in **Paper IV**. Three common direct transesterification methods (Lewis, Lepage and Wahlen) were evaluated and optimized for the efficient lipid extraction and estimation. Three different catalysts were utilized in the direct transesterification methods: hydrochloric acid for Lewis method, sulphuric acid for Wahlen method, and acetyl chloride for Lepage method. The three methods were modified in respect to reaction times and heating, and amount of cosolvents. Some fungal strains can produce extraordinarily high amounts of lipids and there is a competition hydrolysis reaction ongoing on the cell wall biopolymers during the transesterification. Thus, *Mucor circinelloides* as a strain with resilient cell wall, *Umbelopsis vinacea* as a strain with very high lipid production, and olive oil as control substance were used. Different internal standards for GC-FID measurements were applied. FTIR spectroscopy was utilized to estimate the residual lipids in biomass (Figure 2.5) and transesterification efficiency was evaluated by the NMR spectroscopy. In addition, the optimized method was used for six Mucoromycota strains. Exact description of the transesterification methods modifications can be found in the **Paper IV**.

Selected direct transesterification methods provided efficient lipid extraction, while transesterification efficiency differed significantly (Figure 2.6, 2.7). The most optimal method, providing ease of use, as well as efficient lipid extraction and transesterification, was the optimised Lewis method (Lewis 2), where the optimization parameters were solvent to co-solvent ratio, reaction time, and TAG internal standard. The FA profiles of the extracted lipids were comparable between the two Lewis methods. The relation between the solvent used for the internal standard (hexane) and the solvents used for the disintegration of fungal biomass and lipid extraction (methanol in Lewis 1 and chloroform in Lewis 2) play an important role for the correct total lipid content estimation.

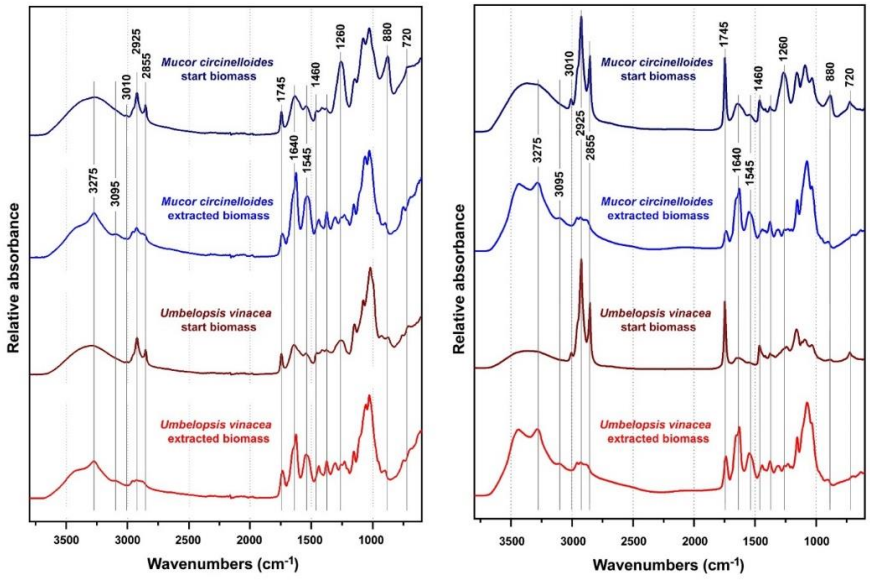

Figure 2.5: ATR (left) and HTS (right) FTIR spectra of Mucor circinelloides and Umbelopsis vinacea fungal biomass before and after transesterification reaction (Lewis 2 method with 90 min reaction time).

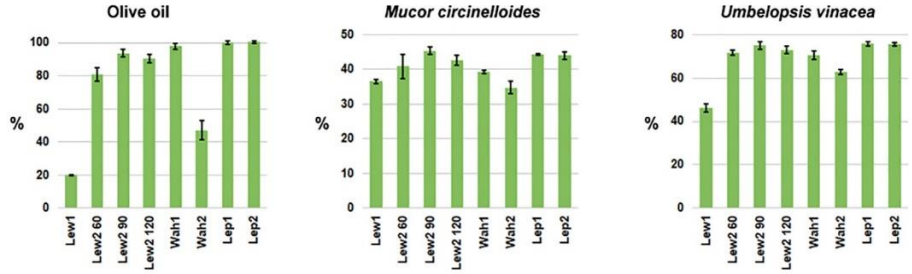

Figure 2.6: Total FAMEs yield estimate based on GC-FID measurements. The yield is calculated as percentage of dry biomass (%w/w), with one standard deviation error bars. Lew: Lewis method (with designated reaction times in minutes for method 2), Wah: Wahlen method, Lep: Lepage method.

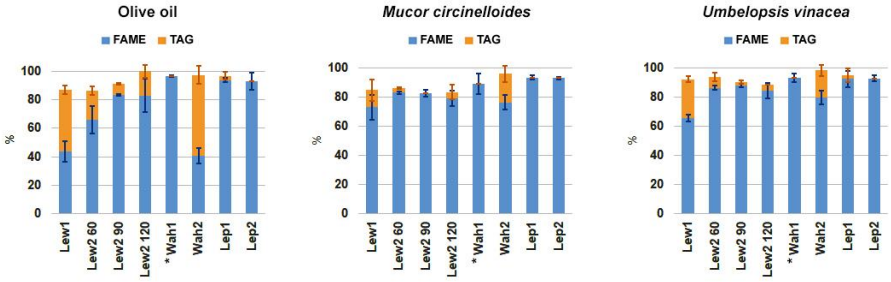

*Figure 2.7: Total yield of FAME and TAG based on NMR analysis, calculated by specific signals in the extracted oil, with one standard deviation error bars. Yield is calculated as mol percentage (%mol). Lew: Lewis method (with designated reaction times in minutes for method 2), Wah: Wahlen method, Lep: Lepage method. *TAGs were not estimated for Wahlen 1 method.*

2.5 Paper V: Calcium affects polyphosphate and lipid accumulation in Mucoromycota fungi.

Calcium (Ca) is important element for fungal metabolism, such as hyphae growth, cell wall synthesis, stress tolerance etc. In **Paper III**, we reported the importance of Ca for polyphosphate and lipid accumulation in *Mucor circinelloides*. In order to examine to what extend the observations of Ca relation to lipid and polyphosphates accumulation observed in **Paper III** are conserved and valid for other Mucoromycota, we have assessed the effect of a lack (Ca0) and presence (Ca1) of calcium on six strains grown under three different phosphorus substrate (Pi) levels in **Paper V**. FTIR spectroscopy was used for biochemical fingerprinting of fungal biomass. Peak ratios lipids-to-proteins and phosphates-to-proteins were calculated to estimate the relative content of lipids-to-proteins and phosphates-to-proteins in the fungal biomass using the following peaks: (i) ester bond (C=O stretch at 1745 cm^{-1}) for lipids, (ii) phosphate functional group (P=O stretch at 1251 cm^{-1}) for polyphosphate and (iii) Amide I (C=O stretch at 1650 cm^{-1}) for proteins. Lipids were analyzed by GC using optimized transesterification protocol. Total cellular P was analyzed by assay-based UV/VIS spectroscopy. Solid-state NMR was utilized to characterize the cellular phosphates (only for *Mucor circinelloides* VI04473).

The results indicate that an extensive polyphosphate accumulation could be possible by polyphosphate accumulating strains only in non-acidic pH conditions. Calcium clearly enhanced the phosphorus uptake in Pi4 and Pi0.5 conditions, since higher cellular phosphorus was detected for all samples (Figure 2.8). The effect of calcium under the Pi1 level has shown to be strain specific. Lack of calcium enhanced lipid accumulation under Pi0.5 condition for all strains except *Mucor circinelloides* FRR5020, where the differences were most prominent for *Mucor circinelloides* VI04773, *Mucor racemosus* and *Amylomyces rouxii* (Table 2.1). In Pi4 and Pi1 conditions, the effect of Ca on the lipid accumulation was strain specific. Further, it was visually detected that the biomass of *Amylomyces rouxii* and both *Mucor circinelloides* strains produced more carotenoids in calcium-lacking media, especially for the Pi0.5 condition. FTIR spectra indicated changes in chitin/chitosan under Pi0.5 condition.

To conclude, calcium is important agent regulating polyphosphate and lipid accumulation in fungal cells and calcium availability can be used as an optimization parameter in fungal biorefineries. Further, it has to be noted that pH and possibly phosphorus availability play important role in involvement of calcium in regulating lipid accumulation in Mucoromycota fungi, and further verification experiments would be needed to confirm these observations.

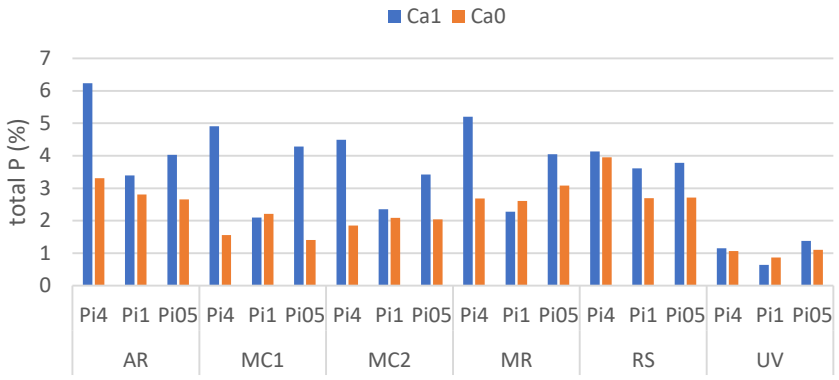

Figure 2.8: Total P (%) in the fungal biomass estimated by assay-based UV-VIS spectroscopy.

Table 2.1: Lipid content in % per cell dry weight

sample		Pi4	Pi1	Pi05
Amylomyces rouxii	Ca1	30.37	46.76	27.36
	Ca0	31.24	40.02	37.48
Mucor circinelloides	Ca1	42.80	47.85	22.67
VI 04473	Ca0	47.42	54.01	48.05
Mucor circinelloides	Ca1	34.37	47.62	37.11
FRR 5020	Ca0	41.01	48.60	35.79
Mucor racemosus	Ca1	31.10	37.85	22.83
	Ca0	30.86	35.04	39.63
Rhizopus stolonifer	Ca1	25.33	24.27	22.78
	Ca0	27.40	26.75	27.90
Umbelopsis vinacea	Ca1	69.90	81.04	52.36
	Ca0	58.43	84.18	66.70

2.6 Paper VI: Assessment of fungal biomass by Fourier transform Raman spectroscopy for application in biotechnology and bioprocessing.

While **Paper V** and **Paper VI** share the experimental design concerning the cultivation, Fourier transform (FT) Raman spectroscopy has been utilized in **Paper VI** for the characterization of fungal biomass. We assessed suitability of FT Raman spectroscopy for screening and process monitoring of filamentous fungi in biotechnology. FT-Raman and FT-infrared (FTIR) spectroscopies data was assessed with respect to the referent analyses of lipids (GC), phosphorus (assay-based UV-VIS), and carotenoids (HPLC) by using principal component analysis (PCA), multiblock consensus PCA, partial least square regression (PLSR), and variation contribution analysis. The study demonstrates that FT-Raman and FTIR spectroscopies provide complementary information on main fungal biomass constituents.

All main chemical biomass constituents were detected by FT-Raman spectra, including lipids, proteins, cell wall carbohydrates, and polyphosphates, as well as carotenoids (Figure 2.9). Lipids showed by far the strongest signals in FT-Raman spectra, unless the biomass contained carotenoids (Figure 2.10). Due to the resonance effect, carotenoids peaks, which are present in very low amounts in the fungal biomass (maximum 1457 $\mu g/g_{dry\ weight}$ in the presented study) became predominant signals in FT-Raman spectra. Biomass grown in media lacking calcium show significantly lower chitin-related signals in Raman spectra when compared to their counterparts cultivated under normal calcium conditions. This is especially noticeable for samples grown under low phosphate conditions that show overexpression of chitin production as a result of acidic conditions.

FT-Raman spectra clearly show effect of growth conditions on fungal biomass (Figure 2.11). PLSR models with high coefficients of determination (0.83–0.94) and low error (approx. 8%) for quantitative determination of total lipids, phosphates and carotenoids were established. In general, the levels of accuracy achieved by vibrational spectroscopy PLSR models are similar to the accuracy achieved by the reference methods involving extraction, transesterification and chromatography. FT-Raman spectroscopy showed great potential for chemical analysis of biomass of oleaginous filamentous fungi.

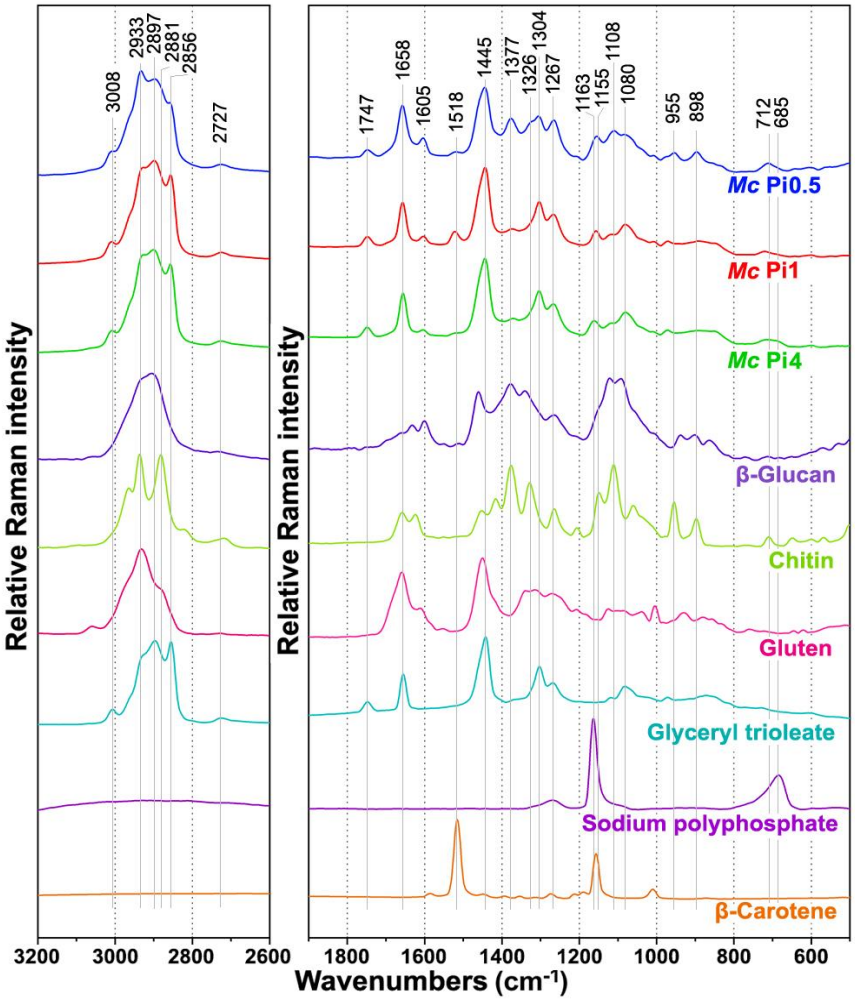

Figure 2.9: FT-Raman spectra of Mucor circinelloides (Mc) strain VI 04473 cultivated under Ca1 conditions and three different phosphate concentrations, and of six reference compounds: β-glucan, chitin, gluten, glyceryl trioleate, sodium polyphosphate, and β-carotene. All spectra were preprocessed and plotted with offset for better viewing.

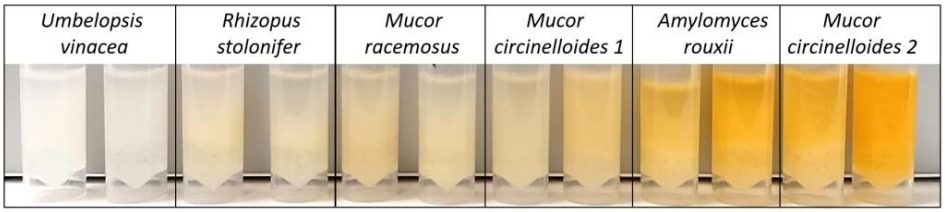

Figure 2.10: Biomass of studied Mucoromycota fungi with different pigment content

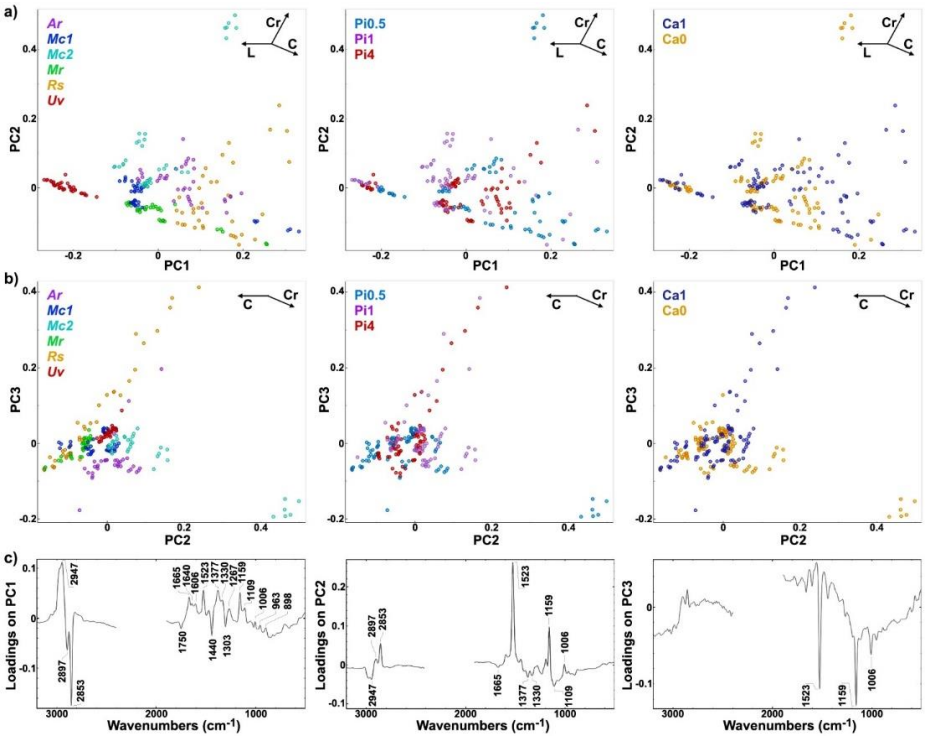

Figure 2.11: PCA of FT-Raman spectra of fungi grown at different phosphates and calcium concentrations. (a) Score plots of PC1 and PC2, and (b) PC2 and PC3, and (c) the first three loading vectors. Score plots are labelled according to strains: Amylomyces rouxii (Ar), Mucor circinelloides VI 04473 (Mc1), Mucor circinelloides FRR 5020 (Mc2), Mucor racemosus (Mr), Rhizopus stolonifer (Rs), and Umbelopsis vinacea (Uv) (left), phosphates concentrations (middle), and calcium availability (right). Vectors are approximating the increase in relative amount of the metabolites: lipids (L), cell wall carbohydrates (C), and carotenoids (Cr). The explained variances for the first five principal components are 47.3%, 26.9%, 15.8%, 3.8% and 1.4%..

3 Conclusions and future prospects

In this PhD work the influence of nitrogen source, phosphorus and metal ions availability on the growth and metabolite production in oleaginous Mucoromycota fungi was examined. High C/N ratio triggering lipid accumulation was applied through the experiments in order to induce lipid accumulation and assess co-production of other valuable metabolites in Mucoromycota. The majority of the tested fungi showed submerged growth in either dispersed or pellet form with no adherent wall growth in Duets MTPS. For *Rhizopus stolonifer*, some wall growth and sporulation were observed.

The influence of nitrogen sources and phosphorus availability on the growth and co-production of valuable metabolites, lipid accumulation and fatty acid profile for the selected oleaginous Mucoromycota fungi was investigated in **Paper I** and **Paper II**, respectively. In **Paper I**, co-production of lipids, chitin/chitosan and polyphosphate in several studied Mucoromycota fungi was identified by using FTIR spectroscopy as a sole analytical method. *Mucor circinelloides, Rhizopus stolonifer, Amylomyces rouxii, Absidia glauca* and *Lichtheimia corymbifera* showed an ability to co-produce lipids and chitin/chitosan, while *Mucor circinelloides, Rhizopus stolonifer* and *Amylomyces rouxii* co-produced lipids and polyphosphate. *Mucor circinelloides* can be considered as a microbial cell factory with a high co-production potential as it showed ability to co-produce lipids, chitin/chitosan and polyphosphate. **Paper II** reports the gravimetrically estimated total lipid production and FA profiles analyzed by GC**.** Lipid accumulation and fatty acid profiles of Mucoromycota grown in yeast extract media were quite consistent irrespective phosphorus availability. Phosphorus availability had a significant impact on the biomass and lipid production in the ammonium sulphate media for all strains except for *Rhizopus stolonifer*. Since *Mucor circinelloides* has shown a great potential for the co-production, its growth and metabolic activity under different metal ions (Ca, Cu, Co, Fe, Mg, Mn, Zn) concentrations were studied in **Paper III.** Mg and Zn are essential for the growth of *Mucor circinelloides.* Further, higher amounts of Zn and Mn and lack of Ca ions can have beneficial impact on lipid accumulation. Increasing Ca availability was shown to be connected to increasing polyphosphate accumulation. In order to understand whether the role of Ca ions can be generally valid for all oleaginous Mucoromycota, a growth and biomass composition for a set of six Mucoromycota fungi was studied under different Ca ions conditions in **Paper V**. The relation between Ca ions availability and accumulation of lipids and

polyphosphate was demonstrated under non-acidic conditions. Increased lipid accumulation was shown in the absence of Ca ions in acidic conditions for all tested fungal strains. Thus, it can be concluded that lipid accumulation in Mucoromycota fungi could be improved by adjusting the availability of Ca ions and pH of the media. Further, high availability of Ca ions contributed to a higher polyphosphate accumulation that is important for phosphorus recovery operations employing filamentous fungi. Further, In **Paper VI**, FT-Raman analysis enabled to detect that Ca affects the carotenoid accumulation in *Mucor circinelloides* and *Amylomyces rouxii*, and chitin/chitosan production in Mucoromycota especially in acidic conditions connected to Pi limitation.

In addition to the main aims of the PhD work focused on the optimizing different media components for production of valuable metabolites in Mucoromycota fungi, studies on the optimization of the lipid extraction and development of rapid non-destructive monitoring of fungal fermentation by vibrational spectroscopy was performed in **Paper IV** and **Paper VI.** It was shown that the direct transesterification method (Lewis 1 method), utilized in **Papers II** and **III,** can result in significant underestimation of the total lipid content, particularly for biomass that is rich in lipids, while FA profiles were accurate. Therefore, in **Paper IV,** the direct transesterification Lewis 1 method was modified in order to increase lipid extraction efficiency and estimation accuracy. The optimized method (Lewis 2 method, with a modified reaction time (90 minutes), solvent and co-solvent ratios (chloroform-methanol 16:5), has shown to be the most suitable method for efficient extraction and estimation of lipids in Mucoromycota.

Vibrational spectroscopy techniques, FTIR-HTS and FTIR-ATR, utilized for biochemical profiling of intracellular fungal metabolites and substrate consumption, showed to be exceptionally powerful in shedding the light on the role of different media components in metabolic activity and co-production in Mucoromycota fungi. In addition, a thorough comparison of two complementary vibrational spectroscopy techniques, FTIR and FT-Raman performed in **Paper VI** demonstrated the high potential of techniques for screening studies, as well as for real-time in-line monitoring and control of fungal fermentations.

The findings of this PhD work deliver important knowledge on oleaginous Mucoromycota physiology and metabolism and their potential as microbial cell factories for sustainable fungal biorefineries. The thesis provides understanding of how media components can be used for optimizing metabolite production and development of the co-production concepts by using Mucoromycota fungi. One of the most exciting findings is related to the

effect of calcium on lipid, carotenoid and polyphosphate accumulation in Mucoromycota. Further studies are needed in order to achieve a more profound understanding of the role of calcium ions in these processes. Further, the effect of pH associated with low phosphorus availability and the role of ammonium sulphate for the co-production of lipids and chitin/chitosan needs to be verified in bioreactor cultivations.

4 Bibliography

1. Cherubini, F. The biorefinery concept: using biomass instead of oil for producing energy and chemicals. *Energy conversion and management* **2010**, *51*, 1412-1421.
2. Lindorfer, J.; Lettner, M.; Hesser, F.; Fazeni, K.; Rosenfeld, D.; Annevelink, B.; Mandl, M. Technical, Economic and Environmental Assessment of Biorefinery Concepts. *Developing a practical approach for characterization. IEA (International Energy Agency). Bioenergy: Task* **2019**, *42*, 01.
3. Meyer, V.; Andersen, M.R.; Brakhage, A.A.; Braus, G.H.; Caddick, M.X.; Cairns, T.C.; de Vries, R.P.; Haarmann, T.; Hansen, K.; Hertz-Fowler, C. Current challenges of research on filamentous fungi in relation to human welfare and a sustainable bio-economy: a white paper. *Fungal biology and biotechnology* **2016**, *3*, 1-17.
4. Moore, D.; Chiu, S.W. Fungal products as food. *eds. Pointing, SB and Hyde, KD in Bio-exploitation of filamentous fungi. Fungal Diversity Research Series* **2001**, *6*, 223-251.
5. Santek, M.I.; Beluhan, S.; Santek, B. Production of microbial lipids from lignocellulosic biomass. *Advances in Biofuels and Bioenergy* **2018**, 137-164.
6. Dashtban, M.; Schraft, H.; Qin, W. Fungal bioconversion of lignocellulosic residues; opportunities & perspectives. *International journal of biological sciences* **2009**, *5*, 578.
7. Karimi, K.; Edebo, L.; Taherzadeh, M.J. Mucor indicus as a biofilter and fermenting organism in continuous ethanol production from lignocellulosic hydrolyzate. *Biochemical engineering journal* **2008**, *39*, 383-388.
8. Liao, W.; Liu, Y.; Frear, C.; Chen, S. Co-production of fumaric acid and chitin from a nitrogen-rich lignocellulosic material–dairy manure–using a pelletized filamentous fungus Rhizopus oryzae ATCC 20344. *Bioresource technology* **2008**, *99*, 5859-5866.
9. Cherubini, F.; Strømman, A.H.; Ulgiati, S. Influence of allocation methods on the environmental performance of biorefinery products—A case study. *Resources, Conservation and Recycling* **2011**, *55*, 1070-1077.
10. Zheng, Y.; Yu, X.; Zeng, J.; Chen, S. Feasibility of filamentous fungi for biofuel production using hydrolysate from dilute sulfuric acid pretreatment of wheat straw. *Biotechnology for biofuels* **2012**, *5*, 50.
11. Qiao, W.; Tao, J.; Luo, Y.; Tang, T.; Miao, J.; Yang, Q. Microbial oil production from solid-state fermentation by a newly isolated oleaginous fungus, *Mucor circinelloides* Q531 from mulberry branches. *Royal Society open science* **2018**, *5*, 180551.
12. Satari, B.; Karimi, K. Mucoralean fungi for sustainable production of bioethanol and biologically active molecules. *Applied microbiology and biotechnology* **2018**, *102*, 1097-1117.
13. Zhang, Z.Y.; Jin, B.; Kelly, J.M. Production of lactic acid from renewable materials by Rhizopus fungi. *Biochemical engineering journal* **2007**, *35*, 251-263.

14. Ferreira, J.A.; Lennartsson, P.R.; Edebo, L.; Taherzadeh, M. Zygomycetes-based biorefinery: Present status and future prospects. *Bioresource technology* **2013**, *135*, 523-532.
15. Zininga, J.T.; Puri, A.K.; Govender, A.; Singh, S.; Permaul, K. Concomitant production of chitosan and lipids from a newly isolated *Mucor circinelloides* ZSKP for biodiesel production. *Bioresource technology* **2019**, *272*, 545-551.
16. Bonfante, P.; Venice, F. Mucoromycota: going to the roots of plant-interacting fungi. *Fungal Biology Reviews* **2020**, *34*, 100-113.
17. Vattem, D.A.; Shetty, K. Solid-state production of phenolic antioxidants from cranberry pomace by *Rhizopus oligosporus*. *Food Biotechnology* **2002**, *16*, 189-210.
18. Carvalho, A.K.F.; da Conceição, L.R.V.; Silva, J.P.V.; Perez, V.H.; de Castro, H.F. Biodiesel production from *Mucor circinelloides* using ethanol and heteropolyacid in one and two-step transesterification. *Fuel* **2017**, *202*, 503-511.
19. Mitra, D.; Rasmussen, M.L.; Chand, P.; Chintareddy, V.R.; Yao, L.; Grewell, D.; Verkade, J.G.; Wang, T.; van Leeuwen, J.H. Value-added oil and animal feed production from corn-ethanol stillage using the oleaginous fungus *Mucor circinelloides*. *Bioresource Technology* **2012**, *107*, 368-375.
20. Andrade, V.S.; Sarubbo, L.A.; Fukushima, K.; Miyaji, M.; Nishimura, K.; Campos-Takaki, G.M.d. Production of extracellular proteases by *Mucor circinelloides* using D-glucose as carbon source/substrate. *Brazilian Journal of Microbiology* **2002**, *33*, 106-110.
21. Rodrigues Reis, C.E.; Bento, H.B.; Carvalho, A.K.; Rajendran, A.; Hu, B.; De Castro, H.F. Critical applications of *Mucor circinelloides* within a biorefinery context. *Critical reviews in biotechnology* **2019**, *39*, 555-570.
22. Singh, A.; Ward, O. Production of high yields of arachidonic acid in a fed-batch system by *Mortierella alpina* ATCC 32222. *Applied microbiology and biotechnology* **1997**, *48*, 1-5.
23. Ruan, Z.; Zanotti, M.; Wang, X.; Ducey, C.; Liu, Y. Evaluation of lipid accumulation from lignocellulosic sugars by *Mortierella isabellina* for biodiesel production. *Bioresource Technology* **2012**, *110*, 198-205.
24. Dyal, S.D.; Bouzidi, L.; Narine, S.S. Maximizing the production of γ-linolenic acid in *Mortierella ramanniana var. ramanniana* as a function of pH, temperature and carbon source, nitrogen source, metal ions and oil supplementation. *Food Research International* **2005**, *38*, 815-829.
25. Gema, H.; Kavadia, A.; Dimou, D.; Tsagou, V.; Komaitis, M.; Aggelis, G. Production of γ-linolenic acid by *Cunninghamella echinulata* cultivated on glucose and orange peel. *Applied Microbiology and Biotechnology* **2002**, *58*, 303-307.
26. Andrade, R.F.; Silva, T.A.; Ribeaux, D.R.; Rodriguez, D.M.; Souza, A.F.; Lima, M.A.; Lima, R.A.; Alves da Silva, C.A.; Campos-Takaki, G.M. Promising biosurfactant produced by *Cunninghamella echinulata* UCP 1299 using renewable resources and its application in cotton fabric cleaning process. *Advances in Materials Science and Engineering* **2018**, *2018*.

27. Grantina-Ievina, L.; Berzina, A.; Nikolajeva, V.; Mekss, P.; Muiznieks, I. Production of fatty acids by *Mortierella* and *Umbelopsis* species isolated from temperate climate soils. *Environ Exp Bio* **2014**, *12*, 15-27.
28. Dourou, M.; Mizerakis, P.; Papanikolaou, S.; Aggelis, G. Storage lipid and polysaccharide metabolism in *Yarrowia lipolytica* and *Umbelopsis isabellina. Applied microbiology and biotechnology* **2017**, *101*, 7213-7226.
29. Tabatabaei, M.; Alidadi, A.; Dehhaghi, M.; Panahi, H.K.S.; Lam, S.S.; Nizami, A.-S.; Aghbashlo, M.; Jouzani, G.S. Fungi as Bioreactors for Biodiesel Production. In *Fungi in Fuel Biotechnology*, Springer: 2020; pp. 39-67.
30. Pawłowska, J.; Okrasińska, A.; Kisło, K.; Aleksandrzak-Piekarczyk, T.; Szatraj, K.; Dolatabadi, S.; Muszewska, A. Carbon assimilation profiles of mucoralean fungi show their metabolic versatility. *Scientific reports* **2019**, *9*, 1-8.
31. El-Esawi, M.A. *Physical Methods for Stimulation of Plant and Mushroom Development*; BoD–Books on Demand: 2018.
32. Karimi, S.; Mahboobi Soofiani, N.; Lundh, T.; Mahboubi, A.; Kiessling, A.; Taherzadeh, M.J. Evaluation of filamentous fungal biomass cultivated on Vinasse as an alternative nutrient source of fish feed: protein, lipid, and mineral composition. *Fermentation* **2019**, *5*, 99.
33. Athenaki, M.; Gardeli, C.; Diamantopoulou, P.; Tchakouteu, S.S.; Sarris, D.; Philippoussis, A.; Papanikolaou, S. Lipids from yeasts and fungi: physiology, production and analytical considerations. *Journal of applied microbiology* **2018**, *124*, 336-367.
34. Ratledge, C.; Cohen, Z. Microbial and algal oils: do they have a future for biodiesel or as commodity oils? *Lipid Technology* **2008**, *20*, 155-160.
35. Ratledge, C. Single cell oils for the 21st century. In *Single cell oils*, Elsevier: 2010; pp. 3-26.
36. Ander, B.P.; Dupasquier, C.M.; Prociuk, M.A.; Pierce, G.N. Polyunsaturated fatty acids and their effects on cardiovascular disease. *Experimental & Clinical Cardiology* **2003**, *8*, 164.
37. Bartnicki-Garcia, S. Cell wall chemistry, morphogenesis, and taxonomy of fungi. *Annual Reviews in Microbiology* **1968**, *22*, 87-108.
38. Bowman, S.M.; Free, S.J. The structure and synthesis of the fungal cell wall. *Bioessays* **2006**, *28*, 799-808.
39. Azuma, K.; Ifuku, S.; Osaki, T.; Okamoto, Y.; Minami, S. Preparation and biomedical applications of chitin and chitosan nanofibers. *Journal of biomedical nanotechnology* **2014**, *10*, 2891-2920.
40. Kumar, M.N.R. A review of chitin and chitosan applications. *Reactive and functional polymers* **2000**, *46*, 1-27.
41. Elieh-Ali-Komi, D.; Hamblin, M.R. Chitin and chitosan: production and application of versatile biomedical nanomaterials. *International journal of advanced research* **2016**, *4*, 411.
42. Safaei, Z.; Karimi, K.; Zamani, A. Impact of phosphate, potassium, yeast extract, and trace metals on chitosan and metabolite production by *Mucor indicus*. *International journal of molecular sciences* **2016**, *17*, 1429.
43. Ruiz-Herrera, J. *Fungal cell wall: structure, synthesis, and assembly*; CRC press: 1991.

44. Hu, K.-J.; Hu, J.-L.; Ho, K.-P.; Yeung, K.-W. Screening of fungi for chitosan producers, and copper adsorption capacity of fungal chitosan and chitosanaceous materials. *Carbohydrate Polymers* **2004**, *58*, 45-52.
45. Synowiecki, J.; Al-Khateeb, N.A.A.Q. Mycelia of *Mucor rouxii* as a source of chitin and chitosan. *Food Chemistry* **1997**, *60*, 605-610.
46. Vaingankar, P.N.; Juvekar, A.R. Fermentative production of mycelial chitosan from zygomycetes: media optimization and physico-chemical characterization. *Advances in Bioscience and Biotechnology* **2014**, *5*, 940.
47. Sebastian, J.; Rouissi, T.; Brar, S.K. Fungal chitosan: prospects and challenges. *Handbook of Chitin and Chitosan: Volume 1: Preparation and Properties* **2020**, 22.
48. Synowiecki, J.; Al-Khateeb, N.A. Production, properties, and some new applications of chitin and its derivatives. **2003**.
49. Elsoud, M.M.A.; El Kady, E. Current trends in fungal biosynthesis of chitin and chitosan. *Bulletin of the National Research Centre* **2019**, *43*, 59.
50. Shari'a, A.E.d.N.; Nascimento, A.E.d.; Lima, M.A.B.d.; Campos-Takaki, G.M.d.; Souza, W.d. Polyphosphate in Zygomycetes: a cytochemical study. *Brazilian Journal of Microbiology* **2002**, *33*, 119-126.
51. Werner, T.P.; Amrhein, N.; Freimoser, F.M. Specific localization of inorganic polyphosphate (poly P) in fungal cell walls by selective extraction and immunohistochemistry. *Fungal Genetics and Biology* **2007**, *44*, 845-852.
52. Beever, R.E.; Burns, D. Phosphorus uptake, storage and utilization by fungi. In *Advances in botanical research*, Elsevier: 1981; Vol. 8, pp. 127-219.
53. Cordell, D.; Rosemarin, A.; Schröder, J.J.; Smit, A. Towards global phosphorus security: A systems framework for phosphorus recovery and reuse options. *Chemosphere* **2011**, *84*, 747-758.
54. He, Q.; Rajendran, A.; Gan, J.; Lin, H.; Felt, C.A.; Hu, B.J. Phosphorus recovery from dairy manure wastewater by fungal biomass treatment. *Water and Environment Journal* **2019**, *33*, 508-517.
55. Mohamed, H.; El-Shanawany, A.-R.; Shah, A.M.; Nazir, Y.; Naz, T.; Ullah, S.; Mustafa, K.; Song, Y. Comparative Analysis of Different Isolated Oleaginous Mucoromycota Fungi for Their γ-Linolenic Acid and Carotenoid Production. *BioMed research international* **2020**, *2020*.
56. Fraser, P.D.; Ruiz-Hidalgo, M.J.; Lopez-Matas, M.A.; Alvarez, M.I.; Eslava, A.P.; Bramley, P.M. Carotenoid biosynthesis in wild type and mutant strains of *Mucor circinelloides. Biochimica et Biophysica Acta (BBA)-General Subjects* **1996**, *1289*, 203-208.
57. Enrique, A.; Papp, T.; Breum, J.; Arnau, J.; Arturo, P. Strain and culture conditions improvement for β-carotene production with *Mucor*. In *Microbial processes and products*, Springer: 2005; pp. 239-256.
58. Khanafari, A.; Tayari, K.; Emami, M. Light Requirement for the Carotenoids Production by *Mucor hiemalis*. *Iranian Journal of Basic Medical Sciences* **2008**, *11*, 25-32.
59. Mosqueda-Cano, G.; Gutiérrez-Corona, J.F. Environmental and developmental regulation of carotenogenesis in the dimorphic fungus *Mucor rouxii*. *Current Microbiology* **1995**, *31*, 141-145.

60. Sahadevan, Y.; Richter-Fecken, M.; Kaerger, K.; Voigt, K.; Boland, W. Early and late trisporoids differentially regulate β-carotene production and gene transcript levels in the mucoralean fungi Blakeslea trispora and *Mucor mucedo*. *Applied and environmental microbiology* **2013**, *79*, 7466-7475.
61. Corrochano, L.M.; Garre, V. Photobiology in the Zygomycota: multiple photoreceptor genes for complex responses to light. *Fungal Genetics and Biology* **2010**, *47*, 893-899.
62. Dexter, Y.; Cooke, R. Fatty acids, sterols and carotenoids of the psychrophile *Mucor strictus* and some mesophilic *Mucor* species. *Transactions of the British Mycological Society* **1984**, *83*, 455-461.
63. Csernetics, Á.; Nagy, G.; Iturriaga, E.A.; Szekeres, A.; Eslava, A.P.; Vágvölgyi, C.; Papp, T. Expression of three isoprenoid biosynthesis genes and their effects on the carotenoid production of the zygomycete Mucor circinelloides. *Fungal Genetics and Biology* **2011**, *48*, 696-703.
64. Zhang, Y.; Navarro, E.; Cánovas-Márquez, J.T.; Almagro, L.; Chen, H.; Chen, Y.Q.; Zhang, H.; Torres-Martinez, S.; Chen, W.; Garre, V. A new regulatory mechanism controlling carotenogenesis in the fungus *Mucor circinelloides* as a target to generate β-carotene over-producing strains by genetic engineering. *Microbial cell factories* **2016**, *15*, 99.
65. Kosa, G.; Zimmermann, B.; Kohler, A.; Ekeberg, D.; Afseth, N.K.; Mounier, J.; Shapaval, V. High-throughput screening of Mucoromycota fungi for production of low-and high-value lipids. *Biotechnology for biofuels* **2018**, *11*, 66.
66. Corrochano, L.M.; Kuo, A.; Marcet-Houben, M.; Polaino, S.; Salamov, A.; Villalobos-Escobedo, J.M.; Grimwood, J.; Álvarez, M.I.; Avalos, J.; Bauer, D. Expansion of signal transduction pathways in fungi by extensive genome duplication. *Current Biology* **2016**, *26*, 1577-1584.
67. Amore, A.; Ciesielski, P.N.; Lin, C.-Y.; Salvachúa, D.; i Nogué, V.S. Development of lignocellulosic biorefinery technologies: recent advances and current challenges. *Australian Journal of Chemistry* **2016**, *69*, 1201-1218.
68. Cooke, W.B. Carbon/nitrogen relationships of fungus culture media. *Mycopathologia* **1968**, *34*, 305-316.
69. Gmoser, R.; Ferreira, J.A.; Lundin, M.; Taherzadeh, M.J.; Lennartsson, P.R. Pigment production by the edible filamentous fungus Neurospora intermedia. *Fermentation* **2018**, *4*, 11.
70. Dulf, F.V.; Vodnar, D.C.; Toşa, M.I.; Dulf, E.-H. Simultaneous enrichment of grape pomace with γ-linolenic acid and carotenoids by solid-state fermentation with Zygomycetes fungi and antioxidant potential of the bioprocessed substrates. *Food Chemistry* **2020**, *310*, 125927.
71. Nisha, A.; Venkateswaran, G. Effect of culture variables on mycelial arachidonic acid production by *Mortierella alpina*. *Food and Bioprocess Technology* **2011**, *4*, 232-240.
72. Moustogianni, A.; Bellou, S.; Triantaphyllidou, I.E.; Aggelis, G. Feasibility of raw glycerol conversion into single cell oil by zygomycetes under non-aseptic conditions. *Biotechnology and Bioengineering* **2015**, *112*, 827-831.

73. Deelai, S.; Suetrong, S.; Damrianant, S.; Unagul, P.; Sakkayawong, N. Isolation and identification of native lower fungi for polyunsaturated fatty acid (PUFA) production in Thailand, and the effect of carbon and nitrogen sources on growth and production. *African Journal of Biotechnology* **2015**, *14*, 1449-1460.
74. Funtikova, N.; Mysyakina, I.; Konova, I. Synthesis of biologically active lipids by the fungus *Mucor lusitanicus* 306D grown on media with various composition. *Applied Biochemistry and Microbiology* **2002**, *38*, 553-557.
75. Certik, M.; Megova, J.; Horenitzky, R. Effect of nitrogen sources on the activities of lipogenic enzymes in oleaginous fungus *Cunninghamella echinulata. The Journal of General and Applied Microbiology* **1999**, *45*, 289-293.
76. Fakas, S.; Papanikolaou, S.; Galiotou-Panayotou, M.; Komaitis, M.; Aggelis, G. Organic nitrogen of tomato waste hydrolysate enhances glucose uptake and lipid accumulation in *Cunninghamella echinulata*. *Journal of applied microbiology* **2008**, *105*, 1062-1070.
77. Chatzifragkou, A.; Fakas, S.; Galiotou-Panayotou, M.; Komaitis, M.; Aggelis, G.; Papanikolaou, S. Commercial sugars as substrates for lipid accumulation in *Cunninghamella echinulata* and *Mortierella isabellina* fungi. *European Journal of Lipid Science and Technology* **2010**, *112*, 1048-1057.
78. Papanikolaou, S.; Galiotou-Panayotou, M.; Fakas, S.; Komaitis, M.; Aggelis, G. Lipid production by oleaginous Mucorales cultivated on renewable carbon sources. *European Journal of Lipid Science and Technology* **2007**, *109*, 1060-1070.
79. Choudhari, S.; Singhal, R. Media optimization for the production of β-carotene by Blakeslea trispora: A statistical approach. *Bioresource Technology* **2008**, *99*, 722-730.
80. Allen, N.S.; Schumm, J.H. Endoplasmic reticulum, calciosomes and their possible roles in signal transduction. *Protoplasma* **1990**, *154*, 172-178.
81. Mohammadi, M.; Zamani, A.; Karimi, K. Effect of phosphate on glucosamine production by ethanolic fungus *Mucor indicus*. *Applied biochemistry and biotechnology* **2013**, *171*, 1465-1472.
82. Gerwien, F.; Skrahina, V.; Kasper, L.; Hube, B.; Brunke, S. Metals in fungal virulence. *FEMS microbiology reviews* **2018**, *42*, fux050.
83. North, M.; Steffen, J.; Loguinov, A.V.; Zimmerman, G.R.; Vulpe, C.D.; Eide, D.J. Genome-wide functional profiling identifies genes and processes important for zinc-limited growth of *Saccharomyces cerevisiae*. *PLoS Genet* **2012**, *8*, e1002699.
84. Gimenez, M.S.; Oliveros, L.B.; Gomez, N.N. Nutritional deficiencies and phospholipid metabolism. *International journal of molecular sciences* **2011**, *12*, 2408-2433.
85. Walker, G.M.; Duffus, J.H. Magnesium ions and the control of the cell cycle in yeast. *journal of cell science* **1980**, *42*, 329-356.
86. Bardi, L. Production of Bio-oils from Microbial Biomasses. In *Mycoremediation and Environmental Sustainability*, Springer: 2018; pp. 61-89.

87. Papanikolaou, S.; Sarantou, S.; Komaitis, M.; Aggelis, G. Repression of reserve lipid turnover in *Cunninghamella echinulata* and *Mortierella isabellina* cultivated in multiple-limited media. *Journal of Applied Microbiology* **2004**, *97*, 867-875.
88. Strain, J.; Culotta, V.C. Copper ions and the regulation ofSaccharomyces cerevisiae metallothionein genes under aerobic and anaerobic conditions. *Molecular and General Genetics MGG* **1996**, *251*, 139-145.
89. Šajbidor, J.; Koželouhov'a, D.; Ĉert'ik, M. Influence of some metal ions on the lipid content and arachidonic acid production by *Mortierella* sp. *Folia Microbiologica* **1992**, *37*, 404-406.
90. Yoo, J.-Y.; Lee, H.-C.; Shin, D.-H.; Min, B.-Y. Production of Fungal Lipids-V. Effects of Vitamins, Metabolic Intermediates and Mineral Salts on the Growth and Lipid Accumulation of *Mucor plumbeus*. *Korean Journal of Food ScienceTechnology* **1982**, *14*, 151-155.
91. Muhid, F.; Nawi, W.; Kader, A.J.A.; Yusoff, W.M.W.; Hamid, A.A. Effects of metal ion concentrations on lipid and gamma linolenic acid production by *Cunninghamella* sp. 2A1. *OnLine Journal of Biological Sciences* **2008**, *8*, 62-67.
92. Fekete, F.A.; Chandhoke, V.; Jellison, J. Iron-binding compounds produced by wood-decaying basidiomycetes. *Applied and environmental microbiology* **1989**, *55*, 2720-2722.
93. Reddi, A.R.; Jensen, L.T.; Naranuntarat, A.; Rosenfeld, L.; Leung, E.; Shah, R.; Culotta, V.C. The overlapping roles of manganese and Cu/Zn SOD in oxidative stress protection. *Free radical biology & medicine* **2009**, *46*, 154.
94. Jackson, S.; Heath, I. Roles of calcium ions in hyphal tip growth. *Microbiology and Molecular Biology Reviews* **1993**, *57*, 367-382.
95. Benčina, M.; Legiša, M.; Read, N.D. Cross-talk between cAMP and calcium signalling in Aspergillus niger. *Molecular microbiology* **2005**, *56*, 268-281.
96. Roy, A.; Kumar, A.; Baruah, D.; Tamuli, R. Calcium signaling is involved in diverse cellular processes in fungi. *Mycology* **2020**, 1-15.
97. Kyrmizi, I.; Ferreira, H.; Carvalho, A.; Figueroa, J.A.L.; Zarmpas, P.; Cunha, C.; Akoumianaki, T.; Stylianou, K.; Deepe, G.S.; Samonis, G. Calcium sequestration by fungal melanin inhibits calcium–calmodulin signalling to prevent LC3-associated phagocytosis. *Nature microbiology* **2018**, *3*, 791-803.
98. Cunningham, K.W. Acidic calcium stores of *Saccharomyces cerevisiae. Cell calcium* **2011**, *50*, 129-138.
99. Lange, M.; Peiter, E. Calcium transport proteins in fungi: the phylogenetic diversity of their relevance for growth, virulence, and stress resistance. *Frontiers in microbiology* **2020**, *10*, 3100.
100. Martinou, A.; Koutsioulis, D.; Bouriotis, V. Expression, purification, and characterization of a cobalt-activated chitin deacetylase (Cda2p) from Saccharomyces cerevisiae. *Protein expression and purification* **2002**, *24*, 111-116.
101. Ruiz-Herrera, J.; Manuel González-Prieto, J.; Ruiz-Medrano, R. Evolution and phylogenetic relationships of chitin synthases from yeasts and fungi. *FEMS yeast research* **2002**, *1*, 247-256.

102. Ruiz-Herrera, J.; Ruiz-Medrano, R. Chitin biosynthesis in fungi. *Handbook of fungal biotechnology* **2004**, 315-330.
103. Kavadia, A.; Komaitis, M.; Chevalot, I.; Blanchard, F.; Marc, I.; Aggelis, G. Lipid and γ-linolenic acid accumulation in strains of Zygomycetes growing on glucose. *Journal of the American Oil Chemists' Society* **2001**, *78*, 341-346.
104. Kosa, G.; Kohler, A.; Tafintseva, V.; Zimmermann, B.; Forfang, K.; Afseth, N.K.; Tzimorotas, D.; Vuoristo, K.S.; Horn, S.J.; Mounier, J. Microtiter plate cultivation of oleaginous fungi and monitoring of lipogenesis by high-throughput FTIR spectroscopy. *Microbial cell factories* **2017**, *16*, 101.
105. Huber, R.; Ritter, D.; Hering, T.; Hillmer, A.-K.; Kensy, F.; Müller, C.; Wang, L.; Büchs, J. Robo-Lector–a novel platform for automated high-throughput cultivations in microtiter plates with high information content. *Microbial cell factories* **2009**, *8*, 42.
106. Duetz, W.A. Microtiter plates as mini-bioreactors: miniaturization of fermentation methods. *Trends in microbiology* **2007**, *15*, 469-475.
107. Kosa, G.; Vuoristo, K.S.; Horn, S.J.; Zimmermann, B.; Afseth, N.K.; Kohler, A.; Shapaval, V. Assessment of the scalability of a microtiter plate system for screening of oleaginous microorganisms. *Applied microbiology and biotechnology* **2018**, *102*, 4915-4925.
108. Burmeister, A.; Hilgers, F.; Langner, A.; Westerwalbesloh, C.; Kerkhoff, Y.; Tenhaef, N.; Drepper, T.; Kohlheyer, D.; von Lieres, E.; Noack, S. A microfluidic co-cultivation platform to investigate microbial interactions at defined microenvironments. *Lab on a Chip* **2019**, *19*, 98-110.
109. Jian, X.; Guo, X.; Wang, J.; Tan, Z.L.; Xing, X.h.; Wang, L.; Zhang, C. Microbial microdroplet culture system (MMC): An integrated platform for automated, high-throughput microbial cultivation and adaptive evolution. *Biotechnology and Bioengineering* **2020**, *117*, 1724-1737.
110. Tunac, J.B. High-aeration capacity shake-flask system. *Journal of fermentation and bioengineering* **1989**, *68*, 157-159.
111. Li-Chan, E.; Chalmers, J.M.; Griffiths, P.R. *Applications of vibrational spectroscopy in food science*; John Wiley & Sons: 2010.
112. Sathyanarayana, D.N. *Vibrational spectroscopy: theory and applications*; New Age International: 2015.
113. Faix, O. Fourier transform infrared spectroscopy. In *Methods in lignin chemistry*, Springer: 1992; pp. 83-109.
114. Barth, A. Infrared spectroscopy of proteins. *Biochimica et Biophysica Acta (BBA)-Bioenergetics* **2007**, *1767*, 1073-1101.
115. Wenning, M.; Scherer, S. Identification of microorganisms by FTIR spectroscopy: perspectives and limitations of the method. *Applied microbiology and biotechnology* **2013**, *97*, 7111-7120.
116. Schuster, K.C.; Mertens, F.; Gapes, J. FTIR spectroscopy applied to bacterial cells as a novel method for monitoring complex biotechnological processes. *Vibrational Spectroscopy* **1999**, *19*, 467-477.
117. Kosa, G.; Shapaval, V.; Kohler, A.; Zimmermann, B. FTIR spectroscopy as a unified method for simultaneous analysis of intra-and extracellular

metabolites in high-throughput screening of microbial bioprocesses. *Microbial cell factories* **2017**, *16*, 195.

118. Shapaval, V.; Brandenburg, J.; Blomqvist, J.; Tafintseva, V.; Passoth, V.; Sandgren, M.; Kohler, A. Biochemical profiling, prediction of total lipid content and fatty acid profile in oleaginous yeasts by FTIR spectroscopy. *Biotechnology for biofuels* **2019**, *12*, 140.
119. Shapaval, V.; Afseth, N.K.; Vogt, G.; Kohler, A. Fourier transform infrared spectroscopy for the prediction of fatty acid profiles in Mucor fungi grown in media with different carbon sources. *Microbial cell factories* **2014**, *13*, 86.
120. Duarte, M.; Ferreira, M.; Marvao, M.; Rocha, J. An optimised method to determine the degree of acetylation of chitin and chitosan by FTIR spectroscopy. *International Journal of Biological Macromolecules* **2002**, *31*, 1-8.
121. Gong, W. A real time in situ ATR-FTIR spectroscopic study of linear phosphate adsorption on titania surfaces. *International journal of mineral processing* **2001**, *63*, 147-165.
122. Khoshmanesh, A.; Cook, P.L.; Wood, B.R. Quantitative determination of polyphosphate in sediments using Attenuated Total Reflectance-Fourier Transform Infrared (ATR-FTIR) spectroscopy and partial least squares regression. *Analyst* **2012**, *137*, 3704-3709.
123. Doyle, W.M. Principles and applications of Fourier transform infrared (FTIR) process analysis. *Process Control Qual* **1992**, *2*, 11-41.
124. Ami, D.; Mereghetti, P.; Doglia, S.M. Multivariate analysis for Fourier transform infrared spectra of complex biological systems and processes. *Multivariate analysis in management, engineering and the sciences* **2013**, 978-953.
125. Thomas, S.; Thomas, R.; Zachariah, A.K.; Kumar, R. *Spectroscopic Methods for Nanomaterials Characterization*; Elsevier: 2017; Vol. 2.
126. Hirschfeld, T.; Chase, B. FT-Raman spectroscopy: development and justification. *Applied spectroscopy* **1986**, *40*, 133-137.
127. John, N.; George, S. Raman spectroscopy. In *Spectroscopic methods for nanomaterials characterization*, Elsevier: 2017; pp. 95-127.
128. Naumann, D. FT-infrared and FT-Raman spectroscopy in biomedical research. *Applied spectroscopy reviews* **2001**, *36*, 239-298.
129. Bowie, B.T.; Chase, D.B.; Griffiths, P.R. Factors affecting the performance of bench-top Raman spectrometers. Part II: Effect of sample. *Applied Spectroscopy* **2000**, *54*, 200a-207a, doi:Doi 10.1366/0003702001950175.
130. Bowie, B.T.; Chase, D.B.; Griffiths, P.R. Factors affecting the performance of bench-top Raman spectrometers. Part I: Instrumental effects. *Applied Spectroscopy* **2000**, *54*, 164a-173a, doi:Doi 10.1366/0003702001949924.
131. Boyaci, I.H.; Temiz, H.T.; Genis, H.E.; Soykut, E.A.; Yazgan, N.N.; Guven, B.; Uysal, R.S.; Bozkurt, A.G.; Ilaslan, K.; Torun, O., et al. Dispersive and FT-Raman spectroscopic methods in food analysis. *Rsc Adv* **2015**, *5*, 56606-56624.
132. He, H.R.; Sun, D.W.; Pu, H.B.; Chen, L.J.; Lin, L. Applications of Raman spectroscopic techniques for quality and safety evaluation of milk: A review of recent developments. *Crit Rev Food Sci* **2019**, *59*, 770-793.

133. Agarwal, U.P. 1064 nm FT-Raman spectroscopy for investigations of plant cell walls and other biomass materials. *Front Plant Sci* **2014**, *5*.
134. Kendel, A.; Zimmermann, B. Chemical Analysis of Pollen by FT-Raman and FTIR Spectroscopies. *Front Plant Sci* **2020**, *11*.
135. Gherman, A.M.R.; Dina, N.E.; Chis, V.; Wieser, A.; Haisch, C. Yeast cell wall - Silver nanoparticles interaction: A synergistic approach between surface-enhanced Raman scattering and computational spectroscopy tools. *Spectrochim Acta A* **2019**, *222*, doi:ARTN 117223 10.1016/j.saa.2019.117223.
136. Noothalapati, H.; Sasaki, T.; Kaino, T.; Kawamukai, M.; Ando, M.; Hamaguchi, H.; Yamamoto, T. Label-free Chemical Imaging of Fungal Spore Walls by Raman Microscopy and Multivariate Curve Resolution Analysis. *Scientific Reports* **2016**, *6*, doi:ARTN 27789 10.1038/srep27789.
137. Edwards, H.G.M.; Russell, N.C.; Weinstein, R.; Wynnwilliams, D.D. Fourier-Transform Raman-Spectroscopic Study of Fungi. *J Raman Spectrosc* **1995**, *26*, 911-916.
138. Meenu, M.; Xu, B.J. Application of vibrational spectroscopy for classification, authentication and quality analysis of mushroom: A concise review. *Food Chemistry* **2019**, *289*, 545-557, doi:10.1016/j.foodchem.2019.03.091.
139. Zajac, A.; Hanuza, J.; Wandas, M.; Dyminska, L. Determination of N-acetylation degree in chitosan using Raman spectroscopy. *Spectrochim Acta A* **2015**, *134*, 114-120.
140. Jehlicka, J.; Edwards, H.G.M.; Orenc, A. Raman Spectroscopy of Microbial Pigments. *Applied and Environmental Microbiology* **2014**, *80*, 3286-3295.
141. Forfang, K.; Zimmermann, B.; Kosa, G.; Kohler, A.; Shapaval, V. FTIR spectroscopy for evaluation and monitoring of lipid extraction efficiency for oleaginous fungi. *PloS one* **2017**, *12*, e0170611.
142. Edebo, L.; Magnusson, K.-E. Disintegration of cells and protein recovery. In *Microbial Engineering*, Elsevier: 1973; pp. 325-338.
143. Sönnichsen, M.; Müller, B. A rapid and quantitative method for total fatty acid analysis of fungi and other biological samples. *Lipids* **1999**, *34*, 1347-1349.
144. Lewis, T.; Nichols, P.D.; McMeekin, T.A. Evaluation of extraction methods for recovery of fatty acids from lipid-producing microheterotrophs. *Journal of Microbiological Methods* **2000**, *43*, 107-116.
145. Wahlen, B.D.; Willis, R.M.; Seefeldt, L.C. Biodiesel production by simultaneous extraction and conversion of total lipids from microalgae, cyanobacteria, and wild mixed-cultures. *Bioresource technology* **2011**, *102*, 2724-2730.
146. Lepage, G.; Roy, C.C. Improved recovery of fatty acid through direct transesterification without prior extraction or purification. *Journal of Lipid research* **1984**, *25*, 1391-1396.
147. Pochanavanich, P.; Suntornsuk, W. Fungal chitosan production and its characterization. *Letters in applied microbiology* **2002**, *35*, 17-21.
148. Subramanyam, C.; Rao, S. An enzymic method for the determination of chitin and chitosan in fungal cell walls. *Journal of Biosciences* **1987**, *12*, 125-129.
149. Wattjes, J.; Niehues, A.; Cord-Landwehr, S.; Hoßbach, J.; David, L.; Delair, T.; Moerschbacher, B.M. Enzymatic production and enzymatic-mass spectrometric fingerprinting analysis of chitosan polymers with different

nonrandom patterns of acetylation. *Journal of the American Chemical Society* **2019**, *141*, 3137-3145.

150. Wattjes, J.; Niehues, A.; Moerschbacher, B.M. Robust enzymatic-mass spectrometric fingerprinting analysis of the fraction of acetylation of chitosans. *Carbohydrate Polymers* **2020**, *231*, 115684.
151. McGrath, J.W.; Quinn, J.P. Intracellular accumulation of polyphosphate by the yeast Candida humicola G-1 in response to acid pH. *Applied and Environmental Microbiology* **2000**, *66*, 4068-4073.
152. Cade-Menun, B.; Liu, C.W. Solution phosphorus-31 nuclear magnetic resonance spectroscopy of soils from 2005 to 2013: A review of sample preparation and experimental parameters. *Soil Science Society of America Journal* **2014**, *78*, 19-37.
153. King, E.J. The colorimetric determination of phosphorus. *Biochemical Journal* **1932**, *26*, 292-297.
154. Staal, L.B.; Petersen, A.B.; Jørgensen, C.A.; Nielsen, U.G.; Nielsen, P.H.; Reitzel, K. Extraction and quantification of polyphosphates in activated sludge from waste water treatment plants by 31P NMR spectroscopy. *Water research* **2019**, *157*, 346-355.
155. Standardization, I.O.f. *Animal Feeding Stuffs: Determination of Phosphorus Content: Spectrometric Method*; International Organization for Standardization: 1998.
156. Demšar, J.; Curk, T.; Erjavec, A.; Gorup, Č.; Hočevar, T.; Milutinovič, M.; Možina, M.; Polajnar, M.; Toplak, M.; Starič, A. Orange: data mining toolbox in Python. *the Journal of machine Learning research* **2013**, *14*, 2349-2353.
157. Hair, J.F. Multivariate Data Analysis: An Overview. *International encyclopedia of statistical science* **2011**, *904907*.
158. Dempster, A.P. An overview of multivariate data analysis. *Journal of Multivariate Analysis* **1971**, *1*, 316-346.
159. Afseth, N.K.; Kohler, A. Extended multiplicative signal correction in vibrational spectroscopy, a tutorial. *Chemometrics and Intelligent Laboratory Systems* **2012**, *117*, 92-99.
160. Zimmermann, B.; Kohler, A. Optimizing Savitzky-Golay parameters for improving spectral resolution and quantification in infrared spectroscopy. *Applied spectroscopy* **2013**, *67*, 892-902.
161. Wold, S.; Esbensen, K.; Geladi, P. Principal component analysis. *Chemometrics and intelligent laboratory systems* **1987**, *2*, 37-52.
162. Zwanenburg, G.; Hoefsloot, H.C.; Westerhuis, J.A.; Jansen, J.J.; Smilde, A.K. ANOVA–principal component analysis and ANOVA–simultaneous component analysis: a comparison. *Journal of Chemometrics* **2011**, *25*, 561-567.
163. Legal, J.; Manfait, M.; Theophanides, T. Applications of FTIR spectroscopy in structural studies of cells and bacteria. *Journal of molecular structure* **1991**, *242*, 397-407.
164. Dean, A.P.; Sigee, D.C.; Estrada, B.; Pittman, J.K. Using FTIR spectroscopy for rapid determination of lipid accumulation in response to nitrogen limitation in freshwater microalgae. *Bioresource technology* **2010**, *101*, 4499-4507.

165. Geladi, P.; Kowalski, B.R. Partial least-squares regression: a tutorial. *Analytica chimica acta* **1986**, *185*, 1-17.
166. Westerhuis, J.A.; Kourti, T.; MacGregor, J.F. Analysis of multiblock and hierarchical PCA and PLS models. *Journal of Chemometrics: A Journal of the Chemometrics Society* **1998**, *12*, 301-321.

Paper I

PLOS ONE

RESEARCH ARTICLE

Microcultivation and FTIR spectroscopy-based screening revealed a nutrient-induced co-production of high-value metabolites in oleaginous *Mucoromycota* fungi

Simona Dzurendova[1]*, Boris Zimmermann[1], Achim Kohler[1], Valeria Tafintseva[1], Ondrej Slany[2], Milan Certik[2], Volha Shapaval[1]

1 Faculty of Science and Technology, Norwegian University of Life Sciences, Ås, Norway, **2** Faculty of Chemical and Food Technology, Slovak Technical University, Bratislava, Slovakia

* simona.dzurendova@gmail.com, simona.dzurendova@nmbu.no

Citation: Dzurendova S, Zimmermann B, Kohler A, Tafintseva V, Slany O, Certik M, et al. (2020) Microcultivation and FTIR spectroscopy-based screening revealed a nutrient-induced co-production of high-value metabolites in oleaginous *Mucoromycota* fungi. PLoS ONE 15(6): e0234870. https://doi.org/10.1371/journal.pone.0234870

Editor: Marie-Joelle Virolle, Universite Paris-Sud, FRANCE

Received: March 6, 2020

Accepted: June 3, 2020

Published: June 22, 2020

Peer Review History: PLOS recognizes the benefits of transparency in the peer review process; therefore, we enable the publication of all of the content of peer review and author responses alongside final, published articles. The editorial history of this article is available here: https://doi.org/10.1371/journal.pone.0234870

Data Availability Statement: All relevant data are within the paper and its Supporting Information files.

Abstract

Mucoromycota fungi possess a versatile metabolism and can utilize various substrates for production of industrially important products, such as lipids, chitin/chitosan, polyphosphates, pigments, alcohols and organic acids. However, as far as commercialisation is concerned, establishing industrial biotechnological processes based on *Mucoromycota* fungi is still challenging due to the high production costs compared to the final product value. Therefore, the development of co-production concept is highly desired since more than one valuable product could be produced at the time and the process has a potentially higher viability. To develop such biotechnological strategy, we applied a high throughput approach consisting of micro-titre cultivation and FTIR spectroscopy. This approach allows single-step biochemical fingerprinting of either fungal biomass or growth media without tedious extraction of metabolites. The influence of two types of nitrogen sources and different levels of inorganic phosphorus on the co-production of lipids, chitin/chitosan and polyphosphates for nine different oleaginous *Mucoromycota* fungi was evaluated. FTIR analysis of biochemical composition of *Mucoromycota* fungi and biomass yield showed that variation in inorganic phosphorus had higher effect when inorganic nitrogen source–ammonium sulphate–was used. It was observed that: (1) *Umbelopsis vinacea* reached almost double biomass yield compared to other strains when yeast extract was used as nitrogen source while phosphorus limitation had little effect on the biomass yield; (2) *Mucor circinelloides*, *Rhizopus stolonifer*, *Amylomyces rouxii*, *Absidia glauca* and *Lichtheimia corymbifera* overproduced chitin/chitosan under the low pH caused by the limitation of inorganic phosphorus; (3) *Mucor circinelloides*, *Amylomyces rouxii*, *Rhizopus stolonifer* and *Absidia glauca* were able to store polyphosphates in addition to lipids when high concentration of inorganic phosphorus was used; (4) the biomass and lipid yield of high-value lipid producers *Mortierella alpina* and *Mortierella hyalina* were significantly increased when high concentrations of inorganic phosphorus were combined with ammonium sulphate, while the same amount of inorganic phosphorus combined with yeast extract showed negative impact on the growth and lipid accumulation. FTIR spectroscopy revealed the co-production potential of several

Funding: The study was funded by the Research Council of Norway - FMETEKN Grant, project number 257622; BIONÆR Grant, project numbers 268305, 305215; DAAD Grant, project number 309220 and by the Slovak Ministry of Education, Science, Research and Sport- grant VEGA 1/0323/19. The funders had no role in study design, data collection and analysis, decision to publish, or preparation of the manuscript.

Competing interests: The authors have declared that no competing interests exist.

oleaginous *Mucoromycota* fungi forming lipids, chitin/chitosan and polyphosphates in a single cultivation process.

Introduction

Biorefinery is the sustainable processing of biomass into a spectrum of marketable products, such as biofuels and biochemicals, through the application of green conversion technologies [1]. *Mucoromycota* filamentous fungi play an important role in developing sustainable biorefinery processes due to their versatile metabolism and ability to utilize a broad range of renewable feedstock, rest and waste materials [2–4]. *Mucoromycota* fungi are able to produce a number of industrially important products, such as alcohols, organic acids and enzymes [5]. Moreover, the biomass of *Mucoromycota* fungi is rich in various high-value metabolites such as lipids, proteins, pigments, polyphosphates and chitosan [6], making it well suited for nutrition purposes as a whole.

It is well known that some filamentous fungi, so-called oleaginous fungi, are able to produce high amounts of lipids. Oleaginous *Mucoromycota* fungi are able to accumulate lipids (Single Cell Oils–SCOs) with up to 80% w/w yield [7]. SCOs are stored in globular intracellular organelles (i.e. lipid bodies) predominantly in the form of triacylglycerides (TAGs) [8, 9]. Depending on a fungal strain, fungal lipids can be very similar to vegetable oils and thus suitable for biodiesel production, or similar to highly nutritious and valuable fish oils with high content of polyunsaturated fatty acids (PUFAs) [10–13]. Although SCOs production by oleaginous *Mucoromycota* fungi has been suggested and up-scaled a century ago [14], industrial process based on *Mucoromycota* fungi are still limited only to production of high-value PUFA-rich oils. For example gamma-linoleic and arachidonic acids rich oils are produced industrially by *Mucor circinelloides* and *Mortierella alpina* [15].

Despite all the developments in the field of fungal SCOs, a commercially sustainable *Mucoromycota*-based biodiesel production has not yet been established. The production of relatively low-valued fungal lipids, such as biodiesels, could become economically feasible if a concept of co-production of lipids and other value-added chemicals is applied [16]. Such co-production concept for oleaginous *Mucoromycota* fungi has been first suggested for production of chitosan and biodiesel lipids by *Mucor circinelloides* [17]. Other co-production strategies using *Mucoromycota* include concomitant production of fumaric acid and chitin by *Rhizopus oryzae* [18], lactic acid and chitin by *Rhizopus oryzae* [19], lipids, proteins, ethanol and chitosan by *Rhizopus oryzae* and *Mucor indicus* [20].

When developing a sustainable co-production strategy for oleaginous *Mucoromycota* fungi, the aim is to co-produce high-value metabolites which are generated in metabolic pathways that are not competing for carbon sources. Thus, co-production of extracellular acids and intracellular lipids is expected to have low sustainability since these metabolic pathways are competing for the carbon source. Notwithstanding, strategies based on the co-production of metabolites of lipid bodies and cell wall are advantageous since metabolic pathways for the production of chemical components of these two organelles are not competing. The major components of the cell wall in *Mucoromycota* fungi are commercially lucrative biopolymers chitin, chitosan and polyphosphates [21].

Chitin (ß-1,4-N-acetyl-D-glucosamine) and its deacetylated form, chitosan (ß-1,4-D-glucosamine), are natural biodegradable polymers with a broad range of applications in food, pharmaceutical and agricultural industries [22]. Chitosan belongs to the most versatile and

promising functional biopolymers, with superior material properties and interesting biological activities. An increasing market demand for high-quality chitosan exceeds the current global production, which is based primarily on deacetylation of chitin from shells of crustaceans. Therefore, production based on *Mucoromycota* fungi could be lucrative, in particular since *Mucoromycota* are among the rather rare natural producers of chitosan. In some cases, the total chitin and chitosan yield in *Mucoromycota* fungi can reach up to 40% w/w [23].

Another important biopolymer of the *Mucoromycota* cell wall is polyphosphate [24], a chain of phosphate units connected by high-energy phospho-anhydride bonds. Polyphosphates have several key functions in fungal cells, such as energy and phosphate storage, controlling of fungal homeostasis via trapping cations and amino acids, and regulation of the hyphal phosphate amount [25]. Phosphorus accumulation takes place in the exponential growth phase, when the source of phosphorus is in high access [26]. Phosphorus accumulating *Mucoromycota* fungi are able to store more polyphosphates than needed for their survival, which is very attractive for the phosphorus recovery. Currently, the global phosphorus market is getting into a critical situation due to the limited availability of rock phosphate, which is a non-renewable phosphorus source. Various waste substrates contain significant amounts of phosphorus that could be recovered if appropriate processes for phosphorus recovery were available. Waste sources of phosphorus are municipal waste or waste-water streams [27]. The traditional phosphorus recovery approach is based on wet-chemistry and thermo-chemical treatment. It requires the use of chemicals and high energy [28]. An alternative and more sustainable way of phosphorus recovery is based on utilizing filamentous fungi that are able to accumulate phosphorus during their growth [26]. Therefore, production of fungal polyphosphate in a biorefinery concept can have a significant contribution to phosphorus recycling. However, not all fungal strains possess the ability to accumulate phosphorus and therefore biotechnologically valuable phosphorus-accumulating strains need to be identified.

The development of sustainable fungal biorefinery for co-production of lipids, chitin/chitosan and polyphosphates depends sensitively on the chemical composition of the substrates since different sources are required for the different metabolic processes needed to reach the target products. When processes are built on the utilization of different rest materials and waste streams as low-cost substrates, theses substrates need to be modified and optimized such that they contain all needed sources in the best possible concentrations. Rest materials and waste streams have a highly diverse chemical composition and there is a need to enrich them with essential macro- and micro-nutrients. Therefore, the optimization of cultivation media or substrates based on rest materials and waste streams is crucial in the fungal biorefinery process development. In order to perform adequate optimizing of rest materials-based substrates, there is a need for deeper understanding the effect of single media components on the synthesis of different intra- and extracellular metabolites in fungal cells. Extensive research has been done on studying the role of different carbon and to some extend nitrogen sources [29–33] for the fungal fermentation in general and for the production of one main metabolite. However, there is a very little known about the role of phosphorus on the production of different metabolites, as this element is mostly examined in the context of polyphosphates accumulation [34]. In addition, to our knowledge no study has been performed so far that investigates the effect of single media nutrients either in excess or in limited amounts on the co-production of several metabolites by fungi.

The traditional approach for monitoring and developing the production of different metabolites in fungal cells is based on the extraction or separation of the produced metabolites followed by further qualitative and quantitative analysis using different analytical procedures. Such approach requires significant amount of biomass for the analysis, since different metabolites need to be extracted and analyzed in different and often expensive and time-consuming ways. Fourier Transform Infrared (FTIR) spectroscopy is a rapid non-invasive technology

allowing biochemical fingerprinting of all cell chemical components [35]. While FTIR spectroscopy has been used for many decades for structural chemical analysis, FTIR spectroscopy became a popular tool for identification and characterization of biological materials in the 90ies. FTIR spectroscopy has been extensively used in applied microbiology and biotechnology of various types of microorganisms, including fungi [36–41], bacteria [42–44], yeasts [45–50] or algae [51–53]. Moreover, FTIR spectroscopy was applied as a tool for measurement of growth media and extracellular metabolites [54, 55]. FTIR spectroscopy has been shown to be precise and reliable method for the identification and analysis of microbial lipids [10, 56–61], chitin/chitosan [62–65] and polyphosphates [66, 67]. Further, this method has been utilized for monitoring lipid extraction in oleaginous filamentous fungi [68, 69]. Thus, FTIR showed the potential to serve as the sole method for the bioprocess monitoring. Combined with the Duetz microtiter plate system (Duetz-MTPS), FTIR can serve as a rapid tool for monitoring of high throughput studies, such as screening of fungal strains for high and low value lipid production [10, 70]. Moreover, high throughput screening was strengthen by a fully automated set-up of the biomass samples preparation for the FTIR-HTS analysis [71–73].

The aim of this study was to assess the biotechnological potential of oleaginous *Mucoromycota* grown on two different nitrogen sources, namely yeast extract and ammonium sulphate, in combination with six different inorganic phosphorus (Pi) concentrations in a high throughput screening using FTIR spectroscopy combined with Duetz-MTPS. The primary goal of presented high throughput screening is the identification of co-producing strains and understanding the role of phosphorus and nitrogen alone and in the interaction in the co-production. Thus, the study provides relative estimation of the high-value metabolites co-produced by *Mucoromycota* fungi and, therefore, can be considered as a basis for further research in developing of co-production concepts.

1. Materials and methods

1.1. Oleaginous filamentous fungi

Nine oleaginous filamentous fungi from the genera *Absidia*, *Amylomyces*, *Cunninghamella*, *Lichthemia*, *Mortierella*, *Mucor*, *Rhizopus* and *Umbelopsis* were used in the study (Table 1). The selection of fungal strains was based on the results of our recent study, where 100 oleaginous filamentous fungi were screened for the ability to accumulate high amount of lipids [10].

Table 1. List of oleaginous filamentous fungi used in the study.

Fungal strain name	Collection №	Short name
Absidia glauca	CCM[1] 451	AGL
Amylomyces rouxii	CCM F220	ARO
Cunninghamella blakesleeana	CCM F705	CBL
Lichtheimia corymbifera	CCM 8077	LCO
Mortierella alpina	ATCC[2] 32222	MAL
Mortierella hyalina	VKM[3] F1629	MHY
Mucor circinelloides	VI[4] 04473	MCI
Rhizopus stolonifer	VKM F-400	RST
Umbelopsis vinacea	CCM F539	UVI

[1]Czech collection of Microorganisms (Brno, Czech Republic)

[2]American Type Culture Collection (Virginia, USA)

[3]All-Russian Collection of Microorganisms (Moscow, Russia), and

[4]Norwegian school of Veterinary Science (Oslo, Norway).

https://doi.org/10.1371/journal.pone.0234870.t001

While some Mucoromycota species have been previously identified as medically important [74], in general they have been utilised at industrial scale as cell factories for example for chitosan, lipids or lactic acid production.

1.2. Design of the experiment

Six different concentrations of phosphate salts–KH_2PO_4 and Na_2HPO_4, and two different nitrogen sources–yeast extract (YE) and ammonium sulphate (AS)–were used for the cultivation of fungi in a full factorial design. The cultivation was performed in Duetz-MTPS [54] in three independent biological replicates for each fungus, phosphorus concentration and nitrogen source, resulting in 324 samples. Biological replicates were prepared on separate microtiter plates and cultivated at different time points for each fungal strain. For every biological replicate, fresh spore suspension was prepared.

1.3. Growth media and cultivation conditions

Growth of the selected fungi was done in two steps: 1) growth on standard agar medium for preparing spore inoculum and 2) growth in nitrogen-limited broth media with different inorganic phosphorus (Pi) concentrations and nitrogen sources in the Duetz-MTPS.

For the preparation of spore inoculum, *Mortierella* and *Umbelopsis* were cultivated on potato dextrose agar, while all other strains were cultivated on malt extract agar. Malt extract agar was prepared by dissolving 30 g of malt extract (Merck, Germany), 5 g of peptone (Amresco, USA) and 15 g of agar powder (Alfa Aesar, ThermoFischer, Germany) in 1L of distilled water and autoclaved at 115˚C for 15 min. Potato dextrose agar was prepared by dissolving 39 g of potato dextrose agar (VWR, Belgium) in 1L of distilled water and autoclaved at 115˚C for 15 min. Agar cultivation was performed for 7 days at 25˚C for all strains except for *Mortierella* (14 days) due to the slower growth of *Mortierella*. Fungal spores were harvested from agar plates with a bacteriological loop after the addition of 10 mL of sterile 0.9% NaCl solution.

The main components of the nitrogen-limited broth media [75] with modifications [76] ($g \cdot L^{-1}$) were: glucose 80, yeast extract 3, MgSO4·7H2O 1.5, CaCl2·2H2O 0.1, FeCl3·6H2O 0.008, ZnSO4·7H2O 0.001, CoSO4·7H2O 0.0001, CuSO4·5H2O 0.0001, MnSO4·5H2O 0.0001. For broth media with ammonium sulphate as a nitrogen source, yeast extract was replaced with 1.5 g/L of $(NH_4)_2SO_4$ in order to keep the same C/N ratio as with yeast extract medium. Broth media with ammonium sulphate contained 0.05g/L thiamin hydrochloride and 0.02 mg/L biotin [77]. Different concentrations of phosphate salts, namely KH_2PO_4 and Na_2HPO_4, were added to the main components of nitrogen-limited broth medium, as described in Table 2. The concentrations of phosphate salts, 7 $g \cdot L^{-1}$ KH_2PO_4 and 2 $g \cdot L^{-1}$ Na_2HPO_4, were selected as a reference value (Pi1) since they have frequently been used in cultivation of oleaginous *Mucoromycota* [75, 76]. The broth media contained higher (up to 8 × Pi1) and lower (up to ¼ × Pi1) amount of phosphate salts compared to the reference value (Table 2). Broth media with

Table 2. The concentration of phosphate salts in the nitrogen-limited broth media.

Sample name	KH_2PO_4 ($g \cdot L^{-1}$)	Na_2HPO_4 ($g \cdot L^{-1}$)
Pi8	56	16
Pi4	28	8
Pi2	14	4
Pi1	7	2
Pi0.5	3.5	1
Pi0.25	1.75	0.5

https://doi.org/10.1371/journal.pone.0234870.t002

the decreased amount of inorganic phosphorus contained KCl and NaCl in a corresponding concentration in order to have equal K^+ and Na^+ ions as in the reference condition (Pi1). Broth media were autoclaved for 15 min at 121˚C. The starting pH of media was 6 ± 0.3 and pH of growth media was measured as well after the cultivation.

Cultivation in broth media was performed in the Duetz-MTPS (Enzyscreen, Netherlands) which consists of 24-square polypropylene deep well microtiter plates, low evaporation sandwich covers and extra high cover clamps, which were placed into the MAXQ 4000 shaker (Thermo Scientific). The autoclaved microtiter plates were filled with 7 ml of sterile broth media per well, and each well was inoculated with 50 μl of spore inoculum. Cultivation was performed for 7 days at 25˚C and 400 rpm agitation (1.9 cm circular orbit). Fungi *Mortierella alpina* and *Mortierella hyalina* were cultivated for 14 days due to their slow growth.

1.4. Analysis

1.4.1. Fourier transform infrared spectroscopy of fungal biomass. Fourier transform infrared (FTIR) spectroscopy analysis of fungal biomass was performed according to [76] with some modifications. The biomass was separated from the growth media by centrifugation and washed with distilled water. Approximately 5 mg of fresh washed biomass was transferred into 2 ml polypropylene tube containing 250±30 mg of acid washed glass beads and 0.5 ml of distilled water for further homogenization. The remaining washed biomass was freeze-dried for 24 hours for determining biomass yield. In total, 312 biomass samples were analysed in three technical replicates by FTIR spectroscopy. *Mortierella alpina* and *Mortierella hyalina* in Pi8 conditions were not measured since no growth was observed.

The homogenization of fungal biomass was performed by using Percellys Evolution tissue homogenizer (Bertin Technologies, France) with the following set-up: 5500 rpm, 6 × 20 s cycle. 10 μl of homogenized fungal biomass was pipetted onto an IR transparent 384-well silica microplate. Samples were dried at room temperature for two hours. For every sample, three technical replicates were prepared. The FTIR spectra were recorded in the region between 4000 cm^{-1} and 500 cm^{-1} with a spectral resolution of 6 cm^{-1}, a digital spacing of 1.928 cm^{-1}, and an aperture of 5 mm. Spectra were recorded in a transmission mode using the High Throughput Screening eXTension (HTS-XT) unit coupled to the Vertex 70 FTIR spectrometer (both Bruker Optik, Germany). For each spectrum, 64 scans were averaged. Spectra were recorded as the ratio of the sample spectrum to the spectrum of the empty IR transparent microplate. In total, 936 biomass spectra were obtained. The OPUS software (Bruker Optik GmbH, Germany) was used for data acquisition and instrument control.

1.4.2. Attenuated total reflectance Fourier transform infrared spectroscopy. Attenuated total reflectance (ATR)-infrared spectra of growth media after cultivation, were recorded using a Vertex 70 FTIR spectrometer (Bruker Optik GmbH, Germany) with a single reflectance-attenuated total-reflectance accessory. For identification of basic biochemicals in the growth media and the biomass a set of model compounds was measured. Spectra of glyceryl trioleate ((9Z)9-Octadecenoic acid 1,2,3-propanetriyl ester), chitin, and sodium polyphosphate were measured. Moreover, spectra of pure water, and water solutions of pure glucose, ammonium sulphate, yeast extract, phosphates, as well as media before cultivation were recorded. All chemicals were purchased from Merck (Darmstadt, Germany) and used without further purification. In addition to growth media, spectra of pure water, and water solutions of pure glucose, ammonium sulphate, yeast extract, phosphates, as well as media before cultivation were recorded. The ATR IR spectra were recorded with a total of 32 scans and spectral resolution of 4 cm^{-1} over the range of 4000–600 cm^{-1}, using the horizontal ATR diamond prism with 45˚ angle of incidence on a High Temperature Golden gate ATR Mk II (Specac, United Kingdom).

For each measurement a 10 μl droplet of sample was placed on the surface of the ATR diamond crystal. 972 samples were measured in total. The OPUS software (Bruker Optik GmbH, Germany) was used for data acquisition and instrument control. Growth media after cultivation were measured with the HTS-XT system as well, in the configuration mentioned above.

1.4.3. Transmission electron microscopy (TEM) of *Mucor circinelloides* hyphae sections. Fresh washed fungal biomass was fixated by applying the fixating solution consisting of 2% paraformaldehyde, 1.25% glutaraldehyde and 0.1 M sodium cacodylate buffer for 1 hour at 4˚C. Subsequently, the fixating solution was removed by centrifugation at 11000 rpm for 15 min and the fixated biomass was washed three times with 0.1 M sodium cacodylate buffer (for 10 min at 4˚C for each washing step). Buffer was removed and the fixated biomass was post-fixated in 1% OsO4 in 0.1 M sodium cacodylate buffer for 1h. After the postfixation, the fungal biomass was dehydrated with ethanol employing each of the following ethanol concentrations for 15 minutes: 70%, 90%, 96% and 100% ethanol. The last concentration was repeated four times for 15 minutes. Thereafter, the LR White resin (LRW) medium grade was infiltrated into the biomass in the mixture with ethanol in following LRW/ethanol ratios: 1:3, over night; 1:1 overnight; 3:1 overnight; 100% LRW overnight. Finally, the fixated biomass was embedded in 100% LRW overnight at 60˚C in the oven. The embedded biomass was sectioned using Leica EM UC6 into 60 nm thin slices and sections were monitored using FEI Morgagni 268 Transmission electron microscope equipped with Olympus Veleta CCD camera.

1.5. Data analysis

The Following software packages were used for the data analysis: Unscrambler X version 10.5.1 (CAMO Analytics, Norway), Orange data mining toolbox version 3.15 (University of Ljubljana, Slovenia) [78, 79], and Matlab R2018a (The Mathworks Inc., Natick, USA).

1.5.1. Pre-processing of FTIR spectra. The pre-processing of FTIR-HTS spectra was performed in two ways:

(1) FTIR-HTS spectra of the biomass were first transformed to second-derivative spectra by the Savitzky–Golay algorithm using a polynomial of degree 2 and a window size of either 11 or 61 points in total. Different window sizes were used in order to emphasize either narrow peaks associated with lipids and chitin/chitosan (window size 11), or broad peaks associated with polyphosphates (window size 61). The second-derivative spectra were pre-processed by extended multiplicative scatter correction (EMSC), an MSC model extended by a linear and quadratic components [80–82]. Technical replicates (936 spectra in total) were averaged in order to remove technical variability of the measurements, resulting into 312 spectra. These spectra were cut and used for the PCA analysis of specific lipid- (3020–2819 cm^{-1}, 1760–1726 cm^{-1}, 1475–1375 cm^{-1}, 1160–1149 cm^{-1}, 730–715 cm^{-1}), polyphosphates- (1301–1203 cm^{-1}, 925–842 cm^{-1}) and chitin/chitosan (3457–3417 cm^{-1}, 3293–3251 cm^{-1}, 3133–3081 cm^{-1}, 1639–1623 cm^{-1}, 1392–1346 cm^{-1}, 962–941 cm^{-1}) spectral regions (Figs 7, 9 and 11) in order to show the reproducibility of the growth experiment (i.e. biological replicates).

(2) In order to get overview of all samples in whole measured spectral region, technical replicates (936 spectra in total) were averaged in order to remove technical variability of the measurements, resulting into 312 spectra (biological replicates). Further, biological replicates were averaged, resulting in 104 FTIR spectra, and pre-processed by EMSC. After pre-processing, spectra were used for PCA analysis (Fig 6) and to plot each fungal strain separately for the observation of the effect of different amounts of phosphate salts on the biochemical composition of biomass (S1–S18 Figs).

1.5.2. Principle component analysis (PCA) and variation contribution analysis. Principle component analysis (PCA) was conducted on the pre-processed FTIR data. To evaluate

influence of different nitrogen sources, PCA analysis was done on the data set split into two parts: 1) samples grown on yeast extract (YE), 2) samples grown on ammonium sulphate (AS). Variation in the data introduced by the different design parameters, specifically N-source, Pi concentration and N-Pi interaction, was calculated for each strain independently in each data set. In ANOVA model a data matrix is represented as a sum of matrices that describe experimental design factors and the residual error. Each of these matrices consists of the means of the spectra that correspond to different levels of the design factor. The variation due to each factor can then be calculated. The ANOVA model for this study contained three design factors: N-source, Pi concentration and N-Pi interaction. The factor "N-source" had two levels (YE, AS), the factor "Pi concentration" consisted of six levels (six different Pi concentrations), the design factor "N-Pi interaction" had 12 levels. Biological and other variations not of interest for this study were kept as a part of residuals. The variation of each factor was normalized by the sum of the variations for the three factors of interest, so they summed up to 100%. Such ANOVA model underlies commonly used ANOVA-PCA and ASCA analysis [83, 84] which in addition to calculating variation contribution of design factors in a data allow analyzing other aspects of the data. The methods were therefore not implemented in this study.

1.5.3. Monitoring of glucose and phosphate consumption. FTIR-ATR spectra of growth media after the cultivation were used for the estimation of glucose and phosphate consumption. ATR spectra of pure water, and water solutions of pure glucose, nitrogen sources, phosphates, as well as media before cultivation were evaluated for characteristic signal of the components (S19 Fig). The peak at 1799 cm^{-1} was selected for the correction of baseline shift, while the peak associated with water at 1637 cm^{-1} was selected for peak normalization of all spectra. All growth media spectra were first baseline corrected ($A_{n\nu}$-A_{n1799}), and then peak normalized ($A_{n\nu}$/ A_{n1637}), where $A_{n\nu}$ is the absorbance value of sample *n* at a specific wavenumber. Finally, growth media spectra were corrected for water absorbance by subtracting the absorbance values of baseline- corrected and peak- normalized water spectrum from the corresponding absorbance values of the preprocessed growth media spectra. The peak associated with glucose at 1034 cm^{-1} (A_{n1034}) and peak associated with phosphates at 937 cm^{-1} (A_{n937}) were used to estimate nutrient consumption in the growth media. Phosphate consumption (P_{FTIR}) was based on the A_{n937} value of the growth media. Glucose consumptions (G_{FTIR}) was calculated according to the equation:

$$\mathbf{G_{FTIR}} = \mathbf{A_{GM1034}} - \mathbf{A_{GM937}}\frac{\mathbf{A_{P1034}}}{\mathbf{A_{P937}}}$$

where A_{GM} and A_P are the absorbance values (at the corresponding wavenumbers) for pre-processed growth media spectrum and water solution of pure phosphate spectrum, respectively. The second term in the equation is taking into consideration that both glucose and phosphate contribute to the absorbance at 1034 cm^{-1} (i.e. the term is estimating phosphate contribution to the total absorbance at 1034 cm^{-1} based on measurement of water solution of pure phosphate). Four media samples, belonging to one biological replicate of *Umbelopsis vinacea* grown in ammonium sulphate with Pi8, Pi4, Pi2, and Pi1 phosphate concentrations, were excluded from the analysis due to a technical error in the preparation of the samples for the FTIR measurements.

2. Results

2.1. Growth characteristics of *Mucoromycota* fungi under different nutrient conditions

2.1.1. Biomass production and pH. Two types of nitrogen (N) sources, yeast extract (YE) and ammonium sulphate (AS), and six concentrations of inorganic phosphorus (Pi) were

applied to study the effect of N source and Pi level on the nutrient-induced co-production of high-value metabolites–lipids, chitin/chitosan and polyphosphates, in *Mucoromycota* fungi.

Fig 1A shows the effect of yeast extract- complex organic multi-component substrate containing both nitrogen and phosphorus, on the cultivation of *Mucoromycota* fungi under different Pi levels. Results indicate that the addition of inorganic phosphorus could be neglected, since it does not have any significant effect on the biomass production. Yeast extract contains approximately 2.5% of total phosphorus. This amount corresponds to approx. 15% in terms of total P contained in added phosphates salts in the lowest examined Pi condition- Pi0.25. The highest biomass yield (18.92–23.67 g/L) was observed for *Umbelopsis vinacea* on both types of nitrogen sources (Fig 1). In case of YE-Pi medium, high *Umbelopsis vinacea* biomass yield was obtained for a wide range of phosphorus concentrations (Pi0.5 –Pi4), while on AS-Pi media Pi2 and Pi4 concentrations showed the highest biomass yield. This indicates that *Umbelopsis vinacea* requires quite high concentration of phosphorus for optimal growth in ammonium sulphate media under nitrogen-limited conditions. The lowest biomass yield was obtained for *Mortierella alpina* on both YE–(5.55–6.10 g/L) and AS-based (0.90–7.03 g/L) media. The biomass yield for *Mucor circinelloides*, *Absidia glauca*, *Lichthemia corymbifera*, and *Amylomyces rouxii* was in a range from 8.52 to 12.92 g/L when grown on yeast extract, and from 2.41 to 12.34 g/L when grown on ammonium sulphate. *Cunninghamella blakesleeana*, *Rhizopus stolonifer* and *Mortierella hyalina* had biomass yields from 4.28 to 9.20 g/L when grown on YE-Pi media, and from 2.11 to 10.05 g/L when grown on AS-Pi media (Fig 1).

The use of different phosphorus (Pi) concentrations resulted in a change of the pH in the media after the cultivation for all studied fungi when ammonium sulphate was used as a nitrogen source. Low phosphorus concentrations caused a significant drop of pH in media for all fungi (Fig 2). In media with yeast extract as a nitrogen source, quite stable pH values where observed for media of several fungi throughout Pi concentration range: *Lichtheimia corymbifera*, *Umbelopsis vinacea*, *Mortierella alpina* and *Mortierella hyalina*. Significantly lower pH values were detected for low Pi concentrations compared to the media with higher Pi concentrations for *Mucor circinelloides*, *Absidia glauca*, *Cunninghamella blakesleeana*, *Amylomyces rouxii* and *Rhizopus stolonifer*. Thus, YE shows higher buffering capacity than AS, which was confirmed by titration of YE-Pi0.25 and AS-Pi0.25 growth media with 1M HCl (S20 Fig).

2.2. Fourier Transform Infrared (FTIR) spectroscopy reveals co-production in oleaginous *Mucoromycota* fungi

FTIR spectroscopy is a non-destructive technique that allows examining the total biochemical profile of intracellular metabolites in fungal cells, as well as extracellular metabolites, by using high-throughput screening (HTS) FTIR measurements. Moreover, monitoring of growth media components (glucose and phosphates) was obtained by using attenuated total reflectance (ATR) FTIR measurements. In infrared spectroscopy, the loss of infrared radiation due to chemical absorption is quantified. In the FTIR-HTS transmission mode, the loss of radiation due to absorption is quantified by transmitting infrared radiation through a sample and quantifying the loss of the radiation by comparing the transmitted radiation with the radiation that impinges on the sample. By covering the complete spectra range of the mid-infrared, biochemical fingerprint of all major chemical building blocks is obtained. The FTIR-HTS system employs a high-throughput setup with microplates and automated measurements allowing the automated analysis of around 180 samples in one measurement run. Relatively large variance in sample thickness results in the difference in optical path length, which can be corrected by standard pre-processing tools developed by us [80, 82]. In FTIR-ATR analysis, the infrared radiation undergoes reflection in an ATR crystal an produces an evanescent field in the sample

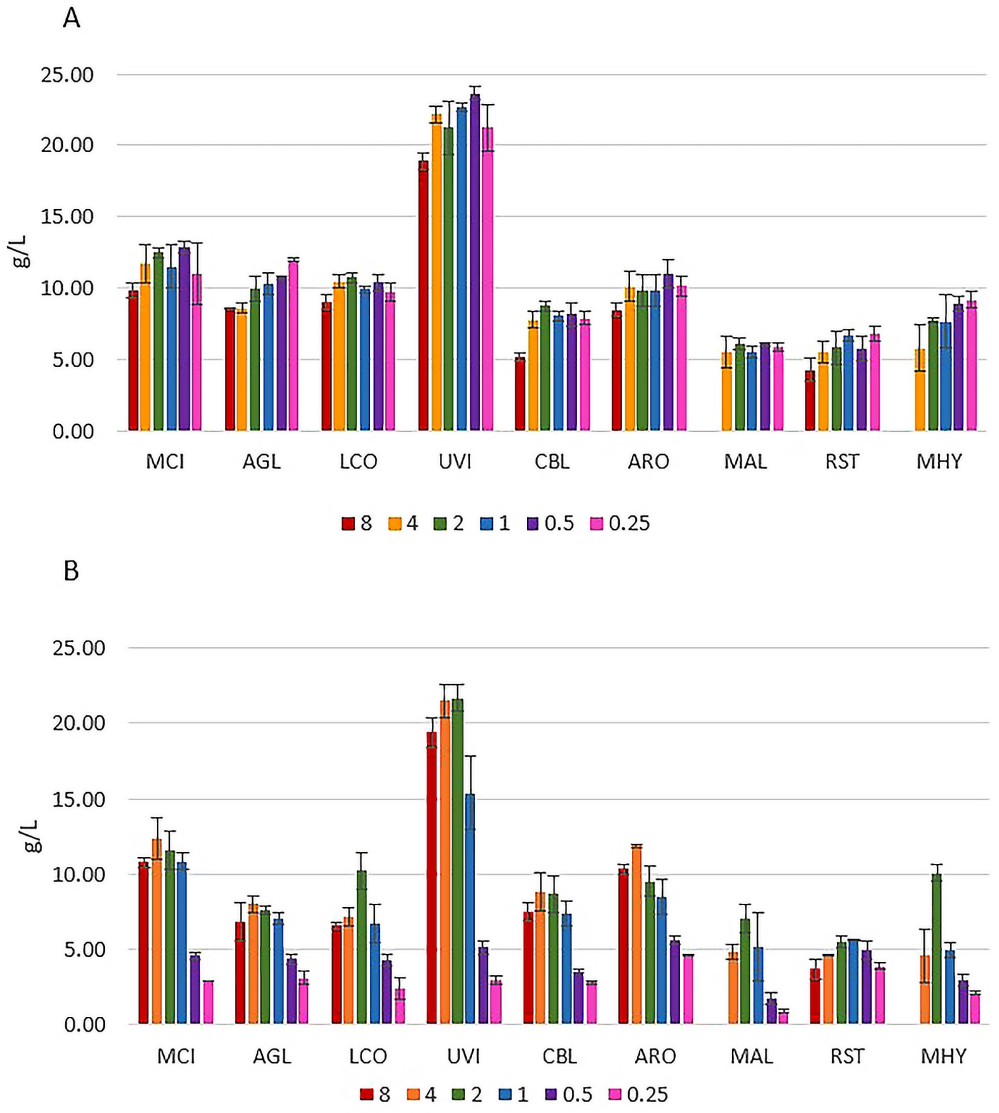

Fig 1. Biomass yield for *Mucoromycota* fungi grown in media with (A) yeast extract (YE) and (B) ammonium sulphate (AS) under different Pi concentrations. Different colors correspond to different Pi concentrations (Table 2). *Absidia glauca*- AGL, *Amylomyces rouxii*- ARO, *Cunninghamella blakesleeana*- CBL, *Lichtheimia corymbifera*- LCO, *Mortierella alpina*- MAL, *Mortierella hyalina*- MHY, *Mucor circinelloides*- MCI, *Rhizopus stolonifer*- RST, *Umbelopsis vinacea*- UVI.

https://doi.org/10.1371/journal.pone.0234870.g001

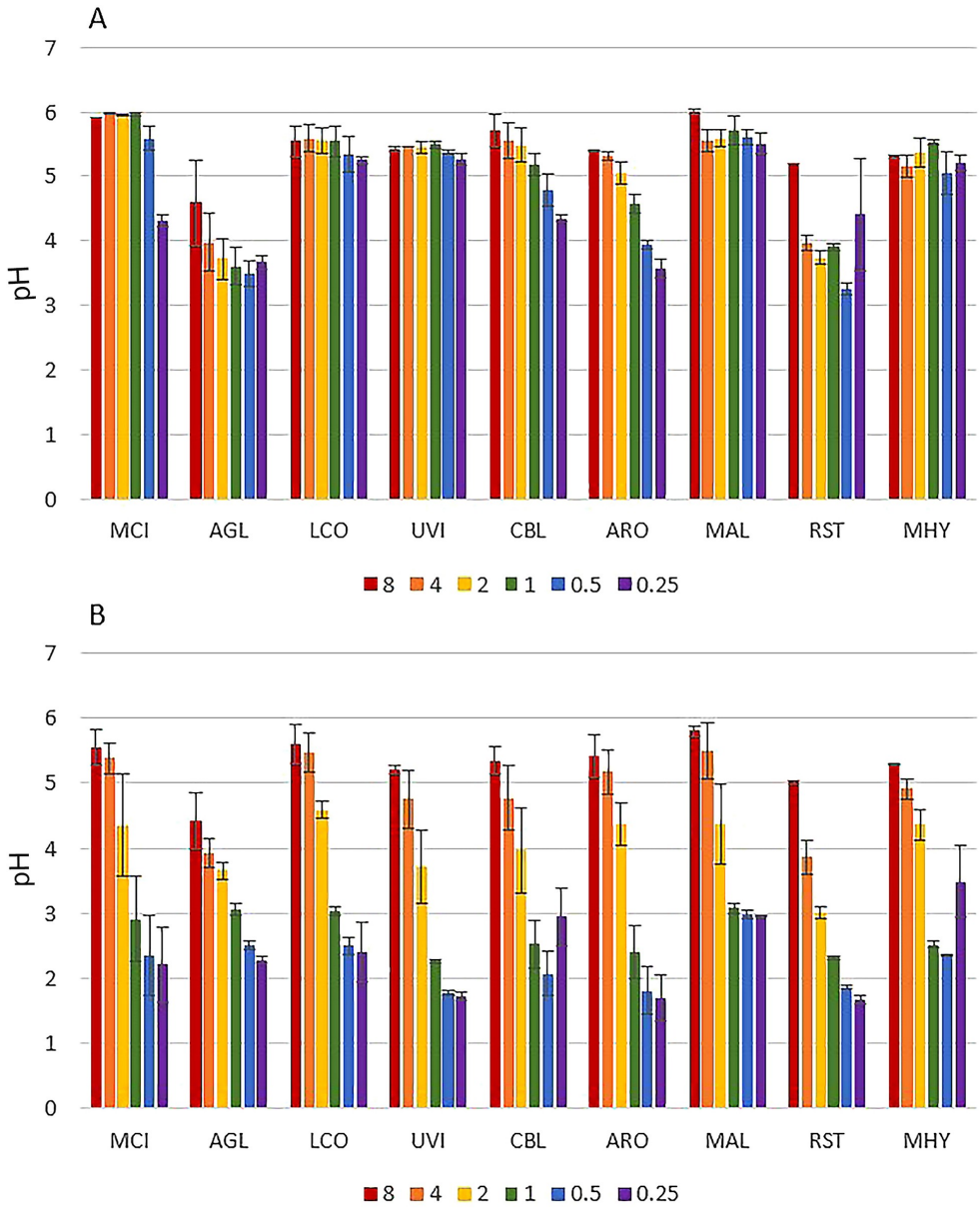

Fig 2. pH values of YE-Pi media with different phosphorus (Pi) levels after the cultivation on YE-Pi (A) and AS-Pi (B) media. The initial pH value at the start of the cultivation was 6±0.3. Different colors correspond to different Pi concentrations (Table 2). *Absidia glauca*- AGL, *Amylomyces rouxii*- ARO, *Cunninghamella blakesleeana*- CBL, *Lichtheimia corymbifera*- LCO, *Mortierella alpina*- MAL, *Mortierella hyalina*- MHY, *Mucor circinelloides*- MCI, *Rhizopus stolonifer*- RST, *Umbelopsis vinacea*- UVI.

https://doi.org/10.1371/journal.pone.0234870.g002

which is located on its surface. The evanescent field is attenuated by the sample die to chemical absorption and the absorption can be quantified by relating the attenuated radiation with the radiation that is obtained in an ATR setup without a sample at the surface of the crystal. The ATR setup is characterized by a high reproducibility caused by a stable penetration depth of the IR beam into the sample, when the sample at the top of the crystal is in tight contact with the surface of the crystal. This is true for liquid and viscous samples such as the culture supernatant in our measurements. Information about intracellular and extracellular metabolites of fungal cells could be read from different spectral regions of HTS FTIR spectra (Fig 3, Table 3): (1) The region from 3010–2800 cm^{-1}, 1800–1700 cm^{-1} and some single peaks related to -CH_2 and -CH_3 scissoring in a region ~1460 cm^{-1} contain detailed information about lipids. One of the most important lipids associated peaks is ~1745 cm^{-1} which is related to the carbonyl bond stretching in esters and indicating the lipid (acylglycerols) content in the cell. The peak around 1715 cm^{-1} is related to the carbonyl bond vibrations in organic acids, and the peak around 3010 cm^{-1} is related to = C-H stretching in lipids and indicating the unsaturation level of lipids in the cell. (2) Proteins have peaks in the region from 1700–1500 cm^{-1}; (3) Polyphosphates–1260–1240 cm^{-1} and 885–880 cm^{-1}; (4) Glucans peaks can be found in the region 1160–1050 cm^{-1}; (5) Chitin/chitosan shows peaks in the region 3440–3100 cm^{-1} and a single peak at 1377 cm^{-1}. A more detailed overview of characteristic peaks can be found in Table 3. For the ATR FTIR monitoring of media (Fig 4), the most important peaks were related to glucose (1151, 1103, 1080, 1034 and 990 cm^{-1}) and phosphates (1161, 1076 and 937 cm^{-1}).

Fourier transform infrared (FTIR) spectroscopy can provide both qualitative and quantitative measures. Quantitative analysis by FTIR requires regression onto reference data. For regression analysis often methods based on latent variables such as partial least square regression are used. As reference data for respective metabolites, e.g. chromatography analyses can be used. Qualitative measures are achieved by spectral assignments (see Fig 3 and Table 3) and by applying unsupervised multivariate data analysis tools (for example principal component analysis or ANOVA-PCA). Although FTIR spectroscopy cannot provide absolute quantifications without establishing calibration models based on reference quantitative data, a semi-quantitative analysis of ratios of chemical constituents (see Fig 13) can be obtained. Nevertheless, the biggest advantage of the FTIR approach is that it allows high-throughput screening of samples and detection of a vast range of different metabolites simultaneously within a single analytical run. Thus, it provides high precision qualitative information allowing to pre-select strains and growth conditions.

The FTIR spectra of *Mucor circinelloides*, grown on a AS nitrogen-source, illustrate the effect of phosphorus availability in media on the intracellular production of lipids, polyphosphates and chitin/chitosan (Fig 3A). Signals of these metabolites clearly correspond to the model components- chitin, glyceryl trioleate and sodium polyphosphate (Fig 3B). *Mucor circinelloides* showed good oleaginous properties when phosphorus was not limited (Pi1 –Pi8), as indicated by strong absorbance peaks related to acylglycerides (3010, 2925, 2854, 1743, and 725 cm^{-1}). Moreover, an increase in the amount of phosphorus in the growth media (Pi2 –Pi8) led to increased polyphosphates accumulation in fungal cells, as indicated by the strong absorbance peaks related to polyphosphates (1265 and 883 cm^{-1}). FTIR results clearly indicated that limitation of phosphorus availability (Pi0.25 and Pi0.5) resulted in low pH and an overproduction of chitin/chitosan which could be explained as an activation of protective mechanisms in the cell wall. The production of chitin and chitosan is strongly supported by an observation of the absorbance peaks related to these biopolymers at 3434, 3274, 3104, 1660, 1629, 1550, 1377, and 952 cm^{-1}. FTIR-HTS spectra of all strains used in the study can be found in the supplementary materials.

The FTIR-HTS spectra of media after growth, in particular of the AS nitrogen-source media, show carbonyl peaks (at approx. 1715 cm^{-1}) (Fig 4A). These carbonyl peaks may relate

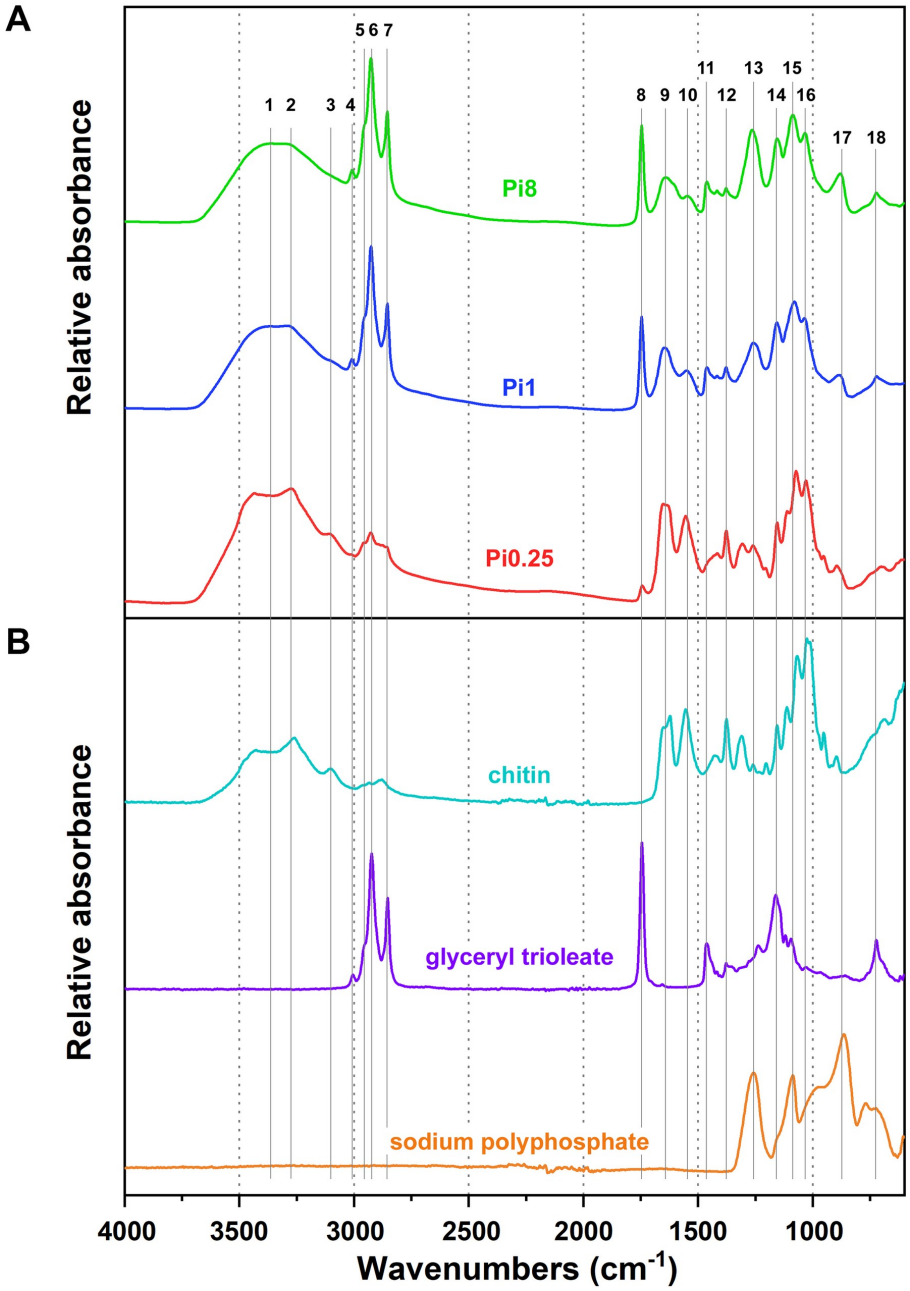

Fig 3. FTIR-HTS spectra of fungal biomass and model compounds. A) Preprocessed FTIR-HTS spectra of *Mucor circinelloides* biomass grown on ammonium sulphate and different Pi levels. B) Preprocessed FTIR-ATR spectra of model compounds: chitin, glyceryl trioleate and sodium polyphosphate. Spectra are plotted with an offset for better viewing. Peak numbers correspond to the numbers given in Table 3.

https://doi.org/10.1371/journal.pone.0234870.g003

Table 3. Peak assignments of the FTIR spectra of the fungal cells (chemical class with the predominant contribution is stated in the parenthesis).

Peak Nr.	Wavenumber (cm^{-1})	Peak assignment	Reference
1	3500–3200	O-H stretching (carbohydrates)	[85]
2	3275	N-H stretching (chitin/chitosan)	[85]
3	3105	N-H stretching (chitin/chitosan)	[85]
4	3010	= C-H stretching (lipids)	[86]
5	2955	-C-H (CH_3) stretching (lipids)	[86]
6	2925	>CH_2 of acyl chain (lipids)	[86]
7	2855	-C-H (CH_2) stretching (lipids)	[86]
8	1745	-C = O stretching in esters (lipids)	[86]
9	1680–1630	-C = O stretching, Amide I (proteins, chitin)	[87, 88]
10	1530–1560	C-N-H deformation, Amide II (proteins, chitin)	[88, 89]
11	1465	-C-H (CH_2, CH_3) bending (lipids)	[86]
12	1377	-C-H (CH_3) bending (chitin)	[86]
13	1265	P = O stretching (polyphosphates)	[66]
14	1160	C-O-C stretching in esters (lipids)	[90]
14–16	1200–1000	C-O and C-O-C stretching (carbohydrates)	[91]
17	885	P-O-P stretching (polyphosphates)	[66]
18	725	>CH_2 rocking in methylene–$(CH_2)_n$-chains (lipids)	[86]

https://doi.org/10.1371/journal.pone.0234870.t003

to production of organic acids coming from the Krebs cycle, for example citric acid. This is in agreement with pH measurements (Fig 2B) and with our previous studies [54], where citric acid was determined by HPLC measurements. In order to confirm this observation, transmission electron microscopy (TEM) of the *Mucor circinelloides* sectioned hyphae, obtained from the growth on ammonium sulphate media with Pi-limited and Pi-non-limited conditions, was performed (Fig 5).

As it can be seen from TEM images, the cell wall of *Mucor circinelloides* hyphae grown on Pi-limited condition (Fig 5A) is much thicker than the cell wall of the hyphae from Pi-non-limited condition (Fig 5B), while size and number of lipid bodies are smaller in a Pi-limited than in Pi-non-limited conditions. This indicates the increase in the cell wall components–chitin/chitosan and decrease in the lipid accumulation for the hyphae obtained from Pi-limited conditions is in accordance with the FTIR-HTS spectroscopy results reported above.

2.2.1. The influence of N-source and Pi-levels on the co-production in *Mucoromycota* fungi. A nitrogen (N) source used for the fungal fermentation can be organic or inorganic. In this study, yeast extract (YE) was used as an organic N-source and ammonium sulphate (AS) as an inorganic N-source. PCA analysis of FTIR-HTS spectral data was performed to reveal the biochemical composition of the samples.

The PCA score plot of the first and second component of FTIR-HTS spectra of fungal biomass grown on YE is shown in Fig 6A, the corresponding loadings are shown in Fig 6C. The PCA score plot shows clear strain-specific clustering. Higher components did not show relevant trends related to the main biomass constituents. This indicates that each fungus has its strain-specific biochemical composition when grown on YE. Different Pi concentrations are not influencing these strain-specific fingerprints considerably. The loadings in Fig 6C show that the strain-specific differences in biomass composition are mostly determined by the ratio of main cellular components, specifically lipids (3010, 2925, 2855 cm^{-1}), polyphosphates (1265, 885 cm^{-1}), chitin/chitosan (3434, 3275, 3105, 1660, 1629, 1550, 1377, and 952 cm^{-1}) and proteins (1680–1630, 1530–1560 cm^{-1}). For example, biomass of *Mucor circinelloides* and *Amylomyces rouxii* have high phosphate (polyphosphates) to nitrogen (chitin, chitosan and proteins)

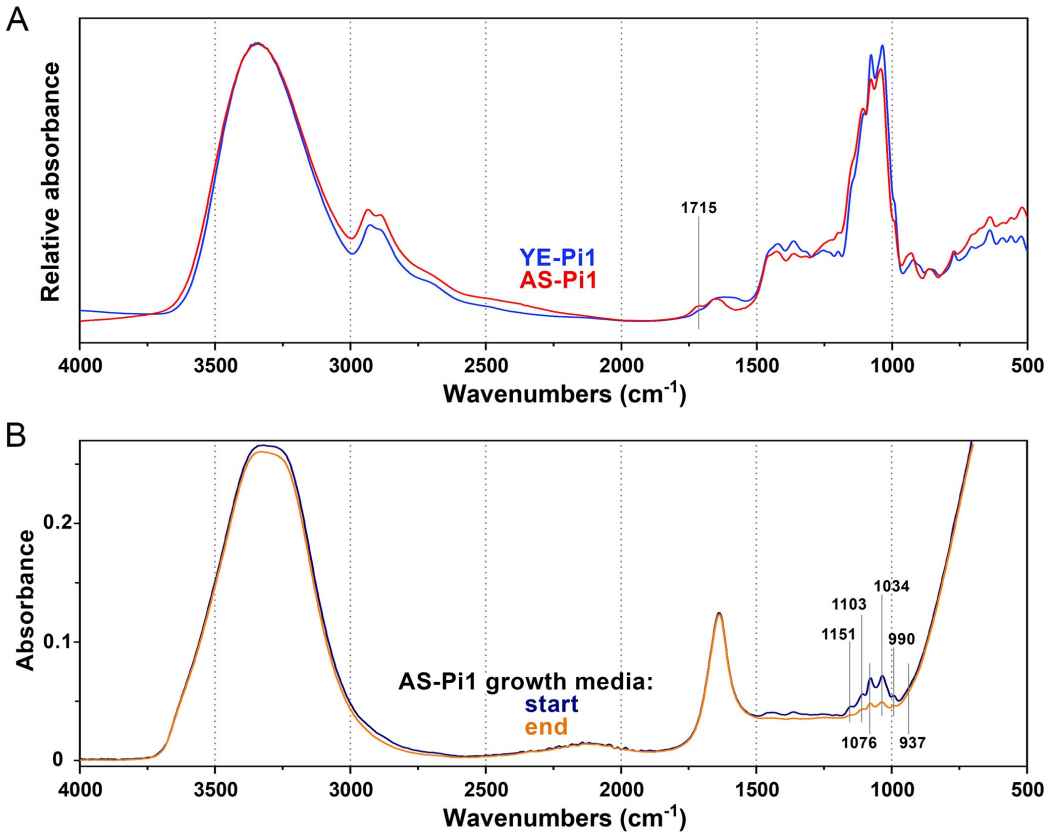

Fig 4. FTIR spectra of growth media. A) Preprocessed FTIR-HTS spectra of ammonium sulphate and yeast extract growth media (both Pi1) at the end of cultivation of *Mucor circinelloides*, B) FTIR-ATR spectra of ammonium sulphate Pi1 growth media at the beginning and end of cultivation of *Mucor circinelloides*.

https://doi.org/10.1371/journal.pone.0234870.g004

ratio, compared to *Cunninghamella blakesleeana* and *Lichtheimia corymbifera*. Compared to all of them, spectra of *Umbelopsis vinacea* show the highest lipids-to-proteins ratio.

The PCA score plot of the first and second component of FTIR-HTS spectra of fungal biomass grown on AS is shown in Fig 6B and the corresponding loadings are shown in Fig 6D. In contrast to the FTIR spectra of fungi grown on YE, the FTIR spectra of fungi grown on AS do not show any clustering with respect to fungal strain (Fig 6B). However, unlike for the YE-Pi media, strong biochemical differences for fungi grown in AS-Pi at different phosphorus levels can be clearly seen. The low effect of phosphorus on the biochemical composition of the strains when grown in yeast extract may be explained by the fact that yeast extract is a complex and rich source of not only nitrogen, sulphur, vitamins and minerals, but also of organic phosphorus. Due to a relatively large starting amount of organic phosphorus in the yeast extract, variation in the concentration of the inorganic phosphorus may not have strong effects on fungal growth in the YE media. In the case of AS-based media, when Pi was the only source of phosphorus for fungal growth, considerable changes in fungal cell chemistry were observed when

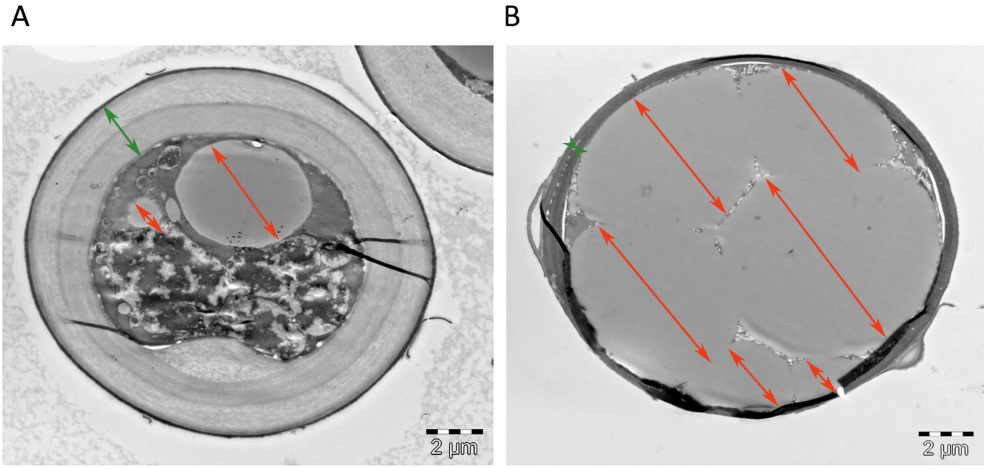

Fig 5. Transmission electron microscopy (TEM) of cross sectioned *Mucor circinelloides* (MCI) hyphae grown on AS media with Pi0.5 (limited) (A) and AS Pi1 (non-limited) (B) conditions. Green arrows indicate cell wall and orange arrows lipid bodies. Images are taken by Lene Cecilie Hermansen, Imaging center NMBU.

https://doi.org/10.1371/journal.pone.0234870.g005

phosphorus levels were changed. Therefore, biochemical differences in the biomass were quite pronounced at already low Pi concentrations (Fig 6A and 6B).

PCA of FTIR-HTS spectra using specific spectral regions that are characteristic for lipids, polyphosphates and chitin/chitosan was performed in order to evaluate the co-production of these components in *Mucoromycota* fungi (Figs 7, 9 and 11). In order to have a deeper understanding on the influence of variations in N-source, Pi concentration and N-Pi interaction on the co-production of lipids, polyP and chitin/chitosan in *Mucoromycota* fungi, Analysis of Variance PCA (ANOVA-PCA) was performed following the approach by Harrington [83]. The analysis of variation in the FTIR-HTS spectra introduced by the different design factors was done using respective spectral regions (Figs 8, 10 and 12).

In Fig 7A, the score values of the first principal component of the lipid region are shown for all strains and the corresponding loading vector is shown in Fig 7C. From the spread of the score values of the first PC, we can see that availability of inorganic phosphorus did not influence the accumulation of lipids in *Umbelopsis vinacea*, *Mortierella hyalina*, *Mucor circineloides*, and only some minor effects could be seen for *Mortierella alpina* (Fig 7A). Thus, results indicate that addition of inorganic phosphorus might be not needed, when complex organic multi-component substrates containing both nitrogen and phosphorus are used for the production of lipids by *Mucoromycota* fungi. In this case, the addition of Pi does not have any significant effect on the biomass and lipid yield. Moreover, in some cases high levels of phosphorus can negatively influence accumulation of lipids, as it was observed for *Cunninghamella blakesleeana*, *Amylomyces rouxii* and *Absidia glauca* (Fig 7A) which is explained by the growth inhibition effect of high Pi-levels of these fungal strains and the accumulation of polyphosphates in case of *Amylomyces rouxii* and *Absidia glauca*. The observed variation in lipid content of *Rhizopus stolonifer* which is not correlated with Pi availability can be explained by a low relative amount of lipids in *Rhizopus stolonifer* biomass, as shown in Fig 6A.

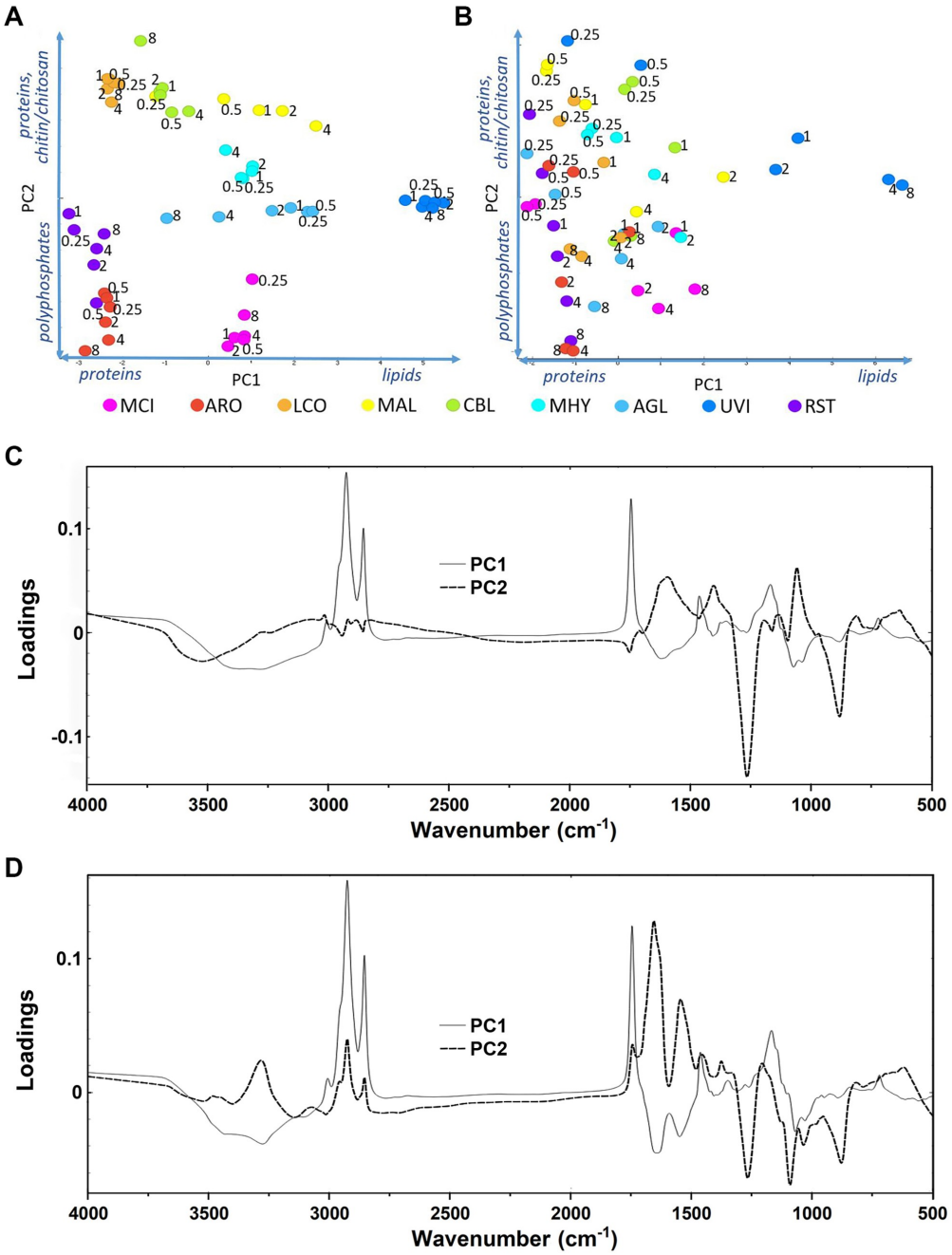
A
B
proteins, chitin/chitosan
polyphosphates
PC2
PC1
proteins
lipids
MCI
ARO
LCO
MAL
CBL
MHY
AGL
UVI
RST
C
D
Loadings
PC1
PC2
Wavenumber (cm-1)
4000
3500
3000
2500
2000
1500
1000
500
0.1
0
-0.1

Fig 6. PCA score plots of FTIR-HTS spectra of fungi grown at different phosphorus concentrations on yeast extract (A) and ammonium sulphate (B). Numbers in PCA score plots indicate the Pi amounts. Vectors on axis describe an observed increase of the metabolites chitin/chitosan, polyphosphates and lipids. Below the scatter plots, loading vectors for PC1 (full line) and PC2 (dashed line) are plotted in C and D, respectively. The explained variance for the first and second principal components are 87% and 7%, respectively, for YE and 69% and 20% for AS.

https://doi.org/10.1371/journal.pone.0234870.g006

The score values of the first principal component of the PCA of the lipid region of FTIR spectra of AS-Pi grown fungi is shown in Fig 7B and the corresponding loading vector in Fig 7D. The spread of the score values indicates that lipid accumulation in *Absidia glauca*, *Amylomyces rouxii* and *Mucor circinelloides* was stronger influenced by the Pi level than in other fungi. The decrease in Pi in AS-Pi media led to the low lipid content for all fungi except *Cunninghamella blakesleeana* (Fig 7B). *Mucor circinelloides* showed the highest decrease in the

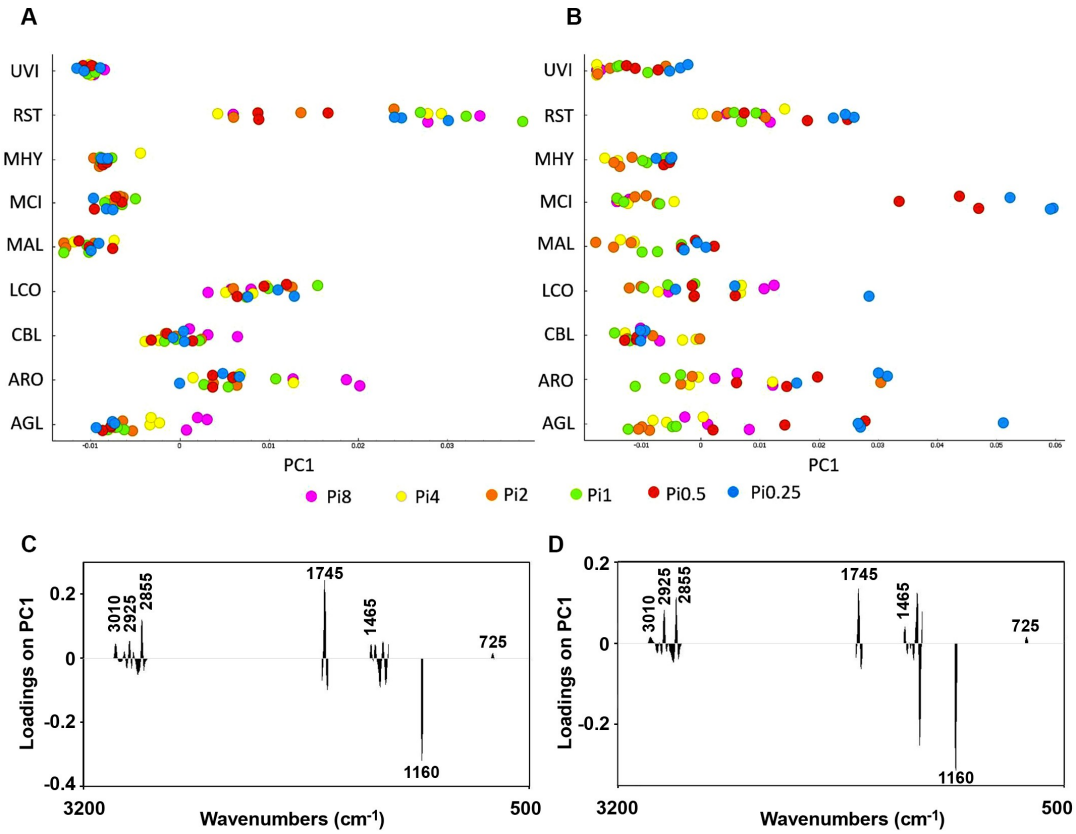

Fig 7. PCA results (first principal component) for the lipid region 3020–2819 cm^{-1}, 1760–1726 cm^{-1}, 1475–1375 cm^{-1}, 1160–1149 cm^{-1}, 730–715 cm^{-1}) of FTIR-HTS spectra (pre-processed by 2nd derivative and EMSC). The scores for the first principal component are plotted for all strains in A and B. In A and C, the score plot and the corresponding loading plot are shown for fungi grown on YE-Pi using different Pi levels. In B and D, the score plot and corresponding loading plot are shown for fungi grown on AS-Pi media using different Pi levels. The color coding is according to the Pi levels. The loading plots show that the total lipid content is increasing from the right to the left in both score plots. The explained variance for the first principal component is 66% and 76% for YE and AS, respectively.

https://doi.org/10.1371/journal.pone.0234870.g007

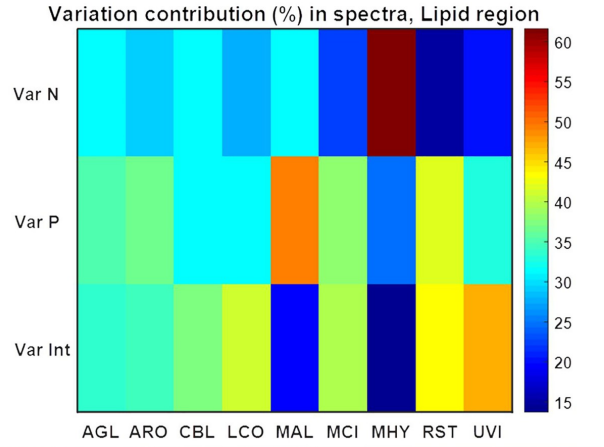

Fig 8. Variation contribution (%) from changes in N, Pi and N-Pi interaction on the lipid region (3020–2819 cm^{-1}, 1760–1726 cm^{-1}, 1475–1375 cm^{-1}, 1160–1149 cm^{-1}, 730–715 cm^{-1}) of FTIR-HTS spectra. Variation contributions due to changes in N and Pi alone are presented in the first two rows (Var N and Var P), whereas contribution from N-Pi interaction (Int) is presented in the last row (Var Int).

https://doi.org/10.1371/journal.pone.0234870.g008

lipid accumulation at low Pi levels (Pi0.5 and Pi0.25). The reason for this is that both cell growth as well as the lipid accumulation process involves a set of phosphorylated molecules, the synthesis of which could be inhibited under Pi-limited conditions. Generally, Pi concentrations Pi1, Pi2 and Pi4 where better suited for the lipid accumulation in *Mucoromycota* fungi (Fig 7B). Based on the biomass yield results, the optimal phosphorus amount for the fungal growth in growth media that are poorer in nutrients is Pi2 for *Mortierella*. Taking in consideration that *Mortierella* are producing high value polyunsaturated fatty acids, this finding has importance for optimization of industrial bioprocesses. *Lichtheimia corymbifera* did not show any specific trend in lipid content with respect to the amount of Pi neither in YE-Pi, nor AS-Pi media.

ANOVA model for spectral data using the lipid region (Fig 8) (3020–2819 cm^{-1}, 1760–1726 cm^{-1}, 1475–1375 cm^{-1}, 1160–1149 cm^{-1}, 730–715 cm^{-1}) showed that variation in N, Pi and N-Pi interaction influences fungal lipids in different ways depending on the fungal strain, and the N-source variation had the least influence on the lipid accumulation in all fungi except *Mortierella hyalina* (Fig 8). For *Absidia glauca*, *Amylomyces rouxii* and *Cunninghamella blakesleeana*, variation of nitrogen, phosphorus and their combination influenced the lipid production to the same extent. For *Lichtheimia corymbifera* and *Umbelopsis vinacea* there was a slightly higher influence of the N-Pi interaction than of each of the nutrients separately. The lipid production of *Mucor circinelloides* and *Rhizopus stolonifer* was not strongly affected by the different nitrogen sources, contrary to *Mortierella hyalina*, where the nitrogen source played an important role in lipid accumulation. Variation of phosphorus caused the biggest changes in the lipid production of *Mortierella alpina*.

The co-production of polyphosphate (polyP) and lipids was studied by PCA analysis of the spectral regions of HTS-FTIR spectra of fungi that have characteristic bands from polyphosphate (1301–1203 cm^{-1}, 925–842 cm^{-1}). The score values of the first principal component of the PCA of the of the spectral regions that have characteristic bands from polyphosphate of fungi grown on YE-Pi media is shown in Fig 9A and the corresponding loading vector in Fig

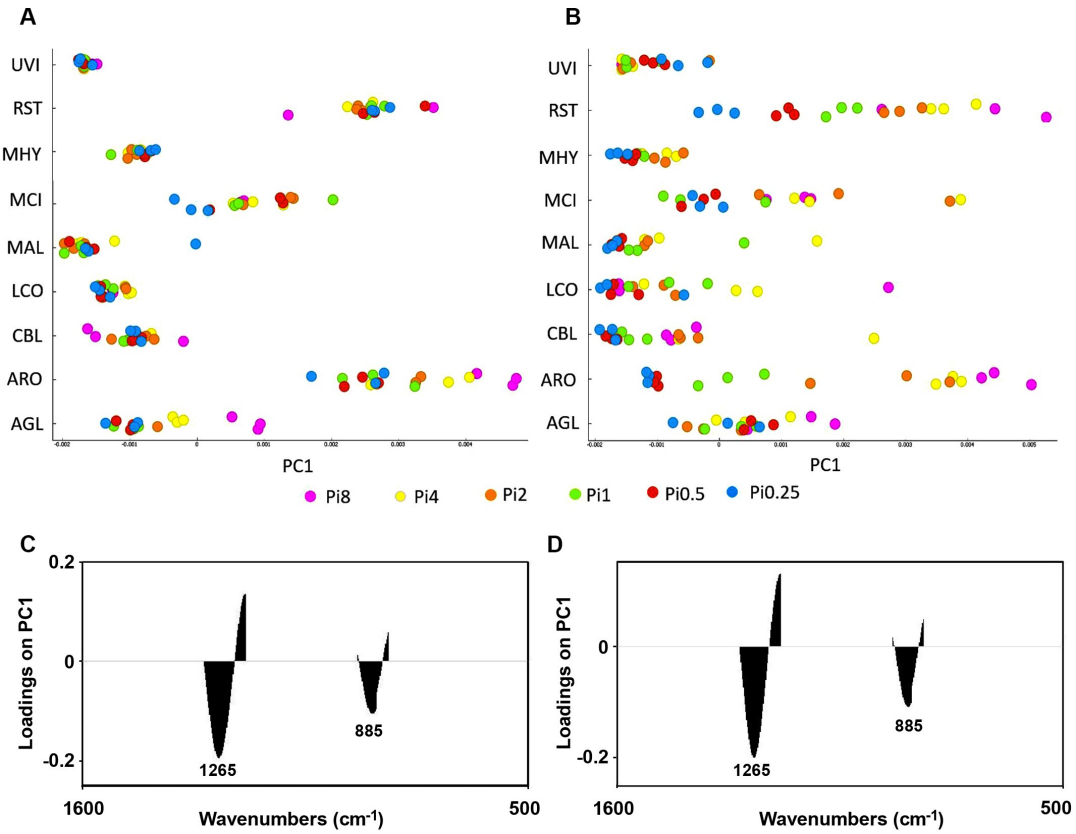

Fig 9. PCA results (first principal component) for the polyphosphate region (1301–1203 cm^{-1}, 925–842 cm^{-1}) of FTIR-HTS (pre-processed by 2nd derivative and EMSC) spectra of fungi grown on (A) YE-Pi and (B) AS-Pi. The scores for the first component is plotted for all strains in A and B. In A and C, the score plot and the corresponding loading plot are shown for fungi grown on YE-Pi using different Pi levels. In B and D, the score plot and corresponding loading plot are shown for fungi grown on AS-Pi media using different Pi levels. The color coding is according to the Pi levels. The loading plots show that the total polyphosphates content is increasing from the left to the right in both score plots. The explained variance for the first principal component is 95% and 93% for YE and AS, respectively.

https://doi.org/10.1371/journal.pone.0234870.g009

9C. It was observed that *Rhizopus stolonifer*, *Mucor circinelloides*, *Amylomyces rouxii* and *Absidia glauca* grown in YE-Pi and AS-Pi media show significant polyP accumulation along with lipid accumulation when a high level of Pi was used (Fig 9).

A co-production of polyP in addition to lipids could not be observed for *Mortierella* fungi and *Umbelopsis vinacea*. While, some polyP accumulation was observed for *Umbelopsis vinacea* with low phosphorus in AS-Pi media., probably due to the high salinity. Specifically, relatively high salinity was observed when phosphorus media were depleted, since KCl and NaCl were used to keep the same K/Na ratio in phosphorus limited media as for the standard conditions. Polyphosphates are reported to be involved in the adaptation mechanisms of microorganisms to stress conditions, namely temperature, radiation, or salinity [92, 93].

By analyzing the variance contribution using ANOVA model in the polyP-related spectral region (Fig 10) (1301–1203 cm^{-1}, 925–842 cm^{-1}) it was possible to identify polyP-accumulating

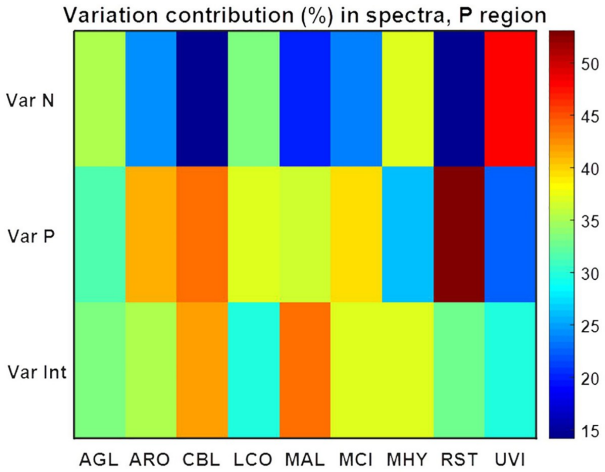

Fig 10. Variation contribution (%) from changes in N, Pi and N-Pi interaction on the polyphosphate region (1301–1203 cm^{-1}, 925–842 cm^{-1}) of FTIR HTS spectra. Variation contributions due to N and Pi alone are presented in the first two rows (Var N and Var P), whereas contribution from N-Pi interaction (Int) is presented in the last row (Var Int).

https://doi.org/10.1371/journal.pone.0234870.g010

strains. Increased variation in the polyphosphate region of FTIR-HTS spectra was observed for *Amylomyces rouxii*, *Cunninghamella blakesleana*, *Mucor circinelloides* and most of all *Rhizopus stolonifer*, for which an extraordinary correlation between variation in phosphorus amount in the growth media and intracellular polyphosphates was already noticed in the PCA (Fig 6, Fig 9). For these strains, the phosphorus variation has much more influence on changes in the polyP region of spectra than variation in nitrogen source. The lowest effect of Pi variation was observed for non-polyP accumulating fungi *Mortierella hyalina* and *Umbelopsis vinacea* (Fig 10). The influence of N-source variation was stronger in the case of spectral region related to polyP than the lipid region for *Absidia glauca*, *Mortierella hyalina*, *Lichtheimia corymbifera* and *Umbelopsis vinacea* (Fig 10). In addition, it could be seen that N-Pi interaction has a higher influence on polyP than on the lipid spectral region. This is associated mainly with Pi variation which occurred in AS-Pi media.

In Fig 11, PCA results (first principal component) are shown for the spectral regions 3457–3417 cm^{-1}, 3293–3251 cm^{-1}, 3133–3081 cm^{-1}, 1639–1623 cm^{-1}, 1392–1346 cm^{-1}, 962–941 cm^{-1}, which show characteristic for chitin/chitosan region of the FTIR-HTS spectra of fungi grown on YE-Pi and AS-Pi. In Fig 11A and Fig 11C the first score and loading are shown for the PCA results for fungi grown on AS-Pi media with Pi concentrations Pi0.5 and Pi0.25. The loading plot (Fig 11C) indicates that chitin and chitosan content increases from the left to the right. In Fig 11B and Fig 11D, the corresponding score plot and loading plot are shown for fungi grown on AS-Pi media. From the score plot in Fig 11B we can see that *Mucor circinelloides*, *Rhizopus stolonifer*, *Amylomyces rouxii*, *Absidia glauca* and *Lichtheimia corymbifera* grown on AS-Pi media with Pi concentrations Pi0.5 and Pi0.25 showed increased content of chitin/chitosan (Fig 11B) while the content of lipids was reduced (Fig 7B). In addition to lipids and polyP, several *Mucoromycota* fungi were able to overproduce chitin/chitosan under phosphorus limited conditions (Fig 11B).

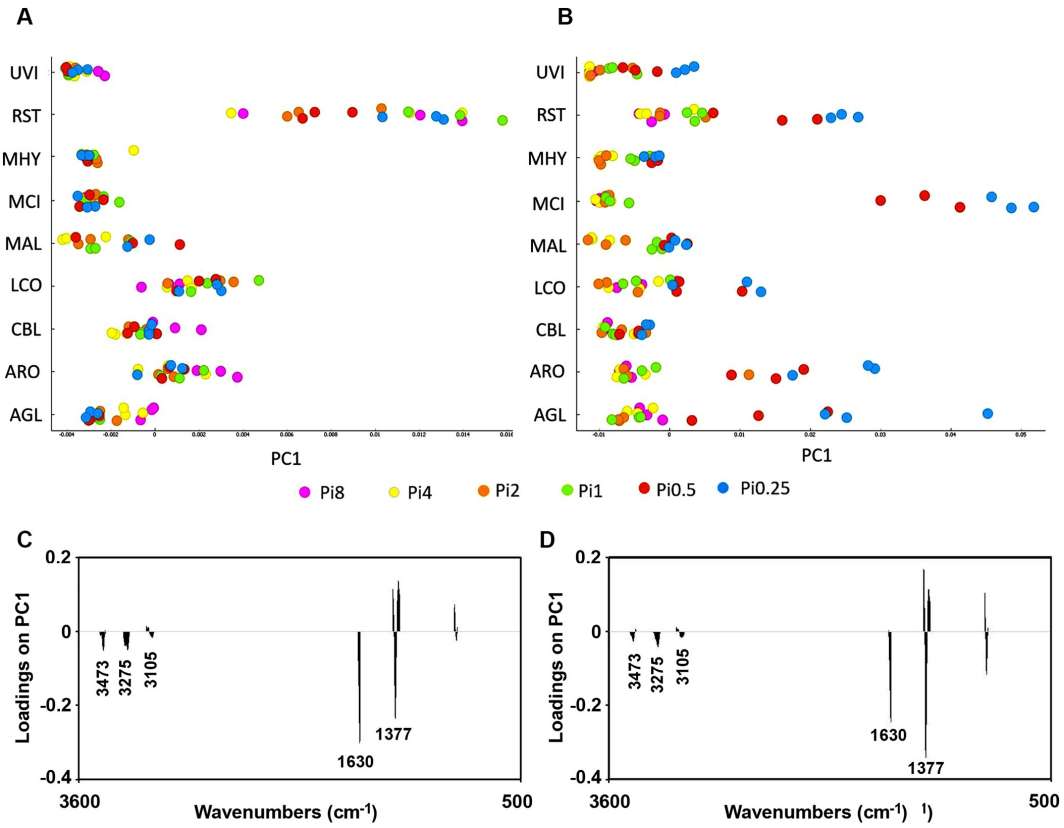

Fig 11. PCA results (first principal component) for the chitin/chitosan region (3457–3417 cm^{-1}, 3293–3251 cm^{-1}, 3133–3081 cm^{-1}, 1639–1623 cm^{-1}, 1392–1346 cm^{-1}, 962–941 cm^{-1}) of FTIR-HTS spectra of fungi (pre-processed by 2nd derivative and EMSC) grown on (A) YE-Pi and (B) AS-Pi. In A and C, the score plot and the corresponding loading plot are shown for fungi grown on YE-Pi using different Pi levels. In B and D, the score plot and the corresponding loading plot are shown for fungi grown on AS-Pi media using different Pi levels. The color coding is according to the Pi levels. The loading plots show that the total chitin/chitosan content is increasing from the left to the right in both score plots. The explained variance for the first principal component is 79% and 80% for YE and AS, respectively.

https://doi.org/10.1371/journal.pone.0234870.g011

ANOVA model for the spectral region related to chitin/chitosan (3457–3417 cm^{-1}, 3293–3251 cm^{-1}, 3133–3081 cm^{-1}, 1639–1623 cm^{-1}, 1392–1346 cm^{-1}, 962–941 cm^{-1}) showed that nature of N-source may have a strong effect for *Absidia glauca* and *Mortierella hyalina*, while variation in the concentration of Pi and N-Pi interaction did not show any significant influence for these fungi (Fig 12). Generally, it could be concluded that the nature of N-source is possibly important for chitin/chitosan content for most of the studied fungi, while the influence from N-Pi interaction seemed to be least important. Variation in Pi affected chitin/chitosan content to some extend for *Amylomyces rouxii*, *Cunninghamella blakesleana*, *Mucor circinelloides* and to a high extend for *Rhizopus stolonifer* (Fig 12). Chitin/chitosan content in *Amylomyces rouxii* was equally affected by the change in N-source and Pi concentrations, while for *Rhizopus stolonifer* little effect was observed from the N-source and most of the changes where related to Pi variation.

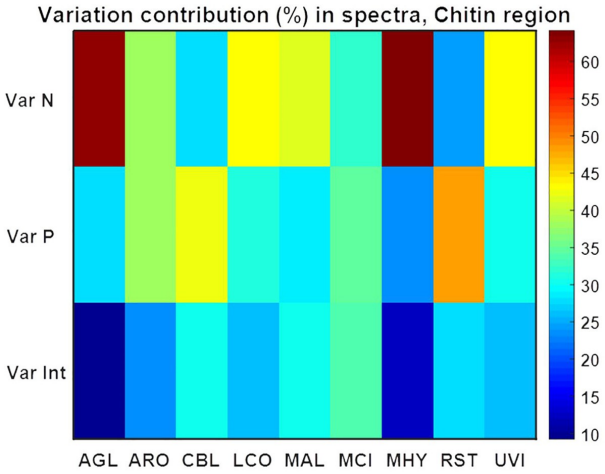

Fig 12. Variation contribution (%) from changes in N, Pi and N-Pi interaction on the chitin/chitosan region (3457–3417 cm^{-1}, 3293–3251 cm^{-1}, 3133–3081 cm^{-1}, 1639–1623 cm^{-1}, 1392–1346 cm^{-1}, 962–941 cm^{-1}) of FTIR HTS spectra. Variation contributions due to N and Pi alone are presented in the first two rows (Var N and Var P), whereas contribution from N-Pi interaction (Int) is presented in the last row (Var Int).

https://doi.org/10.1371/journal.pone.0234870.g012

Absidia glauca and *Lichtheimia corymbifera* modified their cell wall mostly due to a change in nitrogen source, while variations in phosphorus changed to the chitin/chitosan production only weakly. In contrary, the variation in Pi amount induced the chitin/chitosan production in *Rhizopus stolonifer* and just small effect was observed for the contribution of different nitrogen sources. This corresponds to the biomass yield results, where there were no big changes observed with different nitrogen sources, even for the phosphorus limited conditions in the AS-Pi media. For *Amylomyces rouxii* and *Mucor circinelloides*, variation of Pi and N have similar effects on the chitin/chitosan production.

2.2.2. Monitoring of nutrients consumption by FTIR spectroscopy. FTIR-ATR spectra of the growth media after cultivation were used to evaluate the consumption of glucose and phosphate salts (Fig 13). We have shown recently that FTIR-ATR, in combination with multivariate statistical analyses, can be used for analysis of growth media and extracellular metabolites in screening and monitoring of fungal bioprocesses [54]. Here a univariate approach was used with only one variable per analyte (1034 and 937 cm^{-1} for glucose and phosphates, respectively) in order to create a robust model for media monitoring. As shown in Fig 13, this approach allows to estimate concentrations of main nutrients in the media.

The results show that the glucose consumption corresponds to the biomass production (Fig 1). For *Mortierella alpina* and *Mortierella hyalina*, no growth was observed with the Pi8 amount, therefore the glucose content in the growth media after the cultivation was the highest. For AS-Pi media, more glucose was consumed at higher Pi concentrations (Pi1 –Pi4). For example, the double amount of biomass was produced for *Mortierella hyalina* at Pi2, compared to Pi0.25 (Fig 1), and this clearly corresponded to the lowest glucose content. For YE-Pi media, similar biomass yields were obtained irrespective of Pi concentrations, and thus the glucose consumption showed no trend. *Umbelopsis vinacea* utilized nearly all glucose available, which again corresponded to the high biomass yield.

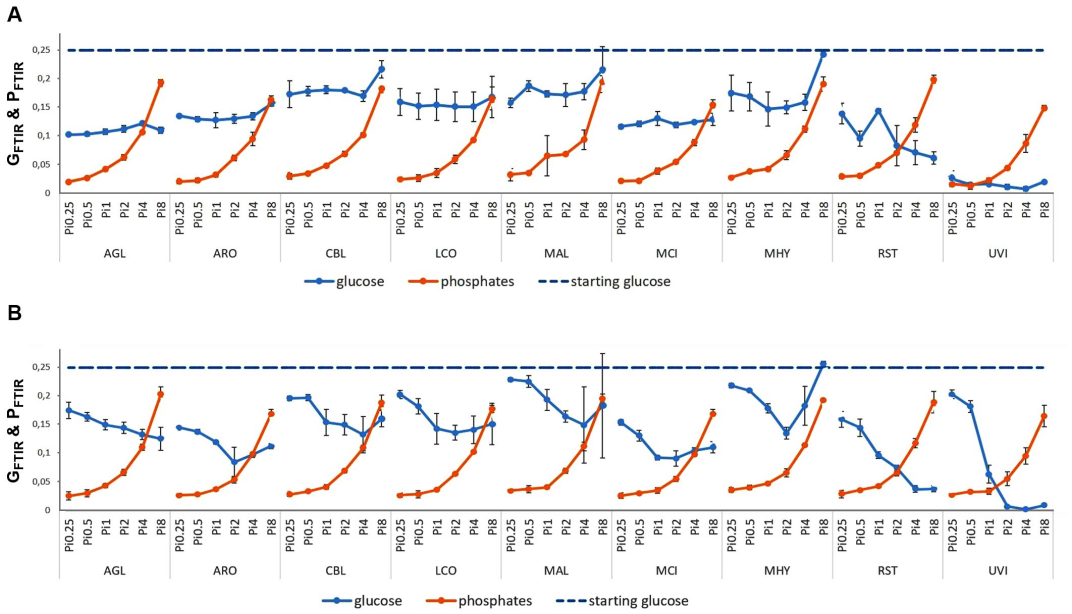

Fig 13. Estimation of the consumption of glucose and phosphate salts in the growth media after cultivation by FTIR-ATR. Starting glucose concentration corresponds to the blue dashed line, final glucose concentration the blue full line and final phosphates concentration are pictured with the orange line. Figure A shows the Ye-Pi media and figure B AS-Pi media.

https://doi.org/10.1371/journal.pone.0234870.g013

3. Discussion

All studied *Mucoromycota* fungi were able to grow in media with different nitrogen sources and inorganic phosphorus concentrations, except *Mortierella* species for which the high concentration of inorganic phosphorus (Pi8) inhibited the growth completely (Fig 1). FTIR-ATR spectra of the growth media after cultivation were used to evaluate the consumption of main nutrients–glucose and phosphate salts and generally, the glucose consumption corresponds to the biomass production (Fig 1, Fig 13). In general, when yeast extract was used as a nitrogen source, no significant changes in biomass yield for different concentrations of inorganic phosphorus were observed. Moreover, biomass yield for fungi grown on yeast extract and low concentrations of inorganic phosphorus was higher compared to when ammonium sulphate was used as nitrogen source. This was mainly due to the fact, that yeast extract is a chemically complex substrate which is a source of not only nitrogen but also phosphorus, sulphur, vitamins, amino acids and trace elements. Therefore, variation in the level of inorganic phosphorus showed small effect on the fungal growth when yeast extract was used as a nitrogen source. This indicates that usage of complex N-source substrates, containing nitrogen, phosphorus and other nutrients for the enrichment of rest materials could be beneficial and sustainable. Such cultivation would provide relatively stable biomass yields without addition of inorganic phosphorus, which is a world limited chemical component. In addition, cultivation of all fungal strains in the presence of yeast extract and various inorganic phosphorus as accompanied by relative stable pH that resulted in high biomass yield.

Combining ammonium sulphate as a nitrogen source with different concentrations of inorganic phosphorus, showed that Pi- requirements for optimal growth varied for different fungi:

(1) *Rhizopus stolonifer* exhibited relatively uniform biomass yield within the used phosphorus concentration range; (2) *Mucor circinelloides*, *Absidia glauca*, *Cunninghamella blakesleeana* and *Amylomyces rouxii* showed the optimal growth and the highest biomass yield within relatively broad concentration range Pi1 –Pi8; (3) *Umbelopsis vinacea* had the highest biomass yield within more narrow concentration range Pi2 –Pi4; (4) *Lichtheimia corymbifera*, *Mortierella alpina* and *Mortierella hyalina* produced the highest biomass yield at Pi2 concentration, and, in case of *Mortierella hyalina*, the biomass yield was double compared to Pi4 and Pi1. Overall, the biomass yield for fungi grown in media with the high phosphorus levels was comparable to the yeast extract media, and in some cases, even higher biomass yields were obtained. The biomass yield clearly showed that the majority of strains, aside from *Rhizopus stolonifer*, have strongly inhibited growth in the low phosphorus media.

When the biomass yield and pH results are compared, it is apparent that low pH caused by the low Pi concentrations inhibited fungal growth. Fungal lipids are accumulated when nitrogen depletion leads to decrease of adenosine monophosphate (AMP) level. This results in the inactivation of isocitrate dehydrogenase and causes the accumulation of citric acid. Citric acid is further converted by ATP citrate lyase to AcetylCoA, which is a precursor for the synthesis of fatty acids (Wynn et al., 2001). Accumulation of citric acid, which was detected by FTIR and HPLC in our previous study (Kosa et al., 2017b), is therefore expected to some extend in the lipogenesis in oleaginous fungi. Other organic acids coming from glycolysis and the Krebs cycle, such as pyruvic or fumaric acid, might be present as well and contribute to the acidic pH. Although decrease in pH is observed in the YE-Pi media as well, the buffering capacity of YE is higher than AS (S20 Fig). Some of the fungal strains activated the protective mechanisms against acidic stress, leading to increased chitin/chitosan production in the cell wall, as it was reported above (Figs 3, 5, 6B and 11). Further studies under pH-controlled conditions are needed to clarify the contribution of low Pi to chitin/chitosan overproduction.

FTIR-HTS spectra of fungi grown on yeast extract and different Pi concentrations showed that *Mucor circinelloides*, *Umbelopsis vinacea*, *Mortierella hyalina*, *Mortierella alpina* and *Absida glauca* had high lipid content in the biomass. The highest lipid content was observed for *Umbelopsis vinacea* (Fig 6). Considering high biomass yield and lipid accumulation, *Umbelopsis vinacea* could be considered as one of the best lipid producers with the potential for industrial application. Several fungi, namely *Absidia glauca*, *Rhizopus stolonifer*, *Amylomyces rouxii*, *Mucor circinelloides*, showed accumulation of polyphosphates in addition to lipids when grown on yeast extract. *Mucor circinelloides* showed the highest content of polyphosphate co-produced along with the relatively high content of lipids (Fig 6). The co-production of lipids along with polyphosphates and chitosan by *Mucor circinelloides* could be considered as one of the co-production concepts for elevating level of sustainability for fungal lipid production, as three products would be produced in a single fermentation process.

PCA of the lipid region of FTIR-HTS spectra showed that when yeast extract was used as N-source, phosphorus availability did not affect the accumulation of lipids in *Umbelopsis vinacea*, *Mortierella hyalina*, and *Mucor circineloides*, and just minimal effect could be seen in case of *Mortierella alpina*. This indicates that for the biotechnological production of lipids by *Mucoromycota* fungi, it would be possible to exclude or limit addition of inorganic phosphorus without any strong effect on biomass and lipid yield when a rich N-source is used. This is of particular importance for reduction of costs in production of lipids for biodiesel. Accumulation of lipids by *Rhizopus stolonifer*, *Cunninghamella blakesleeana*, *Amylomyces rouxii* and *Absidia glauca* was negatively affected when a high concentration of inorganic phosphorus was present in the growth media containing either yeast extract or ammonium sulphate (Fig 7). This can be explained by the ability of co-production of lipids and polyphosphates of these fungi. Polyphosphates were accumulated during the exponential growth phase and therefore

the lipid accumulation might have been suppressed, since both, polyphosphates and lipids serve as energy storage in the fungal cells. The strongest effect of phosphorus was detected when fungi were grown on ammonium sulphate-based media, where the decrease in phosphorus availability led to a lower lipid content for all fungi except *Cunninghamella blakesleeana*. Pi2 condition doubled the biomass yield of *Mortierella* fungi known as excellent producers of high- valued polyunsaturated fatty acids.

Further, FTIR-HTS data were utilized to study nutrient-induced co-production strategies for concomitant production of lipids, polyphosphate and chitin/chitosan in *Mucoromycota* fungi. A co-production of polyphosphate and lipids was observed for fungi *Rhizopus stolonifer*, *Mucor circinelloides*, *Amylomyces rouxii* and *Absidia glauca* grown in both yeast- and ammonium-based media (Fig 6). A big increase in the polyphosphate accumulation was observed in media with the high level of phosphorus (Pi2 –Pi8). Thus, these fungi could be considered as promising strains from the view of increasing sustainability in microbial-lipid biorefinery and phosphorus recovery. The co-production of polyphosphate in addition to lipids was not detected for *Mortierella* fungi and *Umbelopsis vinacea*. The co-production of chitin/chitosan generally occured in all types of media, since these polymers are principle structural components of *Mucoromycota* fungi cell wall. The main reason for the overproduction of chitin/chitosan accompanied with the decreased lipid production in AS-Pi media under low Pi levels could be an acidic stress caused by the low Pi concentrations. The obtained results are in accordance with results reported in literature showing that chitin overproduction in the cell wall of *Mucoromycota* fungi is induced by acidic pH of the growth media [94]. Taking in account high biomass yield, the total chitin/chitosan yield in YE-Pi media could be higher than in AS-Pi media with low Pi levels. When using inorganic nitrogen source, it is possible to stimulate the overproduction of chitin/chitosan in some *Mucoromycota* fungi by limiting inorganic phosphorus. This finding is in agreement with chitosan yield optimization in *Mucor indicus*, where phosphate-free medium was reported to result in the highest chitosan production [95].

Production of chitin and chitosan from fungal mycelium has significant advantages in comparison to traditional way from crustacean waste. For example, microbial production is not dependent on a season and fishing industry, it does not require demineralization process, and the composition of chitin and chitosan is more consistent compared to crustacean waste materials [96, 97]. Chitin/chitosan creates side-stream product and additional value for the process. Although optimization of the biomass yield for chitin/chitosan and lipid co-production was not the primary goal of this study, there is a potential to enhance the yields by modification of C/N ratio, pH, aeration, cultivation temperature and time [22, 98, 99].

Generally, the co-production concept of bioproduction in some cases may lead to the use of different downstream processes, while in the case of oleaginous fungal biomass, co-produced lipids and chitin/chitosan are located in different cell compartments (lipids in lipid droplets, chitin/chitosan in cell wall) and therefore they can be separated relatively easy by using, for example, solvent-based or super critical fluid extraction. Lipids and chitin/chitosan are carbon-based products. Therefore, achieving a high yield of lipids will be at the expense of the yield of chitin/chitosan and vice versa. However, it is important to note that chitin/chitosan are the principle components of the fungal cell wall. Thus, even with the highest possible lipid yield, the cell wall, which is an essential part of the fungal cells, will always constitute a rest product after lipid extraction. The separation of polyphosphate could be challenging since its located both intracellularly and in the cell wall. Further, it's important to note that co-production concept is particularly beneficial for producing microbial biomass to be consumed as a whole, as for example fungal biomass enriched in lipids, chitin/chitosan and polyphosphates could be particularly beneficial as a whole for fish feed applications.

4. Conclusion

The presented study reveals a nutrient-induced co-production of industrially important metabolites, namely lipids, polyphosphates and chitin/chitosan in oleaginous *Mucoromycota* fungi using FTIR spectroscopy. The co-production was shown to depend sensitively on the presence and concentration of macronutrients in the substrates, namely six different phosphorus levels and two nitrogen sources (yeast extract and ammonium sulphate). Since the co-production of different high-value products is closely related to the sustainability of the process, our study can be considered as an assessment of the biotechnological potential of the nine different oleaginous *Mucoromycota* grown on nitrogen-limited conditions. Ammonium sulphate growth media enabled full control over the media composition, and thus the overview of the effect of different phosphorus levels on the fungal growth and metabolism.

As polyphosphate accumulating fungi, we have identified *Mucor circinelloides*, *Amylomyces rouxii*, *Rhizopus stolonifer* and *Absidia glauca*. These fungi showed a potential for the co-production of lipids and polyphosphates. Further, phosphorus limiting conditions led to low pH which induced over co-production of chitin/chitosan for *Rhizopus stolonifer*, *Mucor circinelloides*, *Amylomyces rouxii* and *Absidia glauca* in AS-Pi media. In addition, *Rhizopus stolonifer* showed an obvious advantage in managing Pi deficiency, since its growth in AS-Pi was not remarkably affected by phosphorus limitation. *Mucor circinelloides* has a high biotechnological potential for the co-production of three products, namely chitin/chitosan, lipids and polyphosphates in a single cultivation. *Umbelopsis vinacea* was identified as the best biomass and lipid producer, the yields were almost twice as high as for the other studied fungi. These findings are important for developing sustainable modern microbial lipid biorefineries. This study demonstrates that Fourier transform infrared spectroscopy allows to monitor any chemical bioprocess compound in media and cells without tedious sample preparation and extraction steps and is a powerful tool that can be used for developing and monitoring novel biotechnological processes.

Supporting information

S1 Fig. FTIR-HTS spectra of *Absidia glauca* (EMSC corrected); ammonium sulphate nitrogen source, different Pi-levels.
(DOCX)

S2 Fig. FTIR-HTS spectra of *Absidia glauca* (EMSC corrected); yeast extract nitrogen source, different Pi-levels.
(DOCX)

S3 Fig. FTIR-HTS spectra of *Amylomyces rouxii* (EMSC corrected); ammonium sulphate nitrogen source, different Pi-levels.
(DOCX)

S4 Fig. FTIR-HTS spectra of *Amylomyces rouxii* (EMSC corrected); yeast extract nitrogen source, different Pi-levels.
(DOCX)

S5 Fig. FTIR-HTS spectra of *Cunninghamella blakesleeana* (EMSC corrected); ammonium sulphate nitrogen source, different Pi-levels.
(DOCX)

S6 Fig. FTIR-HTS spectra of *Cunninghamella blakesleeana* (EMSC corrected); yeast extract nitrogen source, different Pi-levels.
(DOCX)

S7 Fig. FTIR-HTS spectra of *Lichtheimia corymbifera* (EMSC corrected); ammonium sulphate nitrogen source, different Pi-levels.
(DOCX)

S8 Fig. FTIR-HTS spectra of *Lichtheimia corymbifera* (EMSC corrected); yeast extract nitrogen source, different Pi-levels.
(DOCX)

S9 Fig. FTIR-HTS spectra of *Mortierella alpina* (EMSC corrected); ammonium sulphate nitrogen source, different Pi-levels.
(DOCX)

S10 Fig. FTIR-HTS spectra of *Mortierella alpina* (EMSC corrected); yeast extract nitrogen source, different Pi-levels.
(DOCX)

S11 Fig. FTIR-HTS spectra of *Mucor circinelloides* (EMSC corrected); ammonium sulphate nitrogen source, different Pi-levels.
(DOCX)

S12 Fig. FTIR-HTS spectra of *Mucor circinelloides* (EMSC corrected); yeast extract nitrogen source, different Pi-levels.
(DOCX)

S13 Fig. FTIR-HTS spectra of *Mortierella hyalina* (EMSC corrected); ammonium sulphate nitrogen source, different Pi-levels.
(DOCX)

S14 Fig. FTIR-HTS spectra of *Mortierella hyalina* (EMSC corrected); yeast extract nitrogen source, different Pi-levels.
(DOCX)

S15 Fig. FTIR-HTS spectra of *Rhizopus stolonifer* (EMSC corrected); ammonium sulphate nitrogen source, different Pi-levels.
(DOCX)

S16 Fig. FTIR-HTS spectra of *Rhizopus stolonifer* (EMSC corrected); yeast extract nitrogen source, different Pi-levels.
(DOCX)

S17 Fig. FTIR-HTS spectra of *Umbelopsis vinacea* (EMSC corrected); ammonium sulphate nitrogen source, different Pi-levels.
(DOCX)

S18 Fig. FTIR-HTS spectra of *Umbelopsis vinacea* (EMSC corrected); yeast extract nitrogen source, different Pi-levels.
(DOCX)

S19 Fig. FTIR-ATR spectra of glucose, ammonium sulphate (AS), phosphate salts, yeast extract (YE) and growth media AS-Pi4 before the cultivation.
(DOCX)

S20 Fig. Titration of 100 ml not autoclaved YE-Pi0.25 (blue) and AS-Pi0.25 (red) with 1M HCl confirmed the buffering properties of yeast extract.
(DOCX)

S1 Table. FTIR raw spectral data: HTS spectra of biomass, ATR spectra of culture supernatant, ATR spectra of reference materials, HTS spectra of culture supernatant MCI_YE_Pi1; MCI_AS_Pi1.
(XLSX)

Acknowledgments

We thank Lene Cecilie Hermansen from Imaging Centre at NMBU for the help with the TEM measurements.

Author Contributions

Conceptualization: Simona Dzurendova, Boris Zimmermann, Achim Kohler, Volha Shapaval.

Data curation: Simona Dzurendova, Boris Zimmermann.

Formal analysis: Simona Dzurendova, Valeria Tafintseva.

Funding acquisition: Achim Kohler, Volha Shapaval.

Investigation: Simona Dzurendova, Boris Zimmermann, Ondrej Slany.

Methodology: Boris Zimmermann, Achim Kohler, Valeria Tafintseva, Volha Shapaval.

Project administration: Achim Kohler, Volha Shapaval.

Resources: Achim Kohler, Volha Shapaval.

Software: Achim Kohler.

Supervision: Boris Zimmermann, Achim Kohler, Volha Shapaval.

Validation: Achim Kohler, Valeria Tafintseva.

Visualization: Simona Dzurendova, Boris Zimmermann, Valeria Tafintseva.

Writing – original draft: Simona Dzurendova.

Writing – review & editing: Simona Dzurendova, Boris Zimmermann, Achim Kohler, Valeria Tafintseva, Ondrej Slany, Milan Certik, Volha Shapaval.

References

1. Cherubini F. The biorefinery concept: using biomass instead of oil for producing energy and chemicals. Energy conversion management. 2010; 51(7):1412–21.
2. Gupta VK, Kubicek CP, Berrin J-G, Wilson DW, Couturier M, Berlin A, et al. Fungal enzymes for bio-products from sustainable and waste biomass. Trends in biochemical sciences. 2016; 41(7):633–45. https://doi.org/10.1016/j.tibs.2016.04.006 PMID: 27211037
3. Karimi S, Mahboobi Soofiani N, Mahboubi A, Taherzadeh M. Use of organic wastes and industrial by-products to produce filamentous fungi with potential as aqua-feed ingredients. Sustainability. 2018; 10 (9):3296.
4. André A, Diamantopoulou P, Philippoussis A, Sarris D, Komaitis M, Papanikolaou S, et al. Biotechnological conversions of bio-diesel derived waste glycerol into added-value compounds by higher fungi: production of biomass, single cell oil and oxalic acid. Industrial Crops. 2010; 31(2):407–16.
5. Meyer V, Andersen MR, Brakhage AA, Braus GH, Caddick MX, Cairns TC, et al. Current challenges of research on filamentous fungi in relation to human welfare and a sustainable bio-economy: a white paper. Fungal biology and biotechnology. 2016; 3(1):6.

6. Ferreira JA, Lennartsson PR, Edebo L, Taherzadeh MJ. Zygomycetes-based biorefinery: Present status and future prospects. Bioresource technology. 2013; 135:523–32. https://doi.org/10.1016/j.biortech.2012.09.064 PMID: 23127833
7. Ochsenreither K, Glück C, Stressler T, Fischer L, Syldatk C. Production Strategies and Applications of Microbial Single Cell Oils. 2016; 7(1539). https://doi.org/10.3389/fmicb.2016.01539 PMID: 27761130
8. Vongsangnak W, Ruenwai R, Tang X, Hu X, Zhang H, Shen B, et al. Genome-scale analysis of the metabolic networks of oleaginous Zygomycete fungi. Gene. 2013; 521(1):180–90. https://doi.org/10.1016/j.gene.2013.03.012 PMID: 23541380
9. Ratledge C. Fatty acid biosynthesis in microorganisms being used for single cell oil production. Biochimie. 2004; 86(11):807–15. https://doi.org/10.1016/j.biochi.2004.09.017 PMID: 15589690
10. Kosa G, Zimmermann B, Kohler A, Ekeberg D, Afseth NK, Mounier J, et al. High-throughput screening of Mucoromycota fungi for production of low-and high-value lipids. Biotechnology for biofuels. 2018; 11(1):66.
11. Sakuradani E, Shimizu S. Single cell oil production by Mortierella alpina. Journal of biotechnology. 2009; 144(1):31–6. https://doi.org/10.1016/j.jbiotec.2009.04.012 PMID: 19409938
12. Shinmen Y, Shimizu S, Akimoto K, Kawashima H, Yamada H. Production of arachidonic acid by Mortierella fungi. Applied Microbiology and Biotechnology. 1989; 31(1):11–6.
13. Khot M, Kamat S, Zinjarde S, Pant A, Chopade B, RaviKumar A. Single cell oil of oleaginous fungi from the tropical mangrove wetlands as a potential feedstock for biodiesel. Microbial Cell Factories. 2012; 11(1):71.
14. Ratledge C. Single cell oils for the 21st century. In: Cohen ZR, C., editor. Single cell oils: microbial and algal oils: Elsevier; 2010. p. 3–26.
15. Yadav AN, Mishra S, Singh S, Gupta A. Recent Advancement in White Biotechnology Through Fungi: Springer; 2019.
16. Santek MI, Beluhan S, Santek BJAiB, Bioenergy. Production of microbial lipids from lignocellulosic biomass. 2018:137–64.
17. Zininga JT, Puri AK, Govender A, Singh S, Permaul KJBt. Concomitant production of chitosan and lipids from a newly isolated Mucor circinelloides ZSKP for biodiesel production. Bioresource technology. 2019; 272:545–51. https://doi.org/10.1016/j.biortech.2018.10.035 PMID: 30391848
18. Liao W, Liu Y, Frear C, Chen S. Co-production of fumaric acid and chitin from a nitrogen-rich lignocellulosic material–dairy manure–using a pelletized filamentous fungus Rhizopus oryzae ATCC 20344. Bioresource technology. 2008; 99(13):5859–66. https://doi.org/10.1016/j.biortech.2007.10.006 PMID: 18006305
19. Liu Y, Liao W, Chen S-l. Co-production of lactic acid and chitin using a pelletized filamentous fungus Rhizopus oryzae cultured on cull potatoes and glucose. Journal of applied microbiology. 2008; 105(5):1521–8. https://doi.org/10.1111/j.1365-2672.2008.03913.x PMID: 19146489
20. Satari B, Karimi K, Taherzadeh M, Zamani A. Co-production of fungal biomass derived constituents and ethanol from citrus wastes free sugars without auxiliary nutrients in airlift bioreactor. International journal of molecular sciences. 2016; 17(3):302. https://doi.org/10.3390/ijms17030302 PMID: 26927089
21. Raghukumar S. Fungi in coastal and oceanic marine ecosystems: Springer; 2017.
22. Tan SC, Tan TK, Wong SM, Khor E. The chitosan yield of zygomycetes at their optimum harvesting time. Carbohydrate Polymers. 1996; 30(4):239–42.
23. Bartnicki-Garcia S, Lippman E. Fungal morphogenesis: cell wall construction in Mucor rouxii. Science. 1969; 165(3890):302–4. https://doi.org/10.1126/science.165.3890.302 PMID: 5787989
24. Werner TP, Amrhein N, Freimoser FM, Biology. Specific localization of inorganic polyphosphate (poly P) in fungal cell walls by selective extraction and immunohistochemistry. Fungal Genetics Biology. 2007; 44(9):845–52. https://doi.org/10.1016/j.fgb.2007.01.008 PMID: 17320430
25. Beever RE, Burns D. Phosphorus uptake, storage and utilization by fungi. Advances in botanical research. 8: Elsevier; 1981. p. 127–219.
26. Ye Y, Gan J, Hu B. Screening of phosphorus-accumulating fungi and their potential for phosphorus removal from waste streams. Applied biochemistry biotechnology. 2015; 177(5):1127–36. https://doi.org/10.1007/s12010-015-1801-1 PMID: 26280802
27. El Wali M, Golroudbary SR, Kraslawski A. Impact of recycling improvement on the life cycle of phosphorus. Chinese Journal of Chemical Engineering. 2019; 27(5):1219–29.
28. Appels L, Degrève J, Van der Bruggen B, Van Impe J, Dewil R. Influence of low temperature thermal pre-treatment on sludge solubilisation, heavy metal release and anaerobic digestion. Bioresource technology. 2010; 101(15):5743–8. https://doi.org/10.1016/j.biortech.2010.02.068 PMID: 20335023

29. Wang L, Ridgway D, Gu T, Moo-Young M. Bioprocessing strategies to improve heterologous protein production in filamentous fungal fermentations. Biotechnology advances. 2005; 23(2):115–29. https://doi.org/10.1016/j.biotechadv.2004.11.001 PMID: 15694123

30. Lu J, Peng C, Ji X-J, You J, Cong L, Ouyang P, et al. Fermentation Characteristics of Mortierella alpina in Response to Different Nitrogen Sources. Applied Biochemistry Biotechnology advances. 2011; 164 (7):979–90. https://doi.org/10.1007/s12010-011-9189-z PMID: 21336613

31. Papanikolaou S, Galiotou-Panayotou M, Fakas S, Komaitis M, Aggelis G. Lipid production by oleaginous Mucorales cultivated on renewable carbon sources. European Journal of Lipid Science Technology. 2007; 109(11):1060–70.

32. Botha A, Strauss T, Kock J, Pohl C, Coetzee D. Carbon source utilization and γ-linolenic acid production by Mucoralean fungi. Systematic applied microbiology. 1997; 20(1):165–70.

33. Lindberg A-M, Hansson L. Production of ψ-linolenic acid by the fungus Mucor rouxii on cheap nitrogen and carbon sources. Applied microbiology biotechnology advances. 1991; 36(1):26–8.

34. Lima MABd, Nascimento AEd, Wd Souza, Fukushima K, Campos-Takaki GMd. Effects of phosphorus on polyphosphate accumulation by Cunninghamella elegans. Brazilian Journal of Microbiology. 2003; 34:363–72.

35. Schmitt J, Flemming H-C. FTIR-spectroscopy in microbial and material analysis. International Biodeterioration and Biodegradation. 1998; 41(1):1–11.

36. Shapaval V, Schmitt J, Møretrø T, Suso H, Skaar I, Åsli A, et al. Characterization of food spoilage fungi by FTIR spectroscopy. Journal of applied microbiology. 2013; 114(3):788–96. https://doi.org/10.1111/jam.12092 PMID: 23210658

37. Shapaval V, Møretrø T, Suso HP, Åsli AW, Schmitt J, Lillehaug D, et al. A high-throughput microcultivation protocol for FTIR spectroscopic characterization and identification of fungi. Journal of biophotonics. 2010; 3(8-9):512–21. https://doi.org/10.1002/jbio.201000014 PMID: 20414905

38. Santos C, Fraga ME, Kozakiewicz Z, Lima N. Fourier transform infrared as a powerful technique for the identification and characterization of filamentous fungi and yeasts. Research in microbiology. 2010; 161 (2):168–75. https://doi.org/10.1016/j.resmic.2009.12.007 PMID: 20079832

39. Salman A, Tsror L, Pomerantz A, Moreh R, Mordechai S, Huleihel M. FTIR spectroscopy for detection and identification of fungal phytopathogenes. Spectroscopy. 2010; 24(3–4):261–7.

40. Lecellier A, Gaydou V, Mounier J, Hermet A, Castrec L, Barbier G, et al. Implementation of an FTIR spectral library of 486 filamentous fungi strains for rapid identification of molds. Food microbiology. 2015; 45:126–34. https://doi.org/10.1016/j.fm.2014.01.002 PMID: 25481069

41. Shaligram NS, Bule M, Bhambure R, Singhal RS, Singh SK, Szakacs G, et al. Biosynthesis of silver nanoparticles using aqueous extract from the compactin producing fungal strain. Process biochemistry. 2009; 44(8):939–43.

42. Erukhimovitch V, Pavlov V, Talyshinsky M, Souprun Y, Huleihel M. FTIR microscopy as a method for identification of bacterial and fungal infections. Journal of pharmaceutical and biomedical analysis. 2005; 37(5):1105–8. https://doi.org/10.1016/j.jpba.2004.08.010 PMID: 15862692

43. Kamnev AAJJoS. FTIR spectroscopic studies of bacterial cellular responses to environmental factors, plant-bacterial interactions and signalling. 2008; 22(2–3):83–95.

44. Tang M, McEwen GD, Wu Y, Miller CD, Zhou AJ. Characterization and analysis of mycobacteria and Gram-negative bacteria and co-culture mixtures by Raman microspectroscopy, FTIR, and atomic force microscopy. Analytical and bioanalytical chemistry. 2013; 405(5):1577–91. https://doi.org/10.1007/s00216-012-6556-8 PMID: 23196750

45. Vongsvivut J, Heraud P, Gupta A, Puri M, McNaughton D, Barrow CJ. FTIR microspectroscopy for rapid screening and monitoring of polyunsaturated fatty acid production in commercially valuable marine yeasts and protists. Analyst. 2013; 138(20):6016–31. https://doi.org/10.1039/c3an00485f PMID: 23957051

46. Corte L, Tiecco M, Roscini L, Germani R, Cardinali G. FTIR analysis of the metabolomic stress response induced by N-alkyltropinium bromide surfactants in the yeasts Saccharomyces cerevisiae and Candida albicans. Colloids and Surfaces B: Biointerfaces. 2014; 116:761–71. https://doi.org/10.1016/j.colsurfb.2014.01.054 PMID: 24582147

47. Correa-García S, Bermúdez-Moretti M, Travo A, Déléris G, Forfar I. FTIR spectroscopic metabolome analysis of lyophilized and fresh Saccharomyces cerevisiae yeast cells. Analytical Methods. 2014; 6 (6):1855–61.

48. Colabella C, Corte L, Roscini L, Shapaval V, Kohler A, Tafintseva V, et al. Merging FT-IR and NGS for simultaneous phenotypic and genotypic identification of pathogenic Candida species. PloS one. 2017; 12(12).

49. Shapaval V, Walczak B, Gognies S, Møretrø T, Suso H, Åsli AW, et al. FTIR spectroscopic characterization of differently cultivated food related yeasts. Analyst. 2013; 138(14):4129–38. https://doi.org/10.1039/c3an00304c PMID: 23741734

50. Kohler A, Böcker U, Shapaval V, Forsmark A, Andersson M, Warringer J, et al. High-throughput biochemical fingerprinting of Saccharomyces cerevisiae by Fourier transform infrared spectroscopy. PLoS One. 2015; 10(2).

51. Wagner H, Liu Z, Langner U, Stehfest K, Wilhelm C. The use of FTIR spectroscopy to assess quantitative changes in the biochemical composition of microalgae. Journal of biophotonics. 2010; 3(8-9):557–66. https://doi.org/10.1002/jbio.201000019 PMID: 20503222

52. Jebsen C, Norici A, Wagner H, Palmucci M, Giordano M, Wilhelm C. FTIR spectra of algal species can be used as physiological fingerprints to assess their actual growth potential. Physiologia plantarum. 2012; 146(4):427–38. https://doi.org/10.1111/j.1399-3054.2012.01636.x PMID: 22540209

53. Mayers JJ, Flynn KJ, Shields RJ. Rapid determination of bulk microalgal biochemical composition by Fourier-Transform Infrared spectroscopy. Bioresource technology. 2013; 148:215–20. https://doi.org/10.1016/j.biortech.2013.08.133 PMID: 24050924

54. Kosa G, Shapaval V, Kohler A, Zimmermann B. FTIR spectroscopy as a unified method for simultaneous analysis of intra-and extracellular metabolites in high-throughput screening of microbial bioprocesses. Microbial cell factories. 2017; 16(1):195. https://doi.org/10.1186/s12934-017-0817-3 PMID: 29132358

55. Veale EL, Irudayaraj J, Demirci A. An on-line approach to monitor ethanol fermentation using FTIR spectroscopy. Biotechnology progress. 2007; 23(2):494–500. https://doi.org/10.1021/bp060306v PMID: 17311406

56. Ami D, Posteri R, Mereghetti P, Porro D, Doglia SM, Branduardi P. Fourier transform infrared spectroscopy as a method to study lipid accumulation in oleaginous yeasts. Biotechnology for biofuels. 2014; 7(1):12. https://doi.org/10.1186/1754-6834-7-12 PMID: 24450603

57. Liu J, Mukherjee J, Hawkes JJ, Wilkinson SJ. Optimization of lipid production for algal biodiesel in nitrogen stressed cells of Dunaliella salina using FTIR analysis. Journal of Chemical Technology and Biotechnology. 2013; 88(10):1807–14.

58. Enshaeieh M, Abdoli A, Nahvi I, Madani M. Bioconversion of different carbon sources in to microbial oil and biodiesel using oleaginous yeasts. Journal of biology and today's world. 2012; 1(2):82–92.

59. Brar K, Sarma A, Aslam M, Polikarpov I, Chadha B. Potential of oleaginous yeast Trichosporon sp., for conversion of sugarcane bagasse hydrolysate into biodiesel. Bioresource technology. 2017; 242:161–8. https://doi.org/10.1016/j.biortech.2017.03.155 PMID: 28438358

60. Yehia R, Ali E, Al-Zahrani A. Feasibility of oleaginous fungi isolated from soil samples of Saudi Arabia for mycodiesel production. Applied biochemistry and microbiology. 2017; 53(1):94–100.

61. Shapaval V, Brandenburg J, Blomqvist J, Tafintseva V, Passoth V, Sandgren M, et al. Biochemical profiling, prediction of total lipid content and fatty acid profile in oleaginous yeasts by FTIR spectroscopy. Biotechnology for biofuels. 2019; 12(1):140.

62. Cardoso A, Lins CIM, dos Santos ER, Silva MCF, Campos-Takaki GM. Microbial enhance of chitosan production by Rhizopus arrhizus using agroindustrial substrates. Molecules. 2012; 17(5):4904–14. https://doi.org/10.3390/molecules17054904 PMID: 22543505

63. Di Mario F, Rapana P, Tomati U, Galli E. Chitin and chitosan from Basidiomycetes. International Journal of Biological Macromolecules. 2008; 43(1):8–12. https://doi.org/10.1016/j.ijbiomac.2007.10.005 PMID: 18023863

64. Teng WL, Khor E, Tan TK, Lim LY, Tan SCJCr. Concurrent production of chitin from shrimp shells and fungi. 2001; 332(3):305–16.

65. Wu T, Zivanovic S, Draughon FA, Conway WS, Sams CE. Physicochemical properties and bioactivity of fungal chitin and chitosan. Journal of agricultural and food chemistry. 2005; 53(10):3888–94. https://doi.org/10.1021/jf048202s PMID: 15884813

66. Khoshmanesh A, Cook PL, Wood BR. Quantitative determination of polyphosphate in sediments using Attenuated Total Reflectance-Fourier Transform Infrared (ATR-FTIR) spectroscopy and partial least squares regression. Analyst. 2012; 137(16):3704–9. https://doi.org/10.1039/c2an35289c PMID: 22801463

67. Ojeda JJ, Dittrich M. Fourier transform infrared spectroscopy for molecular analysis of microbial cells. Microbial Systems Biology: Springer; 2012. p. 187–211.

68. Forfang K, Zimmermann B, Kosa G, Kohler A, Shapaval V. FTIR spectroscopy for evaluation and monitoring of lipid extraction efficiency for oleaginous fungi. PloS one. 2017; 12(1):e0170611. https://doi.org/10.1371/journal.pone.0170611 PMID: 28118388

69. Shapaval V, Afseth NK, Vogt G, Kohler A. Fourier transform infrared spectroscopy for the prediction of fatty acid profiles in Mucor fungi grown in media with different carbon sources. Microbial cell factories. 2014; 13(1):86. https://doi.org/10.1186/1475-2859-13-86 PMID: 25208488

70. Kosa G, Vuoristo KS, Horn SJ, Zimmermann B, Afseth NK, Kohler A, et al. Assessment of the scalability of a microtiter plate system for screening of oleaginous microorganisms. Applied microbiology and biotechnology. 2018; 102(11):4915–25. https://doi.org/10.1007/s00253-018-8920-x PMID: 29644428

71. Xiong Y, Shapaval V, Kohler A, From PJ. A Laboratory-Built Fully Automated Ultrasonication Robot for Filamentous Fungi Homogenization. SLAS TECHNOLOGY: Translating Life Sciences Innovation. 2019:2472630319861361.

72. Li J, Shapaval V, Kohler A, Talintyre R, Schmitt J, Stone R, et al. A modular liquid sample handling robot for high-throughput Fourier transform infrared spectroscopy. Advances in reconfigurable mechanisms and robots II: Springer; 2016. p. 769–78.

73. Xiong Y, Shapaval V, Kohler A, Li J, From PJ. A Fully Automated Robot for the Preparation of Fungal Samples for FTIR Spectroscopy Using Deep Learning. IEEE Access. 2019; 7:132763–74.

74. Walther G, Wagner L, Kurzai O. Updates on the taxonomy of Mucorales with an emphasis on clinically important taxa. Journal of Fungi. 2019; 5(4):106.

75. Kavadia A, Komaitis M, Chevalot I, Blanchard F, Marc I, Aggelis G. Lipid and γ-linolenic acid accumulation in strains of Zygomycetes growing on glucose. Journal of the American Oil Chemists' Society. 2001; 78(4):341–6.

76. Kosa G, Kohler A, Tafintseva V, Zimmermann B, Forfang K, Afseth NK, et al. Microtiter plate cultivation of oleaginous fungi and monitoring of lipogenesis by high-throughput FTIR spectroscopy. Microbial cell factories. 2017; 16(1):101. https://doi.org/10.1186/s12934-017-0716-7 PMID: 28599651

77. Zeng Y, Ji X-J, Chang S-M, Nie Z-K, Huang H. Improving arachidonic acid accumulation in Mortierella alpina through B-group vitamin addition. Bioprocess biosystems engineering. 2012; 35(5):683–8. https://doi.org/10.1007/s00449-011-0648-2 PMID: 22052233

78. Demšar J, Curk T, Erjavec A, Gorup Č, Hočevar T, Milutinovič M, et al. Orange: data mining toolbox in Python. The Journal of Machine Learning Research. 2013; 14(1):2349–53.

79. Toplak M, Birarda G, Read S, Sandt C, Rosendahl S, Vaccari L, et al. Infrared orange: connecting hyperspectral data with machine learning. Synchrotron Radiation News. 2017; 30(4):40–5.

80. Zimmermann B, Kohler A. Optimizing Savitzky-Golay parameters for improving spectral resolution and quantification in infrared spectroscopy. Applied spectroscopy. 2013; 67(8):892–902. https://doi.org/10.1366/12-06723 PMID: 23876728

81. Afseth NK, Kohler A. Extended multiplicative signal correction in vibrational spectroscopy, a tutorial. Chemometrics and Intelligent Laboratory Systems. 2012; 117:92–9.

82. Kohler A, Kirschner C, Oust A, Martens H. Extended multiplicative signal correction as a tool for separation and characterization of physical and chemical information in Fourier transform infrared microscopy images of cryo-sections of beef loin. Applied spectroscopy. 2005; 59(6):707–16. https://doi.org/10.1366/0003702054280649 PMID: 16053536

83. Harrington PdB, Vieira NE, Espinoza J, Nien JK, Romero R, Yergey AL. Analysis of variance–principal component analysis: A soft tool for proteomic discovery. Analytica chimica acta. 2005; 544(1–2):118–27.

84. Smilde AK, Jansen JJ, Hoefsloot HC, Lamers R-JA, Van Der Greef J, Timmerman ME. ANOVA-simultaneous component analysis (ASCA): a new tool for analyzing designed metabolomics data. Bioinformatics. 2005; 21(13):3043–8. https://doi.org/10.1093/bioinformatics/bti476 PMID: 15890747

85. Cárdenas G, Cabrera G, Taboada E, Miranda SP. Chitin characterization by SEM, FTIR, XRD, and 13C cross polarization/mass angle spinning NMR. Journal of Applied Polymer Science. 2004; 93(4):1876–85.

86. Guillen MD, Cabo N. Relationships between the composition of edible oils and lard and the ratio of the absorbance of specific bands of their Fourier transform infrared spectra. Role of some bands of the fingerprint region. Journal of Agricultural and Food Chemistry. 1998; 46(5):1788–93. https://doi.org/10.1021/jf9705274 WOS:000073757800014.

87. Byler DM, Susi H. Examination of the secondary structure of proteins by deconvolved FTIR spectra. Biopolymers: Original Research on Biomolecules. 1986; 25(3):469–87.

88. Barth A. Infrared spectroscopy of proteins. Biochimica et Biophysica Acta -Bioenergetics. 2007; 1767(9):1073–101.

89. Krimm S, Bandekar J. Vibrational spectroscopy and conformation of peptides, polypeptides, and proteins. Advances in protein chemistry. 38: Elsevier; 1986. p. 181–364. https://doi.org/10.1016/s0065-3233(08)60528-8 PMID: 3541539

90. Shurvell H. Handbook of Vibrational Spectroscopy, vol. 1. John Wiley & Sons, New York, NY, USA; 2001.

91. Signori L, Ami D, Posteri R, Giuzzi A, Mereghetti P, Porro D, et al. Assessing an effective feeding strategy to optimize crude glycerol utilization as sustainable carbon source for lipid accumulation in oleaginous yeasts. Microb Cell Fact. 2016; 15:75. https://doi.org/10.1186/s12934-016-0467-x PMID: 27149859; PubMed Central PMCID: PMC4858929.

92. Rothschild LJ, Mancinelli RL. Life in extreme environments. Nature. 2001; 409(6823):1092. https://doi.org/10.1038/35059215 PMID: 11234023

93. Seufferheld MJ, Alvarez HM, Farias ME. Role of polyphosphates in microbial adaptation to extreme environments. Appl Environ Microbiol. 2008; 74(19):5867–74. https://doi.org/10.1128/AEM.00501-08 PMID: 18708516

94. Bignell E. The molecular basis of pH sensing, signaling, and homeostasis in fungi. Advances in applied microbiology. 79: Elsevier; 2012. p. 1–18. https://doi.org/10.1016/B978-0-12-394318-7.00001-2 PMID: 22569515

95. Safaei Z, Karimi K, Zamani A. Impact of phosphate, potassium, yeast extract, and trace metals on chitosan and metabolite production by Mucor indicus. International journal of molecular sciences. 2016; 17 (9):1429.

96. Kumar MNR. A review of chitin and chitosan applications. Reactive functional polymers. 2000; 46(1):1–27.

97. White SA, Farina PR, Fulton I. Production and isolation of chitosan from Mucor rouxii. Appl Environ Microbiol. 1979; 38(2):323–8. PMID: 518086

98. Kim WJ, Lee WG, Theodore K, Chang HN. Optimization of culture conditions and continuous production of chitosan by the fungi, Absidia coerulea. Biotechnology and Bioprocess Engineering. 2001; 6 (1):6–10.

99. Hu K-J, Hu J-L, Ho K-P, Yeung K-W. Screening of fungi for chitosan producers, and copper adsorption capacity of fungal chitosan and chitosanaceous materials. Carbohydrate Polymers. 2004; 58(1):45–52.

Supplementary Material

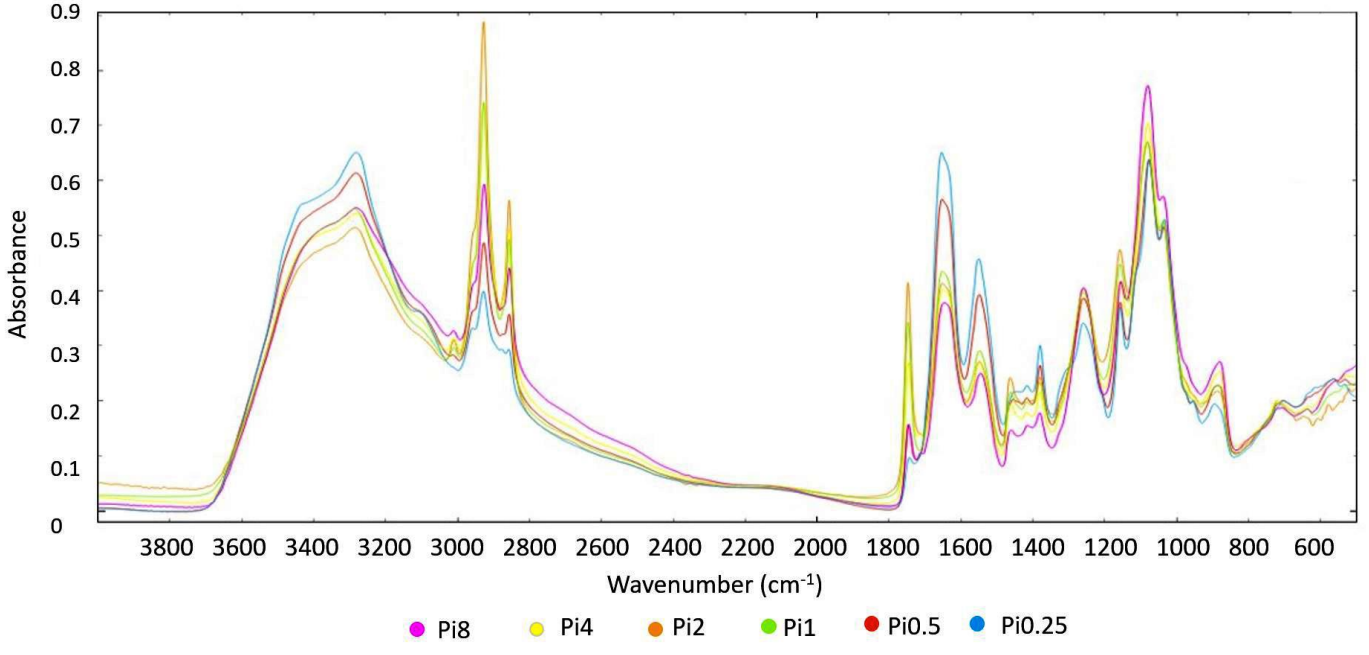

Supplementary Figure 1. FTIR-HTS spectra of *Absidia glauca* (EMSC corrected); ammonium sulphate nitrogen source, different Pi-levels

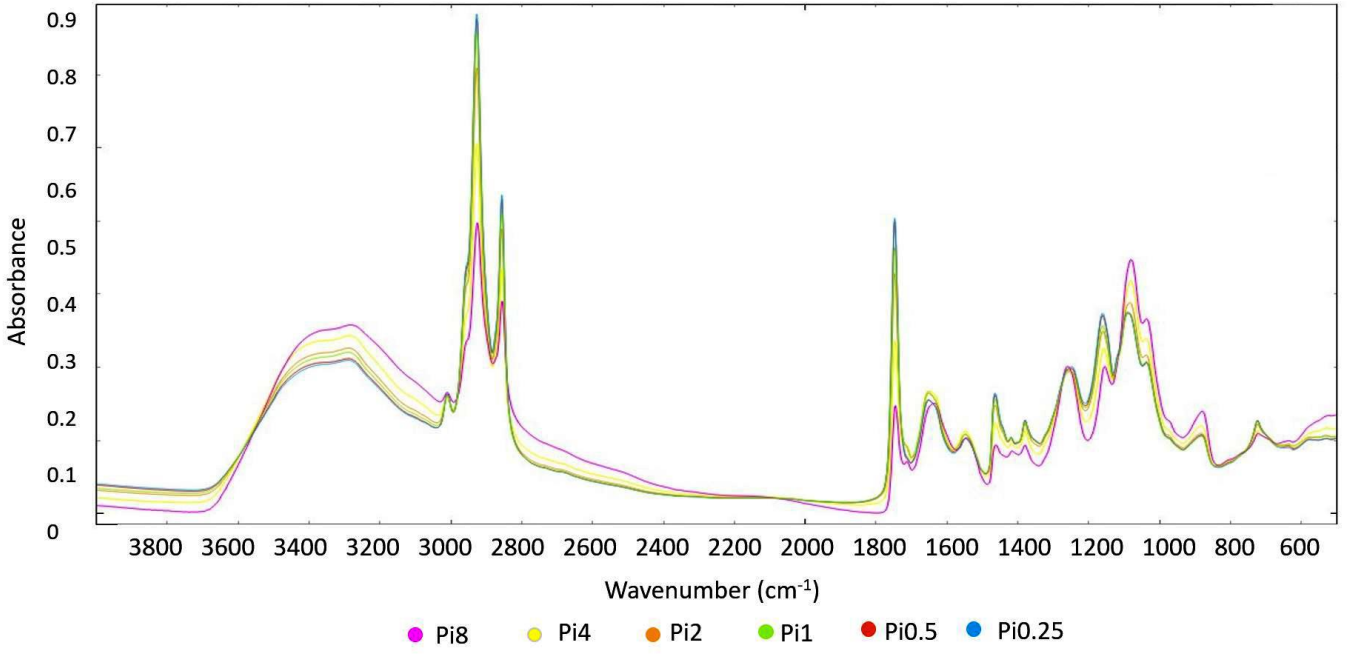

Supplementary Figure 2. FTIR-HTS spectra of *Absidia glauca* (EMSC corrected); yeast extract nitrogen source, different Pi-levels

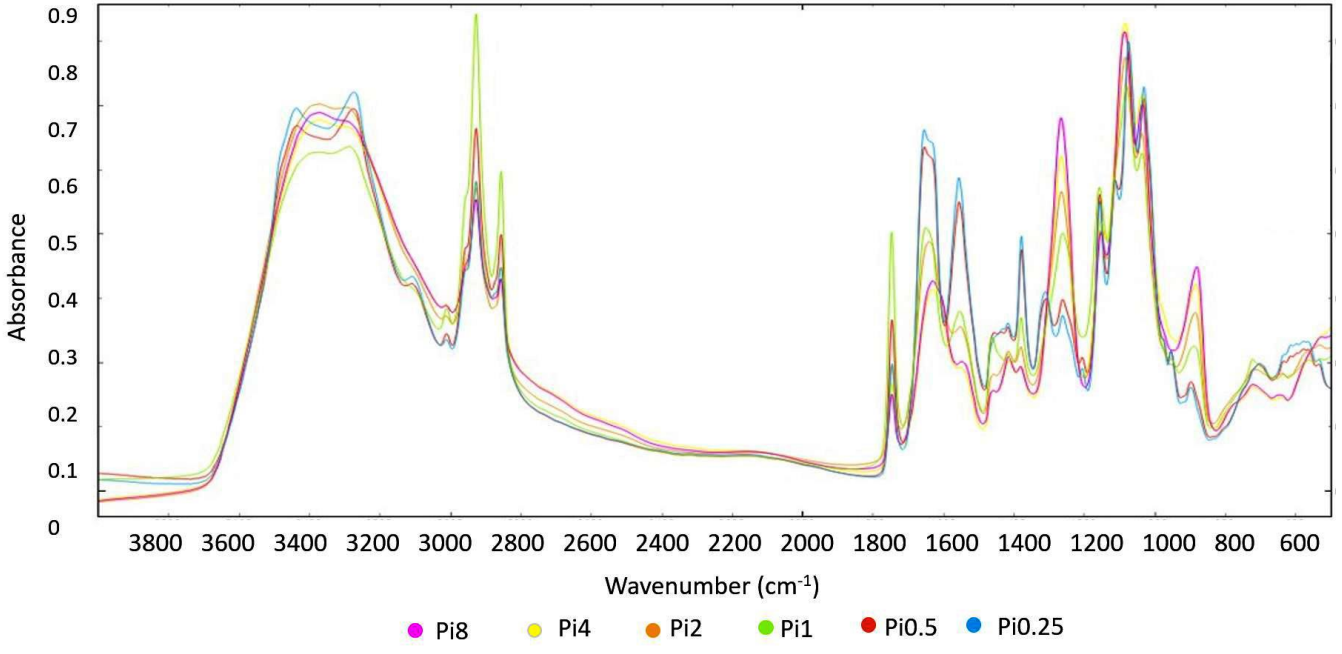

Supplementary Figure 3. FTIR-HTS spectra of *Amylomyces rouxii* (EMSC corrected); ammonium sulphate nitrogen source, different Pi-levels

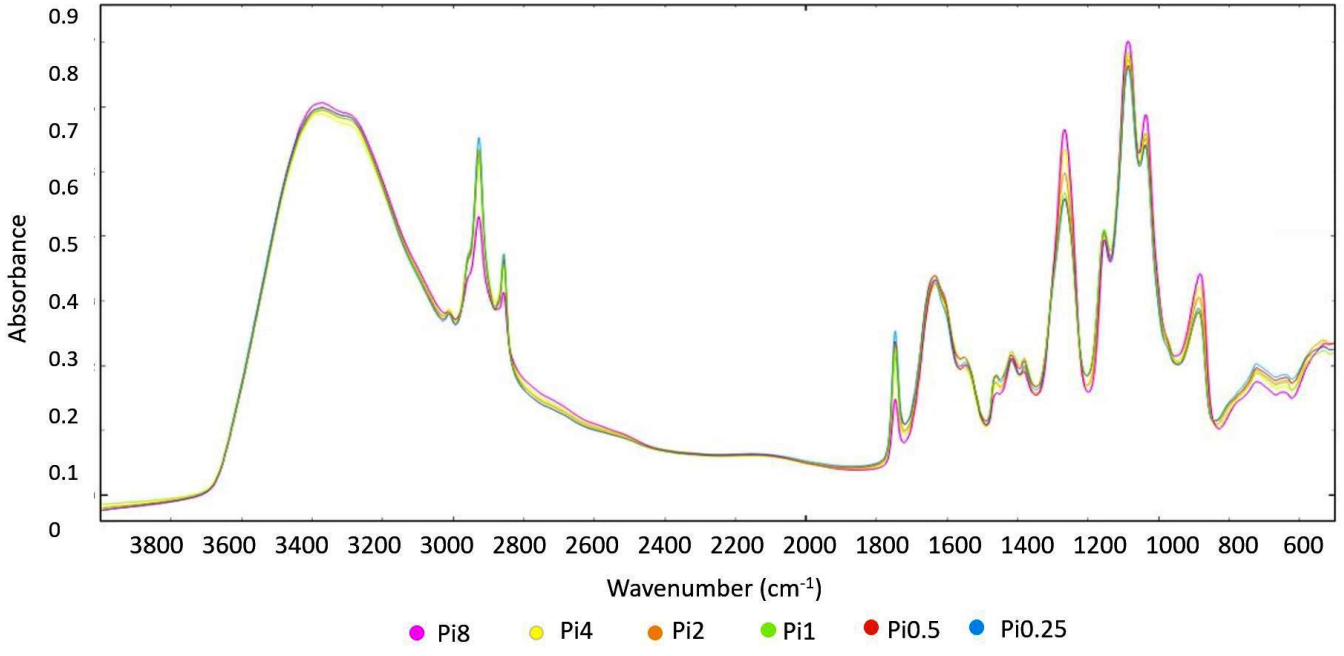

Supplementary Figure 4. FTIR-HTS spectra of *Amylomyces rouxii* (EMSC corrected); yeast extract nitrogen source, different Pi-levels

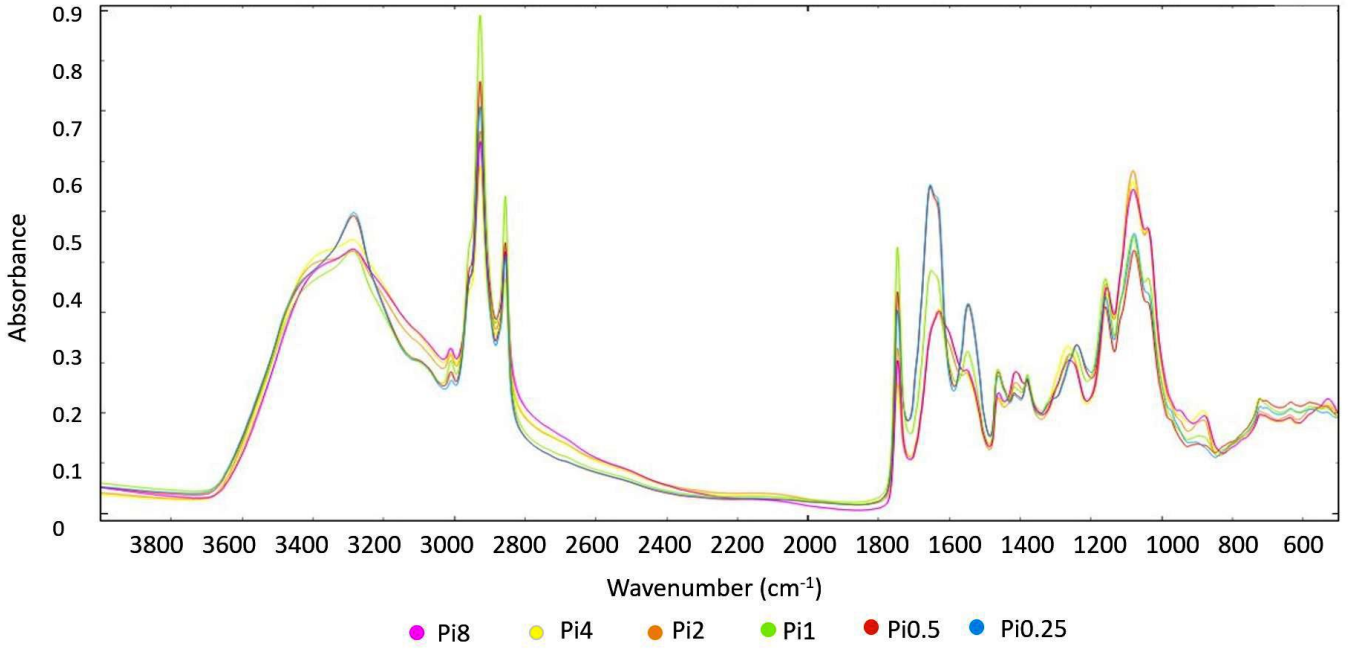

Supplementary Figure 5. FTIR-HTS spectra of *Cunninghamella blakesleeana* (EMSC corrected); ammonium sulphate nitrogen source, different Pi-levels

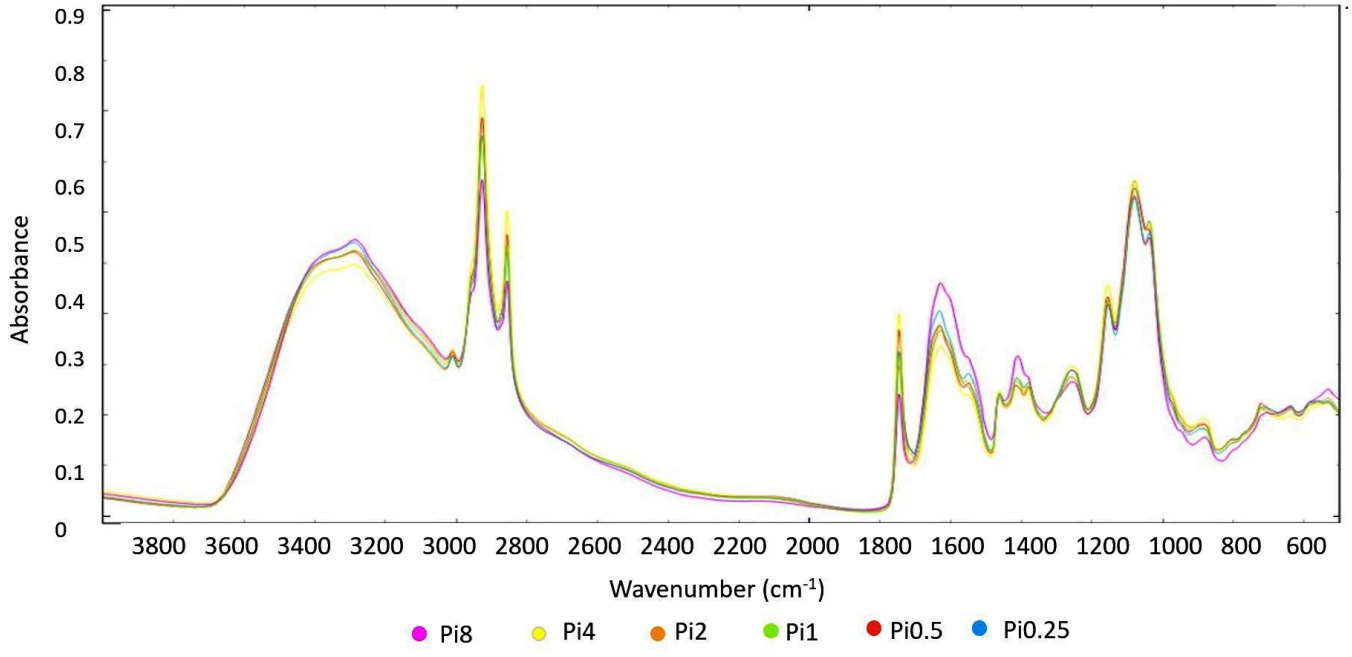

Supplementary Figure 6. FTIR-HTS spectra of *Cunninghamella blakesleeana* (EMSC corrected); yeast extract nitrogen source, different Pi-levels

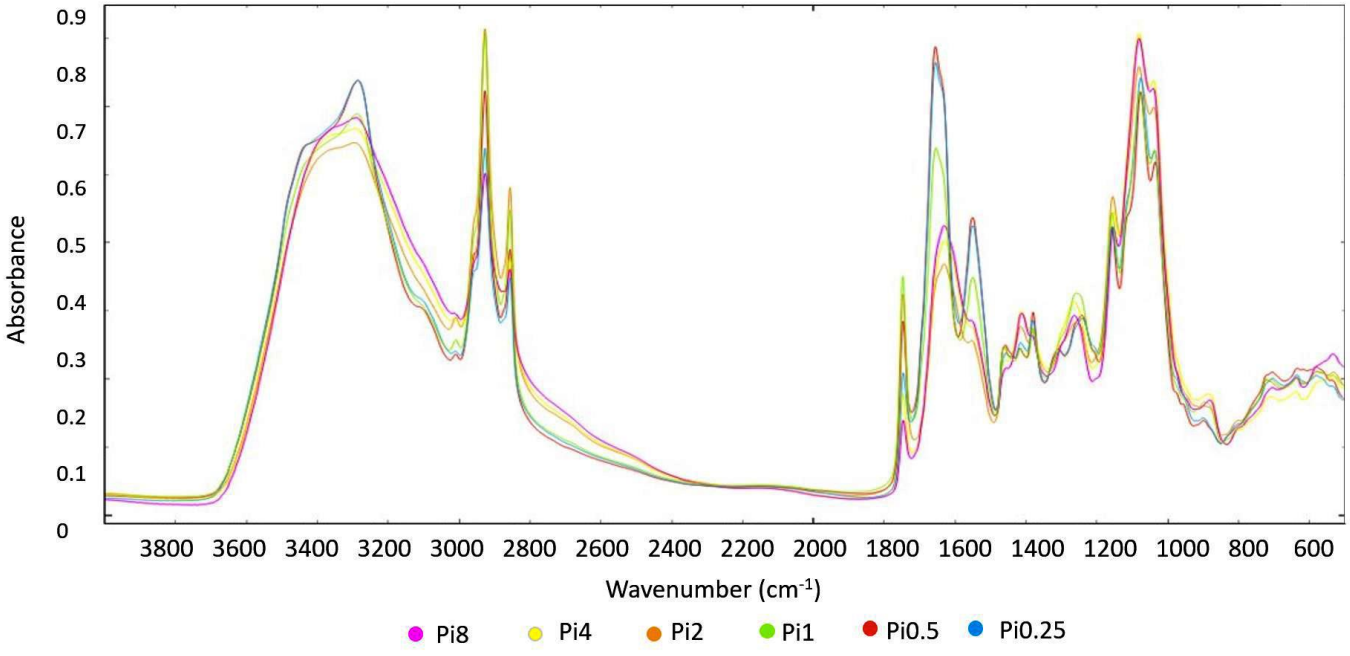

Supplementary Figure 7. FTIR-HTS spectra of *Lichtheimia corymbifera* (EMSC corrected); ammonium sulphate nitrogen source, different Pi-levels

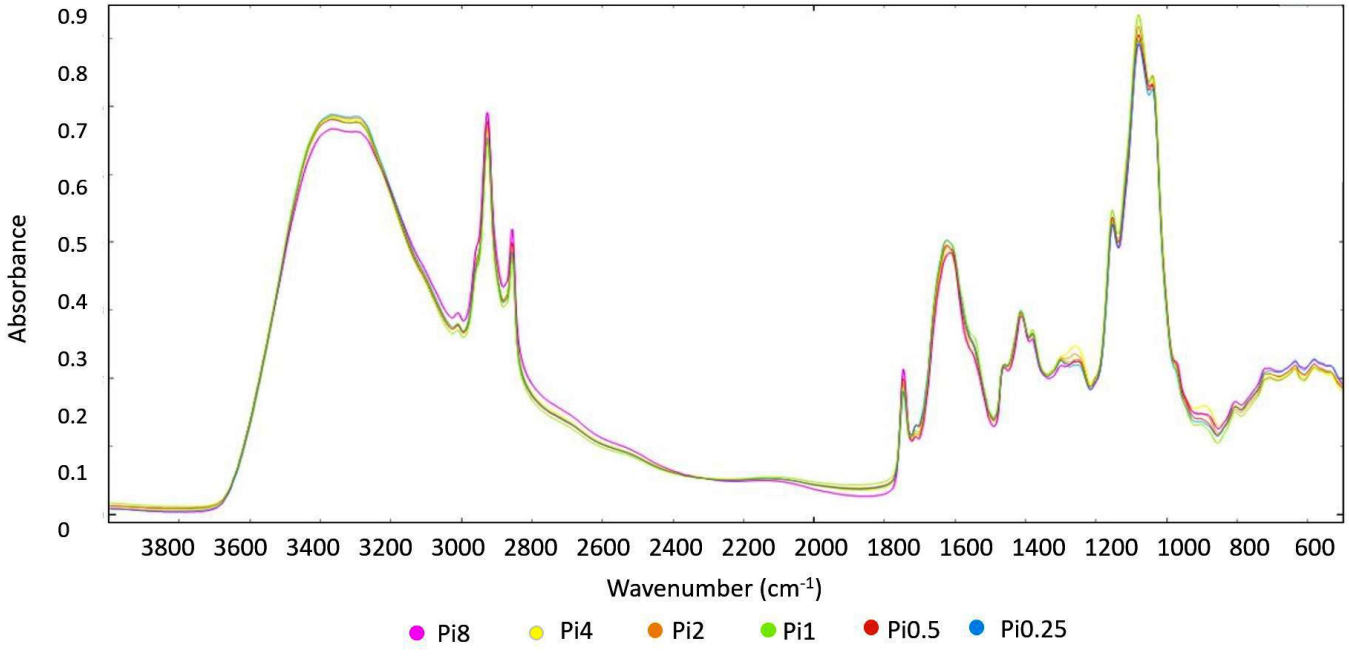

Supplementary Figure 8. FTIR-HTS spectra of *Lichtheimia corymbifera* (EMSC corrected); yeast extract nitrogen source, different Pi-levels

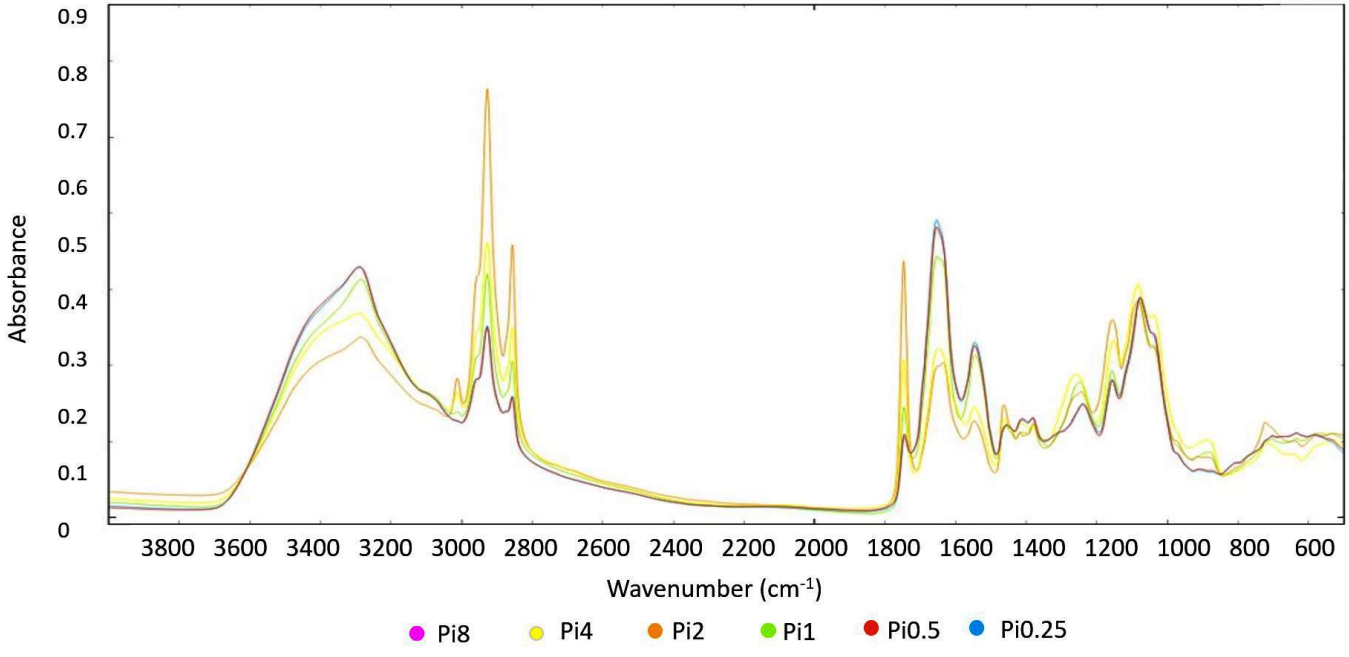

Supplementary Figure 9. FTIR-HTS spectra of *Mortierella alpina* (EMSC corrected); ammonium sulphate nitrogen source, different Pi-levels

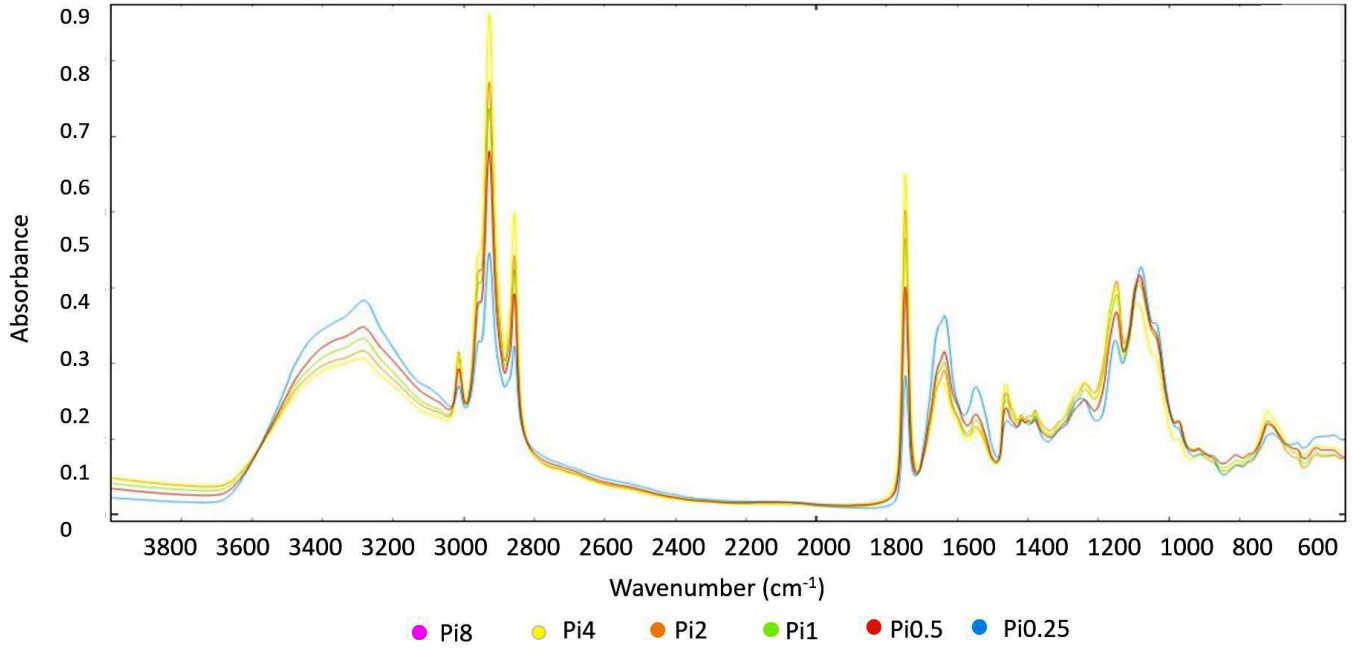

Supplementary Figure 10. FTIR-HTS spectra of *Mortierella alpina* (EMSC corrected); yeast extract nitrogen source, different Pi-levels

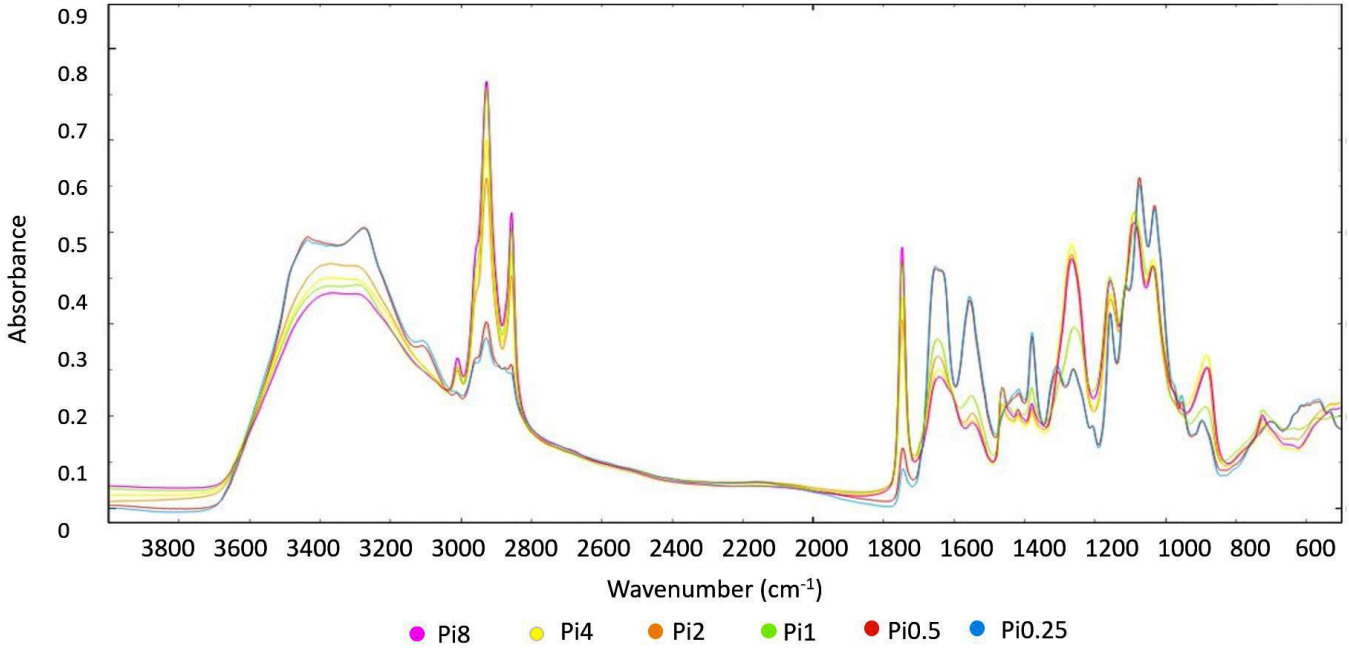

Supplementary Figure 11. FTIR-HTS spectra of *Mucor circinelloides* (EMSC corrected); ammonium sulphate nitrogen source, different Pi-levels

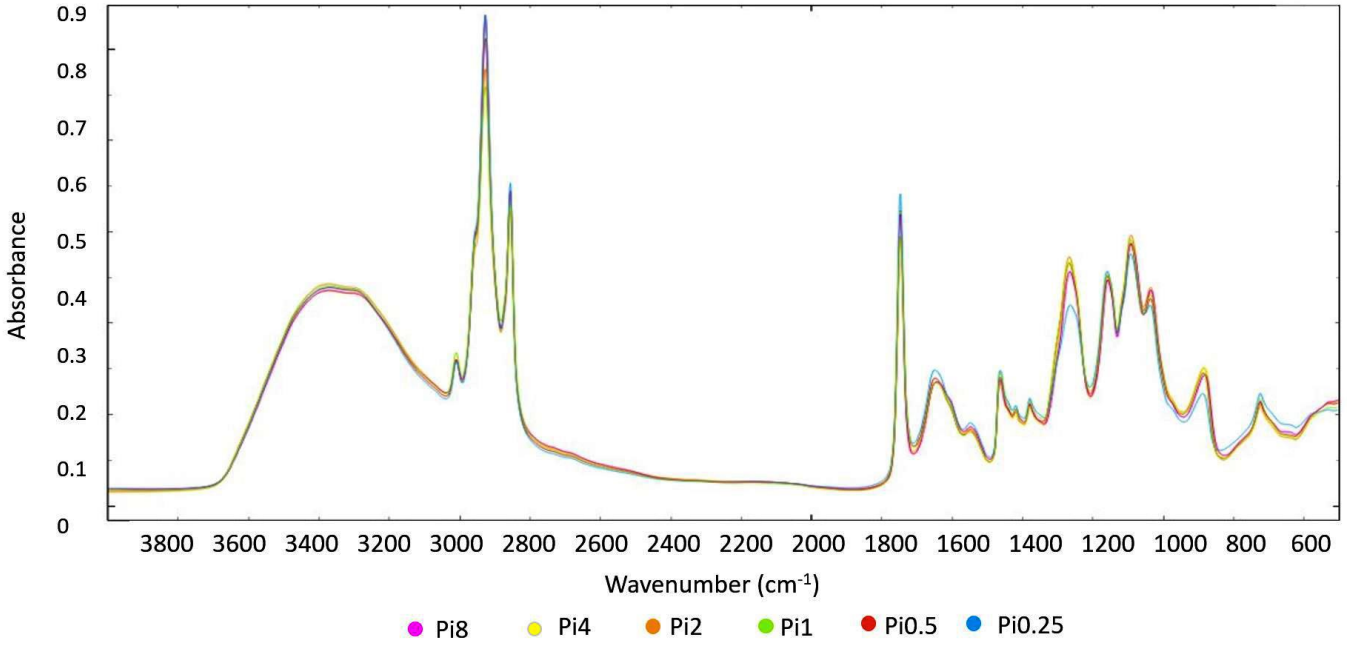

Supplementary Figure 12. FTIR-HTS spectra of *Mucor circinelloides* (EMSC corrected); yeast extract nitrogen source, different Pi-levels

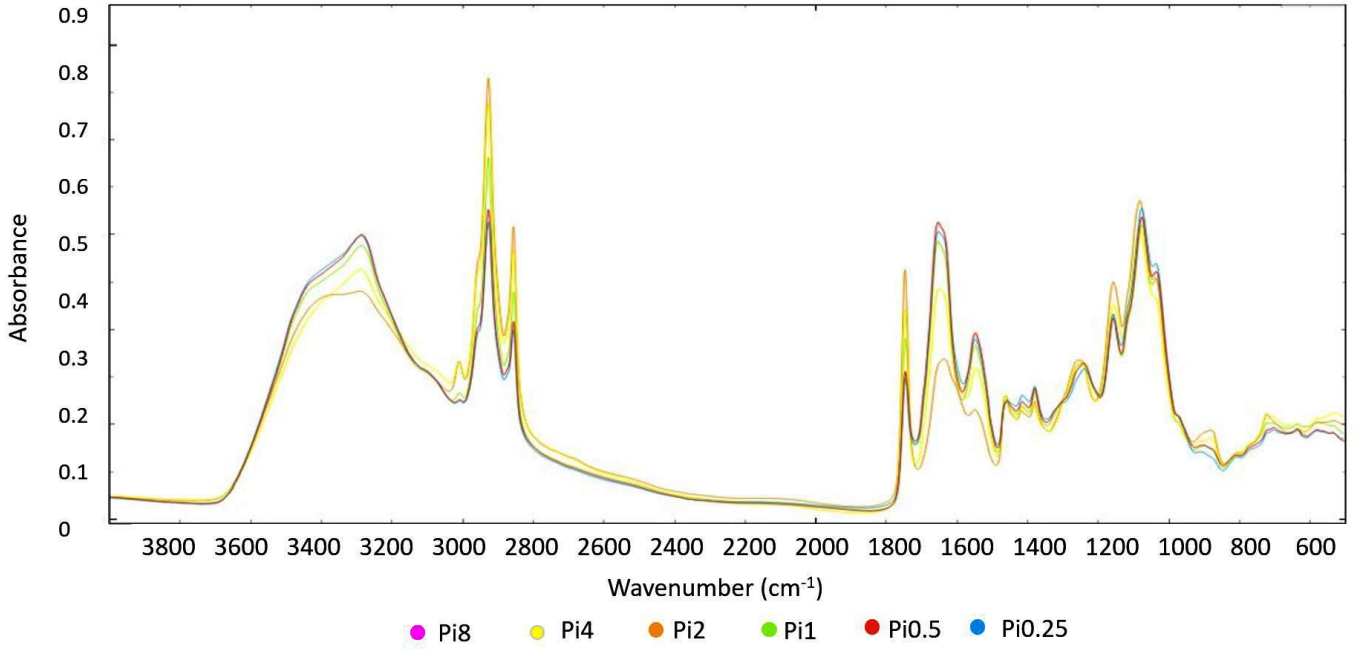

Supplementary Figure 13. FTIR-HTS spectra of *Mortierella hyalina* (EMSC corrected); ammonium sulphate nitrogen source, different Pi-levels

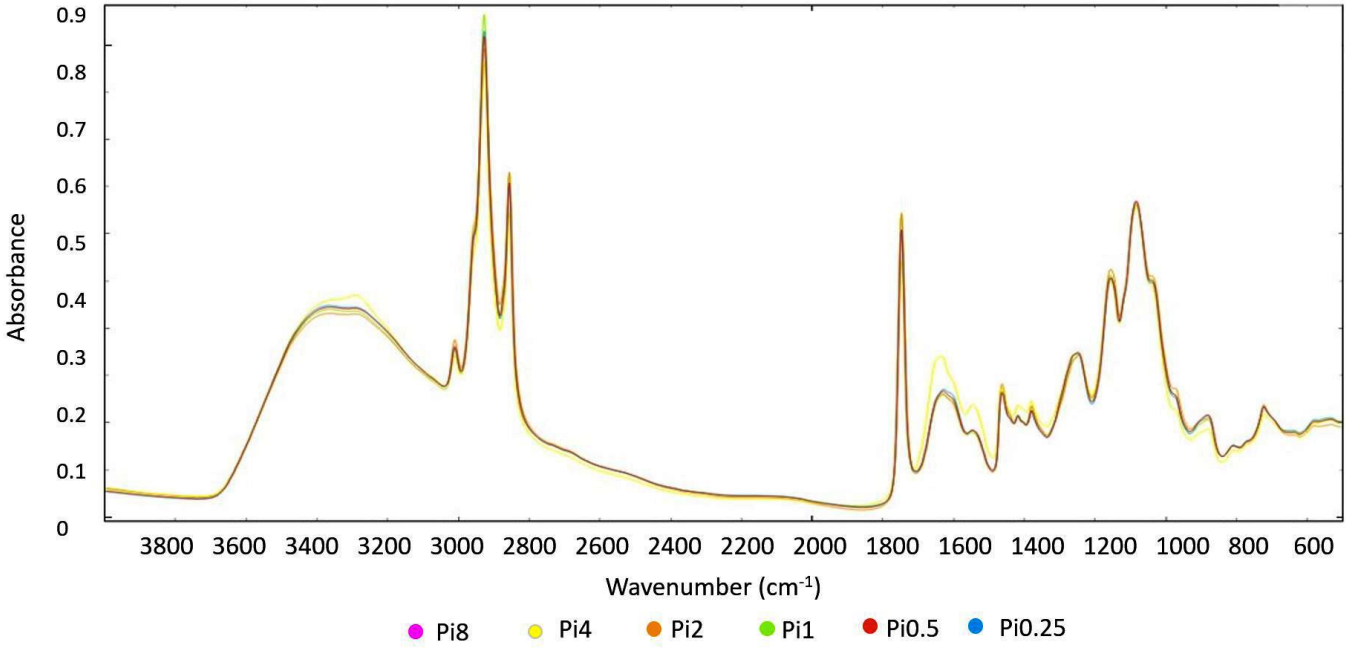

Supplementary Figure 14. FTIR-HTS spectra of *Mortierella hyalina* (EMSC corrected); yeast extract nitrogen source, different Pi-levels

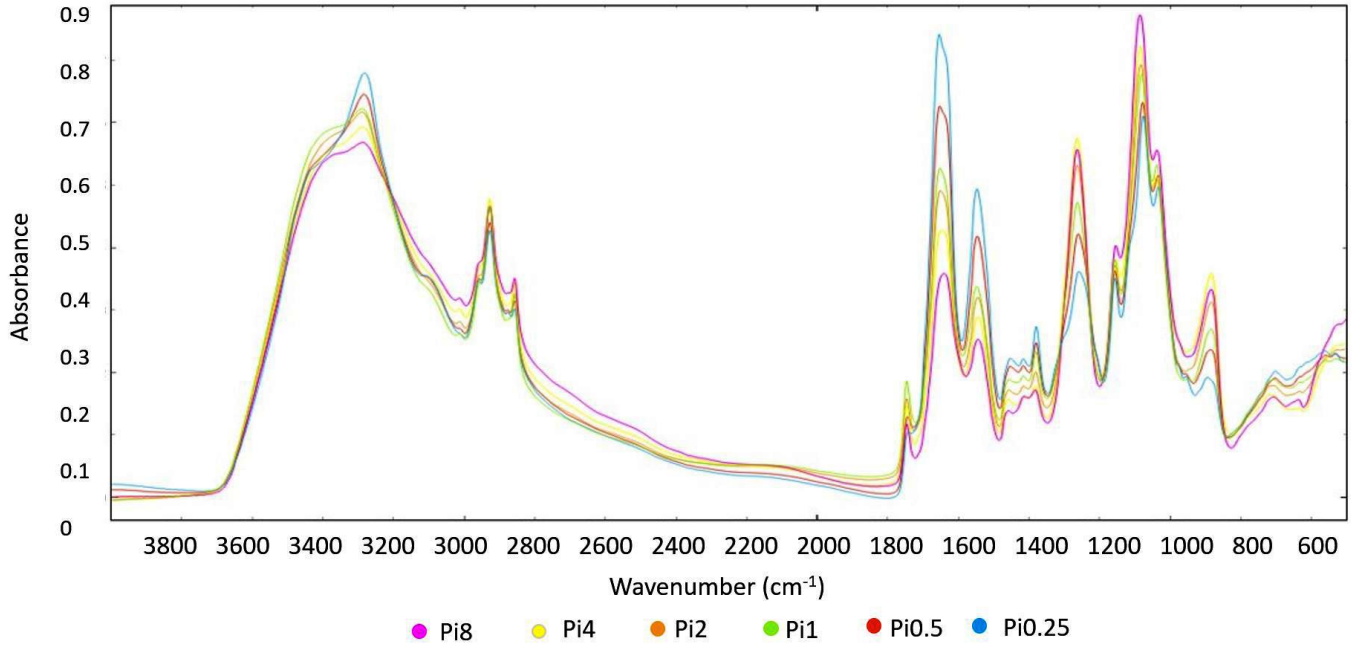

Supplementary Figure 15. FTIR-HTS spectra of *Rhizopus stolonifer* (EMSC corrected); ammonium sulphate nitrogen source, different Pi-levels

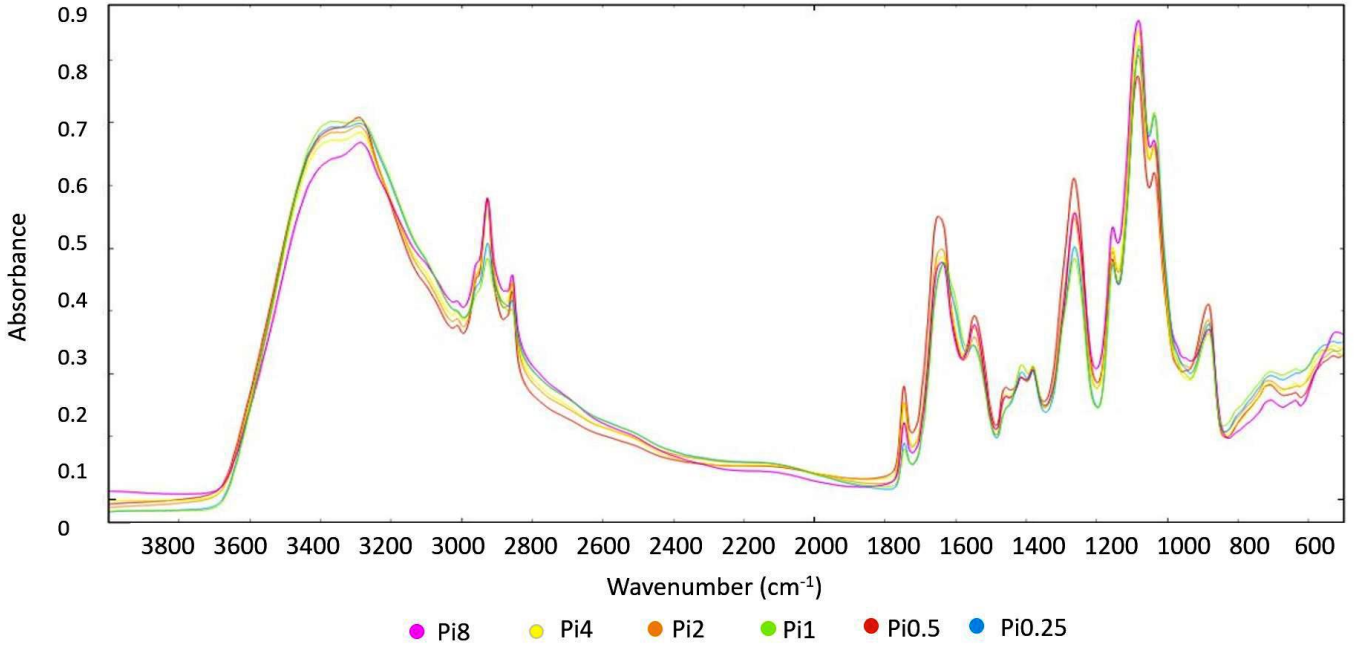

Supplementary Figure 16. FTIR-HTS spectra of *Rhizopus stolonifer* (EMSC corrected); yeast extract nitrogen source, different Pi-levels

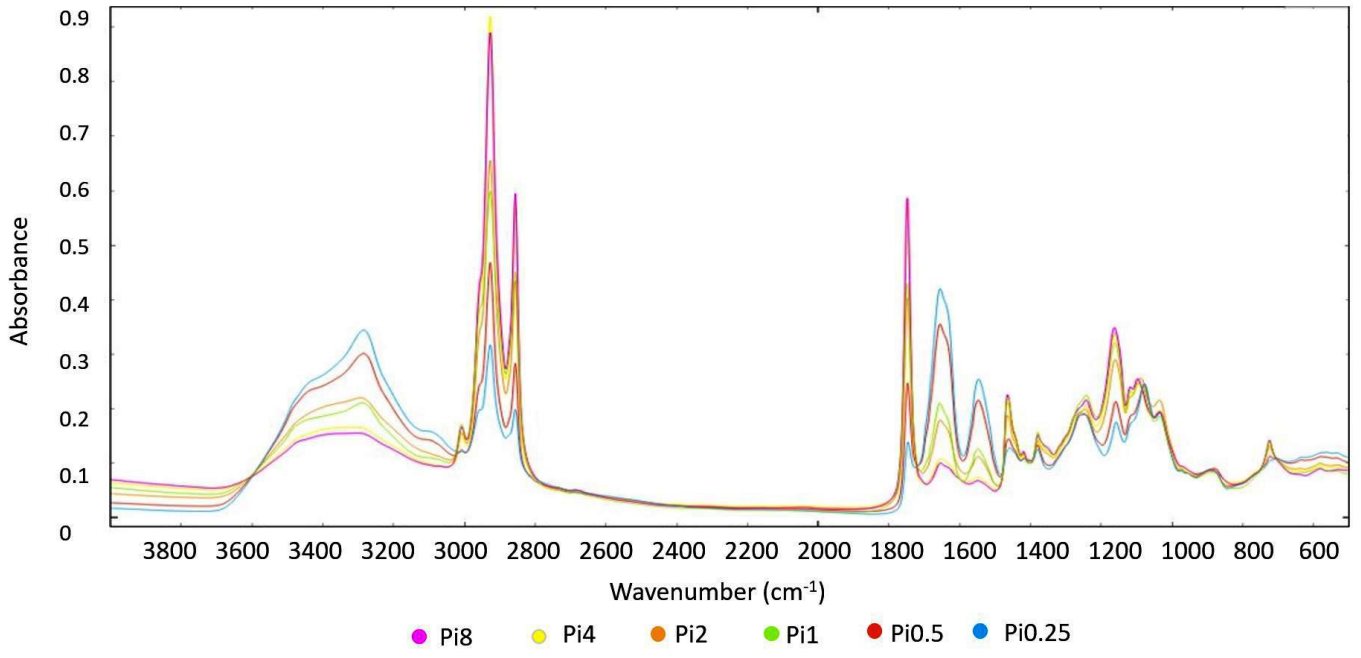

Supplementary Figure 17. FTIR-HTS spectra of *Umbelopsis vinacea* (EMSC corrected); ammonium sulphate nitrogen source, different Pi-levels

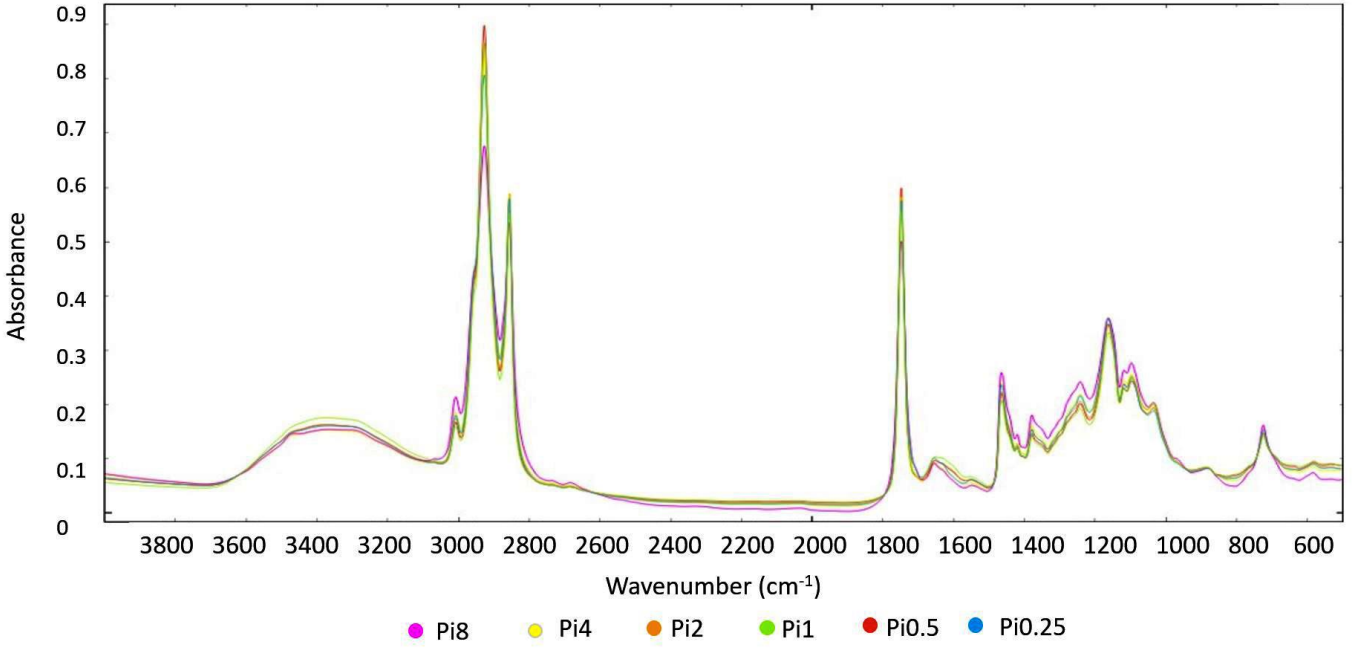

Supplementary Figure 18. FTIR-HTS spectra of *Umbelopsis vinacea* (EMSC corrected); yeast extract nitrogen source, different Pi-levels

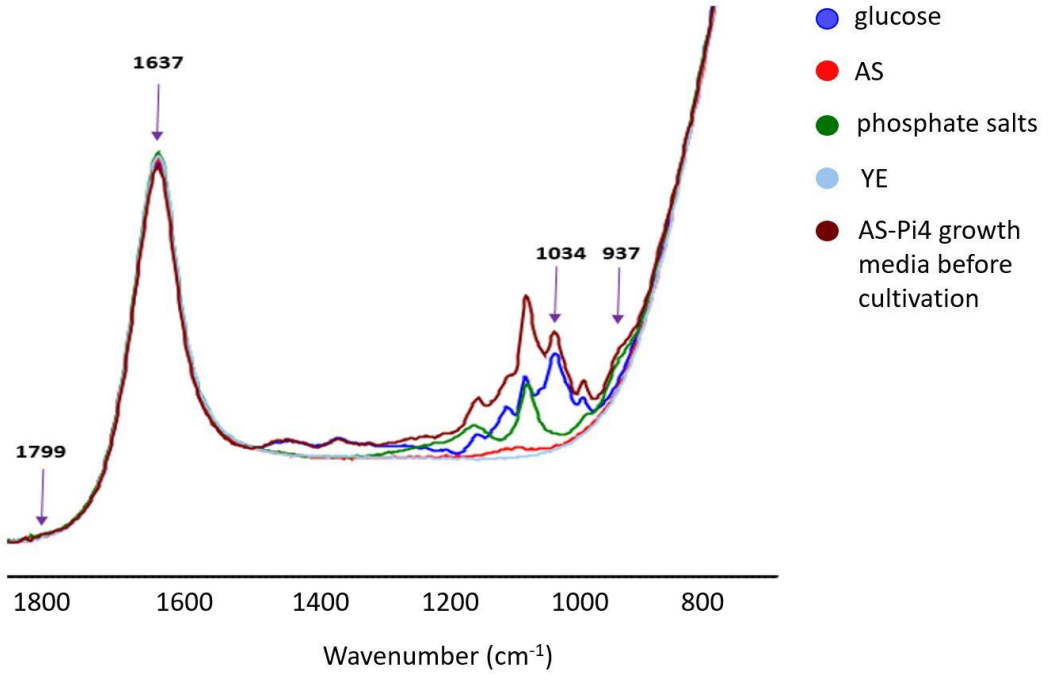

Supplementary Figure 19. FTIR-ATR spectra of glucose, ammonium sulphate (AS), phosphate salts, yeast extract (YE) and growth media AS-Pi4 before the cultivation.

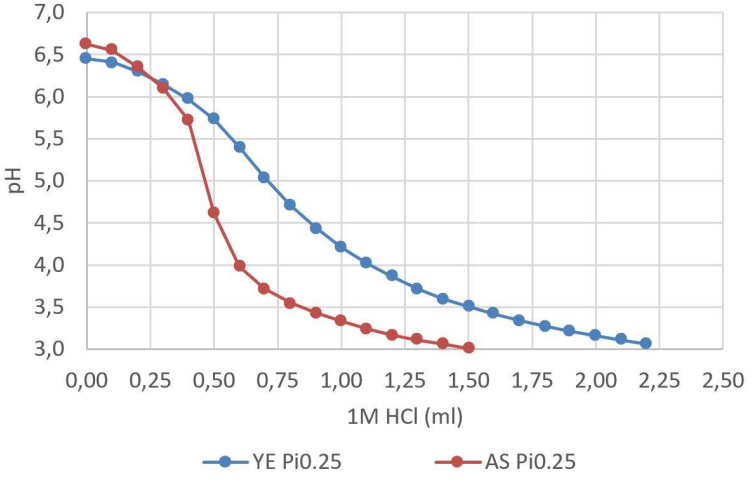

Supplementary Figure 20. Titration of 100 ml not autoclaved YE-Pi0.25 (blue) and AS-Pi0.25 (red) with 1M HCl confirmed the buffering properties of yeast extract.

Paper II

Applied Microbiology and Biotechnology (2020) 104:8065–8076
https://doi.org/10.1007/s00253-020-10821-7

BIOENERGY AND BIOFUELS

The influence of phosphorus source and the nature of nitrogen substrate on the biomass production and lipid accumulation in oleaginous *Mucoromycota* fungi

Simona Dzurendova[1] · Boris Zimmermann[1] · Valeria Tafintseva[1] · Achim Kohler[1] · Dag Ekeberg[2] · Volha Shapaval[1]

Received: 22 May 2020 / Revised: 28 July 2020 / Accepted: 5 August 2020 / Published online: 13 August 2020

Abstract

Oleaginous filamentous fungi grown under the nitrogen limitation, accumulate high amounts of lipids in the form of triacylglycerides (TAGs) with fatty acid profiles similar to plant and fish oils. In this study, we investigate the effect of six phosphorus source concentrations combined with two types of nitrogen substrate (yeast extract and ammonium sulphate), on the biomass formation, lipid production, and fatty acid profile for nine oleaginous *Mucoromycota* fungi. The analysis of fatty acid profiles was performed by gas chromatography with flame ionization detector (GC-FID) and the lipid yield was estimated gravimetrically. Yeast extract could be used as both nitrogen and phosphorus source, without additional inorganic phosphorus supplementation. The use of inorganic nitrogen source (ammonium sulphate) requires strain-specific optimization of phosphorus source amount to obtain optimal lipid production regarding quantity and fatty acid profiles. Lipid production was decreased in ammonium sulphate-based media when phosphorus source was limited in all strains except for *Rhizopus stolonifer*. High phosphorus source concentration inhibited the growth of *Mortierella* fungi. The biomass (22 g/L) and lipid (14 g/L) yield of *Umbelopsis vinacea* was the highest among all the tested strains.

Key points

- *The strain specific P requirements of Mucoromycota depend on the nature of N source.*
- *Yeast extract leads to consistent biomass and lipid yield and fatty acids profiles.*
- *Umbelopsis vinacea showed the highest biomass (22 g/L) and lipid (14 g/L) yield.*
- *High P source amounts inhibit the growth of Mortierella fungi.*

Keywords Oleaginous fungi · Phosphorus · Nitrogen · Lipid profile · Micro-cultivation

Introduction

Unsaturated lipids are essential components in a human and animal nutrition and are traditionally obtained from fish and vegetable oils. Monounsaturated lipids are one of the major raw materials for lipid-based biofuels, which are nowadays mostly derived from vegetable and/or waste cooking oils. Recently, increased attention to the ocean protection and fishing regulations for avoiding the overfishing and preserving fish species highlighted the need to find alternative sources of essential unsaturated lipids (Pinheiro et al. 2018; Sala et al. 2018). Furthermore, on-going transition of the global economy towards renewable bioresources and the continuous discussion on the controversial usage of vegetable oils for biofuel vs food applications, created an increasing need for alternative sources of lipids (Correa et al. 2019; Meyer et al. 2020).

Oleaginous microbial biomass is considered as an alternative source of high- and low-value unsaturated lipids for food, feed, chemical industry, and lipid-based biofuels (Ratledge 2010). Oleaginous microorganisms, such as filamentous fungi, yeast and microalgae, are able to accumulate lipids up to

Electronic supplementary material The online version of this article (https://doi.org/10.1007/s00253-020-10821-7) contains supplementary material, which is available to authorized users.

✉ Simona Dzurendova
simona.dzurendova@gmail.com; simona.dzurendova@nmbu.no

[1] Faculty of Science and Technology, Norwegian University of Life Sciences, Droebakveien 31, 1430 Aas, Norway

[2] Faculty of Chemistry, Biotechnology and Food Science, Norwegian University of Life Sciences, Christian Magnus Falsens vei 1, 1433 Aas, Norway

85% (w/w) of their total cell mass (Bharathiraja et al. 2017). Cellular oils are mainly produced in the form of free fatty acids, acylglycerols (mostly as triglycerides-TAGs) and other fatty acid-based lipids, that are stored in the globular organelles called lipid bodies. TAGs are generally considered as storage lipids. Depending on the fungal producer, accumulated lipids can be very similar to either vegetable oils, where saturated and monounsaturated fatty acids dominate, or to fish oils, where monounsaturated and polyunsaturated fatty acids dominate. Fatty acids derived from fungal lipids range from high-volume/low price to low-volume/high price. Examples for high-volume/low price fatty acids are monounsaturated fatty acids and saturated fatty acids that are used for the production of biodiesel, surfactants, soaps, resins, stabilizers, etc. On the other hand, high-price polyunsaturated fatty acids (ω3-PUFAs) may achieve high market value in pharmaceutical and food industry (van der Voort et al. 2017).

Oleaginous *Mucoromycota* fungi are considered as promising oleaginous microorganisms due to the relatively fast growth and high metabolic activity for utilizing both sugar- and lipid-based substrates. They are able to valorize a broad spectrum of low-cost substrates, including lignocellulose hydrolysates (Qiao et al. 2018; Subhash and Mohan 2015), sugar beet pulp (Ozsoy et al. 2015), wastewater (Bhanja et al. 2014), corncob waste liquor (Subhash and Mohan 2011), oil wastes (Mirbagheri et al. 2015), cheese whey permeate (Chan et al. 2018), and starch hydrolysates (Zhu et al. 2003).

In order to utilize low-cost substrates for the sustainable production of fungal lipids, there is a need to optimize their chemical composition. Carbon, nitrogen and phosphorus are the main components present in different low-cost substrates, and they are the key nutrients involved in the biomass growth and lipid accumulation in oleaginous microorganisms (Ratledge and Wynn 2002). Under the nitrogen-limiting condition, carbon is converted into TAGs which are stored in lipid bodies. Nitrogen is required for the proliferation and growth of fungal cells and as soon as it is depleted, the activity of isocitrate dehydrogenase is inhibited, and overproduced citrate is transported from mitochondria to the cytosol (Jiru and Abate 2014). Furthermore, ATP citrate lyase, which is a key enzyme of lipogenesis, cleaves the citrate into acetyl-CoA, which is reduced by the malic enzyme providing NADPH for fatty acid synthase. Thus, the backbone for fatty acids can be created (Akpinar-Bayizit 2014). Phosphorus is a part of phosphorylated molecules essential in lipid biosynthesis, such as energy transfer molecules adenosine mono-, di-, triphosphate (AMP, ADP, ATP), key lipogenesis enzyme ATP-citrate lyase, and reduced nicotinamide adenine dinucleotide phosphate (NADPH), which is directly involved in fatty acid synthesis as reductant. In addition, phosphorus is involved in the formation of lipid droplets, as it is the part of phospholipids of the lipid droplet membrane (Ratledge 2004).

Extensive number of studies focused on the understanding of the utilization of different carbon and nitrogen sources (Cortes and de Carvalho 2015; Evans and Ratledge 1983; Fakas et al. 2009; Heredia-Arroyo et al. 2011; Papanikolaou et al. 2007) and influence of different C/N ratios on the lipid accumulation in oleaginous microorganisms has been performed (Braunwald et al. 2013; Dyal et al. 2005; Economou et al. 2011; Evans and Ratledge 1984; Prasad et al. 2008; Ykema et al. 1988). The effect of phosphorus on the lipid production in algae has already been addressed (Chiriboga and Rorrer 2019; Esakkimuthu et al. 2016), and it was shown to be specie-dependent. In some cases, phosphorus starvation induced and enhanced the lipid accumulation (Feng et al. 2012; Roopnarain et al. 2014; Wu et al. 2013) while in other cases, it had the opposite effect (Li et al. 2014). Concerning oleaginous yeasts, phosphorus source limitation is beneficial for the lipid accumulation in nitrogen not-limited conditions (Huang et al. 2018; Wang et al. 2018; Wu et al. 2010). In case of filamentous fungi, the effect of phosphorus was investigated in connection to polyphosphate accumulation (Lima et al. 2003) or chitosan production (Safaei et al. 2016). To the authors knowledge, there is no study reported the investigation of the role of phosphorus on the lipid accumulation in oleaginous filamentous fungi.

Most of the reported studies used the traditional approach for triggering lipid accumulation by limiting either nitrogen or phosphorus nutrients when carbon is in excess. Our study is the first investigation of the influence of various phosphorus source concentrations under nitrogen-limiting conditions, when using different nitrogen sources. Two types of nitrogen sources were used—yeast extract (YE) and ammonium sulphate (AS). Yeast extract is a rich organic N-source, containing, in addition to 10% of nitrogen, approx. 2.5% of phosphorus, as well as a broad range of other macro- and micronutrients. Yeast extract was shown to be beneficial for biomass and lipid production for oleaginous *Mucoromycota* fungi (Dyal et al. 2005; Kosa et al. 2018b). Ammonium sulphate is a simple inorganic source of nitrogen, and it allows precise control of the chemical composition of all added nutrients.

The aim of the study was to investigate the influence of nitrogen source nature and the phosphorus source availability under nitrogen-limiting conditions on the biomass growth, lipid accumulation, and fatty acid profile of triacylglycerides for nine oleaginous *Mucoromycota* fungi, which were selected based on previously reported high-throughput screening study (Kosa et al. 2018b). High throughput micro-cultivation setup which employs the Duetz microtiter plates was used for presented screening (Duetz and Witholt 2001; Dzurendova et al. 2020; Kosa et al. 2017a; b; 2018b). A complete biochemical composition of the produced fungal biomass revealing the co-production potential has been assessed by Fourier transform infrared spectroscopy (FTIR-HTS), and the substrate consumption was monitored by FTIR-ATR (Dzurendova et al. 2020).

Materials and methods

Oleaginous *Mucoromycota* fungi

Nine oleaginous *Mucoromycota* fungi from the genera *Absidia*, *Amylomyces*, *Cunninghamella*, *Lichtheimia*, *Mortierella*, *Mucor*, *Rhizopus*, and *Umbelopsis* were used in the study (Table 1).

Growth media and cultivation conditions

The cultivation of the fungi was performed in two steps: (1) cultivation on agar plates for a spore inoculum preparation, and (2) cultivation triggering lipid accumulation by using nitrogen-limited broth media with the different nitrogen sources (ammonium sulphate and yeast extract) and different amounts of inorganic phosphorus salts (Pi). For the preparation of the spore inoculum, malt extract agar (MEA) was used for all fungi with the exception of MAL, MHY, and UVI, which were cultivated on potato dextrose agar (PDA). MEA was prepared by dissolving 30 g of malt extract (Merck, Darmstadt, Germany), 5 g of peptone (Amresco, Solon, Ohio, USA), and 15 g of agar powder (Alfa Aesar, ThermoFischer, Kandel, Germany) in 1 L of distilled water and autoclaved at 115 °C for 15 min. PDA was prepared by dissolving 39 g of potato dextrose agar (VWR, Leuven, Belgium) in 1 L of distilled water and autoclaved at 115 °C for 15 min. Agar cultivations were performed for 7 days at 25 °C for all fungi except MAL and MHY, which were grown for 14 days due to the slower growth. Fungal spores were harvested with a bacteriological loop after the addition of 10 mL of sterile 0.9% NaCl solution.

The main components of the nitrogen-limited broth media were prepared according to the previously published studies on the screening of *Mucoromycota* fungi (Kavadia et al. 2001; Kosa et al. 2017a), with the following modifications (g/L): glucose 80, yeast extract 3, $MgSO_4 \cdot 7H_2O$ 1.5, $CaCl_2 \cdot 2H_2O$ 0.1, $FeCl_3 \cdot 6H_2O$ 0.008, $ZnSO_4 \cdot 7H_2O$ 0.001, $CoSO_4 \cdot 7H_2O$ 0.0001, $CuSO_4 \cdot 5H_2O$ 0.0001, and $MnSO_4 \cdot 5H_2O$ 0.0001. For the media with ammonium sulphate (AS) as a nitrogen source, yeast extract (YE) was replaced with 1.5 g/L of $(NH_4)_2SO_4$ in order to keep the same C/N ratio. Broth media with ammonium sulphate contained 0.05 g/L thiamin hydrochloride and 0.02 mg/L biotin (Zeng et al. 2012). Different concentrations of phosphate salts, namely KH_2PO_4 and Na_2HPO_4, were added to the main components of nitrogen-limited broth media, as described in Table 2. 7 g L^{-1} KH_2PO_4 and 2 g L^{-1} Na_2HPO_4 were selected as a reference concentration values (Pi1) as those have been used in the previous studies (Kavadia et al. 2001; Kosa et al. 2017a, 2018b). The broth media contained higher (up to 8 × Pi1) and lower (down to ¼ × Pi1) amounts of phosphate salts in comparison to the reference value (Table 2). Two salts, KCl and NaCl, have been added in the corresponding concentrations to the broth media with the decreased amount of inorganic phosphorus, in order to have equal K^+ and Na^+ ions as in the reference condition (Pi1). Broth media were autoclaved for 15 min at 121 °C. The starting pH of the media was 6.0 ± 0.3, and pH of the culture supernatant after the growth was recorded (Table S1 in the Supplementary Material).

Cultivation in the nitrogen-limited broth media was performed in the Duetz-MTPS (Enzyscreen, Heemstede, Netherlands) (Kosa et al. 2017b, 2018a), consisting of 24-square polypropylene deep well microtiter plates, low evaporation sandwich covers, and extra high cover clamp system, which were mounted into the shaking incubator MAXQ 4000 (Thermo Scientific, Oslo, Norway). Seven milliliters of the sterile broth media was transferred into the autoclaved microtiter plates, and each well was inoculated with 50 μL of the spore suspension. Cultivations were performed for 7 days at 25 °C and 400 rpm agitation speed (1.9 cm circular orbit). Fungal strains MAL and MHY were cultivated for 14 days due to the slow growth.

Table 1 List of the oleaginous *Mucoromycota* fungi used in the study

Family	Fungal strain name	Short name	Collection no.
Cunninghamellaceae	*Absidia glauca*	AGL	CCM[1] 451
Cunninghamellaceae	*Cunninghamella blakesleeana*	CBL	CCM F705
Cunninghamellaceae	*Lichtheimia corymbifera*	LCO	CCM 8077
Mortierellaceae	*Mortierella alpina*	MAL	ATCC[2] 32222
Mortierellaceae	*Mortierella hyalina*	MHY	VKM[3] F1629
Mucoraceae	*Amylomyces rouxii*	ARO	CCM F220
Mucoraceae	*Mucor circinelloides*	MCI	VI[4] 04473
Mucoraceae	*Rhizopus stolonifer*	RST	VKM F-400
Umbelopsidaceae	*Umbelopsis vinacea*	UVI	CCM F539

[1] Czech collection of Microorganisms (Brno, Czech Republic), [2] American Type Culture Collection (Virginia, USA), [3] All-Russian Collection of Microorganisms (Moscow, Russia), and [4] Norwegian school of Veterinary Science (Oslo, Norway)

Table 2 The list of concentrations of phosphate salts in the nitrogen-limited broth media

Concentration labeling	KH_2PO_4 (g L^{-1})	Na_2HPO_4 (g L^{-1})
Pi8	56	16
Pi4	28	8
Pi2	14	4
Pi1	7	2
Pi0.5	3.5	1
Pi0.25	1.75	0.5

The cultivation was performed in full factorial design in three independent biological replicates for each fungus, phosphorus source concentration, and nitrogen source, resulting in 324 samples. Biological replicates were prepared on a separate microtiter plates at different time points. For every biological replicate, fresh spore suspension was prepared. Two biological replicates were used for the extraction of lipids, while three biological replicates were used for evaluating the biomass production.

Extraction of lipids and GC-FID analysis of fatty acid profile

Direct transesterification was performed according to the Lewis et al. (2000) with modifications. Two milliters screw-cap polypropylene (PP) tubes were filled with 30 ± 3 mg of freeze-dried biomass, 250 ± 30 mg of acid-washed glass beads, and 500 μL of methanol. Further, fungal biomass was disrupted in a tissue homogenizer (Bertin Technologies Percellys Evolution, Montigny-le-Bretonneux, France). The disrupted fungal biomass was transferred into glass reaction tubes by washing the PP tube with 2400 μL methanol–chloroform–hydrochloric acid solvent mixture (7.6:1:1 *v*/v). One milligram of C13:0 TAG internal standard in 100 μL of hexane was added to the glass reaction tube (100 μL from a 10.2 mg/mL glyceryl tritridecanoate ($C_{42}H_{80}O_6$, C13:0 TAG (13:0/13:0/13:0), Sigma-Aldrich, St. Louis, Missouri, USA). Reaction tubes were incubated at 90 °C for 1 h, followed by cooling to room temperature and the addition of 1 mL distilled water. The fatty acid methyl esters (FAMEs) were extracted by the addition of 2 mL hexane–chloroform mixture (4:1 v/v) and 10 s vortex mixing. The reaction tubes were centrifuged at 3000*g* for 5 min at 4 °C and the upper hexane phase was collected in glass tubes. The extraction step was repeated three times for each sample. Subsequently, the solvent was evaporated under nitrogen at 30 °C, and FAMEs were dissolved in 1.5 mL of hexane containing 0.01% of butylated hydroxytoluene (BHT, Sigma-Aldrich, St. Louis, Missouri, USA) and a small amount of anhydrous sodium sulfate (to remove traces of water in the sample). Samples were mixed by vortexing, and finally, dissolved FAMEs were transferred to the GC vials.

Fatty acid profile analysis was performed using gas chromatography system with flame ionization detector (GC-FID) 7820A GC System, Agilent Technologies, controlled by Agilent OpenLAB software (Agilent Technologies, Santa Clara, California, USA). Agilent J&W GC column 121-2323, DB-23, 20 m length; 0.180 mm diameter; 0.20-μm film was used for the separation of FAMEs. One microliter of the sample was injected in the 30:1 split mode with the split flow 30 mL/min. The inlet heater temperature was set on 250 °C and helium was used as the carrier gas. The total runtime for one sample was 36 min with the following oven temperature increase: initial temperature 70 °C for 2 min, after 8 min to 150 °C with no hold time, 230 °C in 16 min with 5 min hold time, and 245 °C in 1 min with 4 min hold time. For identification and quantification of fatty acids, the C4–C24 FAME mixture (Supelco, St. Louis, USA) was used as an external standard, in addition to C13:0 TAG internal standard.

The total lipid yield was estimated gravimetrically. Hexane containing extracted lipids was evaporated under nitrogen at 30 °C and the residuals of the solvent were removed by drying in an oven overnight at 150 °C.

Data analysis

Unscrambler X version 10.5.1 (CAMO Analytics, Oslo, Norway) and Orange data mining toolbox version 3.16 (University of Ljubljana, Slovenia) (Demšar et al. 2013; Toplak et al. 2017) were used for averaging the GC data and performing principal component analysis (PCA). Data for PCA were normalized. Matlab R2018a (The Mathworks Inc., Natick, USA) was used for the analysis of the influence of nitrogen source and phosphorus availability on the total biomass and lipid yield. For each fungal strain, an ANOVA model was established to calculate the variation in the data introduced by the different design factors such as N-source, Pi concentration, and N-Pi interaction. In ANOVA model, one represents the original data matrix as a sum of matrices corresponding to the experimental design factors. Each design matrix consists of means of rows corresponding to the levels of each design factor. The ANOVA model in this study contained three design factors: N-source, Pi concentration, the interaction of N-source and Pi level. All other variation was summarized in a matrix representing residual variation (Harrington et al. 2005).

Results

The influence of the nitrogen source nature and phosphorus availability on the biomass and lipid yield

Two types of nitrogen (N) sources, organic yeast extract (YE) and inorganic ammonium sulphate (AS), and six concentrations of inorganic phosphorus salts (Pi) were used to study the

influence of the nitrogen source nature and Pi substrate availability on the biomass production, lipid accumulation, and fatty acid profile of the accumulated TAGs in oleaginous *Mucoromycota* fungi. High glucose concentration (80 g/L) with low N substrate availability was used in order to induce lipid accumulation. The same glucose amount was used in our previous *Mucoromycota* studies (Kosa et al. 2017a; b; 2018b), and it was shown to be sufficient for cultivation lasting 12 days. HPLC analysis has shown residual glucose remaining after the cultivations. Thus, no glucose starvation, and, consequently, the utilization of produced fungal lipids as a carbon source was expected. The relative amount of residual glucose and phosphates in the culture supernatant was estimated by FTIR-ATR as published previously (Dzurendova et al. 2020). Both, phosphates and glucose were not fully utilized by fungi. UVI showed the highest glucose consumption, which corresponds to highest biomass production.

In the YE-Pi media, the highest biomass 18.92–23.67 g/L and lipid yield 11.46–14.13 g/L was observed for UVI (Fig. 1a). The obtained lipid content (57–63%) is in an agreement with the previously reported 51% (Zheng et al. 2012) and 66% (Meng et al. 2009). While, the biomass production for UVI reported in our study was three times higher than in previously reported studies (7.1 g/L) (Zheng et al. 2012). Furthermore, a high biomass production was observed for MCI, AGL, LCO, and ARO in a range from 8.49 to 12.92 g/L with the lipid content from 2.52 to 6.7 g/L, where the highest biomass and lipid content was observed for MCI 12.92 g/L and 6.7 g/L, respectively (Fig. 1a), that is considerably higher than from previously reported studies (Zheng et al. 2012). Fungal strains CBL, MAL, MHY, and RST showed relatively low biomass production below 10 g/L, and lipid accumulation did not reach more than 3.82 g/L, where MAL had the lowest biomass 5.55–6.10 g/L and lipid 2.74–3.5 g/L yield (Fig. 1a).

High content of Pi source (Pi8) in the growth media led to the slight decrease in the growth and lipid accumulation in comparison to the moderate amounts of Pi source for all fungi, with completely inhibited growth for MAL and MHY. Moderate concentrations of inorganic phosphorus substrate (Pi4, Pi2, and Pi1) were optimal for the biomass and lipid production for the majority of the oleaginous *Mucoromycota* fungi when grown in AS-based media (Fig. 1b). Phosphorus source concentration Pi2 contributed to the highest biomass and lipid yield for LCO, UVI, MAL, and MHY. Pi4 was optimal for MCI, ARO, and AGL (Fig. 1b). Fungal strain RST showed an exceptional growth and lipid accumulation consistency, that was not affected by the Pi source availability and the nature of the nitrogen substrate (Fig. 1a, b).

As already mentioned, high phosphorus source availability showed inhibiting effect in YE-based media. On the other hand, AS-based media with high phosphorus source availability led to the increased biomass production for some fungi, such as CBL with AS-Pi8 (7.47 g/L) and Pi4 (8.83 g/L); ARO with AS-Pi8 (10.32 g/L) and AS-Pi4 (11.88 g/L), and MAL (7.03 g/L) and MHY (10.05 g/L) with AS-Pi2. In addition, lipid accumulation was increased for some fungi grown in AS-Pi media in comparison to the corresponding YE-Pi media, as for example, in the case of CBL with Pi1 (3.02 g/L), ARO Pi non-limited (3.40–4.20 g/L), and MHY with Pi2 (4.61 g/L) (Fig. 1a, b).

ANOVA analysis was applied to perform overall study of the influence of the nitrogen source nature and the availability of inorganic phosphorus source on the variation in biomass and lipid yield (Fig. 2a, b). It was observed that the nature of the nitrogen source and phosphorus availability, both alone and in the interaction, introduce strain-specific and diverse changes in the biomass formation and lipid production in *Mucoromycota* fungi. The most substantial influence was observed from the interaction of both factors. Nature of the nitrogen source as a sole factor showed the biggest influence on the biomass production of AGL and LCO. Conversely, for ARO, CBL, and MCI, the nature of nitrogen substrate did not play the decisive role. The lipid production was significantly influenced by the nitrogen source for LCO, MAL, and UVI.

Variation in phosphorus source availability contributed to the most remarkable changes in the biomass and lipid production for RST. This was probably due to its extensive ability to store intracellular polyphosphates (Werner et al. 2007). The least phosphorus source contribution was observed for AGL. Lipid production for CBL was mostly affected by the interaction of both factors (N and Pi) (Fig. 2a, b).

Fatty acid (FA) profile under different nitrogen sources and phosphorus substrate availability

The fatty acid profiles of *Mucoromycota* TAGs are dominated by the following fatty acids: myristic (C14:0), palmitic (C16:0), palmitolenic (C16:1), stearic (C18:0), oleic (C18:1n9), linoleic (C18:2n6), γ-linolenic (C18:3n6), and arachidonic (C20:4n6) acid. It was observed that fatty acid profiles are strain-specific while some similarities could be observed within the families *Mucoraceae* and *Umbelopsidaceae* (Fig. 3), *Cunninghamellaceae* (Fig. 4), and *Mortierellaceae* (Fig. 5). These results are in accordance with our previous study covering hundred *Mucoromycota* strains (Kosa et al. 2018b). Table S2 in the Supplementary Materials reports the detailed FA profiles.

The principal component analysis (PCA) of gas chromatography fatty acid profile data was performed to get an overview of the influence of phosphorus availability and the nature of the nitrogen source on the fatty acid profile of the TAGs, accumulated in *Mucoromycota* fungi (Fig. S1 in Supplementary Materials). The PCA scatter plot shows that fatty acid profile—sum of saturated (SAT), monounsaturated

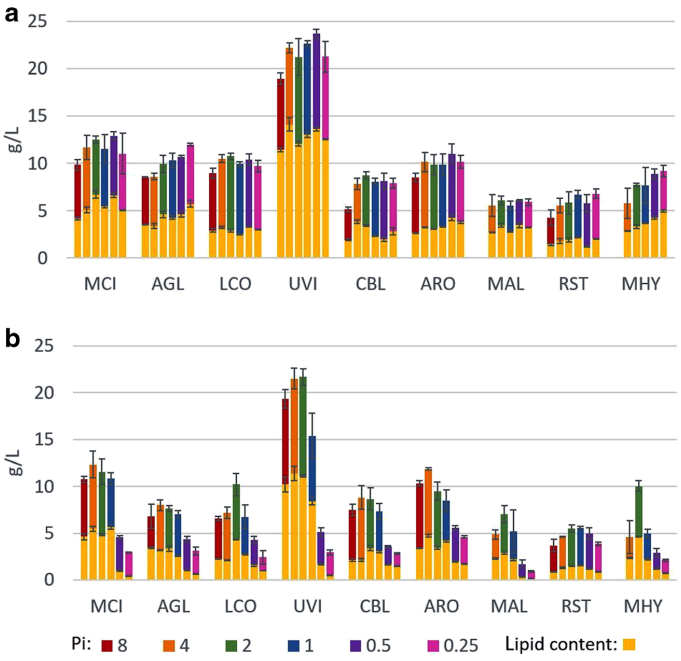

Fig. 1 Biomass and lipid production of oleaginous *Mucoromycota* fungi grown in YE-Pi (**a**) and AS-Pi (**b**) based nitrogen-limited broth media

(MUFA), and polyunsaturated (PUFA) fatty acids—was relatively consistent when *Mucoromycota* fungi were grown in the YE-Pi media (A). The only exception was MAL, which under the high phosphorus source levels produced slightly more saturated TAGs (Fig. S1A in Supplementary Materials) and a decrease in arachidonic acid production (Pi4- 37.75%; Pi0.25–47%) was observed (Fig. 5).

The substantial variation in fatty acid profile of *Mucoromycota* TAGs was observed when fungi were grown in AS-Pi media (Fig. S1B in Supplementary Materials, Figs. 3, 4, and 5). Low phosphorus source availability (Pi0.5 and Pi0.25) led to acidic pH which induced clearly the most remarkable strain-specific changes in FA profiles for all the studied *Mucoromycota* fungi, except for LCO and RST (Fig. 3, Table S1 in Supplementary Materials). Thus, for *Mucoraceae* fungi, except RST, low Pi source amount resulted in the increase of the relative amount of the unsaturated fatty acids (γ-linolenic and linolenic) accompanied with the decrease in the amount of saturated (oleic and stearic) fatty acids (Fig. 3a, b). The opposite effect was observed for

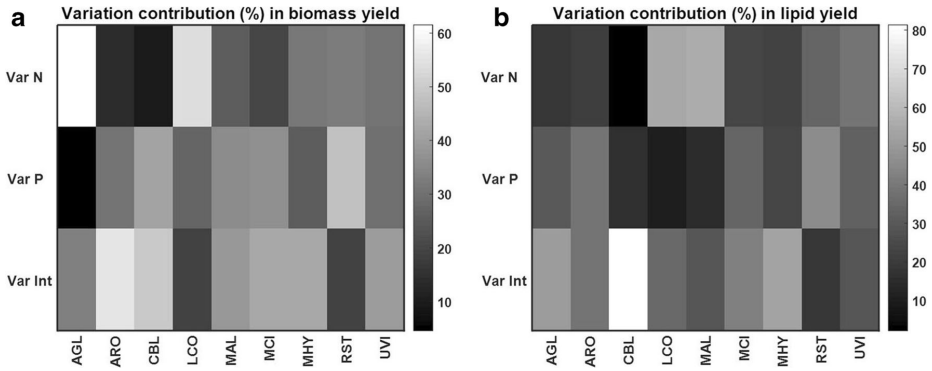

Fig. 2 Variation contribution (%) from the changes in N, Pi, and N-Pi interaction on the biomass (g/L) (**a**) and lipid (% w/w) (**b**) yield. Variation contributions due to the changes in N and Pi alone are presented in the first two rows (Var N and Var P), whereas contribution from the N-Pi interaction (Int) is presented in the last row (Var Int)

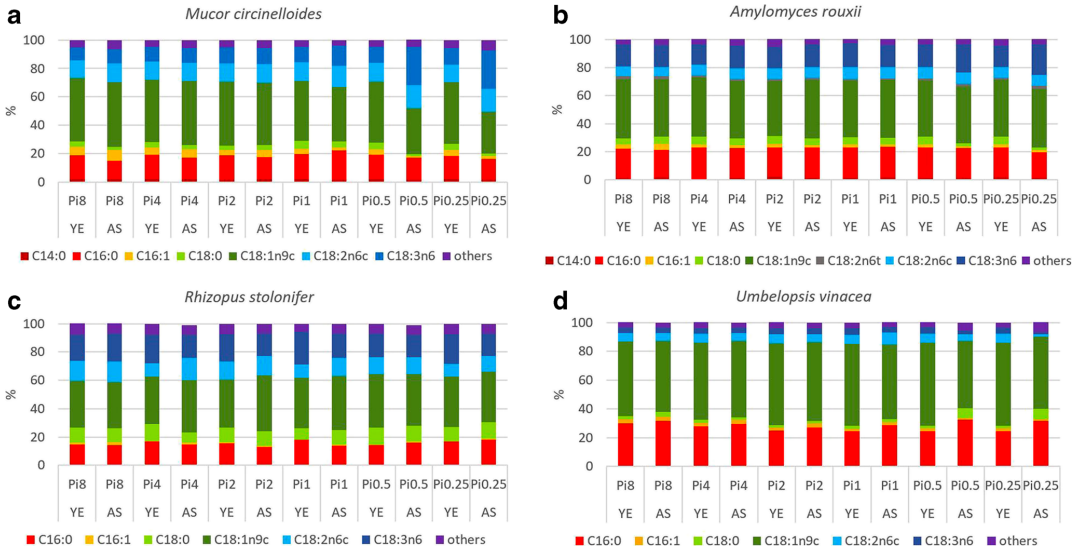

Fig. 3 Fatty acid profiles *Mucoraceae* and *Umbelopsidaceae*. Fatty acids present in the amount higher than 1% are displayed; remaining fatty acids produced in a lower amount are summed up and presented as others

Mortierellaceae fungi, where amount of unsaturated fatty acids, specifically arachidonic fatty acid, decreased under the low phosphorus source availability (Fig. 5). Interestingly, MHY grown under the phosphorus limitation had a similar fatty acid profile as for the reference (Pi1) condition (Fig. 5). Fungi from the family *Cunninghamellaceae* showed diverse responses towards the low amounts of phosphorus source. For CBL, an increase in oleic acid up to 56.87% at Pi0.25 was observed (Fig. 4a). For AGL, a decrease in the content of oleic, linoleic, and γ-linolenic fatty acids, as well as an increase in stearic fatty acid was observed (Fig. 4b, Fig. 4c).

High (Pi8 and Pi4) phosphorus source availability did not have a significant influence on the fatty acid profile of TAGs accumulated in *Mucoraceae* fungi. For *Cunninghamellaceae*, except RST, high phosphorus source concentrations induced decrease in oleic acid accompanied with the increase in stearic

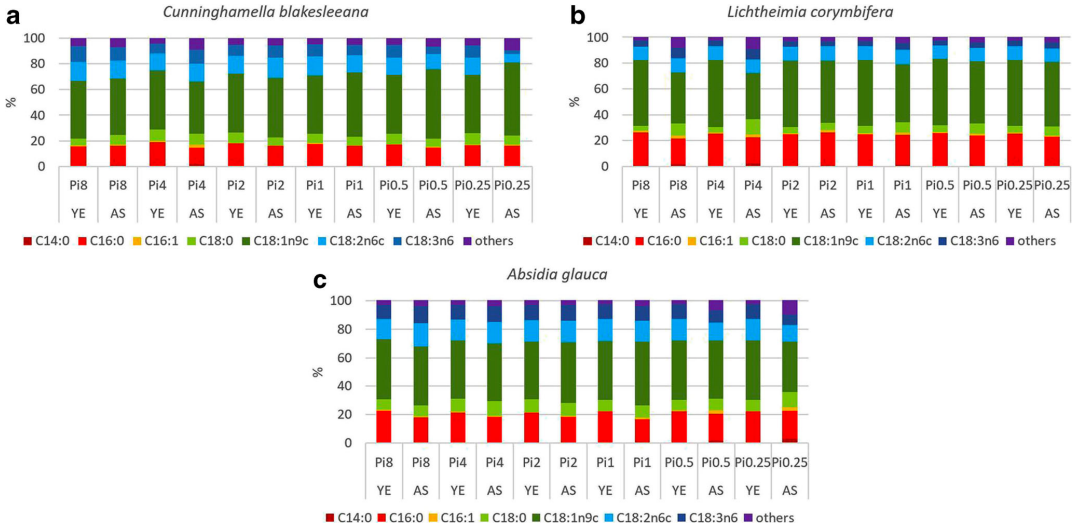

Fig. 4 Fatty acid profile of *Cunninghamellaceae*. Fatty acids present in the amount higher than 1% are displayed; remaining fatty acids produced in a lower amount are summed up and presented as others

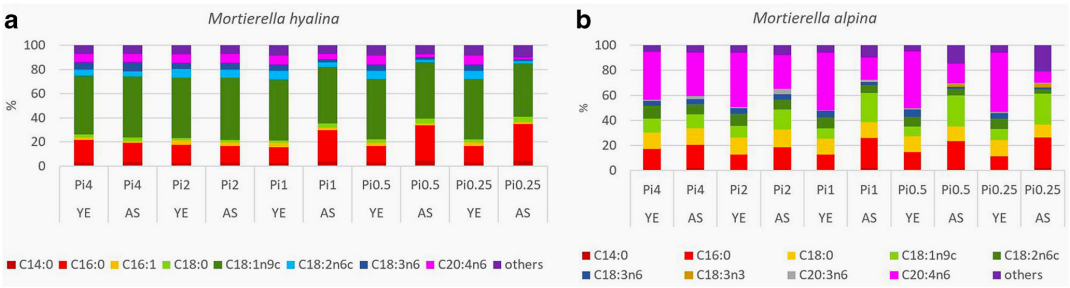

Fig. 5 Fatty acid profiles of *Mortierellaceae*. Fatty acids present in the amount higher than 1% are displayed; remaining fatty acids produced in a lower amount are summed up and presented as others

acid (Fig. 4a, b). Thus, the difference in oleic fatty acid content for LCO and CBL was approximately 10% and 7%, respectively, in comparison to the reference phosphorus source condition (Pi1). Moreover, the relative content of stearic acid was doubled for LCO (Fig. 4). This is an indication that for these fungi high phosphorus source amount is possibly attenuating the activity of enzyme DS9, which is responsible for the desaturation of the bond at C9 position.

For ARO and RST, fatty acid profiles of the accumulated TAGs were not affected by the variation in inorganic phosphorus source and the type of nitrogen substrate. Further, interesting results were observed for UVI and LCO. These strains showed very similar lipid profile in YE-Pi media, while in AS-Pi media, phosphorus source availability affected these fungi in different ways. Increasing Pi source amount induced production of monounsaturated TAGs in UVI, whereas it led to more saturated lipids in LCO (Figs. 3, and 4).

Evaluating *Mucoromycota* lipids for biofuels application

Degree of unsaturation, or unsaturation index (UI), is an important parameter when evaluating the suitability of fatty acids for biofuel applications, and it is closely connected to the oxidation stability of lipids. The calculation of UI was performed for the TAGs of all *Mucoromycota* fungi with the exception of *Mortierella* strains, due to the fact that they produce relatively high amount of long-chain polyunsaturated fatty acids, which are as *tetraene*, not included in the calculation formula of UI. The unsaturation index was calculated as follows:

$$UI = [\Sigma(\%\text{monoene} + 2 \times \%\text{ diene} + 3 \times \%\text{ triene})]/100$$

(Sumner and Morgan 1969).

It was observed that the UI of the produced in *Mucoromycota* TAGs, and respectively, the oxidation stability of the biofuel, increase with the limitation of phosphorus source in the growth medium. The UI was more stable for lipids produced by fungi grown in YE-Pi media, with the exception of UVI, where UI was lower with the increased phosphorus source availability. Limited availability of phosphorus source in the media with the ammonium sulphate resulted in a lower UI for MCI, ARO, CBL, AGL, and UVI (Fig. 6).

Discussion

Fungi grown in YE-based nitrogen-limited broth media showed relatively stable biomass and lipid yield without significant changes depending on the level of inorganic phosphorus source (Pi) in comparison with ammonium sulphate (AS)-based media (Fig.1a, b). Yeast extract (YE) is a complex, nutrient rich N-source which is initially containing approx. 2.5% of organic phosphorus. Thus, the addition of moderate amounts of inorganic phosphorus substrate (Pi1, Pi2, and Pi4) had neglectable effects on the growth and lipid accumulation, while high (Pi8) and low (Pi0.5 and Pi0.25) Pi substrate concentrations influenced the fungal growth and lipid accumulation, as discussed further (Fig. 1a). A decrease in the biomass and lipid yield was observed for all *Mucoromycota* fungi when grown in the presence of high concentration of inorganic phosphorus source (Pi8) and YE as a nitrogen substrate (Fig. 1a). In addition, high Pi source amount (Pi8) was toxic for MAL and MHY strains and inhibited their growth completely. The opposite effect was observed when lower amount of Pi source (Pi 0.5 and Pi 0.25) was present in the media, the biomass and respectively lipid yield was increased for AGL, ARO, RST, and MHY (Fig. 1a). Thus, the observed results indicate that when using a rich organic nitrogen source such as yeast extract, the level of Pi source should not exceed Pi4 in order to achieve high biomass and lipid yield for *Mucoromycota* fungi.

The growth and lipid accumulation of oleaginous *Mucoromycota* fungi, grown in a nitrogen-limited broth-media with the inorganic nitrogen source ammonium sulphate (AS), were strongly influenced by the inorganic phosphorus

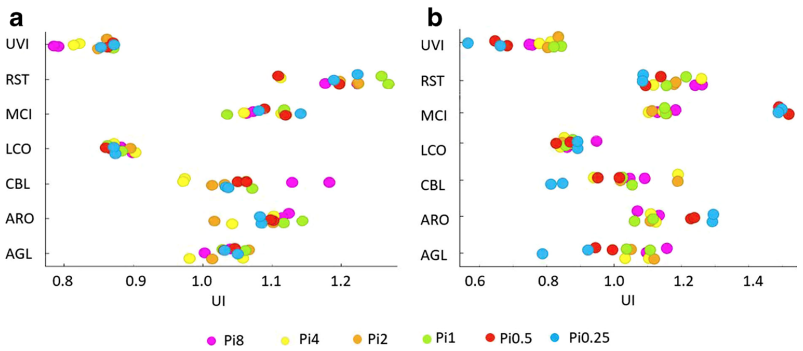

Fig. 6 Unsaturation index of fungal TAGs grown in YE-Pi (**a**) and AS-Pi (**b**) media

source (Pi) availability. It was observed that fungal growth and lipid accumulation in the media with the low Pi source amounts (Pi0.5 and Pi0.25) were substantially lower than in the media with the moderate (Pi1, P2, and Pi4) and high Pi source concentrations (Pi8) (Fig. 1b). Inorganic phosphate salts play buffering role in the growth media, and their low levels led to the decrease of pH (Table S1 in Supplementary Material). Low pH as the consequence of low Pi source therefore negatively affected the growth and lipid accumulation. When decreased amount of phosphate salts (Pi0.5 and Pi0.25) was combined with YE, the buffering function of Pi was substituted by the buffering capacity of YE (Dzurendova et al. 2020). The major advantage of Duetz micro-cultivation setup is the miniaturization of culture volume, which allows high throughput screening of many different media and strains at the same time. Unfortunately, these can only be performed in a set-up with only start-end pH measurement without continuous pH tuning available. Bioreactor cultivation under pH-controlled conditions would shed light on the effect of low Pi concentrations when using AS on the biomass and lipid production, excluding the factor of low pH.

Our study showed that several *Mucoromycota* fungi have relatively low biomass production under lipogenesis conditions. Thus, the results of low biomass for *Rhizopus (oryzae)* and CBL were in accordance with the previously performed study by Janakiraman (2014). Furthermore, the biomass and lipid production of RST were quite low, approx. 5 g/L and 2 g/L, respectively. There are several strategies for the optimization of the biomass production, such as increasing the nitrogen substrate content in the media, addition of stimulators, and/or using different cultivation temperatures. For example, biomass yield and lipid accumulation for *Mortierella* species could be improved by supplementation with soy flour, vegetable oils, temperature switch, and fed-batch cultivation (Singh and Ward 1997). However, those were not tested since they were outside the scope of this study.

The fatty acid profile of fungal lipids is dependent on the growth phase, which was affected by the low pH caused by low Pi source availability in the AS-Pi media. When using above described transesterification method, fatty acids present in different types of lipids (mono-, di-, triglycerides; phospholipids, and free fatty acids) are turned into FAMEs. Our previous studies and reference literature support the fact that majority of lipids present in studied *Mucoromycota* are in the form of TAGs (Forfang et al. 2017; Ratledge 2010). Therefore, the majority of FAMEs obtained after transesterification originate from TAGs. Furthermore, when assessing lipids for biodiesel application, lipids are converted into FAMEs; therefore, the used transesterification protocol was suitable from this point of view. It was observed that low Pi source availability caused changes in the content of stearic, oleic, linoleic, γ-linolenic, and arachidonic acids. Thus, low Pi source concentrations have possibly affected the activity of enzymes DS9, DS12, EL, DS12, and DS6 (Fig. S2 in Supplementary Materials). It can be noted, that based on the fatty acid profiles, the activity of enzymes DS9, DS6, and DS12 seemed inhibited in some cases while for others, it was enhanced under the low Pi source availability. Interestingly, low amount of Pi substrate possibly inhibited the activity of desaturases (DS6, EL, and DS5), resulting in the decrease of polyunsaturated fatty acids. The importance of phosphorus source availability on the activity of desaturase enzymes could be revealed by the increased unsaturation of fatty acids in *Mortierella* strains under the moderate (Pi2) and high Pi (Pi4) source concentrations in AS-based media (Fig. 5). The same Pi source amounts in YE-based media caused decrease in the unsaturation, indicating that *Mortierellaceae* fungi would require a careful optimization of phosphorus source content in the media. Detailed enzymatic study would be needed to confirm the effect of Pi on the lipogenesis enzymes.

Due to the fact that single-cell oil-based biofuels are one of the rapidly growing biofuels sector demanding alternative source of lipids, we performed an evaluation of *Mucoromycota* lipids for possible biofuels application. It is well known, that the more double bonds are present in a fatty acid, the more it is prone towards the oxidation (Yaakob et al. 2014). While, some monounsaturated fatty acids, as for

example, oleic acid, have been reported for being stable towards the oxidation (Hernandez 2016); polyunsaturated fatty acids, which are often produced by *Mucoromycota* fungi, are rapidly oxidizing molecules and therefore need to be avoided and separated from the lipids subjected to the production of lipid-based biofuels. Thus, the lower the UI of the produced fatty acids, the more suitable they are for the production of lipid-based biofuels. Among the studied *Mucoromycota* fungi, strains UVI, LCO, and CBL showed the most suitable UI of lipids for the lipid-based biofuels application. For strains producing TAGs containing increased amount of linolenic acid—ARO, RST, AGL, and MCI, it would possibly require the addition of antioxidants (Botella et al. 2014) when producing biofuels.

To conclude, yeast extract could be considered as a suitable organic N source requiring from very limited to no phosphorus substrate addition for obtaining consistent biomass and lipid yield and fatty acid profile. When inorganic nitrogen source ammonium sulphate was used, it required strain-specific optimization of phosphorus source concentration to achieve optimal biomass and lipid production as well as fatty acid profile. Low Pi source availability in AS-Pi media resulted in low pH which negatively affected the fungal growth. Considering the buffering capacity and the cost of yeast extract and ammonium sulphate, the economical sustainability of these substrates needs to be carefully evaluated. The price is dependent on required quality and amount. The price for yeast extract for use in microbial growth medium is 198 USD per kg (Sigma Aldrich, St. Louis, Missouri, USA; molecular biology grade), while the cost of ammonium sulphate is considerably lower—74 USD per kg (Sigma Aldrich, St. Louis, Missouri, USA; ReagentPlus grade, ≥ 99.0%).

We showed that phosphorus source influence on the biomass yield, lipid product, and fatty acid profile is strain-specific, and both low and/or high phosphorus source availability can have beneficial effects. Among the tested *Mucoromycota* fungi, interesting findings were observed for (i) UVI which showed extraordinary high biomass and lipid yield (22 g/L and 63.55%) at relatively high phosphorus source amount; (ii) RST showed an obvious advantage in managing the acidic pH caused by phosphorus source deficiency, since its growth, lipid accumulation, and fatty acid profile did not change under different phosphorus source amounts; (iii) MAL and MHY showed high sensitivity to the high levels of phosphorus substrate, while moderate amounts resulted in the increase of the lipid accumulation and unsaturation.

Authors' contributions Conceived the research idea: VS, BZ, AK. Designed the experiments: SD, VS, BZ, AK. Methodology: VS, BZ, AK. Performed the growth experiments: SD. Performed the lipid extraction: SD, BZ. Analyzed the data: SD, BZ, VT, VS, AK. Discussed the results: SD, VS, BZ, AK, VT, DE. Wrote the manuscript: SD. Discussed and revised the manuscript: SD, VS, BZ, AK, VT, DE. All authors read and approved the final manuscript.

Funding information Open Access funding provided by Norwegian University of Life Sciences. The study was funded by the Research Council of Norway-FMETEKN grant, project number 257622; BIONÆR grant, project number 305215; DAAD grant, project number 309220; HAVBRUK2 grant, project number 302543/E40; MATFONDAVTALE grant, project number 301834/E50.

Availability of data and materials The datasets generated and/or analyzed during the current study are available in the manuscript and its supplementary materials.

Compliance with ethical standards

Competing interests The authors declare that they have no competing interests.

Ethics approval and consent to participate Not applicable.

Consent for publication Not applicable.

References

Akpinar-Bayizit A (2014) Fungal lipids: the biochemistry of lipid accumulation. Int J Chem Eng Appl 5(5):409

Bhanja A, Minde G, Magdum S, Kalyanraman V (2014) Comparative studies of oleaginous fungal strains (*Mucor circinelloides* and *Trichoderma reesei*) for effective wastewater treatment and bio-oil production. Biotechnol Res Int 2014:479370

Bharathiraja B, Sridharan S, Sowmya V, Yuvaraj D, Praveenkumar R (2017) Microbial oil–a plausible alternate resource for food and fuel application. Bioresour Technol 233:423–432

Botella L, Bimbela F, Martín L, Arauzo J, Sánchez JL (2014) Oxidation stability of biodiesel fuels and blends using the Rancimat and PetroOXY methods. Effect of 4-allyl-2, 6-dimethoxyphenol and catechol as biodiesel additives on oxidation stability. Front Chem 2:43

Braunwald T, Schwemmlein L, Graeff-Hönninger S, French WT, Hernandez R, Holmes WE, Claupein W (2013) Effect of different C/N ratios on carotenoid and lipid production by *Rhodotorula glutinis*. Appl Microbiol Biotechnol 97(14):6581–6588

Chan LG, Cohen JL, Ozturk G, Hennebelle M, Taha AY, de Moura Bell JML (2018) Bioconversion of cheese whey permeate into fungal oil by *Mucor circinelloides*. J Biol Eng 12(1):25

Chiriboga O, Rorrer GL (2019) Phosphate addition strategies for enhancing the co-production of lipid and chitin nanofibers during fed-batch cultivation of the diatom *Cyclotella* sp. Algal Res 38:101403

Correa DF, Beyer HL, Fargione JE, Hill JD, Possingham HP, Thomas-Hall SR, Schenk PM (2019) Towards the implementation of

sustainable biofuel production systems. Renew Sust Energ Rev 107: 250–263

Cortes MAL, de Carvalho CC (2015) Effect of carbon sources on lipid accumulation in *Rhodococcus* cells. Biochem Eng J 94:100–105

Demšar J, Curk T, Erjavec A, Gorup Č, Hočevar T, Milutinovič M, Možina M, Polajnar M, Toplak M, Starič A (2013) Orange: data mining toolbox in Python. J Mach Learn Res 14(1):2349–2353

Duetz WA, Witholt B (2001) Effectiveness of orbital shaking for the aeration of suspended bacterial cultures in square-deepwell microtiter plates. Biochem Eng J 7(2):113–115

Dyal SD, Bouzidi L, Narine SS (2005) Maximizing the production of γ-linolenic acid in *Mortierella ramanniana* var. *ramanniana* as a function of pH, temperature and carbon source, nitrogen source, metal ions and oil supplementation. Food Res Int 38(7):815–829

Dzurendova S, Zimmermann B, Kohler A, Tafintseva V, Slany O, Certik M, Shapaval V (2020) Microcultivation and FTIR spectroscopy-based screening revealed a nutrient-induced co-production of high-value metabolites in oleaginous *Mucoromycota* fungi. PLoS One 15(6):e0234870

Economou CN, Aggelis G, Pavlou S, Vayenas DV (2011) Single cell oil production from rice hulls hydrolysate. Bioresour Technol 102(20): 9737–9742

Esakkimuthu S, Krishnamurthy V, Govindarajan R, Swaminathan K (2016) Augmentation and starvation of calcium, magnesium, phosphate on lipid production of *Scenedesmus obliquus*. Biomass Bioenergy 88:126–134

Evans CT, Ratledge C (1983) A comparison of the oleaginous yeast, *Candida curvata*, grown on different carbon sources in continuous and batch culture. Lipids 18(9):623–629

Evans CT, Ratledge C (1984) Effect of nitrogen source on lipid accumulation in oleaginous yeasts. Microbiol 130(7):1693–1704

Fakas S, Papanikolaou S, Batsos A, Galiotou-Panayotou M, Mallouchos A, Aggelis G (2009) Evaluating renewable carbon sources as substrates for single cell oil production by *Cunninghamella echinulata* and *Mortierella isabellina*. Biomass Bioenergy 33(4):573–580

Feng P, Deng Z, Fan L, Hu Z (2012) Lipid accumulation and growth characteristics of *Chlorella zofingiensis* under different nitrate and phosphate concentrations. J Biosci Bioeng 114(4):405–410

Forfang K, Zimmermann B, Kosa G, Kohler A, Shapaval V (2017) FTIR spectroscopy for evaluation and monitoring of lipid extraction efficiency for oleaginous fungi. PLoS One 12(1):e0170611

Harrington PB, Vieira NE, Espinoza J, Nien JK, Romero R, Yergey AL (2005) Analysis of variance–principal component analysis: a soft tool for proteomic discovery. Anal Chim Acta 544(1–2):118–127

Heredia-Arroyo T, Wei W, Ruan R, Hu B (2011) Mixotrophic cultivation of *Chlorella vulgaris* and its potential application for the oil accumulation from non-sugar materials. Biomass Bioenergy 35(5): 2245–2253

Hernandez EM (2016) In: Sanders T (ed) Specialty oils: functional and nutraceutical properties. Functional dietary lipids. Woodhead Publishing, Sawston, pp 69–101

Huang X, Luo H, Mu T, Shen Y, Yuan M, Liu J (2018) Enhancement of lipid accumulation by oleaginous yeast through phosphorus limitation under high content of ammonia. Bioresour Technol 262:9–14

Janakiraman S (2014) Harnessing indigenous plant seed oil for the production of bio-fuel by an oleaginous fungus, *Cunninghamella blakesleeana*-JSK2, isolated from tropical soil. Appl Biochem Biotechnol 172(2):1027–1035

Jiru TM, Abate D (2014) Oleaginous microorganisms, diversity, lipid biosynthesis pathway and strain improvement. Webpub J Sci Res 2(6):55–65

Kavadia A, Komaitis M, Chevalot I, Blanchard F, Marc I, Aggelis G (2001) Lipid and γ-linolenic acid accumulation in strains of *Zygomycetes* growing on glucose. J Am Oil Chem Soc 78(4):341–346

Kosa G, Kohler A, Tafintseva V, Zimmermann B, Forfang K, Afseth NK, Tzimorotas D, Vuoristo KS, Horn SJ, Mounier J (2017a) Microtiter plate cultivation of oleaginous fungi and monitoring of lipogenesis by high-throughput FTIR spectroscopy. Microb Cell Factories 16(1):101

Kosa G, Shapaval V, Kohler A, Zimmermann B (2017b) FTIR spectroscopy as a unified method for simultaneous analysis of intra-and extracellular metabolites in high-throughput screening of microbial bioprocesses. Microb Cell Factories 16(1):195

Kosa G, Vuoristo KS, Horn SJ, Zimmermann B, Afseth NK, Kohler A, Shapaval V (2018a) Assessment of the scalability of a microtiter plate system for screening of oleaginous microorganisms. Appl Microbiol Biotechnol 102(11):4915–4925

Kosa G, Zimmermann B, Kohler A, Ekeberg D, Afseth NK, Mounier J, Shapaval V (2018b) High-throughput screening of *Mucoromycota* fungi for production of low-and high-value lipids. Biotechnol Biofuels 11(1):66

Lewis T, Nichols PD, McMeekin TA (2000) Evaluation of extraction methods for recovery of fatty acids from lipid-producing microheterotrophs. J Microbiol Methods 43(2):107–116

Li Y, Han F, Xu H, Mu J, Chen D, Feng B, Zeng H (2014) Potential lipid accumulation and growth characteristic of the green alga *Chlorella* with combination cultivation mode of nitrogen (N) and phosphorus (P). Bioresour Technol 174:24–32

Lima MAB, Nascimento AE, Wd S, Fukushima K, Campos-Takaki GM (2003) Effects of phosphorus on polyphosphate accumulation by *Cunninghamella elegans*. Braz J Microbiol 34:363–372

Meng X, Yang J, Xu X, Zhang L, Nie Q, Xian M (2009) Biodiesel production from oleaginous microorganisms. Renew Energy 34(1):1–5

Meyer V, Basenko EY, Benz JP, Braus GH, Caddick MX, Csukai M, de Vries RP, Endy D, Frisvad JC, Gunde-Cimerman N (2020) Growing a circular economy with fungal biotechnology: a white paper. Fungal Biol and Biotechnol 7:1–23

Mirbagheri M, Nahvi I, Emamzade R (2015) Reduction of chemical and biological oxygen demands from oil wastes via oleaginous fungi: an attempt to convert food by products to essential fatty acids. Iran J Biotechnol 13(2):25–30

Ozsoy HD, Arikan EB, Cinkir C, Eryilmaz GD, Kucuk D, van Leeuwen JH (2015) Fungal oil production from oleaginous fungi *Mucor circinelloides* and *Aspergillus oryzae* cultivated on sugar beet pulp. Acad Platform J Eng Sci 3:735–741

Papanikolaou S, Galiotou-Panayotou M, Fakas S, Komaitis M, Aggelis G (2007) Lipid production by oleaginous *Mucorales* cultivated on renewable carbon sources. Eur J Lipid Sci Technol 109(11):1060–1070

Pinheiro H, Teixeira J, Francini-Filho R, Soares-Gomes A, Ferreira C, Rocha L (2018) Hope and doubt for the world's marine ecosystems. Perspect Ecol Conser 17(1):19–25

Prasad G, Girisham S, Reddy S, Srisailam K (2008) Biotransformation of albendazole by *Cunninghamella blakesleeana*: effect of carbon and nitrogen source. World J Microbiol Biotechnol 24(10):2055–2059

Qiao W, Tao J, Luo Y, Tang T, Miao J, Yang Q (2018) Microbial oil production from solid-state fermentation by a newly isolated oleaginous fungus, *Mucor circinelloides* Q531 from mulberry branches. Roy Soc Open Sci 5(11):180551

Ratledge C (2004) Fatty acid biosynthesis in microorganisms being used for single cell oil production. Biochimie 86(11):807–815

Ratledge C (2010) Single cell oils for the 21st century. In: Cohen ZR, C. (eds) Single cell oils: microbial and algal oils. AOCS, Urbana, pp 3–26

Ratledge C, Wynn JP (2002) The biochemistry and molecular biology of lipid accumulation in oleaginous microorganisms. Adv Appl Microbiol 51:1–52

Roopnarain A, Gray V, Sym S (2014) Phosphorus limitation and starvation effects on cell growth and lipid accumulation in *Isochrysis*

galbana U4 for biodiesel production. Bioresour Technol 156:408–411

Safaei Z, Karimi K, Zamani A (2016) Impact of phosphate, potassium, yeast extract, and trace metals on chitosan and metabolite production by *Mucor indicus*. Int J Mol Sci 17(9):1429

Sala E, Lubchenco J, Grorud-Colvert K, Novelli C, Roberts C, Sumaila UR (2018) Assessing real progress towards effective ocean protection. Mar Policy 91:11–13

Singh A, Ward O (1997) Production of high yields of arachidonic acid in a fed-batch system by *Mortierella alpina* ATCC 32222. Appl Microbiol Biotechnol 48(1):1–5

Subhash GV, Mohan SV (2011) Biodiesel production from isolated oleaginous fungi *Aspergillus* sp. using corncob waste liquor as a substrate. Bioresour Technol 102(19):9286–9290

Subhash GV, Mohan SV (2015) Sustainable biodiesel production through bioconversion of lignocellulosic wastewater by oleaginous fungi. Biomass Convers Bior 5(2):215–226

Sumner J, Morgan E (1969) The fatty acid composition of sporangiospores and vegetative mycelium of temperature-adapted fungi in the order *Mucorales*. Microbiology 59(2):215–221

Toplak M, Birarda G, Read S, Sandt C, Rosendahl S, Vaccari L, Demšar J, Borondics F (2017) Infrared orange: connecting hyperspectral data with machine learning. Synchrotron Radiat News 30(4):40–45

van der Voort M, Spruijt J, Potters J, Elissen H (2017) Socio-economic assessment of algae-based PUFA production: the value chain from microalgae to PUFA ('PUFACHAIN'). PUFAChain

Wang Y, Zhang S, Zhu Z, Shen H, Lin X, Jin X, Jiao X, Zhao ZK (2018) Systems analysis of phosphate-limitation-induced lipid accumulation by the oleaginous yeast *Rhodosporidium toruloides*. Biotechnol Biofuels 11(1):148

Werner TP, Amrhein N, Freimoser FM (2007) Specific localization of inorganic polyphosphate (poly P) in fungal cell walls by selective extraction and immunohistochemistry. Fungal Genet Biol 44(9): 845–852

Wu S, Hu C, Jin G, Zhao X, Zhao ZK (2010) Phosphate-limitation mediated lipid production by *Rhodosporidium toruloides*. Bioresour Technol 101(15):6124–6129

Wu Y-H, Yu Y, Hu H-Y (2013) Potential biomass yield per phosphorus and lipid accumulation property of seven microalgal species. Bioresour Technol 130:599–602

Yaakob Z, Narayanan BN, Padikkaparambil S (2014) A review on the oxidation stability of biodiesel. Renew Sust Energ Rev 35:136–153

Ykema A, Verbree EC, Kater MM, Smit H (1988) Optimization of lipid production in the oleaginous yeast *Apiotrichum curvatum* in whey permeate. Appl Microbiol Biotechnol 29(2–3):211–218

Zeng Y, Ji X-J, Chang S-M, Nie Z-K, Huang H (2012) Improving arachidonic acid accumulation in *Mortierella alpina* through B-group vitamin addition. Bioprocess Biosyst Eng 35(5):683–688

Zheng Y, Yu X, Zeng J, Chen S (2012) Feasibility of filamentous fungi for biofuel production using hydrolysate from dilute sulfuric acid pretreatment of wheat straw. Biotechnol Biofuels 5(1):50

Zhu M, Yu L-J, Wu Y-X (2003) An inexpensive medium for production of arachidonic acid by *Mortierella alpina*. J Ind Microbiol 30(1):75–79

Applied Microbiology and Biotechnology

The influence of phosphorus source and the nature of nitrogen substrate on the biomass production and lipid accumulation in oleaginous *Mucoromycota* fungi

Simona Dzurendova[1*], Boris Zimmermann[1], Valeria Tafintseva[1], Achim Kohler[1], Dag Ekeberg[2], Volha Shapaval[1]

[1]Norwegian University of Life Sciences, Faculty of Science and Technology,

Droebakveien 31, 1430 Aas, Norway

[2]Norwegian University of Life Sciences, Faculty of Chemistry, Biotechnology and Food Science, Christian Magnus Falsens vei 1, 1433 Aas, Norway

*Correspondence:

Simona Dzurendova

email: simona.dzurendova@gmail.com; simona.dzurendova@nmbu.no

phone: +47 94785832

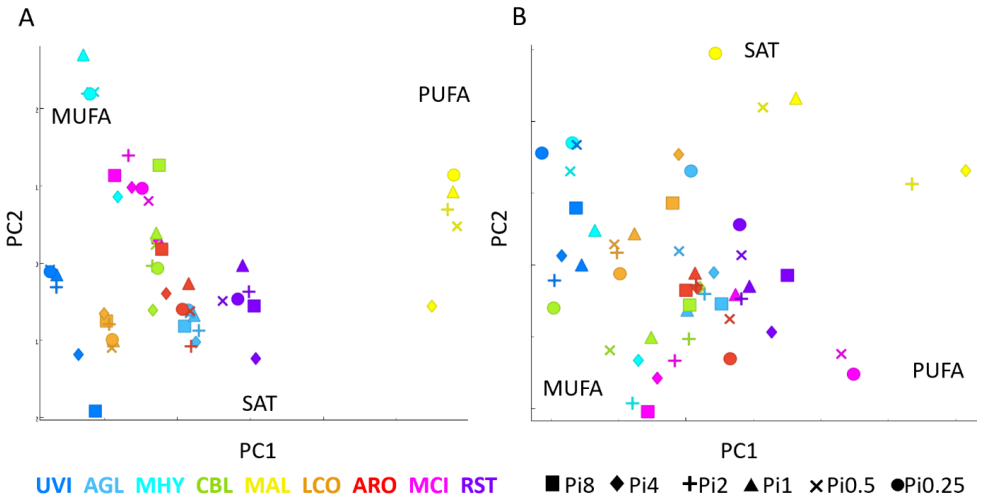

Fig. S1: PCA scatter plot of fatty acid profile of the accumulated TAGs in *Mucoromycota* fungi grown in the presence of different phosphorus amounts in the growth media with YE (A) and AS (B) as nitrogen source.

Table S1: Average pH of culture supernatant

Average pH		**Pi 8**	**Pi 4**	**Pi 2**	**Pi 1**	**Pi 0.5**	**Pi 0.25**
MCI	YE	5.91	5.98	5.95	5.97	5.59	4.30
	AS	5.55	5.38	4.34	2.91	2.34	2.21
AGL	YE	4.59	3.98	3.72	3.61	3.49	3.67
	AS	4.41	3.91	3.65	3.05	2.50	2.28
LCO	YE	5.54	5.59	5.56	5.54	5.33	5.25
	AS	5.61	5.46	4.59	3.03	2.50	2.41
UVI	YE	5.42	5.46	5.44	5.49	5.37	5.26
	AS	5.21	4.76	3.72	2.26	1.78	1.72
CBL	YE	5.72	5.56	5.48	5.19	4.78	4.35
	AS	5.35	4.77	3.96	2.52	2.07	2.94
ARO	YE	5.39	5.32	5.06	4.58	3.95	3.57
	AS	5.42	5.17	4.36	2.40	1.81	1.69
MAL	YE	6.00	5.55	5.59	5.72	5.61	5.51
	AS	5.80	5.49	4.36	3.08	2.97	2.95
RST	YE	5.19	3.97	3.74	3.90	3.26	4.41
	AS	5.02	3.87	3.01	2.32	1.86	1.66
MHY	YE	5.31	5.16	5.37	5.52	5.05	5.21
	AS	5.29	4.91	4.36	2.51	2.35	3.49

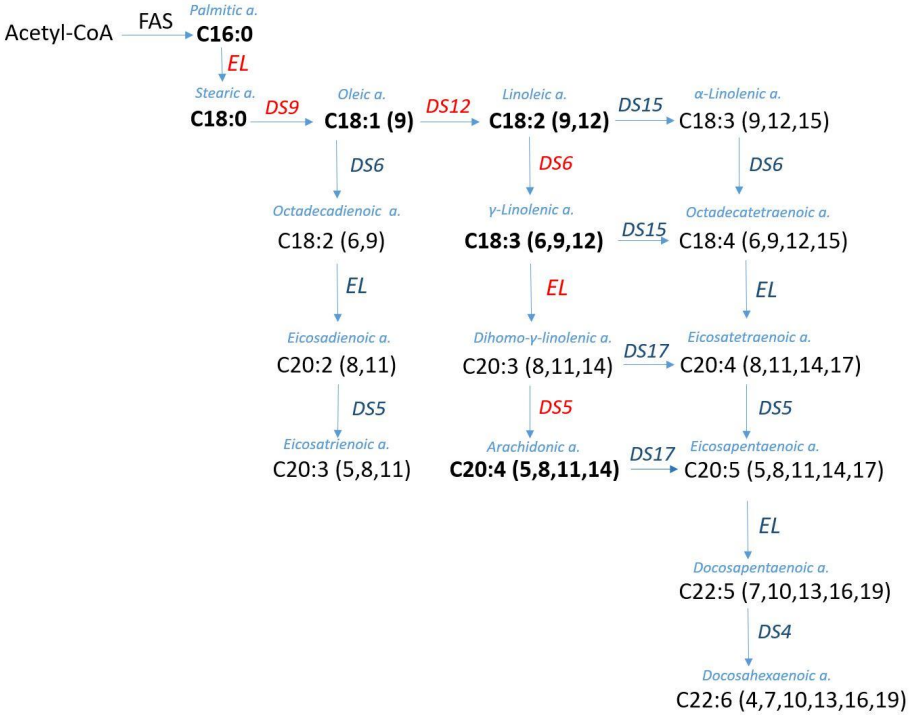

Fig. S2: Fatty acid synthesis in oleaginous microorganisms, adapted from (Ratledge and Wynn 2002). Fatty acids produced by strains used in the study are marked in bold. FAS- fatty acid synthase; DS- desaturase; EL- elongase. Enzymes affected by Pi variation are marked red.

Ratledge C, Wynn JP (2002) The biochemistry and molecular biology of lipid accumulation in oleaginous microorganisms Adv Appl Microbiol 51:1-52

Table S2: Fatty acid profiles

			C14:0	C16:0	C16:1	C18:0	C18:1n9c	C18:2n6t	C18:2n6c	C18:3n6	C20:4n6
MCI	**YE**	**Pi8**	2.05	16.67	6.03	3.53	45.13	0.75	12.22	9.09	0.04
MCI	**YE**	**Pi4**	1.91	17.17	4.94	3.98	44.23	0.66	12.84	10.10	0.04
MCI	**YE**	**Pi2**	1.74	16.90	4.07	2.77	45.37	0.61	12.96	10.95	0.05
MCI	**YE**	**Pi1**	1.88	17.74	3.69	5.61	42.28	0.52	13.23	10.70	0.04
MCI	**YE**	**Pi0.5**	1.98	17.08	3.99	4.66	43.18	0.62	13.10	11.22	0.06
MCI	**YE**	**Pi0.25**	2.02	16.39	4.16	4.26	43.53	0.74	12.59	11.38	0.02
MCI	**AS**	**Pi8**	1.97	12.89	7.73	2.05	45.71	0.86	13.08	10.04	0.03
MCI	**AS**	**Pi4**	1.88	15.05	6.10	2.88	45.34	0.68	12.98	10.23	0.07
MCI	**AS**	**Pi2**	1.96	15.47	4.94	3.51	44.10	0.67	13.19	11.32	0.06
MCI	**AS**	**Pi1**	1.52	20.71	1.82	4.41	38.37	0.28	15.09	14.24	0.06
MCI	**AS**	**Pi0.5**	1.63	15.49	0.92	1.40	32.63	0.68	16.06	27.08	0.07
MCI	**AS**	**Pi0.25**	1.67	14.59	2.06	1.51	29.79	0.75	16.07	26.92	0.14
AGL	**YE**	**Pi8**	0.55	22.16	0.73	7.36	42.32	0.11	13.95	9.98	0.02
AGL	**YE**	**Pi4**	0.52	21.10	0.65	9.04	40.91	0.13	14.57	9.96	0.02
AGL	**YE**	**Pi2**	0.48	20.87	0.59	8.97	40.60	0.12	14.59	10.75	0.03
AGL	**YE**	**Pi1**	0.51	21.74	0.58	7.64	41.34	0.10	15.08	10.42	0.02
AGL	**YE**	**Pi0.5**	0.54	21.81	0.60	7.47	41.83	0.10	14.86	10.15	0.02
AGL	**YE**	**Pi0.25**	0.54	21.64	0.58	7.53	42.07	0.10	14.90	10.17	0.02
AGL	**AS**	**Pi8**	0.39	17.72	0.75	7.81	41.43	0.25	15.89	12.26	0.04
AGL	**AS**	**Pi4**	0.36	18.23	0.71	10.08	40.57	0.23	14.89	11.36	0.04
AGL	**AS**	**Pi2**	0.42	18.15	0.76	8.82	42.73	0.24	14.79	11.29	0.03
AGL	**AS**	**Pi1**	0.90	15.81	1.32	8.59	44.68	0.42	14.42	10.18	0.02
AGL	**AS**	**Pi0.5**	1.98	18.61	2.62	8.06	40.86	0.82	12.49	8.49	0.09
AGL	**AS**	**Pi0.25**	2.93	19.67	2.52	10.66	35.53	0.74	11.67	6.91	0.06
MHY	**YE**	**Pi4**	2.76	18.88	1.92	2.68	48.24	0.14	5.09	6.07	7.50
MHY	**YE**	**Pi2**	2.53	14.93	3.58	2.01	50.31	0.09	6.80	5.02	7.31
MHY	**YE**	**Pi1**	2.58	12.93	3.43	2.04	50.74	0.06	7.25	4.81	7.67
MHY	**YE**	**Pi0.5**	2.63	13.88	2.69	2.71	50.10	0.06	6.81	4.99	7.73
MHY	**YE**	**Pi0.25**	2.70	14.05	2.83	2.46	50.33	0.07	6.54	4.91	7.44
MHY	**AS**	**Pi4**	3.24	15.71	1.49	3.37	50.55	0.26	3.89	7.69	7.19
MHY	**AS**	**Pi2**	2.89	13.74	3.15	2.03	51.47	0.08	6.36	5.90	7.21
MHY	**AS**	**Pi1**	3.78	25.94	1.97	3.43	46.94	0.14	3.64	2.79	4.68
MHY	**AS**	**Pi0.5**	4.37	29.13	1.62	4.31	46.29	0.18	2.34	1.62	2.62
MHY	**AS**	**Pi0.25**	4.21	30.28	1.78	4.61	44.02	0.10	1.93	1.39	1.86
LCO	**YE**	**Pi8**	0.71	25.44	1.72	3.62	51.07	0.06	10.11	4.86	0.02
LCO	**YE**	**Pi4**	0.61	24.55	1.29	4.24	51.88	0.06	10.64	4.33	0.02
LCO	**YE**	**Pi2**	0.57	24.19	1.05	4.89	51.37	0.05	10.88	4.21	0.02
LCO	**YE**	**Pi1**	0.54	24.56	0.96	5.25	50.92	0.06	10.75	4.14	0.02
LCO	**YE**	**Pi0.5**	0.59	25.11	1.03	5.26	51.16	0.06	10.49	4.00	0.03
LCO	**YE**	**Pi0.25**	0.56	24.76	0.98	5.15	51.11	0.06	10.65	4.17	0.03
LCO	**AS**	**Pi8**	2.06	19.53	2.36	9.56	39.20	0.27	10.84	8.24	0.05
LCO	**AS**	**Pi4**	2.53	20.11	2.18	11.62	36.20	0.26	10.31	7.82	0.04
LCO	**AS**	**Pi2**	0.77	25.75	1.68	5.65	48.10	0.07	11.25	3.97	0.04
LCO	**AS**	**Pi1**	1.31	22.93	2.25	7.79	44.69	0.18	11.20	5.15	0.03
LCO	**AS**	**Pi0.5**	0.89	23.23	1.39	7.74	48.20	0.16	10.24	4.45	0.04
LCO	**AS**	**Pi0.25**	0.37	22.69	0.95	6.95	49.77	0.11	10.64	4.82	0.07

			C14:0	C16:0	C16:1	C18:0	C18:1n9c	C18:2n6t	C18:2n6c	C18:3n6	C20:4n6
CBL	**YE**	**Pi8**	0.49	15.09	0.72	5.55	45.06	0.76	14.41	12.49	0.08
CBL	**YE**	**Pi4**	0.64	18.29	0.76	9.28	46.03	0.40	13.29	7.25	0.05
CBL	**YE**	**Pi2**	0.57	17.24	0.64	7.97	45.95	0.51	13.69	8.48	0.07
CBL	**YE**	**Pi1**	0.61	17.09	0.58	7.16	45.73	0.55	14.37	9.59	0.04
CBL	**YE**	**Pi0.5**	0.59	16.33	0.54	8.11	45.85	0.62	13.49	9.84	0.03
CBL	**YE**	**Pi0.25**	0.59	16.06	0.49	9.04	45.49	0.63	12.91	9.55	0.06
CBL	**AS**	**Pi8**	1.09	14.78	1.02	7.59	44.23	0.72	13.53	10.50	0.05
CBL	**AS**	**Pi4**	2.02	12.57	2.33	8.85	40.53	0.82	13.69	10.79	0.03
CBL	**AS**	**Pi2**	0.60	15.26	0.67	6.32	46.42	0.70	15.48	9.73	0.04
CBL	**AS**	**Pi1**	0.49	15.47	0.58	6.78	50.09	0.60	13.41	7.87	0.04
CBL	**AS**	**Pi0.5**	0.42	14.43	0.84	5.98	54.21	0.47	11.57	5.79	0.03
CBL	**AS**	**Pi0.25**	0.45	15.71	0.91	6.94	56.87	0.37	6.68	2.80	0.09
UVI	**YE**	**Pi8**	0.77	30.21	2.57	2.39	51.60	0.12	6.05	3.79	0.04
UVI	**YE**	**Pi4**	0.74	27.73	2.59	2.20	53.57	0.16	6.16	3.95	0.04
UVI	**YE**	**Pi2**	0.68	24.89	2.21	1.81	56.77	0.14	6.25	4.18	0.03
UVI	**YE**	**Pi1**	0.69	24.40	2.05	1.85	56.80	0.15	6.45	4.54	0.03
UVI	**YE**	**Pi0.5**	0.69	24.49	2.12	1.73	57.75	0.15	6.25	4.34	0.03
UVI	**YE**	**Pi0.25**	0.72	24.60	2.25	1.63	57.49	0.16	6.12	4.27	0.03
UVI	**AS**	**Pi8**	0.84	31.82	2.67	3.64	48.96	0.15	5.78	3.68	0.04
UVI	**AS**	**Pi4**	0.82	29.51	2.88	2.05	52.56	0.22	5.64	3.84	0.03
UVI	**AS**	**Pi2**	0.82	27.25	2.71	1.78	54.62	0.21	5.49	4.05	0.03
UVI	**AS**	**Pi1**	0.82	28.81	2.11	1.94	51.92	0.11	8.17	3.93	0.04
UVI	**AS**	**Pi0.5**	0.71	32.69	1.30	6.60	46.61	0.12	4.77	2.53	0.04
UVI	**AS**	**Pi0.25**	0.79	31.66	1.48	6.90	50.04	0.51	1.66	1.28	0.10
RST	**YE**	**Pi8**	0.73	14.88	1.16	10.82	32.91	0.49	14.07	18.22	0.07
RST	**YE**	**Pi4**	0.63	16.97	0.51	11.92	33.34	0.99	9.39	20.12	0.06
RST	**YE**	**Pi2**	0.66	15.77	0.65	10.33	33.93	0.67	12.60	19.43	0.03
RST	**YE**	**Pi1**	0.61	18.06	0.22	8.11	35.41	1.02	9.34	22.90	0.02
RST	**YE**	**Pi0.5**	0.61	14.11	0.69	11.97	37.49	0.63	12.10	16.79	0.02
RST	**YE**	**Pi0.25**	0.58	16.74	0.30	9.89	35.74	1.07	8.92	21.00	0.07
RST	**AS**	**Pi8**	0.92	14.47	1.82	10.05	32.54	0.40	14.38	19.85	0.05
RST	**AS**	**Pi4**	0.59	11.90	0.99	7.33	35.51	0.38	15.55	16.27	0.07
RST	**AS**	**Pi2**	0.60	13.01	0.76	10.23	39.28	0.41	13.87	16.01	0.04
RST	**AS**	**Pi1**	0.62	14.03	0.70	10.42	37.86	0.52	12.98	17.18	0.08
RST	**AS**	**Pi0.5**	0.69	15.95	0.83	11.08	36.52	0.49	11.92	15.88	0.04
RST	**AS**	**Pi0.25**	0.76	18.14	0.89	11.42	35.52	0.47	11.39	15.68	0.07
ARO	**YE**	**Pi8**	1.54	20.59	3.18	4.15	42.57	1.83	7.22	15.54	0.05
ARO	**YE**	**Pi4**	0.69	22.27	2.45	5.23	42.65	1.24	7.73	14.30	0.06
ARO	**YE**	**Pi2**	2.20	20.91	2.36	5.80	39.37	1.31	7.71	14.82	0.06
ARO	**YE**	**Pi1**	1.69	21.43	2.13	5.20	40.33	1.26	8.42	16.67	0.02
ARO	**YE**	**Pi0.5**	1.52	21.73	2.00	5.57	40.08	1.21	8.24	15.88	0.06
ARO	**YE**	**Pi0.25**	1.77	21.29	2.32	5.26	40.63	1.33	8.05	14.97	0.06
ARO	**AS**	**Pi8**	2.10	19.34	4.06	5.48	40.69	2.15	6.54	15.53	0.05
ARO	**AS**	**Pi4**	1.55	20.91	2.40	4.70	40.97	1.41	7.62	16.20	0.04
ARO	**AS**	**Pi2**	1.50	21.41	1.85	4.78	41.76	1.20	8.09	15.89	0.03
ARO	**AS**	**Pi1**	1.75	21.84	1.49	4.70	41.47	0.83	8.51	15.26	0.04
ARO	**AS**	**Pi0.5**	1.60	20.87	1.48	2.34	40.44	1.49	8.30	20.12	0.04
ARO	**AS**	**Pi0.25**	1.50	18.14	1.67	1.76	41.93	1.94	8.05	21.22	0.05

			C14:0	C16:0	C16:1	C18:0	C18:1n9c	C18:2n6t	C18:2n6c	C18:3n6	C20:4n6
MAL	**YE**	**Pi4**	0.96	16.01	0.14	13.54	11.18	0.09	9.96	4.27	37.75
MAL	**YE**	**Pi2**	0.57	12.02	0.10	13.86	9.40	0.09	9.75	4.42	43.54
MAL	**YE**	**Pi1**	0.61	12.02	0.10	12.65	8.68	0.08	8.72	4.99	45.58
MAL	**YE**	**Pi0.5**	0.76	13.95	0.12	12.52	8.22	0.08	7.77	5.69	45.07
MAL	**YE**	**Pi0.25**	0.46	10.73	0.08	13.35	8.61	0.07	8.45	4.47	47.00
MAL	**AS**	**Pi4**	1.87	18.60	0.16	13.50	10.86	0.18	8.23	4.26	34.30
MAL	**AS**	**Pi2**	1.72	17.00	0.19	14.13	15.84	0.07	7.88	4.28	27.12
MAL	**AS**	**Pi1**	2.05	23.73	0.26	13.10	23.25	0.05	6.07	2.41	17.47
MAL	**AS**	**Pi0.5**	1.73	21.98	0.28	11.53	25.07	0.11	5.13	1.69	15.57
MAL	**AS**	**Pi0.25**	2.06	24.52	0.41	10.34	24.53	0.36	3.53	1.39	8.75

Paper III

Journal of *Fungi*

MDPI

Article

Metal and Phosphate Ions Show Remarkable Influence on the Biomass Production and Lipid Accumulation in Oleaginous *Mucor circinelloides*

Simona Dzurendova [1,*], Boris Zimmermann [1], Valeria Tafintseva [1], Achim Kohler [1], Svein Jarle Horn [2] and Volha Shapaval [1]

[1] Faculty of Science and Technology, Norwegian University of Life Sciences, Drøbakveien 31, 1430 As, Norway; boris.zimmermann@nmbu.no (B.Z.); valeria.tafintseva@nmbu.no (V.T.); achim.kohler@nmbu.no (A.K.); volha.shapaval@nmbu.no (V.S.)

[2] Faculty of Chemistry, Biotechnology and Food Science, Norwegian University of Life Sciences, Christian Magnus Falsens vei 1, 1433 As, Norway; svein.horn@nmbu.no

* Correspondence: simona.dzurendova@gmail.com or simona.dzurendova@nmbu.no

Received: 6 October 2020; Accepted: 27 October 2020; Published: 30 October 2020

Abstract: The biomass of *Mucor circinelloides,* a dimorphic oleaginous filamentous fungus, has a significant nutritional value and can be used for single cell oil production. Metal ions are micronutrients supporting fungal growth and metabolic activity of cellular processes. We investigated the effect of 140 different substrates, with varying amounts of metal and phosphate ions concentration, on the growth, cell chemistry, lipid accumulation, and lipid profile of *M. circinelloides*. A high-throughput set-up consisting of a Duetz microcultivation system coupled to Fourier transform infrared spectroscopy was utilized. Lipids were extracted by a modified Lewis method and analyzed using gas chromatography. It was observed that Mg and Zn ions were essential for the growth and metabolic activity of *M. circinelloides*. An increase in Fe ion concentration inhibited fungal growth, while higher concentrations of Cu, Co, and Zn ions enhanced the growth and lipid accumulation. Lack of Ca and Cu ions, as well as higher amounts of Zn and Mn ions, enhanced lipid accumulation in *M. circinelloides*. Generally, the fatty acid profile of *M. circinelloides* lipids was quite consistent, irrespective of media composition. Increasing the amount of Ca ions enhanced polyphosphates accumulation, while lack of it showed fall in polyphosphate.

Keywords: *Mucor circinelloides*; high-throughput screening; metal ions; phosphorus; lipids; biofuel; FTIR spectroscopy; bioremediation; co-production

1. Introduction

Mucor circinelloides is a dimorphic oleaginous filamentous fungus with a fully sequenced genome [1]. It has a versatile metabolism, allowing utilization of a variety of feedstocks, making this fungus widely applicable in a range of biotechnological processes [2]. *M. circinelloides* is well known as a robust cell factory, where extracellular products include enzymes (cellulases, lipases, proteases, phytases, and amylases) [2,3] and ethanol [4]. Further, *M. circinelloides* can synthesize and accumulate a number of valuable intracellular components, such as lipids, polyphosphates, carotenoids, and chitin/chitosan [5–9]. The biomass of *M. circinelloides* has a significant nutritional value and can be used as a feed ingredient [10]. Chitosan exhibits great chelating properties, mainly due to the low level of acetylation and the abundance of hydroxyl groups [9,11,12]. Due to the presence of chitin and

chitosan in the cell wall of *M. circinelloides*, the biomass of this fungus can be used as bioabsorbent for heavy metals and applied as a bioremediation agent, for example in the wastewater treatment [13].

M. circinelloides has been extensively studied for the production of lipids for different applications [14–16]. The lipids are mainly in the form of triacylglycerides (TAGs) and contain palmitic, stearic, oleic, linoleic acid, and y-linoleic acids that make it particularly suitable for biodiesel production [17]. Therefore, the biomass of *M. circinelloides* could be considered as an important alternative feedstock for the biodiesel industry [18]. However, the cost of the *M. circinelloides* biomass production for biodiesel as a sole product is still too high compared to competitive bioprocesses. Thus, there is a need to further optimize lipid and biomass yield for *M. circinelloides*, and develop a coproduction concept, where other valuable components could be produced along with lipids in a single fermentation process [19,20].

Lipid accumulation, as well as biomass formation, can be affected by many different cultivation parameters, such as the nutrient composition of the growth medium, temperature, pH, aeration, or parameter shift during the fermentation (temperature/pH) [2,21,22]. Optimization of the nutrient composition of the growth medium is one of the most important aspects in improving fungal lipid production. In order to increase lipid and biomass yields, it is crucial to understand the role and effect of all media components. Many studies have assessed the effect of different carbon (C) and nitrogen (N) sources on the fungal lipid production in *Mucoromycota* fungi [23–29], where nitrogen limitation in carbon-rich media is the most frequently used strategy for inducing lipid accumulation and achieving high lipid yields. Macro- and micronutrients, such as phosphorus (P), potassium (K), sulfur (S), calcium (Ca), sodium (Na), iron (Fe), and magnesium (Mg), have previously been reported as essential for optimal fungal growth and metabolic activity [30].

Metal ions play an important role in fungal metabolism as they provide necessary redox and catalytic activities for the cellular processes [31]. The role of metal ions in yeast metabolism has been widely studied [32–35]. Bivalent metal ions are often reported as cofactors for different enzymes [36,37]. Metal ions are usually examined in the context of bioremediation capabilities of *M. cicrcinelloides* [9,38], while the role of metal ions in lipid accumulation of *Mucoromycota* fungi have been examined only to a limited extent. Different metal ions have shown strain-specific influence on lipid accumulation in *Mucoromycota* fungi, where either fatty acid profiles or total lipid content is affected. For example, manganese (Mn) has shown positive effects on the lipogenesis in *Mucor plumbeus* and *Mortierella sp*. [39,40]. Iron had an inhibiting effect on the arachidonic acid production in *Mortierella sp*. [39], while together with magnesium and zinc (Zn), it was enhancing lipid accumulation in *Cunninghamella sp*. Furthermore, zinc increased the gamma-linoleic acid production in *Cunninghamella sp*. [41], while iron, zinc, and copper (Cu) were reported as enhancers of arachidonic acid production in *Mortierella alpina* [42]. To the authors' knowledge, the effect of calcium and cobalt (Co) on the lipid accumulation in the oleaginous *Mucoromycota* fungi has not been investigated before. Moreover, there have been no studies reporting the effect of metal ions on the lipogenesis in *M. circinelloides*.

In our previous studies, we have assessed the chemical composition of nine different oleaginous filamentous fungi (including *M. circinelloides*) and revealed nutrient-induced coproduction of lipids, chitin/chitosan, and polyphosphates [43,44]. We reported that *M. circinelloides* has an ability to coproduce lipids, polyphosphate, and chitin/chitosan at different phosphorus concentrations and showed a versatile metabolism with a high adaptability level to different stress conditions. Thus, this fungus can be utilized in phosphorus recovery processes, while the co-production concept greatly contributes to the economic feasibility of such processes.

The aim of this study was to assess the effect of 140 different substrates, with varying amounts of metal and phosphate ions, on the growth, cell chemistry, and lipid production in *M. circinelloides*. Different concentrations of phosphorus source were used in order to study the effect of metal ions on the co-production of lipids, polyphosphates and cell wall polysaccharides, such as chitin/chitosan, triggered by phosphorus availability. Analogous to our previous studies, the study was performed in a high-throughput set-up using a Duetz microtiter plate system (Duetz-MTPs) combined with Fourier transform infrared (FTIR) spectroscopy [43–46]. FTIR spectroscopy was applied to obtain a

biochemical fingerprint of the microbial cells [43,47–52], while gas chromatography was used to analyze the lipid yield and fatty acid profiles of the extracted lipids.

2. Materials and Methods

2.1. Growth Media and Cultivation Conditions

Fungal strain *M. circinelloides* VI04473, provided by the Veterinary Institute, Oslo, Norway was selected based on the previous study of 100 oleaginous fungal strains, as it showed the highest lipid and biomass yield of all tested *Mucor* strains [50]. Moreover, this strain has also shown coproduction potential for lipids, chitin/chitosan, and polyphosphates [43]. *M. circinelloides* was cultivated on malt extract agar (MEA) for 7 days at 25 °C in order to obtain fresh spores for the inoculation into nitrogen-limited broth media with various metal and phosphorus ion concentrations. Spores were collected from agar plates using 10 ml of saline solution and a bacteriological loop. The composition of the reference medium, used and modified in our previous studies [27,43–45], was the following: 80 g/L of glucose, 1.5 g/L of $(NH_4)_2SO_4$, 7 g/L of KH_2PO_4, 2 g/L of Na_2HPO_4, 1.5 g/L of $MgSO_4{\cdot}7H_2O$, 0.1 g/L of $CaCl_2{\cdot}2H_2O$, 0.008 g/L of $FeCl_3{\cdot}6H_2O$, 0.001 g/L of $ZnSO_4{\cdot}7H_2O$, 0.0001 g/L of $CoSO_4{\cdot}7H_2O$, 0.0001 g/L of $CuSO_4{\cdot}5H_2O$, 0.0001 g/L of $MnSO_4{\cdot}5H_2O$, where the listed concentrations of the metal ions Ca, Cu, Co, Fe, Mg, Mn, and Zn were assigned as reference concentration and marked as "R" (Table 1). The higher—1000; 100; 10 × R and lower—0.1; 0.01 and 0 × R concentrations of the metal ions were assessed in the study as described in Table 1. The reference medium was modified by using four relative levels of metal and phosphate ions (Table 1). KH_2PO_4 and Na_2HPO_4 were used as phosphates substrate, and their total concentration is hereafter referred as "phosphates concentration" (Pi). Phosphate concentrations KH_2PO_4 7 g/L, Na_2HPO_4 2 g/L have been assigned as Pi1. In addition to Pi1 concentration, the higher—4 and 2 × Pi1 and lower—0.5 and 0.25 × Pi1 concentrations of phosphates were assessed in the study as described in Table 1. Broth media, with the lower than Pi1 amount of Pi—Pi0.5 and Pi0.25, contained KCl and NaCl in a corresponding concentration in order to have equal amounts of K^+ and Na^+ ions as in the Pi1 condition. Different media were prepared by modifying one metal ion concentration at a time for every level of Pi ions. The only exception was for the condition 0Mg10Ca, which was tested in order to examine a possibility of substitution of Mg by Ca. Thus, in total, 140 different media were prepared. The concrete concentrations of all media components can be found in the Supplementary Materials (Table S1).

Table 1. Overview over the relative levels of concentration of metal ions and inorganic phosphate in the media. The exact concentrations can be found in the Supplementary Materials (Table S1).

Ca	Mg	Cu	Co	Fe	Mn	Zn	Pi
0	0Mg 10Ca	0	0	0	0	0	0.25
0.01	0.01	R	R	R	R	R	0.5
0.1	0.1	10	10	10	10	10	Pi1
R	R	100	100	100	100	100	2
10		1000	1000	1000	1000	1000	4

Considering the high-throughput set-up of the study and consequently high number of samples, the reproducibility of the *M. circinelloides* growth was controlled by four biological replicates for the reference medium R with Pi1 concentration, two biological replicates for the reference metal ion concentrations, and the following phosphate ion concentrations: Pi4, Pi2, Pi0.5, and Pi0.25, and two biological replicates for the medium with 0Ca under all tested phosphate concentrations. The reproducibility of lipid accumulation was controlled under the reference metal concentrations by four biological replicates for the reference medium R-Pi1, two biological replicates for Pi4, Pi2, Pi0.5, and Pi0.25 media, and two biological replicates for the media with 0Ca-Pi2 and Pi1 levels. The biological variability is represented by error bars in Figure 1 and standard deviation in Table 3.

Cultivation was performed in Duetz-MTPS (Enzyscreen, Heemstede, The Netherlands) [43,45,47,50,53,54], consisting of 24-square well polypropylene deep well microtiter plates (MTPs), low evaporation sandwich covers with a clamp system. A total of 7 ml of sterile media broth was transferred into the autoclaved microtiter plates and each well was inoculated with 50 µL of the spore suspension. MTPs were placed on the shaking platform of the incubator MAXQ 4000 (Thermo Scientific, Oslo, Norway). Cultivations were performed for 7 days at 25 °C and 400 rpm agitation speed (1.9 cm circular orbit).

2.2. Lipid Extraction and GC-FID Analysis of Lipid Concentration and Fatty Acid Profile

Direct transesterification was performed according to Lewis et al. [55], with some modifications [44]: 2 mL screw-cap polypropylene (PP) tubes were filled with 30 ± 3 mg of freeze-dried biomass, 250 ± 30 mg of acid-washed glass beads, and 500 µL of methanol. Further, the fungal biomass was disrupted in a tissue homogenizer (Bertin Technologies Percellys Evolution, Montigny-le-Bretonneux, France). The disrupted fungal biomass was transferred into glass reaction tubes by washing the PP tube with 2400 µL of a methanol–chloroform–hydrochloric acid solvent mixture (7.6:1:1 v/v). Then, 1 mg of C13:0 TAG internal standard in 100 µL of hexane was added to the glass reaction tubes (100 µL from a 10.2 mg/mL^{-1} glyceryl tritridecanoate ($C_{42}H_{80}O_6$, C13:0 TAG (13:0/13:0/13:0), Sigma-Aldrich, St. Louis, Missouri, USA). Reaction tubes were incubated at 90 °C for 1 h, followed by cooling to room temperature and the addition of 1 mL distilled water. The fatty acid methyl esters (FAMEs) were extracted by the addition of 2 mL of a hexane–chloroform mixture (4:1 v/v) and applying 10 s of vortex mixing. The reaction tubes were centrifuged at 3000 g for 5 min at 4 °C and the upper hexane phase was collected in glass tubes. The extraction step was repeated three times for each sample. Subsequently, the solvent was evaporated under nitrogen at 30 °C and FAMEs were dissolved in 1.5 mL of hexane containing 0.01% of butylated hydroxytoluene (BHT, Sigma-Aldrich, St. Louis, Missouri, USA) and a small amount of anhydrous sodium sulfate (to remove traces of water in the sample). Samples were mixed by vortexing and, finally, dissolved FAMEs were transferred to the GC vials.

Fatty acid profile analysis was performed using a gas chromatography system with flame ionization detector (GC-FID) 7820A GC System, Agilent Technologies, controlled by Agilent OpenLAB software (Agilent Technologies, Santa Clara, CA, USA). Agilent J and W GC column 121–2323, DB-23, 20 m length; 0.180 mm diameter; 0.20 µm film was used for the separation of FAMEs. Then, 1 µL of the sample was injected in the 30:1 split mode with the split flow 30 mL/min. The inlet heater temperature was set on 250 °C and helium was used as the carrier gas. The flow of helium through the column was 1 mL/min. The total runtime for one sample was 36 min with the following oven temperature increase: initial temperature 70 °C for 2 min, after 8 min to 150 °C with no hold time, 230 °C in 16 min with 5 min hold time, and 245 °C in 1 min with 4 min hold time. For identification and quantification of fatty acids, the C4–C24 FAME mixture (Supelco, St. Louis, MO, USA) was used as an external standard, in addition to C13:0 TAG internal standard. The weight of individual FAs was calculated based on the peak areas, relative response factors (RRF), and C13 internal standard. The total lipids in the fungal biomass were the sum of FA (the weight of C13 IS was subtracted) divided by the weight of dry biomass.

2.3. Fourier Transform Infrared Spectroscopy of Fungal Biomass

Fourier transform infrared (FTIR) spectroscopy analysis of fungal biomass was performed according to Kosa et al. [45], with some modifications [43]. The biomass was separated from the growth media by centrifugation and washed with distilled water. Approximately 5 mg of washed biomass was transferred into a 2 ml polypropylene tube containing 250 ± 30 mg of acid washed glass beads and 0.5 ml of distilled water for further homogenization. The remaining washed biomass was freeze-dried for 24 h for determining biomass yield. The homogenization of fungal biomass was performed by using Percellys Evolution tissue homogenizer (Bertin Technologies, Aix-en-Provence, France) with the following set-up: 5500 rpm, 6 × 20 s cycle. Then, 10 µL of homogenized fungal biomass was pipetted onto an IR transparent 384-well silica microplate. Samples were dried at room

temperature for 2 h. In total, 140 biomass samples were analyzed in three technical replicates by FTIR spectroscopy.

FTIR spectra were recorded in a transmission mode using the high throughput screening extension (HTS-XT) unit coupled to the Vertex 70 FTIR spectrometer (both Bruker Optik, Leipzig, Germany). Spectra were recorded as the ratio of the sample spectrum to the spectrum of the empty IR transparent microplate in the region between 4000 cm^{-1} and 500 cm^{-1}, with a spectral resolution of 6 cm^{-1}, a digital spacing of 1.928 cm^{-1}, and an aperture of 5 mm. For each spectrum, 64 scans were averaged. In total, 420 biomass spectra were obtained.

The OPUS software (Bruker Optik GmbH, Leipzig, Germany) was used for data acquisition and instrument control.

2.4. Data Analysis

The following software packages were used for the data analysis: Unscrambler X version 10.5.1 (CAMO Analytics, Oslo, Norway) and Matlab R2019a (The Mathworks Inc., Natick, MA, USA).

2.4.1. Analysis of FTIR Spectral Data

To evaluate the correlation of lipid content results obtained from FTIR and GC data and, further, investigate media associated changes of the lipid content in biomass, FTIR spectra were preprocessed by 2nd derivative using Savitzky–Golay algorithm with 2nd order polynomial and windows size 13, followed by spectral region of interest (SROI) selection 3050–2800 and 1800–1700 cm^{-1} and normalization by extended multiplicative signal correction (EMSC) [56] with linear and quadratic terms. Preprocessed FTIR data were then analyzed by principal component analysis (PCA) and score plots were used to compare the lipid related information in FTIR and GC data.

Different preprocessing was applied in order to evaluate the cell chemistry changes that occurred under different media conditions. To do so, SROI 3300–2800 and 1800–800 cm^{-1} was selected and normalized by EMSC using linear and quadratic terms and up-weighting the region 2800–1800 cm^{-1}. The up-weighting of the inactive region 2800–1800 cm^{-1} helped in reducing baselines by EMSC in the SROI. Afterwards, the dataset was split according to the concentrations of inorganic phosphorus (Pi) and separately analyzed by PCA. Correlation loading plots were obtained for Pi1, Pi2, and Pi4 in order to analyze the most pronounced correlation patterns in the data. To obtain such a plot, we used scores of each separate PCA model corresponding to one Pi concentration and projected on them variables of interest such as certain relevant peaks of FTIR data and other reference variables, such as pH, biomass yield, and lipid content from GC data, in addition to experimental design factors. The maxima of the corresponding chemical bonds selected for correlation loading plots based on the FTIR spectra of reference materials were pure sodium polyphosphate, chitin, and glyceryl trioleate (Table 2, Figure S3 in the Supplementary Materials). These compounds were the main cell components of interest. For plotting the peaks on the correlation loading plots, the preselected peaks of the preprocessed spectra were used (Table 2).

Table 2. The maxima of the corresponding chemical bonds selected for correlation loading plots based on FTIR data.

Cell Component	Peak Maxima	Molecular Vibration
Chitin/chitosan	3261	N-H stretching
	3105	N-H stretching
	2879	-C-H stretching
	1656	-C=O stretching (Amide I)
	1620	-C=O stretching (Amide I)
	1554	C-N-H deformation (Amide II)
	1375	$-CH_3$ deformation
	1305	C-N-H deformation (Amide III)
	1027	C-O-C str., C-O-H def. C-O-C def.

	950	-CH_3 def.
Lipids	3004	=C-H stretching
	2921	-C-H stretching
	2852	-C-H stretching
	1743	-C=O stretching
	1463	-CH_2 bending
	723	>CH_2 rocking
Polyphosphates	1263	P=O stretching
	885	P-O-P stretching

2.4.2. Analysis of GC Data

The detailed fatty acid profiles from the GC analysis were analyzed and compared to FTIR data. Fatty acid profiles were represented by both single fatty acids and sum of fatty acids—saturated fatty acids (SAT), monounsaturated fatty acids (MUFA), and polyunsaturated fatty acids (PUFA). Each data column was standardized (x/std (x)) and then analyzed by PCA. The scatter plot was used to compare the information related to total lipid content and profile obtained by GC and FTIR.

To find differences in fatty acid composition at different Pi concentrations, after standardization, the GC dataset was split into three datasets: Pi1, Pi2, Pi4, and analyzed separately by PCA. To learn about the correlation patterns in the data, the correlation loading plots for GC data were obtained using scores of GC based PCA models. The fatty acid profile of *M. circinelloides* is dominated by myristic (C14:0), palmitic (C16:0), palmitoleic (C16:1), stearic (C18:0), oleic (C18:1n9), linoleic (C18:2n6), and γ-linolenic (C18:3n6) acid, therefore these were presented in the correlation loading plots.

3. Results

3.1. Growth of Oleaginous M. Circinelloides in Metal Ion-Regulated Media With Different Pi Levels

In order to assess the variation between bioreplicates, cultivation of *M. circinelloides* in the reference medium R with Pi1 concentration was performed 11 times (part of the data were published previously [43]). Cultivations were performed at different timepoints and by using different MTPs. The results of statistical analysis of 11 bioreplicates show that the mean for the biomass production in the reference medium (R-Pi1) was 10.08 g/L (range: 9.35–11.52 g/L, median: 9.90 g/L), with 0.62 g/L standard deviation, and 0.19 g/L standard error. Therefore, it can be considered that all deviations higher than two standard deviations (13% of the average biomass concentration) are statistically significant and can be assigned as the effect of various metal and phosphates concentrations.

Growth of *M. circinelloides* in different media was strongly affected by the availability of phosphates. Low availability of phosphates (Pi0.25 and Pi0.5) led to a substantial decrease in pH (Table S2, Supplementary Materials) causing a significantly reduced growth of *M. circinelloide*s (Figure 1, Table S3). Biomass yields in all Pi0.25 and Pi0.5 media were in the range from 0.51 g/L to 2.79 g/L and from 0.73 g/L to 4.70 g/L, respectively (Figure 1). The biomass production under moderate and high levels of phosphates (Pi1–Pi4) was substantially higher and in the range from 7.84 g/L to 12.90 g/L for Pi1, from 7.54 g/L to 12.47 g/L for Pi2, and from 7.89 g/L to 13.23 g/L for Pi4 (Figure 1). The biomass yield of *M. circinelloides* was, in several cases, higher than in the reference medium with Pi1 concentration (Figure 1, Table S3).

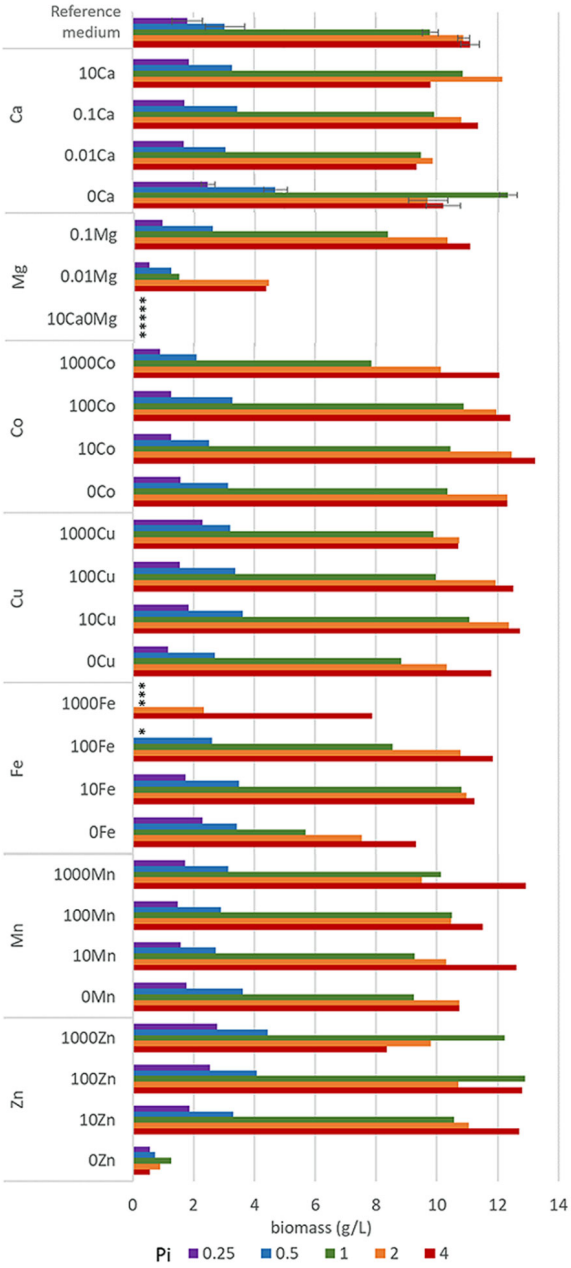

Figure 1. Final biomass concentrations after 7 days of incubation of *M. circinelloides* in the media with different concentrations of metal and phosphorus ions. * Empty slots indicate no growth.

Metal ions affected the growth of *M. circinelloides* differently and the strongest effect was observed at moderate and high levels of phosphates (Pi1, Pi2, and Pi4). Metal ions' starvation for most of the tested metal ions led to a reduced fungal growth. Thus, Zn and Mg starvation resulted in a low or no growth of *M. ciricinelloides* in all tested Pi conditions (Figure 1, Table S3). Further, removal of Cu ions led to a slight biomass decrease. Removal and low concentrations of Ca ions resulted in a slight biomass decrease at Pi2 and Pi4 and increase at Pi0.25, Pi0.5, and Pi1 levels (Figure 1, Table S3). Similar increase in the biomass yield was observed for the media without Fe ions at Pi0.25, and it was significantly decreased at higher Pi levels −44% for Pi1, −30% Pi2, and −16% for Pi4 compared to the reference amount of Fe (Figure 1, Table S3). Deficiency of Co ions did not result in any significant change in biomass formation of *M. circinelloides* in comparison with high concentrations of Co ions (100Co).

Generally, increased availability of metal ions showed either no effect or both growth-stimulating and -inhibiting effects, depending on the metal type and phosphates concentration. Thus, high metal ions concentration in the media with low Pi levels did not lead to any significant changes in the biomass formation of *M. ciricinelloides* (Figure 1), with the exception of Fe and Zn ions. High amount of Fe ions in a combination with the low concentration of phosphates showed a negative effect on the biomass formation, and no or very limited growth was observed for the following Fe conditions: 1000Fe-Pi 0.25, 1000Fe-Pi1, and 100Fe-Pi0.25. Low growth under these conditions can be connected to the acidic pH ranging from 2.79 for Pi4 to 1.62 for Pi0.25 (Table S2 in the supplementary materials). The opposite effect was observed for the media with elevated concentration of Zn ions, which enhanced growth of *M. circinelloides*, resulting in a higher biomass yield under Pi limitation, with the highest biomass yield of 4.44 g/L observed for 1000Zn condition (1 g/L $ZnSO_4 \cdot 7H_2O$) (Figure 1, Table S3).

A considerable effect of the increased metal ions availability was recorded for the media with moderate and high Pi levels (Figure 1). For example, high concentrations of Mn provided higher biomass at Pi4, with the highest yield of 12.93 g/L for 1000Mn condition, while the effect of other Mn conditions on the growth of M. *circinelloides* was generally negligible. Increasing amount of Fe ions up to the 100Fe condition positively affected the biomass production of *M. circinelloides* in the media with Pi4 and Pi2, and the highest yield of 11.84 g/L was observed for the condition 100Fe with Pi4 (Figure 1). However, very high iron concentration (1000Fe) showed an inhibiting effect at Pi1 and significantly decreased biomass at Pi2 and Pi4 (Figure 1). While increased concentration of Zn ions positively affected the growth of *M. circinelloides* in the media with low phosphates concentration (Pi0.5 and Pi0.25), it slightly decreased the growth in media with high phosphates concentration (Pi2 and Pi4). Generally, it can be concluded that increased concentrations of Zn ions (10Zn and 100Zn) in the media have beneficial effects, since under all Pi levels the biomass yield was increased compared to the standard conditions (R) (Figure 1). A similar effect can be seen for Cu and Co ions, where media with 10Cu condition provided the highest biomass yield for moderate and high Pi levels (Figure 1). Moreover, the highest biomass yield of 13.23 g/L of all tested conditions was observed for 10Co (0.001 g/L $CoSO_4 \cdot 7H_2O$) with Pi4 level of phosphorus substrate (Figure 1, Table S3).

3.2. Effect of Metal Ions on Lipid Accumulation and Fatty Acid Profile of M. Circinelloides TAGs

Lipid content in oleaginous *M. circinelloides* biomass grown in the different media is reported in Table 3. Due to the low growth and not sufficient amount of biomass for lipid extraction, samples Pi0.25 and Pi0.5 for all metal ions conditions, and samples 1000Fe, 0Mg, 0Zn, 10Ca0Mg were excluded from the lipid extraction and further data analysis.

Table 3. Lipid accumulation (% of lipids per dry cell weight) for *M. circinelloides* grown in nitrogen-limited metal ion-regulated media with different amounts of inorganic phosphorus substrates (Pi1, Pi2, and Pi4).

Metal Ion Condition	Pi1	Pi2	Pi4
Reference medium	41.13 ± 1.19	33.44 ± 1.28	33.15 ± 0.01
0Ca	61.16 ± 0.16	40.15 ± 2.31	31.51
0.01Ca	34.00	39.61	34.93
0.1Ca	60.55	37.22	43.70
10Ca	44.37	33.50	27.95
0.01Mg	11.43	20.57	22.80
0.1Mg	30.38	32.90	39.40
0Co	38.78	37.24	31.46
10Co	30.25	34.40	29.87
100Co	30.31	38.52	29.60
1000Co	31.49	35.08	29.38
0Cu	61.27	53.80	52.24
10Cu	47.11	37.75	35.63
100Cu	46.70	41.27	38.27
1000Cu	43.11	42.46	38.36
0Fe	37.27	37.00	30.62
10Fe	36.73	34.36	29.19
100Fe	30.77	33.00	27.11
0Mn	46.78	37.94	38.74
10Mn	34.52	31.67	33.21
100Mn	35.16	39.13	34.22
1000Mn	33.23	30.58	33.61
10Zn	49.78	38.31	37.65
100Zn	43.84	41.94	34.72
1000Zn	42.36	41.85	38.04

Lipid accumulation in *M. circinelloides* grown under the reference metal ion conditions reached approximately 41% for Pi1 and 33% for Pi2 and Pi4 (Table 3). Lack of several metals resulted in an increase of lipid content for several Pi conditions. For example, removal of Ca, Co, and Fe ions in the media with Pi2 and Pi1 and Cu and Mn ions in the media with Pi1, Pi2, and Pi4 resulted in an increase in lipid accumulation in *M. circinelloides*, compared to the reference conditions. The most significant increase in lipid accumulation was recorded for 0Ca-Pi1 and 0Cu-Pi1 conditions. Interestingly, the removal of some metal ions, such as Ca, Co, and Fe, enhanced lipid accumulation only at moderate phosphate concentrations in the media (Pi1 and Pi2), and decreased lipid accumulation at high phosphate concentrations (Pi4). Removal of Mn, and especially Cu, ions resulted in increased lipid accumulation at moderate and high phosphate concentrations (Pi1, Pi2, and Pi4) (Table 3).

Variation in the availability of metal ions showed diverse and metal-specific effects on the lipid accumulation in *M. circinelloides* (Table 3). Lack of Mn ions has resulted in relatively high lipid accumulation in *M. circinelloides* for all tested Pi levels. The inhibiting effect of higher Mn ion concentrations was more visible in the media with reference amounts of phosphates (Pi1). Similar results were recorded for the media with increased levels of Fe ions, where lipid yield was lower than under the reference Fe condition (R). Two tested concentrations of Mg ions provided low lipid yield in *M. circinelloides* with the lowest values of 11.43% at 0.01Mg-Pi1 condition, while lipid yield of 39.4% was observed in the biomass grown in the 0.1Mg-Pi4 condition. When increasing the amount of Co ions in the media with Pi4 and Pi2, a decrease in lipid accumulation was recorded, while the opposite effect was seen for the medium with Pi4. An increase in the concentration of Zn ions showed a triggering effect on lipid accumulation in *M. circinelloides* grown at different levels of phosphorus substrate, with the highest lipid yield of 49.78% at 10Zn-Pi1 (0.01 g/L $ZnSO_4 \cdot 7H_2O$), which was 9%

higher than for the reference condition. A similar lipogenesis triggering effect was observed for increasing concentration of Cu ions at all tested Pi levels, while the highest lipid yield was recorded when Cu ions were removed. The most diverse effect on lipid accumulation in *M. circinelloides* was observed for different concentrations of Ca ions. Increase in Ca ion availability from 0Ca to 0.01Ca resulted in the decrease of lipid yield for condition 0.01Ca-Pi1, while a further increase in Ca ions to 0.1Ca resulted in the increase of lipid yield for biomass grown in the media with Pi1, Pi2, and Pi4. A high concentration of Ca ions (10Ca) resulted in the decrease in lipid accumulation in the medium with Pi4 and slight increase in the media with Pi2 and Pi1 (Table 3).

The fatty acid profile of *M. circinelloides* grown under the reference condition was dominated by oleic acid (C18:1n9; 38%), followed by palmitic (C16:0; 22%), linoleic (C18:2n6; 14%), and γ-linolenic (C18:3n6; 12%) acids. Further, stearic (C18:0; 5%), palmitoleic (C16:1; 1.75%), and myristic (C14:0; 1.5%) acids were recorded in smaller amounts (Figure 2, Table S4). An example chromatogram can be found in the Supplementary materials (Figure S1). The fatty acid profile of *M. circinelloides*, grown under reference metal ion conditions, slightly changed depending on the phosphorus availability in the media. Thus, we observed an increase in the unsaturation and amount of palmitoleic acid with the increasing amount of phosphorus (Figure 2, Table S4). An opposite effect of phosphorus availability (and the associated changes in pH of media) was recorded for the unsaturation of stearic acid into oleic and γ-linolenic acid, where decreasing unsaturation was evident with increasing Pi concentrations and higher pH. This pattern can be visible through all the samples, with some exceptions for 10Fe-Pi1/Pi2/Pi4, 100Fe-Pi1/Pi2, 1000Zn, 1000Co, 10Cu-Pi2, and 0.01Mg-Pi1conditions (Figure 2, Table S4). Minimal content of myristic acid (C14:0) was observed in 10Fe and 100Fe conditions, except for the 100Fe-Pi4 sample (Figure 2). Further, media with high amounts of Zn (1000Zn) and Co (1000Co) ions led to the synthesis of TAGs with the increased relative amount of stearic acid (Figure 2, Table S4).

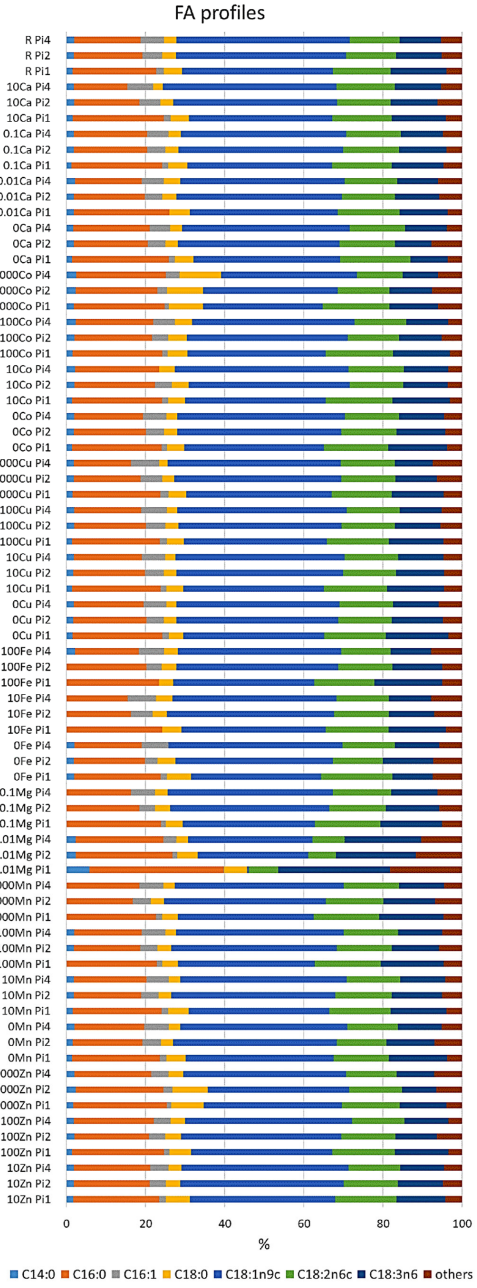

Figure 2. Fatty acid profile of lipids accumulated in *M. circinelloides* grown in media with Pi1, Pi2, and Pi4 levels of phosphorus. Only fatty acids present in amounts of more than 1% are displayed. The rest is summed up as 'others'. An example chromatogram can be found in the Supplementary Materials (Figure S1).

To reveal underlying correlations among certain fatty acids, design variables, and reference variables, as well as sum of saturated (SAT), monounsaturated (MUFA), and polyunsaturated (PUFA) fatty acids, PCA analysis of fatty acid (FA) profiles was done for each Pi substrate level separately. The separation of data into different Pi concentrations was done in order to focus on the effect of metal ions only on FA profile, excluding the effect of phosphorus substrate availability. The results, in the form of correlation loading plots, are presented in Figure 3. Generally, the fatty acid profile of *M. circinelloides* was quite consistent, irrespective of media composition.

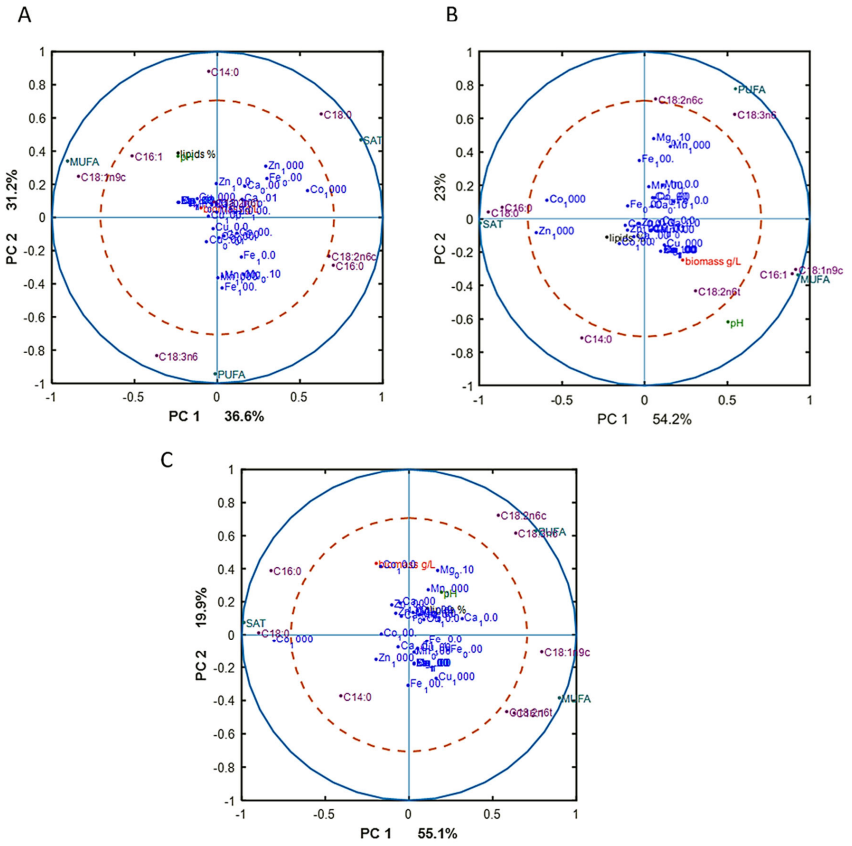

Figure 3. Correlation loading plots based on the PCA analysis of fatty acid (FA) profiles of lipids accumulated in *M. circinelloides* grown in metal ion-regulated media under Pi1 (**A**), Pi2 (**B**), and Pi4 (**C**) levels of phosphorus substrate.

In the biomass obtained from the media with Pi1 and Pi2 amounts of phosphorus, high concentrations of Co (1000 Co) and Zn (1000 Zn) ions were positively correlated with the saturated fatty acids (SAT) (Figure 3A). This was also evident from the detailed FA profiles, where the relative amount of palmitic and stearic acid was increased under these conditions (Figure 2). Further, some tendency of positive correlation between increasing concentration of Fe ions and content of polyunsaturated fatty acids (PUFA) was observed in the media with Pi1 level (Figure 3A). In the

media with high amounts of phosphorus substrate (Pi4 and Pi2), 1000 Mn and 0.01 Mg conditions were positively correlated with the polyunsaturated fatty acids (PUFAs) (Figure 3B,C).

3.3. Chemical Composition of M. Circinelloides Biomass

In order to study differences in the compositional profile of the *M. circinelloides* biomass, high-throughput Fourier transform infrared (FTIR-HTS) spectroscopy was used. Spectral regions and peaks related to three types of metabolites—lipids, chitin/chitosan, and polyphosphates were used in the analysis. The FTIR-HTS spectra (Figures S2 and S3 in the Supplementary Materials) showed that fungal biomass was dominated by signals of these intracellular metabolites. The spectra of reference materials can be found in the supplementary materials (Figure S2). The maxima of the peaks selected for the correlation loading plots are listed in Table 2. Due to the insufficient growth (Figure 1), the following samples have been disregarded from the FTIR-HTS spectral data analysis: (i) all samples grown under Pi0.25 and Pi0.5 levels; (ii) samples grown in the media with 1000Fe, 0Mg, 0.01Mg, 0Zn, and 10Ca0Mg.

First, we examined the lipid region of FTIR-HTS spectra (3050–2800 and 1800–1700 cm^{-1}) and analyzed the correspondence of it with GC data by PCA analysis (Figure 4). On the PCA score plots we can observe similar pattern for FTIR and GC data, indicating similarity in the obtained information about lipid yield and profile from the data of these analytical techniques.

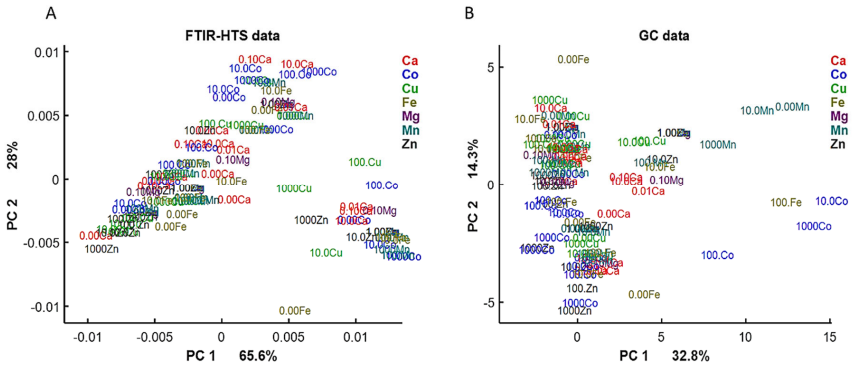

Figure 4. PCA score plots of FTIR-HTS (**A**) and GC (**B**) data. PCA analysis was performed on the preprocessed FTIR-HTS data (2nd derivative, polynomial order 2, window size 13; SROI: 3050–2800 and 1800–1700 cm^{-1}, EMSC) and normalized GC data.

The correlation loading plots from the PCA analysis visualize the relation between the presence of lipids, chitin/chitosan, and polyphosphate and different media (Figure 5). PCA analysis of EMSC preprocessed spectra was performed separately for different Pi concentrations in order to emphasize the effect of different metal ions and disconnect it from the effect of inorganic phosphorus substrate. The loading vectors and FTIR spectral scores are displayed in Figures S4–S6 in the Supplementary materials. The first principle component (PC1), which explained the highest variance in the FTIR data, was represented by lipids to proteins and to chitin and chitosan ratio. The second principle component (PC2) was represented by the polyphosphate peaks, which were strongly visible in the cases of polyphosphate accumulation triggering conditions when Pi4 and Pi2 phosphate concentrations were used in the media (Figures S5A and S6A), while no strong characteristic signals representing any of the studied metabolite were visible in the PC2 for Pi1 condition (Figure S4A).

Lipids and chitin/chitosan are both carbon-rich metabolites, therefore their synthesis processes are competing for the C source. In all correlation loading plots, we can observe that lipids and chitin/chitosan were anticorrelated, indicating that these metabolites cannot be produced

simultaneously at high yields, while they still can be coproduced with one of them dominating (Figure 5). Further, we see that peaks 2879 cm^{-1} (-C-H stretching) and 950 cm^{-1} (C-O str, C-C str., C-O-H def. C-O-C def), responsible for chitin/chitosan, have been shown to be correlated with the lipid-related peaks (Figure 4). The reason is that the chemical bonds, represented by these peaks, are also present in lipids and the contribution of the lipid associated peaks was stronger than the contribution of chitin/chitosan peaks. The chitin/chitosan formation could also be negatively affected by the N-limitation. The biomass concentration was correlated with the lipid peaks, revealing that a good lipid accumulation can be achieved only with the optimal growth conditions providing good growth and biomass formation and that high biomass concentration was the result of the increased lipid accumulation (Figure 5).

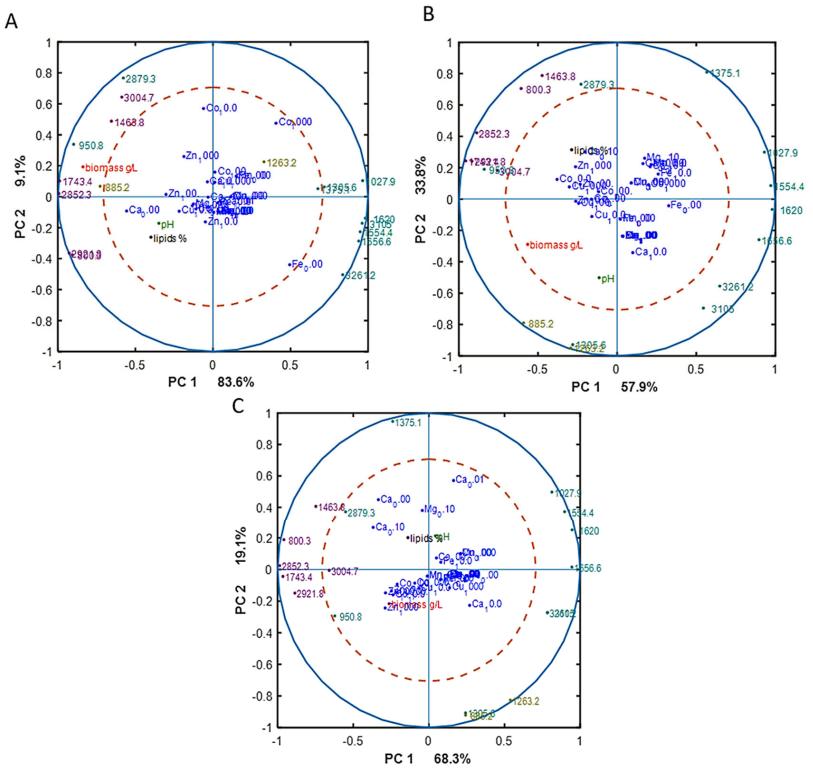

Figure 5. Correlation loading plots based on the PCA analysis of FTIR-HTS spectra of *M. circinelloides* biomass grown in metal ion-regulated media with Pi1 (**A**), Pi2 (**B**), and Pi4 (**C**) levels. Main peaks corresponding to the lipids (purple), chitin/chitosan (green), and polyphosphates (yellow) are presented.

The effect of metal ions on the *M. circinelloides* biomass composition in the media with reference level of phosphorus (Pi1) is displayed in a PCA score plot with loading vectors (Figure S4 in the Supplementary materials). Due to the fact that PC2 was not representing any clear relation between FTIR-HTS peaks and studied metabolites, we analyzed only PC1 representing the ratio of lipids to protein and to chitin and chitosan peaks. PCA score plots show that lipid content correlated with the absence of Ca ions (0Ca) (Figure S4B), which is in agreement with the lipid yield data presented in Table 3. Further, the PCA score plot shows that increasing Co amount displayed an inhibiting effect

on the lipid accumulation (Figure S4B). The same results were observed for the lipid yield, where the highest lipid production was recorded for 0Co-Pi1 condition (Table 3). FTIR-HTS spectra of biomass grown in the media with reference level of inorganic phosphorus substrate (Pi1) did not exhibit significant absorbance for polyphosphate peaks. The correlation loading plot (Figure 5A) shows some effect of two metal ions—Fe and Co. Namely, a decrease in the concentration of Fe ions was correlated with the chitin/chitosan peaks, indicating that higher amounts of this metabolites is expected in the fungal biomass when Fe ions are in a low availability, while the absence of Fe ions (0Fe) was anticorrelated with the lipid peaks and biomass concentration (Figure 5A). This corresponds well to the biomass production results, where it is obvious that lack of Fe ions caused a significant decrease of biomass formation (Figure 1). A high concentration of Co ions (1000 Co) showed correlation with chitin/chitosan peaks of FTIR-HTS spectra, indicating that the relative content of this metabolite in the fungal biomass increased with the increased concentration of Co ions. Absence of Ca ions (0Ca) was correlated with the high lipid and biomass concentration. This is in agreement with the reference biomass and lipid concentration results, where 0Ca-Pi1condition provided the highest biomass and lipid production from all the tested Ca ions conditions (Figures 1 and 2).

The effect of metal ions on the synthesis of studied *M. circinelloides* metabolites in the media with Pi2 level of phosphorus is displayed on the Figure 5B, where we can see that increased amounts of Zn and Cu ions were corelated with the lipid yield. Similar correlation results were observed for Co ions, except for the condition of 1000Co-Pi2, which was slightly anticorrelated with lipid peaks. Correlation between polyphosphate spectral peaks and the highest tested Ca ions amount (10Ca) was observed (Figure 4B). Further, we can see correlation between amount of Zn ions and polyphosphate peaks. Finally, metal ions conditions 0.1Ca, 1000Zn, 100Zn, 10Zn, 10Co, 100Co, and 10Cu correlated with the lipid yield.

When examining the effect of metal ions under the high amounts of inorganic phosphorus substrate level (Pi4), on the PCA score plot it is seen that increasing amount of Ca ions corelated with the decrease of the relative lipid content and increase of the polyphosphate content (Figure S6 in the Supplementary materials). Further, in Figure 5C we observed that: (i) decreasing Cu ion availability and high concentration of Zn ions correlated with the increase of relative lipid content; (ii) low amount of Ca ions (0,1Ca) correlated with the lipid peaks and lipid yield and anticorrelated with polyphosphates peaks, while high amount of Ca ions (10Ca- 1 g/L $CaCl_2.2H_2O$) correlated with polyphosphate and chitin/chitosan peaks; (iii) low concentration of Mg ions (0,1Mg) correlated with lipid peaks and anticorrelates with polyphosphate peaks; (iv) there was no correlation observed for Co and Mn ions (Figure 5C).

4. Discussion

For half of a century, *M. circinelloides* has been studied as a microbial cell factory for production of a series of metabolites and valorization of different substrates. Today, this dimorphic oleaginous fungus is positioned as one of the most robust fungal cell factories for the biotech, biorefinery, and bioremediation industries [2].

Despite the deep understanding of *M. circinelloides* physiology and metabolic processes, the role and the effect of metal ions on the lipid accumulation and the cellular composition of this fungus have not been systematically investigated. The effect of metal ions on the growth and metabolic activity of *M. circinelloides* has, to the authors knowledge, only been assessed in the connection to bioremediation abilities of this fungus [11,12,57]. Therefore, in this study we performed an extensive screening of the growth, lipid accumulation, and compositional profile of *M. circinelloides* on 140 different media with variations in the concentrations of metals ions and phosphorus. Lipid accumulation and fatty acid profiles were determined by the GC-FID. The composition of the fungal biomass was investigated by the quantification of lipids, polyphosphates, and chitin/chitosan, as these components previously have been suggested for a coproduction concept involving *M. circinelloides* [43]. For the evaluation of biomass composition, the modern high-throughput analytical technique FTIR spectroscopy was applied. The main advantage of FTIR spectroscopy is that all biochemical components of the sample can be profiled in a single measurement run, without tedious

extraction procedures [58–62]. FTIR spectroscopy provides detailed relative quantitative information about different chemical components of the samples and it has been previously utilized for the characterization of lipids [50,51,63], polyphosphates [64], and chitin/chitosan [65,66]. In this study, we have demonstrated that the FTIR analysis as a sole method coupled to multivariate data analysis can be applied for a fast and simple analysis of microbial biomass.

Efficiency of microbial biomass production, the yield of the targeted metabolite(s), and a coproduction potential are important assessment parameters in bioprocess development [19,20]. Biomass production is affected by factors such as pH, temperature, aeration, media composition, and cultivation mode [2]. For example, culture volume and mode of cultivation were reported by Carvalho et al. as factors strongly affecting the final biomass yield of *M. circinelloides* [67]. The reported biomass production of *M. circinelloides*, depending on the culture conditions, varied greatly, from 5 g/L to 20 g/L [10,17,68]. In our previous studies, the biomass concentration for different *M. circinelloides* strains was between 10 g/L and 15 g/L for the cultivations performed in microtiter plates, and 15.8 g/L in bioreactors [54]. The biomass production of the *M. circinelloides* VI04473 strain in this study varied from 0.5 to 13.2 g/L (Figure 1). The standard growth medium containing reference amount of inorganic phosphorus substrate (Pi1) and the reference amounts of metal ions resulted in 9.8 g/L of biomass, significantly lower than in our previous screening study [50]. The reason for the lower biomass production in the reference medium in the present study was probably due to utilization of ammonium sulphate as a nitrogen source, instead of yeast extract as in the previous study [50]. Ammonium sulphate is a pure inorganic source of nitrogen, lacking any additional macro- and micronutrients, vitamins, and growth factors that are present in yeast extract. Buffering capacity of ammonium sulfate is lower than for yeast extract and, as it has been previously reported, the uptake of ammonium ions causes the release of H^+ by the fungal cells into the media, which accelerates pH lowering [69,70]. Further, possible formation of sulfuric acid during the uptake of ammonium could occur [71]. In addition, formation of organic acids by fungal cells either during exponential or during the stationary growth phase [72] significantly contributes to the acidity of the growth media. Thus, in the media with the low Pi levels we detected considerably low pH and suppressed growth and lipid accumulation in *M. circinelloides* (Figure 1). Acidic pH is a stress factor for many cellular organelles, especially for endoplasmic reticulum (ER), which is connected to protein folding and lipogenesis in fungal cells. It has been previously reported that acidic pH causes ER stress and induces unfolded protein response (UPR). This results in the accumulation of misfolded proteins in the ER and activation of the ER-stress sensor (Ire1p) and ER stress-responsive transcription factor (Hac1p), leading to the inhibition of growth and metabolic activity [73]. In our previous studies, we have showed that acidic pH affects cell wall and increasing chitin/chitosan production in *M. circinelloides* [43]. Cultivation in Duetz-MTPS does not allow continuous adjustment of pH and only start- and end-point measurements are possible, therefore the effect of low phosphorus concentrations was directly linked to drop in pH. Due to the fact, that acidic pH is quite an aggressive stress factor inhibiting fungal growth, the effect of metal ions on the growth and lipid accumulation under low phosphorus substrate availability was difficult to assess. Only two observations could be considered as significant—increase of biomass under higher Zn ion availability and Ca deficiency. Moreover, under Pi conditions lower than the reference (Pi0.5 and Pi0.25), K and Na ions were compensated with KCl and NaCl salts in order to provide the same Na and K amounts as in the reference Pi1 condition [43,44]. It has been reported that chlorides could have negative effect on the mycelium formation of some fungi [74,75]. Moreover, much higher concentrations of Cl (10–15% NaCl) than used in our study (KCl and NaCl in total below 5%) have shown some negative impact on fungal growth [76]. No negative impact of increased Cl^- on the biomass and lipid production has been observed when yeast extract was used as N-source [43,44]. Thus, we can hypothesize that in addition to pH-stress, increased Cl^- ions possibly negatively impacted the growth under low pH conditions. Therefore, these samples were excluded from further data analysis.

Variation in metal ion availability showed diverse and often metal- and pH-specific effects on biomass production and biomass composition of *M. circinelloides*. Growth of *M. circinelloides* was severely inhibited in media lacking Zn and Mg, indicating that these metal ions are essential for the

growth and metabolic activity of the fungus. Inhibition of fungal growth in the media lacking Zn ions can be related to the fact that Zn plays an important role in the regulation of all genes in the eukaryotic cells [31]. Deficiency of Zn is detrimental for the fungal spore germination and further cell proliferation. Our study shows that elevated concentration of Zn ions has a beneficial effect on the biomass formation under phosphorus limitation. Low concentrations of Mg (0.01Mg condition) led to a decrease in biomass production and lipid yield, especially for Pi1 condition, where a lipid content of only 11.43% was reached (Figure 1, Table 3, Table S4). This can be explained by the fact that magnesium deficiency in eukaryotic cells can result in the decrease of glucose-6-phosphate, total content of phospholipids, and a remarkable decrease in oxygen and substrate delivery to the cells with further concomitant changes in membrane phospholipids, leading to the reduced cell growth, delay in the cell cycle, and metabolic activity [77]. It has been shown that long-term Mg deficiency for yeast may result in distortion of cell division, production of aberrant cell forms, and a decrease in viability that can lead to a delay or change of cell cycle [78]. Therefore, the difference in the FA profile of *M. circinielloides* grown under the Mg deficiency (0.01Mg condition) could be explained by disruption of the cell cycle [79].

In addition to Zn and Mg, Ca and Fe are known to be essential for fungal growth [31,80]. In our study, an absence of Fe ions in the medium suppressed the growth of *M. circinelloides* under conditions of moderate and high phosphorus concentrations. While these metals did not affect lipid accumulation. This is an interesting observation, due to the fact that Fe is an important cofactor of many enzymes, it is essential during DNA synthesis and cleavage, and, thus, Fe deficiency should strongly affect growth and metabolic activity of fungal cells.

An absence of Ca ions affected growth of *M. circinelloides* depending on the phosphorus concentration and associated pH of the growth media. A considerable increase in the biomass production of *M. circinelloides* was observed in the media lacking Ca ions and containing moderate (Pi1) and low concentrations of phosphates (Pi0.5 and Pi0.25). Elevated biomass production under the condition Ca0-Pi1 could be partially explained by the fact that the absence of Ca ions in the medium enhanced lipid yield up to 61% (*w*/*w*). Increase in lipid accumulation with the decrease of concentration of Ca ions was observed also for media containing Pi2 and Pi4 levels of phosphates. Calcium starvation enhancing lipid accumulation in oleaginous microorganisms has been reported for algae [81], where the lipid production was increased by 30% in Ca deprived media. To the authors knowledge, a similar effect of Ca ions deficiency on lipid accumulation has never been reported for oleaginous fungi. Currently, there is no clear understanding of the mechanisms behind Ca deficiency-induced lipid accumulation in oleaginous microorganisms, and the direct link between calcium and lipid accumulation and TAGs synthesis has not been clearly demonstrated yet. Similar observations have been reported for adipocyte cells, where low cellular availability of Ca ions mediated antilipolytic pathways through a calcium-sensing receptor (CaSR), resulting in enhancing of lipid content in adipose tissue [82]. Due to the fact that lipolytic pathways are functionally conserved from mammalian cells to fungi [83], we suggest that Ca deficiency is mediating similar antilipolytic pathways in oleaginous microorganisms. Further, Wang. W.A. et al. [83] showed that Ca ions are important for the basal sensitivity of the sterol sensing mechanism of the sterol response element binding proteins (SREBPs) pathway. Wang W.A. et al. discovered that reduction of Ca concentration in endoplasmic reticulum changes the distribution of intracellular sterol/cholesterol, resulting in the enhancement of SREBPs activation and triggering synthesis of neutral lipids. Sterol response element binding proteins (SREBP) are transcription factors that are synthesized on endoplasmic reticulum (ER) and considered as ER-associated integral membrane proteins [83]. SREBP were reported for eukaryotic cells, including mammalian and fungal cells [84]. The studies show that SREBP are involved in lipid homeostasis, while SREBP isoforms control the expression of genes responsible for the biosynthesis of sterol/cholesterol, fatty acids, triacylglycerols, and phospholipid in the cell [85]. Further, detailed studies would be needed to confirm if these two events are valid also for oleaginous fungi grown under calcium deficiency.

Increase in *M. circinelloides* biomass yield was observed also at high concentrations of Ca ions in the media with high phosphate concentrations (Pi2). Infrared spectra of *M. circinelloides* biomass

grown in this medium showed strong absorbance values for polyphosphate peaks (Figure S5 in the Supplementary Materials). Thus, we can assume that increase in biomass production is associated with the intracellular accumulation of available inorganic phosphorus substrate in the form of polyphosphate. It has been previously reported that, in media with excess phosphorus source, *M. circinelloides* is able to perform so called luxury uptake of phosphorus and accumulate it in the form of polyphosphates either in the cell wall or in the form of intracellular polyphosphate granules [6]. Polyphosphate (polyP) is a polyanionic compound, and it has been reported by Kikuchi Y. et al. that in the fully dissociated form, polyP has one negative charge per Pi residue and two extra charges of terminal residues [85]. Therefore, accumulation of polyP in the cell results in the accumulation of a large amount of negative charge, which is probably compensated by an existence of a regulatory mechanism for maintaining charge neutrality of the cell. The studies involving temporal and quantitative analyses of cationic components of the fungal cells revealed that Na, K, Ca, and Mg ions were taken up by polyP, providing strong evidence that these ions play a major role in the neutralization of the negative charge of polyP in the fungal cell [85,86]. Thus, it is likely that with the higher availability of calcium ions in the medium, the neutralization of the polyP negative charge is more efficient and a higher amount of phosphorus can be stored intracellularly in the form of polyP. Due to fact that polyphosphate accumulation takes place in the exponential growth phase, while lipid accumulation in the stationary growth phase [87,88], it could be possible to perform a coproduction of these two components by manipulation of the availability of calcium and phosphorus substrate in the medium. Therefore, *M. circinelloides* can be utilized in the phosphorus recycling processes.

In addition to Ca-deprived media, lack of Cu and higher amounts of Zn and Mn considerably enhanced lipid accumulation in *M. circinelloides*. While elevated lipid production observed due to Ca deficiency could be explained by the above-mentioned hypothesis, there is no clear explanation of the high lipid accumulation under the copper deficiency condition that was significantly higher at all Pi levels. It has to be noted that the highest lipid yield was obtained under deficiency of Ca and Cu ions. In the literature, there has only been only one study, conducted on the liver cells, reporting Cu deficiency enhancing lipid storage [89], while metabolic pathways linking copper to lipid homeostasis have not been reported for fungal and any other microbial cells.

The FA profile of the accumulated in *M. circinelloides* TAGs was not significantly affected by the availability of metal ions and phosphorus. Only some tendency in increase of saturation with high Co and Zn amount was observed, but further enzymatic study would be needed to assess the activity of desaturases at these conditions.

By applying FTIR spectroscopy, we revealed that Ca, Co, and Zn ions at different concentrations correlated with lipid peaks; Ca and Zn correlated with polyphosphate, while Fe and Co with chitin/chitosan peaks of *M. circinelloides* biomass spectra. Thus, these ions could be considered as important components in optimizing and developing coproduction of lipids, polyphosphate, and chitin/chitosan by *M. circineloides.* However, further studies are needed to fully understand the role of these metal ions in the metabolic pathways of *M. circineloides* metabolites.

5. Conclusions

The aim of the study was to evaluate the effect of different metal ions and their concentration on biomass production, composition, and the lipid production in the oleaginous fungus *M. circinelloides*. Moreover, the growth experiments were conducted at different concentrations of phosphates. It can be concluded that, among tested metals, Mg and Zn are essential metals required for the optimal growth of *M. circinelloides*. Calcium availability is important for optimizing polyphosphate accumulation, while calcium and copper deficiency is important for lipid accumulation in *M. circinelloides*. Tested metal ions did not affect fatty acid profile of the accumulated TAGs. However, Ca, Co, Mg, and Zn ions have affected the cellular biochemical profile of *M. circinelloides*. Thus, metal ions are an important tool for optimizing lipid accumulation and coproduction of lipids, polyphosphate, and chitin/chitosan in *M. circinelloides*.

Supplementary Materials: www.mdpi.com/2309-608X/6/4/260/s1. Table S1: Concentrations of salts used for regulating metal ions and inorganic phosphorus levels in the growth media. Table S2: pH of culture supernatant. Table S3: Biomass concentration (g/L). Table S4: Fatty acid profiles (%).Figure S1: Example chromatogram, *Mucor circinelloides* grown in Pi1-R condition. Figure S2: EMSC corrected FTIR-HTS spectra of *Mucor circinelloides* biomass. Figure S3: FTIR spectra of reference materials. Adapted from Dzurendova et al. Figure S4: PCA analysis of FTIR-HTS spectra of *Mucor circinelloides* biomass grown under Pi1 level. The loadings of spectral PCA (A), the score plot (B). Figure S5: PCA analysis of FTIR-HTS spectra of *Mucor circinelloides* biomass grown under Pi2 level. The loadings of spectral PCA (A), the score plot (B). Figure S6: PCA analysis of FTIR-HTS spectra of *Mucor circinelloides* biomass grown under Pi4 level. The loadings of spectral PCA (A), the score plot (B).

Author Contributions: Conceived the research idea, V.S., B.Z., and A.K.; Designed the experiments, B.Z., S.D., V.S., and A.K.; methodology, V.S., B.Z., and A.K.; performed the experimental work, S.D.; analyzed the data, V.T. and S.D.; discussed the results, S.D., V.S., B.Z., A.K., and V.T.; wrote the manuscript, S.D.; discussed and revised the manuscript, S.D., V.S., B.Z., V.T., S.J.H., and A.K. All authors have read and agreed to the published version of the manuscript.

Funding: This research was funded by Research Council of Norway—FMETEKN Grant, project number 257622; BIONÆR Grant, project numbers 268305, 305215; DAAD Grant, project number 309220; HAVBRUK2 Grant, project number 302543/E40; MATFONDAVTALE Grant, project number 301834/E50.

Conflicts of Interest: The authors declare no conflict of interest. The funders had no role in the design of the study; in the collection, analyses, or interpretation of data; in the writing of the manuscript; or in the decision to publish the results.

References

1. Corrochano, L.M.; Kuo, A.; Marcet-Houben, M.; Polaino, S.; Salamov, A.; Villalobos-Escobedo, J.M.; Grimwood, J.; Álvarez, M.I.; Avalos, J.; Bauer, D. Expansion of signal transduction pathways in fungi by extensive genome duplication. *Curr. Biol.* **2016**, *26*, 1577–1584.
2. Rodrigues Reis, C.E.; Bento, H.B.; Carvalho, A.K.; Rajendran, A.; Hu, B.; De Castro, H.F. Critical applications of *Mucor circinelloides* within a biorefinery context. *Crit. Rev. Biotechnol.* **2019**, *39*, 555–570.
3. Carvalho, A.K.F.; Bento, H.B.; Reis, C.E.; De Castro, H.F. Sustainable enzymatic approaches in a fungal lipid biorefinery based in sugarcane bagasse hydrolysate as carbon source. *Bioresour. Technol.* **2019**, *276*, 269–275.
4. Lübbehüsen, T.L.; Nielsen, J.; Mcintyre, M. Aerobic and anaerobic ethanol production by *Mucor circinelloides* during submerged growth. *Appl. Microbiol. Biotechnol.* **2004**, *63*, 543–548.
5. Enrique, A.; Papp, T.; Breum, J.; Arnau, J.; Arturo, P. Strain and culture conditions improvement for β-carotene production with *Mucor*. In *Microbial Processes and Products*; Springer: Berlin/Heidelberg, Germany, 2005; pp. 239–256.
6. Ye, Y.; Gan, J.; Hu, B. Screening of phosphorus-accumulating fungi and their potential for phosphorus removal from waste streams. *Appl. Biochem. Biotechnol.* **2015**, *177*, 1127–1136.
7. Carvalho, A.K.; Rivaldi, J.D.; Barbosa, J.C.; de Castro, H.F. Biosynthesis, characterization and enzymatic transesterification of single cell oil of *Mucor circinelloides*–A sustainable pathway for biofuel production. *Bioresour. Technol.* **2015**, *181*, 47–53.
8. Fai, A.E.C.; Stamford, T.; Stamford-Arnaud, T.M.; Santa-Cruz, P.D.; Silva, M.C.; Campos-Takaki, G.M.; Stamford, T.L. Physico-chemical characteristics and functional properties of chitin and chitosan produced by *Mucor circinelloides* using yam bean as substrate. *Molecules* **2011**, *16*, 7143–7154.
9. Hu, K.-J.; Hu, J.-L.; Ho, K.-P.; Yeung, K.-W. Screening of fungi for chitosan producers, and copper adsorption capacity of fungal chitosan and chitosanaceous materials. *Carbohydr. Polym.* **2004**, *58*, 45–52.
10. Mitra, D.; Rasmussen, M.L.; Chand, P.; Chintareddy, V.R.; Yao, L.; Grewell, D.; Verkade, J.G.; Wang, T.; van Leeuwen, J.H. Value-added oil and animal feed production from corn-ethanol stillage using the oleaginous fungus *Mucor circinelloides*. *Bioresour. Technol.* **2012**, *107*, 368–375.
11. Zhang, X.; Yang, H.; Cui, Z. *Mucor circinelloides*: Efficiency of bioremediation response to heavy metal pollution. *Toxicol. Res.* **2017**, *6*, 442–447.
12. Cui, Z.; Zhang, X.; Yang, H.; Sun, L. Bioremediation of heavy metal pollution utilizing composite microbial agent of *Mucor circinelloides*, *Actinomucor* sp. and *Mortierella* sp. *J. Environ. Chem. Eng.* **2017**, *5*, 3616–3621.
13. He, Q.; Rajendran, A.; Gan, J.; Lin, H.; Felt, C.A.; Hu, B.J. Phosphorus recovery from dairy manure wastewater by fungal biomass treatment. *Water Environ. J.* **2019**, *33*, 508–517.

14. Tauk-Tornisielo, S.M.; Arasato, L.S.; Almeida, A.F.d.; Govone, J.S.; Malagutti, E.N. Lipid formation and γ-linolenic acid production by *Mucor circinelloides* and *Rhizopus* sp., grown on vegetable oil. *Braz. J. Microbiol.* **2009**, *40*, 342–345.
15. Tang, X.; Chen, H.; Gu, Z.; Zhang, H.; Chen, Y.Q.; Song, Y.; Chen, W.J. Comparative proteome analysis between high lipid-producing strain *Mucor circinelloides* WJ11 and low lipid-producing strain CBS 277.49. *J. Agric. Food Chem.* **2017**, *65*, 5074–5082.
16. Zhang, Y.; Adams, I.P.; Ratledge, C. Malic enzyme: The controlling activity for lipid production? Overexpression of malic enzyme in *Mucor circinelloides* leads to a 2.5-fold increase in lipid accumulation. *Microbiology* **2007**, *153*, 2013–2025.
17. Vicente, G.; Bautista, L.F.; Rodríguez, R.; Gutiérrez, F.J.; Sádaba, I.; Ruiz-Vázquez, R.M.; Torres-Martínez, S.; Garre, V. Biodiesel production from biomass of an oleaginous fungus. *Biochem. Eng. J.* **2009**, *48*, 22–27.
18. Ratledge, C.; Cohen, Z. Microbial and algal oils: Do they have a future for biodiesel or as commodity oils? *Lipid Technol.* **2008**, *20*, 155–160.
19. Santek, M.I.; Beluhan, S.; Santek, B. Production of microbial lipids from lignocellulosic biomass. *Adv. Biofuels Bioenergy* **2018**, 137–164.
20. Meyer, V.; Basenko, E.Y.; Benz, J.P.; Braus, G.H.; Caddick, M.X.; Csukai, M.; de Vries, R.P.; Endy, D.; Frisvad, J.C.; Gunde-Cimerman, N.; et al. Growing a circular economy with fungal biotechnology: A white paper. *Fungal Biol. Biotechnol.* **2020**, *7*, 1–23.
21. Mironov, A.A.; Nemashkalov, V.A.; Stepanova, N.N.; Kamzolova, S.V.; Rymowicz, W.; Morgunov, I.G. The Effect of pH and Temperature on Arachidonic Acid Production by Glycerol-Grown *Mortierella alpina* NRRL-A-10995. *Fermentation* **2018**, *4*, 17.
22. Kamisaka, Y.; Kikutsugi, H.; Yokohichi, T.; Nakahara, T.; Suzuki, O. Studies on Production of Lipids in Fungi. XX. *J. Jpn. Oil Chem. Soc.* **1988**, *37*, 344–348.
23. Papanikolaou, S.; Galiotou-Panayotou, M.; Fakas, S.; Komaitis, M.; Aggelis, G. Lipid production by oleaginous Mucorales cultivated on renewable carbon sources. *Eur. J. Lipid Sci. Technol.* **2007**, *109*, 1060–1070.
24. Bellou, S.; Makri, A.; Sarris, D.; Michos, K.; Rentoumi, P.; Celik, A.; Papanikolaou, S.; Aggelis, G. The olive mill wastewater as substrate for single cell oil production by Zygomycetes. *J. Biotechnol.* **2014**, *170*, 50–59.
25. Bellou, S.; Moustogianni, A.; Makri, A.; Aggelis, G. Lipids containing polyunsaturated fatty acids synthesized by Zygomycetes grown on glycerol. *Appl. Biochem. Biotechnol.* **2012**, *166*, 146–158.
26. Vamvakaki, A.N.; Kandarakis, I.; Kaminarides, S.; Komaitis, M.; Papanikolaou, S. Cheese whey as a renewable substrate for microbial lipid and biomass production by Zygomycetes. *Eng. Life Sci.* **2010**, *10*, 348–360.
27. Kavadia, A.; Komaitis, M.; Chevalot, I.; Blanchard, F.; Marc, I.; Aggelis, G. Lipid and γ-linolenic acid accumulation in strains of Zygomycetes growing on glucose. *J. Am. Oil Chem. Soc.* **2001**, *78*, 341–346.
28. Fakas, S.; Papanikolaou, S.; Galiotou-Panayotou, M.; Komaitis, M.; Aggelis, G. Organic nitrogen of tomato waste hydrolysate enhances glucose uptake and lipid accumulation in *Cunninghamella Echinulata*. *J. Appl. Microbiol.* **2008**, *105*, 1062–1070.
29. Dyal, S.D.; Bouzidi, L.; Narine, S.S. Maximizing the production of γ-linolenic acid in *Mortierella ramanniana* var. *ramanniana* as a function of pH, temperature and carbon source, nitrogen source, metal ions and oil supplementation. *Food Res. Int.* **2005**, *38*, 815–829.
30. Moo-Young, M.; Chisti, Y. Biochemical engineering in biotechnology (Technical Report). *Pure Appl. Chem.* **1994**, *66*, 117–136.
31. Gerwien, F.; Skrahina, V.; Kasper, L.; Hube, B.; Brunke, S. Metals in fungal virulence. *Fems Microbiol. Rev.* **2018**, *42*, fux050.
32. Chandrasena, G.; Walker, G.M.; Staines, H.J. Use of response surfaces to investigate metal ion interactions in yeast fermentations. *J. Am. Soc. Brew. Chem.* **1997**, *55*, 24–29.
33. Walker, G.M. Metals in yeast fermentation processes. *Adv. Appl. Microbiol.* **2004**, *54*, 197–230.
34. Birch, R.M.; Ciani, M.; Walker, G.M. Magnesium, calcium and fermentative metabolism in wine yeasts. *J. Wine Res.* **2003**, *14*, 3–15.
35. Gadd, G.M.; Griffiths, A.J. Microorganisms and heavy metal toxicity. *Microb. Ecol.* **1977**, *4*, 303–317.
36. Guchhait, R.B.; Polakis, S.E.; Dimroth, P.; Stoll, E.; Moss, J.; Lane, M.D. Acetyl coenzyme A carboxylase system of *Escherichia coli* purification and properties of the biotin carboxylase, carboxyltransferase, and carboxyl carrier protein components. *J. Biol. Chem.* **1974**, *249*, 6633–6645.

37. Gooday, G. Cell walls. In *The Growing Fungus*; Springer: Berlin/Heidelberg, Germany, 1995; pp. 43–62.
38. Albert, Q.; Baraud, F.; Leleyter, L.; Lemoine, M.; Heutte, N.; Rioult, J.-P.; Sage, L.; Garon, D. Use of soil fungi in the biosorption of three trace metals (Cd, Cu, Pb): Promising candidates for treatment technology? *Environ. Technol.* **2019**, *41*, 3166–3177.
39. Šajbidor, J.; Koželouhova, D.; Ĉertik, M. Influence of some metal ions on the lipid content and arachidonic acid production by *Mortierella* sp. *Folia Microbiol.* **1992**, *37*, 404–406.
40. Yoo, J.-Y.; Lee, H.-C.; Shin, D.-H.; Min, B.-Y. Production of Fungal Lipids-V. Effects of Vitamins, Metabolic Intermediates and Mineral Salts on the Growth and Lipid Accumulation of *Mucor plumbeus*. *Korean J. Food Sci. Technol.* **1982**, *14*, 151–155.
41. Muhid, F.; Nawi, W.; Kader, A.J.A.; Yusoff, W.M.W.; Hamid, A.A. Effects of metal ion concentrations on lipid and gamma linolenic acid production by *Cunninghamella* sp. 2A1. *Online J. Biol. Sci.* **2008**, *8*, 62–67.
42. Kyle, D.J. Arachidonic Acid and Methods for the Production and Use Thereof. U.S. Patent 5,658,767, 19 August 1997; assigned to Martek Corporation.
43. Dzurendova, S.; Zimmermann, B.; Kohler, A.; Tafintseva, V.; Slany, O.; Certik, M.; Shapaval, V. Microcultivation and FTIR spectroscopy-based screening revealed a nutrient-induced co-production of high-value metabolites in oleaginous Mucoromycota fungi. *PLoS ONE* **2020**, *15*, e0234870.
44. Dzurendova, S.; Zimmermann, B.; Tafintseva, V.; Kohler, A.; Ekeberg, D.; Shapaval, V. The influence of phosphorus source and the nature of nitrogen substrate on the biomass production and lipid accumulation in oleaginous Mucoromycota fungi. *Appl. Microbiol. Biotechnol.* **2020**, *104*, 8065–8076.
45. Kosa, G.; Kohler, A.; Tafintseva, V.; Zimmermann, B.; Forfang, K.; Afseth, N.K.; Tzimorotas, D.; Vuoristo, K.S.; Horn, S.J.; Mounier, J.; et al. Microtiter plate cultivation of oleaginous fungi and monitoring of lipogenesis by high-throughput FTIR spectroscopy. *Microb. Cell Factories* **2017**, *16*, 101.
46. Kosa, G.; Shapaval, V.; Kohler, A.; Zimmermann, B. FTIR spectroscopy as a unified method for simultaneous analysis of intra-and extracellular metabolites in high-throughput screening of microbial bioprocesses. *Microb. Cell Factories* **2017**, *16*, 195.
47. Shapaval, V.; Møretrø, T.; Suso, H.P.; Åsli, A.W.; Schmitt, J.; Lillehaug, D.; Martens, H.; Böcker, U.; Kohler, A. A high-throughput microcultivation protocol for FTIR spectroscopic characterization and identification of fungi. *J. Biophotonics* **2010**, *3*, 512–521.
48. Shapaval, V.; Schmitt, J.; Møretrø, T.; Suso, H.; Skaar, I.; Åsli, A.; Lillehaug, D.; Kohler, A. Characterization of food spoilage fungi by FTIR spectroscopy. *J. Appl. Microbiol.* **2013**, *114*, 788–796.
49. Shapaval, V.; Afseth, N.K.; Vogt, G.; Kohler, A. Fourier transform infrared spectroscopy for the prediction of fatty acid profiles in *Mucor* fungi grown in media with different carbon sources. *Microb. Cell Factories* **2014**, *13*, 86.
50. Kosa, G.; Zimmermann, B.; Kohler, A.; Ekeberg, D.; Afseth, N.K.; Mounier, J.; Shapaval, V. High-throughput screening of Mucoromycota fungi for production of low-and high-value lipids. *Biotechnol. Biofuels* **2018**, *11*, 66.
51. Forfang, K.; Zimmermann, B.; Kosa, G.; Kohler, A.; Shapaval, V. FTIR spectroscopy for evaluation and monitoring of lipid extraction efficiency for oleaginous fungi. *PLoS ONE* **2017**, *12*, e0170611.
52. Zimmermann, B.; Kohler, A. Optimizing Savitzky-Golay parameters for improving spectral resolution and quantification in infrared spectroscopy. *Appl. Spectrosc.* **2013**, *67*, 892–902.
53. Duetz, W.A. Microtiter plates as mini-bioreactors: Miniaturization of fermentation methods. *Trends Microbiol.* **2007**, *15*, 469–475.
54. Kosa, G.; Vuoristo, K.S.; Horn, S.J.; Zimmermann, B.; Afseth, N.K.; Kohler, A.; Shapaval, V. Assessment of the scalability of a microtiter plate system for screening of oleaginous microorganisms. *Appl. Microbiol. Biotechnol.* **2018**, *102*, 4915–4925.
55. Lewis, T.; Nichols, P.D.; McMeekin, T.A. Evaluation of extraction methods for recovery of fatty acids from lipid-producing microheterotrophs. *J. Microbiol. Methods* **2000**, *43*, 107–116.
56. Kohler, A.; Kirschner, C.; Oust, A.; Martens, H. Extended multiplicative signal correction as a tool for separation and characterization of physical and chemical information in Fourier transform infrared microscopy images of cryo-sections of beef loin. *Appl. Spectrosc.* **2005**, *59*, 707–716.
57. Zhu, S.-C.; Tang, J.-X.; Zeng, X.-X.; Wei, B.-J.; Huang, B. Isolation of *Mucor circinelloides* Z4 and *Mucor racemosus* Z8 from heavy metal-contaminated soil and their potential in promoting phytoextraction with Guizhou oilseed rap. *J. Cent. South Univ.* **2015**, *22*, 88–94.

58. Bağcıoğlu, M.; Kohler, A.; Seifert, S.; Kneipp, J.; Zimmermann, B. Monitoring of plant–environment interactions by high-throughput FTIR spectroscopy of pollen. *Methods Ecol. Evol.* **2017**, *8*, 870–880.
59. Kenđel, A.; Zimmermann, B. Chemical analysis of pollen by FT-Raman and FTIR spectroscopies. *Front. Plant Sci.* **2020**, *11*, 352.
60. Kohler, A.; Böcker, U.; Shapaval, V.; Forsmark, A.; Andersson, M.; Warringer, J.; Martens, H.; Omholt, S.W.; Blomberg, A. High-throughput biochemical fingerprinting of *Saccharomyces cerevisiae* by Fourier transform infrared spectroscopy. *PLoS ONE* **2015**, *10*, e0118052.
61. Shapaval, V.; Brandenburg, J.; Blomqvist, J.; Tafintseva, V.; Passoth, V.; Sandgren, M.; Kohler, A. Biochemical profiling, prediction of total lipid content and fatty acid profile in oleaginous yeasts by FTIR spectroscopy. *Biotechnol. Biofuels* **2019**, *12*, 140.
62. Byrtusová, D.; Shapaval, V.; Holub, J.; Šimanský, S.; Rapta, M.; Szotkowski, M.; Kohler, A.; Márová, I. Revealing the Potential of Lipid and β-Glucans Coproduction in Basidiomycetes Yeast. *Microorganisms* **2020**, *8*, 1034.
63. Dean, A.P.; Sigee, D.C.; Estrada, B.; Pittman, J.K. Using FTIR spectroscopy for rapid determination of lipid accumulation in response to nitrogen limitation in freshwater microalgae. *Bioresour. Technol.* **2010**, *101*, 4499–4507.
64. Khoshmanesh, A.; Cook, P.L.; Wood, B.R. Quantitative determination of polyphosphate in sediments using Attenuated Total Reflectance-Fourier Transform Infrared (ATR-FTIR) spectroscopy and partial least squares regression. *Analyst* **2012**, *137*, 3704–3709.
65. Kasaai, M. A review of several reported procedures to determine the degree of N-acetylation for chitin and chitosan using infrared spectroscopy. *Carbohydr. Polym.* **2008**, *71*, 497–508.
66. Cárdenas, G.; Cabrera, G.; Taboada, E.; Miranda, S.P. Chitin characterization by SEM, FTIR, XRD, and 13C cross polarization/mass angle spinning NMR. *J. Appl. Polym. Sci.* **2004**, *93*, 1876–1885.
67. Carvalho, A.K.F.; da Conceição, L.R.V.; Silva, J.P.V.; Perez, V.H.; de Castro, H.F. Biodiesel production from *Mucor circinelloides* using ethanol and heteropolyacid in one and two-step transesterification. *Fuel* **2017**, *202*, 503–511.
68. Andrade, V.S.; Sarubbo, L.A.; Fukushima, K.; Miyaji, M.; Nishimura, K.; Campos-Takaki, G.M.d. Production of extracellular proteases by *Mucor circinelloides* using D-glucose as carbon source/substrate. *Braz. J. Microbiol.* **2002**, *33*, 106–110.
69. Peña, A.; Pardo, J.P.; Ramírez, J. Early metabolic effects and mechanism of ammonium transport in yeast. *Arch. Biochem. Biophys.* **1987**, *253*, 431–438.
70. Torija, M.J.; Beltran, G.; Novo, M.; Poblet, M.; Rozès, N.; Mas, A.; Guillamón, J.M. Effect of organic acids and nitrogen source on alcoholic fermentation: Study of their buffering capacity. *J. Agric. Food Chem.* **2003**, *51*, 916–922.
71. Beaulieu, M.; Beaulieu, Y.; Melinard, J.; Pandian, S.; Goulet, J. Influence of Ammonium Salts and Cane Molasses on Growth of *Alcaligenes eutrophus* and Production of Polyhydroxybutyrate. *Appl. Environ. Microbiol.* **1995**, *61*, 165–169.
72. Papagianni, M.; Wayman, F.; Mattey, M. Fate and role of ammonium ions during fermentation of citric acid by *Aspergillus niger*. *Appl. Environ. Microbiol.* **2005**, *71*, 7178–7186.
73. Kawazoe, N.; Kimata, Y.; Izawa, S. Acetic acid causes endoplasmic reticulum stress and induces the unfolded protein response in *Saccharomyces cerevisiae*. *Front. Microbiol.* **2017**, *8*, 1192.
74. Diyaolu, S.; Adebajo, L. Effects of sodium chloride and relative humidity on growth and sporulation of moulds isolated from cured fish. *Food/Nahr.* **1994**, *38*, 311–317.
75. Babich, H.; Stotzky, G. Toxicity of zinc to fungi, bacteria, and coliphages: Influence of chloride ions. *Appl. Environ. Microbiol.* **1978**, *36*, 906–914.
76. Al Tamie, M.S. Sodium chloride stress induced morphological changes in some halotolerant fungi. *Egypt. J. Hosp. Med.* **2016**, *62*, 109–126.
77. Gimenez, M.S.; Oliveros, L.B.; Gomez, N.N. Nutritional deficiencies and phospholipid metabolism. *Int. J. Mol. Sci.* **2011**, *12*, 2408–2433.
78. Walker, G.M.; Duffus, J.H. Magnesium ions and the control of the cell cycle in yeast. *J. Cell Sci.* **1980**, *42*, 329–356.
79. Certik, M.; Shimizu, S. Kinetic analysis of oil biosynthesis by an arachidonic acid-producing fungus, *Mortierella alpina* 1S-4. *Appl. Microbiol. Biotechnol.* **2000**, *54*, 224–230.

80. Aiba, S.; Humphrey, A.E.; Millis, N.F. *Biochemical Engineering*; 1973; Academic Press: New York, USA. ISBN 0120450526.
81. Gorain, P.C.; Bagchi, S.K.; Mallick, N. Effects of calcium, magnesium and sodium chloride in enhancing lipid accumulation in two green microalgae. *Environ. Technol.* **2013**, *34*, 1887–1894.
82. Wang, W.-A.; Liu, W.-X.; Durnaoglu, S.; Lee, S.-K.; Lian, J.; Lehner, R.; Ahnn, J.; Agellon, L.B.; Michalak, M. Loss of calreticulin uncovers a critical role for calcium in regulating cellular lipid homeostasis. *Sci. Rep.* **2017**, *7*, 1–15.
83. Kurat, C.F.; Natter, K.; Petschnigg, J.; Wolinski, H.; Scheuringer, K.; Scholz, H.; Zimmermann, R.; Leber, R.; Zechner, R.; Kohlwein, S.D. Obese yeast: Triglyceride lipolysis is functionally conserved from mammals to yeast. *J. Biol. Chem.* **2006**, *281*, 491–500.
84. Bien, C.M.; Espenshade, P.J. Sterol regulatory element binding proteins in fungi: Hypoxic transcription factors linked to pathogenesis. *Eukaryot. Cell* **2010**, *9*, 352–359.
85. Kikuchi, Y.; Hijikata, N.; Yokoyama, K.; Ohtomo, R.; Handa, Y.; Kawaguchi, M.; Saito, K.; Ezawa, T. Polyphosphate accumulation is driven by transcriptome alterations that lead to near-synchronous and near-equivalent uptake of inorganic cations in an arbuscular mycorrhizal fungus. *New Phytol.* **2014**, *204*, 638–649.
86. Allen, N.S.; Schumm, J.H. Endoplasmic reticulum, calciosomes and their possible roles in signal transduction. *Protoplasma* **1990**, *154*, 172–178.
87. Beever, R.E.; Burns, D. Phosphorus uptake, storage and utilization by fungi. In *Advances in Botanical Research*; Elsevier: Amsterdam, The Netherlands, 1981; Volume 8, pp. 127–219.
88. Ratledge, C. Microorganisms for lipids. *Acta Biotechnol.* **1991**, *11*, 429–438.
89. Burkhead, J.L.; Lutsenko, S. The role of copper as a modifier of lipid metabolism. In *Lipid Metabolism*; IntechOpen: London, UK, 2013.

Supplementary Materials

Metal and phosphate ions show remarkable influence on the biomass production and lipid accumulation in oleaginous Mucor circinelloides

Table S1: Concentrations of salts used for regulating metal ions and inorganic phosphorus levels in the growth media

	Condition label and salt concentration (g/L)									
Salts	**0.01**	**0.10**	**0.25**	**0.5**	**1 (R)**	**2**	**4**	**10**	**100**	**1000**
$MgSO_4.7H_2O$	0.015	0.15	-	-	1.5	-	-	15	150	1500
$CaCl_2.2H_2O$	0.001	0.01	-	-	0.1	-	-	1	10	100
$FeCl_3 \cdot 6H_2O$	-	-	-	-	0.008	-	-	0.08	0.8	8
$ZnSO_4 \cdot 7H_2O$	-	-	-	-	0.001	-	-	0.01	0.1	1
$CoSO_4 \cdot 7H_2O$	-	-	-	-	0.0001	-	-	0.001	0.01	0.1
$CuSO_4 \cdot 5H_2O$	-	-	-	-	0.0001	-	-	0.001	0.01	0.1
$MnSO_4 \cdot 5H_2O$	-	-	-	-	0.0001	0.0002	-	0.001	0.01	0.1
KH_2PO_4	-	-	1.75	3.5	7	14	28	-	-	-
Na_2HPO_4	-	-	0.5	1	2	4	8	-	-	-

Table S2: pH of culture supernatant

Pi	0.25	0.5	1	2	4
R	2.17	2.33	2.88	4.81	5.67
0Ca	2.23	2.35	2.86	4.33	5.72
0.01Ca	2.25	2.41	2.94	4.60	5.54
0.1Ca	2.23	2.37	2.93	4.62	5.56
10Ca	2.17	2.31	2.83	4.25	5.30
10Ca0Mg	4.01	4.76	5.54	5.89	5.96
0.01Mg	2.30	2.56	3.15	4.63	5.73
0.1Mg	2.17	2.39	2.92	4.27	5.59
0Co	2.17	2.33	2.89	4.61	5.68
10Co	2.24	2.35	2.86	4.24	5.71
100Co	2.25	2.39	2.87	4.04	5.57
1000Co	2.22	2.37	2.81	3.85	5.38
0Cu	2.19	2.30	2.76	4.20	5.75
10Cu	2.18	2.33	2.94	4.75	5.67
100Cu	2.20	2.34	2.95	4.50	5.60
1000Cu	2.14	2.32	2.93	4.30	5.54
0Fe	2.09	2.23	2.82	3.97	5.56
10Fe	2.10	2.26	2.77	4.05	5.45
100Fe	2.08	2.22	2.65	3.50	5.26
1000Fe	1.62	1.62	1.85	2.35	2.79
10Ca0Mg	4.01	4.76	5.54	5.89	5.96
10Mn	2.20	2.33	2.86	3.97	5.67
100Mn	2.11	2.28	2.88	4.19	5.56
1000Mn	2.11	2.26	2.80	3.89	5.60
0Zn	2.99	3.49	4.19	5.70	5.81
10Zn	2.12	2.28	2.85	4.37	5.67
100Zn	2.07	2.25	2.85	4.05	5.70
1000Zn	2.03	2.25	2.86	3.78	4.97

Table S3: Biomass concentration (g/L)

Pi	0.25	0.5	1	2	4
R	1.81	3.05	9.80	10.89	11.10
0Ca	2.47	4.70	12.37	9.73	10.24
0.01Ca	1.70	3.07	9.49	9.87	9.34
0.1Ca	1.73	3.44	9.91	10.80	11.37
1Ca	1.81	3.05	9.80	10.89	11.10
10Ca	1.87	3.29	10.86	12.16	9.80
10Ca0Mg	0.00	0.00	0.00	0.00	0.00
0.01Mg	0.51	1.24	1.50	4.47	4.36
0.1Mg	0.94	2.60	8.39	10.36	11.10
1Mg	1.81	3.05	9.80	10.89	11.10
0Co	1.59	3.14	10.34	12.33	12.31
1Co	1.81	3.05	9.80	10.89	11.10
10Co	1.26	2.51	10.44	12.47	13.23
100Co	1.27	3.29	10.89	11.97	12.41
1000Co	0.90	2.11	7.84	10.13	12.06
0Cu	1.17	2.71	8.84	10.33	11.79
1Cu	1.81	3.05	9.80	10.89	11.10
10Cu	1.83	3.61	11.07	12.37	12.74
100Cu	1.56	3.37	9.97	11.94	12.51
1000Cu	2.30	3.20	9.89	10.73	10.71
0Zn	0.57	0.73	1.27	0.90	0.57
1Zn	1.81	3.05	9.80	10.89	11.10
10Zn	1.86	3.30	10.56	11.06	12.70
100Zn	2.54	4.09	12.90	10.70	12.81
1000Zn	2.79	4.44	12.21	9.80	8.36
0Fe	2.30	3.43	5.69	7.54	9.31
1Fe	1.81	3.05	9.80	10.89	11.10
10Fe	1.74	3.50	10.81	10.97	11.24
100Fe	0.00	2.61	8.54	10.77	11.84
1000Fe	0.00	0.00	0.00	2.34	7.89
0Mn	1.76	3.61	9.24	10.73	10.73
1Mn	1.81	3.05	9.80	10.89	11.10
2Mn	1.49	2.50	10.13	10.24	12.60
3Mn	1.66	1.60	8.26	7.71	11.27
10Mn	1.57	2.73	9.27	10.30	12.60
100Mn	1.47	2.90	10.49	10.47	11.50
1000Mn	1.71	3.13	10.13	9.51	12.93

Table S4: Fatty acid profiles (%)

Sample	C14:0	C16:0	C16:1	C18:0	C18:1n9c	C18:2n6c	C18:3n6	others
R Pi1	1.51	21.23	1.80	4.68	38.07	14.70	13.99	4.02
R Pi2	1.86	17.35	4.97	3.49	42.91	12.74	11.44	5.24
R Pi4	1.90	16.82	6.00	3.08	43.87	12.45	10.60	5.30
0Ca Pi1	1.39	24.51	1.46	4.72	37.17	17.69	9.44	3.62
0Ca Pi2	1.79	18.75	4.46	3.13	40.84	14.09	9.26	7.67
0Ca Pi4	1.76	19.29	5.20	3.00	42.39	13.97	10.55	3.85
0.01Ca Pi1	1.85	24.12	0.03	5.21	37.33	15.58	12.28	3.61
0.01Ca Pi2	1.86	17.89	4.54	3.45	41.83	13.51	11.17	5.73
0.01Ca Pi4	2.12	16.86	5.62	4.20	41.55	13.25	10.28	6.13
0.1Ca Pi1	1.32	22.86	1.45	4.85	36.60	15.12	13.05	4.74
0.1Ca Pi2	1.79	18.63	4.59	3.27	41.74	14.01	11.95	4.02
0.1Ca Pi4	1.88	18.56	5.36	3.09	41.82	13.70	10.68	4.90
10Ca Pi1	1.55	23.02	1.73	4.68	36.25	14.92	13.76	4.08
10Ca Pi2	1.91	16.53	5.22	3.31	41.41	13.54	11.92	6.16
10Ca Pi4	1.84	13.46	6.65	2.41	43.80	14.81	11.70	5.34
0.01Mg Pi1	5.83	33.89	0.12	5.88	0.46	7.27	28.30	18.26
0.01Mg Pi2	2.34	24.42	1.24	5.13	27.93	7.04	20.27	11.64
0.01Mg Pi4	2.32	22.17	3.26	3.02	31.36	8.18	19.28	10.41
0.1Mg Pi1	0.04	23.86	1.26	4.26	33.39	16.45	15.67	5.06
0.1Mg Pi2	0.05	18.36	4.00	3.82	40.24	14.30	13.45	5.77
0.1Mg Pi4	0.05	16.29	6.03	3.15	41.81	14.72	11.76	6.20
0Co Pi1	1.35	22.64	1.48	4.27	35.28	16.22	14.99	3.77
0Co Pi2	1.78	18.32	4.63	3.25	41.47	13.95	12.44	4.17
0Co Pi4	1.92	17.34	6.01	2.75	42.37	13.68	11.42	4.51
10Co Pi1	1.43	22.70	1.49	4.38	35.45	16.94	14.53	3.08
10Co Pi2	2.04	20.34	4.26	4.25	40.76	13.44	11.24	3.68
10Co Pi4	2.21	21.26	0.02	3.82	44.00	13.95	11.19	3.56
100Co Pi1	1.47	22.76	1.34	5.04	34.84	17.05	14.39	3.11
100Co Pi2	2.09	19.52	4.12	4.70	40.67	12.90	10.78	5.22
100Co Pi4	2.39	19.59	5.47	4.32	41.11	13.08	10.48	3.57
1000Co Pi1	1.79	22.97	1.14	8.63	30.24	16.85	12.34	6.06
1000Co Pi2	2.26	20.71	2.53	9.00	34.01	13.07	10.85	7.58
1000Co Pi4	2.49	22.66	3.42	10.56	34.29	11.53	9.03	6.02
0Cu Pi1	1.50	22.73	1.61	3.64	35.60	15.65	15.85	3.41
0Cu Pi2	1.72	18.45	4.38	3.24	40.87	13.50	12.98	4.85
0Cu Pi4	1.88	17.59	5.77	2.56	41.17	13.50	11.59	5.93
10Cu Pi1	1.36	22.43	1.49	4.27	35.53	15.84	14.56	4.52
10Cu Pi2	1.69	18.15	4.70	3.18	42.27	13.26	12.19	4.56
10Cu Pi4	1.78	17.31	5.86	2.56	42.84	13.51	11.39	4.76
100Cu Pi1	1.39	22.15	1.77	4.37	36.06	15.75	13.72	4.78
100Cu Pi2	1.90	18.18	4.93	3.29	41.19	13.42	11.53	5.56
100Cu Pi4	1.90	16.99	6.44	2.67	42.90	13.36	10.53	5.22
1000Cu Pi1	1.50	22.23	2.09	4.47	36.75	15.17	13.19	4.61
1000Cu Pi2	1.84	16.94	5.45	3.00	42.20	13.71	10.49	6.37
1000Cu Pi4	1.80	14.52	7.20	2.06	43.68	13.69	9.64	7.40

Sample	C14:0	C16:0	C16:1	C18:0	C18:1n9c	C18:2n6c	C18:3n6	others
0Fe Pi1	1.98	21.77	1.60	6.20	32.80	17.98	10.27	7.40
0Fe Pi2	1.82	18.01	3.20	4.50	39.79	12.65	12.75	7.27
0Fe Pi4	2.09	16.86	6.78	0.00	44.02	13.22	11.24	5.79
10Fe Pi1	0.04	24.21	0.02	4.78	36.40	15.94	14.48	4.12
10Fe Pi2	0.05	16.33	5.32	3.63	42.27	13.90	11.39	7.10
10Fe Pi4	0.05	15.44	7.10	4.24	41.37	13.34	10.68	7.79
100Fe Pi1	0.06	23.33	0.02	3.59	35.60	15.11	17.29	4.99
100Fe Pi2	0.06	20.13	3.80	3.81	40.83	13.76	12.67	4.94
100Fe Pi4	2.18	16.08	6.45	3.39	41.35	12.46	10.27	7.81
0Mn Pi1	1.41	22.15	1.66	4.84	37.52	13.97	14.74	3.71
0Mn Pi2	1.64	17.55	4.71	2.96	41.40	12.60	12.12	7.00
0Mn Pi4	2.01	17.58	6.35	2.85	42.22	12.68	11.07	5.24
10Mn Pi1	1.66	22.34	1.69	5.14	35.63	15.50	14.12	3.93
10Mn Pi2	1.79	17.10	4.34	3.20	41.52	14.16	12.83	5.05
10Mn Pi4	1.86	18.29	5.79	2.87	42.05	13.51	11.30	4.34
100Mn Pi1	0.04	22.80	1.39	3.97	34.53	16.73	15.90	4.63
100Mn Pi2	1.80	16.79	4.36	3.48	41.88	13.84	11.95	5.90
100Mn Pi4	1.93	17.08	5.95	2.69	42.43	13.77	11.21	4.94
1000Mn Pi1	0.06	22.55	1.53	3.92	34.40	16.52	16.25	4.77
1000Mn Pi2	0.05	16.67	4.54	3.47	40.81	14.53	13.12	6.81
1000Mn Pi4	0.05	18.37	6.08	2.86	42.68	14.04	11.34	4.59
10Zn Pi1	1.68	21.81	1.68	5.98	36.69	15.52	12.44	4.19
10Zn Pi2	1.87	19.15	4.11	3.57	41.41	13.56	11.41	4.91
10Zn Pi4	1.78	19.36	4.61	3.38	42.13	13.14	11.03	4.58
100Zn Pi1	1.43	23.30	1.24	5.54	35.65	15.78	13.61	3.44
100Zn Pi2	2.01	18.81	4.07	4.04	40.54	13.74	10.37	6.43
100Zn Pi4	1.88	20.14	4.27	3.66	42.25	13.28	11.10	3.42
1000Zn Pi1	1.69	23.70	1.05	8.28	34.89	14.64	11.77	3.98
1000Zn Pi2	2.39	22.11	2.30	8.90	35.68	13.47	8.60	6.54
1000Zn Pi4	2.03	19.34	4.41	3.77	41.08	12.82	9.45	7.09

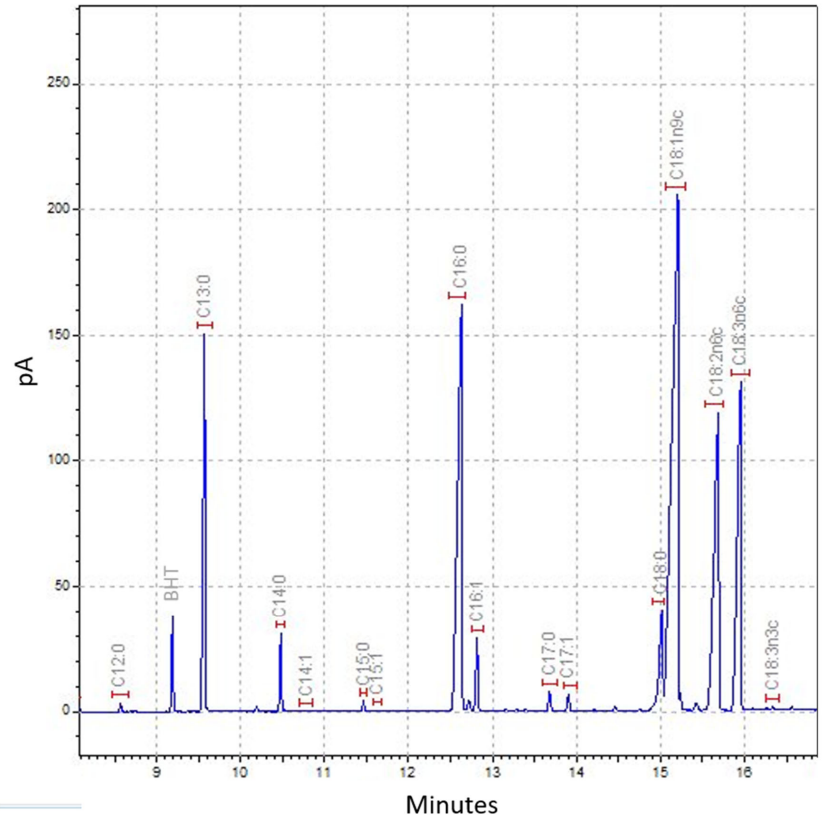

Figure S1: Example chromatogram, *Mucor circinelloides* grown in Pi1-R condition.

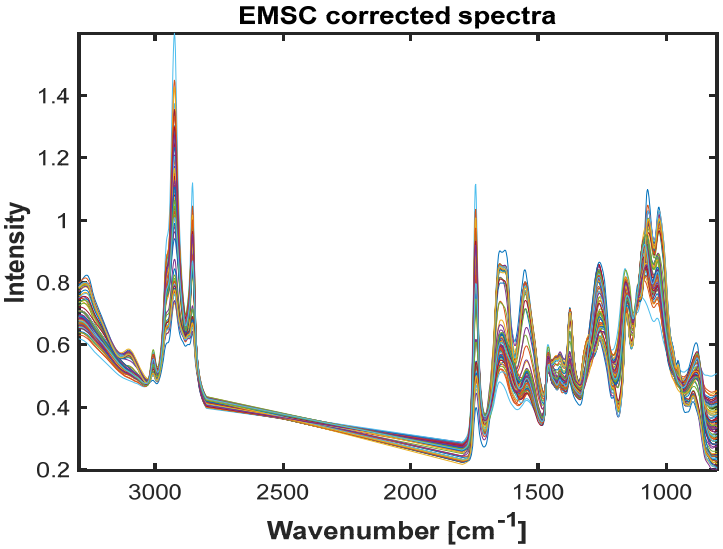

Figure S2: EMSC corrected FTIR-HTS spectra of *Mucor circinelloides* biomass

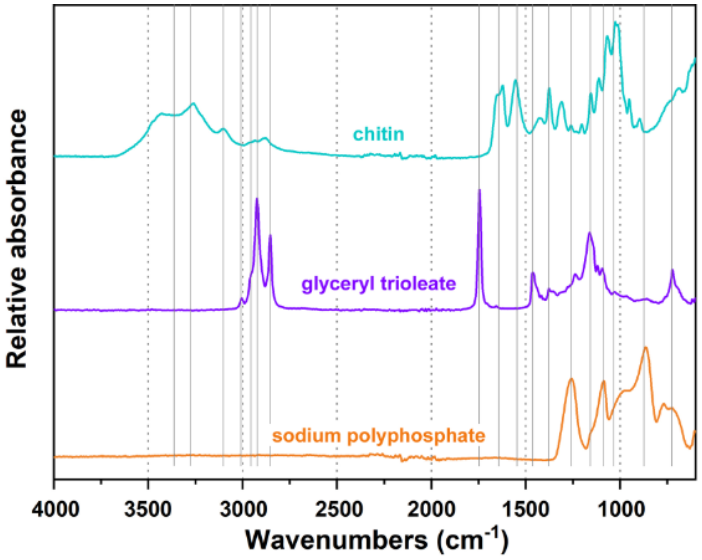

Figure S3: FTIR spectra of reference materials. Adapted from Dzurendova et al. [1]

[1] Dzurendova, S.; Zimmermann, B.; Kohler, A.; Tafintseva, V.; Slany, O.; Certik, M.; Shapaval, V. Microcultivation and FTIR spectroscopy-based screening revealed a nutrient-induced co-production of high-value metabolites in oleaginous Mucoromycota fungi. *PloS one* **2020**, *15*, e0234870

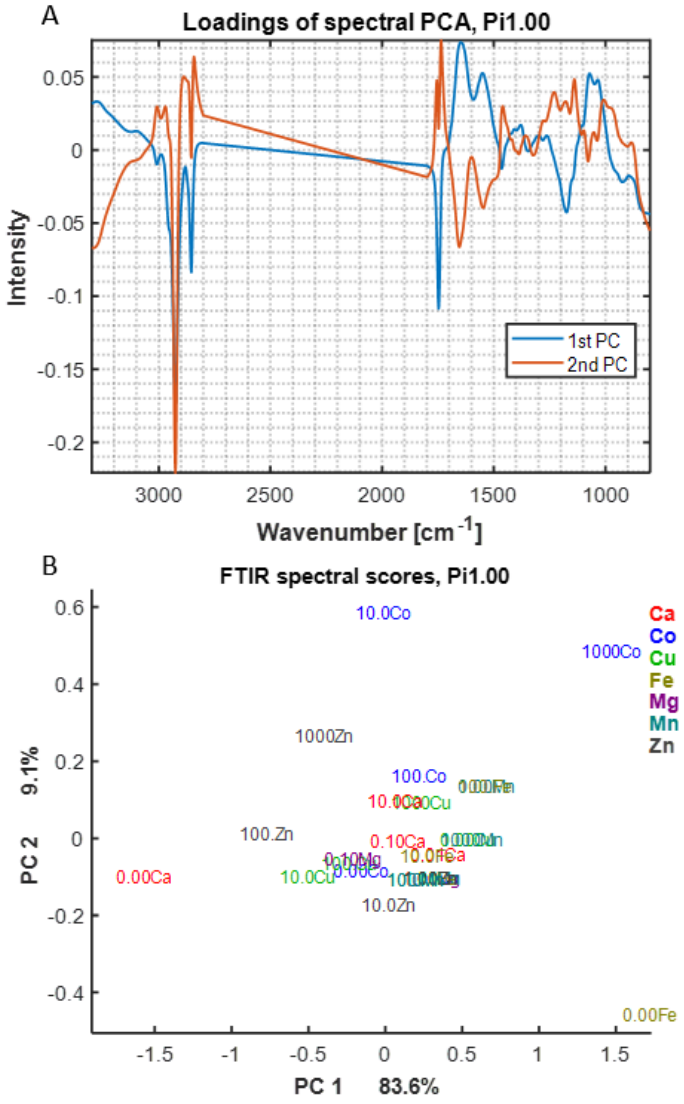

Figure S4: PCA analysis of FTIR-HTS spectra of *Mucor circinelloides* biomass grown under Pi1 level. The loadings of spectral PCA (A), the score plot (B).

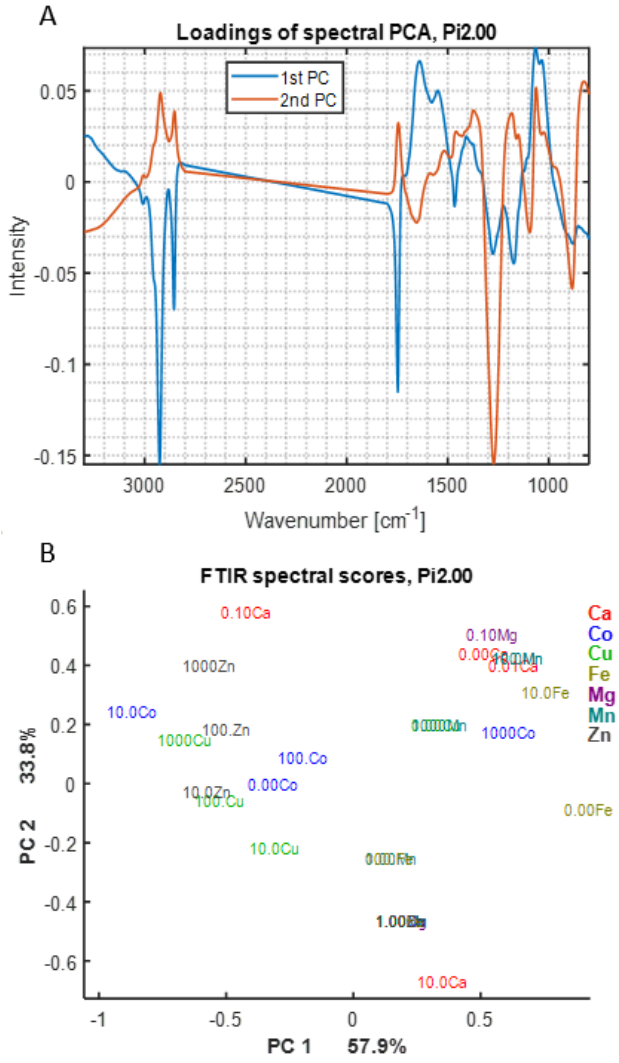

Figure S5: PCA analysis of FTIR-HTS spectra of *Mucor circinelloides* biomass grown under Pi2 level. The loadings of spectral PCA (A), the score plot (B).

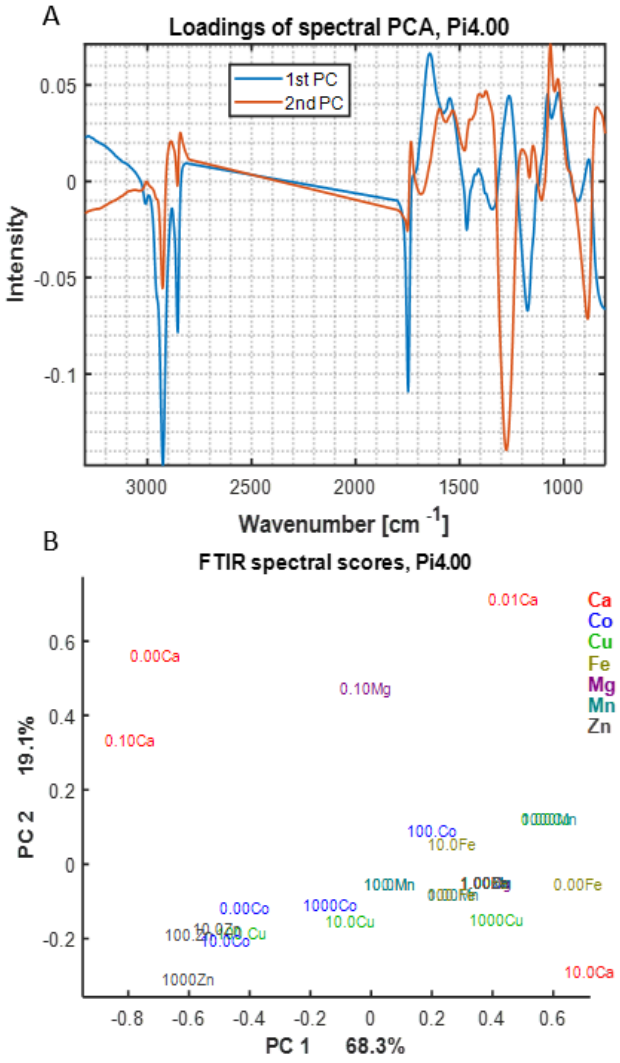

Figure S6: PCA analysis of FTIR-HTS spectra of *Mucor circinelloides* biomass grown under Pi4 level. The loadings of spectral PCA (A), the score plot (B).

Paper IV

Evaluation and optimisation of direct transesterification methods for the assessment of lipid accumulation in oleaginous filamentous fungi

Anne Marie Langseter[1] (anne.langseter@nmbu.no), Simona Dzurendova[1] (simona.dzurendova@nmbu.no), Volha Shapaval[1] (volha.shapaval@nmbu.no), Achim Kohler[1] (achim.kohler@nmbu.no), Dag Ekeberg[2] (dag.ekeberg@nmbu.no), Boris Zimmermann[1]* (boris.zimmermann@nmbu.no).

[1]Faculty of Science and Technology, Norwegian University of Life Sciences, Postbox 5003, 1432 Ås, Norway
[2]Faculty of Chemistry, Biotechnology and Food Science, Norwegian University of Life Sciences, P.O. Box 5003, 1432 Ås, Norway
Correspondence address: Faculty of Science and Technology, Norwegian University of Life Sciences, Postbox 5003, 1432 Ås, Norway

ABSTRACT

Background: Oleaginous filamentous fungi can accumulate large amount of cellular lipids and potentially serve as a major source of oleochemicals for food, feed, chemical, pharmaceutical, and transport industries. Transesterification of microbial oils is an essential step in microbial lipid production at both laboratory and industrial scale. Direct transesterification can considerably reduce costs, increase sample throughput and improve lipid yields (in particular fatty acid methyl esters, FAMEs). There is a need for the assessment of the direct transesterification methods on a biomass of filamentous fungi due to their unique properties, specifically resilient cell wall and wide range of lipid content and composition. In this study we have evaluated and optimised three common direct transesterification methods and assessed their suitability for processing of fungal biomass.

Results: The methods, based on hydrochloric acid (Lewis method), sulphuric acid (Wahlen method), and acetyl chloride (Lepage method), were evaluated on six different strains of Mucoromycota fungi by using different internal standards for gas chromatography measurements. Moreover, Fourier transform infrared (FTIR) spectroscopy was used for the detection of residual lipids in the biomass after the transesterification reaction/extraction, while transesterification efficiency was evaluated by nuclear magnetic resonance spectroscopy. The results show that the majority of lipids, in particular triglycerides, were extracted for all methods, though several methods had substandard transesterification yields. Lewis method, optimised with respect to solvent to co-solvent ratio and reaction time, as well as Lepage method, offer precise estimate of FAME-based lipids in fungal biomass.

Conclusions: The results show that Lepage and Lewis methods are suitable for lipid analysis of oleaginous filamentous fungi. The significant difference in lipid yields results, obtained by optimised and standard Lewis methods, indicates that some of the previously reported lipid yields for oleaginous filamentous fungi must be corrected upwards. The study demonstrates value of biomass monitoring by FTIR, importance of optimal solvent to co-solvent ratio, as well as careful selection and implementation of internal standards for gas chromatography.

Keywords: Oleaginous microorganisms, biodiesel, biofuel, methyl esters, *in situ* transesterification

INTRODUCTION

Microbial oils, produced by a range of oleaginous microorganisms, are being considered as one of the primary sources of oleochemicals for food, feed, chemical, pharmaceutical, and transport industries. Oleaginous microorganisms, such as algae, bacteria and fungi, can accumulate cellular oils in amounts above 20 % of dry biomass (%w/w), and often in 50-80 %w/w range [1, 2]. The cellular oils are mainly produced in the form of free fatty acids and acylglycerols (mostly as triglycerides) and are stored in the globular organelles called lipid bodies. Microbial oils can have similar chemical composition to animal and vegetable oils, ranging from the valuable and highly nutritious omega-3 and omega-6 long-chain polyunsaturated fatty acids (PUFAs), to the biodiesel-compatible monounsaturated and saturated fatty acids (MUFAs and SFAs). Amongst various types of oleaginous microorganisms, Mucoromycota fungi have gained interest due to their versatile metabolism capable to utilize a wide range of feedstock, including waste materials and industrial raw rest materials [3-5]. These filamentous fungi are powerful cell factories able to valorize various feedstocks into a range of marketable products, such as lipids, biopolymers, pigments, proteins, enzymes, and organic acids [6, 7]. Biomass of these oleaginous filamentous fungi can contain large amount of lipids, up to 86 % of dry weight [1, 7], which is often significantly higher than in oleaginous plants and single cell phototrophs, such as green algae, diatoms and cyanobacteria [1, 2].

Microbial lipid production at both laboratory and industrial scale includes several upstream and downstream stages, such as cultivation, separation of biomass, cell disruption, oil extraction, and transesterification. At both research and industrial scale, microbial oils are usually extracted by employing various solvents of different polarities [8-10]. However, compared to the plant and animal lipids, extraction of lipids from the microbial biomass is often hindered by the strong and resilient cell wall, which can lead to the reduced extraction performance [11]. Therefore, cell disruption methods are often employed in order to break up the cellular wall and membrane as a precondition for the effective extraction of oils from the microbial biomass. Cell disruption methods include different mechanical and chemical pretreatments, such as bead beating (bead milling), ultrasonication, microwave, enzymes, and acid or base hydrolysis [12, 13]. Recently, we have demonstrated that Fourier transform infrared (FTIR)

spectroscopy could be used to evaluate and monitor lipid extraction processes, and to identify cell wall components, such as polyphosphates, polyuronides (polymers of glucuronic acid such as glucuronans), and polyglucosamines (such as chitin and chitosan) biopolymers in Mucoromycota fungi, that may negatively affect the extraction process [14].

Once the extraction of lipids from the microbial biomass is accomplished, lipid yield and chemical composition is analysed. Transesterification is a key step in the lipid analysis since chemical composition of extracted oils is predominantly based on the qualitative and quantitative analysis of methyl esters of fatty acids (FAMEs) due to their volatility and thermal stability. After conversion of lipids to FAMEs, the extracted mixture is routinely analysed by gas chromatography (GC) coupled with various detectors [15, 16]. However, total lipid yield can be estimated by the total FAMEs yield only if the predominant lipid classes present in the biomass can be converted into FAMEs, which is the case for free fatty acids and their derivatives, such as acylglycerols and glycerophospholipids. Moreover, the conversion of acylglycerols and other fatty acid-based lipids into FAMEs is essential for industrial production of biodiesel. Both laboratory and industrial researches are exploring process of direct transesterification, where disruption, extraction and transesterification processes are combined into one operation [13]. Direct transesterification can considerably reduce costs, increase sample throughput and improve yields. There is a number of methods for the direct transesterification of microbial biomass, and they differ mainly by the choice of catalyst, usually either acid or base [10, 15, 17-20], though some methods use both [21, 22]. Compared to the standard two-step extraction-transesterification methods, such as Folch and Bligh & Dyer methods [8, 9], direct transesterification often results in higher FAMEs yields [17, 18, 21]. It should be noted that direct transesterification also includes chemical cell disruption obtained by an acid or base catalyst, and that acid/base hydrolysis of various cell components (other than lipids) can compete with transesterification reaction. Our recent study has demonstrated that acid hydrolysis can significantly increase extraction efficiency during a lipid analysis of filamentous fungal biomass [14]. Moreover, we have recently demonstrated that the combination of microtiter plate-based cultivation, with the direct transesterification monitored by high-throughput FTIR spectroscopy, can be used for high-throughput screening of filamentous fungi and other oleaginous microorganisms for the production of low and high-value lipids [23-26]. Application of such high-throughput methodology saves valuable time and decreases costs in the development of bioprocesses for both nutraceutical and biofuel industries.

There is a need for the assessment of the direct transesterification methods on a biomass of filamentous fungi due to the unique properties of these oleaginous microorganisms. Specifically, oleaginous filamentous fungi have resilient cell wall made of various biopolymers [27], in particular glucosamines (chitin and chitosan). For example, *Mucor* can have cell wall thickness of 2 μm [28], and both *Mucor* and *Absidia* have been identified as one of the most promising chitin and chitosan producers, with the maximum reported yield of about 35% of dry weight [29, 30]. Another common cell wall biopolymer in Mucoromycota is polyphosphate, which functions as energy storage component

and an anion counter-ion for chitin and chitosan [31]. In our previous study, we have found that the presence of these biopolymers hampers extraction of lipids in Mucoromycota biomass by standard lipid analysis methods [14]. Finally, standard direct transesterification methods were developed on biomass with relatively low content of lipids (approx. 5-25% of dry weight), while Mucoromycota can have extraordinary high content of lipids, regularly exceeding 30% of dry weight and reaching over 80 % [1, 7]. In general, standard direct transesterification methods were not developed to tackle biomasses with extremely resilient and chemically complex cell wall, and extremely high content of lipids. Although a number of direct transesterification methods have been tested on filamentous fungi, they either failed [32], or were focused on the industrial processes rendering them overly time-consuming for routine research analyses [18, 33-36]. This is unfortunate given that incentive for applying these methods for analysis of filamentous fungi is high, as exemplified by the two recent studies showing clear advantage of direct transesterification methods, compared with standard two-step methods, in routine analysis of fungal biomass [14, 37].

Therefore, the aim of this study was to evaluate and optimise several common direct transesterification methods, and to assess their suitability for processing of fungal biomass of oleaginous Mucoromycota filamentous fungi in screening studies. In addition to fungal biomass, pure vegetable oil (olive oil) was used as a control sample to assess these methods. Several modifications of the three common direct transesterification methods were employed, namely methods based on hydrochloric acid (Lewis method) [10], sulphuric acid (Wahlen method) [19], and acetyl chloride (Lepage method) [38]. The modifications included variations in pretreatments, reaction times, and addition of co-solvents for improved reaction conditions. Different internal standards for GC-FID measurement were used to evaluate the transesterification efficiency and optimise the methods. Moreover, the methods were evaluated by using FTIR spectroscopy for the detection of residual lipids in the biomass after the transesterification reaction. Furthermore, transesterification efficiency of conversion of acylglycerols to FAME was evaluated by nuclear magnetic resonance (NMR) spectroscopy. The methods were compared in terms of the FAMEs yield and fatty acid composition. Finally, the optimised direct transesterification method was demonstrated in a typical high-throughput screening-study workflow, involving microreactor cultivation and routine assessment of biomass lipids by FTIR and GC-FID.

MATERIALS AND METHODS

Fungal strains

Six strains of Mucoromycota oleaginous filamentous fungi were used in the study: *Mucor circinelloides* VI 04473, *Umbelopsis vinacea* CCM F539, *Absidia glauca* CCM 451, *Lichtheimia corymbifera* CCM 8077, *Cunninghamella blakesleeana* CCM F705, and *Amylomyces rouxii* CCM F220. Fungi were obtained in agar slants and dishes or in lyophilized form, from the Czech Collection of Microorganisms, Brno, Czech Republic (CCM) and the Norwegian School of Veterinary Science,

Oslo, Norway (VI). All the selected oleaginous filamentous fungi were identified as a potentially good fungal lipid producers and were able to accumulate between 23 and 47 % of lipids [26].

Cultivation of fungi in high-throughput Duetz-MTP screening system

All six fungal strains were cultivated in the Duetz microtiter plate screening (Duetz-MTPS) system (Enzyscreen, Netherlands). Growth was done in two steps – first, growth on standard agar medium for preparing spore inoculum and second, growth in nitrogen limited broth media in Duetz-MTPS. The cultivation was performed in two independent biological replicates for each fungal strain. Biological replicates were prepared on separate MTPS plates and cultivated at different time points for each fungal strain. For every biological replicate, fresh spore suspension was prepared.

For the preparation of spore inoculum, *Umbelopsis vinacea* was cultivated on potato dextrose agar (PDA), while all other strains were cultivated on malt extract agar (MEA). MEA was prepared by dissolving 30 g of malt extract (Merck, Germany), 5 g of peptone (Amresco, USA) and 15 g of agar powder (Alfa Aesar, ThermoFischer, Germany) in 1L of distilled water and autoclaved at 115 °C for 15 min. PDA was prepared by dissolving 39 g of potato dextrose agar (VWR, Belgium) in 1L of distilled water and autoclaved at 115 °C for 15 min. Agar cultivation was performed 7 days at 25 °C. Fungal spores were harvested from agar plates with a bacteriological loop after the addition of 10 mL of sterile 0.9 % NaCl solution.

The main components of the nitrogen limited broth media were according to the Kavadia *et al.* [39] with modifications ($g \cdot L^{-1}$) [24]: glucose 80, yeast extract 3, KH_2PO_4 7, Na_2HPO_4 2, $MgSO4 \cdot 7H2O$ 1.5, $CaCl2 \cdot 2H2O$ 0.1, $FeCl3 \cdot 6H2O$ 0.008, $ZnSO4 \cdot 7H2O$ 0.001, $CoSO4 \cdot 7H2O$ 0.0001, $CuSO4 \cdot 5H2O$ 0.0001, $MnSO4 \cdot 5H2O$ 0.0001. Media were autoclaved for 15 min at 121 °C. pH of broth media was 6.0 ± 0.3. Cultivation in broth media was performed in Duetz-MTPS, consisting of 24 square polypropylene deep-well microtiter plates, low evaporation sandwich covers and extra high cover clamps, which were placed into the shaker MAXQ 4000 (Thermo Scientific, Germany). 7 ml of sterile broth media was filled into the autoclaved microtiter plates and each well was inoculated with 50 µl of spore inoculum. Cultivation was performed for 7 days at 25 °C and 400 rpm agitation (1.9 cm circular orbit). *Absidia glauca*, *Lichtheimia corymbifera* and *Cunninghamella blakesleeana* were growing in a pellet form, while other strains were growing in a form of dispersed mycelium.

Cultivation of fungi in Erlenmeyer flasks

In addition to the Duetz-MTPS cultivation, two selected fungi, namely *Mucor circinelloides* and *Umbelopsis vinacea*, were also cultivated in Erlenmeyer flasks. Same as Duetz-MTPS cultivation, flask cultivation was done in two steps – first, growth on standard agar medium for preparing spore inoculum and second, growth in nitrogen limited broth media in Erlenmeyer flasks. 100 ml of sterile broth media (see above) was placed into 500 ml Erlenmeyer flasks and inoculated with 100 µl of abovementioned spore inoculum. Cultivation was performed for 7 days at 25 °C and 130 rpm agitation

(2.25 cm circular orbit) in the shaking incubator Climo-Shaker ISF1-X (Kuhner, Germany). Both strains were growing in a form of dispersed mycelium.

Preparation of biomass

The growth media were separated from the fungal biomass by transferring the fermentation broth with plastic Pasteur pipettes into 15 ml Falcon tubes and the subsequent centrifugation at 13500 rpm for 15 min at 4 °C. Fungal biomass from Falcon tubes was washed three times with cold distilled water and filtered under vacuum using a Whatman No. I filter paper (GE Whatman, USA). Washed fungal biomass was frozen at − 20 °C and then lyophilized 24 h in a FreeZone 2.5 freeze-dryer (Labconco, USA) at − 50 °C and 0.01 mbar pressure. All samples were stored at −20 °C until analysis.

Direct transesterification

We have used three standard transesterification methods. Prior to each transesterification process, the samples were preprocessed by bead beating for cell wall disruption and homogenization. Shortly, the main difference between the transesterification methods is acid catalyst: hydrochloric acid in Lewis method, sulphuric acid in Wahlen method, and acetyl chloride in Lepage method. As an additional difference, Wahlen 1 method was performed in a microwave oven, while all other methods (including Wahlen 2 method) were conducted in a heating block. Finally, all methods were modified by either adding chloroform co-solvent (Lepage 2 method) or by increasing the amount of chloroform co-solvent (Lewis 2 method). The detailed description of the methods is provided below.

The following direct transesterification methods were applied on either fungal biomass from flask cultivations (*Mucor circinelloides* and *Umbelopsis vinacea*) or on pure vegetable (olive) oil. Each sample was processed in triplicate per each direct transesterification method.

Hydrochloric acid method 1 (Lewis 1): Direct transesterification was performed according to Lewis *et al*. [10] with the modifications: 2 mL screw-cap polypropylene (PP) tube was filled with 30 ± 5 mg freeze dried biomass or vegetable oil, approx. 250 ± 30 mg (710–1180 μm diameter) acid-washed glass beads and 600 μL of methanol. The fungal biomass was homogenized in a Percellys Evolution tissue homogenizer (Bertin Technologies, France) at 5500 rpm, 6×20 s cycles. The processed biomass was transferred into glass reaction tube by washing the PP tube with 2400 μL of methanol–chloroform–hydrochloric acid solvent mixture (7.6:1:1v/v) (3×800 μL). 1.02 mg of C13:0 TAG internal standard in 100 μL of hexane was added to the glass reaction tube (100 μL from a 10.2 mg/mL^{-1} glyceryl tridecanoate ($C_{42}H_{80}O_6$, C13:0 TAG (13:0/13:0/13:0), Sigma-Aldrich, USA)). The reaction mixture was incubated at 90 °C for 1 h in a heating block, followed by cooling to room temperature. 0.88±3 mg of C15:1 FAME internal standard in 100 μL of hexane was added to the glass reaction tube (100 μL from a 9.1 mg/mL^{-1} methyl 10(Z)-pentadecenoate; $C_{16}H_{30}O_2$, C15:1 FAME, Larodan, Sweden), followed by addition of 1 mL of distilled water. FAMEs were extracted by the addition of 2 mL hexane–chloroform (4:1 v/v) followed by 10 s vortex mixing. The reaction tube was centrifuged at 3000 rpm for 5 min at 4

°C, and the upper (organic) phase was collected in glass tube. The hexane–chloroform extraction (extractive workup) was performed thrice. The residual biomass was stored at −20 ˚C for FTIR measurements. The solvent in glass tube was evaporated under nitrogen at 30 °C, and small amount of anhydrous sodium sulphate (approx. 5 mg) was added in glass tube. FAMEs were transferred into GC vial by washing the glass tube with 1500 µL hexane (2×750 µL) containing 0.01% butylated hydroxytoluene (BHT, Sigma-Aldrich, USA) followed by 5 s vortex mixing.

Hydrochloric acid method 2 (Lewis 2): Direct transesterification was performed according to Lewis *et al.* [10] with modifications: 2 mL screw-cap PP tube was filled with 30 ± 5 mg freeze dried biomass or vegetable oil, approx. 250 ± 30 mg (710–1180 µm diameter) acid-washed glass beads, and 500 µL of chloroform. 1.02 mg of C13:0 TAG internal standard in 100 µL of hexane was added to the PP tube. The fungal biomass was homogenized in a Percellys Evolution tissue homogenizer at 5500 rpm, 6×20 s cycles. The processed biomass was transferred into glass reaction tube by washing the PP tube with 2400 µL of methanol–chloroform–hydrochloric acid solvent mixture (7.6:1:1v/v) (3×800 µL). Finally, 500 µL of methanol was added into glass reaction tube. The reaction mixture was incubated at 90 °C for either 60, 90 or 120 min in a heating block, followed by cooling to room temperature. 0.88±3 mg of C15:1 FAME internal standard in 100 µL of hexane was added to the glass reaction tube, followed by addition of 1 mL of distilled water. The fatty acid methyl esters (FAMEs) were extracted by the addition of 2 mL hexane followed by 10 s vortex mixing. The reaction tube was centrifuged at 3000 rpm for 5 min at 4 °C, and the upper (organic) phase was collected in glass tube. The lower (water phase) was extracted two more times, but now by the addition of 2 mL hexane–chloroform mixture (4:1 v/v). The residual biomass was stored at −20 ˚C for FTIR measurements. The organic phase in the glass tube was dried and prepared for the GC measurement according to Hydrochloric acid method 1.

Sulphuric acid method 1 (Wahlen 1): Direct transesterification was performed according to Wahlen *et al.*[19] with modifications: 2 mL screw-cap PP tube was filled with 30 ± 5 mg freeze dried biomass or vegetable oil, approx. 250 ± 30 mg (710–1180 µm diameter) acid-washed glass beads, and 600 µL of chloroform. 1.02 mg of C13:0 TAG internal standard in 100 µL of hexane was added to the PP tube. The fungal biomass was homogenized in a Percellys Evolution tissue homogenizer at 5500 rpm, 6×20 s cycles. The processed biomass was transferred into microwave glass reaction vessel by washing the PP tube with 2400 µL of chloroform (3×800 µL). The solvent in the microwave vessel was evaporated under nitrogen at 30 °C, and 2 mL of freshly prepared MeOH with 2 % H_2SO_4 was added. A stir bar was added to the microwave-vessel, capped and microwaved at 80°C for 20 min, with 10 sec pre-stirring in an Initiator microwave synthesizer (Biotage AB, Sweden). After cooling to room temperature, 1 mL of saturated $NaHCO_3$ solution, 1mL of distilled water, and 0.88±3 mg of C15:1 FAME internal standard in 100 µL of hexane were added to the reaction tube. The fatty acid methyl esters (FAMEs) were extracted by the addition of 2 mL hexane–chloroform (4:1 v/v) followed by 10 s vortex mixing. The reaction tube was centrifuged at 3000 rpm for 5 min at 4 °C, and the upper (organic) phase was collected in glass tubes. The hexane–chloroform extraction was performed thrice. The residual biomass was

stored at −20 ˚C for FTIR measurements. The organic phase in the glass tube was prepared for the GC measurement according to Hydrochloric acid method 1.

Sulphuric acid method 2 (Wahlen 2): Direct transesterification was performed according to Sulphuric acid method 1, with one modification: The reaction was conducted at 80°C for 60 min in a heating block, instead of at 80°C for 20 min in a microwave oven.

Acetyl chloride method 1 (Lepage 1): Direct transesterification was performed according to Lepage and Roy [38] with modifications: 2 mL screw-cap PP tube was filled with 30 ± 5 mg freeze dried biomass or vegetable oil, approx. 250 ± 30 mg (710–1180 µm diameter) acid-washed glass beads, and 600 µL of chloroform. 1.02 mg of C13:0 TAG internal standard in 100 µL of hexane was added to the PP tubes. The fungal biomass was homogenized in a Percellys Evolution tissue homogenizer at 5500 rpm, 6×20 s cycles. The processed biomass was transferred into a glass reaction tube by washing the PP tube with 2400 µL of chloroform (3×800 µL). The solvent in glass tube was evaporated under nitrogen at 30 °C, and 2 mL of freshly prepared acetyl chloride-methanol (5:100, v/v) was added. The reaction mixture was incubated at 90 °C for 1 h in a heating block, followed by cooling to room temperature. After cooling to room temperature, 2 mL of hexane, 1mL of distilled water, and 0.88 ± 3 mg of C15:1 FAME internal standard in 100 µL of hexane were added to the reaction tube. After 10 s vortex mixing, the reaction tube was centrifuged at 3000 rpm for 5 min at room temperature, and the organic phase was collected in a separate glass tube. The water phase was extracted two more times, but now by the addition of 2 mL hexane–chloroform mixture (4:1 v/v). The residual water phase (with residual biomass) was stored at −20 ˚C for FTIR measurements. The organic phase in glass tubes was prepared for the GC measurement according to Hydrochloric acid method 1.

Acetyl chloride method 2 (Lepage 2): Direct transesterification was performed according to Acetyl chloride method 1, with one modification: 2 mL of chloroform was added to the reaction mixture as co-solvent in addition to 2 mL of acetyl chloride-methanol.

Direct transesterification of fungal biomass from the microtiter plate cultivations: For the direct transesterification of fungal biomass from microtiter plate cultivations (*Mucor circinelloides*, *Umbelopsis vinacea*, *Absidia glauca*, *Lichtheimia corymbifera*, *Cunninghamella blakesleeana*, and *Amylomyces rouxii*) only Hydrochloric acid method 1 and Hydrochloric acid method 2 (with 90 min reaction time) were conducted. The Hydrochloric acid method 1 was implemented as stated above, while the Hydrochloric acid method 2 was slightly modified in respect to the internal standards. Specifically, 0.93 mg of C17:1 FAME internal standard in 100 µL of hexane were added to the GC vial (100 µL from a 9.3 mg/mL^{-1} methyl 10(Z)-heptadecenoate; $C_{18}H_{34}O_2$, C17:1 FAME, Larodan, Sweden). Each biological replicate was processed once with each of the two direct transesterification methods (i.e. two independent biological replicate measurements were obtained per method and per fungal strain).

FTIR spectroscopy analysis

FTIR analyses of fungal biomass were performed before and after lipid extraction by both, the reflectance and transmittance infrared measurements. For measurement of the biomass after lipid extraction, biomass was washed and dried before FTIR measurement as described previously [14]. FTIR measurements were performed using a Vertex 70 FTIR spectrometer (Bruker Optik GmbH, Germany) equipped with a globar mid-IR source and a DTGS detector. The FTIR reflectance spectra were measured with a single reflectance-attenuated total-reflectance (SR-ATR) accessory High Temperature Golden gate ATR Mk II (Specac, United Kingdom). The ATR IR spectra were recorded with a total of 32 scans, spectral resolution of 4 cm^{-1}, and digital spacing of 1.928 cm^{-1}, over the range of 4000–600 cm^{-1}, using the horizontal SR-ATR diamond prism with 45° angle of incidence. Approximately 1 mg of sample was deposited onto the ATR crystal for each measurement, and each sample was measured in triplicates. Between each measurement a background (reference) spectrum was recorded using the sample-free setup. The FTIR transmittance spectra were measured using the High Throughput Screening eXTension (HTS-XT) unit (Bruker Optik GmbH, Germany) as described previously [28]. Fungal biomass was homogenized prior to the HTS FTIR measurements. Approximately 5 mg of biomass was transferred into 2 ml polypropylene tube containing 250 ± 30 mg of acid washed glass beads and 0.5 ml of distilled water, and homogenized by using Percellys Evolution tissue homogenizer (Bertin Technologies, France) with the following set-up: 5500 rpm, 6 × 20 s cycle. 10 µl of homogenized fungal biomass was pipetted onto an IR transparent 384-well silica microplate and dried at room temperature for two hours. The HTS-FTIR spectra were recorded with a total of 64 scans, spectral resolution of 6 cm^{-1}, and digital spacing of 1.928 cm^{-1}, over the range of 4000–500 cm^{-1}, and an aperture of 5 mm. Spectra were recorded as the ratio of the sample spectrum to the spectrum of the empty IR transparent microplate. The OPUS software (Bruker Optik GmbH, Germany) was used for data acquisition and instrument control. ATR correction was performed by using *Extended ATR correction* algorithm of the OPUS software (see Figure S3 in the Supplementary Materials).

For chemical characterization of fungal biomass, a set of model compounds was measured by FTIR-ATR. Chitin, glyceryl trioleate (1,2,3-tri(cis-9-octadecenoyl)glycerol), and glucoronate (methyl 1,2,3,4-tetra-O-acetyl-β-D-glucuronate) were purchased from Merck-Sigma-Aldrich (Darmstadt, Germany) and used without further purification.

GC-FID total lipid content and fatty acid analysis

Determination of total lipid content (expressed as the wt% of total fatty acid methyl esters (FAMEs) of sample dry weight) and fatty acid composition (expressed as wt% of individual FAME of total FAMEs) were performed by using gas chromatography 7820A System (Agilent Technologies, USA), equipped with an Agilent J&W 121-2323 DB-23 column, 20m × 180 µm × 0.20 µm and a flame ionization detector (FID). Helium was used as a carrier gas. The total runtime for one sample was 36 minutes with the following oven temperature increase: initial temperature 70 °C for 2 minutes, after 8

minutes to 150 °C with no hold time, 230 °C in 16 minutes with 5 minutes hold time, and 245 °C in one minute with 4 minutes hold time. The injector temperature was 250 °C and 1 µl of a sample was injected (30:1 split ratio, with split flow 30 mL/min). For the identification and quantification of fatty acids, the Supelco 37 Component FAME Mix (C4–C24 FAME mixture, Sigma-Aldrich, USA) was used as an external standard, in addition to C13:0 TAG and C15:1 FAME internal standards (see above, Direct transesterification of the fungal biomass). Measurements were controlled by the Agilent OpenLAB software (Agilent Technologies, USA).

NMR spectroscopy analysis

Estimation of unreacted TAGs in the oil product after transesterification (expressed as the mole % of total FAMEs and TAGs) were performed by using nuclear magnetic resonance (NMR). The ^{1}H-NMR spectra were recorded by an Ascend 400 spectrometer (Bruker BioSpin, Germany) at 400 MHz. Deuterated chloroform ($CDCl_3$) was used as solvent for all the samples and the chloroform signal at 7.26 ppm was used as an internal standard. The conversion to FAMEs in the transesterification reaction was calculated based on the previously published methods [40, 41], by the methoxy protons of FAMEs at 3.65 ppm, and of the α-carbonyl methylene signals at 2.26 ppm.

The presence of unreacted TAGs was identified by the characteristic two doublet of doublets at 4.05-4.40 ppm from the methylene groups of the glycerol moiety of the triglyceride. Unreacted TAGs were quantified by the stoichiometric comparison of the integrals of the total α-carbonyl methylene signals of the total acyl lipids (FAMEs, free fatty acids and their derivatives, such as acylglycerols and glycerophospholipids, as well as minor components, such as fatty alcohols) and the signal of the glycerol moiety left after reaction. Error in the ^{1}H-NMR measurement is estimated up to 5% [42]. TAGs were not estimated for Wahlen 1 method due to the overlap of many signals belonging to the microwave reaction products with the TAG-specific signals.

RESULTS AND DISCUSSION

Fungal strains

The studied species of filamentous fungi, namely *Mucor circinelloides*, *Umbelopsis vinacea*, *Absidia glauca*, *Lichtheimia corymbifera*, *Cunninghamella blakesleeana*, and *Amylomyces rouxii*, are considered as either model organisms (*Mucor circinelloides*) or oleaginous filamentous fungi of high industrial potential for production of microbial oils [43]. All species were grown under nitrogen-limitation to facilitate accumulation of lipids in the biomass. The assessment of the transesterification methods was conducted by using biomass of *M. circinelloides*, *U. vinacea*. These two Mucoromycota species are characterised by complex and resilient cell wall made of glucosamine and glucuronate biopolymers, and ability to accumulate extraordinarily high amount of lipids under the nitrogen-limited conditions. Moreover, they can store high amounts of intracellular polyphosphates in fungal cell wall

and intracellular granules [28, 44]. The assessment of the optimised Lewis method was demonstrated on all six fungal strains.

Direct transesterification methods and FAME yields

Research on transesterification is often focused on the base-catalysts, since they offer faster and milder reaction conditions compared to acid-catalysts [45]. However, base-catalysts have problems when dealing with a high content of free fatty acids and moisture in the sample. In addition to acylglycerols, biomass of oleaginous filamentous fungi and yeasts can contain high concentration of free fatty acids [14, 18, 46]. While transesterification of acylglycerols can be achieved with base-catalysts, esterification of free fatty acids cannot [47]. Since this can result in significant underestimate of total lipid yield in fungal biomass, transesterification methods for fungal biomass are almost exclusively acid-catalysed [18, 32-37].

Three common acid-catalysed direct transesterification methods were tested in this study: Lewis method (with hydrochloric acid catalyst) [10], Wahlen method (with sulphuric acid catalyst) [19], and Lepage method (with acetyl chloride catalyst) [38]. Out of the three methods, Lewis method is the simplest for handling since it requires relatively safe reagents that are tolerable to moisture (including wet biomass). Wahlen method has limited moisture tolerance and requires microwave heating which is a serious limitation for high-throughput analyses. Lepage method includes use of acetyl chloride, a highly flammable and corrosive substance, and the method requires a safe handling due to reactive nature of the acetyl chloride and water [19, 20, 38, 48]. In all three direct transesterification methods, hexane was used either as a co-solvent during the reaction or for extractive workup. Since hexane is a hazardous chemical, a safer alternatives, such as heptane, could be considered in future studies [49].

First, the three methods were used with minimal modifications, henceforth referred to as Lewis 1, Wahlen 1, and Lepage 1. Second, the three methods were extensively modified:

1) Lewis 2 had higher concentration of chloroform co-solvent: the standard method (Lewis 1) has solvent/co-solvent ratio 10:1, while the method 2 has this ratio 16:5. Moreover, non-polar solvent (chloroform) was added first, prior to bead beating preprocessing, followed by polar solvent (methanol) prior to the transesterification reaction. This modification was made to adjust the polarity of the extraction media for better solvation of the reacting lipids. Moreover, different reaction times were tested to optimise transesterification: 60, 90 and 120 min.
2) Wahlen 2 was conducted for 60 min in a heating block, instead for 20 min in a microwave oven as in the standard method (Wahlen 1). In both cases the reaction was conducted at 80°C.
3) Lepage 2 was conducted with co-solvent (chloroform in 1:1 ratio to the main solvent), instead of conducting the reaction in pure acetyl chloride-methanol as in the standard method (Lepage 1).

The gas chromatography (GC-FID) results show clear differences between the methods (Figure 1, and Table S1 in the Supplementary Materials). For pure olive oil, the results show superiority of

Wahlen 1 and both Lepage methods over Lewis methods. In particular, the difference is striking for Lewis 1, where lipid content was estimated to be only 20 %, compared to 98 % and 100 % estimates for Wahlen 1 and Lepage 1 methods respectively. These results are consistent with the previously published studies that show superiority of Lepage method over Lewis method in lipid analysis of algal biomass [15, 16]. Modification of Lewis method (Lewis 2) resulted in greatly improved total lipid estimate, reaching 94 % for 90 min reaction time (Figure 1). However, modification of Wahlen method (Wahlen 2) resulted in halving of the lipid estimate (47 %). Modification of Lepage method (Lepage 2) resulted in equally optimal lipid estimate of 100 % as obtained by the standard method.

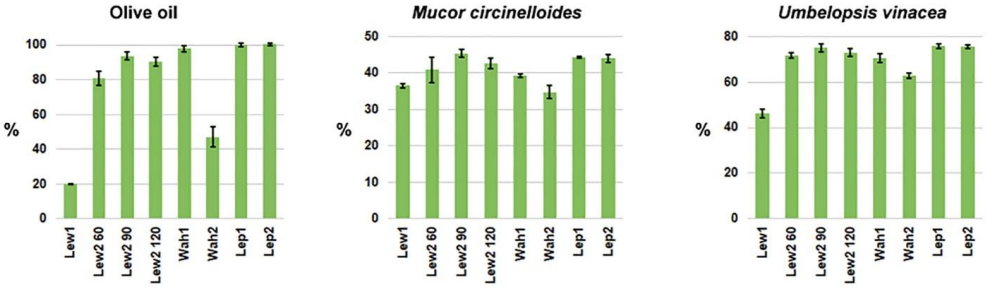

Figure 1. Total FAMEs yield estimate based on GC-FID measurements. The yield is calculated as percentage of dry biomass ($\%_{w/w}$), with one standard deviation error bars. Lew: Lewis method (with designated reaction times in minutes for method 2), Wah: Wahlen method, Lep: Lepage method.

When transesterification was conducted on the fungal biomass, the differences between the methods were not so prominent as compared to the transesterification of pure oil (Figure 1). Here, Lewis 2 and both Lepage methods were clearly superior to other methods. Regarding Lewis 2, the optimal reaction time was 90 min for all three types of samples (olive oil, and two types of fungal biomass). The optimal Lewis 2 (90 min), as well as Lepage methods, have estimated the same total lipid content in the dry biomass (i.e. total FAMEs) of approx. 45 $\%_{w/w}$ for *Mucor circinelloides*, and 75 $\%_{w/w}$ for *Umbelopsis vinacea*. Compared to these numbers, Wahlen 1 is underestimating the total FAME-converted lipids by 13 % in case of *Mucor circinelloides* (39 $\%_{w/w}$ total FAMEs), and 7% in case of *Umbelopsis vinacea* (70 $\%_{w/w}$ total FAMEs). Lewis 1 is faring even worse, underestimating the total FAME-converted lipids by 18 % in case of *Mucor circinelloides* (37 $\%_{w/w}$ total FAMEs), and 39 % in case of *Umbelopsis vinacea* (46 $\%_{w/w}$ total FAMEs).

For the Lewis 1, the estimate of the total FAME-converted lipids was decreasing with the increase of oil content in the sample, dropping to only 20 $\%_{w/w}$ in the case of pure vegetable oil (Figure 1). The FAMEs yield has increased dramatically by modifying the solvent to co-solvent ratio. Thus, the proper amount of co-solvent is critical for optimal transesterification of samples by the Lewis method, and it can be concluded that the main problem with Lewis 1 was ineffective solvation. This is in agreement with the similar study on direct transesterification of microalgal biomass by a modified

Lewis method [50]. It should be mentioned that the importance of solvation was noticed already in the original Lewis *et al.* study [10]. That study has shown that the order of solvent addition can influence the method yields, with better results obtained when the order was from non-polar to polar solvents, similar to our results.

An interesting result was observed with Wahlen 1, where the estimate of the total FAMEs-converted lipids was higher for the vegetable oil than for the fungal biomass. In particular, the total-FAMEs estimate for Wahlen 1 analysis of *Mucor circinelloides* biomass was just 39 $\%_{w/w}$, compared to 44-45 $\%_{w/w}$ obtained by Lepage and Lewis 2 methods (Figure 1). It is known that *Mucor circinelloides* biomass has high content of polyphosphates [14]. These polyphosphates, as well as other cell wall biopolymers (glucosamines and glucuronates), probably compete with acylglycerols for acid-based catalyst during the reaction. Thus, higher concentration of catalyst is perhaps needed in the Wahlen method in order to compensate for this competing reaction. In the original study, Wahlen *et al.* have studied the influence of catalyst concentration on the transesterification, varying the amount of H_2SO_4 within the range 1.2-2.4 $\%_{v/v}$ [19]. Although Wahlen *et al.* study showed that the concentration of the catalyst had a modest effect on the transesterification process, it should be noted that their study was conducted on very different type of biomass, specifically on green algae and diatoms than was the case in our study. Algae and diatoms in that study had significantly lower content of lipids (i.e. 7-27 $\%_{w/w}$ relative to dry mass), than it was the case with *Mucor circinelloides* and *Umbelopsis vinacea* filamentous fungi (45 and 75 % relative to dry mass, respectively). Modification of the Wahlen method (Wahlen 2), where the reaction was performed in a heating block instead of a microwave, showed that the microwave is a critical step for the efficient transesterification.

Composition of extracted fungal lipids

In addition to the GC-FID analyses, we have conducted the NMR analyses of the extracted oils to verify the FAMEs yields, as well as to detect the residual triglycerides in the oils (Figure 2). In general, the results are in agreement with the GC analyses. The small differences between the GC and NMR results can be ascribed to the inherent error of the NMR methodology [42], as well as to the difference in lipid estimate, reported as $\%_{weight}$ in the GC, and $\%_{mol}$ in the ^{1}H-NMR. The NMR results confirm relatively low FAMEs yields for Lewis 1 and Wahlen 2 (Figure 2). The NMR estimates of FAME and TAG for the analysis of *Mucor circinelloides* biomass by Lewis 1 are in agreement with the results from our previous study when lipid class composition was estimated by thin layer chromatography [14]. Furthermore, the NMR results show good transesterification yields for Wahlen 1, and both Lepage methods. Moreover, and as already indicated by the GC-FID results, modification of Lewis method resulted with greatly improved FAMEs yield and relatively small TAG residuals. In particular, TAG residuals were small when Lewis 2 method was conducted on the fungal biomass with 90 min reaction time.

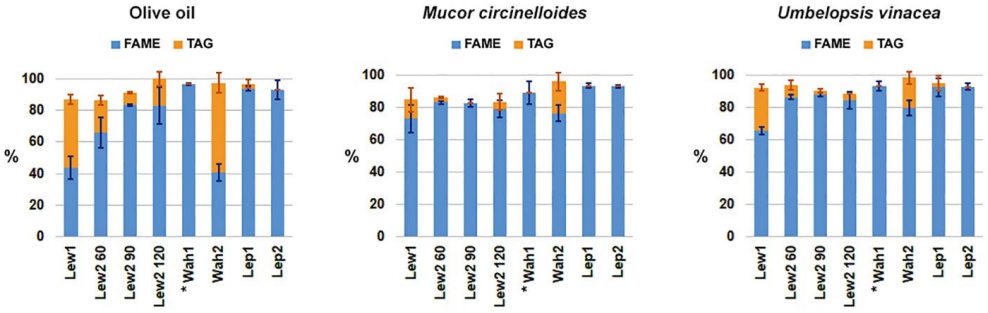

Figure 2. Total yield of FAME and TAG based on NMR analysis, calculated by specific signals in the extracted oil, with one standard deviation error bars. Yield is calculated as mol percentage ($\%_{mol}$) of total acyl lipids. Lew: Lewis method (with designated reaction times in minutes for method 2), Wah: Wahlen method, Lep: Lepage method. *TAGs were not estimated for Wahlen 1 method.

Although the transesterification methods differed substantially regarding the total FAMEs yield, the fatty acid profiles of extracted fungal FAMEs were in agreement across the methods (Table 1). This shows that the transesterification conversion was proportional across all types of fatty acids, even for the methods with relatively low conversion rates, such as Lewis 1. For the pure vegetable oil, the differences in FAMEs profiles between the suboptimal methods (i.e. Lewis 1 and Wahlen 2) and the other methods were noticeable, but not extensive (approx. 3-12 % relative difference in fatty acid compositions).

Table 1. Fatty acid profiles (%, normalized to total FAME), with one standard deviation error. Lew: Lewis method (with designated reaction times in minutes for method 2), Wah: Wahlen method, Lep: Lepage method.

FAME	Lew1	Lew2 60	Lew2 90	Lew2 120	Wah1	Wah2	Lep1	Lep2
Olive oil								
C16:0	11.58 ±0.12	11.59 ±0.01	11.18 ±0.07	11.43 ±0.12	11.19 ±0.01	11.58 ±0.03	11.19 ±0.02	11.07 ±0.00
C16:1	1.09 ±0.04	0.91 ±0.01	0.90 ±0.01	0.88 ±0.01	0.87 ±0.00	1.01 ±0.01	0.88 ±0.01	0.86 ±0.00
C18:0 + C18:1n9c	76.39 ±0.15	78.48 ±0.17	78.54 ±0.31	78.31 ±0.98	79.58 ±0.08	78.05 ±0.06	79.50 ±0.08	79.28 ±0.02
C18:2n6c	7.26 ±0.12	6.58 ±0.04	6.64 ±0.05	6.47 ±0.08	6.38 ±0.01	7.05 ±0.05	6.43 ±0.04	6.81 ±0.01
C18:3n3	0.83 ±0.03	0.68 ±0.01	0.70 ±0.01	0.66 ±0.00	0.66 ±0.00	0.78 ±0.01	0.67 ±0.00	0.65 ±0.00
M. circinelloides								
C14:0	1.54 ±0.01	1.48 ±0.14	1.48 ±0.26	1.49 ±0.00	1.51 ±0.03	1.63 ±0.00	1.49 ±0.04	1.49 ±0.05
C16:0	17.33 ±0.06	17.18 ±0.12	17.17 ±0.03	17.25 ±0.03	17.32 ±0.00	17.33 ±0.04	17.35 ±0.04	17.41 ±0.15
C16:1	4.35 ±0.01	4.18 ±0.05	4.23 ±0.03	4.19 ±0.06	4.34 ±0.02	4.54 ±0.03	4.29 ±0.02	4.28 ±0.03
C17:0	0.81 ±0.01	0.84 ±0.01	0.82 ±0.00	0.84 ±0.01	0.85 ±0.01	0.80 ±0.01	0.82 ±0.00	0.83 ±0.01
C17:1	0.71 ±0.00	0.70 ±0.01	0.71 ±0.00	0.71 ±0.01	0.69 ±0.00	0.72 ±0.00	0.71 ±0.01	0.71 ±0.01
C18:0 + C18:1n9c	50.14 ±0.15	50.20 ±0.30	50.28 ±0.09	50.41 ±0.22	50.56 ±0.03	49.44 ±0.19	50.85 ±0.14	51.05 ±0.48

C18:2n6t	0.69 ±0.02	0.65 ±0.01	0.69 ±0.00	0.66 ±0.01	0.65 ±0.00	0.67 ±0.00	0.65 ±0.00	0.65 ±0.01
C18:2n6c	12.51 ±0.02	12.28 ±0.07	12.36 ±0.04	12.31 ±0.05	12.36 ±0.01	12.74 ±0.02	12.38 ±0.04	12.73 ±0.10
C18:3n6	9.92 ±0.02	9.54 ±0.05	9.62 ±0.03	9.56 ±0.01	9.71 ±0.04	10.38 ±0.07	9.69 ±0.06	9.65 ±0.07
U. vinacea								
C14:0	0.71 ±0.00	0.65 ±0.00	0.64 ±0.01	0.64 ±0.00	0.64 ±0.03	0.69 ±0.00	0.63 ±0.01	0.64 ±0.02
C16:0	27.85 ±0.10	27.49 ±0.01	27.34 ±0.03	27.40 ±0.03	27.52 ±0.01	27.76 ±0.06	27.60 ±0.03	27.41 ±0.07
C16:1	3.09 ±0.02	2.92 ±0.00	2.88 ±0.00	2.90 ±0.01	2.93 ±0.02	3.06 ±0.01	2.92 ±0.01	2.87 ±0.01
C18:0 + C18:1n9c	57.11 ±0.11	58.13 ±0.04	57.96 ±0.05	58.13 ±0.12	58.33 ±0.06	57.88 ±0.07	58.50 ±0.14	58.24 ±0.15
C18:2n6c	5.17 ±0.01	4.93 ±0.02	4.92 ±0.03	4.94 ±0.01	4.84 ±0.03	5.01 ±0.03	4.83 ±0.02	5.17 ±0.01
C18:3n6	3.60 ±0.01	3.29 ±0.01	3.30 ±0.01	3.28 ±0.02	3.27 ±0.02	3.49 ±0.03	3.28 ±0.01	3.25 ±0.01
C20:0	0.62 ±0.00	0.72 ±0.00	0.72 ±0.00	0.74 ±0.00	0.72 ±0.01	0.65 ±0.00	0.72 ±0.01	0.73 ±0.00

Assessment of the residual lipids in the biomass after the transesterification

Assessment of the residual lipids in the fungal biomass after the transesterification reaction was done by FTIR spectroscopy, as demonstrated recently [14]. Following the transesterification reaction, the reaction mixture was processed by the follow-up extractive workup, specifically organic-water biphasic extraction. For all direct transesterification methods, the residual fungal biomass was isolated from the water phase by centrifugation, washed three times with distilled water, and measured by the FTIR spectroscopy (Figure 3 and Figure S1 in the Supplementary Materials). The lipid content of the intact fungal biomass can be estimated based on the signals associated with triglycerides: C− H stretching vibrations (=C−H stretching at 3010 cm^{-1}; C−H stretching in -CH_3 and -CH_2 at 2954, 2925 and 2855 cm^{-1}), C=O stretching in esters (1745 cm^{-1}), CH_2 bending (1460 cm^{-1}), C−O−C stretching in esters (1200-1070 cm^{-1}) and CH_2 rocking (720 cm^{-1}) [14, 23]. In addition to the lipid-related signals, the biomass before extraction shows signals at 1640 and 1545 cm^{-1} related to proteins (C=O stretching in amides (amide I), and C−N−H vibration (amide II) respectively). Finally, signals at 1260 and 880 cm^{-1}, related to polyphosphate P−O and P=O stretching [51], could be explained by the accumulation of polyphosphates in Mucoromycota fungi [28, 52, 53]. The FTIR spectra indicate that biomass of *Mucor circinelloides* has higher content of polyphosphates than *Umbelopsis vinacea* (Figure 3, Figure S2).

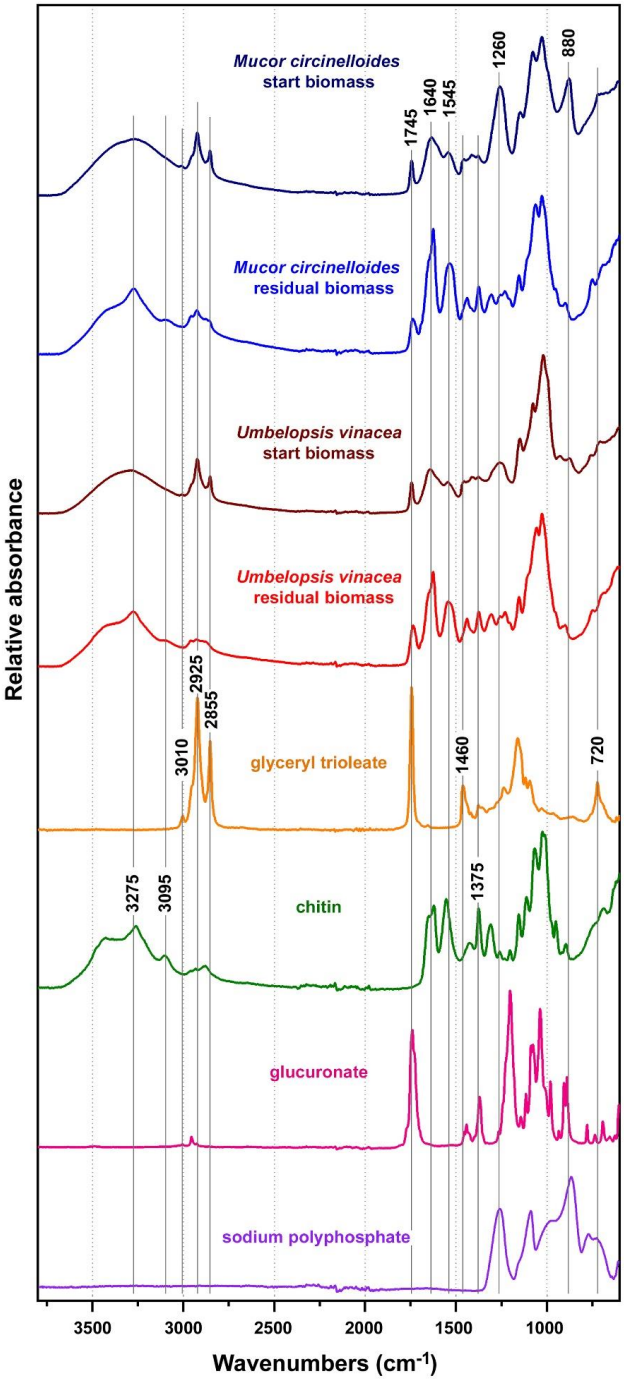
Mucor circinelloides
start biomass
1745
1640
1545
1260
880
Mucor circinelloides
residual biomass
Umbelopsis vinacea
start biomass
Umbelopsis vinacea
residual biomass
2925
2855
3010
glyceryl trioleate
1460
720
3275
3095
chitin
1375
glucuronate
sodium polyphosphate
Relative absorbance
3500
3000
2500
2000
1500
1000
Wavenumbers (cm-1)

504

Figure 3. FTIR spectra of fungal biomass before and after direct transesterification (Lewis 2 method with 90 min reaction time), and of model compounds (glyceryl trioleate, chitin, glucuronate, and sodium polyphosphate). Spectra are plotted with an offset for better viewing.

The infrared spectra of residual biomass (biomass after extraction) show that the majority of lipids, in particular triglycerides, were extracted for all direct transesterification methods (Figure 3). The predominant spectral features are signals associated with cell wall carbohydrates, namely chitin and chitosan (N−H stretching at 3275 and 3095 cm^{-1}, C=O stretching in amides at 1660 and 1625 cm^{-1} (amide I), and C−N−H vibration at 1524 cm^{-1} (amide II), CH and CH_3 bending at 1375 cm^{-1}, C−O and C−O−C stretching at 1200-1000 cm^{-1}, CH_3 bending at 950 cm^{-1}), glucans (C−O and C−O−C stretching at 1200-1000 cm^{-1}) and glucuronans (C=O stretching in esters at 1735 cm^{-1}, C−O and C−O−C stretching at 1200-1000 cm^{-1}) [54-56]. The spectra of biomass after extraction are clearly devoid of signals associated with triglycerides and polyphosphates. It can be presumed that acidic conditions of all tested direct transesterification methods have led to hydrolysis of cell-wall polyphosphates. Thus, acid catalyst is not only important for the transesterification reaction, but it also facilitate degradation of cell wall, leading to efficient extraction of lipids. This is in agreement with our recent study that showed satisfactory degradation of fungal cell wall by bead beating and acid pretreatment [14].

However, the presence of high concentration of polyphosphates in fungal biomass, in particular in *Mucor circinelloides*, probably hinders the transesterification process of TAGs due to the competing acid-based hydrolysis of polyphosphates. All the direct transesterification methods are conducted in relatively polar solvent, which facilitates extraction of phosphate compounds. It has been reported that phosphates, in the form of phospholipids and polyphosphates, hinder transesterification of acylglycerols [57]. This can result in lower FAME yields, as already commented for Wahlen 1 method.

In this study we have used both reflectance (ATR) and transmittance (HTS) FTIR methods for obtaining the IR spectra. Considering that the two methods result with qualitatively different spectra (see Figure S2 in the Supplementary Materials), it is important to clarify why these differences occur. The main difference between the ATR and HTS infrared spectra is the difference in intensity of the absorption bands. The high-wavenumber bands have significantly lower intensity when measured with the ATR method than with the HTS method. The reason for this effect is wavelength-dependence of the IR-beam penetration depth when measuring with the ATR method. The penetration depth (i.e. IR-beam pathlength through the sample) is higher for higher wavelengths, thus the spectra show higher intensity of the low-wavenumber absorbance bands. The effect of the wavelength dependency of the penetration depth is routinely corrected with spectral acquisition software (in our case with Bruker OPUS software) when one wants to compare spectra measured using reflectance (ATR-FTIR) and transmittance (HTS-FTIR) techniques. Thusly corrected ATR spectrum of *Mucor circinelloides* intact biomass is shown in the Figure S3 in the Supplementary Materials. However, such correction is valid only for homogenous samples, for example *Mucor circinelloides* residual biomass (due to homogenization step with bead

beating). In case of intact fungal biomass, chemical components have uneven spatial allocation. For example, cell wall of *Mucor circinelloides* is predominantly made of glucosamine polysaccharides (chitin and chitosan), while cell interior is dominated by lipids [28]. As a result, ATR spectrum will overrepresent chemical components present in the surface area of the sample, such as chitin, and underestimate lipids and other chemical components present in the interior of fungal hyphae. Since HTS transmittance method requires sample homogenization, the resulting spectra show less bias towards different chemical components present in the sample. In general, it is easier to notice spectral differences related to lipids when using HTS method [14], though both FTIR methods are equally useful for assessment of residual lipids in fungal biomass after transesterification reaction.

Importance of the internal standard

All studied transesterification methods have three crucial steps: 1) biomass pretreatment, 2) transesterification reaction, and 3) extractive workup (Figure 4). In this study, all three main steps where controlled by the internal standards for the GC-FID analysis. All three internal standards comprised fatty acids (C13:0, C15:1 and C17:1) that are either not present in fungal oils or present as minor components.

Internal standard is crucial for estimating the total FAME-converted lipids. Namely, total lipid yield is often being estimated as total FAMEs yield by GC-FID [10, 15, 16, 20, 21, 32, 50]. As stated previously, this is valid only if the predominant lipid classes present in the biomass can be converted into FAMEs (for example, fatty acids, acylglycerols and glycerophospholipids). In general, oleaginous microorganisms contain mainly such type of lipids, in particular triacylglycerols. The total lipid yield can be also estimated gravimetrically [18, 34-36, 44]. However, gravimetric lipid quantification is inherently variable and inaccurate due to the extraction of non-lipid compounds, such as proteins, and thus can over- or underestimate the lipid content [58].

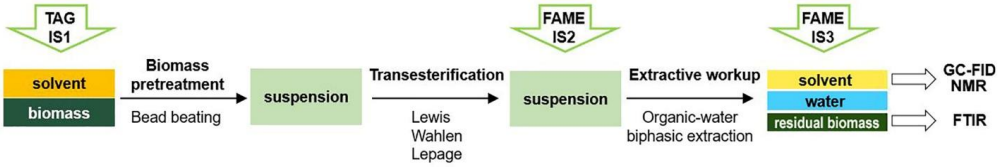

Figure 4. Schematic overview of the study design, with direct transesterification steps and methods, and internal standards (IS1 – C13:0 TAG; IS2 – C15:1 FAME; IS3 – C17:1 FAME).

For the accurate assessment of FAMEs from fungal biomass it is important that the appropriate internal standard (i.e. the internal standard of similar chemical composition to the predominant analyte lipids) is added prior to the transesterification reaction [16]. In our study, the main internal standard was C13:0 TAG (glyceryl tritridecanoate), since the predominant class of lipids in oleaginous filamentous fungi are triacylglycerols [14, 59], and it was added at the very beginning of all transesterification

methods, before the biomass pretreatment (Figure 4). Biomass pretreatment was done by bead beating in order to accomplish cell wall disruption, biomass grinding and homogenization. Moreover, the pretreatment also served to provide good homogenization of the biomass (or vegetable oil sample) with the C13:0 TAG internal standard.

The second internal standard was C15:1 FAME (methyl 10(Z)-pentadecenoate), which was added after the transesterification reaction in order to assess the transesterification yield into FAMEs (Figure 4). To be precise, by comparing the actual value of the added C15:1 FAME with the calculated estimate of the C15:1 FAME based on the C13:0 TAG internal standard, we were able to estimate the conversion of C13:0 TAG into C13:0 FAME (Table 2). The results show that both Lepage methods were able to convert almost all C13:0 TAG into C13:0 FAME, as previously indicated by the NMR analysis (Table 2 and Figure 2). Lewis methods had internal standard conversion into FAME of approx. 90%, while Wahlen methods had between 79 and 96%, depending on the type of sample (Table 2). Interestingly, Wahlen 1 had much lower conversion yield in the presence of fungal biomass than what was the case for the vegetable oil. This is yet another indication that polyphosphates and cell wall polysaccharides are probably competing with acylglycerols for acid-based catalyst, thus hindering the transesterification.

Table 2. GC-FID estimate of conversion of C13:0 TAG internal standard into C13:0 FAME, expressed as percentage with one standard deviation error. (based on the C15:1 FAME internal standard).

	Lew1	Lew2 60	Lew2 90	Lew2 120	Wah1	Wah2	Lep1	Lep2
Olive oil	89 ±4	88 ±3	91 ±1	88 ±3	96 ±2	79 ±10	96 ±1	97 ±0
M. circinelloides	94 ±2	92 ±2	92 ±0	92 ±2	84 ±1	91 ±2	97 ±1	96 ±0
U. vinacea	91 ±2	91 ±2	92 ±1	89 ±1	84 ±3	90 ±2	96 ±1	97 ±1

Importantly, high conversion yield of the internal standard C13:0 TAG into C13:0 FAME was accomplished even for rather ineffective direct transesterification methods, such as Lewis 1 and Wahlen 2 methods. For example, for these two methods the conversion yield of the internal standard into FAME was approx. 80-90%, while the conversion of vegetable oil TAGs into FAMEs was only 20-40%. In general, incomplete transesterification is not detrimental for estimating total FAME content in the biomass since the error created by incomplete transesterification can be corrected by the use of the internal standard [60]. However, this is only valid as long as both internal standard and the biomass lipids have the same conversion yield into FAMEs, which was not the case here. Therefore, our finding is of great importance for the lipid research studies based on the lipid yield determination by GC analysis since it demonstrates that extremely inaccurate total FAME content estimates are obtained when an internal standard and lipid analytes have different conversion yields into FAMEs. For example, for the Lewis 1, the total FAMEs content was underestimated by 20-40 % in fungal biomass, and by 80 % (i.e. five times lower) in vegetable oil.

It can be presumed that the reason for the difference in conversion yield between the vegetable oil TAGs and the internal standard C13:0 TAG is due to the different solvation of these triacylglycerols. Specifically, the internal standard was already well solvated in hexane when it was added to the sample, while solvation of sample lipids commenced during the pretreatment step. In the lipid research studies, an internal standard is often being added completely solvated in a solution. In most cases, such internal standard solution is based on the reaction solvent [15, 21, 38]. Alternatively, internal standard solution is based on a third type of solvent, different than in the main solvent/co-solvent system [16, 32]. The reason for this is ease of handling and time-saving. However, as indicated by our results, this can lead to incorrect estimate of total FAMEs content in the biomass. It is worth noting that a number of studies use internal standard in the form of FAME [10, 50], instead of TAG or free fatty acid, which can result in underestimate of the total FAME content in the biomass if analyte lipids are not completely converted into FAMEs.

Lewis 2 method clearly demonstrates that addition of co-solvent at the very beginning of the pretreatment phase enables good solvation and extraction of lipids from the biomass during the bead beating cell disruption and subsequent reaction. Moreover, it enables good homogenization of cellular (and vegetable) lipids with the internal standard. Thus, even though Lewis 2 has somewhat lower conversion yield of TAGs to FAMEs, compared to the Lepage methods, it offers precise estimate of lipids in the biomass since the internal standard and the biomass lipids have the same conversion yield. However, this only demonstrates that Lewis 2 is reliable in the lipid research, where total lipid yields (i.e. FAME content) and fatty acid compositions are of main importance. Regarding industrial production of biodiesel, Lewis 2 is not as suitable as Lepage method due to lower conversion yield of TAGs into FAMEs, as indicated by the NMR analysis (Figure 2).

The third internal standard used in the study was C17:1 FAME (methyl 10(Z)-heptadecenoate), which was added directly before the GC measurements to assess the lipid losses during the extractive workup (Figure 4 and Table S3). The extractive workup includes water-phase treatment of the reaction media following the transesterification reaction in order to facilitate separation of the hydrophobic lipids from the hydrophilic compounds. This internal standard control was conducted only for the transesterification of fungal biomass from the microtiter plate cultivations. Comparison of the actual values of the added C15:1 and C17:1 FAMEs showed that there was no noteworthy loss of lipids during the workup (Table S2 in the Supplementary Materials). For *Mucor circinelloides* and *Umbelopsis vinacea*, the minor difference between the measured FAME internal standards can be attributed to small intrinsic amount of C17:1 in the fungal biomass, which was detected by analysing the biomass with Lewis 1 without C17:1 internal standard (Table S3 in the Supplementary Materials).

Modified Lewis method and screening of oleaginous filamentous fungi

Our previous study has identified several promising filamentous fungal strains for the production of high-value PUFA and biodiesel [26]. However, these results were obtained by applying

Lewis 1 as described here. The assessment of fungal biomass after transesterification reaction by FTIR indicates complete extraction of triglyceride lipids and hydrolysis of cell-wall polyphosphates (Figure S4 in the Supplementary Materials). Implementation of Lewis 2 on the selected fungal strains cultivated in the high-throughput Duetz-MTP screening system, indicates that the previous study has underestimated total FAME yields by a large extent (Table 3). Specifically, the estimates for the lipid yields obtained by Lewis 2 are 34-84 % higher than the values obtained by Lewis 1. The difference in total FAMEs yield had no impact on the fatty acid profiles of extracted fungal FAMEs since for both Lewis methods the FAME profiles were in large agreement (Table S3 in the Supplementary Materials). This was expected considering our other results (Table 1).

Table 3. Lipid yield (%) from GC-FID for two different biological replicates per strain. Lew: Lewis 1 and 2 methods (with designated reaction time in minutes for method 2).

	Biological replicate 1		Biological replicate 2	
Sample \ Method	**Lew1**	**Lew2 90**	**Lew1**	**Lew2 90**
Mucor circinelloides	38.25	48.31	29.73	44.45
Umbelopsis vinacea	37.57	64.02	33.99	65.22
Cunninghamella blakesleeana	23.42	42.90	22.67	42.00
Lichtheimia corymbifera	24.29	37.59	33.07	37.18
Amylomyces rouxii	23.50	36.61	27.62	36.43
Absidia glauca	44.40	56.33	39.23	59.86

CONCLUSIONS

The study has shown that standard Lepage method (Lepage 1) and the optimised Lewis method (Lewis 2 at 90 ºC) are suitable for lipid analysis of oleaginous filamentous fungi. Comparing the two methods, the optimised Lewis method uses reagents which are easier to prepare and are much less water-sensitive than the reagent (acetyl chloride) in Lepage method. Water sensitivity of acetyl chloride requires drying of solvents as well as thorough freeze-drying of biomass. Wahlen method shows certain deficiencies when dealing with the fungal biomass, indicating a significant matrix effect probably caused by the presence of polyphosphates and polysaccharides in the fungal cells. The significant difference in lipid yields results, obtained by optimised and standard Lewis methods, indicates that some of the previously reported lipid yields must be corrected upwards. This could have important biotechnological implications for production of high-value (PUFA-rich) oils, as well as biodiesel, since it would indicate that some fermentation processes are more economically viable than previously estimated. Finally, the study demonstrates value of biomass monitoring by FTIR, importance of optimal solvent to co-solvent ratio, as well as careful selection and implementation of internal standards for gas chromatography.

Funding

The study was funded by the Research Council of Norway - FMETEKN Grant, project number 257622, BIONÆR Grant, projects number 268305 and 305215, HAVBRUK2 Grant, project number 302543, and IS-DAAD Grant, project number 309220.

Author Contributions

Conceived the research idea: AK, BZ, VS. Designed the experiments: AML, BZ. Methodology: AML, BZ, DE. Performed the growth experiments: SD. Performed the transesterification experiments: AML, SD. Conducted GC and FTIR measurements: AML, SD. Conducted NMR measurements: AML. Analysed the data: AML, BZ, SD. Discussed the results: AK, AML, BZ, DE, SD, VS. Wrote the manuscript: BZ. Discussed and revised the manuscript: AK, AML, BZ, DE, SD, VS. All authors read and approved the final manuscript.

Data Availability

The data generated for this study are available in the Supplementary Materials

Competing interests

The authors declare that they have no competing interests.

Consent for publication

Not applicable.

Ethics approval and consent to participate

Not applicable.

Acknowledgements

Not applicable.

Supplementary Materials

Table S1. Lipid yield from GC-FID

Figure S1. FTIR spectra of fungal biomass before and after transesterification reactions

Figure S2. FTIR spectra of *Mucor circinelloides* and *Umbelopsis vinacea* fungal biomass before and after transesterification reaction

Figure S3. FTIR ATR spectra with ATR correction for IR-beam penetration depth

Table S2. Ratio of normalised measured FAME internal standards

Figure S4. FTIR HTS spectra of fungal biomass after transesterification reaction

Table S3 Fatty acid profiles for Lewis 1 and the optimal Lewis 2 methods

References:

1. Meng X, Yang JM, Xu X, Zhang L, Nie QJ, Xian M: **Biodiesel production from oleaginous microorganisms.** *Renewable Energy* 2009, **34:**1-5.
2. Bharathiraja B, Sridharan S, Sowmya V, Yuvaraj D, Praveenkumar R: **Microbial oil - A plausible alternate resource for food and fuel application.** *Bioresource Technology* 2017, **233:**423-432.
3. Qiao WC, Tao JQ, Luo Y, Tang TH, Miao JH, Yang QW: **Microbial oil production from solid-state fermentation by a newly isolated oleaginous fungus, *Mucor circinelloides* Q531 from mulberry branches.** *Royal Society Open Science* 2018, **5**.
4. Mirbagheri M, Nahvi I, Emamzade R: **Reduction of Chemical and Biological Oxygen Demands from Oil Wastes via Oleaginous Fungi: An Attempt to Convert Food by Products to Essential Fatty Acids.** *Iranian Journal of Biotechnology* 2015, **13:**25-30.
5. Papanikolaou S, Galiotou-Panayotou M, Fakas S, Komaitis M, Aggelis G: **Lipid production by oleaginous Mucorales cultivated on renewable carbon sources.** *European Journal of Lipid Science and Technology* 2007, **109:**1060-1070.
6. Ferreira JA, Lennartsson PR, Edebo L, Taherzadeh MJ: **Zygomycetes-based biorefinery: Present status and future prospects.** *Bioresource Technology* 2013, **135:**523-532.
7. Zhu S, Bonito G, Chen Y, Du Z-Y: **Oleaginous Fungi in Biorefineries.** In *Reference Module in Life Sciences.* Elsevier; 2020.
8. Bligh EG, Dyer WJ: **A Rapid Method of Total Lipid Extraction and Purification.** *Canadian Journal of Biochemistry and Physiology* 1959, **37:**911-917.
9. Folch J, Lees M, Stanley GHS: **A Simple Method for the Isolation and Purification of Total Lipides from Animal Tissues.** *Journal of Biological Chemistry* 1957, **226:**497-509.
10. Lewis T, Nichols PD, McMeekin TA: **Evaluation of extraction methods for recovery of fatty acids from lipid-producing microheterotrophs.** *Journal of Microbiological Methods* 2000, **43:**107-116.
11. Hidalgo P, Toro C, Ciudad G, Navia R: **Advances in direct transesterification of microalgal biomass for biodiesel production.** *Reviews in Environmental Science and Bio-Technology* 2013, **12:**179-199.

12. Patel A, Mikes F, Matsakas L: **An Overview of Current Pretreatment Methods Used to Improve Lipid Extraction from Oleaginous Microorganisms.** *Molecules* 2018, **23**.
13. Yousuf A, Khan MR, Islam MA, Ab Wahid Z, Pirozzi D: **Technical difficulties and solutions of direct transesterification process of microbial oil for biodiesel synthesis.** *Biotechnology Letters* 2017, **39:**13-23.
14. Forfang K, Zimmermann B, Kosa G, Kohler A, Shapaval V: **FTIR Spectroscopy for Evaluation and Monitoring of Lipid Extraction Efficiency for Oleaginous Fungi.** *Plos One* 2017, **12**.
15. Tran HL, Hong SJ, Lee CG: **Evaluation of extraction methods for recovery of fatty acids from *Botryococcus braunii* LB 572 and *Synechocystis* sp PCC 6803.** *Biotechnology and Bioprocess Engineering* 2009, **14:**187-192.
16. Chu PN, Chu FF, Zhang Y, Wu C, Zeng RJ: **A Robust Direct-transesterification Method for Microalgae.** *Energy Sources Part a-Recovery Utilization and Environmental Effects* 2015, **37:**2583-2590.
17. Johnson MB, Wen ZY: **Production of Biodiesel Fuel from the Microalga *Schizochytrium limacinum* by Direct Transesterification of Algal Biomass.** *Energy & Fuels* 2009, **23:**5179-5183.
18. Vicente G, Bautista LF, Gutierrez FJ, Rodriguez R, Martinez V, Rodriguez-Frometa RA, Ruiz-Vazquez RM, Torres-Martinez S, Garre V: **Direct Transformation of Fungal Biomass from Submerged Cultures into Biodiesel.** *Energy & Fuels* 2010, **24:**3173-3178.
19. Wahlen BD, Willis RM, Seefeldt LC: **Biodiesel production by simultaneous extraction and conversion of total lipids from microalgae, cyanobacteria, and wild mixed-cultures.** *Bioresource Technology* 2011, **102:**2724-2730.
20. Cavonius LR, Carlsson NG, Undeland I: **Quantification of total fatty acids in microalgae: comparison of extraction and transesterification methods.** *Analytical and Bioanalytical Chemistry* 2014, **406:**7313-7322.
21. Griffiths MJ, van Hille RP, Harrison STL: **Selection of Direct Transesterification as the Preferred Method for Assay of Fatty Acid Content of Microalgae.** *Lipids* 2010, **45:**1053-1060.
22. Soares AT, da Costa DC, Silva BF, Lopes RG, Derner RB, Antoniosi NR: **Comparative Analysis of the Fatty Acid Composition of Microalgae Obtained by Different Oil Extraction Methods and Direct Biomass Transesterification.** *Bioenergy Research* 2014, **7:**1035-1044.
23. Kosa G, Kohler A, Tafintseva V, Zimmermann B, Forfang K, Afseth NK, Tzimorotas D, Vuoristo KS, Horn SJ, Mounier J, Shapaval V: **Microtiter plate cultivation of oleaginous fungi and monitoring of lipogenesis by high-throughput FTIR spectroscopy.** *Microbial Cell Factories* 2017, **16**.

24. Kosa G, Shapaval V, Kohler A, Zimmermann B: **FTIR spectroscopy as a unified method for simultaneous analysis of intra- and extracellular metabolites in high-throughput screening of microbial bioprocesses.** *Microbial Cell Factories* 2017, **16**.
25. Kosa G, Vuoristo KS, Horn SJ, Zimmermann B, Afseth NK, Kohler A, Shapaval V: **Assessment of the scalability of a microtiter plate system for screening of oleaginous microorganisms.** *Applied Microbiology and Biotechnology* 2018, **102:**4915-4925.
26. Kosa G, Zimmermann B, Kohler A, Ekeberg D, Afseth NK, Mounier J, Shapaval V: **High-throughput screening of Mucoromycota fungi for production of low- and high-value lipids.** *Biotechnology for Biofuels* 2018, **11**.
27. Lecointe K, Cornu M, Leroy J, Coulon P, Sendid B: **Polysaccharides Cell Wall Architecture of Mucorales.** *Frontiers in Microbiology* 2019, **10**.
28. Dzurendova S, Zimmermann B, Kohler A, Tafintseva V, Slany O, Certik M, Shapaval V: **Microcultivation and FTIR spectroscopy-based screening revealed a nutrient-induced co-production of high-value metabolites in oleaginous Mucoromycota fungi.** *PLoS One* 2020, **15:**e0234870.
29. Hu KJ, Hu JL, Ho KP, Yeung KW: **Screening of fungi for chitosan producers, and copper adsorption capacity of fungal chitosan and chitosanaceous materials.** *Carbohydrate Polymers* 2004, **58:**45-52.
30. Synowiecki J, AlKhateeb NAAQ: **Mycelia of *Mucor rouxii* as a source of chitin and chitosan.** *Food Chemistry* 1997, **60:**605-610.
31. Shari'a AED, do Nascimento AE, de Lima MAB, de Campos-Takaki GM, de Souza W: **Polyphosphate in zygomycetes: A cytochemical study.** *Brazilian Journal of Microbiology* 2002, **33:**119-126.
32. Sonnichsen M, Muller BW: **A rapid and quantitative method for total fatty acid analysis of fungi and other biological samples.** *Lipids* 1999, **34:**1347-1349.
33. Liu B, Zhao Z: **Biodiesel production by direct methanolysis of oleaginous microbial biomass.** *Journal of Chemical Technology and Biotechnology* 2007, **82:**775-780.
34. Vicente G, Bautista LF, Rodriguez R, Gutierrez FJ, Sadaba I, Ruiz-Vazquez RM, Torres-Martinez S, Garre V: **Biodiesel production from biomass of an oleaginous fungus.** *Biochemical Engineering Journal* 2009, **48:**22-27.
35. Subhash GV, Mohan SV: **Biodiesel production from isolated oleaginous fungi *Aspergillus* sp. using corncob waste liquor as a substrate.** *Bioresource Technology* 2011, **102:**9286-9290.
36. Kakkad H, Khot M, Zinjarde S, RaviKumar A: **Biodiesel Production by Direct In Situ Transesterification of an Oleaginous Tropical Mangrove Fungus Grown on Untreated Agro-Residues and Evaluation of Its Fuel Properties.** *Bioenergy Research* 2015, **8:**1788-1799.

37. Hoarau J, Caro Y, Petit T, Grondin I: **Evaluation of Direct Wet Transesterification Methods on Yeast and Fungal Biomass Grown on Sugarcane Distillery Spent Wash.** *Chemical Engineering & Process Techniques* 2016, **2:**1032.

38. Lepage G, Roy CC: **Improved Recovery of Fatty-Acid through Direct Trans-Esterification without Prior Extraction or Purification.** *Journal of Lipid Research* 1984, **25:**1391-1396.

39. Kavadia A, Komaitis M, Chevalot I, Blanchard F, Marc I, Aggelis G: **Lipid and gamma-linolenic acid accumulation in strains of zygomycetes growing on glucose.** *Journal of the American Oil Chemists Society* 2001, **78:**341-346.

40. Gelbard G, Bres O, Vargas RM, Vielfaure F, Schuchardt UF: **H-1 Nuclear-Magnetic-Resonance Determination of the Yield of the Transesterification of Rapeseed Oil with Methanol.** *Journal of the American Oil Chemists Society* 1995, **72:**1239-1241.

41. Tariq M, Ali S, Ahmad F, Ahmad M, Zafar M, Khalid N, Khan MA: **Identification, FT-IR, NMR (H-1 and C-13) and GC/MS studies of fatty acid methyl esters in biodiesel from rocket seed oil.** *Fuel Processing Technology* 2011, **92:**336-341.

42. Knothe G, Kenar JA: **Determination of the fatty acid profile by H-1-NMR spectroscopy.** *European Journal of Lipid Science and Technology* 2004, **106:**88-96.

43. Diwan B, Gupta P: **Lignocellulosic Biomass to Fungal Oils: A Radical Bioconversion Toward Establishing a Prospective Resource.** In *Recent Advancement in White Biotechnology Through Fungi.* Edited by Yadav A, Singh S, Mishra S, Gupta A: Springer, Cham; 2019.

44. Dzurendova S, Zimmermann B, Tafintseva V, Kohler A, Ekeberg D, Shapaval V: **The influence of phosphorus source and the nature of nitrogen substrate on the biomass production and lipid accumulation in oleaginous Mucoromycota fungi.** *Applied Microbiology and Biotechnology* 2020, **104:**8065-8076.

45. Vicente G, Martinez M, Aracil J: **Integrated biodiesel production: a comparison of different homogeneous catalysts systems.** *Bioresource Technology* 2004, **92:**297-305.

46. Tamano K, Miura A: **Further increased production of free fatty acids by overexpressing a predicted transketolase gene of the pentose phosphate pathway in *Aspergillus oryzae* faaA disruptant.** *Bioscience Biotechnology and Biochemistry* 2016, **80:**1829-1835.

47. Christie WW: **Preparation of Ester Derivatives of Fatty Acids for Chromatographic Analysis.** In *Advances in Lipid Methodology 2.* Edited by Christie WW. Dundee: Oily Press; 1993.

48. Ichihara K, Fukubayashi Y: **Preparation of fatty acid methyl esters for gas-liquid chromatography.** *Journal of Lipid Research* 2010, **51:**635-640.

49. Prat D, Hayler J, Wells A: **A survey of solvent selection guides.** *Green Chemistry* 2014, **16:**4546-4551.

50. Armenta RE, Scott SD, Burja AM, Radianingtyas H, Barrow CJ: **Optimization of Fatty Acid Determination in Selected Fish and Microalgal Oils.** *Chromatographia* 2009, **70:**629-636.
51. Khoshmanesh A, Cook PLM, Wood BR: **Quantitative determination of polyphosphate in sediments using Attenuated Total Reflectance-Fourier Transform Infrared (ATR-FTIR) spectroscopy and partial least squares regression.** *Analyst* 2012, **137:**3704-3709.
52. Ye YL, Gan J, Hu B: **Screening of Phosphorus-Accumulating Fungi and Their Potential for Phosphorus Removal from Waste Streams.** *Applied Biochemistry and Biotechnology* 2015, **177:**1127-1136.
53. Werner TP, Amrhein N, Freimoser FM: **Specific localization of inorganic polyphosphate (poly P) in fungal cell walls by selective extraction and immunohistochemistry.** *Fungal Genetics and Biology* 2007, **44:**845-852.
54. Cardenas G, Cabrera G, Taboada E, Miranda SP: **Chitin characterization by SEM, FTIR, XRD, and C-13 cross polarization/mass angle spinning NMR.** *Journal of Applied Polymer Science* 2004, **93:**1876-1885.
55. Signori L, Ami D, Posteri R, Giuzzi A, Mereghetti P, Porro D, Branduardi P: **Assessing an effective feeding strategy to optimize crude glycerol utilization as sustainable carbon source for lipid accumulation in oleaginous yeasts.** *Microbial Cell Factories* 2016, **15**.
56. Pau-Roblot C, Petit E, Sarazin C, Courtois J, Courtois B, Barbotin JN, Seguin JP: **Studies of low molecular weight samples of glucuronans with various acetylation degree.** *Biopolymers* 2002, **64:**34-43.
57. Williams PJL, Laurens LML: **Microalgae as biodiesel & biomass feedstocks: Review & analysis of the biochemistry, energetics & economics.** *Energy & Environmental Science* 2010, **3:**554-590.
58. Laurens LML, Quinn M, Van Wychen S, Templeton DW, Wolfrum EJ: **Accurate and reliable quantification of total microalgal fuel potential as fatty acid methyl esters by in situ transesterification.** *Analytical and Bioanalytical Chemistry* 2012, **403:**167-178.
59. Khot M, Katre G, Zinjarde S, RaviKumar A: **Single Cell Oils (SCOs) of Oleaginous Filamentous Fungi as a Renewable Feedstock: A Biodiesel Biorefinery Approach.** In *Fungal biorefineries.* Edited by Kumar S, Dheeran P, Taherzadeh M, Khanal S. New York, NY: Springer Science+Business Media; 2018.
60. O'Fallon JV, Busboom JR, Nelson ML, Gaskins CT: **A direct method for fatty acid methyl ester synthesis: Application to wet meat tissues, oils, and feedstuffs.** *Journal of Animal Science* 2007, **85:**1511-1521.

Supplementary Material

Evaluation and optimisation of direct transesterification methods for the assessment of lipid accumulation in oleaginous filamentous fungi

Anne Marie Langseter[1] (anne.langseter@nmbu.no), Simona Dzurendova[1] (simona.dzurendova@nmbu.no), Volha Shapaval[1] (volha.shapaval@nmbu.no), Achim Kohler[1] (achim.kohler@nmbu.no), Dag Ekeberg[2] (dag.ekeberg@nmbu.no), Boris Zimmermann[1]* (boris.zimmermann@nmbu.no).

[1]Faculty of Science and Technology, Norwegian University of Life Sciences, Postbox 5003, 1432 Ås, Norway
[2]Faculty of Chemistry, Biotechnology and Food Science, Norwegian University of Life Sciences, P.O. Box 5003, 1432 Ås, Norway
Correspondence address: Faculty of Science and Technology, Norwegian University of Life Sciences, Postbox 5003, 1432 Ås, Norway

*Corresponding author:
Boris Zimmermann
Faculty of Science and Technology
Norwegian University of Life Sciences
Drøbakveien 31, 1432 Ås, Norway.
Tel: +47 6723 1576
Fax: +47 6496 5001
E-mail: boris.zimmermann@nmbu.no

Table of Contents **Page**

Table S1. Lipid yield from GC-FID (with standard deviation values)

	Lew1	Lew2 60	Lew2 90	Lew2 120	Wah1	Wah2	Lep1	Lep2
Olive oil	20.08 ±0.26	80.75 ±4.18	93.62 ±2.14	90.37 ±2.51	97.96 ±1.73	47.02 ±5.76	100.11 ±1.18	100.44 ±0.80
M. circinelloides	36.54 ±0.61	40.78 ±3.59	45.24 ±1.09	42.29 ±1.46	39.24 ±0.52	34.72 ±1.79	44.32 ±0.30	43.92 ±1.09
U. vinacea	46.20 ±1.80	71.65 ±1.21	74.90 ±1.60	72.90 ±1.81	70.44 ±1.83	62.58 ±1.14	75.66 ±0.88	75.54 ±0.78

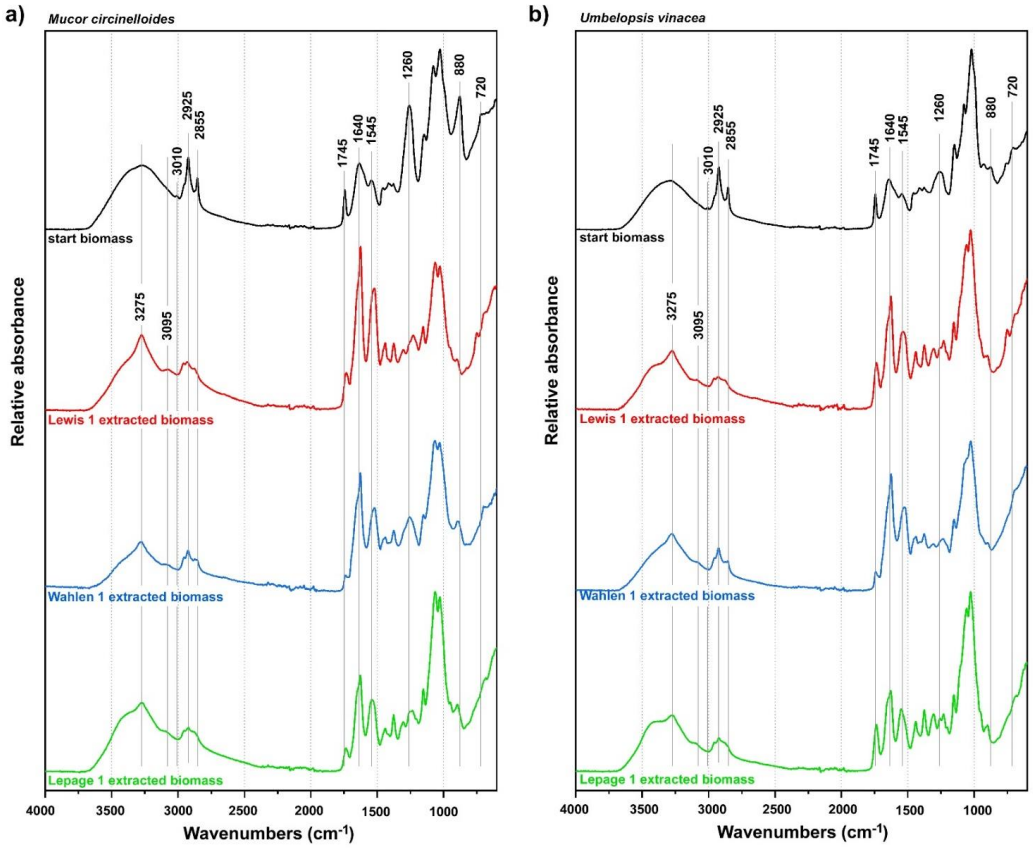

Figure S1. FTIR spectra of fungal biomass before and after transesterification reactions (Lewis 1, Wahlen 1, and Lepage 1 methods): a) *Mucor circinelloides*, b) *Umbelopsis vinacea*.

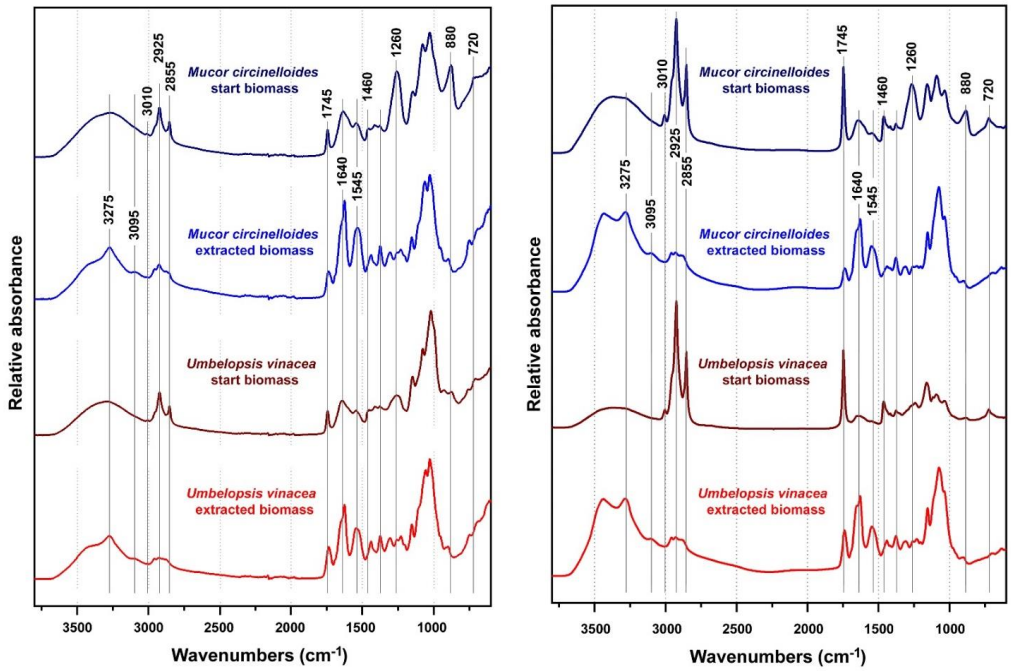

Figure S2. ATR (left) and HTS (right) FTIR spectra of *Mucor circinelloides* and *Umbelopsis vinacea* fungal biomass before and after transesterification reaction (Lewis 2 method with 90 min reaction time).

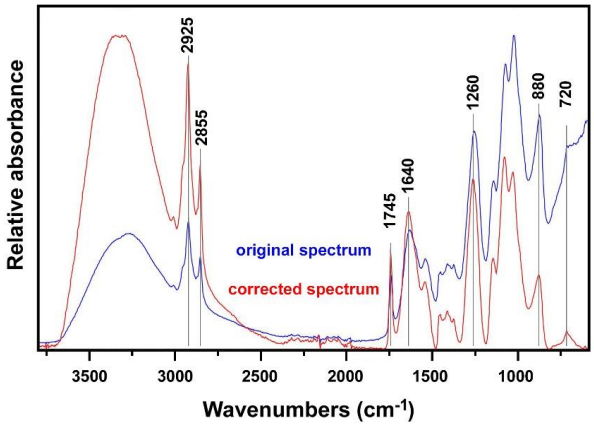

Figure S3. FTIR ATR spectra of *Mucor circinelloides* fungal biomass before transesterification reaction: original measured spectrum (blue) and after ATR correction for IR-beam penetration depth.

Table S2. The ratio of normalised measured FAME internal standards (C15:1 and C17:1) for Lewis 1 and optimal Lewis 2 methods (Lewis 2 method, 90 min reaction time). Normalised values were obtained by dividing the GC-FID measured values (based on C13:0 TAG internal standard) with the actual values of added FAME internal standards.

	Biological replicate 1	
Sample \ Method	**Lew1**	**Lew2 90**
Mucor circinelloides	0.94	0.93
Umbelopsis vinacea	0.95	0.96
Cunninghamella blakesleeana	0.95	0.96
Lichtheimia corymbifera	1.00	0.99
Amylomyces rouxii	0.98	0.96
Absidia glauca	0.97	0.99

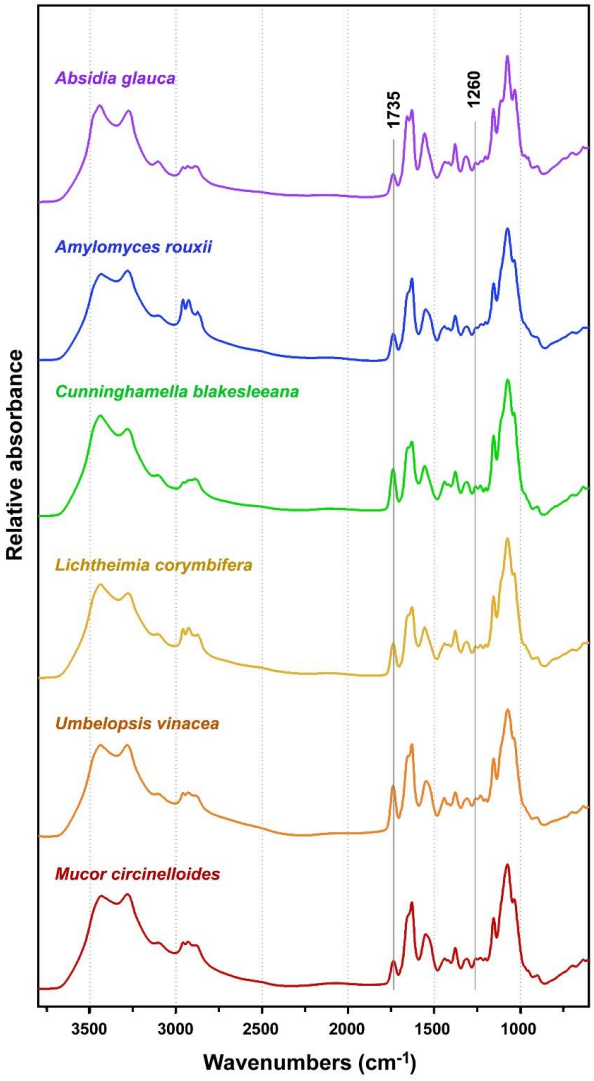

Figure S4. HTS FTIR spectra of *Absidia glauca*, *Amylomyces rouxii*, *Cunninghamella blakesleeana*, *Lichtheimia corymbifera*, *Umbelopsis vinacea*, and *Mucor circinelloides* fungal biomass after transesterification reaction (Lewis 2 method with 90 min reaction time).

Table S3a Fatty acid profiles for Lewis 1 and the optimal Lewis 2 methods (90 min reaction time for method 2). IS designates internal standard.

	Biological replicate 1		Biological replicate 2	
FAME	Lew1	Lew2 90	Lew1	Lew2 90
M. circinelloides				
C14:0	2.14	1.79	1.62	1.44
C16:0	17.95	17.76	17.53	17.48
C16:1	3.78	3.76	3.59	3.42
C17:0	0.97	0.97	0.73	0.76
C17:1	0.56	IS	0.50	IS
C18:0 + C18:1n9c	47.96	48.96	47.82	50.13
C18:2n6t	0.56	0.60	0.47	0.47
C18:2n6c	12.77	13.29	13.68	13.36
C18:3n6	10.06	10.13	11.33	10.47
U. vinacea				
C14:0	0.67	0.59	0.70	0.59
C16:0	24.87	25.10	23.92	24.25
C16:1	2.07	1.98	2.03	1.87
C17:1	0.23	IS	0.25	IS
C18:0 + C18:1n9c	57.71	59.81	55.89	60.46
C18:2n6c	6.32	6.00	6.58	5.91
C18:3n6	4.28	3.88	4.80	3.97
C20:0	0.79	0.89	0.74	0.91
C. blakesleeana				
C14:0	0.69	0.63	0.53	0.64
C16:0	16.51	15.44	17.66	18.56
C16:1	0.56	0.58	0.59	0.58
C18:0 + C18:1n9c	53.59	54.32	52.18	54.86
C18:2n6c	14.36	13.45	14.38	12.84
C18:3n6	9.36	8.81	9.83	7.74
C20:1n9	0.67	0.68	0.65	0.57
C22:0	0.51	0.65	0.53	0.62
C24:0	1.79	2.29	1.75	1.89

Table S3b Fatty acid profiles for Lewis 1 and the optimal Lewis 2 methods (90 min reaction time for method 2). IS designates internal standard.

	Biological replicate 1		Biological replicate 2	
FAME	Lew1	Lew2 90	Lew1	Lew2 90
L. corymbifera				
C14:0	0.56	0.49	0.52	0.54
C16:0	24.60	24.00	24.51	24.96
C16:1	0.99	0.98	0.92	0.97
C18:0 + C18:1n9c	55.31	56.94	57.02	57.07
C18:2n6c	11.05	10.57	10.44	10.45
C18:3n6	4.38	4.02	3.90	3.81
C20:0	0.46	0.54	0.55	0.51
A. rouxii				
C14:0	1.83	1.39	1.55	1.39
C16:0	21.32	21.54	21.53	21.48
C16:1	2.27	1.88	1.99	1.90
C17:1	0.38	IS	0.27	IS
C18:0 + C18:1n9c	45.57	46.55	45.48	46.66
C18:2n6t	1.30	1.17	1.21	1.22
C18:2n6c	8.50	8.22	8.34	8.35
C18:3n6	16.99	15.54	16.34	15.81
A. glauca				
C14:0	0.50	0.48	0.52	0.48
C16:0	21.21	21.20	22.27	21.94
C16:1	0.57	0.59	0.59	0.59
C18:0 + C18:1n9c	49.40	49.74	48.55	49.39
C18:2n6c	15.06	14.60	15.09	14.61
C18:3n6	10.62	10.23	10.21	9.85
C24:0	0.88	1.16	0.99	1.11

Paper V

Calcium affects polyphosphate and lipid accumulation in Mucoromycota fungi

Simona Dzurendova[1]*, Boris Zimmermann[1], Achim Kohler[1], Kasper Reitzel[2], Ulla Gro Nielsen[3], Benjamin Xavier Dupuy—Galet[1], Shaun Allan Leivers[4], Svein Jarle Horn[4], Volha Shapaval[1]

[1]Norwegian University of Life Sciences, Faculty of Science and Technology, Drøbakveien 31, 1433 Ås, Norway
[2]Department of Biology, University of Southern Denmark, Campusvej 55, DK-5230, Odense M, Denmark
[3]Department of Physics, Chemistry and Pharmacy, University of Southern Denmark, Campusvej 55, DK-5230, Odense M, Denmark
[4]Norwegian University of Life Sciences, Faculty of Chemistry, Biotechnology and Food Science, Christian Magnus Falsens vei 1, 1433 Ås, Norway

* Correspondence: simona.dzurendova@gmail.com; simona.dzurendova@nmbu.no

ABSTRACT

Calcium controls important processes in fungal metabolism, such as hyphae growth, cell wall synthesis, and stress tolerance. Recently, it was reported that calcium affects polyphosphate and lipid accumulation in fungi. The purpose of this study is to assess the effect of calcium on accumulation of lipids and polyphosphate for six oleaginous Mucoromycota fungi grown under different phosphorus/pH conditions. Duetz microtiter plate system (Duetz MTPS) was used for the cultivation. The biochemical cellular profile was analysed by Fourier transform infrared spectroscopy (FTIR-HTS). Lipid content and fatty acid profiles were determined by gas chromatography (GC). Cellular phosphorus was determined by assay-based UV-VIS spectroscopy, and accumulated phosphates were characterized by solid state nuclear magnetic resonance spectroscopy (SS NMR). Glucose consumption was estimated by FTIR attenuated total reflection (FTIR-ATR). The obtained results indicate that calcium availability enhances polyphosphate accumulation in Mucoromycota fungi, while calcium deficiency increases lipid production especially under the acidic conditions caused by the phosphorus limitation. In addition, it was observed that under acidic conditions, calcium deficiency leads to increase in carotenoid production. It can be concluded that calcium availability can be used as an optimization parameter in fungal biorefineries to enhance production of lipids or polyphosphates.

Keywords: Mucoromycota, Calcium, lipids, polyphosphates, carotenoids, biorefinery, fungi

1. INTRODUCTION

Mucoromycota fungi are powerful cell factories widely applicable in developing modern biorefineries [1,2]. Mucoromycota fungi can accumulate a wide range of high-value metabolites, among of which lipids and polyphosphates gained a high interest in the last decade [3].

In order to optimize production of Mucoromycota lipids and polyphosphate, and maximize biomass yield, it is crucial to understand the role of single media components on fungal growth and metabolic activity [4,5]. In our recent study we investigated the effect of metal and phosphorus ions on the growth, lipid accumulation and cell chemistry of *Mucor circinelloides* [6]. We showed that calcium starvation enhanced lipid accumulation in *Mucor circinelloides*, while increased calcium availability positively affected polyphosphate accumulation.

Calcium (Ca) is unique universal signaling element in prokaryotic and eukaryotic cells. Calcium signaling is evolutionary conserved process and in fungal cells it regulates multiple cell functions ranging from growth [7-9], hyphae development, sporulation, chitin synthesis [10], intracellular pH signaling [11], stress tolerance, and virulence [12]. The level of Ca ions in cytosol is important for signaling and regulation of above-mentioned processes. In fungal cells, calcium is mainly stored in vacuoles, which can contain approx. 95% of the cellular Ca [13].

For supporting Ca-signaling, cells maintain cytosolic Ca at a low concentration. There are different protein transporters managing the level of Ca ions in cytosol and mediating entry or exit from vacuoles. In eukaryotic cells Ca is required at the endoplasmic reticulum (ER), where it provides the correct function of protein folding and secretory machinery [14].

Since polyphosphate and lipid accumulation are associated with ER, calcium could be directly or indirectly involved into their accumulation. It has been reported that calcium and several other cations neutralize the negative charge of polyphosphate in fungal cells [15,16]. Thus, it can be hypothesized that with the higher availability of calcium ions in the medium, more efficient neutralizing of polyphosphate negative charge occurs and, subsequently, a higher amount of phosphorus can be stored intracellularly in the form of polyphosphate [6]. Further, it has been reported that calcium starvation enhances lipid accumulation in oleaginous algae [17] and mammalian adipocyte cells [18]. Currently, there are several hypotheses on the mechanisms behind Ca deficiency induced lipid accumulation in oleaginous microorganisms. The first hypothesis is related to the study by Cifuentes *et al.* [19]. It is based on mediation of antilipolytic pathways through a calcium-sensing receptor (CaSR) triggered by the low cellular availability of Ca ions. This results in enhanced lipid accumulation in cells. Due to the evolutional conservancy of lipolytic pathways and Ca signaling [20], it was suggested that Ca deficiency can mediate similar antilipolytic pathways in oleaginous microorganisms [6]. The second hypothesis was suggested by Wang. W.A. et al. [18] and it is based on the importance of calcium ions in the basal sensitivity of the sterol

sensing mechanism of the sterol response element binding proteins (SREBPs) pathway. Wang W.A. et al. discovered that reduction of Ca concentration in endoplasmic reticulum changes the distribution of intracellular sterol/cholesterol, resulting in the enhancement of SREBPs activation and triggering synthesis of neutral lipids. Sterol response element binding proteins (SREBP) are transcription factors that are synthesized on endoplasmic reticulum (ER), and are considered as ER-associated integral membrane proteins [18]. SREBP were reported for eukaryotic cells, including mammalian and fungal cells [21].

As mentioned above, in our recent study we reported that variation in the availability of Ca ions affects lipid and polyphosphate accumulation in oleaginous *Mucor circinelloides* [6]. In order to investigate whether the role of calcium ions in lipid and polyphosphate accumulation is conserved for different Mucoromycota fungi, six Mucoromycota strains have been grown in the presence and absence of Ca ions under three phosphorus levels creating different pH conditions. High phosphate concentration was used in order to buffer the growth media and provide conditions for polyphosphate accumulation. Duetz microtiter plate system (Duetz MTPS) was used for high-throughput cultivation [22-24]. The biochemical fingerprint of the fungal biomass was recorded by Fourier transform infrared spectroscopy in high throughput system (FTIR-HTS), lipid content and fatty acid profile was estimated by gas chromatography, total phosphorus was estimated by assay-based UV-VIS spectrometry. The glucose consumption was estimated using the FTIR attenuated total reflection (FITR-ATR) of culture supernatants.

To the authors' knowledge, this is the first study assessing the role of Ca ions on the polyphosphate and lipid accumulation in Mucoromycota fungi under different phosphorus substrate availability.

2. MATERIALS AND METHODS

2.1 Fungal strains

Six oleaginous Mucoromycota fungi from the genera *Amylomyces*, *Mucor*, *Rhizopus* and *Umbelopsis* obtained from the Czech Collection of Microorganisms (CCM; Brno, Czech Republic), Norwegian School of Veterinary Science (VI; Ås, Norway), Food Fungal Culture Collection (FRR; North Ryde, Australia) and Universitè de Bretagne Occidentale Culture Collection (UBOCC; Brest, France) were used in the study (Table 1). The selection of fungal strains was based on the results of our previous studies, where a set of Mucoromycota fungi was examined for the co-production of lipids, chitin/chitosan and polyphosphate [4,5,24].

Table 1: Fungal strains used in the study

Fungal strain	Collection №	Short name
Amylomyces rouxii	CCM F220	AR
Mucor circinelloides	VI 04473	MC1
Mucor circinelloides	FRR 5020	MC2
Mucor racemosus	UBOCC A 102007	MR
Rhizopus stolonifer	CCM F445	RS
Umbelopsis vinacea	CCM F539	UV

2.2 Growth media and cultivation conditions

Cultivation media was formulated by using full factorial design, where three different concentrations of inorganic phosphorus substrate (Pi) – phosphate salts KH_2PO_4 and Na_2HPO_4 – and two Ca conditions – Ca1 (presence) and Ca0 (absence) – were used. The cultivation was performed in Duetz-MTPS [23] in four independent biological replicates for each fungus and condition, resulting in 144 samples. Cultivation was done in two steps: 1) growth on standard agar medium for preparing spore inoculum, and 2) growth in Duetz-MTPS in nitrogen-limited broth media with ammonium sulphate as nitrogen source and different concentrations of phosphorus substrate (Pi) and Ca.

For the preparation of spore inoculum, all strains, except *Umbelopsis vinacea*, were cultivated on malt extract agar (MEA). *Umbelopsis vinacea* was cultivated on potato dextrose agar (PDA). MEA was prepared by dissolving 30 g of malt extract agar (Merck, Germany) in 1L of distilled water and autoclaved at 115 °C for 15 min. PDA was prepared by dissolving 39 g of potato dextrose agar (VWR, Belgium) in 1L of distilled water and autoclaved at 115°C for 15 min. Agar cultivation was performed for 7 days at 25 °C for all strains. Fungal spores were harvested from agar plates with a bacteriological loop after the addition of 10 mL of sterile 0.9 % NaCl solution.

The main components of the nitrogen-limited broth media [25] with modifications [22] ($g \cdot L^{-1}$) were: glucose 80, $(NH_4)_2SO_4$ 1.5, MgSO4·7H2O 1.5, CaCl2·2H2O 0.1, FeCl3·6H2O 0.008, ZnSO4·7H2O 0.001, CoSO4·7H2O 0.0001, CuSO4·5H2O 0.0001, MnSO4·5H2O 0.0001. The concentrations of phosphate salts, 7 $g \cdot L^{-1}$ KH_2PO_4 and 2 $g \cdot L^{-1}$ Na_2HPO_4, were selected as a reference value (Pi1) since they have frequently been used in cultivation of oleaginous Mucoromycota [22,25]. The broth media contained in addition to Pi1, higher Pi4 (4 × Pi1) and lower Pi0.5 (0.5 × Pi1) amount of phosphate salts. Cultivation in broth media was performed in the Duetz-MTPS (Enzyscreen, Netherlands), which consists of 24-square polypropylene deep well microtiter plates, low evaporation sandwich covers and extra high cover clamps. The autoclaved microtiter plates were filled with 7 ml of sterile broth media per well, and each well was

inoculated with 50 µl of spore inoculum. Duetz-MTPS were placed into the MAXQ 4000 shaker (Thermo Scientific), and cultivation was performed for 7 days at 25 °C and 400 rpm agitation (1.9 cm circular orbit).

2.3 Fourier transform infrared spectroscopy

2.3.1 FTIR-HTS of fungal biomass

Fourier transform infrared (FTIR) spectroscopy analysis of fungal biomass was performed according to Kosa et al. [22] with some modifications [4]. The biomass was separated from the growth media by centrifugation and washed with distilled water. Approximately 5 mg of fresh washed biomass was transferred into 2 ml polypropylene tube containing 250±30 mg of acid washed glass beads and 0.5 ml of distilled water for further homogenization. The remaining washed biomass was freeze-dried for 24 hours for determining biomass yield.

The homogenization of fungal biomass was performed by using Percellys Evolution tissue homogenizer (Bertin Technologies, France) with the following set-up: 5500 rpm, 6 × 20 s cycle. 10 µl of homogenized fungal biomass was pipetted onto an IR transparent 384-well silica microplate. Each biomass sample was analysed in 3 technical replicates. Samples were dried at room temperature for 2 h.

FTIR Spectra were recorded in a transmission mode using the High Throughput Screening eXTension (HTS-XT) unit coupled to the Vertex 70 FTIR spectrometer (both Bruker Optik, Germany). Spectra were recorded in the region between 4000 cm^{-1} and 500 cm^{-1} with a spectral resolution of 6 cm^{-1}, a digital spacing of 1.928 cm^{-1}, and an aperture of 5 mm. For each spectrum, 64 scans were averaged. Spectra were recorded as the ratio of the sample spectrum to the spectrum of the empty IR transparent microplate. In total, 432 biomass spectra were obtained. The OPUS software (Bruker Optik GmbH, Germany) was used for data acquisition and instrument control.

2.3.2 FTIR-ATR of culture supernatant

10 µl of culture supernatant was deposited on the ATR crystal. The FTIR reflectance spectra were measured with a single reflectance-attenuated total-reflectance (SR-ATR) accessory High Temperature Golden gate ATR Mk II (Specac, United Kingdom) coupled to the Vertex 70 FTIR spectrometer (Bruker Optik, Germany). The FTIR-ATR spectra were recorded with a total of 32 scans, spectral resolution of 4 cm^{-1}, and digital spacing of 1.928 cm^{-1}, over the range of 4000–600 cm^{-1}, using the horizontal SR-ATR diamond prism with 45° angle of incidence. All samples were analyzed in three technical replicates, and background measurement of empty crystal was conducted between every sample measurement. The OPUS software (Bruker Optik GmbH, Germany) was used for data acquisition and instrument control.

2.4 Analysis of cellular phosphorus

2.4.1 Analysis of total P in fungal biomass

Total P was estimated by assay-based UV-VIS spectrometry. Biomass samples were freeze-dried and decomposed in the muffle oven at 550° C for 16 hours. 5 mL of 6M HCl was added to each sample. Samples were boiled on a heating-plate for 20 minutes, 7.5 mL MilliQ water were added, and samples were left overnight in the acid/water mixture. Next day, samples were diluted up to 100 mL with MilliQ water, centrifuged and analysed using RX Daytona+ with kit PH8328 (Randox) [26].

2.4.2 Solid state NMR (SSNMR) characterization of phosphates in fungal biomass

Quantitative ^{31}P SSNMR spectra were recorded on a 500 MHz JEOL ECZ 500R spectrometer using a 3.2 mm triple resonance magic angle spinning (MAS) NMR probe, 15 kHz spinning speed, a 45° pulse, and proton decoupling. Relaxation delays were optimized on each sample, typically 200–300 s and 410 s, which served as an external intensity reference for spin counting experiments. The ^{31}P SSNMR spectra were referenced relative to H_3PO_4 ($\delta(^{31}P) = 0$ ppm) and analyzed with 100 Hz line broadening using MestReNova (Mestrelab Research) by absolute integration of the spinning side band manifold. The ^{31}P SSNMR spectra of samples extracted by water/hexanol or water were recorded on a 600 MHz Agilent spectrometer using a 3.2 mm triple resonance MAS NMR probe, 15 kHz spinning speed, 22.5° pulse and proton decoupling. [27]

2.5 Lipid extraction and GC-FID analysis of fatty acid profile

Direct transesterification was performed according to Lewis et al. [28] with modifications [29]: 2 mL screw-cap PP tube was filled with 20 ± 5 mg freeze dried biomass, approx. 250 ± 30 mg (710–1180 µm diameter) acid-washed glass beads, and 500 µL of chloroform. 1.05 mg of C13:0 TAG internal standard in 100 µL of hexane was added to the PP tube. The fungal biomass was homogenized in a Percellys Evolution tissue homogenizer at 5500 rpm, 6×20 s cycles. The processed biomass was transferred into a glass reaction tube by washing the PP tube with 2400 µL of methanol–chloroform–hydrochloric acid solvent mixture (7.6:1:1v/v) (3×800 µL). Finally, 500 µL of methanol was added into a glass reaction tube. The reaction mixture was incubated at 90 °C for 90 min in a heating block, followed by cooling to room temperature. 1 mL of distilled water was added to the glass reaction tube. The fatty acid methyl esters (FAMEs) were extracted by the addition of 2 mL hexane followed by 10 s vortex mixing. The reaction tube was centrifuged at 3000 rpm for 5 min at 4 °C, and the upper (organic) phase was collected in glass tube. The lower (water phase) was extracted two more times, but now by the addition of 2 mL hexane–chloroform mixture (4:1 v/v).

2.6 Data analysis

The following software packages were used for the data analysis: Unscrambler X version 11 (CAMO Analytics, Oslo, Norway) and Orange data mining toolbox version 3.20 (University of Ljubljana, Slovenia) [30].

2.6.1 Analysis of FTIR spectral data of fungal biomass

FTIR-HTS spectra of fungal biomass were preprocessed with extended multiplicative signal correction (EMSC) with linear, quadratic and cubic terms. Amide I peak, mainly related to proteins, was selected as a relatively stable reference band, used for estimating the relative content of cellular lipids and phosphates. Further, ester bond in the FTIR spectra (C=O stretching at 1745 cm^{-1}) was selected for estimation of lipids and phosphate functional group bond (P=O stretching at 1251 cm^{-1}) was selected for estimation of polyphosphate. Thus, lipid-to-protein (LP) and polyphosphate-to-protein (PP) ratios were estimated.

2.6.2 FTIR-ATR spectral data of culture supernatants-glucose estimation

The residual glucose in the culture supernatants was estimated from the FTIR-ATR spectra of culture supernatants by the prediction model based on the standard solutions with known glucose and phosphates concentration. All FTIR-ATR spectra were preprocessed by selecting the region of interest 900-700 cm^{-1}, baseline was corrected by vertical offset, and peaks were normalized using the water band at 1637 cm^{-1}. The reference solutions included glucose concentrations from 10 to 100 g/L (with the step 10 g/L), each with 4 different Pi source levels (Pi4, Pi2, Pi1, Pi05) [4]. The dataset used for building the partial least square regression (PLSR) model was divided into two sub-sets: calibration sub-set (70%) and validation sub-set (30%). The validation sub-set contained samples with glucose concentrations 20, 50 and 70 g/L and all Pi concentrations. The model was further externally validated with additional set of reference glucose solutions with known glucose concentration and culture supernatants from our previous study [31], where the glucose concentrations were estimated by ultra high-performance liquid chromatograph (UHPLC).

3. RESULTS

3.1 Growth characteristics of Mucoromycota fungi

Fungal biomass formation for Mucoromycota fungi grown under different calcium source availability and Pi substrate concentrations is presented on Figure 1, and pH data measured at the end of cultivations presented on Figure S1 (Supplementary Materials). The biomass concentration data represent average of 4 bio-replicates and error bars show the standard deviation. Generally, the biomass formation was

reproducible within the bio-replicates. Initial pH of the culture media was 6.0±0.3 and it stayed relatively stable in Ca-Pi4 conditions, while drop in pH down to 3.0 and 2.0 in Pi1 and Pi0.5 conditions was observed.

Fungi grown in non-acidic conditions when pH was relatively stable (Pi4 media) reached higher biomass concentration than in the media with the acidic pH and lower phosphorus availability. This observation was valid for all tested fungi except *Rhizopus stolonifer*, which showed relatively consistent biomass production from 4.11 to 6.10 g/L on all conditions (Figure 1). The lowest biomass production for the studied Mucoromycota was observed in Pi0.5 media when pH was acidic. When comparing two calcium conditions, calcium ions deprivation (Ca0) combined with high (Pi4) and reference (Pi1) amounts of phosphorus substrate led to the slight decrease in the biomass production for all fungi. Opposite to the fungal growth in Pi0.5 media, where the biomass production was increased in Ca0 condition, except for *Mucor circinelloides* FRR 5020. The most significant effect of calcium ions deficiency on the biomass production was recorded for *Umbelopsis vinacea*, where the difference between Ca1 and Ca0 conditions resulted in about 4 g/L difference in biomass concentration. Further, interesting observation was obtained for *Mucor circinelloides* strains which reacted differently on the absence of Ca ions in acidic Pi0.5 media. Thus, *Mucor circinelloides* VI 04473 (MC1) formed significantly more biomass in Ca0-Pi0.5 (8.70 g/L) medium than in Ca1-Pi0.5 (6.24 g/L), while *Mucor circinelloides* FRR 5020 (MC2) did not show any significant differences in biomass production for Ca1 (6.97 g/L) and Ca0 (6.10 g/L) conditions. Ca availability had no significant effect on the fungal strains *Amylomyces rouxii* and *Rhizopus stolonifer* in Pi0.5 media.

Among all studied Mucoromycota, the highest biomass concentration in all conditions was recorded for *Umbelopsis vinacea*, which produced from 20.56 g/L to 24.49 g/L of biomass. Fungi from *Mucor* and *Amylomyces* genera produced biomass in range of 7.52 g/L – 12.00 g/L in Ca-Pi4 and Ca-Pi1 media, respectively and 5.41 g/L – 8.70 g/L in Ca-Pi0.5 conditions. The lowest biomass concentration was observed for *Rhizopus stolonifer*.

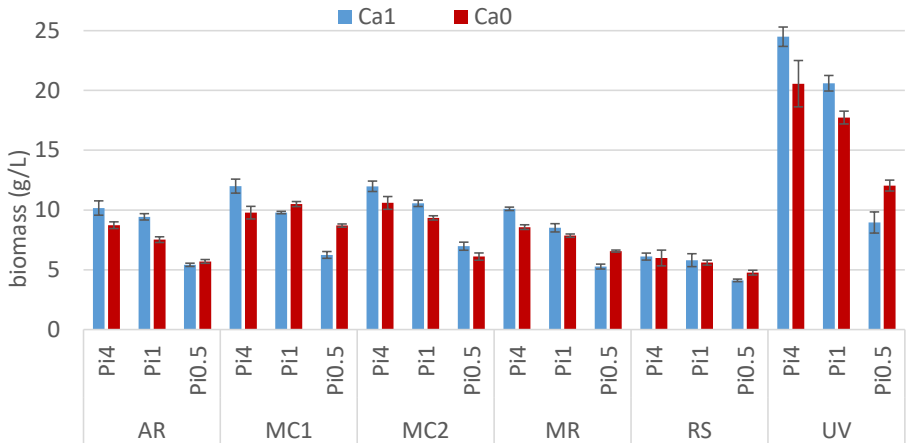

Figure 1: Biomass concentration (g/L) of fungi grown in presence (Ca1)-blue; and absence (Ca0)- red of calcium under three phosphorus substrate levels (Pi4, Pi1, Pi0.5).

The residual glucose was estimated by regression model based on the FTIR-ATR media of culture supernatants and is shown on the Figure 2.

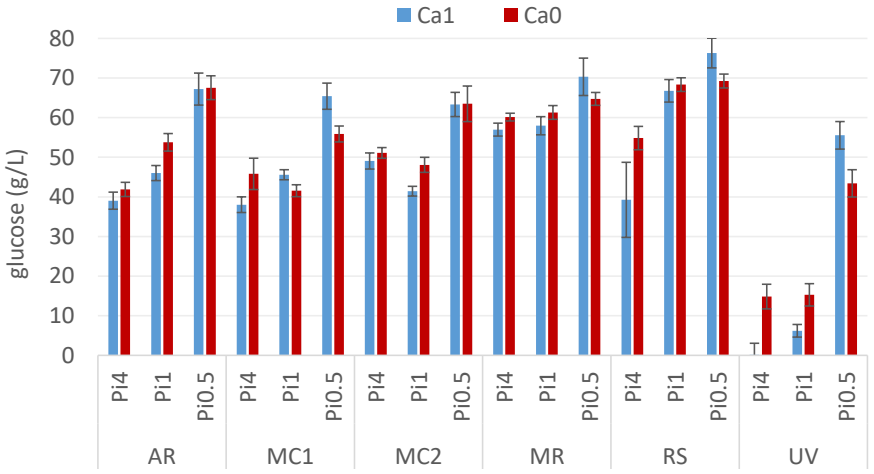

Figure 2: The residual glucose in g/L in the culture supernatants. The glucose concentration was estimated using partial least square regression model based on the FTIR-ATR spectra of culture supernatants and reference glucose solutions.

Generally, the glucose consumption rates correspond well to the biomass production results. The lowest residual glucose was recorded for *Umbelopsis vinacea* in Ca0-Pi4 media that correlates well with the highest biomass production detected for this condition (Figure 2). Strain *Rhizopus stolonifer* showed the lowest glucose consumption, as well the lowest biomass formation. Interestingly, *Rhizopus stolonifer* grown in Pi4 media with the presence of Ca ions consumed more glucose and lower pH was detected in the supernatants compared to the condition when Ca was absent. This could be due to carbon assimilation, not only in the form of biomass but also in the form of organic acids released in the media, since *Rhizopus* genus is known for extracellular acid production. Strain *Amylomyces rouxii* and both *Mucor circinelloid*es strains grown in Pi4 media showed similar glucose requirements, with approximately half of initial glucose amount left (40 g/L) for the production of 10-12 g/L of biomass. In contrast, when grown in Pi0.5 media, these fungi consumed approximately 20 g/L of glucose for the production of 5-8 g/L biomass. While *Mucor racemosus* biomass concentration was similar to *Amylomyces rouxii* in Pi4 and Pi1 media, significantly less glucose was consumed by *Mucor racemosus* (Figure 2).

3.2 Importance of Ca ions availability for polyphosphate accumulation in Mucoromycota

For studying the influence of Ca ions on the lipid and polyphosphate accumulation in Mucoromycota fungi, we performed FTIR spectroscopic profiling of the total cellular biochemical composition of the obtained fungal biomass. Total phosphorus was estimated using assay-based UV/VIS spectroscopy, and phosphates were characterized by solid state NMR. Lipid content and fatty acid profiles were assessed by GC-FID.

When examining FTIR-HTS spectra of fungal biomass grown on different calcium ions conditions, substantial changes are observed for bands associated with lipids (=C-H stretching at 3010 cm^{-1}, -C-H stretching at 2920 cm^{-1} and 2850 cm^{-1}, -C=O stretching at 1745 cm^{-1}) and polyphosphates (P=O stretching 1251 at cm^{-1}, P-O-P stretching at 885 cm^{-1}) (Figure 3). An example of such changes is shown on the spectra of *Mucor circinelloides* VI 04473 grown in Ca0-Pi4 and Ca1-Pi4 media (Figure 3).

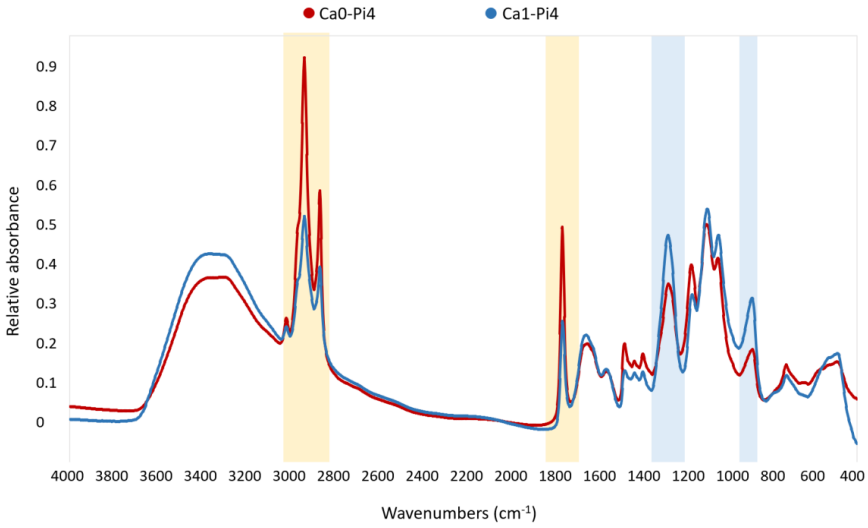

Figure 3: FTIR-HTS spectra of Mucor circinelloides VI 04473 biomass produced in Ca0-Pi4 (red) and Ca1-Pi4 (blue) media. The main characteristic lipid-related peaks are highlighted in yellow, while the polyphosphate-related spectral regions are highlighted blue.

The analysis of the total phosphorus content in % per cell dry weight of fungal biomass (Figure 4) shows that the highest total phosphorus content was recorded for *Amylomyces rouxii* (2.65% – 6.24%), followed by *Mucor racemosus* (2.28% – 5.20%), *Mucor circinelloides* VI 04473 (1.4% – 4.91%) and *Mucor circinelloides* FRR 5020 (1.86% – 4.50%). *Rhizopus stolonifer* and *Umbelopsis vinacea* showed the most uniform cellular phosphorus content (2.7% – 4.13%) and (0.64% – 1.37%), respectively, and the total phosphorus content was lowest in *Umbelopsis vinacea* (Figure 4). In the vast majority of samples, it is visible that the phosphorus uptake was enhanced with Ca availability.

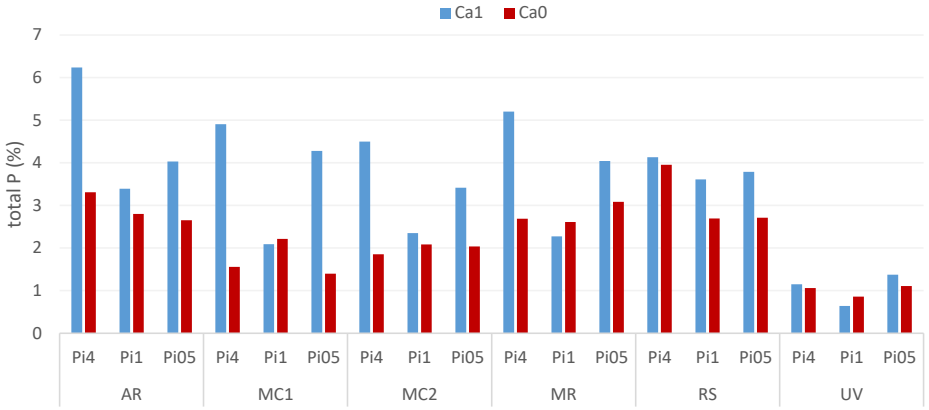

Figure 4: The total cellular P in % of biomass, estimated by assay-based UV-VIS spectroscopy.

In order to confirm that the accumulated phosphorus is stored in the form of polyphosphate, characterization of cellular phosphates was performed by solid state NMR spectroscopy (SSNMR) (Figure 5). Due to the fact, that SSNMR is very expensive and time demanding, one representative strain *Mucor circinelloides* VI 04473 has been selected for this analysis. SSNMR showed that *Mucor circinelloides* VI 04473 under all tested Ca-Pi conditions contained mainly polyphosphate (more than 90%). While for biomass obtained from the media with Pi4 and Pi05, more polyphosphates were present in Ca1 condition (97-98%), and for the biomass from Pi1 media the amount of orthophosphates was comparable for Ca1 and Ca0 conditions (7-8%) (Figure 5).

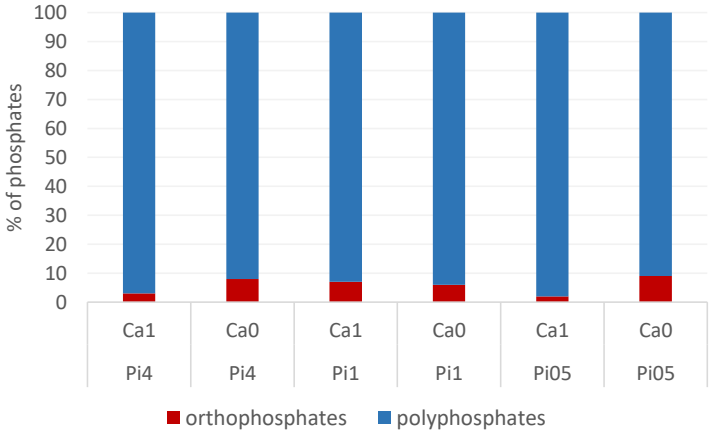

Figure 5: The characterization of cellular phosphates in Mucor circinelloides VI 04473 biomass.

As mentioned above, since SSNMR analysis is expensive and time consuming, it was not possible to use it for all samples. Nevertheless, polyphosphates have strong signals in the FTIR spectra (P=O stretching peak at 1251 cm^{-1} and P-O-P stretching at 885 cm^{-1}), and so FTIR spectroscopy was utilized for the analysis of fungal phosphates for all samples.

Evaluation of the underlying correlations between Ca ions availability with polyphosphate and lipid accumulation, as well as estimation of the relative content of these metabolites in fungal biomass, was based on peak ratios of lipid/polyphosphate- to protein-related bands (Figure 6). Proteins were selected as relatively stable component of fungal biomass, since under nitrogen limiting conditions cell proliferation stops at the end exponential growth phase and, therefore, protein content stays consistent in the lipogenesis phase. For estimating chemical composition of the biomass, the following representative lipid, polyphosphate and proteins peaks were used: (i) ester bond C=O stretching peak at 1745 cm^{-1} for lipids, (ii) phosphate functional group P=O stretching peak at 1251 cm^{-1} for polyphosphate, and (iii) Amide I C=O stretching peak at 1650 cm^{-1} for proteins. The estimated lipid-to-protein (LP) and phosphate-to-protein (PP) ratios are shown on Figure 6.

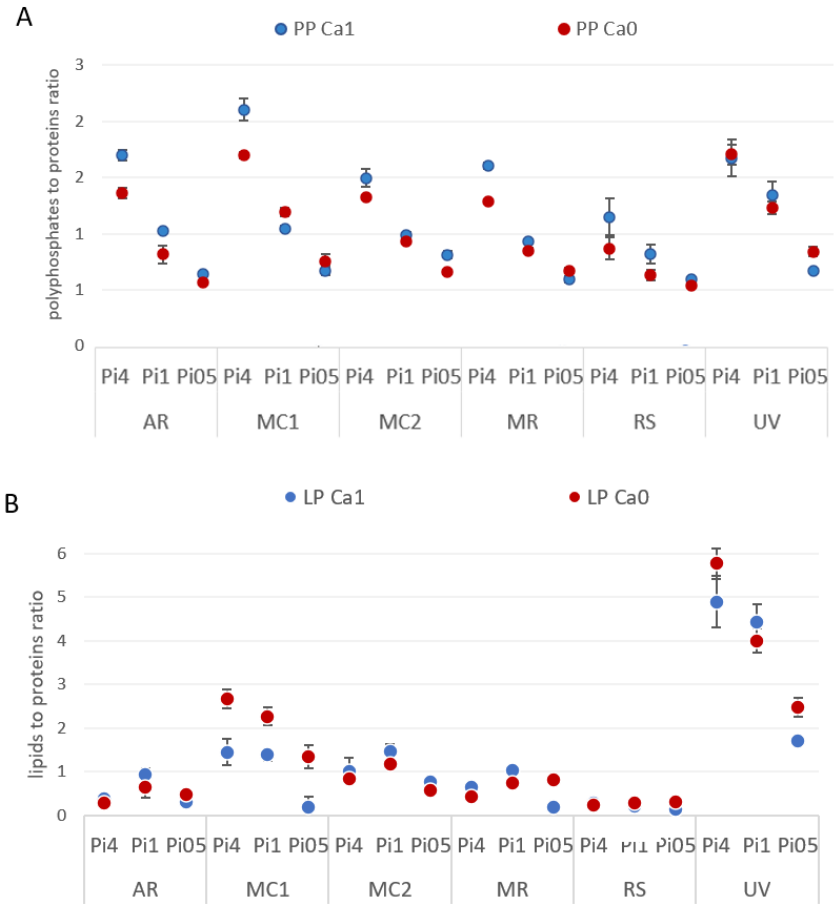

Figure 6: A: polyphosphate-to-protein (PP) and B: the lipid-to-protein (LP) ratios of characteristic bands in FTIR spectra of fungal biomass. Both shown for presence (Ca1)-blue and absence (Ca0)- red of calcium in the growth media.

It can be seen that the effect of Ca ions on lipid and polyphosphate accumulation is pH and strain specific. PP ratio obtained for biomass grown in Ca-Pi4 media was higher than for other Pi conditions indicating high polyphosphate accumulation occurring in Mucoromycota fungi under high phosphorus availability. In the media with the high phosphorus availability (Pi4), for all strains except *Umbelopsis vinacea*, high PP ratio and respectively higher amount of polyphosphate could be observed in the presence of Ca (Figure

6A). These observations were in accordance with the results obtained from the analysis of the total phosphorus content (Figure 5). When reference amount of phosphorus (Pi1) was used, the influence of Ca on the polyphosphate accumulation was less visible and more strain specific. Thus, PP ratio of *Amylomyces rouxii*, *Mucor circinelloides* FRR 5020, *Mucor racemosus*, *Rhizopus stolonifer* and *Umbelopsis vinacea* grown in Ca1-Pi1 medium was higher than in the case of Ca0-Pi1 medium, while it was lower for *Mucor circinelloides* VI 04473 (Figure 6A). Similar results were observed from the total phosphorus content analysis, except for strains *Mucor racemosus* and *Umbelopsis vinacea* which showed higher total phosphorus content in the absence of Ca ions (Figure 4). Strain specific influence of Ca ions was also obtained for Pi0.5 condition, where higher PP ratio in the presence of Ca ions was detected for biomass of *Amylomyces rouxii*, *Mucor circinelloides* FRR 5020 and *Rhizopus stolonifer* and lower for *Mucor circinelloides* VI 04473, *Mucor racemosus* and *Umbelopsis vinacea.* Interestingly, according to the PP ratio, the lowest polyphosphate accumulation was recorded for the biomass grown in Pi0.5 media. Total phosphorus content in fungal biomass grown in Ca1-Pi0.5 medium was higher than in Ca1-Pi1 for all tested fungi (Figure 4). Such discrepancies between FTIR-HTS and reference total phosphorus analysis could be explained by the possible variation in total protein and polysaccharide content in different Mucoromycota fungi under different pH/Pi conditions that affected the estimation of peak ratios from FTIR spectra. In addition, possible explanation for this difference is that the FTIR-based analysis shows phosphate content, while the assay-based UV/VIS analysis reports the total P. Further, the biomass grown in Pi0.5 media is poorer in the cellular content of lipids, thus the results in % show higher P content. It is important to note that when the total P values in % recalculated to absolute values in g/L, it becomes apparent that highest phosphates concentrations were achieved in Pi4 condition (Figure S2 in Supplementary materials, with concentrations in g/L) and comparable results were obtained for Pi1 and Pi0.5 samples. This observation can indicate that majority of phosphorus uptake takes place in the exponential growth phase. To confirm this observation, we investigated the biochemical composition of *Mucor circinelloides* VI 04473 in time-after 1 and 5 days of growth (Figure 7). As it is can be seen in Figure 7, the polyphosphate related peaks of FTIR-HTS spectra of *Mucor circinelloides* biomass can be detected already after first day of cultivation, indicating that polyphosphate accumulation occurred from the start of the exponential growth phase. Further explanation of lower P content in % for Pi1 than Pi0.5 media is that the biomass grown in Pi1 showed higher lipid content, as indicated by the lipid-related peaks in the FTIR spectrum (Figure 7).

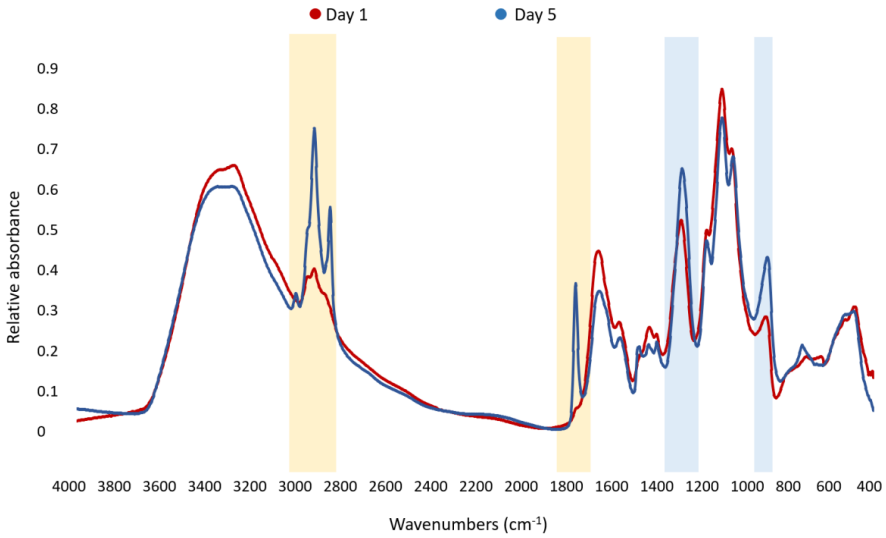

Figure 7: FTIR-HTS spectra of Mucor circinelloides VI04473 biomass grown in Pi4-Ca1 media for 1 day (red) and 5 days (blue). Lipid-related peaks are highlighted yellow, polyphosphate-related peaks are highlighted blue.

3.3 Ca ions deficiency can trigger lipid accumulation in Mucoromycota

All tested strains exhibited oleaginous properties in all assessed media. Generally, the reference phosphorus amount (Pi1) was the most suitable for the lipid accumulation, since the highest lipid content was recorded for all strains except for *Rhizopus stolonifer*. Lipid-to-protein (LP) ratio derived from the FTIR-HTS spectra and total lipid content (in % per cell dry weight) of fungal biomass grown in the absence of Ca ions was higher than in the presence of Ca ions for several fungi and Pi conditions (Figure 4B, Table 2). Thus, lipid triggering effect of Ca deprivation was remarkably pronounced in *Mucor circinelloides* VI 04473 and *Rhizopus stolonifer* under all Pi conditions, *Amylomyces rouxii* and *Mucor circinelloides* FRR5020 in media with Pi4, *Mucor circinelloides* FRR5020 and *Umbelopsis vinacea* in media with Pi1 and all fungi, except *Mucor circinelloides* FRR5020 in Pi0.5 conditions (Figure 4B, Table 2 and Figure S2 in the Supplementary materials). The effect of Ca ions availability was to some extend strain specific, where the highest difference in total lipid content of fungal biomass grown in Ca1 and Ca0 conditions was recorded for *Mucor circinelloides* VI 04473, *Umbelopsis vinacea* and *Mucor racemosus*, while lower differences occurred in *Amylomyces rouxii* and *Rhizopus stolonifer*. Calcium deficiency led to the highest lipid content in all studied Mucoromycota fungi grown in Pi0.5 media.

Among the studied Mucoromycota fungi, *Umbelopsis vinacea* accumulated the highest lipid amount, ranging from 52 to 84% (w/w). Interestingly, the least favorable growth condition Pi05, which resulted in very acidic pH of the growth media, was the most preferable for lipid accumulation in Ca0 condition for *Mucor racemosus*.

Table 2: Lipid content in % per cell dry weight

sample		**Pi4**	**Pi1**	**Pi05**
Amylomyces rouxii	Ca1	30.37	46.76	27.36
	Ca0	31.24	40.02	37.48
Mucor circinelloides	Ca1	42.80	47.85	22.67
VI 04473	Ca0	47.42	54.01	48.05
Mucor circinelloides	Ca1	34.37	47.62	37.11
FRR 5020	Ca0	41.01	48.60	35.79
Mucor racemosus	Ca1	31.10	37.85	22.83
	Ca0	30.86	35.04	39.63
Rhizopus stolonifer	Ca1	25.33	24.27	22.78
	Ca0	27.40	26.75	27.90
Umbelopsis vinacea	Ca1	69.90	81.04	52.36
	Ca0	58.43	84.18	66.70

As it was observed in FTIR and GC analyses, the most pronounced differences related to the Ca availability were truly observed in Pi05 condition for *Mucor circinelloides VI04473* (22.67% Ca1 - 48.05% Ca0), *Mucor racemosus* (22.83% Ca1 – 39.63% Ca0) and *Umbelopsis vinacea* (52.36% Ca1 – 66.70% Ca0). Further, higher lipid content was recorded for all Pi conditions for *Mucor circinelloides* VI04473 (Table 1) in Ca deprived media. The fatty acid (FA) profiles were quite consistent irrespective the Ca availability (Figure S3 in Supplementary materials). Some minor variation in FA profiles can be mostly assigned to variation of Pi availability, which resulted in the different pH conditions.

4. DISCUSSION

Calcium is an important second messenger in the transduction of cellular signals and cell growth under stress conditions. Exposure of fungal cells to environmental stress triggers an immediate response in cytoplasmic calcium levels. This process is fundamental for the survival of eukaryotic cells. Through a

variety of calcium signal transduction mechanisms, fungal cells can tolerate numerous environmental changes, including pH stress [32]. There are at least two calcium-based signal transduction pathways regulating the processes necessary for pH adjustment and ion homeostasis in eukaryotic cells [32]. In this study, fungi were grown in the media with ammonium sulphate as nitrogen source and various phosphorus substrate concentrations combined with different calcium availability. Due to the low buffering capacity of ammonium sulphate, and the fact that the uptake of ammonium ions causes an increase in the release of H+ by the fungal cells, variation in phosphorus substrate concentration caused significant change in pH from 6.0 to 2.0. The biomass concentration results showed that calcium deficiency negatively affected adaptation of fungal cells to the different phosphorus/pH conditions. Thus, a reduced growth and biomass formation at lower phosphorus/pH levels were observed. A large number of studies on a variety eukaryotic cell types, including fungal cells, reported interactions between changes in pH and calcium cellular signals, where both cytosolic acidification and alkalization cause increase in cytoplasmic calcium for providing ion homeostasis in the cell [33]. Therefore, calcium availability is critical for pH stress tolerance as it was also shown in our study. While significant growth inhibiting effect of calcium deficiency was recorded at high (Pi4) and reference (Pi1) phosphorus substrate concentrations, resulting in pH 5.0 and 3.0, respectively, an increase in biomass concentration was observed when calcium was absent in the media with low phosphorus level (Pi0.5) and pH 2.0. Such twisting effect of calcium deficiency could be explained by the higher lipid accumulation under Ca0-Pi0.5 condition, meaning that biomass increase at this condition was due to the higher lipid content and not elevated growth rate.

In addition to the pH stress tolerance, it has been reported that calcium ions are involved in lipid and phosphorus metabolism of eukaryotic cells [15,20]. Thus, synthesis and accumulation of phosphorus in the form of energy storage compounds polyphosphates is linked to the storage of cellular calcium. Polyphosphate granules, also known as acidocalciosomes, are membrane-bounded evolutionary conserved organelles, found in prokaryotic and eukaryotic cells and whose main function is the accumulation of polyphosphate and cations such as calcium, magnesium, zinc and natrium [34]. Calcium, as well as other cations, are functioning as neutralizing agents for negative charge of polyphosphate in the formation of acidocalciosomes. Therefore, calcium availability is important prerequisite for the formation of polyphosphate granules. In our study, calcium deprivation led to the significant decrease in the total phosphorus content in Mucoromycota fungi. Some exceptions, where total phosphorus content in calcium deficient conditions was higher than when calcium was present in the media were recorded for *Mucor circinelloides* FRR 5020, *Mucor racemosus* and *Umbelopsis vinacea*. This could be explained by the possible involvement of other cations present in the media, such as magnesium and zinc, in polyphosphate accumulation. Further, it was reported that for the cells grown under alkaline pH 7.5, the activity of a microbial polyphosphate synthesis enzyme- polyphosphate kinase (PPK), and polyphosphate hydrolysis

enzyme- exopolyphosphatases (PPX) was approximately equal. In contrast to slightly acidic pH (5.5), PPK activity increased sixfold, while PPX activity remained unchanged [35]. The elevation in PPK activity could be responsible for the increased intracellular accumulation of polyphosphate at pH 5.5. This observation is in accordance with our study, where the highest polyphosphate accumulation was observed at pH 5.5.

The positive effect of calcium-lacking growth media on lipid accumulation was observed for oleaginous algae [17], while, to the authors knowledge, there is no study reporting the role of calcium in lipogenesis of oleaginous Mucoromycota fungi. Recently, we reported the first indication on the influence of calcium ions on lipid accumulation in oleaginous *Mucor circinelloides* [6]. The aim of this study was to investigate whether calcium has some general or strain-specific patterns in lipid accumulation in Mucoromycota fungi. In this study, lipid triggering effect of calcium deprivation was remarkably pronounced in all fungi depending on the phosphorus substrate/pH condition. Interestingly, the absence of calcium in the medium with Pi0.5/pH 2.0 showed general effect in increased lipid accumulation in all fungi except *Mucor circinelloides* FRR 5020. Concerning the effect of pH on lipid accumulation in fungal cells, the reference literature indicates that pH variation in the culture medium affects the lipid composition rather than the total lipid content [36]. The response to pH variations is suspected to be strain- and species-specific. Therefore, variation in the calcium availability effect on lipid accumulation in Mucoromycota fungi observed in this study could be associated with the strain-specific response to pH changes in the culture media associated with the different levels of phosphorus substrate.

The observation of a higher total lipid content in Mucoromycota fungi under calcium deficiency at low pH 2.0 could be presumably explained by the activation of the unfolded protein response (UPR). UPR is known as a signal transduction pathway activated in a response to endoplasmic reticulum (ER) stress. ER stress can be mediated by the extremely low pH of the surrounding environment (for example culture medium) or calcium deficiency and it is resulting in the disruption in ER protein-folding capacity [37]. The disruption of ER protein-folding capacity leads to the activation of UPR signaling system for restoring ER homeostasis. Further, activation of the UPR pathways modulating lipid metabolism in the cells triggers lipogenesis, which leads to the higher accumulation of lipids. Based on our results, calcium might have important function in activating UPR pathways, as lipid triggering effect under acidic pH was observed when calcium was removed from the culture medium. In addition to the UPR-based hypothesis, there are two other hypothesis explaining lipid triggering effect of calcium deficiency. One is related to the mediation of antilipolytic pathways through a calcium-sensing receptor (CaSR) triggered by the low cellular availability of calcium ions. This results in enhanced lipid accumulation in cells [20]. The second hypothesis is based on the importance of calcium ions in the basal sensitivity of the sterol sensing mechanism of the sterol response element binding proteins (SREBPs) pathway [18]. The reduction of calcium concentration in endoplasmic reticulum changes the distribution of intracellular sterol/cholesterol, resulting in the

enhancement of SREBPs activation and triggering synthesis of neutral lipids. Currently, there is no clear evidence which of the hypothesis is valid for fungal cells and more profound investigation is needed to understand calcium role in lipogenesis of oleaginous fungi. Moreover, it is worth exploring if there is a link between the polyphosphate and lipid accumulation, and if calcium simultaneously affects both accumulation mechanisms.

In addition to the observations related to the calcium involvement in the accumulation of polyphosphate and lipids in Mucoromycota fungi, several other interesting observations arose in this study. When harvesting and washing the fungal biomass, it was observed that biomass of *Amylomyces rouxii* and the two *Mucor circinelloides* strains had yellow color, indicating possible high content of carotenoids (Figure 8). The biomass obtained from Ca0-Pi0.5 media showed the highest pigmentation. It is interesting that the two strains of the same specie *Mucor circinelloides* showed different metabolic responses. Biomass production and lipid accumulation in calcium deficient Pi0.5 condition significantly differed for these strains. Further, strain *Mucor circinelloides* FRR 5020 showed higher carotenoid production than *Mucor* circinelloides VI 04473 (Figure 8). The ability of carotenoid production by *Mucor circinelloides* FRR 5020 is most likely the cause of the difference in metabolic behavior of this strain compared to *Mucor circinelloides* VI 04473.

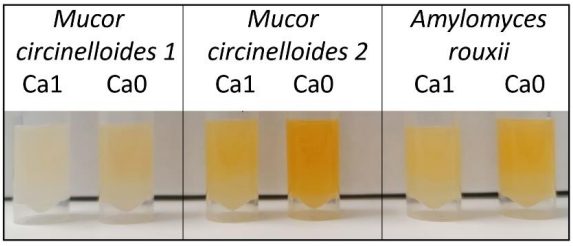

Figure 4: Fungal biomass grown in Pi0.5 media showed carotenoids content. Visibly higher content of carotenoids is observed in biomass grown in Ca-lacking media.

Carotenoid production for *Mucor circinelloides* was reported in the literature before [38,39], and the main factors triggering carotenoid production are light, temperature and aeration [40,41]. To the authors knowledge, this is a first indication of the triggering activity of calcium deficiency on the carotenoid production. Carotenoid pigments are not detectable in FTIR spectroscopy, and since assessment of carotenoids was outside the scope of this study, no further analysis on estimating carotenoids content was conducted. A follow-up study on influence of calcium on carotenoids is scheduled.

5. CONCLUSIONS

The aim of this study was to investigate the effect of calcium availability on lipids and polyphosphates accumulation in Mucoromycota fungi. Calcium availability is important for polyphosphate accumulation, while calcium deficiency could be beneficial for triggering lipid accumulation in Mucoromycota fungi. It can be concluded that calcium is an important nutrient for regulation of polyphosphate and lipid accumulation in fungal cells. Thus, calcium availability can be used as an important optimization parameter in bioprocesses utilizing Mucoromycota for lipid and polyphosphate accumulation. Further, it has to be noted that pH and possibly phosphorus availability play an important role in involvement of calcium in regulation of lipid, polyphosphate and carotenoids accumulation in Mucoromycota fungi. Further investigations are needed to understand the role of calcium availability on carotenoid synthesis in fungal cells.

Supplementary Materials:

Figure S1: Figure S1: pH of culture supernatants at the end of the cultivation.

Figure S2: The total concentrations (in g/L) of fungal biomass, lipids and phosphates.

Figure S3: The fatty acid profiles of FAMEs extracted from fungal biomass. Fatty acids which were present in amount higher than 1% are shown, the rest is summed up into 'others'.

Author Contributions: Conceived the research idea, S.D., V.S., B.Z., and A.K.; Designed the experiments, S.D., V.S., B.Z.; methodology, S.D., V.S., B.Z., and A.K.; performed the experimental work, S.D., B.X.D.G:, U.G.N; analyzed the data, S.D. and B.Z.; discussed the results, S.D., V.S., B.Z. and A.K.; wrote the manuscript, S.D. and V.S.; discussed and revised the manuscript, S.D., V.S., B.Z., A. K., S.J.H., B.X.D.G., K.R., S.A.L. and U.G.N. All authors have read and agreed to the published version of the manuscript.

Funding: The study was funded by the Research Council of Norway - FMETEKN Grant, project number 257622, BIONÆR Grant, projects number 268305 and 305215, HAVBRUK2 Grant, project number 302543, MATFONDAVTALE Grant, project number 301834 and IS-DAAD Grant, project number 309220.

Conflicts of Interest: The authors declare no conflict of interest. The funders had no role in the design of the study; in the collection, analyses, or interpretation of data; in the writing of the manuscript, or in the decision to publish the results.

References

1. Meyer, V.; Basenko, E.Y.; Benz, J.P.; Braus, G.H.; Caddick, M.X.; Csukai, M.; de Vries, R.P.; Endy, D.; Frisvad, J.C.; Gunde-Cimerman, N. Growing a circular economy with fungal biotechnology: a white paper. *Fungal biology and biotechnology* **2020**, *7*, 1-23.
2. Gupta, V.K.; Treichel, H.; Shapaval, V.O.; de Oliveira, L.A.; Tuohy, M.G. *Microbial functional foods and nutraceuticals*; John Wiley & Sons: 2017.

3. Rodrigues Reis, C.E.; Bento, H.B.; Carvalho, A.K.; Rajendran, A.; Hu, B.; De Castro, H.F. Critical applications of *Mucor circinelloides* within a biorefinery context. *Critical reviews in biotechnology* **2019**, *39*, 555-570.
4. Dzurendova, S.; Zimmermann, B.; Kohler, A.; Tafintseva, V.; Slany, O.; Certik, M.; Shapaval, V. Microcultivation and FTIR spectroscopy-based screening revealed a nutrient-induced co-production of high-value metabolites in oleaginous Mucoromycota fungi. *PloS one* **2020**, *15*, e0234870.
5. Dzurendova, S.; Zimmermann, B.; Tafintseva, V.; Kohler, A.; Ekeberg, D.; Shapaval, V. The influence of phosphorus source and the nature of nitrogen substrate on the biomass production and lipid accumulation in oleaginous Mucoromycota fungi. *Applied Microbiology and Biotechnology* **2020**, 1-12.
6. Dzurendova, S.; Zimmermann, B.; Tafintseva, V.; Kohler, A.; Horn, S.J.; Shapaval, V. Metal and Phosphate Ions Show Remarkable Influence on the Biomass Production and Lipid Accumulation in Oleaginous *Mucor circinelloides*. *Journal of Fungi* **2020**, *6*, 260.
7. Jackson, S.; Heath, I. Roles of calcium ions in hyphal tip growth. *Microbiology and Molecular Biology Reviews* **1993**, *57*, 367-382.
8. Benčina, M.; Legiša, M.; Read, N.D. Cross-talk between cAMP and calcium signalling in *Aspergillus niger*. *Molecular microbiology* **2005**, *56*, 268-281.
9. Meyer, V.; Arentshorst, M.; Flitter, S.J.; Nitsche, B.M.; Kwon, M.J.; Reynaga-Pena, C.G.; Bartnicki-Garcia, S.; van den Hondel, C.A.; Ram, A.F. Reconstruction of signaling networks regulating fungal morphogenesis by transcriptomics. *Eukaryotic cell* **2009**, *8*, 1677-1691.
10. Nguyen, Q.B.; Kadotani, N.; Kasahara, S.; Tosa, Y.; Mayama, S.; Nakayashiki, H. Systematic functional analysis of calcium-signalling proteins in the genome of the rice-blast fungus, *Magnaporthe oryzae*, using a high-throughput RNA-silencing system. *Molecular microbiology* **2008**, *68*, 1348-1365.
11. Benčina, M.; Bagar, T.; Lah, L.; Kraševec, N. A comparative genomic analysis of calcium and proton signaling/homeostasis in *Aspergillus* species. *Fungal Genetics and Biology* **2009**, *46*, S93-S104.
12. Roy, A.; Kumar, A.; Baruah, D.; Tamuli, R. Calcium signaling is involved in diverse cellular processes in fungi. *Mycology* **2020**, 1-15.
13. Tisi, R.; Rigamonti, M.; Groppi, S.; Belotti, F. Calcium homeostasis and signaling in fungi and their relevance for pathogenicity of yeasts and filamentous fungi. *AIMS Molecular Science* **2016**, *3*, 505-549.
14. Puigpinós, J.; Casas, C.; Herrero, E. Altered intracellular calcium homeostasis and endoplasmic reticulum redox state in *Saccharomyces cerevisiae* cells lacking Grx6 glutaredoxin. *Molecular biology of the cell* **2015**, *26*, 104-116.
15. Kikuchi, Y.; Hijikata, N.; Yokoyama, K.; Ohtomo, R.; Handa, Y.; Kawaguchi, M.; Saito, K.; Ezawa, T. Polyphosphate accumulation is driven by transcriptome alterations that lead to near-synchronous and near-equivalent uptake of inorganic cations in an arbuscular mycorrhizal fungus. *New Phytologist* **2014**, *204*, 638-649.
16. Allen, N.S.; Schumm, J.H. Endoplasmic reticulum, calciosomes and their possible roles in signal transduction. *Protoplasma* **1990**, *154*, 172-178.

17. Gorain, P.C.; Bagchi, S.K.; Mallick, N. Effects of calcium, magnesium and sodium chloride in enhancing lipid accumulation in two green microalgae. *Environmental technology* **2013**, *34*, 1887-1894.
18. Wang, W.-A.; Liu, W.-X.; Durnaoglu, S.; Lee, S.-K.; Lian, J.; Lehner, R.; Ahnn, J.; Agellon, L.B.; Michalak, M. Loss of calreticulin uncovers a critical role for calcium in regulating cellular lipid homeostasis. *Scientific reports* **2017**, *7*, 1-15.
19. Cifuentes, M.; Rojas, C.V. Antilipolytic effect of calcium-sensing receptor in human adipocytes. *Molecular and cellular biochemistry* **2008**, *319*, 17-21.
20. Kurat, C.F.; Natter, K.; Petschnigg, J.; Wolinski, H.; Scheuringer, K.; Scholz, H.; Zimmermann, R.; Leber, R.; Zechner, R.; Kohlwein, S.D. Obese yeast: triglyceride lipolysis is functionally conserved from mammals to yeast. *Journal of Biological Chemistry* **2006**, *281*, 491-500.
21. Bien, C.M.; Espenshade, P.J. Sterol regulatory element binding proteins in fungi: hypoxic transcription factors linked to pathogenesis. *Eukaryotic cell* **2010**, *9*, 352-359.
22. Kosa, G.; Kohler, A.; Tafintseva, V.; Zimmermann, B.; Forfang, K.; Afseth, N.K.; Tzimorotas, D.; Vuoristo, K.S.; Horn, S.J.; Mounier, J. Microtiter plate cultivation of oleaginous fungi and monitoring of lipogenesis by high-throughput FTIR spectroscopy. *Microbial cell factories* **2017**, *16*, 101.
23. Kosa, G.; Vuoristo, K.S.; Horn, S.J.; Zimmermann, B.; Afseth, N.K.; Kohler, A.; Shapaval, V. Assessment of the scalability of a microtiter plate system for screening of oleaginous microorganisms. *Applied microbiology and biotechnology* **2018**, *102*, 4915-4925.
24. Kosa, G.; Zimmermann, B.; Kohler, A.; Ekeberg, D.; Afseth, N.K.; Mounier, J.; Shapaval, V. High-throughput screening of Mucoromycota fungi for production of low-and high-value lipids. *Biotechnology for biofuels* **2018**, *11*, 66.
25. Kavadia, A.; Komaitis, M.; Chevalot, I.; Blanchard, F.; Marc, I.; Aggelis, G. Lipid and γ-linolenic acid accumulation in strains of Zygomycetes growing on glucose. *Journal of the American Oil Chemists' Society* **2001**, *78*, 341-346.
26. ISO. Animal Feeding Stuffs—Determination of Phosphorus Content—Spectrometric Method, ISO 6491: 1998. International Organisation for Standardization Geneva: 1998.
27. Staal, L.B.; Petersen, A.B.; Jørgensen, C.A.; Nielsen, U.G.; Nielsen, P.H.; Reitzel, K. Extraction and quantification of polyphosphates in activated sludge from waste water treatment plants by 31P NMR spectroscopy. *Water research* **2019**, *157*, 346-355.
28. Lewis, T.; Nichols, P.D.; McMeekin, T.A. Evaluation of extraction methods for recovery of fatty acids from lipid-producing microheterotrophs. *J Microbiol Meth* **2000**, *43*, 107-116, doi:Doi 10.1016/S0167-7012(00)00217-7.
29. Anne Marie Langseter, S.D., Volha Shapaval, Achim Kohler, Dag Ekeberg, Boris Zimmermann. Evaluation and optimisation of direct transesterification methods for the assessment of lipid accumulation in oleaginous filamentous fungi. 2021.*Manuscript.*

30. Demšar, J.; Curk, T.; Erjavec, A.; Gorup, Č.; Hočevar, T.; Milutinovič, M.; Možina, M.; Polajnar, M.; Toplak, M.; Starič, A. Orange: data mining toolbox in Python. *the Journal of machine Learning research* **2013**, *14*, 2349-2353.
31. Kosa, G.; Shapaval, V.; Kohler, A.; Zimmermann, B. FTIR spectroscopy as a unified method for simultaneous analysis of intra-and extracellular metabolites in high-throughput screening of microbial bioprocesses. *Microbial cell factories* **2017**, *16*, 1-11.
32. Liang, Y.; Zhang, B.; Zheng, W.; Xing, L.; Li, M. Alkaline stress triggers an immediate calcium fluctuation in *Candida albicans* mediated by Rim101p and Crz1p transcription factors. *FEMS Yeast Research* **2011**, *11*, 430-439.
33. Speake, T.; Elliott, A.C. Modulation of calcium signals by intracellular pH in isolated rat pancreatic acinar cells. *The Journal of physiology* **1998**, *506*, 415-430.
34. Ramos, I.B.; Miranda, K.; Pace, D.A.; Verbist, K.C.; Lin, F.-Y.; Zhang, Y.; Oldfield, E.; Machado, E.A.; De Souza, W.; Docampo, R. Calcium-and polyphosphate-containing acidic granules of sea urchin eggs are similar to acidocalcisomes, but are not the targets for NAADP. *Biochemical Journal* **2010**, *429*, 485-495.
35. McGrath, J.W.; Quinn, J.P. Intracellular accumulation of polyphosphate by the yeast Candida humicola G-1 in response to acid pH. *Applied and environmental microbiology* **2000**, *66*, 4068-4073.
36. Barth, G.; Gaillardin, C. Physiology and genetics of the dimorphic fungus *Yarrowia lipolytica. FEMS microbiology reviews* **1997**, *19*, 219-237.
37. Kawazoe, N.; Kimata, Y.; Izawa, S. Acetic acid causes endoplasmic reticulum stress and induces the unfolded protein response in *Saccharomyces cerevisiae*. *Frontiers in microbiology* **2017**, *8*, 1192.
38. Mohamed, H.; El-Shanawany, A.-R.; Shah, A.M.; Nazir, Y.; Naz, T.; Ullah, S.; Mustafa, K.; Song, Y. Comparative analysis of different isolated oleaginous Mucoromycota fungi for their γ-linolenic acid and carotenoid production. *BioMed research international* **2020**, *2020*.
39. Fraser, P.D.; Ruiz-Hidalgo, M.J.; Lopez-Matas, M.A.; Alvarez, M.I.; Eslava, A.P.; Bramley, P.M. Carotenoid biosynthesis in wild type and mutant strains of *Mucor circinelloides. Biochimica et Biophysica Acta (BBA)-General Subjects* **1996**, *1289*, 203-208.
40. Enrique, A.; Papp, T.; Breum, J.; Arnau, J.; Arturo, P. Strain and culture conditions improvement for β-carotene production with *Mucor*. In *Microbial processes and products*, Springer: 2005; pp. 239-256.
41. Khanafari, A.; TAYARI, K.; Emami, M. Light requirement for the carotenoids production by *Mucor hiemalis*. **2008**.

Supplementary materials

Calcium affects polyphosphate and lipid accumulation in Mucoromycota fungi

Simona Dzurendova[1]*, Boris Zimmermann[1], Achim Kohler[1], Kasper Reitzel[2], Ulla Gro Nielsen[3], Benjamin Xavier Dupuy—Galet[1], Shaun Allan Leivers[4], Svein Jarle Horn[4], Volha Shapaval[1]

[1]Norwegian University of Life Sciences, Faculty of Science and Technology, Drøbakveien 31, 1433 Ås, Norway

[2]Department of Biology, University of Southern Denmark, Campusvej 55, DK-5230, Odense M, Denmark

[3] Department of Physics, Chemistry and Pharmacy, University of Southern Denmark, Campusvej 55, DK-5230, Odense M, Denmark

[4]Norwegian University of Life Sciences, Faculty of Chemistry, Biotechnology and Food Science, Christian Magnus Falsens vei 1, 1433 Ås, Norway

* Correspondence: simona.dzurendova@gmail.com; simona.dzurendova@nmbu.no

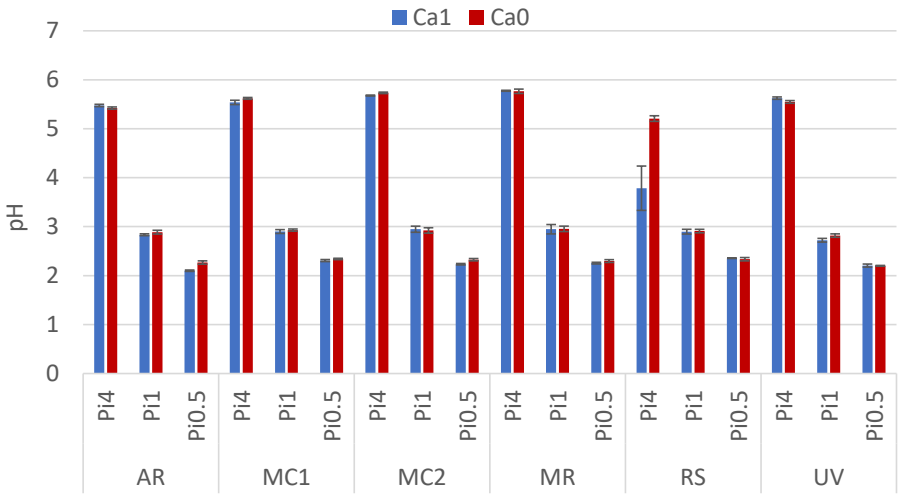

Figure S1: pH of culture supernatants at the end of the cultivation.

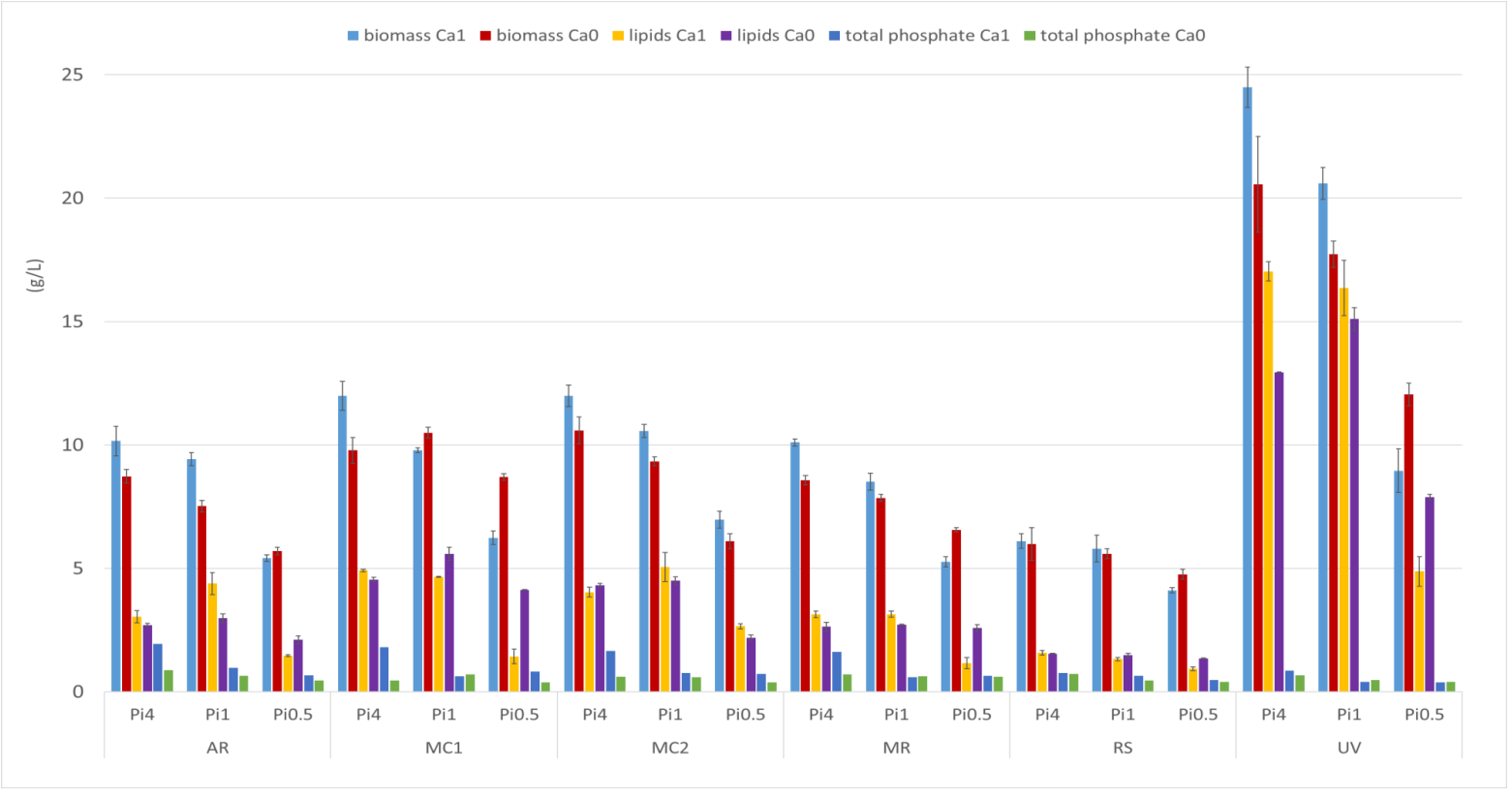

Figure S2: The total concentrations (in g/L) of fungal biomass, lipids and phosphates.

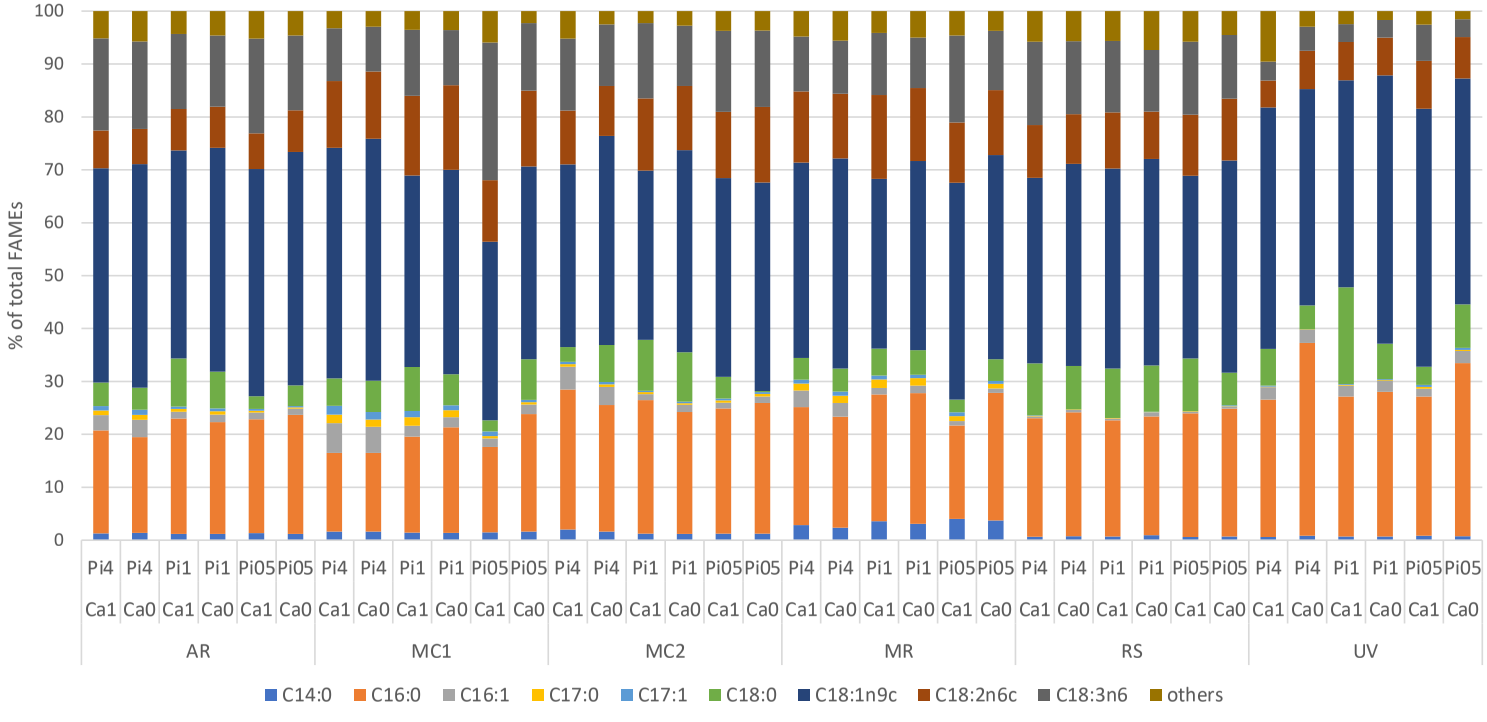

Figure S3: The fatty acid profiles of FAMEs extracted from fungal biomass. Fatty acids which were present in amount higher than 1% are shown, the rest is summed up into ‘others’.

Paper VI

Assessment of filamentous fungal biomass by Fourier transform Raman spectroscopy for application in biotechnology and bioprocessing

Simona Dzurendová[1] (simona.dzurendova@nmbu.no), Volha Shapaval[1] (volha.shapaval@nmbu.no), Valeria Tafintseva[1] (valeria.tafintseva@nmbu.no), Achim Kohler[1] (achim.kohler@nmbu.no), Dana Byrtusová[1,2] (dana.byrtusova@nmbu.no), Martin Szotkowski[2] (xcszotkowski@fch.vut.cz), Ivana Márová[2] (marova@fch.vut.cz), Boris Zimmermann[1]* (boris.zimmermann@nmbu.no)

[1]Faculty of Science and Technology, Norwegian University of Life Sciences, Postbox 5003, 1432 Ås, Norway
[2]Faculty of chemistry, Brno University of Technology, Purkyňova 464/118, 61200 Brno, Czechia

*Correspondence address: Faculty of Science and Technology, Norwegian University of Life Sciences, Postbox 5003, 1432 Ås, Norway

ABSTRACT

Oleaginous filamentous fungi can accumulate large amount of cellular lipids, as well as biopolymers and pigments, and potentially serve as a major source of biochemicals for food, feed, chemical, pharmaceutical, and transport industries. We assessed suitability of Fourier transform (FT) Raman spectroscopy for screening and process monitoring of filamentous fungi in biotechnology. Six Mucoromycota strains were cultivated in microbioreactors under six growth conditions (three phosphate concentrations in presence and absence of calcium). FT-Raman and FT-infrared (FTIR) spectroscopic data was assessed in respect to referent analyses of lipids, phosphorus, and carotenoids by using principal component analysis (PCA), multiblock or consensus PCA, partial least square regression (PLSR), and analysis of spectral variation due to different design factors by ANOVA model. All main chemical biomass constituents were detected by FT-Raman spectra, including lipids, proteins, cell wall carbohydrates, and polyphosphates, as well as carotenoids. FT-Raman spectra clearly show effect of growth conditions on fungal biomass. PLSR models with high coefficients of determination (0.83–0.94) and low error (approx. 8%) for quantitative determination of total lipids, phosphates and carotenoids were established. FT-Raman spectroscopy showed great potential for chemical analysis of biomass of oleaginous filamentous fungi. The study demonstrates that FT-Raman and FTIR spectroscopies provide complementary information on main fungal biomass constituents.

Keywords: Oleaginous microorganisms, biodiesel, pigments, biopolymers, carotenoids, fatty acids, chitin, chitosan, phosphorus, fungi

INTRODUCTION

Filamentous fungi have been commercially used in biotechnology for over a century, creating a range of products from organic acids, enzymes and oleochemicals to antibiotics, statins and steroids for applications in food, pharma and chemical industry [1-3]. Some of the most important filamentous fungal cell factories, such as *Mortierella*, *Mucor*, *Rhizopus* and *Umbelopsis* genera, belong to Mucoromycota taxon. Mucoromycota have gained interest due to their versatile metabolism that enables fermentation process on a wide range of feedstock, such as waste and rest materials [4,5]. When cultivated in a carbon-rich and nitrogen-limited growth conditions, Mucoromycota fungi can accumulate high amount of lipids, up to 85 % of dry weight [6]. The fermentation is the most complex individual process within biotech-manufacturing and it poses a number of challenges related to productivity and quality. The main challenges are related to the variability and heterogeneity of a fermentation growth medium, as well as to the variability in the cellular population, such as natural population heterogeneity [7]. Thus, online monitoring of fermentation is a crucial requirement for an efficient bioprocess. Unfortunately, process monitoring is still dependent on a limited number of standard sensors for pH, temperature and gasses, while the critical process parameters, such as biomass, product and substrate concentrations and compositions, are rarely assessable on-line. Thus, there is a need for rapid methods that provide detailed chemical information for bioprocess monitoring and optimization. Process optimization and monitoring will greatly benefit from advanced spectroscopy-based sensors that will enable real-time monitoring and control of bioprocesses.

Vibrational spectroscopy, comprising infrared and Raman spectroscopies, is considered as a rapid, inexpensive and highly sensitive method for analysis of biological samples [8,9]. These techniques are excellent for obtaining comprehensive and detailed information in biotechnology since they can simultaneously measure broad chemical profiles of the chemical constituents present in the bioprocess via detection of numerous functional groups. This rich spectroscopic data is interpreted by using chemometrics, classical machine learning and deep learning methods [10-16]. Although most of the studies involving filamentous fungi and yeasts have been conducted by Fourier transform infrared (FTIR) spectroscopy, as of late, Raman spectroscopy has been applied to study fungi, in particular regarding pigments [17-25], lipids [21,26-29], and cell wall [30,31]. Compared to FTIR spectroscopy, Raman spectroscopy is based on fundamentally different principle; While infrared spectroscopy relies on absorption of light by molecules, Raman spectroscopy is based on an inelastic Raman scattering phenomenon. In Raman spectroscopy, molecular vibrations originate from the interaction of the sample and the excitation radiation, typically from a laser in the ultraviolet, visible, or near-infrared region of the electromagnetic spectrum. In case of biological samples, the resulting Raman spectrum usually displays broad range of signals related to various types of cellular analytes, such as lipids, proteins, pigments, and carbohydrates [19,28,30,32]. Raman spectroscopy is very suitable for biotechnology applications since it does not require special sample pretreatment, it is non-destructive, and it is fast. Unlike FTIR (mid-IR) spectroscopy, Raman spectroscopy is not hindered by water and glass, which is

extremely useful property for application of the technique in biotechnology. Moreover, it is very versatile, from in-situ monitoring of bioprocesses in bioreactors by a Raman fibre-optic probe [33], to the detailed cellular imaging by a confocal Raman microscope [29]. The advances in Raman instrumentation, in combination with multivariate data analysis, have shown the potential of this technique in bioprocess monitoring [17,34,35] and rapid identification and classification of fungal species [36-40].

In general, Raman scattering intensities are weak, and thus it is difficult to detect molecules that are not present in high concentration in the sample. However, if the excitation radiation is in resonance with the electronic transitions, so called resonance Raman effect will occur. In that case, the Raman scattering will be tremendously enhanced, enabling detection of molecules present in relatively low concentrations. This is often the case of certain pigments, such as carotenoids, enabling measurement of analytes that are undetectable by FTIR [41]. Unfortunately, in addition to Raman and resonant Raman effect, excitation laser can often create resonance fluorescence effect. The fluorescence effect occurs when the energy of the excitation photon is close to the transition energy between two electronic states. The presence of intensive fluorescence can significantly hamper detection of the Raman effect. Another common problem in Raman spectroscopy is sample heating that leads to emission of longer-wavelength radiation and thermal interference to the Raman spectrum, and can even result in thermal degradation of the sample. Both fluorescence and thermal interferences can be minimised by using different excitation lasers, with simultaneous optimization of Raman effect [42,43]. In general, electronic transitions are weaker at longer wavelengths, and thus detrimental effects can be avoided by use of near-infrared (NIR) lasers, such as neodymium doped yttrium aluminium garnet (Nd:YAG) laser with excitation at 1064 nm. Moreover, use of such long-wavelength excitation laser can significantly increase penetration depth, compared to visible (short-wavelength) lasers, thus allowing more comprehensive analysis of a sample [44]. However, NIR excitation lasers offer significantly lower Raman sensitivity compared to ultraviolet and visible lasers, and thus they often require Fourier transform (FT) Raman spectrometers with a Michelson interferometer and a FT processor for signal enhancement. In the last decade, FT-Raman spectroscopy gained momentum in analyses of biological samples [45-48]. However, FT-Raman spectroscopy remains unexplored in analysis of filamentous fungi, although the potential of this technique for chemical characterization of filamentous fungi was demonstrated almost three decades ago by Edwards et al [32]. In the meantime, only one other study, with limited focus on cinnabarin production by *Pycnoporus sanguineus*, has been conducted [22].

A number of our studies have shown that FTIR spectroscopy can be used for chemical characterization of Mucoromycota fungi [49-52]. The Duetz-microtiter plate system (Duetz-MTPS) for microbial cultivation, in combination with FTIR spectroscopy and multivariate data analysis, can be used as a powerful high-throughput low-cost method for the screening of filamentous fungi for biotechnological production of various biochemicals, such as single cell lipids, polyphosphates, and

polyglucosamines (chitin and chitosan) [49]. In this study, we have assessed the potential of FT-Raman spectroscopy for chemical characterization of biomass of Mucoromycota filamentous fungi in biotechnology research and production. Moreover, the same sample set was measured by FTIR spectroscopy, as well as high performance liquid chromatography (HPLC) for pigment analysis, gas chromatography (GC) for lipid analysis, and assay-based UV/VIS spectroscopy and nuclear magnetic resonance spectroscopy for analysis of cellular phosphorus. Thus, advantages and disadvantages of FT-Raman spectroscopy over FTIR spectroscopy were evaluated in respect to various chemical constituents in the fungal biomass, such as lipids, proteins, cell wall carbohydrates, polyphosphates, and carotenoid pigments.

MATERIALS AND METHODS

Fungal strains

Six strains of Mucoromycota oleaginous filamentous fungi were used in the study: *Amylomyces rouxii* CCM F220, *Mucor circinelloides* VI 04473, *Mucor circinelloides* FRR 5020, *Mucor racemosus* UBOCC A 102007, *Rhizopus stolonifer* CCM F445, and *Umbelopsis vinacea* CCM F539. Fungi were obtained in agar slants and Petri dishes or in lyophilized form, from the Czech Collection of Microorganisms, Brno, Czech Republic (CCM), Food Fungal Culture Collection, North Ryde, Australia (FRR), Universitè de Bretagne Occidentale Culture Collection (UBOCC; Brest, France), and the Norwegian School of Veterinary Science, Oslo, Norway (VI).

Cultivation of fungi

Cultivation media was formulated by using full factorial design, where three different concentrations of phosphorus substrate (high, medium and low) and two calcium conditions (presence and absence) were used. The cultivation was performed in Duetz-MTPS [51] in two independent biological replicates for each fungus and condition, resulting in 72 samples. Cultivation of the selected fungi was done in two steps: 1) growth on standard agar medium for preparing spore inoculum, and 2) growth in Duetz-MTPS in nitrogen-limited broth media with ammonium sulphate as nitrogen source and different concentrations of phosphorus substrate (Pi) and calcium (Ca).

For the preparation of spore inoculum, all strains except *Umbelopsis* were cultivated on malt extract agar (MEA) and *Umbelopsis* was cultivated on potato dextrose agar (PDA). MEA was prepared by dissolving 30 g of malt extract agar (Merck, Germany) in 1L of distilled water and autoclaved at 115 °C for 15 min. PDA was prepared by dissolving 39 g of potato dextrose agar (VWR, Belgium) in 1L of distilled water and autoclaved at 115°C for 15 min. Agar cultivation was performed for 7 days at 25 °C for all strains. Fungal spores were harvested from agar plates with a bacteriological loop after the addition of 10 mL of sterile 0.9 % NaCl solution.

The main components of the nitrogen-limited broth media [53] with modifications [49,50] were: 80 $g \cdot L^{-1}$ glucose, 1.5 $g \cdot L^{-1}$ $(NH_4)_2SO_4$, 1.5 $g \cdot L^{-1}$ $MgSO_4 \cdot 7H_2O$, 0.008 $g \cdot L^{-1}$ $FeCl_3 \cdot 6H_2O$, 0.001 $g \cdot L^{-1}$

$ZnSO_4 \cdot 7H_2O$, 0.0001 $g \cdot L^{-1}$ $CoSO_4 \cdot 7H_2O$, 0.0001 $g \cdot L^{-1}$ $CuSO_4 \cdot 5H_2O$, and 0.0001 $g \cdot L^{-1}$ $MnSO_4 \cdot 5H_2O$. The concentration of calcium salt designated as Ca1, with 0.1 $g \cdot L^{-1}$ $CaCl_2 \cdot 2H_2O$, was considered as a reference value for calcium salt, while broth media designated as Ca0 had no calcium salt present. The concentrations of phosphate salts, 7 $g \cdot L^{-1}$ KH_2PO_4 and 2 $g \cdot L^{-1}$ Na_2HPO_4, were selected as a reference value (Pi1) since they have frequently been used in cultivation of oleaginous Mucoromycota [50,53] . The broth media contained higher (four times higher than the standard concentration Pi1, designated as Pi4), standard (Pi1), and lower (half of the standard concentration Pi1, designated as Pi0.5) amount of phosphate salts. Cultivation in broth media was performed in the Duetz-MTPS (Enzyscreen, Netherlands) which consists of 24-square polypropylene deep well microtiter plates, low evaporation sandwich covers and extra high cover clamps [54], which were placed into the MAXQ 4000 shaker (Thermo Scientific). The autoclaved microtiter plates were filled with 7 ml of sterile broth media per well, and each well was inoculated with 50 µl of spore inoculum. Cultivation was performed for 7 days at 25 °C and 400 rpm agitation (1.9 cm circular orbit).

Preparation of fungal biomass for vibrational spectroscopy analyses

The growth media were separated from the fungal biomass by transferring the fermentation broth with plastic Pasteur pipettes into 15 ml Falcon tubes and the subsequent centrifugation at 13500 rpm for 15 min at 4 °C. Fungal biomass from Falcon tubes was washed three times with cold distilled water and filtered under vacuum using a Whatman No. I filter paper (GE Whatman, USA). Approximately 5 mg of fresh washed biomass was transferred into 2 ml polypropylene tube containing 250±30 mg of acid washed glass beads and 0.5 ml of distilled water, and homogenized by using Percellys Evolution tissue homogenizer (Bertin Technologies, France) with the following set-up: 5500 rpm, 6 × 20 s cycle. Freshly homogenized biomass was measured by FTIR. The remaining washed biomass was freeze-dried for 24 hours, and stored at −20 °C until FT-Raman measurements.

FT-Raman spectroscopy analysis

Raman spectra were recorded in backscattering geometry using MultiRAM FT-Raman spectrometer (Bruker Optik GmbH, Germany) equipped with a neodymium-doped yttrium aluminum garnet (Nd:YAG) laser (1064 nm, 9394 cm^{-1}), and germanium detector cooled with liquid nitrogen. For each measurement, 0.5 – 1 mg of freeze-dried sample was deposited in aluminium sample container and pressed with pestle. The spectra were recorded with a total of 128 scans, using Blackman–Harris 4-term apodization, spectral resolution of 4 cm^{-1}, with a digital resolution of 1.928 cm^{-1}, over the range of 3785-50 cm^{-1}, at 500 mW laser power. Since some samples of *Amylomyces rouxii* and *Rhizopus stolonifer* have shown strong heating and burning effects, those samples were measured with the reduced laser power of 200 mW. Each biomass sample was analysed in three technical replicates, resulting in 216 spectra. The OPUS software (Bruker Optik GmbH, Germany) was used for data acquisition and instrument control.

FTIR spectroscopy analysis

The FTIR transmittance spectra were measured using the High Throughput Screening eXTension (HTS-XT) unit coupled to the Vertex 70 FTIR spectrometer (both Bruker Optik, Germany). 10 µl of homogenized fungal biomass was pipetted onto an IR transparent 384-well silica microplate and dried at room temperature for two hours. The HTS-FTIR spectra were recorded with a total of 64 scans, spectral resolution of 6 cm^{-1}, and digital spacing of 1.928 cm^{-1}, over the range of 4000–400 cm^{-1}, and an aperture of 5 mm. Spectra were recorded as the ratio of the sample spectrum to the spectrum of the empty IR transparent microplate. Each biomass sample was analysed in three technical replicates, resulting in 216 spectra. The OPUS software (Bruker Optik GmbH, Germany) was used for data acquisition and instrument control.

Spectral preprocessing and data analysis

All preprocessing methods and data analyses were performed using Matlab R2019a (The Mathworks Inc., Natick, MA, USA), Unscrambler 11.0 (CAMO Software, Oslo, Norway), and Orange data mining toolbox version 3.26 (University of Ljubljana, Slovenia) [55,56].

Spectral preprocessing

Each spectral dataset (FTIR and FT-Raman) was preprocessed with two different procedures, resulting in nonderivative and derivative spectral data. For nonderivative FT-Raman data, FT-Raman spectra were smoothed by using Savitzky-Golay (SG) algorithm (polynomial 2, window size 15, derivative order 0), followed by the rubber band baseline correction, truncation of data to 3200-2400 and 1900-500 cm^{-1} regions, and normalization by extended multiplicative signal correction (EMSC), an MSC model extended by a linear, quadratic and cubic components [57,58]. For nonderivative FTIR data, FTIR spectra were corrected and normalized by using EMSC (MSC with linear, quadratic and cubic components). In the analysis of spectral variation due to design factors by ANOVA model, the nonderivative data were preprocessed further, as stated below. For derivative FT-Raman data, FT-Raman spectra were converted into second derivatives by using SG algorithm (polynomial 2, window size 15, derivative order 2), followed by the EMSC (MSC with linear, quadratic and cubic components), and truncation of data to 1800-900 cm^{-1} region. For derivative FTIR data, FTIR spectra were converted into second derivatives by using SG algorithm (polynomial 2, window size 15, derivative order 2), followed by the EMSC (MSC with linear and quadratic components), and truncation of data to 1800-900 cm^{-1} region.

Principal component analysis

Biochemical similarities between samples were estimated by using principal component analysis (PCA). PCA was conducted on the nonderivative spectral data. The variability test based on Pearson correlation coefficients (PCC) was used to estimate reproducibility of technical replicate measurements. The PCC test was conducted on the preprocessed non-derivative FT-Raman data. Consensus Principal Component analysis (CPCA) was used on multiblock spectral data, consisting of

preprocessed derivative FTIR and FT-Raman data blocks. In CPCA, technical replicates were averaged after the preprocessing in order to obtain sample-to-sample correspondence between the data blocks [59-61].

Quantitative determination of chemical constituents of fungal biomass based on vibrational spectra

Ratios of Raman intensities at different wavenumbers related to chemical constituents of fungal biomass (1747 cm^{-1} for lipids; 1163 cm^{-1} for phosphates, 1523 cm^{-1} for carotenoids) were used for the initial estimation of their content. Nonderivative FT-Raman data was used for this estimation.

Partial least square regression (PLSR) was used to establish calibration models for lipids, phosphates and carotenoids. PLSR models were established by using a data set of either GC (lipids), UV/Vis (phosphorus) or HPLC (carotenoids) reference measurements (responses) as a Y matrix, which was regressed onto an X matrix containing FT-Raman measurements (predictors). Optimal number of PLSR components (i.e. PLSR factors) of the calibration models (*AOpt*), root-mean-square error (RMSE) and coefficient of determination (R^2) were calculated, and the optimal model was selected based on the lowest *AOpt* having insignificantly higher RMSE than the model with the minimum RMSE. PLSR analyses were conducted on both the preprocessed non-derivative and derivative FT-Raman data. PLSR models for total lipids and total phosphorus predictions were based on FT-Raman measurements of either all six fungal strains or the three *Mucor* strains, while the models for determination of carotenoids were based on the measurements of the two *Mucor circinelloides* strains. Model validation was performed by using independent biological replicates for test set, where PLSR models were built by using one set of bioreplicate samples (bioreplicate 1) while validation was performed on the second set of bioreplicate samples (bioreplicate 2).

Multiblock and analysis of spectral variation by ANOVA model of FTIR and FT-Raman data

FTIR and FT-Raman data was used to assess influence of various experimental parameters. Spectral variation in the data introduced by the different design parameters, specifically Pi concentration, calcium availability, phosphates-calcium (Ca-Pi) interactions, and biological replicates, was calculated for each strain independently in each data set. In analysis of variance (ANOVA) model a data matrix is represented as a sum of matrices that describe experimental design factors and the residual error. Each of these matrices consists of the means of the spectra that correspond to different levels of the design factor. The variation due to each factor can then be calculated. The ANOVA model for this study contained five design factors: calcium availability, phosphates concentration, Ca-Pi interaction, biological replicates and unexplained residual variance. The factor “calcium availability” had two levels (Ca1, Ca0), the factor “phosphates concentration” consisted of three levels (three different Pi concentrations), the design factor “Ca-Pi interaction” had therefore six levels, while biological replicates had two levels (bioreplicate 1 and 2). Technical replicate variations and other variations irrelevant for this study were kept as a part of residuals. The variation of each factor was normalized by the sum of the variations for the four factors of interest, meaning that they were summed up to 100%. Such ANOVA model underlies commonly used ANOVA-PCA and ASCA analysis [62,63],

which in addition to calculating variation contribution of design factors in a data allow analyzing other aspects of the data. The methods were therefore not implemented in this study. Such analysis was conducted on the preprocessed derivative FTIR and FT-Raman spectral data, where technical replicates were averaged after the preprocessing, and both FTIR and FT-Raman data were truncated to 1800-900 cm^{-1} region.

Reference compounds and reference chemical analyses

For chemical characterization of fungal biomass, a set of reference compounds was measured by FT-Raman and FTIR spectroscopies. Chitin, β-glucan (from *Saccharomyces cerevisiae*, predominantly β1,3-glucan linear structure with a small number of β1,6-glucan branches), gluten, glyceryl trioleate (1,2,3-tri(cis-9-octadecenoyl)glycerol), and sodium polyphosphate were purchased from Merck-Sigma-Aldrich (Darmstadt, Germany) and used without further purification.

Details on lipid extraction and gas chromatography analysis of fatty acid profiles and total lipids, as well as analysis of cellular phosphorus by assay-based UV/VIS spectroscopy and nuclear magnetic resonance (NMR) spectroscopy, were reported previously [64].

Carotenoid analysis

Total carotenoid content was determined for the two *Mucor circinelloides* strains (VI 04473 and FRR 5020) by using method based on high performance liquid chromatography equipped with photodiode array detector (HPLC-PDA). 15±3 mg of freeze-dried biomass was weighed and rehydrated with 1 ml of miliQ water for 30 minutes. Excess water was removed by centrifugation at 10 000 rpm for 5 min, and 1 ml of methanol and about 0.5 ml of glass beads (0.2-0.5 mm diameter, Roth, Germany) were added to the sample. The sample was vortexed for 20 min, transferred to a 15 ml tube with 2 ml of chloroform, and vortexed for 10 minutes. 1 ml of water was added to the sample, vortexed for 10 seconds, and centrifuged at 3000 rpm for 5 min. The lower (chloroform) phase was transferred to a clean tube and dried under an inert nitrogen atmosphere. The dried sample was dissolved in 1 mL of ethyl acetate: acetonitrile 1:3 and filtered through a 0.45 μm polytetrafluoroethylene (PTFE) filter into a vial. Samples were measured on Dionex Ultimate series HPLC with Vanquish diode array detector (Thermo Fischer Scientific, USA) on Kinetex C18-EVO column 150 mm × 4.6 mm × 5 μm (Phenomenex, USA) using gradient separation with mobile phase A (acetonitrile : methanol : 0.1M tris hydrochloride pH=8; 84:2:14) and mobile phase B (methanol : ethyl acetate; 60:40) at flowrate 1.2 ml/min and 25 °C. The following gradient program was used: 0-13 min from 100% A to 100% B, 13-19 min 100% B, 19-20 min from 100% B to 100% A, 20-25 min 100% A. Carotenoid pigments were detected at 445 nm. Chromatographic data were evaluated using Chromeleon 7.2 software. Carotenoids were identified and evaluated using commercial standards (Sigma Aldrich) and external calibration. Only β-carotene was identified based on standards, while the remaining unidentified carotenoids were quantified via β-carotene calibration curve.

RESULTS AND DISCUSSION

Chemical composition of fungal biomass

The fungal samples, belonging to the subset of samples presented in our previous study [64], were selected for the vibrational spectroscopy study due to their high variation in chemical composition. The selected oleaginous filamentous fungi were identified as a potentially good producers of valuable metabolites, such as lipids, carbohydrates (chitin, chitosan and beta-glucan), polyphosphates and carotenoid pigments [49,52]. Under nitrogen-limitation these fungi accumulate lipids in the form of free fatty acids and their derivatives, such as acylglycerols and glycerophospholipids, where triacylglycerols make by far the biggest fraction [65]. For all samples, determination of total lipids (as fatty acid methyl esters) was conducted by direct transesterification and GC-FID analysis, as reported in our previous study [64]. The samples contained the following range of amounts of the total lipids (expressed as percentage of a dry weight): *Amylomyces rouxii* 27-49%, *Mucor circinelloides* (strain VI 04473) 20-49%, *Mucor circinelloides* (strain FRR 5020) 34-52%, *Mucor racemosus* 19-41%, *Rhizopus stolonifer* 22-28%, and *Umbelopsis vinacea* 49-83% (Figure 1).

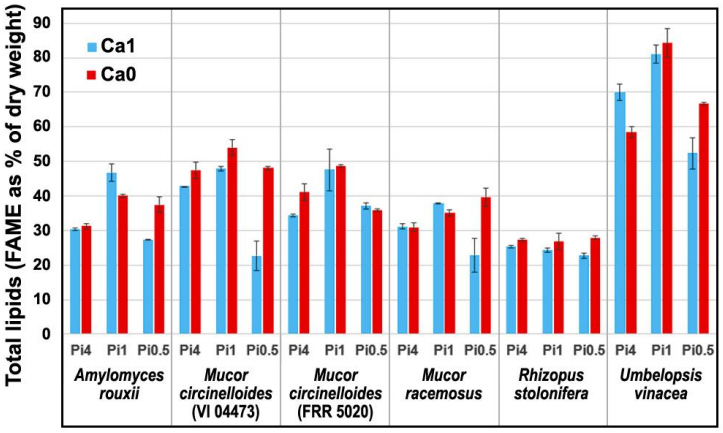

Figure 1. Total lipids content of the fungal samples grown under six different conditions (average values and range based on measurements of two biological replicates).

Moreover, accumulation of other metabolites in the fungal strains was influenced by changing concentrations of phosphate and calcium ions in the media. The samples contained the following range of amounts of the total phosphorus (expressed as percentage of a dry weight): *Amylomyces rouxii* 2.65-6.24%, *Mucor circinelloides* (strain VI 04473) 1.40-4.91%, *Mucor circinelloides* (strain FRR 5020) 1.86-4.50%, *Mucor racemosus* 2.28-5.20%, *Rhizopus stolonifer* 2.70-4.13%, and *Umbelopsis vinacea* 0.64-1.37% [64]. NMR spectroscopy measurements have shown that the majority of phosphorus in *Mucor circinelloides* VI 04473 samples were accumulated in the form of polyphosphates [64]. These results correspond to previously reported studies that have shown average polyphosphate accumulation

of Mucoromycota biomass within 0.31-0.93% range [66], with higher accumulation for *Mucor* strains, approx. within 4-7% range [67]. Our previous studies have indicated that some Mucoromycota strains have extensive polyphosphate accumulation in non-acidic growth conditions [49,64,68]. In growth media lacking calcium, there is a decrease in polyphosphate accumulation [64], which is related to the formation of acidocalcisomes granules (polyphosphate granules) which is calcium dependent process [64,69]. In the formation of acidocalciosomes calcium as well as other cations functioning as neutralizing agent for neutralizing negative charge of polyphosphate molecules, therefore calcium availability is important prerequisite for the formation of polyphosphate granules.

In our previous study, we have observed that Amylomyces, Mucor, and Rhizopus can overproduce chitin/chitosan under low phosphate growth conditions [49]. Cell wall of Mucoromycota fungi is typically composed of fibrillar, rigid and shape determining polyglucosamines, in particular chitin, chitosan and chitin–glucan complexes. These carbohydrates are embedded in an amorphous matrix of glucans and glycoproteins, and, in some cases, substructures of glucuronans and polyphosphates [70-72]. One of the main functions of cell wall is protection against environmental stress [72], such as acidic stress that was present in our study under low phosphate growth conditions [49,64,73]. More specifically, limitation of phosphates availability in the growth media, in combination with ammonium sulphate as nitrogen source, leads to acidity of the growth media, and the subsequent acidic stress results with overproduction of chitin/chitosan in the fungal cell walls. Calcium is directly involved in chitin synthesis as it activates the chitin synthase enzyme in fungi [74].

In addition to changes in polyphosphates accumulation, some fungal strains have shown the influence of media nutrients on carotenoid production (Figure 2a). HPLC analysis of carotenoid content of biomasses of two *Mucor circinelloides* strains shows significant change in carotenoid production under different growth conditions. In particular, *Mucor circinelloides* strain FRR 5020, shows approx. tenfold increase in production of carotenoids, with accumulation of 0.14%$_{\text{dry weight}}$ (1457 µg/g$_{\text{dry weight}}$) total carotenoids in growth media with low phosphate and absence of calcium (Figure 2b). *Mucor circinelloides* was reported as a good candidate for carotenoid production [75], with the production of 98-378 µg/g$_{\text{dry weight}}$ [76] (ref.). The previously reported carotenoid production for other species covered by our study were 192 *Amylomyces rouxii* and 50-200 µg/g$_{\text{dry weight}}$ for *Rhizopus stolonifer* [76]. In addition, several studies have shown that elevated temperature and light intensity will result with higher production of carotenoids in *Mucor* fungi [76,77]. Since our result for *Mucor circinelloides* strain FRR 5020 shows exceedingly high carotenoid production compared to other non-GMO Mucoromycota fungi, it strongly indicates that calcium and phosphates concentrations, as well as acidic stress, should be taken into account in carotenoid-production studies, alongside temperature and light conditions.

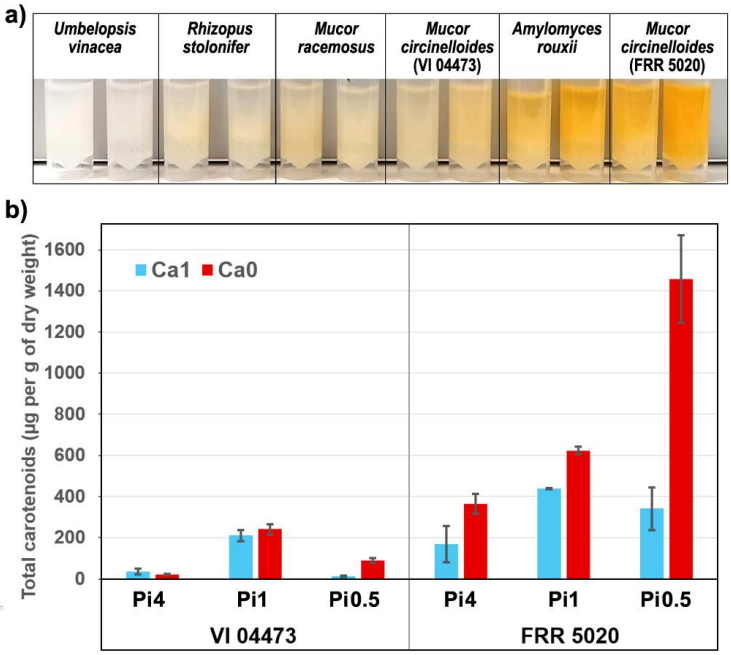

Figure 2. (a) Image of disintegrated fungal biomass of samples grown under Pi0.5 condition, with (Ca1, tube1) and without (Ca0, tube 2) calcium. (b) Total carotenoid content of the two *Mucor circinelloides* strains grown under six different conditions (average values and range based on measurements of two biological replicates).

FT-Raman chemical profiling of fungal biomass

As already mentioned, although Raman spectroscopy requires simple sample preparation and measurement, the resulting spectrum is often dominated by interference signals caused by fluorescence and sample heating. The longer wavelength excitation lasers, such as Nd:YAG laser used in this study, significantly reduce those obstructing effects. Out of 72 samples, only ten have shown interfering signals as a result of sample heating. Sample heating is a well-known problem in Raman spectroscopy, and, in this study, it was primarily caused by absorbance of the excitation laser radiation by fungal spores. More specifically, under moderate and high phosphate concentrations, cultivations of *Rhizopus stolonifer* have resulted with slight sporulation on the walls of microbioreactor. In all cases, small presence of dark fungal spores has led to sample heating during the FT-Raman measurements, resulting with suboptimal FT-Raman spectra (Figure 3). In addition to *Rhizopus stolonifer*, the heating interference was noticeable for several *Amylomyces rouxii* samples although those samples presented no visible sporulation. In total, ten samples were measured with the reduced laser power in order to decrease the rate of heating, the heating emission spectrum, and, in particular, the sample burning.

Overall, the FT-Raman measurements have resulted with high-quality spectra (Figure 4). The corresponding FTIR spectra are presented in Figure S1 in the Supplemental Materials.

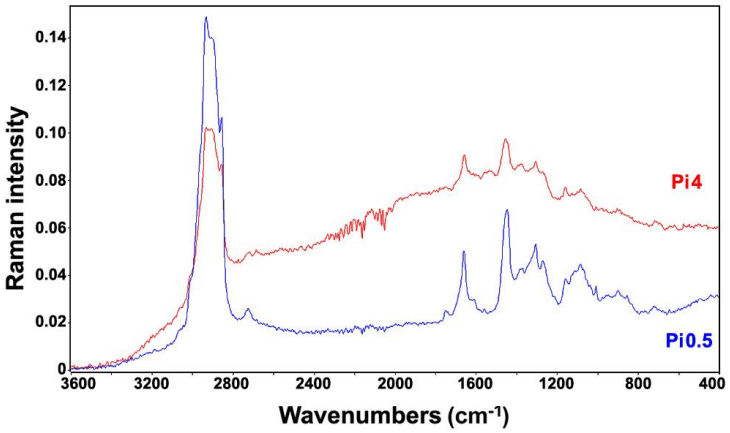

Figure 3. FT-Raman spectra of *Rhizopus stolonifer* cultivated under Ca1 condition and two different phosphate concentrations. The spectrum of the sample cultivated under high phosphate concentration (Pi4, red) shows significant heating effect resulting with distorted baseline even when measured under low excitation laser power (200 mW), compared to the spectrum of the sample cultivated under low phosphate concentration (Pi0.5, blue) which was measured under the standard laser power (500 mW).

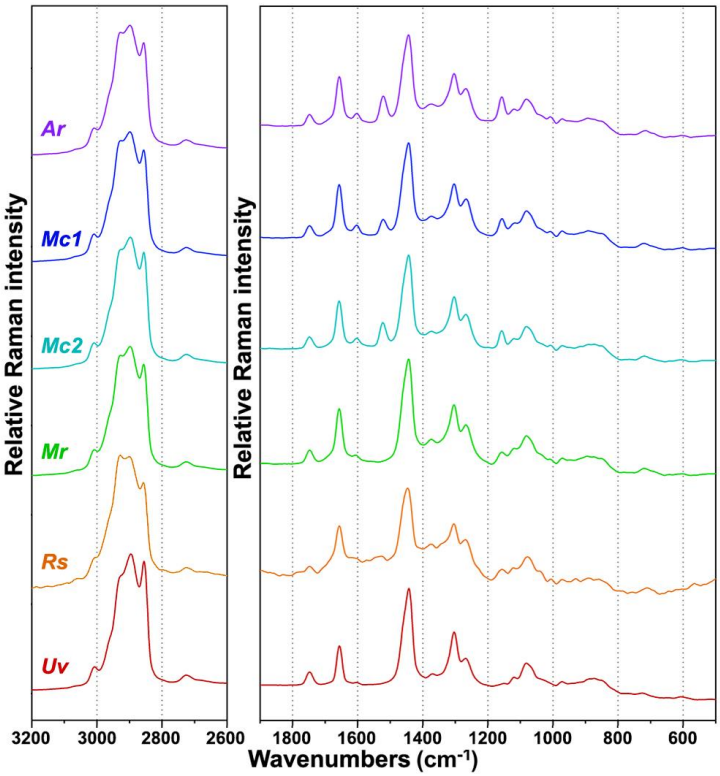

Figure 4. FT-Raman spectra of Mucoromycota oleaginous filamentous fungi cultivated under the standard growth condition (Ca1 and Pi1): *Amylomyces rouxii* (*Ar*), *Mucor circinelloides* VI 04473 (*Mc1*), *Mucor circinelloides* FRR 5020 (*Mc2*), *Mucor racemosus* (*Mr*), *Rhizopus stolonifer* (*Rs*), and *Umbelopsis vinacea* (*Uv*). All spectra were preprocessed and plotted with offset for better viewing.

To analyse reproducibility of measurements, we used Pearson correlation coefficients (PCC) calculated for each set of the three technical replicates of FT-Raman spectra. The coefficient measures correlation between variables, where PCC value of 1 indicates high positive correlation. Therefore, small variability is indicated by small 1-PCC values. As expected, the analysis result shows that samples exhibiting heating effect, which were measured with lower laser power, have lower reproducibility (Figure S2 in the Supplemental Materials). Nevertheless, it can be concluded that all six fungal strains were successfully measured by FT-Raman, even the highly challenging ones. In general, optimisation of measurement parameters is needed when fluorescence and heating effects are present, in particular, excitation laser power and number of scans, in order to acquire quality spectra.

FT-Raman spectra contain rich information on intracellular metabolites (Figure 5). The detailed overview of characteristic Raman bands of main components of fungal biomass is presented in Table 1, alongside the characteristic infrared bands. In general, the most intensive Raman bands are associated

with triglyceride lipids: C−H stretching vibrations (=C−H stretching at 3008 cm^{-1}; C−H stretching in -CH_3 and -CH_2 at 2933, 2895 and 2855 cm^{-1}), C=O stretching in esters (1750 cm^{-1}), C=C stretching (1660 cm^{-1}), CH_2 and CH_3 deformations (1460-1440, and 1305 cm^{-1}), and C−C and C−O stretching (1080-1060 cm^{-1}). In addition to the lipid-related bands, the samples show Raman bands related to cell wall carbohydrates, namely glucosamines (chitin and chitosan), glucans and glucuronans: C− H stretching vibrations (C−H stretching in -CH_3 and -CH_2 at 2933, 2895 and 2885 cm^{-1}), C=O stretching in esters (1755 cm^{-1}, glucuronans) and amides (1680-1620 cm^{-1}, Amide I, chitin), NH_2 deformations (1620-1570 cm^{-1}), CH_2 and CH_3 deformations (1460-1440, 1380-1320 cm^{-1}), C-C, C-O, C-O-C, C-N, CH, COH stretching, deformations and combination bands (1260-700 cm^{-1}). Furthermore, minor spectral contributions are related to vibrations of proteins: C=O stretching in amides (1660 cm^{-1}, Amide I), NH_2 deformations (1620-1580 cm^{-1}), phenyl ring C=C stretching (1605 cm^{-1}) and deformations (1005 cm^{-1}) in tyrosine and phenylalanine, CH_2 and CH_3 deformations (1460-1440 cm^{-1}), and C-N-H deformations (1310-1250 cm^{-1}, Amide III). The spectral bands associated with polyphosphates, namely P=O stretching (1165 cm^{-1}) and P−O−P stretching (685 cm^{-1}), are weak and barely visible in the FT-Raman spectra. This is in stark contrast to the similar bands in the FTIR spectra (at 1263 and 885 cm^{-1}, respectively) that show strong absorbance.

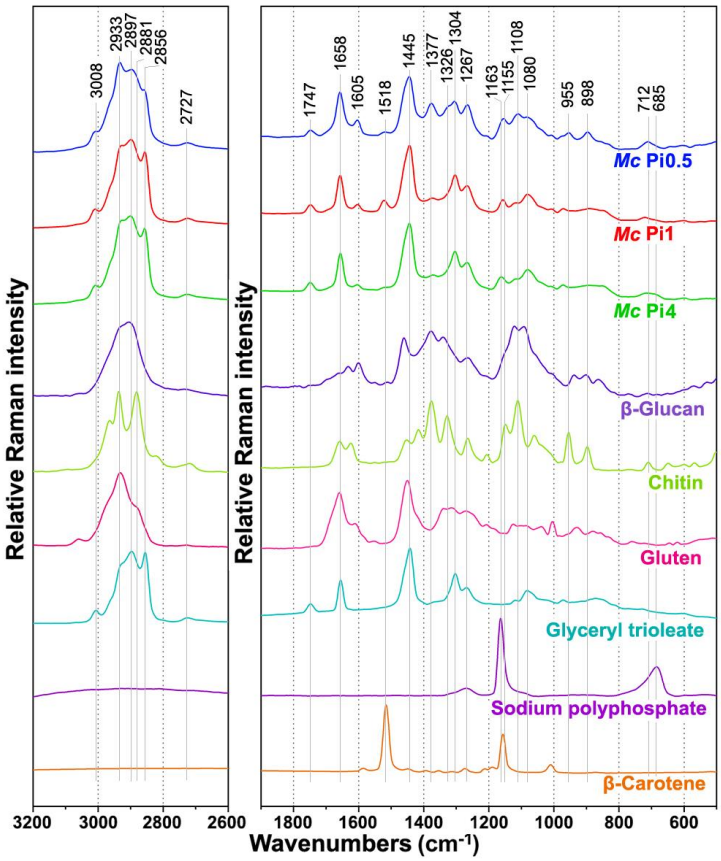

Figure 5. FT-Raman spectra of *Mucor circinelloides* (*Mc*) strain VI 04473 cultivated under Ca1 conditions and three different phosphate concentrations, and of six reference compounds: β-glucan, chitin, gluten, glyceryl trioleate, sodium polyphosphate, and β-carotene. All spectra were preprocessed and plotted with offset for better viewing.

Table 1. Assignments of infrared and Raman bands: str. – stretching, def. – deformation [30-32,37,52,65,78,79].

Cell component	Infrared		Raman	
	Wavenumbers (cm^{-1})	**Molecular vibration**	**Wavenumbers (cm^{-1})**	**Molecular vibration**
Carbohydrates (glucosamines, glucans, glucuronans)	3300	O-H str.	2933 and 2895	-C-H str. (CH_3)
	3400-3100	N-H str., N-H_2 str.	2855	-C-H str. (CH_2, glucan)
	2879	-C-H str. (CH_3)	1680-1620	-C=O str. (Amide I, chitin)
	1730	-C=O str. (glucuronans)	1755	-C=O str. (glucuronan)
	1680-1620	-C=O str. (Amide I, chitin)	1620-1570	NH_2 def. (chitosan)
	1600-1550	NH_2 def. (chitosan)	1460-1440	CH_2 and CH_3 def.
	1554	C-N str. & NH def. (Amide II, chitin)	1377	CH_2, CH, COH def.
	1375	-CH_3 def.	1327	CH_2, CH, COH def.
	1305	C-N-H def. (Amide III, chitin)	1256	C-C, C-O, CH, CH_2
	1200-1000	C-O-C str., COH def. COC def.	1200-1150	C-O-C str.
	950	-CH_3 def.	1050-1150	C-N str. & C-C str.
			950-850	C-C str, C-O-C str. & def., COH def.
			715	O-C-O str. & CH def.
Acylglycerol lipids (triglycerides)	3010	=C-H str.	3008	=C-H str.
	2921	-C-H str. (CH_3)	2933 and 2895	-C-H str. (CH_3)
	2852	-C-H str. (CH_2)	2855	-C-H str. (CH_2)
	1743	-C=O str.	1750	C=O str.
	1463	-CH_2 def.	1660	C=C str.
	1160	C-O-C str.	1460-1440	CH_2 and CH_3 def.
	723	-CH_2 def.	1305	CH_2 def.
			1080-1060	C-C str. C-O str.
Polyphosphates	1263	P=O str (PO_2^-)	1165	P=O str. (PO_2^-)
	885	P-O-P str.	685	P-O-P str.
Proteins	1680-1630	-C=O str. (Amide I)	1660	-C=O str. (Amide I)
	1560-1530	C-N-H def. (Amide II)	1620-1580	NH_2 def.
	1310-1250	C-N-H def. (Amide III)	1605	C=C str. (phenyl ring)
			1460-1440	CH_2 and CH_3 def.
			1310-1250	C-N-H def. (Amide III)
			1005	phenyl ring def.
Carotenoids	*Not detectable at concentrations present in fungal biomass*		1525	C=C str. (polyene chain)
			1155	C-C str. & CH def.
			1005	C-CH_3 def.

Unlike in FTIR spectra (Figure S1), where phosphate accumulation in fungal biomass is very noticeable thanks to strong phosphate-related IR bands [64], phosphate accumulation in FT-Raman spectra is less noticeable. Nevertheless, these weak phosphate-related Raman bands, at 1163 and 685 cm^{-1}, can be detected in the FT-Raman spectra (Figure 6a). As mentioned previously, calcium is directly involved in chitin synthesis, and thus strains cultivated in the absence of calcium show significantly lower chitin-related signals in Raman spectra when compared to their counterparts cultivated under normal calcium conditions. This is especially noticeable for samples grown under low phosphate conditions that show overexpression of chitin production as a result of acidic conditions, as exemplified by *Mucor circinelloides* strain VI 04473 (Figure 6b).

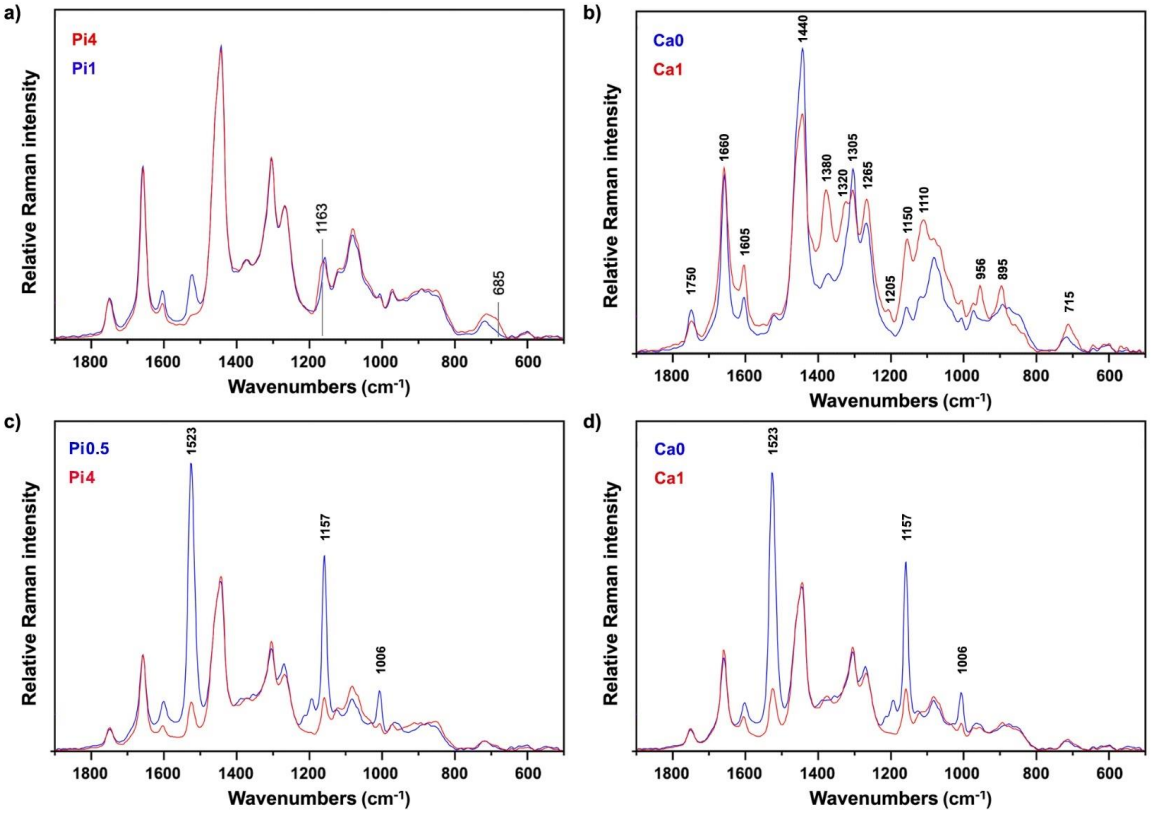

Figure 6. Influence of growth conditions on FT-Raman spectra of fungal biomass. Preprocessed FT-Raman spectra of: (a) *Mucor circinelloides* strain VI 04473 cultivated under reference calcium condition (Ca1) and two different phosphate concentrations, (b) *Mucor circinelloides* strain VI 04473 cultivated under low phosphates (Pi0.5) and two different calcium conditions (Ca0 and Ca1), (c) *Mucor circinelloides* strain FRR 5020 cultivated under absence of calcium (Ca0) and two different phosphate conditions (Pi0.5 and Pi4), (d) *Mucor circinelloides* strain FRR 5020 cultivated under low phosphates (Pi0.5) and two different calcium conditions (Ca0 and Ca1).

Compared to FTIR spectra of fungal biomass (Figure S1), FT-Raman spectra provide information on one additional group of chemicals: carotenoid pigments. These chemicals cannot be measured by FTIR due to their low concentration in fungal biomass. However, they can be measured with FT-Raman spectroscopy because carotenoids exhibit resonance Raman effect. In carotenoids, the conjugated nature of p-electrons from the polyene backbone causes electronic states of lower energy. Because of this, carotenoids often have absorption in the visible part of the spectrum, and they usually display strong yellow, orange and red colours (Figure 2). The resonant Raman effect causes strong enhancement of vibrational bands in carotenoids, in particular those at 1525 cm^{-1} (related to -C=C- stretching), 1155 cm^{-1} (related to -C-C- stretching and CH deformation), and 1005 cm^{-1} (related to C-CH_3 deformations) that have strong electronphonon coupling [79]. Out of the six studied strains, three strains show strong signals related to carotenoids: *Amylomyces rouxii* and the two *Mucor circinelloides* strains (Figure 4). These Raman bands can be used to assess influence of growth conditions on carotenoid production, and we have assessed them via regression analysis based on reference carotenoid measurements (Figure 2). As visible from Figures 6c and 6d, high carotenoid bands are present in FT-Raman spectra of biomass of *Mucor circinelloides* strain FRR 5020 grown in media with low phosphate concentrations and in the absence of calcium. Compared to *Mucor circinelloides* strain VI 04473, that shows overexpression of chitin, it is likely that *Mucor circinelloides* strain FRR 5020 is coping with acidic stress in absence of calcium by overexpression of carotenoids. This is consistent with a number of studies that have shown stress related overexpression of carotenoids in filamentous fungi [80].

In order to obtain general assessment of spectral variances within the whole FT-Raman spectral set, multivariate data analysis was conducted. Both FTIR and FT-Raman data are multivariate data with high collinearity. Therefore, methods based on latent variables, such as principal component analysis and partial least square regression are often used to process such data. In PCA, graphical representations of correlations between samples, principal components, and wavenumbers allow visual detection of groups of related samples (in this case, based on sample strains and growth conditions) and consequent identification of major spectral features that are causing this differentiation. The PCA of FT-Raman data shows that the predominant spectral differences are the result of variations of bands associated with lipids, carotenoids, and cell wall carbohydrates (Figure 7). The PCA plots have high factor loadings associated with carotenoids at 1523, 1159, and 1006 cm^{-1} (positive loadings in PC1 and PC2, and negative loadings in PC3), lipids at 2897, 2853, 1750, 1440, and 1303 cm^{-1} (negative loadings in PC1), and cell wall carbohydrates (in particular chitin) at 2947, 1665, 1377, 1330, and 1109 cm^{-1} (positive loadings in PC1 and negative loadings in PC2). In particular, the signals associated with carotenoids dominate in the first three principal components. Therefore, it is evident that the FT-Raman spectral data provides complementary information to the FTIR data.

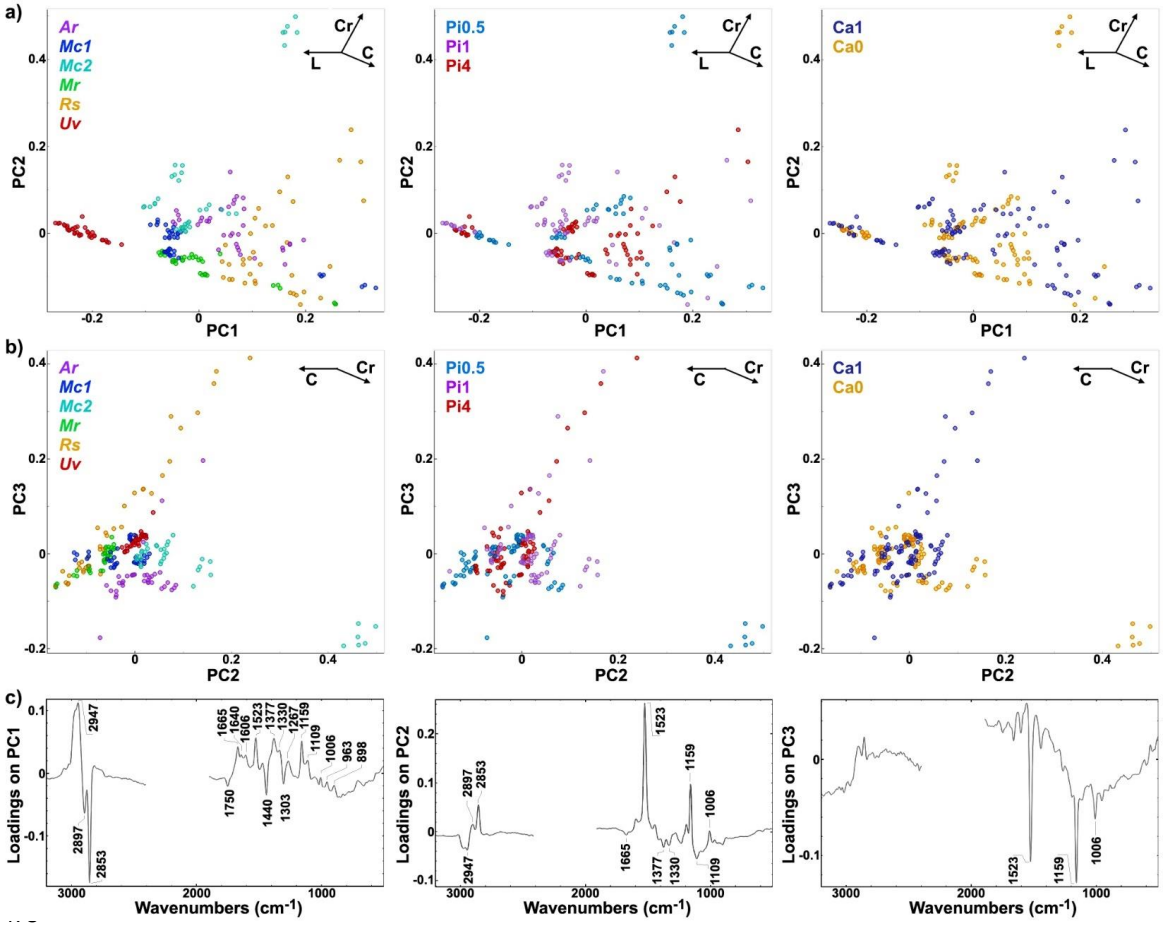

Figure 7. PCA of FT-Raman spectra of fungi grown at different phosphates and calcium concentrations. (a) Score plots of PC1 and PC2, and (b) PC2 and PC3, and (c) the first three loading vectors. Score plots are labelled according to strains: *Amylomyces rouxii* (*Ar*), *Mucor circinelloides* VI 04473 (*Mc1*), *Mucor circinelloides* FRR 5020 (*Mc2*), *Mucor racemosus* (*Mr*), *Rhizopus stolonifer* (*Rs*), and *Umbelopsis vinacea* (*Uv*) (left), phosphates concentrations (middle), and calcium availability (right). Vectors are approximating the increase in relative amount of the metabolites: lipids (L), cell wall carbohydrates (C), and carotenoids (Cr). The explained variances for the first five principal components are 47.3%, 26.9%, 15.8%, 3.8% and 1.4%.

Quantitative determination of chemical constituents of fungal biomass based on vibrational spectra

The influence of growth conditions on chemical composition of fungal biomass can be estimated by using Raman intensity ratios of Raman bands related to specific chemical constituents. Figure 8a shows that ratio of Raman intensities at 1747 cm^{-1} (related to lipids) and 1445 cm^{-1} (related to

total biomass) provides satisfactory estimate of total fungal lipids (compare to Figure 1). Ratio of Raman intensities at 1163 cm^{-1} (related to polyphosphates) and 1155 cm^{-1} (related to chitin) can be used to monitor accumulation of polyphosphates (Figure 8b), while ratio of Raman intensities at 1523 cm^{-1} (related to carotenoids) and 1445 cm^{-1} (related to total biomass) can be used to monitor production of carotenoids (Figure 8c; compare to Figure 2).

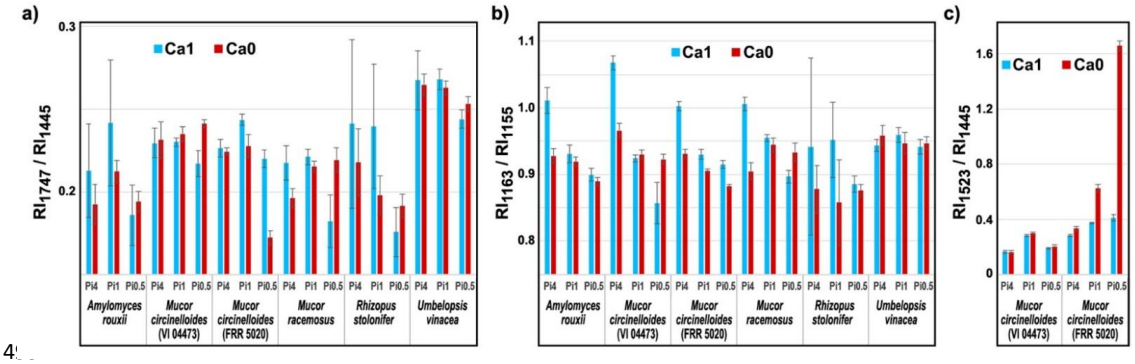

Figure 8. Ratio of Raman intensities at different wavenumbers related to chemical constituents of fungal biomass cultivated in six different growth conditions (phosphates concentrations and calcium availability). Ratio of Raman intensities at: (a) 1747 and 1445 cm^{-1} related to lipids, (b) 1163 and 1155 cm^{-1} related to polyphosphates, and (c) 1523 and 1445 cm^{-1} related to carotenoids (average values and error is based on measurements of two biological replicates and three technical replicates). Analysis was based on nonderivative FT-Raman data.

We have demonstrated previously that PLSR of FTIR data can provide accurate assessments of intra- and extracellular fungal metabolites [51]. Therefore, quantitative estimates of total lipids, total phosphorus, and carotenoids in the fungal biomass were obtained by PLSR analyses of FT-Raman and FTIR data. The results show high level of correlation between the vibrational data and referent measurements (Tables 2 and 3). The RMSE values for assessment of total lipids by FT-Raman are approx. 10% for the PLSR models based on all six strains, and approx. 8% for the models based on *Mucor* strains (Table 2). Similar results were obtained for FTIR-based PLSR models (Table 3), further corroborating our previous findings that FTIR spectroscopy is a practical method for quantitative analysis of total lipids in fungal biomass [50]. In general, the levels of accuracy achieved by vibrational spectroscopy PLSR models are similar to accuracy achieved by the reference method involving extraction, transesterification and chromatography.

Table 2. PLSR coefficients of determination (R^2) and root mean square errors (RMSE) for determination of total lipids, phosphorus and carotenoids, with the number of components in parenthesis (*Aopt*), for the regression analyses based on nonderivative and derivative preprocessed FT-Raman data.

Analysis	Range	Nonderivative		Derivative	
		R^2 (*Aopt*)	RMSE	R^2 (*Aopt*)	RMSE
Total lipids (6 strains)	19.42-87.13 $\%_{dry\ weight}$	0.83 (5)	6.60 $\%_{dry\ weight}$	0.75 (3)	8.06 $\%_{dry\ weight}$
Total lipids (*Mucor*)	19.42-55.57 $\%_{dry\ weight}$	0.88 (5)	2.94 $\%_{dry\ weight}$	0.88 (5)	2.90 $\%_{dry\ weight}$
Total phosphorus (6 strains)	0.64-6.24 $\%_{dry\ weight}$	0.86 (7)	0.50 $\%_{dry\ weight}$	0.79 (5)	0.60 $\%_{dry\ weight}$
Total phosphorus (*Mucor*)	1.40-5.20 $\%_{dry\ weight}$	0.89 (6)	0.38 $\%_{dry\ weight}$	0.89 (5)	0.37 $\%_{dry\ weight}$
Total carotenoids	10.21-1669.88 $\mu g/g_{dry\ weight}$	0.84 (1)	134.69 $\mu g/g_{dry\ weight}$	0.84 (2)	137.34 $\mu g/g_{dry\ weight}$

Moreover, the RMSE values for assessment of total phosphorus by FT-Raman are approx. 10% for the PLSR models based on all six strains and on *Mucor* strains (Table 2). Similar results are obtained for PLSR models based on FTIR data (Table 3). Finally, the RMSE values for assessment of total carotenoids by FT-Raman are approx. 8% for the PLSR models based on the two *Mucor circinelloides* strains (Table 2). The application of Raman spectroscopy for monitoring of carotenoids was hypothesised a decade ago, with preliminary studies on filamentous fungi *Blakeslea trispora* [23], and our results certainly confirm that quantitative analysis of total carotenoids is feasible by FT-Raman spectroscopy. The PLSR models for assessment of total carotenoids by FTIR were unstable, with large difference between prediction values of model and validation data. This is unsurprising considering that direct detection of such small content of carotenoids by FT-Raman spectroscopy was only achieved because of Resonant Raman effect, and the corresponding phenomena is not present in FTIR spectroscopy.

Table 3. PLSR coefficients of determination (R^2) and root mean square errors (RMSE) for determination of total lipids and phosphorus, with the number of components in parenthesis (*Aopt*), for the regression analyses based on nonderivative and derivative preprocessed FTIR data.

Analysis	Range	Nonderivative		Derivative	
		R^2 (*Aopt*)	RMSE	R^2 (*Aopt*)	RMSE
Total lipids (6 strains)	19.42-87.13 $\%_{dry\ weight}$	0.86 (2)	6.02 $\%_{dry\ weight}$	0.85 (8)	6.12 $\%_{dry\ weight}$
Total lipids (*Mucor*)	19.42-55.57 $\%_{dry\ weight}$	0.79 (7)	3.93 $\%_{dry\ weight}$	0.82 (5)	3.59 $\%_{dry\ weight}$
Total phosphorus (6 strains)	0.64-6.24 $\%_{dry\ weight}$	0.87 (9)	0.47 $\%_{dry\ weight}$	0.84 (5)	0.53 $\%_{dry\ weight}$
Total phosphorus (*Mucor*)	1.40-5.20 $\%_{dry\ weight}$	0.94 (6)	0.29 $\%_{dry\ weight}$	0.84 (4)	0.46 $\%_{dry\ weight}$

The number of components (PLS factors) used for building the PLSR models for both type of preprocessed FT-Raman data was low, indicating high stability and reliability of the developed models. The PLS factors clearly show contributions of relevant spectral signals, specifically signals related to

lipids, polyphosphates, and carotenoids (Figures S3-S5 in the Supplemental Materials). Moreover, it can be assumed that large part of error of the PLS models is a result of measurement error in the reference data, and not spectral data. It is important to notice that all reference methods require large amount of biomass sample and several time-consuming processing steps involving wet chemistry. In comparison, vibrational spectroscopy methods are extremely fast and simple to implement.

Multiblock and analysis of spectral variation by ANOVA model of FTIR and FT-Raman data

After averaging of technical replicates, FTIR and FT-Raman spectral sets can be analysed as a multiblock data with a sample-to-sample correspondence between the data blocks. Consensus Principal Component analysis (CPCA) is a frequently used multi-block data analysis method since it allows assessment of the co-variance patterns using more than one block of data [60,81]. CPCA provides global scores that describe the consensus of all data blocks involved in the CPCA. In addition, block scores and block loadings are calculated, showing individual sample and variable variation patterns for each block. Analysis of individual block scores and global scores, as well as block loadings, provides assessment of variation patterns and the molecular insights, related to sample chemistry, obtained by each of the two vibrational spectroscopic techniques (Figure 9 and Figure S6 in the Supplementary Materials). The global scores are presented in Figure 8, and they show that the main variance is predominantly driven by variance in the FT-Raman data. The first two loadings in FTIR data block are highly correlated. Similar result, with high correlation of loadings, was presented previously on simulated data [82]. Such effect is caused by similar variable variation patterns in one data block, while the second block shows different effect of underlying parameters on the variable variation pattern. In our study, the reason for this is high variation in the data caused by carotenoids, which dominate variation in FT-Raman data, and are undetectable by FTIR spectroscopy. Thus, the CPCA results clearly show that FT-Raman spectra reveal additional level of chemical information about fungal biomass that is not present in FTIR data.

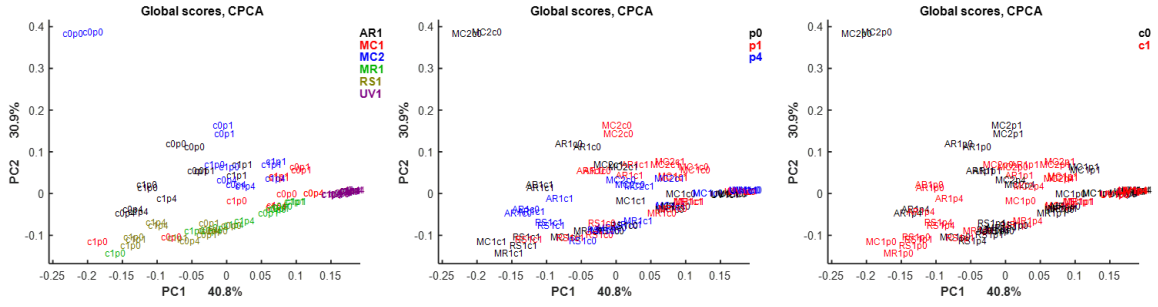

Figure 9. Multiblock or consensus principal component analysis (CPCA) of FTIR and FT-Raman spectroscopic data. Global score values of the CPCA are labelled according to strains: *Amylomyces rouxii* (*Ar*), *Mucor circinelloides* VI 04473 (*Mc1*), *Mucor circinelloides* FRR 5020 (*Mc2*), *Mucor*

racemosus (*Mr*), *Rhizopus stolonifer* (*Rs*), and *Umbelopsis vinacea* (*Uv*) (left), phosphates concentrations (middle), and calcium availability (right).

Both spectral data sets show that phosphate concentrations have the biggest influence on the variation of biochemical profile of fungal biomass (Figure 10). This is probably related not only to the intracellular accumulation of phosphorus in the form of polyphosphates, but also to the influence of phosphate concentration on the pH of the growth media, as discussed in our previous studies [49,64,68,73]. Since the phosphate-related signals (P=O and P-O-P stretching bands) are much more prominent in the FTIR spectra than in the FT-Raman spectra (Figure 4 and Figure S02 in the Supplementary Material), the contribution of phosphates is higher in FTIR dataset for strains that have significant accumulation of polyphosphates, such as *Mucor circinelloides* strain VI 04473. In general, higher contribution of calcium-phosphates interaction is present in FT-Raman data than in FTIR. Possible explanation is relatively high sensitivity of FT-Raman to detection of changes in the chemical composition of cell wall polysaccharides and pigments, the two type of chemical constituents that are affected by both calcium and phosphates. Amongst the six cultivated strains, *Rhizopus stolonifer* was the least sensitive to different cultivation conditions (Figure 1 and [64]). Due to sporulation under higher phosphate concentrations, and the associated problems with acquiring reproducible FT-Raman spectra, this strain shows the highest residual variability in FT-Raman data. *Amylomyces rouxii* and *Mucor circinelloides* strain FRR 5020 have relatively high calcium-dependent production of carotenoid pigments (Figure 2). Since carotenoids have strong signals in FT-Raman spectra, the spectral variation due to calcium availability is higher in FT-Raman than in FTIR data. Of all the studied strains, *Umbelopsis vinacea* was able to accumulate by far the highest content of lipids. On the other hand, this strain shows no significant production of pigments and chitin/chitosan, nor accumulation of polyphosphates. Since lipid accumulation is predominantly affected by phosphates concentration, this design parameter had the highest contribution into variation in spectra of this strain in both FTIR and FT-Raman data. *Mucor racemosus* and *Mucor circinelloides* strain VI 04473 show relatively similar variation contribution profiles due to different design parameters in both spectral data sets. *Mucor circinelloides* strain VI 04473 is quite unique amongst the six cultivated strains due to significant change in polyphosphate, lipid, pigment accumulation, as well as cell wall chemistry, as a result of phosphate and calcium concentrations modifications. For this strain in particular, both FTIR and FT-Raman data provide valuable contribution in discerning the complex changes in biomass chemistry.

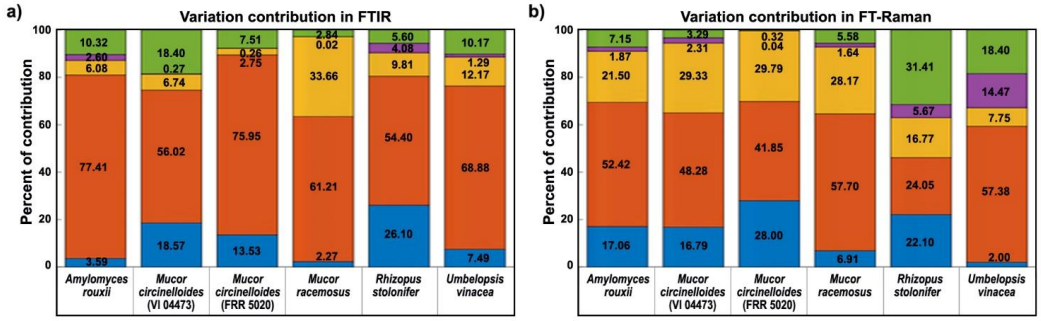

Figure 10. Variation contribution (%) of the design factors in FTIR and FT-Raman data sets. Spectral variation from calcium availability (blue), phosphates concentration (red), calcium-phosphates interaction (yellow), biological replicates (purple), and residuals (green) in: (a) FTIR, and (b) FT-Raman spectral data (nonderivative data, averaged technical replicates).

CONCLUSIONS

The study, conducted on six strains of Mucoromycota filamentous fungi, demonstrates that quality Raman spectra of fungal biomass can be acquired by FT-Raman spectroscopy. In case of sample heating and fluorescence, optimisation of excitation laser power and number of scans is needed to reduce noise and baseline interference. FT-Raman spectra are rich in chemical information and provide data on all main chemical constituents of fungal biomass, including acylglycerol lipids, proteins, cell wall carbohydrates (glucosamines, glucans, and glucuronans), and polyphosphates. In addition, resonant Raman effect enables detection of biomass constituents generally present in low concentrations, namely carotenoids. Effects of growth conditions (phosphorus concentration and calcium availability) on fungal biomass were clearly detectable by FT-Raman spectroscopy. Detection of fungal carotenoids, obtainable by FT-Raman and unattainable by FTIR spectroscopy, is the main difference between the two vibrational spectroscopy methods. Further, the sensitivity of the two methods in detection of other chemical constituents varies; For example, polyphosphates and proteins have strong bands in FTIR spectra, and relatively weak bands in Raman spectra. PLSR models based on FT-Raman and FTIR data were established for quantitative determination of total lipids, phosphates and carotenoids. The results of PLSR analyses indicate that these vibrational spectroscopies, in combination with multivariate regression models, could be utilised as a simple, rapid and non-destructive method for quantitative assessment of phosphorus (polyphosphates) and lipids (both FTIR and FT-Raman), as well as carotenoids (only FT-Raman), in intact fungal biomass.

Funding

The study was funded by the Research Council of Norway - FMETEKN Grant, project number 257622, BIONÆR Grant, projects number 268305 and 305215, HAVBRUK2 Grant, project number 302543, MATFONDAVTALE Grant, project number 301834 and IS-DAAD Grant, project number 309220.

Author Contributions

Conceived the research idea: AK, BZ, VS. Designed the experiments: BZ, SD, VS. Methodology: BZ. Performed the growth experiments: SD. Conducted FT-Raman measurements: BZ. Conducted FTIR measurements: SD. Conducted carotenoid analysis: DB, MS. Analysed the data: BZ, SD, VT. Discussed the results: AK, BZ, SD, VS, VT. Wrote the manuscript: BZ. Discussed and revised the manuscript: AK, BZ, DB, IM, MS, SD, VS, VT. All authors read and approved the final manuscript.

Data Availability

The data generated for this study are available in the Supplementary materials

SUPPLEMENTARY MATERIALS

Figure S1. FTIR spectra of fungal biomass

Figure S2. Reproducibility analysis of FT-Raman spectra

Figure S3. PLSR coefficients for determination of total lipids

Figure S4. PLSR coefficients for determination of total phosphorus

Figure S5. PLSR coefficient for determination of total carotenoids

Figure S6. CPCA score and loading plots for individual blocks

References:

1. Meyer, V.; Basenko, E.Y.; Benz, J.P.; Braus, G.H.; Caddick, M.X.; Csukai, M.; de Vries, R.P.; Endy, D.; Frisvad, J.C.; Gunde-Cimerman, N., et al. Growing a circular economy with fungal biotechnology: a white paper. *Fungal Biology and Biotechnology* **2020**, *7*, 5, doi:10.1186/s40694-020-00095-z.
2. Meyer, V.; Andersen, M.R.; Brakhage, A.A.; Braus, G.H.; Caddick, M.X.; Cairns, T.C.; de Vries, R.P.; Haarmann, T.; Hansen, K.; Hertz-Fowler, C., et al. Current challenges of research on filamentous fungi in relation to human welfare and a sustainable bio-economy: a white paper. *Fungal Biology and Biotechnology* **2016**, *3*, 6, doi:10.1186/s40694-016-0024-8.
3. Gupta, V.K.; Treichel, H.; Shapaval, V.; Oliveira, L.A.d.; Tuohy, M.G. Microbial functional foods and nutraceuticals. John Wiley & Sons,: Hoboken, NJ, 2017; p 1 online resource.
4. Papanikolaou, S.; Galiotou-Panayotou, M.; Fakas, S.; Komaitis, M.; Aggelis, G. Lipid production by oleaginous Mucorales cultivated on renewable carbon sources. *Eur J Lipid Sci Tech* **2007**, *109*, 1060-1070, doi:10.1002/ejlt.200700169.

5. Qiao, W.C.; Tao, J.Q.; Luo, Y.; Tang, T.H.; Miao, J.H.; Yang, Q.W. Microbial oil production from solid-state fermentation by a newly isolated oleaginous fungus, *Mucor circinelloides* Q531 from mulberry branches. *Roy Soc Open Sci* **2018**, *5*, doi:ARTN 180551 10.1098/rsos.180551.
6. Meng, X.; Yang, J.M.; Xu, X.; Zhang, L.; Nie, Q.J.; Xian, M. Biodiesel production from oleaginous microorganisms. *Renew Energ* **2009**, *34*, 1-5, doi:10.1016/j.renene.2008.04.014.
7. Formenti, L.R.; Norregaard, A.; Bolic, A.; Hernandez, D.Q.; Hagemann, T.; Heins, A.L.; Larsson, H.; Mears, L.; Mauricio-Iglesias, M.; Kruhne, U., et al. Challenges in industrial fermentation technology research. *Biotechnol J* **2014**, *9*, 727-738.
8. Kuhar, N.; Sil, S.; Verma, T.; Umapathy, S. Challenges in application of Raman spectroscopy to biology and materials. *Rsc Adv* **2018**, *8*, 25888-25908.
9. Baker, M.J.; Trevisan, J.; Bassan, P.; Bhargava, R.; Butler, H.J.; Dorling, K.M.; Fielden, P.R.; Fogarty, S.W.; Fullwood, N.J.; Heys, K.A., et al. Using Fourier transform IR spectroscopy to analyze biological materials. *Nat Protoc* **2014**, *9*, 1771-1791.
10. Tafintseva, V.; Shapaval, V.; Smirnova, M.; Kohler, A. Extended multiplicative signal correction for FTIR spectral quality test and pre-processing of infrared imaging data. *J Biophotonics* **2020**, *13*.
11. Tahir, H.E.; Zou, X.B.; Xiao, J.B.; Mahunu, G.K.; Shi, J.Y.; Xu, J.L.; Sun, D.W. Recent Progress in Rapid Analyses of Vitamins, Phenolic, and Volatile Compounds in Foods Using Vibrational Spectroscopy Combined with Chemometrics: a Review. *Food Anal Method* **2019**, *12*, 2361-2382.
12. Biancolillo, A.; Marini, F. Chemometric Methods for Spectroscopy-Based Pharmaceutical Analysis. *Front Chem* **2018**, *6*.
13. Salzer, R.; Siesler, H.W. *Infrared and Raman spectroscopic imaging*; Wiley-VCH: Weinheim, 2009; pp. xx, 510 p.
14. Tafintseva, V.; Vigneau, E.; Shapaval, V.; Cariou, V.; Qannari, E.; Kohler, A. Hierarchical classification of microorganisms based on high-dimensional phenotypic data. *J Biophotonics* **2018**, *11*.
15. Zhang, X.L.; Lin, T.; Xu, J.F.; Luo, X.; Ying, Y.B. DeepSpectra: An end-to-end deep learning approach for quantitative spectral analysis. *Anal Chim Acta* **2019**, *1058*, 48-57.
16. Liland, K.H.; Kohler, A.; Shapaval, V. Hot PLS-a framework for hierarchically ordered taxonomic classification by partial least squares. *Chemometr Intell Lab* **2014**, *138*, 41-47.
17. Cannizzaro, C.; Rhiel, M.; Marison, I.; von Stockar, U. On-line monitoring of Phaffia rhodozyma fed-batch process with in situ dispersive Raman spectroscopy. *Biotechnol Bioeng* **2003**, *83*, 668-680, doi:DOI 10.1002/bit.10698.
18. Horiue, H.; Sasaki, M.; Yoshikawa, Y.; Toyofuku, M.; Shigeto, S. Raman spectroscopic signatures of carotenoids and polyenes enable label-free visualization of microbial distributions within pink biofilms. *Sci Rep-Uk* **2020**, *10*, doi:10.1038/s41598-020-64737-3.
19. Tauber, J.P.; Matthaus, C.; Lenz, C.; Hoffmeister, D.; Popp, J. Analysis of basidiomycete pigments in situ by Raman spectroscopy. *J Biophotonics* **2018**, *11*, doi:10.1002/jbio.201700369.
20. Li, F.W.; Xue, F.; Yu, X.H. GC-MS, FTIR and Raman Analysis of Antioxidant Components of Red Pigments from *Stemphylium lycopersici*. *Curr Microbiol* **2017**, *74*, 532-539, doi:10.1007/s00284-017-1220-3.

21. Li, K.; Cheng, J.; Ye, Q.; He, Y.; Zhou, J.H.; Cen, K.F. In vivo kinetics of lipids and astaxanthin evolution in *Haematococcus pluvialis* mutant under 15% CO2 using Raman microspectroscopy. *Bioresource Technol* **2017**, *244*, 1439-1444, doi:10.1016/j.biortech.2017.04.116.
22. de Oliveira, L.F.C.; Le Hyaric, M.; Berg, M.M.; de Almeida, M.V.; Edwards, H.G.M. Raman spectroscopic characterization of cinnabarin produced by the fungus *Pycnoporus sanguineus* (Fr.) Murr. *J Raman Spectrosc* **2007**, *38*, 1628-1632, doi:10.1002/jrs.1881.
23. Papaioannou, E.H.; Liakopoulou-Kyriakides, M.; Christofilos, D.; Arvanitidis, I.; Kourouklis, G. Raman Spectroscopy for Intracellular Monitoring of Carotenoid in Blakeslea trispora. *Appl Biochem Biotech* **2009**, *159*, 478-487, doi:10.1007/s12010-008-8472-0.
24. Culka, A.; Jehlicka, J.; Ascaso, C.; Artieda, O.; Casero, C.M.; Wierzchos, J. Raman microspectrometric study of pigments in melanized fungi from the hyperarid Atacama desert gypsum crust. *J Raman Spectrosc* **2017**, *48*, 1487-1493, doi:10.1002/jrs.5137.
25. Arcangeli, C.; Cannistraro, S. In situ Raman microspectroscopic identification and localization of carotenoids: Approach to monitoring of UV-B irradiation stress on antarctic fungus. *Biopolymers* **2000**, *57*, 179-186, doi:Doi 10.1002/(Sici)1097-0282(2000)57:3<179::Aid-Bip6>3.3.Co;2-W.
26. Munchberg, U.; Wagner, L.; Spielberg, E.T.; Voigt, K.; Rosch, P.; Popp, J. Spatially resolved investigation of the oil composition in single intact hyphae of *Mortierella* spp. with micro-Raman spectroscopy. *Bba-Mol Cell Biol L* **2013**, *1831*, 341-349, doi:10.1016/j.bbalip.2012.09.015.
27. Chiu, Y.F.; Huang, C.K.; Shigeto, S. In Vivo Probing of the Temperature Responses of Intracellular Biomolecules in Yeast Cells by Label-Free Raman Microspectroscopy. *Chembiochem* **2013**, *14*, 1001-1005, doi:10.1002/cbic.201300096.
28. Munchberg, U.; Wagner, L.; Rohrer, C.; Voigt, K.; Rosch, P.; Jahreis, G.; Popp, J. Quantitative assessment of the degree of lipid unsaturation in intact *Mortierella* by Raman microspectroscopy. *Anal Bioanal Chem* **2015**, *407*, 3303-3311, doi:10.1007/s00216-015-8544-2.
29. Kochan, K.; Peng, H.D.; Gwee, E.S.H.; Izgorodina, E.; Haritos, V.; Wood, B.R. Raman spectroscopy as a tool for tracking cyclopropane fatty acids in genetically engineered *Saccharomyces cerevisiae*. *Analyst* **2019**, *144*, 901-912, doi:10.1039/c8an01477a.
30. Gherman, A.M.R.; Dina, N.E.; Chis, V.; Wieser, A.; Haisch, C. Yeast cell wall - Silver nanoparticles interaction: A synergistic approach between surface-enhanced Raman scattering and computational spectroscopy tools. *Spectrochim Acta A* **2019**, *222*, doi:ARTN 117223 10.1016/j.saa.2019.117223.
31. Noothalapati, H.; Sasaki, T.; Kaino, T.; Kawamukai, M.; Ando, M.; Hamaguchi, H.; Yamamoto, T. Label-free Chemical Imaging of Fungal Spore Walls by Raman Microscopy and Multivariate Curve Resolution Analysis. *Sci Rep-Uk* **2016**, *6*, doi:ARTN 27789 10.1038/srep27789.
32. Edwards, H.G.M.; Russell, N.C.; Weinstein, R.; Wynnwilliams, D.D. Fourier-Transform Raman-Spectroscopic Study of Fungi. *J Raman Spectrosc* **1995**, *26*, 911-916.
33. Esmonde-White, K.A.; Cuellar, M.; Uerpmann, C.; Lenain, B.; Lewis, I.R. Raman spectroscopy as a process analytical technology for pharmaceutical manufacturing and bioprocessing. *Anal Bioanal Chem* **2017**, *409*, 637-649.
34. De Gussem, K.; Vandenabeele, P.; Verbeken, A.; Moens, L. Raman spectroscopic study of Lactarius spores (Russulales, Fungi). *Spectrochim Acta A* **2005**, *61*, 2896-2908.

35. McGovern, A.C.; Broadhurst, D.; Taylor, J.; Kaderbhai, N.; Winson, M.K.; Small, D.A.; Rowland, J.J.; Kell, D.B.; Goodacre, R. Monitoring of complex industrial bioprocesses for metabolite concentrations using modern spectroscopies and machine learning: Application to gibberellic acid production. *Biotechnol Bioeng* **2002**, *78*, 527-538.

36. De Gussem, K.; Vandenabeele, P.; Verbeken, A.; Moens, L. Chemotaxonomical identification of spores of macrofungi: possibilities of Raman spectroscopy. *Anal Bioanal Chem* **2007**, *387*, 2823-2832, doi:10.1007/s00216-007-1150-1.

37. Meenu, M.; Xu, B.J. Application of vibrational spectroscopy for classification, authentication and quality analysis of mushroom: A concise review. *Food Chem* **2019**, *289*, 545-557, doi:10.1016/j.foodchem.2019.03.091.

38. Witkowska, E.; Jagielski, T.; Kaminska, A. Genus- and species-level identification of dermatophyte fungi by surface-enhanced Raman spectroscopy. *Spectrochim Acta A* **2018**, *192*, 285-290, doi:10.1016/j.saa.2017.11.008.

39. Dina, N.E.; Gherman, A.M.R.; Chis, V.; Sarbu, C.; Wieser, A.; Bauer, D.; Haisch, C. Characterization of Clinically Relevant Fungi via SERS Fingerprinting Assisted by Novel Chemometric Models. *Anal Chem* **2018**, *90*, 2484-2492, doi:10.1021/acs.analchem.7b03124.

40. Lee, C.M.; Cho, E.M.; Ochir, E.G.; Dembereldorj, U.; Yang, S.I. Chemotaxonomic Raman Spectroscopy Investigation of Ascomycetes and Zygomycetes. *B Korean Chem Soc* **2013**, *34*, 1240-1242, doi:10.5012/bkcs.2013.34.4.1240.

41. Baranska, M.; Roman, M.; Dobrowolski, J.C.; Schulz, H.; Baranski, R. Recent Advances in Raman Analysis of Plants: Alkaloids, Carotenoids, and Polyacetylenes. *Curr Anal Chem* **2013**, *9*, 108-127, doi:Doi 10.2174/157341113804486455.

42. Bowie, B.T.; Chase, D.B.; Griffiths, P.R. Factors affecting the performance of bench-top Raman spectrometers. Part II: Effect of sample. *Appl Spectrosc* **2000**, *54*, 200a-207a, doi:Doi 10.1366/0003702001950175.

43. Bowie, B.T.; Chase, D.B.; Griffiths, P.R. Factors affecting the performance of bench-top Raman spectrometers. Part I: Instrumental effects. *Appl Spectrosc* **2000**, *54*, 164a-173a, doi:Doi 10.1366/0003702001949924.

44. Moester, M.J.B.; Zada, L.; Fokker, B.; Ariese, F.; de Boer, J.F. Stimulated Raman scattering microscopy with long wavelengths for improved imaging depth. *J Raman Spectrosc* **2019**, *50*, 1321-1328, doi:10.1002/jrs.5494.

45. Boyaci, I.H.; Temiz, H.T.; Genis, H.E.; Soykut, E.A.; Yazgan, N.N.; Guven, B.; Uysal, R.S.; Bozkurt, A.G.; Ilaslan, K.; Torun, O., et al. Dispersive and FT-Raman spectroscopic methods in food analysis. *Rsc Adv* **2015**, *5*, 56606-56624.

46. He, H.R.; Sun, D.W.; Pu, H.B.; Chen, L.J.; Lin, L. Applications of Raman spectroscopic techniques for quality and safety evaluation of milk: A review of recent developments. *Crit Rev Food Sci* **2019**, *59*, 770-793.

47. Agarwal, U.P. 1064 nm FT-Raman spectroscopy for investigations of plant cell walls and other biomass materials. *Front Plant Sci* **2014**, *5*.

48. Kendel, A.; Zimmermann, B. Chemical Analysis of Pollen by FT-Raman and FTIR Spectroscopies. *Front Plant Sci* **2020**, *11*.

49. Dzurendova, S.; Zimmermann, B.; Kohler, A.; Tafintseva, V.; Slany, O.; Certik, M.; Shapaval, V. Microcultivation and FTIR spectroscopy-based screening revealed a nutrient-induced co-production of high-value metabolites in oleaginous Mucoromycota fungi. *PLoS One* **2020**, *15*, e0234870, doi:10.1371/journal.pone.0234870.

50. Kosa, G.; Kohler, A.; Tafintseva, V.; Zimmermann, B.; Forfang, K.; Afseth, N.K.; Tzimorotas, D.; Vuoristo, K.S.; Horn, S.J.; Mounier, J., et al. Microtiter plate cultivation of oleaginous fungi and monitoring of lipogenesis by high-throughput FTIR spectroscopy. *Microb Cell Fact* **2017**, *16*, doi:ARTN 101 10.1186/s12934-017-0716-7.

51. Kosa, G.; Shapaval, V.; Kohler, A.; Zimmermann, B. FTIR spectroscopy as a unified method for simultaneous analysis of intra- and extracellular metabolites in high-throughput screening of microbial bioprocesses. *Microb Cell Fact* **2017**, *16*, doi:ARTN 195 10.1186/s12934-017-0817-3.

52. Kosa, G.; Zimmermann, B.; Kohler, A.; Ekeberg, D.; Afseth, N.K.; Mounier, J.; Shapaval, V. High-throughput screening of Mucoromycota fungi for production of low- and high-value lipids. *Biotechnol Biofuels* **2018**, *11*, doi:ARTN 66 10.1186/s13068-018-1070-7.

53. Kavadia, A.; Komaitis, M.; Chevalot, I.; Blanchard, F.; Marc, I.; Aggelis, G. Lipid and γ-linolenic acid accumulation in strains of Zygomycetes growing on glucose. *Journal of the American Oil Chemists' Society* **2001**, *78*, 341-346.

54. Kosa, G.; Vuoristo, K.S.; Horn, S.J.; Zimmermann, B.; Afseth, N.K.; Kohler, A.; Shapaval, V. Assessment of the scalability of a microtiter plate system for screening of oleaginous microorganisms. *Appl Microbiol Biot* **2018**, *102*, 4915-4925.

55. Demsar, J.; Curk, T.; Erjavec, A.; Gorup, C.; Hocevar, T.; Milutinovic, M.; Mozina, M.; Polajnar, M.; Toplak, M.; Staric, A., et al. Orange: Data Mining Toolbox in Python. *J Mach Learn Res* **2013**, *14*, 2349-2353.

56. Toplak, M.; Birarda, G.; Read, S.; Sandt, C.; Rosendahl, S.M.; Vaccari, L.; Demšar, J.; Borondics, F. Infrared Orange: Connecting Hyperspectral Data with Machine Learning. *Synchrotron Radiation News* **2017**, *30*, 40-45, doi:10.1080/08940886.2017.1338424.

57. Guo, S.X.; Kohler, A.; Zimmermann, B.; Heinke, R.; Stockel, S.; Rosch, P.; Popp, J.; Bocklitz, T. Extended Multiplicative Signal Correction Based Model Transfer for Raman Spectroscopy in Biological Applications. *Anal Chem* **2018**, *90*, 9787-9795, doi:10.1021/acs.analchem.8b01536.

58. Zimmermann, B.; Kohler, A. Optimizing Savitzky-Golay Parameters for Improving Spectral Resolution and Quantification in Infrared Spectroscopy. *Appl Spectrosc* **2013**, *67*, 892-902.

59. Curtasu, M.V.; Tafintseva, V.; Bendiks, Z.A.; Marco, M.L.; Kohler, A.; Xu, Y.T.; Norskov, N.P.; Laerke, H.N.; Knudsen, K.E.B.; Hedemann, M.S. Obesity-Related Metabolome and Gut Microbiota Profiles of Juvenile Gottingen Minipigs-Long-Term Intake of Fructose and Resistant Starch. *Metabolites* **2020**, *10*.

60. Hassani, S.; Martens, H.; Qannari, E.M.; Hanafi, M.; Borge, G.I.; Kohler, A. Analysis of -omics data: Graphical interpretation- and validation tools in multi-block methods. *Chemometr Intell Lab* **2010**, *104*, 140-153.

61. Westerhuis, J.A.; Kourti, T.; MacGregor, J.F. Analysis of multiblock and hierarchical PCA and PLS models. *J Chemometr* **1998**, *12*, 301-321.
62. Harrington, P.D.; Vieira, N.E.; Espinoza, J.; Nien, J.K.; Romero, R.; Yergey, A.L. Analysis of variance-principal component analysis: A soft tool for proteomic discovery. *Anal Chim Acta* **2005**, *544*, 118-127.
63. Smilde, A.K.; Jansen, J.J.; Hoefsloot, H.C.J.; Lamers, R.J.A.N.; van der Greef, J.; Timmerman, M.E. ANOVA-simultaneous component analysis (ASCA): a new tool for analyzing designed metabolomics data. *Bioinformatics* **2005**, *21*, 3043-3048.
64. Dzurendova, S.Z., B.; Kohler, A.; Reitzel, K.; Gro Nielsen, U.; Dupuy--Galet, B.X.; Leivers, S. A.; Horn, S. J.; Shapaval, V. Calcium affects polyphosphate and lipid accumulation in Mucoromycota fungi. 2021.*Manuscript.*
65. Forfang, K.; Zimmermann, B.; Kosa, G.; Kohler, A.; Shapaval, V. FTIR Spectroscopy for Evaluation and Monitoring of Lipid Extraction Efficiency for Oleaginous Fungi. *Plos One* **2017**, *12*, doi:ARTN e017061110.1371/journal.pone.0170611.
66. Beever, R.E.; Burns, D.J.W. Phosphorus Uptake, Storage and Utilization by Fungi. In *Advances in Botanical Research*, Woolhouse, H.W., Ed. Academic Press: 1981; Vol. 8, pp. 127-219.
67. Ye, Y.L.; Gan, J.; Hu, B. Screening of Phosphorus-Accumulating Fungi and Their Potential for Phosphorus Removal from Waste Streams. *Appl Biochem Biotech* **2015**, *177*, 1127-1136.
68. Dzurendova, S.; Zimmermann, B.; Tafintseva, V.; Kohler, A.; Horn, S.J.; Shapaval, V. Metal and Phosphate Ions Show Remarkable Influence on the Biomass Production and Lipid Accumulation in Oleaginous *Mucor circinelloides*. *J Fungi (Basel)* **2020**, *6*, doi:10.3390/jof6040260.
69. Ramos, I.B.; Miranda, K.; Ulrich, P.; Ingram, P.; LeFurgey, A.; Machado, E.A.; de Souza, W.; Docampo, R. Calcium- and polyphosphate-containing acidocalcisomes in chicken egg yolk. *Biol Cell* **2010**, *102*, 421-434.
70. Fontaine, T.; Mouyna, I.; Hartland, R.P.; Paris, S.; Latge, J.P. From the surface to the inner layer of the fungal cell wall. *Biochem Soc T* **1997**, *25*, 194-199.
71. Cabib, E.; Bowers, B.; Sburlati, A.; Silverman, S.J. Fungal Cell-Wall Synthesis - the Construction of a Biological Structure. *Microbiol Sci* **1988**, *5*, 370-375.
72. Bartnick.S. Cell Wall Chemistry Morphogenesis and Taxonomy of Fungi. *Annu Rev Microbiol* **1968**, *22*, 87-+.
73. Dzurendova, S.; Zimmermann, B.; Tafintseva, V.; Kohler, A.; Ekeberg, D.; Shapaval, V. The influence of phosphorus source and the nature of nitrogen substrate on the biomass production and lipid accumulation in oleaginous Mucoromycota fungi. *Appl Microbiol Biot* **2020**, *104*, 8065-8076, doi:10.1007/s00253-020-10821-7.
74. Martinezcadena, G.; Ruizherrera, J. Activation of Chitin Synthetase from *Phycomyces-Blakesleeanus* by Calcium and Calmodulin. *Arch Microbiol* **1987**, *148*, 280-285.
75. Papp, T.; Velayos, A.; Bartok, T.; Eslava, A.; Vagvolgyi, C.; Iturriaga, E. Heterologous expression of astaxanthin biosynthesis genes in Mucor circinelloides. *Appl Microbiol Biot* **2006**, *69*, 526-531.
76. Papp, T.; Nagy, G.; Csernetics, Á.; Szekeres, A.; Vágvölgyi, C. BETA-CAROTENE PRODUCTION BY MUCORALEAN FUNGI.

77. Naz, T.; Nosheen, S.; Li, S.; Nazir, Y.; Mustafa, K.; Liu, Q.; Garre, V.; Song, Y. Comparative Analysis of β-Carotene Production by *Mucor circinelloides* Strains CBS 277.49 and WJ11 under Light and Dark Conditions. *Metabolites* **2020**, *10*, 38, doi:10.3390/metabo10010038.
78. Zajac, A.; Hanuza, J.; Wandas, M.; Dyminska, L. Determination of N-acetylation degree in chitosan using Raman spectroscopy. *Spectrochim Acta A* **2015**, *134*, 114-120.
79. Jehlicka, J.; Edwards, H.G.M.; Orenc, A. Raman Spectroscopy of Microbial Pigments. *Appl Environ Microb* **2014**, *80*, 3286-3295.
80. Avalos, J.; Limon, M.C. Biological roles of fungal carotenoids. *Curr Genet* **2015**, *61*, 309-324.
81. Diehn, S.; Zimmermann, B.; Tafintseva, V.; Seifert, S.; Bagcioglu, M.; Ohlson, M.; Weidner, S.; Fjellheim, S.; Kohler, A.; Kneipp, J. Combining Chemical Information From Grass Pollen in Multimodal Characterization. *Front Plant Sci* **2020**, *10*.
82. Hassani, S.; Hanafi, M.; Qannari, E.; Kohler, A. Deflation strategies for multi-block principal component analysis revisited. *Chemometr Intell Lab* **2013**, *120*, 154-168.

Supplementary Material

Assessment of filamentous fungal biomass by Fourier transform Raman spectroscopy for application in biotechnology and bioprocessing

Simona Dzurendová[1] (simona.dzurendova@nmbu.no), Volha Shapaval[1] (volha.shapaval@nmbu.no), Valeria Tafintseva[1] (valeria.tafintseva@nmbu.no), Achim Kohler[1] (achim.kohler@nmbu.no), Dana Byrtusová[1,2] (dana.byrtusova@nmbu.no), Martin Szotkowski[2] (xcszotkowski@fch.vut.cz), Ivana Márová[2] (marova@fch.vut.cz), Boris Zimmermann[1]* (boris.zimmermann@nmbu.no)

[1]Faculty of Science and Technology, Norwegian University of Life Sciences, Postbox 5003, 1432 Ås, Norway
[2]Faculty of chemistry, Brno University of Technology, Purkyňova 464/118, 61200 Brno, Czechia

Correspondence address: Faculty of Science and Technology, Norwegian University of Life Sciences, Postbox 5003, 1432 Ås, Norway

*Corresponding author:
Boris Zimmermann
Faculty of Science and Technology
Norwegian University of Life Sciences
Drøbakveien 31, 1432 Ås, Norway.
Tel: +47 6723 1576
Fax: +47 6496 5001
E-mail: boris.zimmermann@nmbu.no

Table of Contents **Page**

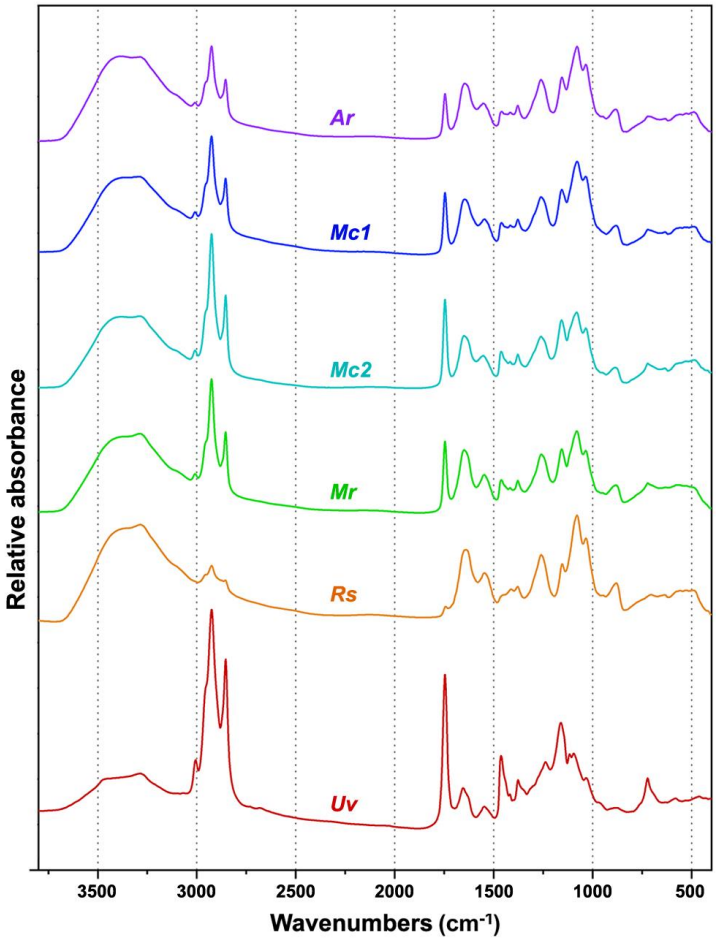

Figure S1. FTIR spectra of Mucoromycota oleaginous filamentous fungi cultivated under the standard growth condition (Ca1 and Pi1): *Amylomyces rouxii* (*Ar*), *Mucor circinelloides* VI 04473 (*Mc1*), *Mucor circinelloides* FRR 5020 (*Mc2*), *Mucor racemosus* (*Mr*), *Rhizopus stolonifer* (*Rs*), and *Umbelopsis vinacea* (*Uv*). All spectra were preprocessed and plotted with offset for better viewing.

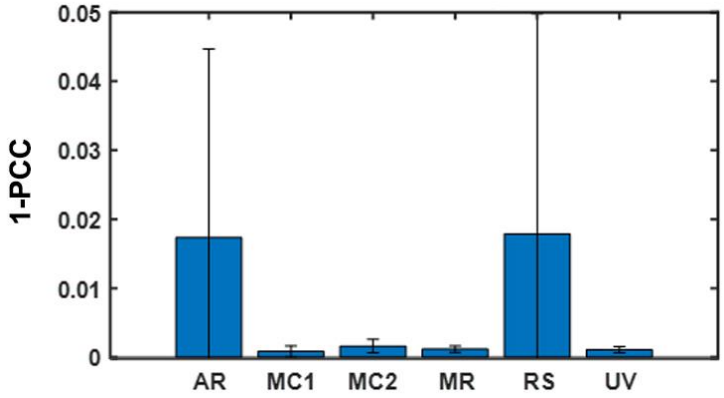

Figure S2. Reproducibility analysis of FT-Raman spectra based on PCC calculation for three technical replicates. *Amylomyces rouxii* (AR), *Mucor circinelloides* VI 04473 (MC1), *Mucor circinelloides* FRR 5020 (MC2), *Mucor racemosus* (MR), *Rhizopus stolonifer* (RS), and *Umbelopsis vinacea* (UV). Bars show 1-PCC with standard deviation. Higher bar values indicate less correlation of the technical replicates.

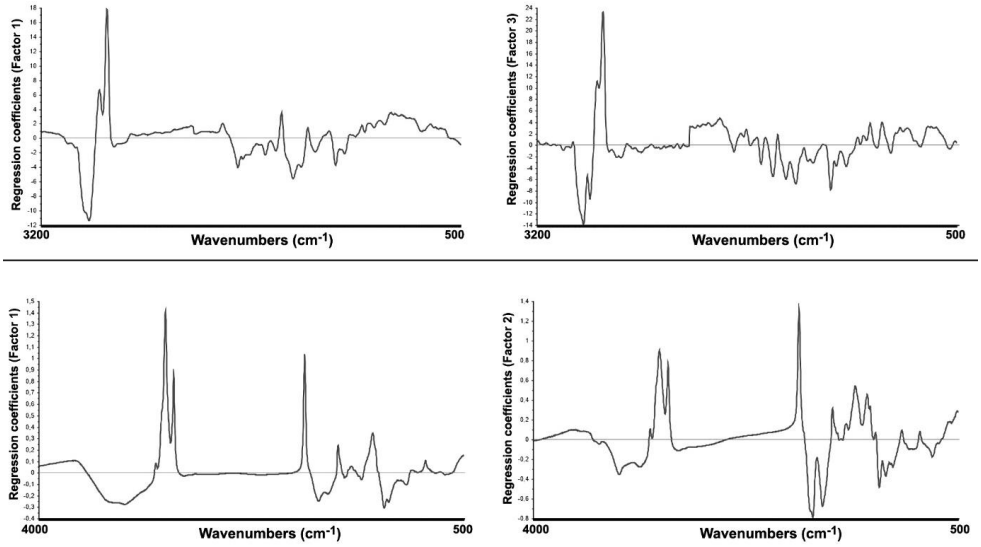

Figure S3. Plot of partial least-squares regression (PLSR) coefficients for determination of total lipids for all six strains, based on nonderivative preprocessed: FT-Raman data (up) and FTIR data (down).

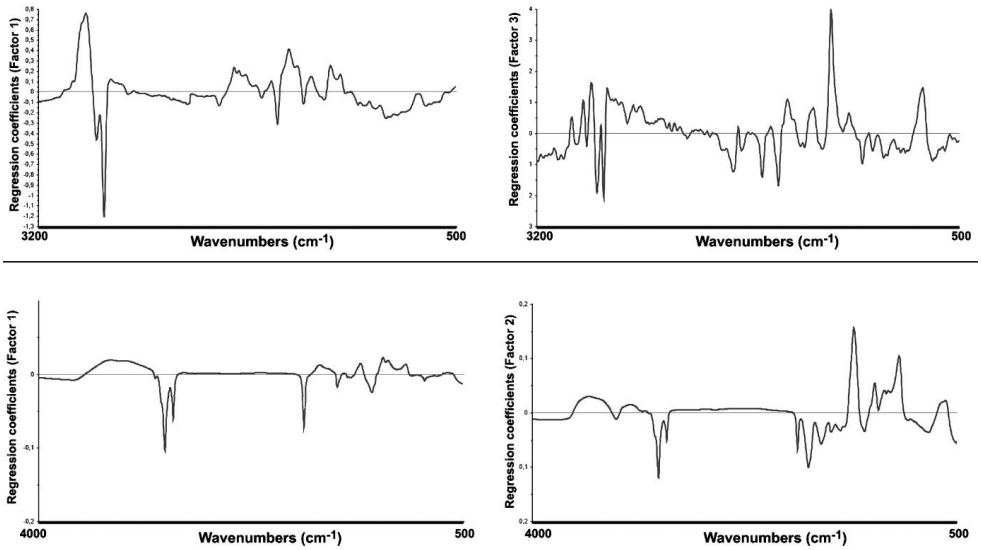

Figure S4. Plot of partial least-squares regression (PLSR) coefficients for determination of total phosphorus for all six strains, based on nonderivative preprocessed: FT-Raman data (up) and FTIR data (down).

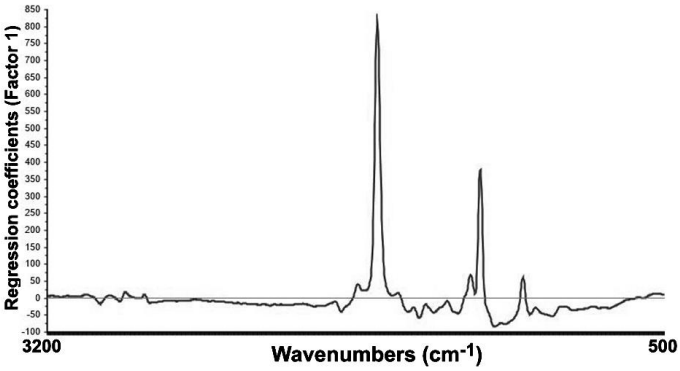

Figure S5. Plot of partial least-squares regression (PLSR) coefficient for determination of total carotenoids for *Mucor circinelloides* strains, based on nonderivative preprocessed: FT-Raman data.

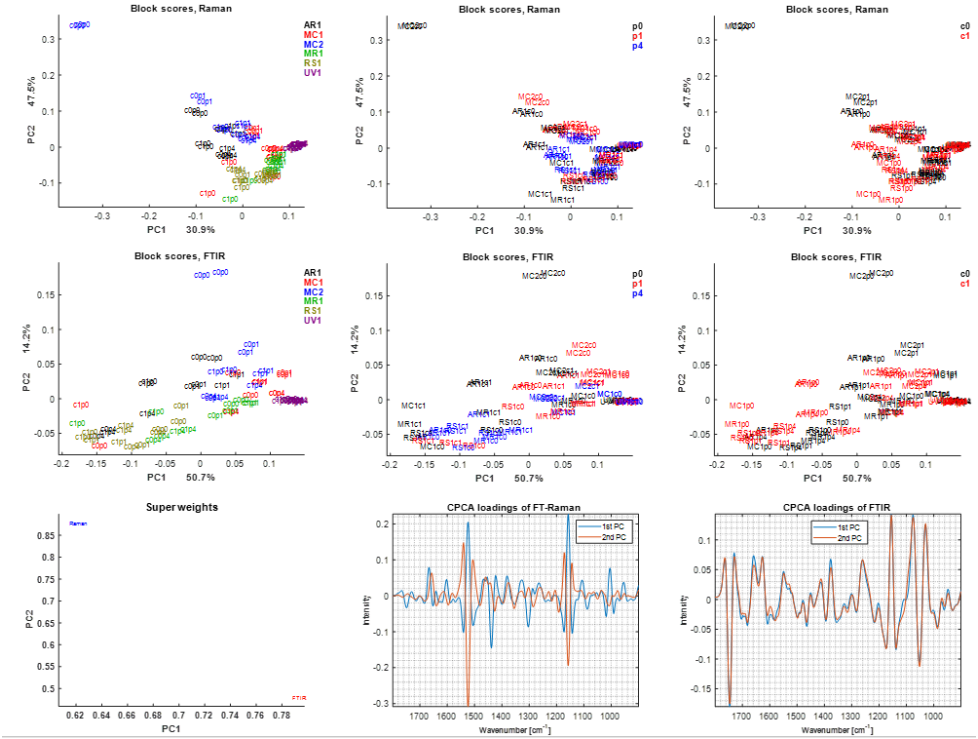

Figure S6. Multiblock consensus principal component analysis of FTIR and FT-Raman spectroscopic data. Score plots of CPCA individual blocks: FT-Raman block (top row), and FTIR block (middle row). Score values of individual data blocks of the CPCA are labelled according to strains: *Amylomyces rouxii* (*Ar*), *Mucor circinelloides* VI 04473 (*Mc1*), *Mucor circinelloides* FRR 5020 (*Mc2*), *Mucor racemosus* (*Mr*), *Rhizopus stolonifer* (*Rs*), and *Umbelopsis vinacea* (*Uv*) (left), phosphates concentrations (middle), and calcium availability (right). CPCA weights of individual blocks (bottom left). CPCA loading plots of individual blocks: FT-Raman block (bottom middle), and FTIR block (bottom right).

ISBN: 978-82-575-1797-7
ISSN: 1894-6402

Norwegian University
of Life Sciences

Postboks 5003
NO-1432 Ås, Norway
+47 67 23 00 00
www.nmbu.no